BIOCATALYSIS OF PRECURSORS TO NEW-GENERATION SB-T-TAXANES EFFECTIVE AGAINST PACLITAXEL-RESISTANT CANCER CELLS

By

Aimen Sabah Al-Hilfi

A DISSERTATION

Submitted to
Michigan State University
in partial fulfillment of the requirements
for the degree of

Chemistry – Doctor of Philosophy

2024

ABSTRACT

Taxus acyltransferases of the BAHD acyltransferases plant superfamily were used as an alternative method for the biocatalytic production of the next-generation paclitaxel analog precursors.

A *Taxus* 10-deacetylbaccatin III: 10-*O*-acetyltransferase (DBAT) was used to install cyclopropane carbonyl and propionyl groups at the C10 position of 10-deacetylbaccatin III (10-DAB). The k_{cat} and K_M of the acyltransferase for cyclopropanecarbonyl CoA (0.83 s^{-1}, 0.15 M) and *n*-propionyl CoA (1.2 s^{-1}, 0.15 M) guided scale-up efforts. The 10-acyl-10-*O*-deacetylbaccatin III analogs (~45 mg each) were made by the acyltransferase when incubated with the commercial taxane 10-*O*-deacetylbaccatin III and synthesized cyclopropanecarbonyl or *n*-propionyl CoA. The structures of the 10-acyl products were verified by NMR analyses that confirmed C10 acylation of the taxane substrate. LC/ESI-MS/MS analysis also supported the identities of the 10-*O*-*n*-propionyl-10-*O*-deacetylbaccatin III and 10-*O*-cyclopropanecarbonyl-10-*O*-deacetylbaccatin III biocatalyzed products. This effort provides a biocatalysis framework to produce new-generation taxane precursors.

A *Taxus* taxane-2-*O*-benzoyltransferase (*m*TBT) biocatalyzed the de-aroylation and re-aroylation of next-generation taxane precursors of drugs effective against multidrug-resistant cancer cells. Various taxanes bearing an acyl, hydroxyl, or oxo group at C13 were screened to assess their turnover by *m*TBT catalysis. The 13-oxotaxanes were the most productive where 2-*O*-debenzoylation of 13-oxobaccatin III was turned over faster compared to 13-oxo-10-*O*-(n-propanoyl)-10-*O*-deacetylbaccatin III and 13-oxo-10-*O*-(cyclopropane carbonyl)-10-*O*-deacetylbaccatin III, yielding ~20 mg of each. *m*TBT catalysis was likely affected by an intramolecular hydrogen bond with the C13-hydroxyl; oxidation to the 13-oxo recovered catalysis.

The experimental data for the debenzoylation reaction was supported by Gaussian-accelerated molecular dynamics simulations that evaluated the conformational changes caused by different functional groups at C13 of the substrate. These findings also helped postulate where the 2-*O*-benzoylation reaction occurs on the paclitaxel pathway in nature. *m*TBT rearoylated the debenzoylated 13-oxobaccatin III acceptors fastest with a non-natural 3-fluorobenzoyl CoA among the other aroyl CoA thioesters evaluated, yielding ~10 mg of each with excellent regioselectivity at laboratory scale. Reducing the 13-oxo group to a hydroxyl yielded key modified baccatin III precursors (~10 mg at laboratory scale) of new-generation taxoids.

The role of Mg^{2+} ions in the *Taxus* baccatin III: 3-amino-3-phenylpropanoyltransferase (BAPT) catalysis has been studied. This hypothesis was tested by screening phenylisoserine CoA with baccatin III. The results suggested that Mg^{2+} ions are critical for the BAPT catalysis by interrupting the intramolecular hydrogen bond between C13 hydroxyl group and OAc, organizing the amino acid active site, and act as oxyanion hole by stabilizing the negative charge form in the tetrahedral intermediate. Further, the BAPT, Mg^{2+} independent catalysis was able to transfer the isobutenylisoserinyl at C13 position of taxnne cores selectively and product the next generation paclitaxel precursors (~10 mg at laboratory scale).

ACKNOWLEDGEMENTS

During my journey at Michigan State University, there were so many people to thank for helping me and making my study a lot easier than I expected it to be. I would like to acknowledge my adviser, Dr. Kevin Walker, for his help and support during my time here at Michigan State University. Also, I would like to acknowledge my committee members: Dr. Heedeok Hong, Dr. Tuo Wang, and Dr. Karen Draths for their help, time, and insightful comments.

I would like to thank the Michigan State University Chemistry Department for giving me this opportunity to pursue my PhD degree thesis work. My gratitude also goes to the dedicated faculty and staff members, especially Dr. Gary Blanchard, Dr. Melaine Cooper, Ms. Nancy Lavrik. Your friendly smiles added great value to every help you gave me.

Finally, I would like to express my profound gratitude to my parents and family. I am extremely grateful to my father for his wisdom, support, and advice now and throughout my life. Also, I would like to dedicate this thesis to my mother for being a constant source of support and encouragement and always believing in me. I would like to thank my brothers and sister for supporting me spiritually and bringing me breaks of laughter during my research.

Last, but not least, I would like to thank my lovely wife Seana for standing by my side while I poured my focus into achieving my goal. I cannot forget the unconditional love provided by my son William Ali. He gave light to the hardest days and was a driving force behind everything including reaching the finish line of my dissertation. I'm here now because they were there with me along the way.

TABLE OF CONTENTS

LIST OF ABBREVIATIONS

Ac_2O	Acetic anhydride
ATP	Adenosine triphosphate
BAPT	baccatin III: 3-amino-3- phenylpropanoyltransferase
Boc	*tert*-Butoxycarbonyl
Bz	Benzoyl
CAN	Cerium (IV) ammonium nitrate
$CDCl_3$	Deuterated chloroform
10-CPCDAB	10-*O*-Cyclopropane carbonyl-10-deacetylbaccatin III
CoA	Coenzyme A
$CDCl_3$	Deuterated chloroform
D_2O	Deuterated water
DMF	Dimethylformamide
DIC	*N*, *N*′-Diisopropylcarbodiimide
10-DAB	10-*O*- deacetylbaccatin III
DMAP	4-Dimethylaminopyridine
DBAT	10-deacetylbaccatin III: 10-*O*-acetyltransferase
DFGWG	Aspartate; phenylalanine; glycine; tryptophan; glycine motif
DBz	Debenzoyl
E. coli	*Escherichia coli*
ESI-MS/MS	Electrospray ionization tandem mass spectrometer
EtOAc	Ethyl acetate
FDA	U.S. Food and Drug Administration

h	Hour(s)
IDP	Isopentenyl diphosphate
IPTG	Isopropyl β–D–1–thiogalactopyranoside
J	NMR coupling constant
k_{cat}	catalytic turnover
K_M	Michaelis constant
kDa	kilodalton
LB	Luria-Bertani medium
LC	Liquid chromatography
LDA	Lithium diisopropylamide
LiHMDS	Lithium bis(trimethylsilyl)amide
m	multiplet
MeCN	Acetonitrile
MeOH	Methanol
min	minute
mg	milligram
mL	milliliter
*m*TBT	modified wild-type 2-*O*-benzoyltransferase
MHz	Megahertz
m/z	mass to charge ratio
MS	Mass Spectrometer
MDR	Multiple-drug resistant
MnO_2	Manganese dioxide

$NaBH_4$	Sodium borohydride
Ni-NTA	Nickel nitrilotriacetic acid
Na_2SO_4	Sodium sulphate
$NaHCO_3$	Sodium bicarbonate
NMR	Nuclear Magnetic Resonance
NDTNBT	*N*-debenzoyltaxol-*N*-benzoyltransferase
OD	Optical density
PMSF	Phenylmethylsulfonyl fluoride
PheAT	Phenylisoserine CoA ligase
10-PDAB	10-*O*-Propionyl-10-deacetylbaccatin III
RT	Room temperature
Red-Al	Sodium bis (2-methoxy ethoxy) aluminum hydride
SAR	Structure-activity relationship
SDS-PAGE	Sodium dodecyl sulfate polyacrylamide gel electrophoresis
SB-T	Stony Brook-Taxol
TAT	Taxadien-5α-ol *O*-acetyltransferase from T. cuspidata
TBT	2-*O*-debenzoylbaccatin III 2-*O*-benzoyltransferase from T. cuspidata
t-BuOH	*tert*-Butyl alcohol
TES-Cl	Triethyl silane chloride
THF	Tetrahydrofuran

CHAPTER 1: INTRODUCTION

Cancer

Cancer is a group of diseases where the abnormal cells grow out of control and invade or spread to other tissue in the body.[1,2] Under normal conditions, cells will grow, divide, and undergo apoptosis to maintain tissue homeostasis and repair damage.[1,3,4] However, in cancer cells, this orderly process is altered. The abnormal cells will survive by evading the cell death mechanism and new cells will grow even when it is not needed leading to uncontrolled cell growth.[3-5]

Cancer was and still is the leading cause of death in both sexes and all ages with an estimated number of new cases increasing every year globally.[6] According to the American Cancer Society (ACS), there are 158,333 new cancer cases and 50,714 cancer-related deaths per day in the United States. The estimated number of new cases and deaths in the world is expected to rise by 2040 to 2.458 million new cancer cases and 1.367 million cancer-related deaths per day. With the increasing numbers of cancer cases and deaths, there will be an urge to look for new treatments or enhance the existing conventional treatments.

There are many conventional treatments used to treat cancer such as surgery, radiotherapy, chemotherapy, and immunotherapy.[7,8] Chemotherapy remains one of the most important treatments among all the conventional treatments to combat cancer. Chemotherapy is the use of drugs to kill cancer cells.[9,10] The chemotherapeutic drugs work by interfering with the microtubule which is responsible for cell division to produce new cells.[11-13] The most important chemotherapy drugs are the taxane analogs.[14,15] The first-generation taxane chemotherapy agents such as paclitaxel and its analogs docetaxel and cabazitaxel are approved by the FDA and applied for various cancer types.[14,16-20] The new generation taxane chemotherapy agents show promising results for treating previously chemo-resistant cancers.[21,22]

Microtubule-Targeting Agents (MTAs)

Microtubules are important components of the cytoskeleton in all the eukaryotic cells. They are key to different cellular activities including maintenance of cell shape, intracellular transport, cell signaling, and cell motility.[23] Microtubules form by the polymerization of tubulin dimers. Tubulin is a heterodimeric protein that consists of two polypeptide subunits, α- and β-tubulin subunits.[24] As the dimers polymerize, they form rings, then uncoil into protofilaments, which associate side-by-side into sheets.[25] The microtubule forms when the sheet grow and reache 13 aligned protofilaments.[26] After that microtubule elongates by the addition of dimers to the ends of the protofilaments which bundle together to form hollow cylinders that are approximately 25 nm in diameter.[26] Since microtubules can interfere with several cellular processes, many microtubule-targeting agents (MTAs) are developed and used in cancer chemotherapy.[27-30] Microtubule-targeting agent drugs act by interfering with the exchange of tubulin subunits between the microtubules and the free tubulin in the mitotic spindle.[28,30] There are two different kinds of microtubule-targeting agents, microtubule destabilizing agents and microtubule stabilizing agents.

Microtubule destabilizing agents such as Vinca alkaloids (**1.1**, **1.2**, and **1.3**), colchicine (**1.4**), and combretastatin (**1.5** and **1.6**) (Figure 1.1), prevent the polymerization of microtubules. These compounds bind to tubulin and prevent microtubule polymerization. This action will result in the rapid disappearance of the mitotic spindle and lead many abnormally dividing cells to die which casing to cell death.[23,31]

Microtubule stabilizing agents such as paclitaxel (**1.7**), docetaxel (**1.8**), cabazitaxel (**1.9**), epothilones A (**1.11**), epothilones B (**1.10**), and dictyostatin (**1.11**) (Figure 1.2), promote the polymerization of microtubules. These compounds bind tubulin and achieve their effect by increasing tubulin polymerization and stabilizing microtubule polymers.[23,32]

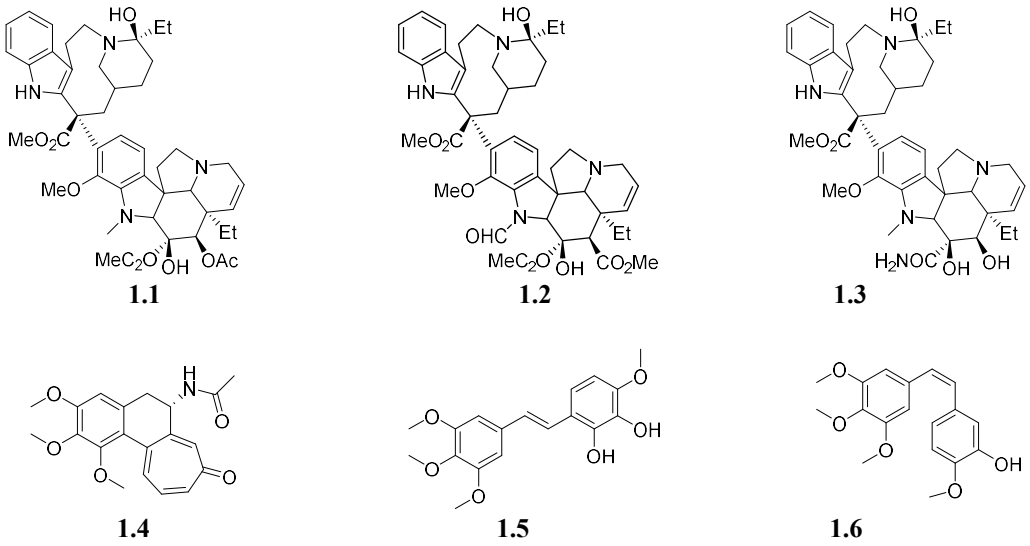

Figure 1.1: Structures of microtubule destabilizing agents.

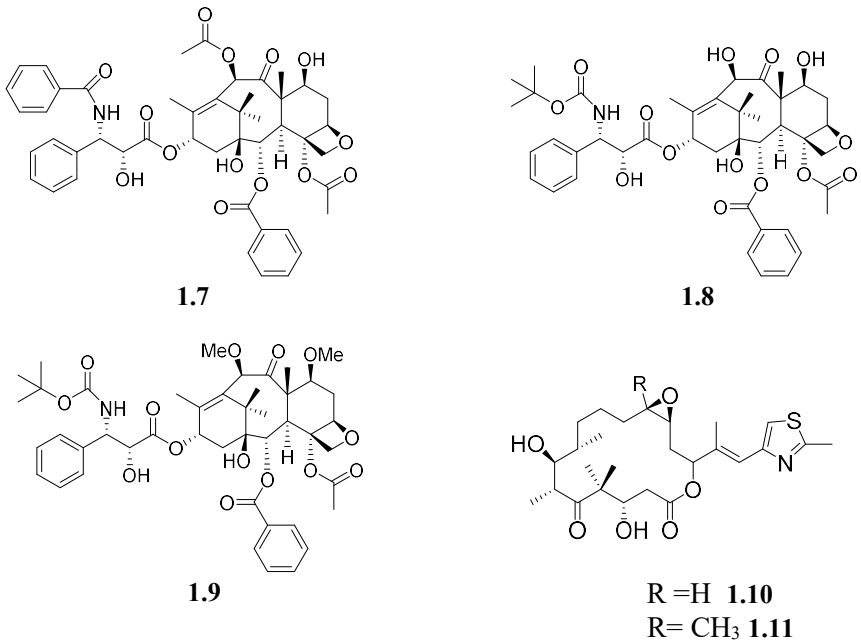

Figure 1.2: Structures of microtubule stabilizing agents.

Brief History of Paclitaxel and Its Analogs

Paclitaxel (Taxol®) (1.7) (Figure 1.2) is one of the most important anticancer drugs in chemotherapy. Paclitaxel was isolated from the bark of the Pacific Yew tree, *Taxus brevifolia* by Monroe E. Wall and Mansukh C. Wani at the National Cancer Institute in North Carolina in 1967.[33] The chemical structure of paclitaxel was characterized in 1971 when it was named Taxol®.[34] The

unique mechanism of action of Taxol as an antimitotic drug was discovered in 1979 by Susan Horwitz, P. Schiff, and J. Fant.[28] They found that Taxol binds to the β-tubulin and stabilizes microtubules by blocking the tubulin assembly.[28,34] In 1983, paclitaxel was put into phase I clinical trials and moved to phase II trials in 1985 which proved to be clinically active against ovarian cancer and breast cancer.[35] The term paclitaxel was used as generic name in 1992. Paclitaxel (Taxol®) was approved by the U.S. Food and Drug Administration (FDA) for the treatment of ovarian cancer in 1992 and breast cancer in 1994.[36] Docetaxel (Taxotere®) (**1.8**) (Figure 1.2) is the water-soluble semisynthetic paclitaxel analog, and it was proved by the FDA for treatment of lung cancer in 1999.[20] Cabazitaxel (Jevtana®) (**1.9**) (Figure 1.2) the second semisynthetic paclitaxel analog was also approved by the FDA for the treatment of metastatic castration-resistant prostate cancer.[19]

Paclitaxel Mechanism of Action

Paclitaxel is a microtubule inhibitor that promotes the assembly of microtubules from tubulin dimers.[37,38] Microtubules have highly dynamic structures assembled from a polymer chain of α and β tubulin subunits, which polymerize head to tail as α/β heterodimers (Figure 1.3).[39] Microtubules undergo continual polymerization and depolymerization as cells grow and divide and this process is called dynamic instability.[40] This dynamic instability of microtubules requires GTP-hydrolysis to function.[40] Microtubule dynamic instability facilitates normal chromosomal segregation and intracellular transport.[40] Paclitaxel binds to the β tubulin and this binding stabilizes microtubules by interrupting the dynamic balance between polymerization and depolymerization. This stability results in the inhibition of the normal dynamic reorganization of microtubule network leading to cell cycle arrest at the G_2/M phase and ultimately cell death.[40-42]

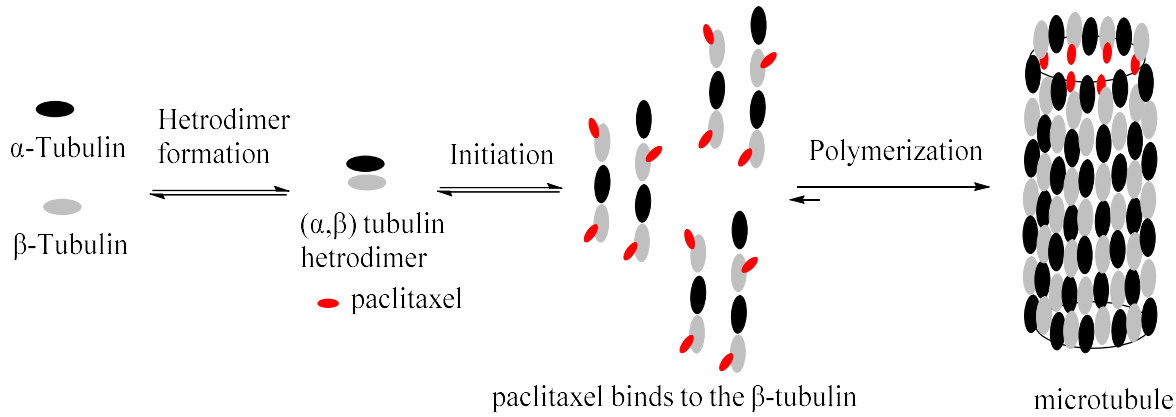

Figure 1.3: Paclitaxel mode of action. Structure of α/β tubulin, microtubule, and paclitaxel-bound microtubule. [43]

Paclitaxel Drug Resistant

Over three decades, cancer cells have been found to develop chemotherapeutic resistance because of multiple-drug resistance (MDR).[44,45] It has been shown that multiple-drug resistance limits the therapeutic use of cancer chemotherapeutic agents such as paclitaxel.[46] Drug resistance in cancers is a multifactorial phenomenon induced through different cellular mechanisms including the overexpression of p-glycoproteins (p-gp) drug-efflux pumps, and overexpression of βIII-tubulin isotype.[44,45]

P-glycoprotein (p-gp) is one of the most important aspects responsible for causing multiple-drug resistances.[47] P-gp is often overexpressed in resistant cancer cells.[47-49] P-gp is an efflux pump powered by ATP that can extrude different drugs outside the cells, which gives protection and monitors the survival of cells.[50,51] The p-gp gene is expressed in different cell types such as liver, kidney, and intestinal cells as well as on the blood-brain barrier.[52,53] P-gp has two transmembrane domains (TMDs). Each domain has six membrane-spanning α-helices where the drug binds and one nucleotide-binding domain (NBD) where the ATP binds (Figure 1.4).[54]

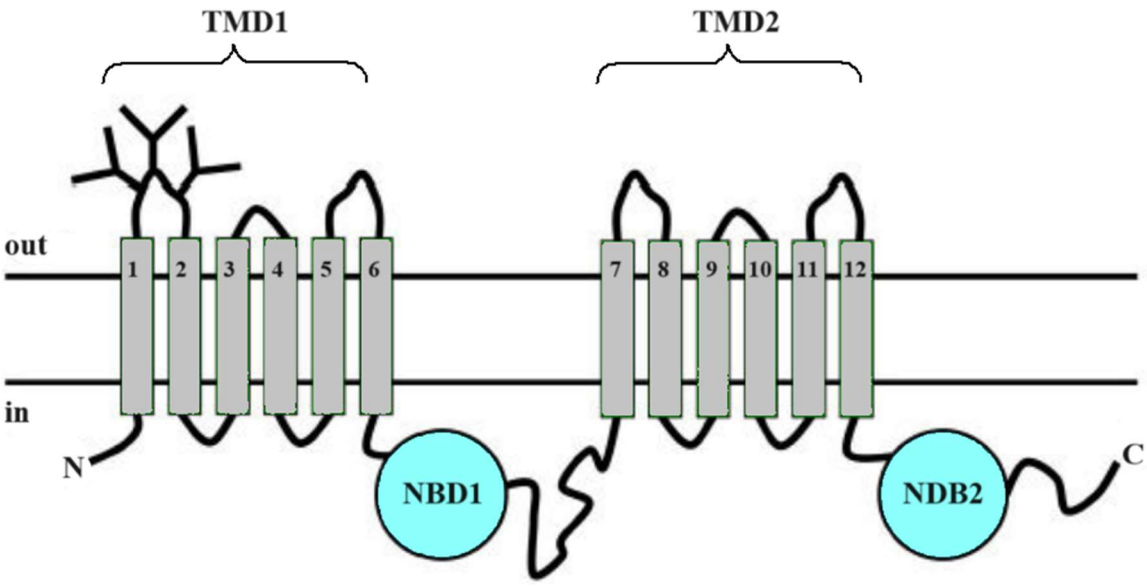

Figure 1.4: Topology structure of P-gp. The topology of P-gp showed that it is formed by a single protein strand with two homologous halves. Each half contains six transmembrane (TM) segments (gray) and a nucleotide binding (NB) domain (blue) on the cytoplasmic side which can bind and hydrolyze ATP.[54]

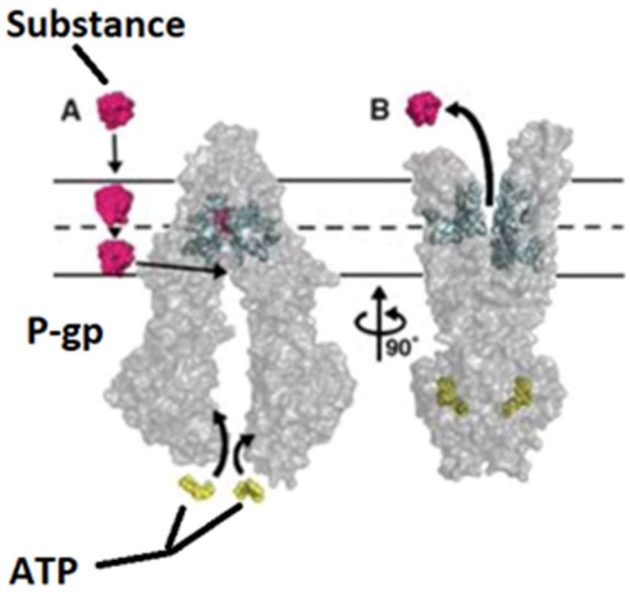

Figure 1.5: Two p-gp transporters in different conformations across the phospholipid bilayer. The inward-facing structure (**left**) promotes drug binding, while the outward-facing structure (**right**) facilitates the efflux process. The channel pore for the outward-facing structure is narrow, hence the drug is actively pumped out into the extracellular environment.[55]

P-gp is an energy-driven transporter, and the efflux of its substrates requires the hydrolysis of ATP.[55] P-gp has an open conformation in the intracellular region (inward facing). When the drug

substrate binds to it, the protein conformational changes to outward facing which causes dimerization of the NBD followed by ATP hydrolysis to convert the first ATP binds into ADP. This will expel the drug molecules outside the cancer cells. After that, the second ATP molecule binds and hydrolyzes to return the conformation of p-gp to its original shape and orientation (Figure 1.5).[55,56] P-gp efflux activity has become a serious problem in drug discovery and their application in chemotherapy by reducing their intracellular concentration.[57,58] Many molecules have been carried out to develop compounds that can bind to p-gp and inhibit its efflux action by blocking its ATPase activity so that other drugs can accumulate, and their therapeutic effect is enhanced.[59,60]

There are eight different β-tubulin isotypes designated as βI, βIIa, βIIb, βIII, βIVa, βIVb, βV, and βVI expressed in mammalian cells. These β-tubulin isoforms differ from each other within the C-terminal amino acids (Figure 1.6).[61,62] The biological roles of these isoforms in microtubule functions in cells are still unclear.

However, many studies on different cancer cell lines have shown that overexpression of βIII-tubulin isotype correlates with the multiple-drug resistance to a subset of anticancer drugs including taxane analogs (paclitaxel, docetaxel, and cabazitaxel) by increasing the microtubule dynamic instability. Moreover, the overexpression of βIII-tubulin isotype is also responsible for increasing aggressiveness in some tumors. The mechanism of how βIII-tubulin overexpression enhances microtubule dynamics remains unclear.[63]

Several studies, however, have been examining the M-loop residues and comparing the leucine cluster region near the paclitaxel binding site of all the eight β-tubulin isoforms.[64-66] The results show that the βIII-tubulin leucine cluster region has an alanine (A218) residue while the other β-tubulin isotype has a threonine (T218) residue (Figure 1.7).[64] This finding could maybe explain why the anticancer drugs do not bind to βIII-tubulin and increase microtubule dynamic instability.

βI ^{430}YQDATAEEEEDFGEEAEEEA^{450}

βIIa ^{430}YQDATAEEEEDFGEEAEEEA^{450}

βIIb ^{430}YQDATADEQGEFEEEEGEDEA^{451}

βIII ^{430}YQDATAEEEGEMYEDDEEESEAQGPK^{456}

βIVa ^{430}YQDATAEEGEFEEEAEEEVA^{450}

βIVb ^{430}YQDATAEEEGEFEEEAEEEVA^{451}

βV ^{430}YQDATANDGEEAFEDEEEEIDG^{452}

βVI ^{430}FQDAKAVLEEDEEVTEEAEMEPEDKGH^{457}

Figure 1.6: Sequence alignment of part of the C-terminal of human β-tubulin isotypes. [61]

βI ^{212}FRTLKLTTPTYGDLNHLVS^{230}

βIIa ^{212}FRTLKLTTPTYGDLNHLVS^{230}

βIIb ^{212}FRTLKLTTPTYGDLNHLVS^{230}

βIII ^{212}FRTLKLATPTYGDLNHLVS^{230}

βIVa ^{212}FRTLKLTTPTYGDLNHLVS^{230}

βIVb ^{212}FRTLKLTTPTYGDLNHLVS^{230}

βV ^{212}FRTLKLTTPTYGDLNHLVS^{230}

βVI ^{212}FRTLKLTTPTYGDLNHLVS^{230}

Figure 1.7: Sequence alignment of part of the leucine cluster of human β-tubulin isotypes. Structure-Activity. [64]

Structure-Activity Relationships (SAR) of Paclitaxel

Since the discovery of paclitaxel, many chemical modifications and biological activities have been carried out to provide structural bioactivity information (Figure 1.8)[43,67] as well as develop analogs with high anticancer drug efficacy.[43,67] Paclitaxel is a very complex diterpenoid with 11 chiral centers and 5 acylations.[67] The core structure of paclitaxel is made up of two major parts. The first part is the C13 side chain containing 2′*R*, 3′*S* stereochemistry, one free hydroxy group at C2′, and an *N*-acyl group at C3′. The second part is the tetracyclic ring containing two free hydroxyl groups at (C1 and C7), two acetates groups at (C4 and C10), and an *O*-benzoyl group at C2.[67,68]

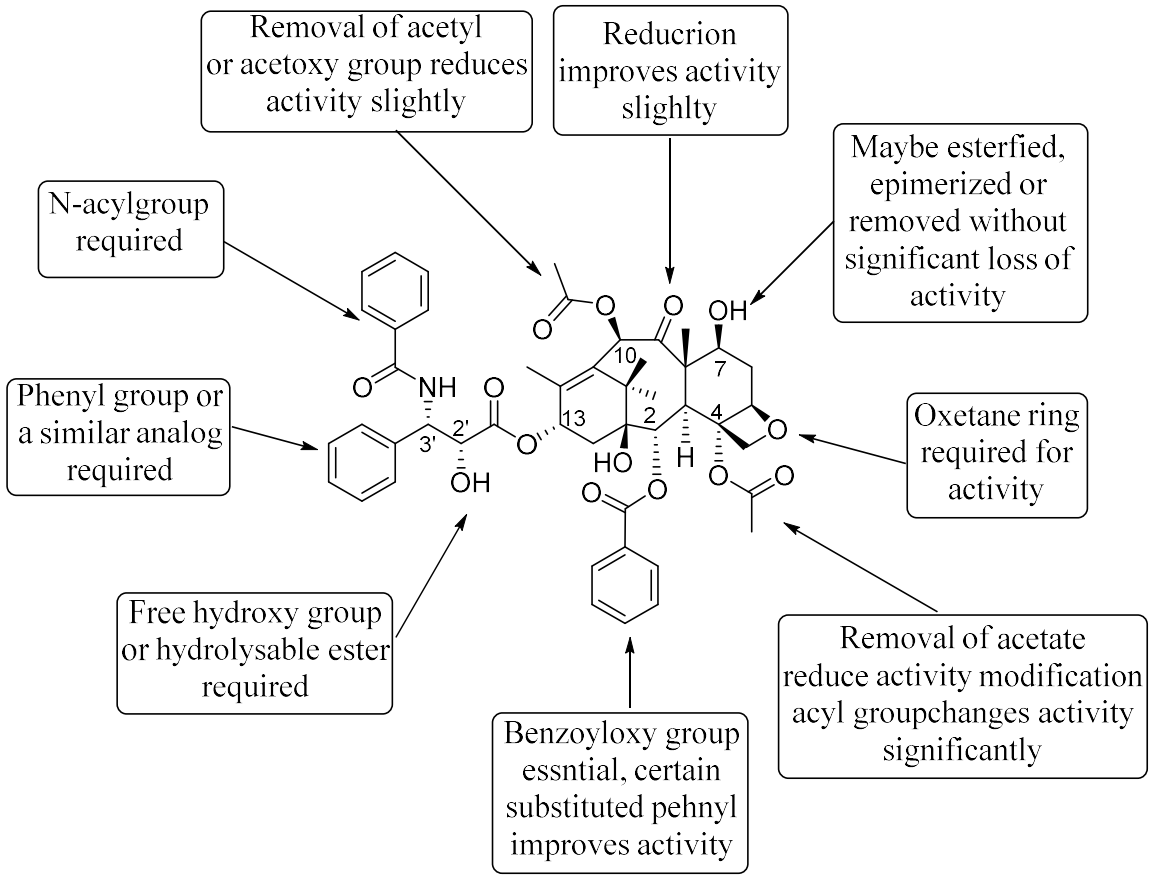

Figure 1.8: The Structure-Activity Relationships (SAR) of paclitaxel. [43]

Several modifications or removal have been constructed on each functional group separately or in combination, and the resulting compounds have been tested for tubulin binding affinity and cytotoxicity.[68-72] It has been shown that the C2′ free hydroxy and C3′ *N*-acyl group at the C13 side chain are required to promote the microtubule assembly and cytotoxicity.[70-72] The free hydroxy at C2′ will form a hydrogen bond with an arginine residue of β-tubulin. Also, modification of C3′ with alkyl or alkenoyl substituted increases the activity significantly.[70-72]

The SAR studies on baccatin III core (tetracyclic ring) show that opening the oxetane reduces the activity significantly. In addition, replacing the acyl group at C4 changed the activity slightly.[70-72] Acylation and dehydroxylation of the C7 position does not change the activity.[70-72] However, oxidation of the C7 hydroxy group to a ketone significantly decreased the activity of paclitaxel because it facilitated the opening of the oxetane ring at the C4-C5 position.[70-72] The carbonyl group

at the C9 position can be reduced to a hydroxyl group without loss of bioactivity.[70-72] Deacetylation at the C10 position will reduce the activity significantly. The C2 benzoyloxy group was proved to be important for the cytotoxicity bioactive conformation of paclitaxel.[70-72]

The recent structure-activity relationship studies show that modifications at the following paclitaxel core carbons: C2 benzoate with *meta*-substituted-(F, Cl, OCH_3, OCF_3, and $OCHF_2$) aroyl group; C10 with (cyclopropane carbonyl, and propionyl); C3′ with (isobutenyl, and 2,2-difluorovinyl); and *N*-acyl group at C3′ with *N*-Boc group enhance the cytotoxicity and potency against multiple-drug resistant (MDR)-cancer cell lines over the parent drug paclitaxel.[21,73]

Semisynthesis of Paclitaxel

Initially, paclitaxel was isolated from the inner bark of the pacific yew tree, *Taxus brevifolia* at very low yields approximately (0.01% w/w).[33] The supply issue of paclitaxel in its early development could not satisfy the market requirement and became an urgent problem.[43] Fortunately, the isolation of 10-deacetylbaccatin III (10-DAB) (**1.12**)[74] (Figure 1.9) by Potier and coworkers from the needles of the European yew, *Taxus baccata* with approximately (0.1% w/w) yield and low labor harvesting cost makes 10-DAB a perfect precursor for the semisynthesis of paclitaxel.[74]

In 1988, several semisynthetic methods were developed using 10-deacetylbaccatin III as precursors to produce paclitaxel.[75-80] These developed methods used a protected 10-DAB at the more reactive sites at C7 and C10 and acylated at C13 by coupling it with a suitable side chain precursor to produce paclitaxel. For instance, Bourzat's method using oxazolidines (**1.13**),[75] Holton and Swindell motheds both used an oxazinone **(1.14)**[77,78] as the protected side chain, Kingston's method using oxazoline (**1.15**)[76] and Holton's and Ojime's method both used β-lactam (**1.16**)[79,80] (Figure 1.10) as a precursor for the side chain coupling. Among all the developed semisynthetic methods, Holton's, and Ojime's method (Figure 1.11) proved to be the most

efficient method which was then licensed to Bristol-Myers Squibb (BMS) for commercial production of paclitaxel.[81]

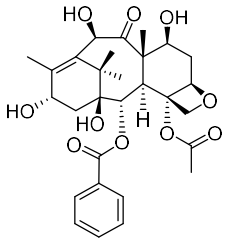

1.12

Figure 1.9: Structure of 10-deacetylbaccatin III (10-DAB).

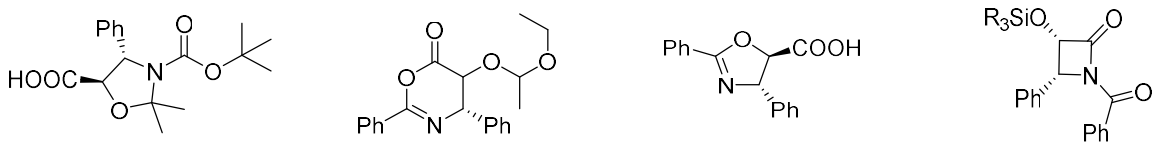

1.13 **1.14** **1.15** **1.16**

Figure 1.10: Structures of oxazolidines, oxazoline, oxazinones, β-lactam.

The Ojima-Holton method coupled *N*-benzoylisoserinyl side chain to baccatin III that is derived synthetically from 10-DAB. However, this semisynthetic method required silyl protection at the C7 hydroxyl group, acetylation of 10-deacetylbaccatin III at C10 to afford 7-*O*-protected baccatin III, synthetic attachment of the *N*-benzoyl phenylisoserine side chain at the C13 hydroxyl group, and, finally, deprotection to yield paclitaxel (Figure 1.11).

Paclitaxel Biosynthesis

Paclitaxel is biosynthesized in *Taxus* plants by a complex metabolic pathway involving 19 enzymatic steps.[82-84] The first step in the pathway starts with the geranylgeranyl diphosphate (GGPP) (**1.28**) which is constructed through the coupling between isopentenyl diphosphate (IDP) (**1.26**) and dimethylallyl diphosphate (DMADP) (**1.27**) by geranylgeranyl diphosphate synthase.[83] GGPP is then cyclized by taxadiene synthetase to generate the tricyclic taxane skeleton (taxadiene). Taxadiene goes through a series of reactions including eight cytochrome P450-mediated oxygenations, three acyl CoA-dependent acylations, an oxidation at C9, and oxetane (D-ring) formation to provide 10-deacetylbaccatin III (Figure 1.12).[83,84]

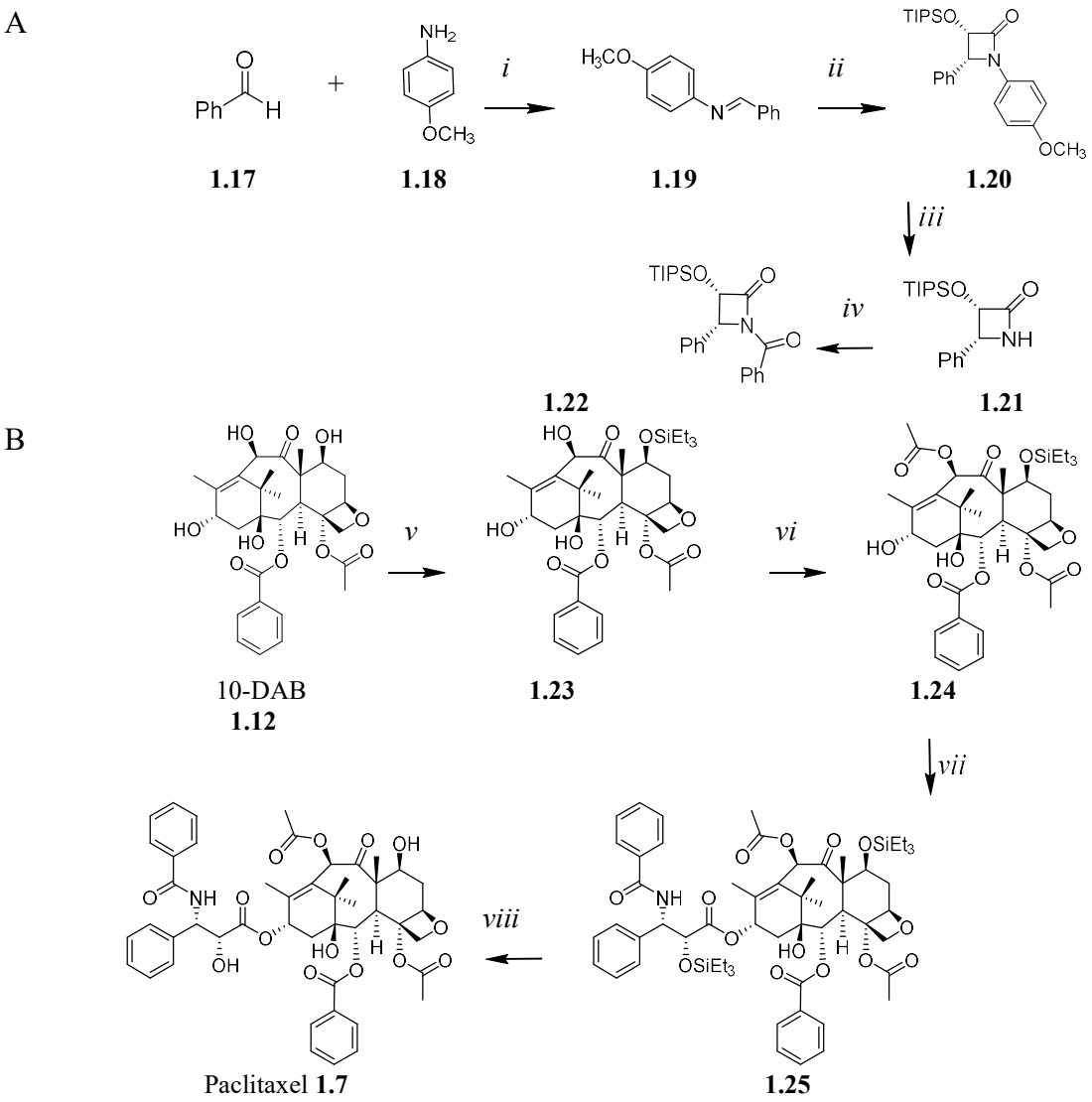

Figure 1.11: Ojima-Holton coupling for the synthesis of Paclitaxel. Reagent and conditions: (i) $MgSO_4$, CH_2Cl_2, r.t., 6h; (ii) LDA, cis-(2)-cyclohexyltriisopropylsilyloxy, THF -40 °C, 8h; (iii) CAN, CH_3CN, H_2O, r.t. 4h; (iv) benzoyl chloride, TEA, DMAP, CH_2Cl_2, r.t.; (v) TES-Cl (3 equiv.), imidazole (4 equiv.), dry DMF, 0 °C to r.t. over 6 h; (vi) acetyl chloride, LiHMDS (1.5 equiv.), dry THF, -40 °C to r.t.over 2 h; (vii) NaHMDS, THF, -30 °C, 2h; (viii) HF/pyridine, pyridine/MeCN, 0 °C to r.t., overnight.

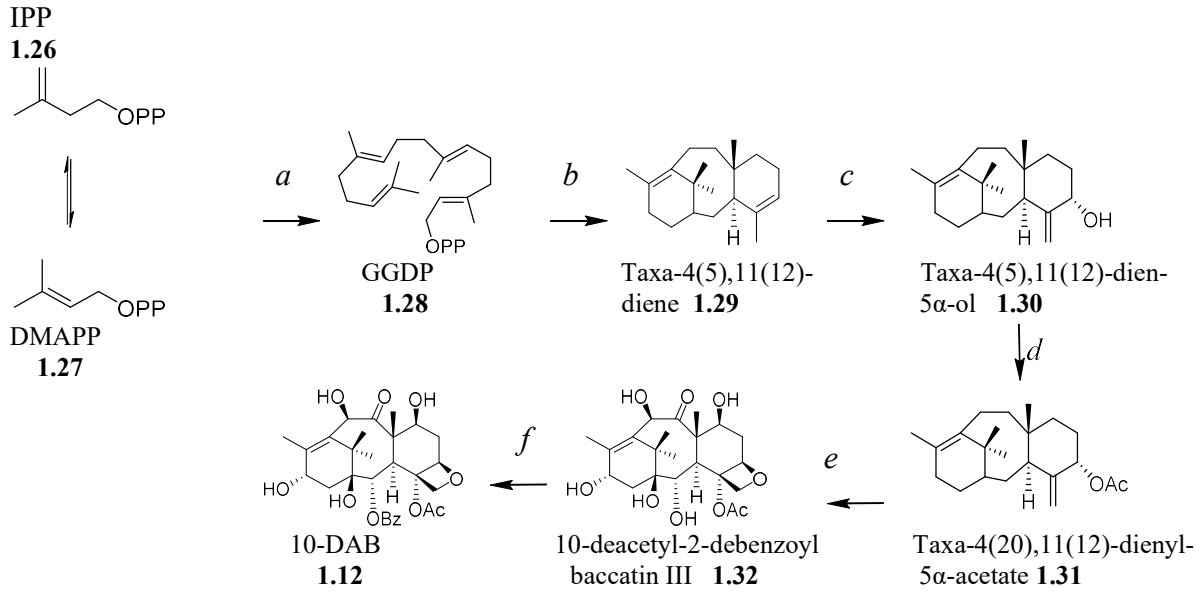

Figure 1.12: Biosynthetic pathway to paclitaxel starting from primary metabolite precursors to the 10-DAB. (a) geranylgeranyl diphosphate synthase, (b) GGDP cyclization by taxadiene synthase, (c) P450 oxygenase, (d) 5-*O*-acetylation by a taxa-5α-ol acetyltransferase, (e) P450 oxygenases, (f) 2-*O*-benzoylation by a 2-*O*-debenzoylbaccatin III benzoyltransferase.

The second half of the paclitaxel biosynthesis pathway starting from 10-deacetylbaccatin III is well-characterized.[85,86] The 10-deacetylbaccatin III 10-*O*-acetyltransferase (DBAT) acetylates 10-DAB to form baccatin III (**1.36**).[85] The baccatin III: 3-amino-13-*O*-phenylpropanoyl CoA transferase (BAPT) transfers the (3*R*)-β-phenylalanyl sidechain resulting (**1.37**).[86] Then P450 hydroxylase the C2′ position on the sidechain[87] and, *N*-debenzoyltaxol-*N*-benzoyltransferase (NDTNBT) benzoylate the 3'*N* side chain on the *N*-debenzoylpaclitaxel to form paclitaxel (Figure 1.13).[88]

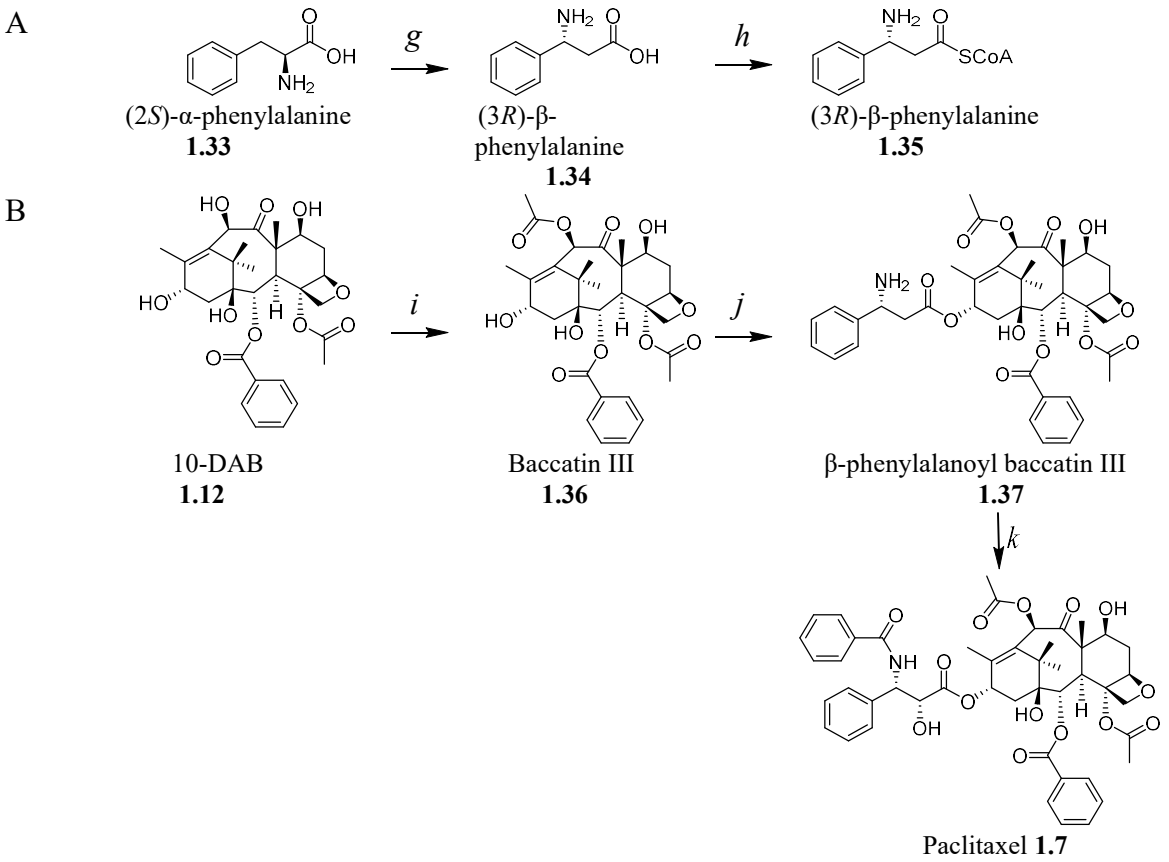

Figure 1.13: Biosynthesis of paclitaxel C-13 side chain (A) and the enzyme catalyzed transfer to the 10-DAB (B); (g) the conversion of (2*S*)-α-phenylalanine to its (3*R*)-β isomer is catalyzed by an aminomutase (PAM); (h) phenylpropanoyl CoA is catalyzed by unidentified phenylalanyl CoA ligase in Taxus plants; (i) 10-*O*-acetylation by a 10-deacetylbaccatin III acyltransferase (DBAT); (j) 13-*O*-acylation with (**1.35**) by a phenylpropanoyltransferase (BAPT); (k) C-2'-oxidation by a P450 hydroxylase; (l) *N*-benzoylation by a taxane *N*-benzoyltransferase (NDTNBT).

BAHD Acyltransferase Superfamily

BAHD acyltransferases belong to a large family of enzymes that are involved in a large diversity of acyl-CoA dependent reactions of secondary metabolites and important natural products.[89-91] Enzymes in this family utilize acyl-coenzyme A as acyl donor substrate and the amino or hydroxy group acceptors as cosubstrates. The BAHD-ATs were named after the first four biochemically characterized enzymes of this superfamily (BEAT, AHCT, HCBT, and DAT). Benzylalcohol-*O*-acetyltransferase (**BEAT**) was isolated from the flower petals of *Clarkia*

breweri[92] and this enzyme catalyzes the formation of benzyl acetate.[92] Anthocyanin-*O*-hydroxycinnamoyltransferases (**A**HCT) isolated from *Petunia*, *Senecio*, *Gentiana*, *Perilla*, and *Lavandula*.[93] AHCT enzyme transfers caffeoyl-CoA to the 5-α- glucoside of the anthocyanin delphinidin.[93] Anthranilate *N*-hydroxycinnamoyl/benzoyltransferase (**H**CBT) from *Dianthus caryophyllus* catalyzes the formation of *N*-benzoylanthranilate.[94] Deacetylvindoline-4-*O*-acetyltransferase (**D**AT) from *Catharanthus roseus* catalyzes the final reaction in the biosynthesis of the important anti-cancer alkaloid, vindoline.[95]

BAHD acyltransferases have molecular masses ranging from 48-55 kD and relatively low protein sequence similarities (10 - 30%).[91,96] However, these enzymes share two conserved motifs, the the catalytic (HXXXD) motif located towards the center of the molecule and the (DFGWG) motif located near the carboxy terminus and plays a structural role.[91,96] The solved x-ray crystal structure of vinorine synthase shows that the monomer is composed of two approximately equal-sized domains with a solvent channel running between them.[97] The HXXXD motif is found in the solvent channel, with the catalytically active His residue occupying the direct center and is accessible from both sides of the channel.[97] This discovery led to the proposed reaction mechanism for the vinorine synthase and all the BAHD acyltransferases.[98] In the mechanism of the vinorine synthase catalysis, the histidine residue of the catalytic (HXXXD) motif acts as a base and deprotonates the oxygen atom of the acyl acceptor substrate, thereby creating a nucleophile.[97,98] The resulting nucleophile attacks the carbonyl carbon of the acyl-CoA donor substrate, forming an unstable tetrahedral intermediate. In the final step of the catalytic cycle, the CoASH is released from the intermediate to produce the ester product (Figure 1.14).[97,98]

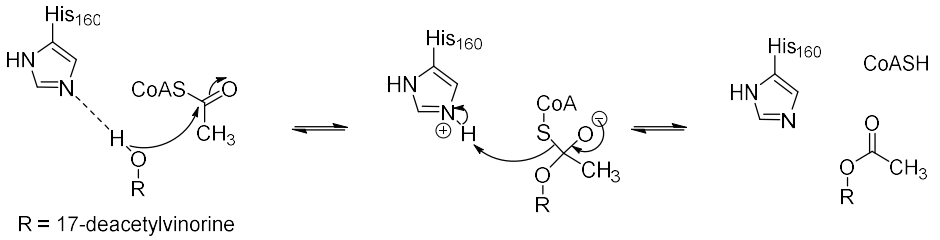

Figure 1.14: The proposed catalytic mechanism of vinorine synthase involves His_{160} as a general base.

Taxus acyltransferases are members of the BAHD acyltransferases superfamily.[91] To date, only five Taxus acyltransferases have been identified, characterized, and are involved in paclitaxel biosynthesis.[99-101] The five acyltransferases involved in paclitaxel biosynthesis are taxadien-5-ol-(9-acetyltransfease (TAT), taxane-2-*O*-benzoyltransferase (TBT), 10-deacetylbaccatin III: 10-*O*-acetyltransferase (DBAT), *N*-debenzoylpaclitaxel-*N*-benzoyltransferase (NDTBT), and baccatin III: 3-amino-3- phenylpropanoyltransferase (BAPT).[100,101] *Taxus* acyltransferases differ in substrate specificities for both acyl donor and acceptor substrates.[101] These enzymes use acetyl-CoA, benzoyl-CoA, or phenylalanoyl- CoA for *O*- and *N*-acylation of various taxanes. *Taxus* acyltransferases share the same catalytic (HXXXD) motif except BAPT.[101] BAPT sequence has a unique catalytic motif containing a natural (GXXXD).[86] Earlier studies proposed that the mechanism of BAPT utilizes the free amine of the β-amino-3- phenylpropanoyl CoA thioester (Figure 1.15).[86]

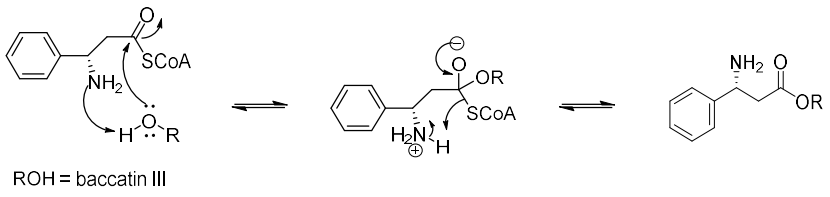

Figure 1.15: Previous substrate-assisted mechanism for BAPT catalysis.

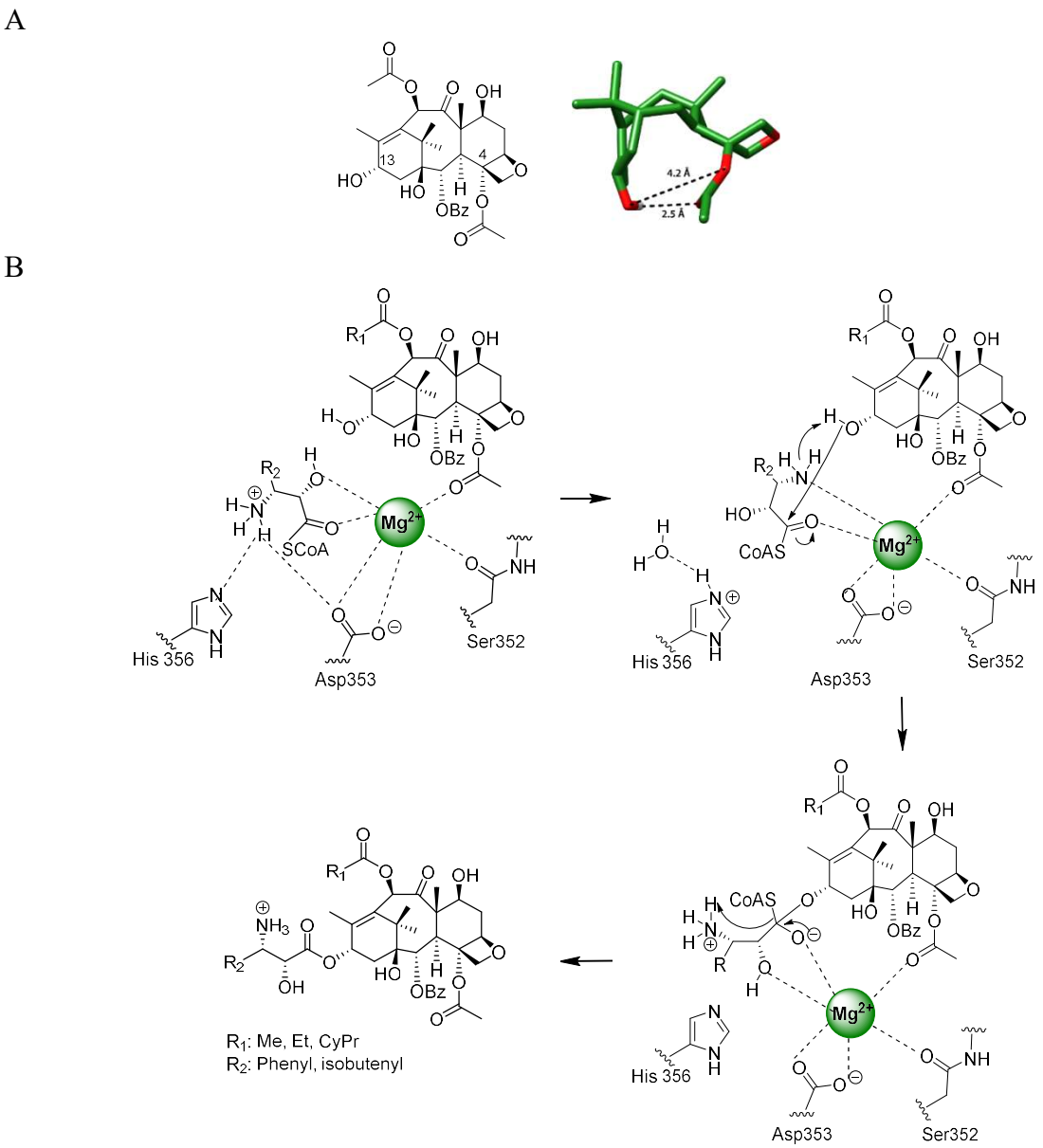

Figure 1.16: Proposed BAPT mechanism catalysis. (A) baccatin III structure and (B) the role of Mg ions as cofactor in BAPT catalysis.

However, our substrates specificity, Gaussian structure optimizations, and molecular dynamics (MD) simulation studies of *Taxus m*TBT catalysis, suggested that baccatin III (**1.36**) C13 hydroxyl group forms an intermolecular hydrogen bond with the oxygen connected to the C4 OAc group (Figure 1.16A). Studies on how metal ions such as Mg^{2+} and Ca^{2+} can prevent intramolecular hydrogen bonding show that introducing metal cations effectively disrupt the intermolecular hydrogen bond.[102,103] These findings inspire us to interrupt the hydrogen bonding between C13

(OH) and C21 (OAc) of taxane analogs by using metal ions such as Mg^{2+} so C13(OH) will be free and ready after deprotonation for nucleophilic attack on the carbonyl carbon of acyl-CoA accepter in the BAPT catalysis. Based on these findings, we propose a new BAPT catalysis mechanism that uses Mg^{2+} ions as a cofactor not just interrupting the hydrogen bonding but also as BAPT structural function by reorganizing the enzyme amino acids active site (Figure 1.16B). We believe that understanding the role of Mg^{2+} ion in the *Taxus* BAPT acyltransferase catalysis in greater detail is vital not only to produce the next-generation paclitaxel analogs but also to add another information of understanding and may help to repropose the mechanism of the BAHD acytransferase members.

Biocatalysis of the Next Generation Paclitaxel Precursor Analogs

Since the discovery of paclitaxel as a powerful anticancer drug, several structure-activity relationship studies (SAR) have been carried out to understand the role of each functional group and conformations in the biological activity of paclitaxel.[72] It has been shown that modification at C2 with *meta*-substituted benzoyl groups, C10 with (cyclopropane carbonyl and propionyl) groups, C13 with (isobutenyl, and *N*-Boc at C3') increase the cytotoxicity 7-fold over exhibit 7-fold over paclitaxel against the drug-sensitive cancer cell and 3-fold over paclitaxel against drug-resistant cancer cells.[21,72] These next-generation paclitaxel analogs are made from a decades-old, nine-step semisynthetic route starting from an abundant taxane natural product, for example, 10-deacetylbaccatin III (10-DAB, **1.12**) (Figure 1.17). Briefly, the reactive hydroxyl groups at C7, 10, and 13 of 10-DAB are silyl ether protected, followed by reductive ester cleavage to remove the naturally occurring benzoyl group at the C2 hydroxyl group.[21,72] Then selectively acylation at the C2 hydroxyl group with the *meta*-substituted benzoic acid substrates, followed by the deprotection of C7, 10, and 13 hydroxyl groups, forming (**1.42**).[21,72] After that selective re-protecting of the hydroxyl group at C7 is achieved before the acylation of the hydroxyl group at C10 with (acetic, propionic, or cyclopropane carboxylic) anhydride, forming (**1.43**).[21,72] Then selective acylation at

the C13 hydroxyl group with enantiopure β-lactam (**1.45**) followed by deprotection of C2, and 7 hydroxyl groups form the next generation paclitaxel analogs (Figure 1.17).[21,72]

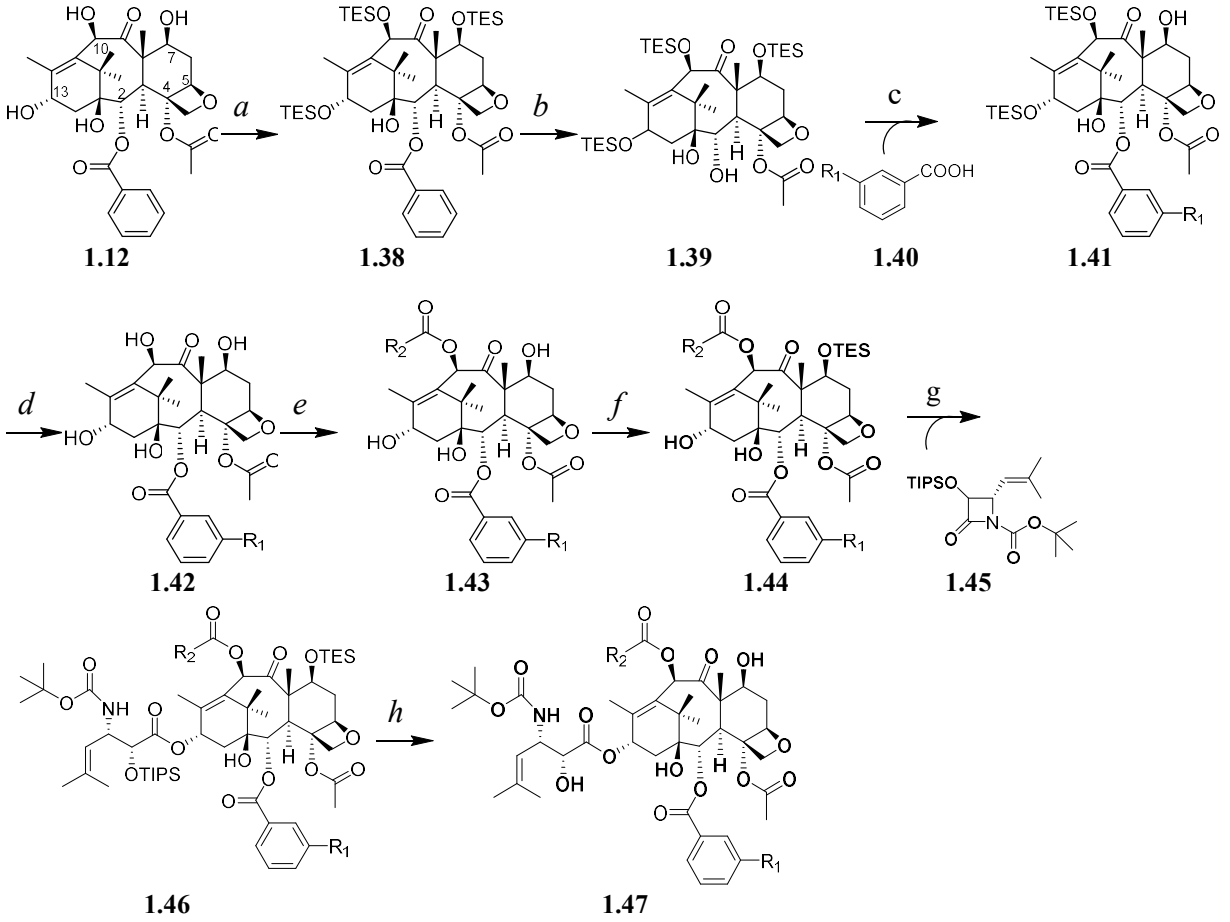

Figure 1.17: An example synthesis of the next-generation paclitaxel analogs. *Reagents and conditions*: (a) TES-Cl (20 equiv), imidazole (12 equiv), dry DMF, 0 °C to rt over 6 h; (b) Red-Al, dry THF, –10 °C, 20 min; (c) a m-benzoic acid analog (1.**40**) (8 equiv), DIC (8 equiv), DMAP (8 equiv), CH_2Cl_2, rt, 2-5 days; (d) HF/pyridine, pyridine/AcCN, 0 °C to rt, overnight; (e) acetic, propanoic, or cyclopropane carboxylic anhydride (10 equiv), $CeCl_3$•$7H_2O$ (0.1 equiv), THF, rt, 20 h; (f) TES-Cl (3 equiv), imidazole (4 equiv), dry DMF, 0 °C to rt, over 45 min; (g) LiHMDS (1.5 equiv), dry THF, –40 °C, 2 h; (h) HF/pyridine, pyridine/AcCN, 0 °C to rt, overnight.

Biocatalysis has emerged as a promising technology for the assembly of fine chemicals. Biocatalytic acylation and deacylation could be key to reducing the number of protection and deprotection steps required to produce the next-generation paclitaxel precursor analogs.[86,88,101,104,105] Herein, we propose to use *Taxus* acyltransferases to transfer next-generation paclitaxel acyl groups to the paclitaxel core. In this method, 10-DAB is selectively acylated with

the (cyclopropane carbonyl or propionyl) groups by DBAT without any prior protection of other free hydroxyl groups in the molecule. Then selective oxidation at the C13 hydroxyl group by MnO_2 form (**1.49**). After that *m*TBT catalyzes both reverse and forward reactions. *m*TBT selectively removes the naturally occurring benzoyl group at C2 to form (**1.50**), then *m*TBT regio-specifically acylates the C2 hydroxyl group with the *meta*-substituted benzoyl groups. BAPT will transfer the isobutenylisoserine substrates to the C13 hydroxyl group (Figure 1.18).

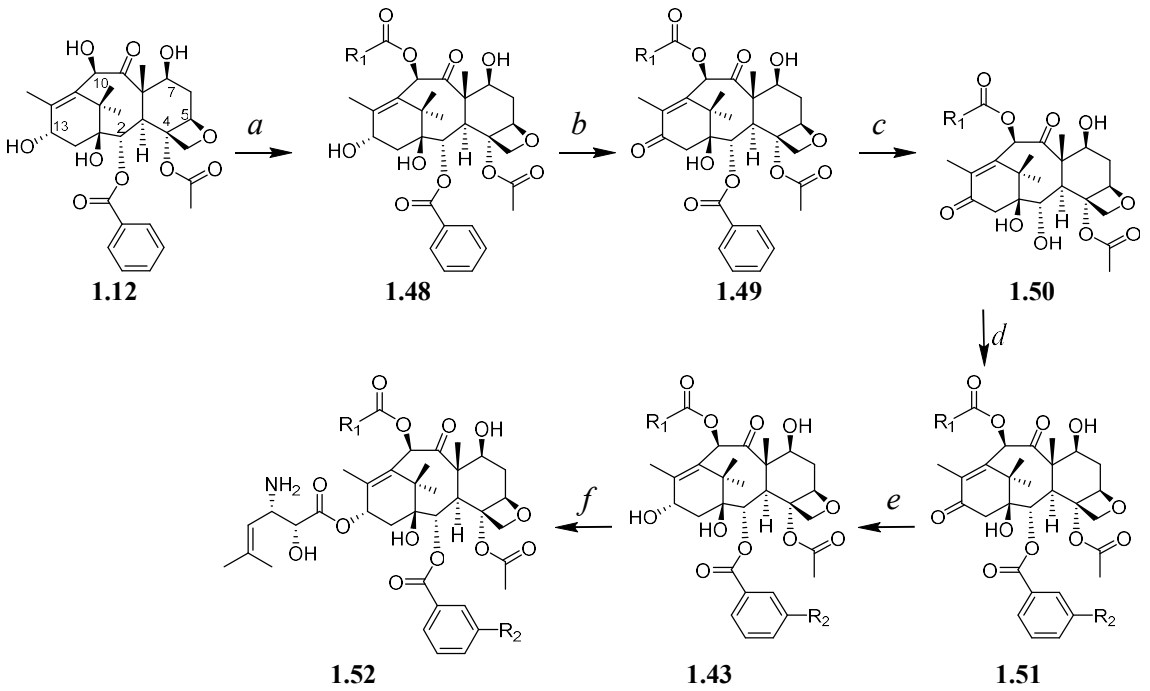

Figure 1.18: Biocatalysis of baccatin III analogs modified at C10, C2, and C13 to make precursors of next-generation paclitaxel analogs. Reagent and conditions: (a) DBAT, (cyclopropane carbonyl or propionyl) CoA thioesters, 50 mM NaH_2PO_4/Na_2HPO_4 buffer (pH 7.4), 31 °C, 4 h; (b) MnO_2, MeOH, rt, 8 h; (c) mTBT, CoA, 50 mM NaH_2PO_4/Na_2HPO_4 buffer (pH 7.4), 31 °C, 4 h; (d) mTBT, m-benzoyl CoA thioesters, 50 mM NaH_2PO_4/Na_2HPO_4 buffer (pH 7.4), 31 °C, 4 h; (e) $NaBH_4$, (1:1) dry MeOH/dry THF, 0 °C to rt 7 h; (f) BAPT, isobutenyl CoA thioester, $MgCl_2$, 50 mM NaH_2PO_4/Na_2HPO_4 buffer (pH 7.4), 31 °C, 4 h.

REFERENCES

(1) Hanahan, D.; Weinberg, R. A. The Hallmarks of Cancer. *Cell.* **2000**, *100*, 57-70.

(2) Anand, U.; Dey, A.; Chandel, A. K. S.; Sanyal, R.; Mishra, A.; Pandey, D. K.; De Falco, V.; Upadhyay, A.; Kandimalla, R.; Chaudhary, A.; Dhanjal, J. K.; Dewanjee, S.; Vallamkondu, J.; Pérez de la Lastra, J. M. Cancer chemotherapy and beyond: Current status, drug candidates, associated risks and progress in targeted therapeutics. *GENES DIS.* **2023**, *10*, 1367-1401.

(3) Elmore, S. Apoptosis: a review of programmed cell death. *Toxicol. Pathol.* **2007**, *35*, 495-516.

(4) Hanahan, D.; Weinberg, Robert A. Hallmarks of Cancer: The Next Generation. *Cell.* **2011**, *144*, 646-674.

(5) Fares, J.; Fares, M. Y.; Khachfe, H. H.; Salhab, H. A.; Fares, Y. Molecular principles of metastasis: a hallmark of cancer revisited. *Signal Transduct Target Ther.* **2020**, *5*, 28.

(6) Sung, H.; Ferlay, J.; Siegel, R. L.; Laversanne, M.; Soerjomataram, I.; Jemal, A.; Bray, F. Global Cancer Statistics 2020: GLOBOCAN Estimates of Incidence and Mortality Worldwide for 36 Cancers in 185 Countries. *CA Cancer J. Clin.* **2021**, *71*, 209-249.

(7) Global variation in postoperative mortality and complications after cancer surgery: a multicentre, prospective cohort study in 82 countries. *Lancet.* **2021**, *397*, 387-397.

(8) Roy, A.; Li, S. D. Modifying the tumor microenvironment using nanoparticle therapeutics. *Wiley Interdiscip. Rev. Nanomed. Nanobiotechnol.* **2016**, *8*, 891-908.

(9) DeVita, V. T., Jr.; Chu, E. A history of cancer chemotherapy. *Cancer Res.* **2008**, *68*, 8643-8653.

(10) Sun, S.-Y.; Hail, N., Jr.; Lotan, R. Apoptosis as a Novel Target for Cancer Chemoprevention. *J. Natl. Cancer Inst.* **2004**, *96*, 662-672.

(11) Rodrigues, D.; Souza, T.; Jennen, D. G. J.; Lemmens, L.; Kleinjans, J. C. S.; de Kok, T. M. Drug-induced gene expression profile changes in relation to intestinal toxicity: State-of-the-art and new approaches. *Cancer Treat. Rev.* **2019**, *77*, 57-66.

(12) Jordan, M. A.; Wilson, L. Microtubules as a target for anticancer drugs. *Nat. Rev. Cancer.* **2004**, *4*, 253-265.

(13) Checchi, P. M.; Nettles, J. H.; Zhou, J.; Snyder, J. P.; Joshi, H. C. Microtubule-interacting drugs for cancer treatment. *Trends Pharmacol. Sci.* **2003**, *24*, 361-365.

(14) Barbuti, A. M.; Chen, Z. S. Paclitaxel Through the Ages of Anticancer Therapy: Exploring Its Role in Chemoresistance and Radiation Therapy. *Cancers (Basel)* **2015**, *7*, 2360-2371.

(15) Singh, S.; Dash, A. K. Paclitaxel in cancer treatment: perspectives and prospects of its delivery challenges. *Crit. Rev. Ther. Drug Carrier Syst.* **2009**, *26*, 333-372.

(16) Ojima, I.; Lichtenthal, B.; Lee, S.; Wang, C.; Wang, X. Taxane anticancer agents: a patent perspective. *Expert Opin. Ther. Pat.* **2016**, *26*, 1-20.

(17) Ojima, I.; Wang, X.; Jing, Y.; Wang, C. Quest for Efficacious Next-Generation Taxoid Anticancer Agents and Their Tumor-Targeted Delivery. *J. Nat. Prod.* **2018**, *81*, 703-721.

(18) Weaver, B. A. How Taxol/paclitaxel kills cancer cells. *Mol. Biol. Cell.* **2014**, *25*, 2677-2681.

(19) De Bono, J. S.; Oudard, S.; Ozguroglu, M.; Hansen, S.; Machiels, J. H.; Shen, L.; Matthews, P.; Sartor, A. O. Cabazitaxel or mitoxantrone with prednisone in patients with metastatic castration-resistant prostate cancer (mCRPC) previously treated with docetaxel: Final results of a multinational phase III trial (TROPIC). *J. Clin. Oncol.* **2010**, *28*, 4508-4508.

(20) Bissery, M. C.; Nohynek, G.; Sanderink, G. J.; Lavelle, F. Docetaxel (Taxotere): a review of preclinical and clinical experience. Part I: Preclinical experience. *Anticancer Drugs.* **1995**, *6*, 339-355, 363-338.

(21) Wang, C.; Wang, X.; Sun, Y.; Taouil, A. K.; Yan, S.; Botchkina, G. I.; Ojima, I. Design, synthesis and SAR study of 3rd-generation taxoids bearing 3-CH(3), 3-CF(3)O and 3-CHF(2)O groups at the C2-benzoate position. *Bioorg. Chem.* **2020**, *95*, 103523.

(22) Wang, C.; Chen, L.; Sun, Y.; Guo, W.; Taouil, A. K.; Ojima, I. Design, synthesis and SAR study of Fluorine-containing 3rd-generation taxoids. *Bioorg. Chem.* **2022**, *119*, 105578.

(23) Singh, P.; Rathinasamy, K.; Mohan, R.; Panda, D. Microtubule assembly dynamics: an attractive target for anticancer drugs. *IUBMB life.* **2008**, *60*, 368-375.

(24) Valiron, O.; Caudron, N.; Job, D. Microtubule dynamics. *Cell. Mol. Life Sci.* **2001**, *58*, 2069-2084.

(25) Burns, R. G. Alpha-, beta-, and gamma-tubulins: sequence comparisons and structural constraints. *Cell motil. cytoskelet.* **1991**, *20*, 181-189.

(26) van der Vaart, B.; Akhmanova, A.; Straube, A. Regulation of microtubule dynamic instability. *Biochem. Soc. Trans.* **2009**, *37*, 1007-1013.

(27) Čermák, V.; Dostál, V.; Jelínek, M.; Libusová, L.; Kovář, J.; Rösel, D.; Brábek, J. Microtubule-targeting agents and their impact on cancer treatment. *Eur. J. Cell Biol.* **2020**, *99*, 151075.

(28) Schiff, P. B.; Fant, J.; Horwitz, S. B. Promotion of microtubule assembly in vitro by taxol. *Nature.* **1979**, *277*, 665-667.

(29) Field, J. J.; Kanakkanthara, A.; Miller, J. H. Microtubule-targeting agents are clinically successful due to both mitotic and interphase impairment of microtubule function. *Bioorg. Med. Chem.* **2014**, *22*, 5050-5059.

(30) Kaul, R.; Risinger, A. L.; Mooberry, S. L. Microtubule-Targeting Drugs: More than Antimitotics. *J. Nat. Prod.* **2019**, *82*, 680-685.

(31) Jordan, M. A.; Wilson, L. Microtubules as a target for anticancer drugs. *Nat. Rev. Cancer.* **2004**, *4*, 253-265.

(32) Bell, A. Microtubule Inhibitors as Potential Antimalarial Agents. *Parasitology Today.* **1998**, *14*, 234-240.

(33) Wani, M. C.; Taylor, H. L.; Wall, M. E.; Coggon, P.; McPhail, A. T. Plant antitumor agents. VI. The isolation and structure of taxol, a novel antileukemic and antitumor agent from Taxus brevifolia. *J. Am. Chem. Soc.* **1971**, *93*, 2325-2327.

(34) Fuchs, D. A.; Johnson, R. K. Cytologic evidence that taxol, an antineoplastic agent from Taxus brevifolia, acts as a mitotic spindle poison. *Cancer treat. rep.* **1978**, *62*, 1219-1222.

(35) McGuire, W. P.; Rowinsky, E. K.; Rosenshein, N. B.; Grumbine, F. C.; Ettinger, D. S.; Armstrong, D. K.; Donehower, R. C. Taxol: a unique antineoplastic agent with significant activity in advanced ovarian epithelial neoplasms. *Ann. Intern. Med.* **1989**, *111*, 273-279.

(36) Holmes, F. A.; Walters, R. S.; Theriault, R. L.; Buzdar, A. U.; Frye, D. K.; Hortobagyi, G. N.; Forman, A. D.; Newton, L. K.; Raber, M. N. Phase II Trial of Taxol, an Active Drug in the Treatment of Metastatic Breast Cancer. *J. Natl. Cancer Inst.* **1991**, *83*, 1797-1805.

(37) Torres, K.; Horwitz, S. B. Mechanisms of Taxol-induced cell death are concentration dependent. *Cancer Res.* **1998**, *58*, 3620-3626.

(38) Horwitz, S. B.; Lothstein, L.; Manfredi, J. J.; Mellado, W.; Parness, J.; Roy, S. N.; Schiff, P. B.; Sorbara, L.; Zeheb, R. Taxol: mechanisms of action and resistance. *Ann. N. Y. Acad. Sci.* **1986**, *466*, 733-744.

(39) Nogales, E. Structural insights into microtubule function. *Annu. Rev. Biochem.* **2000**, *69*, 277-302.

(40) Subramanian, R.; Kapoor, T. M. Building complexity: insights into self-organized assembly of microtubule-based architectures. *Dev. Cell.* **2012**, *23*, 874-885.

(41) Alushin, G. M.; Lander, G. C.; Kellogg, E. H.; Zhang, R.; Baker, D.; Nogales, E. High-resolution microtubule structures reveal the structural transitions in αβ-tubulin upon GTP hydrolysis. *Cell.* **2014**, *157*, 1117-1129.

(42) Weaver, B. A. How Taxol/paclitaxel kills cancer cells. *Mol. Biol. Cell.* **2014**, *25*, 2677-

2681.

(43) Cragg, G. M.; Kingston, D. G. I.; Newman, D. J. *Anticancer Agents from Natural Products*; CRC, **2005**, p 89-122.

(44) Gottesman, M. M.; Pastan, I. Biochemistry of multidrug resistance mediated by the multidrug transporter. *Annu. Rev. Biochem.* **1993**, *62*, 385-427.

(45) Hansen, E.; Woods, R. J.; Read, A. F. How to Use a Chemotherapeutic Agent When Resistance to It Threatens the Patient. *PLOS Biol.* **2017**, *15*, e2001110.

(46) Kesharwani, S. S.; Kaur, S.; Tummala, H.; Sangamwar, A. T. Overcoming multiple drug resistance in cancer using polymeric micelles. *Expert Opin. Drug Deliv.* **2018**, *15*, 1127-1142.

(47) Sun, S.-S.; Hsieh, J.-F.; Tsai, S.-C.; Ho, Y.-J.; Lee, J.-K.; Kao, C.-H. Expression of mediated P-glycoprotein multidrug resistance related to Tc-99m MIBI scintimammography results. *Cancer Lett.*. **2000**, *153*, 95-100.

(48) Housman, G.; Byler, S.; Heerboth, S.; Lapinska, K.; Longacre, M.; Snyder, N.; Sarkar, S. Drug resistance in cancer: an overview. *Cancers (Basel)* **2014**, *6*, 1769-1792.

(49) Sharom, F. J. The P-glycoprotein efflux pump: how does it transport drugs? *J. Membr. Biol.* **1997**, *160*, 161-175.

(50) Leonard, G. D.; Fojo, T.; Bates, S. E. The role of ABC transporters in clinical practice. *Oncologist.* **2003**, *8*, 411-424.

(51) Siegsmund, M.; Brinkmann, U.; Schäffeler, E.; Weirich, G.; Schwab, M.; Eichelbaum, M.; Fritz, P.; Burk, O.; Decker, J.; Alken, P.; Rothenpieler, U.; Kerb, R.; Hoffmeyer, S.; Brauch, H. Association of the P-glycoprotein transporter MDR1(C3435T) polymorphism with the susceptibility to renal epithelial tumors. *J. Am. Soc. Nephrol.* **2002**, *13*, 1847-1854.

(52) Thiebaut, F.; Tsuruo, T.; Hamada, H.; Gottesman, M. M.; Pastan, I.; Willingham, M. C. Cellular localization of the multidrug-resistance gene product P-glycoprotein in normal human tissues. *Proc. Natl. Acad. Sci. U.S.A.* **1987**, *84*, 7735-7738.

(53) Schinkel, A. H. P-Glycoprotein, a gatekeeper in the blood–brain barrier. *Adv. Drug Deliv. Rev.* **1999**, *36*, 179-194.

(54) Sharom, F. J. Complex Interplay between the P-Glycoprotein Multidrug Efflux Pump and the Membrane: Its Role in Modulating Protein Function. *Front. Oncol.* **2014**, *4*, 41.

(55) Aller, S. G.; Yu, J.; Ward, A.; Weng, Y.; Chittaboina, S.; Zhuo, R.; Harrell, P. M.; Trinh, Y. T.; Zhang, Q.; Urbatsch, I. L.; Chang, G. Structure of P-glycoprotein reveals a molecular basis for poly-specific drug binding. *Science* **2009**, *323*, 1718-1722.

(56) Dawson, R. J.; Locher, K. P. Structure of a bacterial multidrug ABC transporter. *Nature.* **2006**, *443*, 180-185.

(57) Tian, Y.; Lei, Y.; Wang, Y.; Lai, J.; Wang, J.; Xia, F. Mechanism of multidrug resistance to chemotherapy mediated by P-glycoprotein (Review). *Int. J. Oncol.* **2023**, *63*.

(58) Attia, M. S.; Elsebaey, M. T.; Yahya, G.; Chopra, H.; Marzouk, M. A.; Yahya, A.; Abdelkhalek, A. S. Pharmaceutical polymers and P-glycoprotein: Current trends and possible outcomes in drug delivery. *Mater. Today Commun.* **2023**, *34*, 105318.

(59) Yang, C.-P. H.; Wang, C.; Ojima, I.; Horwitz, S. B. Taxol Analogues Exhibit Differential Effects on Photoaffinity Labeling of β-Tubulin and the Multidrug Resistance Associated P-Glycoprotein. *J. Nat. Prod.* **2018**, *81*, 600-606.

(60) Jelínek, M.; Balušíková, K.; Daniel, P.; Němcová-Fürstová, V.; Kirubakaran, P.; Jaček, M.; Wei, L.; Wang, X.; Vondrášek, J.; Ojima, I.; Kovář, J. Substituents at the C3′ and C3′N positions are critical for taxanes to overcome acquired resistance of cancer cells to paclitaxel. *Toxicol. Appl. Pharmacol.* **2018**, *347*, 79-91.

(61) Ludueña, R. F.: Chapter Two - A Hypothesis on the Origin and Evolution of Tubulin. In *Int. Rev. Cell Mol. Biol.*; Jeon, K. W., Ed.; Academic Press, **2013**; Vol. 302; pp 41-185.

(62) Gadadhar, S.; Bodakuntla, S.; Natarajan, K.; Janke, C. The tubulin code at a glance. *J. Cell. Sci.* **2017**, *130*, 1347-1353.

(63) Kavallaris, M. Microtubules and resistance to tubulin-binding agents. *Nat. Rev. Cancer.* **2010**, *10*, 194-204.

(64) Yang, C. H.; Horwitz, S. B. Taxol(®): The First Microtubule Stabilizing Agent. *Int. J. Mol. Sci.* **2017**, *18*.

(65) Rao, S.; He, L.; Chakravarty, S.; Ojima, I.; Orr, G. A.; Horwitz, S. B. Characterization of the Taxol Binding Site on the Microtubule: IDENTIFICATION OF Arg282 IN β-TUBULIN AS THE SITE OF PHOTOINCORPORATION OF A 7-BENZOPHENONE ANALOGUE OF TAXOL*. *J. Biol. Chem.* **1999**, *274*, 37990-37994.

(66) Rao, S.; Krauss, N. E.; Heerding, J. M.; Swindell, C. S.; Ringel, I.; Orr, G. A.; Horwitz, S. B. 3'-(p-azidobenzamido)taxol photolabels the N-terminal 31 amino acids of beta-tubulin. *J. Biol. Chem.* **1994**, *269*, 3132-3134.

(67) Kingston, D. G. Taxol: the chemistry and structure-activity relationships of a novel anticancer agent. *Trends Biotechnol.* **1994**, *12*, 222-227.

(68) Nicolaou, K. C.; Dai, W.-M.; Guy, R. K. Chemistry and Biology of Taxol. *Angew. Chem. Int. Ed.* **1994**, *33*, 15-44.

(69) Xue, M.; Long, B. H.; Fairchild, C.; Johnston, K.; Rose, W. C.; Kadow, J. F.; Vyas, D. M.;

Chen, S.-H. Structure–activity relationships study at the 3′-N position of paclitaxel. part 2: synthesis and biological evaluation of 3′-N-thiourea- and 3′-N-thiocarbamate-bearing paclitaxel analogues. *Bioorganic Med. Chem. Lett.* **2000**, *10*, 1327-1331.

(70) Guéritte-Voegelein, F.; Guénard, D.; Lavelle, F.; Le Goff, M. T.; Mangatal, L.; Potier, P. Relationships between the structure of taxol analogues and their antimitotic activity. *J. Med. Chem.* **1991**, *34*, 992-998.

(71) Fang, W. S.; Liang, X. T. Recent progress in structure activity relationship and mechanistic studies of taxol analogues. *Mini Rev. Med. Chem.* **2005**, *5*, 1-12.

(72) Ojima, I.; Chen, J.; Sun, L.; Borella, C. P.; Wang, T.; Miller, M. L.; Lin, S.; Geng, X.; Kuznetsova, L.; Qu, C.; Gallager, D.; Zhao, X.; Zanardi, I.; Xia, S.; Horwitz, S. B.; Mallen-St Clair, J.; Guerriero, J. L.; Bar-Sagi, D.; Veith, J. M.; Pera, P.; Bernacki, R. J. Design, synthesis, and biological evaluation of new-generation taxoids. *J. Med. Chem.* **2008**, *51*, 3203-3221.

(73) Wang, C.; Chen, L.; Sun, Y.; Guo, W.; Taouil, A. K.; Ojima, I. Design, synthesis and SAR study of Fluorine-containing 3rd-generation taxoids. *Bioorg. Chem.* **2022**, *119*, 105578.

(74) Guéritte-Voegelein, F.; Sénilh, V.; David, B.; Guénard, D.; Potier, P. Chemical studies of 10-deacetyl baccatin III: Hemisynthesis of taxol derivatives. *Tetrahedron.* **1986**, *42*, 4451-4460.

(75) Kanazawa, A. M.; Denis, J.-N.; Greene, A. E. Highly Stereocontrolled and Efficient Preparation of the Protected, Esterification-Ready Docetaxel (Taxotere) Side Chain. *J. Org. Chem.* **1994**, *59*, 1238-1240.

(76) Kingston, D. G. I.; Chaudhary, A. G.; Gunatilaka, A. A. L.; Middleton, M. L. Synthesis of taxol from baccatin III via an oxazoline intermediate. *Tetrahedron Lett.* **1994**, *35*, 4483-4484.

(77) Holton Robert, A. Method for preparation of taxol using an oxazinone.

(78) Swindell, C.; Krauss, N.: Synthesis of taxol, analogs and intermediates with variable a-ring side chains. Google Patents, 1994.

(79) Holton, R. A.; Somoza, C.; Kim, H. B.; Liang, F.; Biediger, R. J.; Boatman, P. D.; Shindo, M.; Smith, C. C.; Kim, S. First total synthesis of taxol. 1. Functionalization of the B ring. *J. Am. Chem. Soc.* **1994**, *116*, 1597-1598.

(80) Ojima, I.; Habus, I.; Zhao, M.; Zucco, M.; Park, Y. H.; Sun, C. M.; Brigaud, T. New and efficient approaches to the semisynthesis of taxol and its C-13 side chain analogs by means of β-lactam synthon method. *Tetrahedron.* **1992**, *48*, 6985-7012.

(81) Patel, R. N. Tour de paclitaxel: biocatalysis for semisynthesis. *Annu. Rev. Microbiol.* **1998**, *52*, 361-395.

(82) Ketchum, R. E. B.; Croteau, R. B.: The Taxus Metabolome and the Elucidation of the Taxol® Biosynthetic Pathway in Cell Suspension Cultures. In *Plant Metabolomics*; Saito, K., Dixon, R. A., Willmitzer, L., Eds.; Springer Berlin Heidelberg: Berlin, Heidelberg, **2006**; pp 291-309.

(83) Croteau, R.; Ketchum, R. E.; Long, R. M.; Kaspera, R.; Wildung, M. R. Taxol biosynthesis and molecular genetics. *Phytochem. Rev.* **2006**, *5*, 75-97.

(84) Heinig, U.; Jennewein, S. Taxol: A complex diterpenoid natural product with an evolutionarily obscure origin. *Afr. J. Biotechnol.* **2009**, *8*, 1370-1385.

(85) Loncaric, C.; Merriweather, E.; Walker, K. D. Profiling a Taxol Pathway 10β-Acetyltransferase: Assessment of the Specificity and the Production of Baccatin III by In Vivo Acetylation in E. coli. *Chem. Biol.* **2006**, *13*, 309-317.

(86) Walker, K.; Fujisaki, S.; Long, R.; Croteau, R. Molecular cloning and heterologous expression of the C-13 phenylpropanoid side chain-CoA acyltransferase that functions in Taxol biosynthesis. *Proc. Natl. Acad. Sci. U.S.A.* **2002**, *99*, 12715-12720.

(87) Chau, M.; Croteau, R. Molecular cloning and characterization of a cytochrome P450 taxoid 2α-hydroxylase involved in Taxol biosynthesis. *Arch. Biochem. Biophys.* **2004**, *427*, 48-57.

(88) Walker, K.; Long, R.; Croteau, R. The final acylation step in Taxol biosynthesis: Cloning of the taxoid C13-side-chain N-benzoyltransferase from Taxus. *Proc. Natl. Acad. Sci.* **2002**, *99*, 9166-9171.

(89) Baloglu, E.; Kingston, D. G. The taxane diterpenoids. *J. Nat. Prod.* **1999**, *62*, 1448-1472.

(90) De Luca, V.; St Pierre, B. The cell and developmental biology of alkaloid biosynthesis. *Trends Plant Sci.* **2000**, *5*, 168-173.

(91) D'Auria, J. C. Acyltransferases in plants: a good time to be BAHD. *Curr. Opin. Plant Biol.* **2006**, *9*, 331-340.

(92) Dudareva, N.; Raguso, R. A.; Wang, J.; Ross, J. R.; Pichersky, E. Floral scent production in Clarkia breweri. III. Enzymatic synthesis and emission of benzenoid esters. *Plant Physiol.* **1998**, *116*, 599-604.

(93) Fujiwara, H.; Tanaka, Y.; Fukui, Y.; Ashikari, T.; Yamaguchi, M.; Kusumi, T. Purification and characterization of anthocyanin 3-aromatic acyltransferase from Perilla frutescens. *Plant Sci.* **1998**, *137*, 87-94.

(94) Yang, Q.; Reinhard, K.; Schiltz, E.; Matern, U. Characterization and heterologous expression of hydroxycinnamoyl/benzoyl-CoA:anthranilate N-hydroxycinnamoyl/benzoyltransferase from elicited cell cultures of carnation, Dianthus

caryophyllus L. *Plant Mol. Biol.* **1997**, *35*, 777-789.

(95) St-Pierre, B.; Laflamme, P.; Alarco, A.-M.; D, V.; Luca, E. The terminal O-acetyltransferase involved in vindoline biosynthesis defines a new class of proteins responsible for coenzyme A-dependent acyl transfer. *Plant J.* **1998**, *14*, 703-713.

(96) Lucchetta, L.; Manriquez, D.; El-Sharkawy, I.; Flores, F. B.; Sanchez-Bel, P.; Zouine, M.; Ginies, C.; Bouzayen, M.; Rombaldi, C.; Pech, J. C.; Latché, A. Biochemical and catalytic properties of three recombinant alcohol acyltransferases of melon. sulfur-containing ester formation, regulatory role of CoA-SH in activity, and sequence elements conferring substrate preference. *J. Agric. Food Chem.* **2007**, *55*, 5213-5220.

(97) Bayer, A.; Ma, X.; Stöckigt, J. Acetyltransfer in natural product biosynthesis--functional cloning and molecular analysis of vinorine synthase. *Bioorg. Med. Chem.* **2004**, *12*, 2787-2795.

(98) Ma, X.; Koepke, J.; Panjikar, S.; Fritzsch, G.; Stöckigt, J. Crystal structure of vinorine synthase, the first representative of the BAHD superfamily. *J. Biol. Chem.* **2005**, *280*, 13576-13583.

(99) Malik, S.; Cusido, R. M.; Mirjalili, M. H.; Moyano, E.; Palazón, J.; Bonfill, M. Production of the anticancer drug taxol in Taxus baccata suspension cultures: A review. *Process Biochem.* **2011**, *46*, 23-34.

(100) Hampel, D.; Mau, C. J.; Croteau, R. B. Taxol biosynthesis: Identification and characterization of two acetyl CoA:taxoid-O-acetyl transferases that divert pathway flux away from Taxol production. *Arch. Biochem. Biophys.* **2009**, *487*, 91-97.

(101) Walker, K.; Croteau, R. Taxol biosynthesis: molecular cloning of a benzoyl-CoA:taxane 2alpha-O-benzoyltransferase cDNA from taxus and functional expression in Escherichia coli. *Proc. Natl. Acad. Sci. U.S.A.* **2000**, *97*, 13591-13596.

(102) Chen, J.; Huang, X.; Fang, X.; Yan, C.; Gao, Z.; Shao, H. Disassembly of intermolecular hydrogen bond induced by cations on self-assembled monolayer. *J. Electroanal. Chem.* **2020**, *876*, 114476.

(103) Majerz, I. The influence of potassium cation on a strong OHO hydrogen bond. *Org. Biomol. Chem.* **2011**, *9 5*, 1466-1473.

(104) Nawarathne, I. N.; Walker, K. D. Point mutations (Q19P and N23K) increase the operational solubility of a 2alpha-O-benzoyltransferase that conveys various acyl groups from CoA to a taxane acceptor. *J. Nat. Prod.* **2010**, *73*, 151-159.

(105) Al-Hilfi, A.; Walker, K. D. Biocatalysis of precursors to new-generation SB-T-taxanes effective against paclitaxel-resistant cancer cells. *Arch. Biochem. Biophys.* **2022**, *719*, 109165.

Chapter 2 is adapted from our published work in Archives of Biochemistry and Biophysics

Al-Hilfi, A.; Walker, K. D. Biocatalysis of precursors to new-generation SB-T-taxanes effective against paclitaxel-resistant cancer cells. *Arch. Biochem. Biophys*. **2022**, *719*, 109165. https://doi.org/10.1016/j.abb.2022.109165

CHAPTER 2: BIOCATALYSIS OF 10-CYCLOPROPANE CARBONYL AND RPOPIONYL-10-DEACETYLBACCATIN III PRECURSORS OF NEXT-GENERATION PACLITAXEL ANALOGS

Introduction

Paclitaxel and its analogs are used worldwide, and with their continued use, a serious drug-resistance challenge can develop.[1,2] Multiple-drug resistances caused by overexpression of the p-gp efflux pump and overexpression of βIII-tubulin isotype are significant obstacles that have limited the application of some cancer chemotherapeutic agents.[3] Fundamental mechanisms that promote drug resistance in cancer cells include drug-target modification, drug efflux from the cell, and the epithelial-mesenchymal transition that contributes to metastasis.[4] Toxicodynamic studies have identified the mechanisms of resistance for specific cancer cells against microtubule-stabilizing agents, such as taxane chemotherapeutics.[5,6] Taxanes, such as paclitaxel (**2.1**), docetaxel (**2.2**), and cabazitaxel (**2.3**) (Figure 2.1), are widely used to treat breast,[7,8] ovarian,[9,10] lung cancers[11,12] or prostate cancers.[13-16].

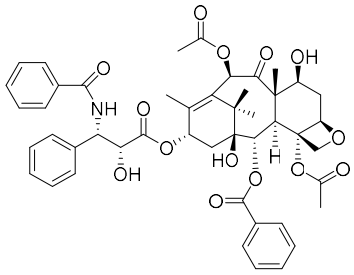

2.1

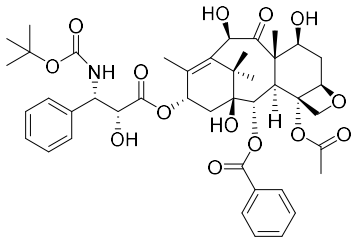

2.2

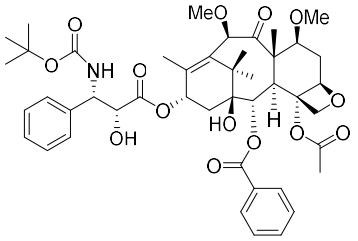

2.3

Figure 2.1: Structures of natural products paclitaxel and it is semisynthsis analogs docetaxel and cabazitaxel.

In drug-sensitive cancer cell lines, the taxane drug family binds the β-tubulin subunit to disrupt microtubule dynamics.[17] Cancer cells resistant to taxane treatment typically express unusually high levels of βIII-tubulin, which confers drug resistance.[5] Besides variations in the β-tubulin target conferring taxane drug-resistance, the P-glycoproteins (P-gp) drug-efflux pumps are often overexpressed in resistant tumor cells.[4,18]

Recent structure-activity relationship studies show that new paclitaxel analogs with modification at C10 with (cyclopropanecarbonyl and propionyl) groups, C2 benzoate with *meta*-substituted-(F, Cl, OCH_3, OCF_3, and $OCHF_2$), and C13 with (isobutenyl, and *N*-Boc at C3') (Figure 2.3).[19,20] SB-T-12 taxane analogs exhibit 7-fold over paclitaxel against the drug-sensitive cancer cell and 3-fold over paclitaxel against drug-resistant cancer cells.[19] Some SB-T-taxanes bind and block the efflux action of the P-gp so that other drugs can accumulate, and their therapeutic effect is enhanced.[21,22] SB-T-1214 was 104- and 18-fold more cytotoxic than the market drugs paclitaxel and docetaxel, respectively, against taxane-resistant human ovarian cancer that overexpressed P-gp.[22-25] Other mechanisms of action of an SB-T-compound (SB-T-121303) (Figure 2.2) include suppressing the phosphatidylinositol 3-kinase/serine-threonine kinase pathway that contributes to chemoresistance and tumor metastasis in paclitaxel-resistant human breast cancer cells.[26,27]

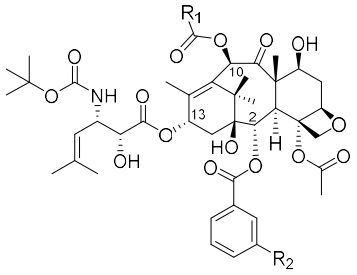

SB-T-1214 (**2.4**) R_1= cyclopropyl, R_2 = H
SB-T-1213303 (**2.5**) R_1= ethyl, R_2 = OCH_3

Figure 2.2: Structure of SB-T-12 taxane substrates (next-generation paclitaxel analogs).

Acylation at the C10 hydroxy group of 10-deacetylbaccatin III (10-DAB) (**2.6**) with cyclopropanecarbonyl or n-propionyl substrates was performed by the two coupling reaction methods.[28] The first method, coupling 7-triethylsilyl-10-DAB (**2.5**) with cyclopropanecarbonyl chloride (**2.8**) or propionyl chloride (**2.9**) using sodium bis(trimethylsilyl)amide (NaHMDS) (Figure 2.3).[28]

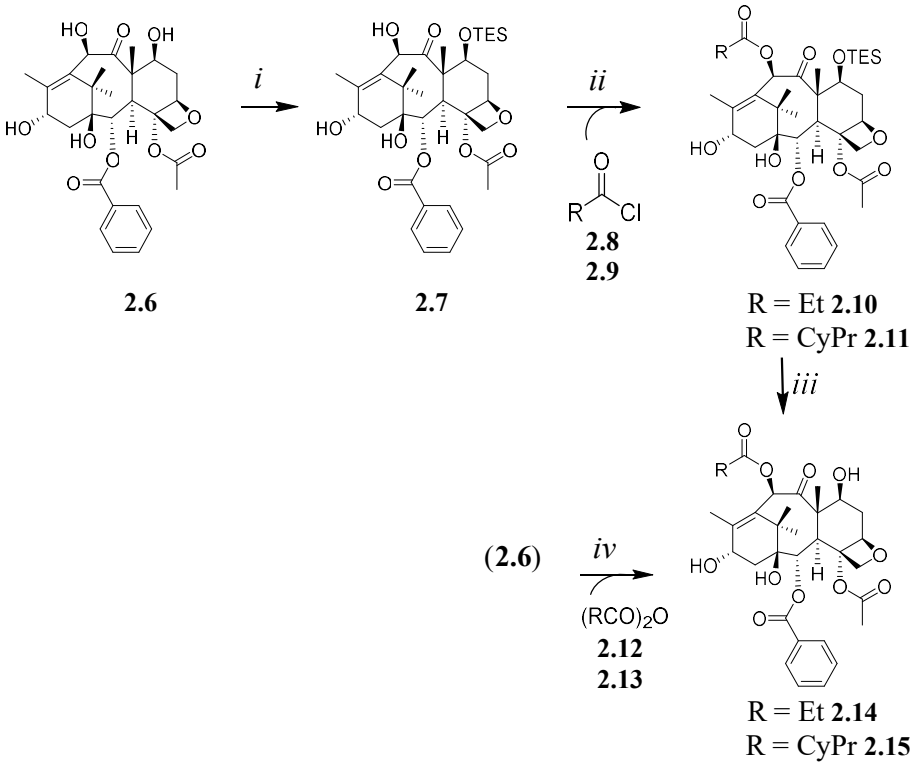

Figure 2.3: Synthesis of the key intermediates of the next generation taxoids. *Reagent and conditions*: (i) TES-Cl (3 equiv.), imidazole (4 equiv.), dry DMF, 0 °C to r.t. over 6 h; (ii) LiHMDS (1.5 equiv.), dry THF, -40 °C to r.t.over 2 h; (iii) HF/pyridine, pyridine/MeCN, 0 °C to r.t., overnight; (iv) $CeCl_3.7H_2O$ (0.1 equiv), THF, r.t., 20 h.

The second method, coupling 10-DAB (**2.6**) with cyclopropanecarboxylic anhydride (**2.12**) or propanoic anhydride (**2.13**) using cerium chloride (Figure 2.3).[28] Several studies show that long-term exposure to cerium chloride resulted in damage to the liver, kidney, and heart. In addition, Ce^{3+} has high oxidative stress and toxicity on the brain which can cause neurotoxicological and damage the brain.[29-31] Therefore, it is important to find or develop an environmentally friendly method to couple these acyl groups with 10-DAB.

Over a decade biocatalysis has become an essential component for the synthesis of fine chemicals.[32-36] Previous biocatalytic acylation studies show that *Taxus* 10-*O*-acyltransferase (DBAT) transfers the acetyl group to the 10-DAB selectively and produces baccatin III.[37,38] This finding could be key to reducing the number of protection and deprotection steps or the use of heavy cerium required to produce the next-generation paclitaxel precursor analogs.

A

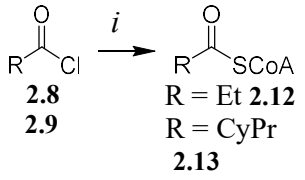

2.8
2.9

R = Et **2.12**
R = CyPr
2.13

B

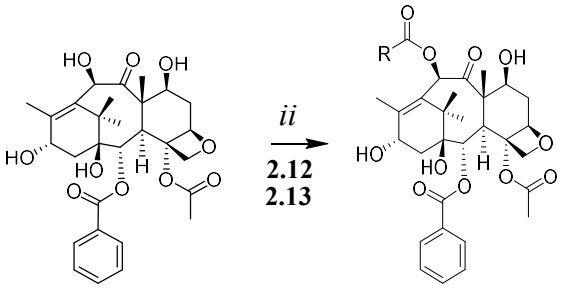

2.12
2.13

2.6

R = Et **2.14**
R = CyPr **2.15**

Figure 2.4: (A) Synthesis of CoA thioesters. (B) Biocatalysis of the 10-DAB analogs modification at C10 to make key intermediate of generation taxoids. *Reagent and conditions*: (i) *t*-BuOH, CoA, 0.4 M $NaHCO_3$, H_2O, 23 °C, 4 h; (ii) DBAT, 50 mM NaH_2PO_4/Na_2HPO_4 buffer (pH 7.4), 31 °C, 4 h.

In this proof of principle study, we used an in vivo method utilizing *E. coli*, expressing an acyl CoA-dependent taxane 10-*O*-acyltransferase (DBAT) enzyme, to assess whether the non-natural product cyclopropanecarbonyl CoA was a cosubstrate of DBAT. Encouraged by the results, we used the DBAT catalyst in vitro to transfer a cyclopropanecarbonyl and an *n*-propionyl group from CoA thioesters to 10-deacetylbaccatin III (10-DAB) (Figure 2.4). The biocatalyzed products were characterized by NMR and mass spectrometry, and the Michaelis-Menten parameters of DBAT are reported.

Experimental

Chemicals and Reagents

Cyclopropanecarbonyl chloride (98%), propionyl chloride (98%), *tert*-butanol (*t*-BuOH) (≥99%), methanol (>99.5%), hexane (>99.5%), and ethyl acetate (EtOAc) (>99.5%) were purchased from Sigma Aldrich (St. Louis, MO). Coenzyme A, sodium salt (95%), was obtained from AmBeed (Arlington Hts, IL). HisPur^{TM} Ni-NTA (nickel-nitrilotriacetic acid) resin was purchased from Thermo Fisher Scientific (Waltham, MA). Isopropyl β-D-1-thiogalactopyranoside (IPTG), kanamycin, and phenylmethylsulfonyl fluoride (PMSF) were purchased from Gold Bio (St. Louis, MO). Taxanes baccatin III (>98%) and 10-deacetyl baccatin III (>98%) were purchased from Natland International Corporation (Research Triangle Park, NC). C18 reverse-phase silica gel resin (carbon 23%, 40-63 μm) was purchased from Silicycle (Quebec City, Quebec, Canada).

In vivo Substrate-Screen of Recombinant DBAT for 10-DAB and Cyclopropanecarbonyl CoA

10-Deacetylbaccatin III (100 μM) was fed to a 100 ml culture of transformed *E. coli* BL-21(DE3) engineered to express the DBAT protein from the pET-28 vector. The bacteria were grown to $A_{600} \approx 1.0$ at 37 °C with ampicillin selection. Cyclopropanecarboxylic acid (2 mM final concentration) and isopropyl-D-thiogalactoside (1 mM final concentration), to induce protein expression, were added, and the transformed bacteria were grown at 31 °C for 18 h. The bacteria cells were harvested by centrifugation at 5000*g* (10 min), and the supernatant was isolated. NaCl (∼30 g) was added to the supernatant to minimize emulsion, and the resulting brine solution was extracted with ethyl acetate (3 × 50 ml). The organic fractions from the supernatant extract were processed separately, dried with sodium sulfate, and filtered. The filtrate was evaporated, and the sample was dissolved in 200 μl of acetonitrile and analyzed by reverse-phase liquid chromatography/electrospray-ionization tandem mass spectrometry (LC/ESI-MS/MS) in selected-

ion mode. An earlier study informed that the cell pellets retained a small proportion of the diterpene substrate or its 10-acylated products made biocatalytically;[39] therefore, the cells were not evaluated further.

Synthesis of Acyl CoA Thioesters

Cyclopropanecarbonyl chloride or propionyl chloride (54 μmol) was dissolved in 1 mL of *t*-BuOH, and the solution was stirred for 30 min at 23 °C. Coenzyme A, sodium salt (60 μmol, 46 mg dissolved in 1 mL of 0.4 M $NaHCO_3$ in distilled H_2O), was added dropwise to the acyl chloride solution. The mixture was stirred for 4 h at 23 °C, and the reaction was quenched with dropwise addition of 1 M HCl to pH 3. The solvent was evaporated under vacuum, and the residue was dissolved in distilled H_2O (5 mL) and loaded on a C18 reverse-phase silica gel column washed previously with 100% MeOH (25 mL) and pre-equilibrated with distilled H_2O (25 mL). The sample was eluted with a step gradient of distilled H_2O (25 mL) and then with 10% (v/v) MeOH in distilled H_2O (25 mL). As determined by C18 thin-layer chromatography with uv-quench tracking, the fractions containing the CoA thioesters were combined, and the solvent was evaporated under a vacuum. The remaining residue was extracted with diethyl ether (4 × 2 mL) to remove residual *t*-BuOH to yield the acyl CoA product.

NMR Data for Cyclopropanecarbonyl CoA (210 mg, 95% yield). ^{1}H NMR (500 MHz, D_2O) δ: 8.49 (s, 1H), 8.29 (s, 1H), 6.04 (d, J = 6.2 Hz, 1H), 4.72 (m, 1H), 4.68 (d, J = 5.9 Hz, 1H), 4.47 (t, J = 2.7 Hz, 1H), 4.11 – 4.07 (m, 2H), 3.88 (s, 1H), 3.73 (dd, J = 9.8, 4.9 Hz, 1H), 3.48 (dd, J = 9.8, 4.8 Hz, 1H), 3.31 (t, J = 6.6 Hz, 2H), 3.17 (t, J = 6.6 Hz, 2H), 2.46 (t, J = 6.6 Hz, 2H), 2.34 (t, J = 6.6 Hz, 2H), 1.47 (tt, J = 7.7, 4.8 Hz, 1H), 0.82 (dd, J = 5.3, 3.3 Hz, 2H), 0.79 (s, 3H), 0.78 (dd, J = 6.8, 4.7 Hz, 2H), 0.68 (s, 3H) (Figure 2.8). ^{13}C NMR (126 MHz, D_2O) δ: 198.5, 178.9, 178.6, 156.1, 154.6, 152.1, 143.2, 121.4, 89.8, 86.4, 76.3, 76.1, 74.9, 67.1, 44.7, 41.5, 37.9, 31.8, 25.2, 23.4, 21.8, 10.1 (Figure 2.9).

NMR Data for Propionyl CoA (224 mg, 96% yield). ^{1}H NMR (500 MHz, D_2O) δ: 8.51 (s, 1H), 8.29 (s, 1H), 6.08 (d, *J* = 6.2 Hz, 1H), 4.72 (m, 1H), 4.69 (d, *J* = 5.9 Hz, 1H), 4.49 (t, *J* = 2.7 Hz, 1H), 4.14 – 4.09 (m, 2H), 3.89 (s, 1H), 3.74 (dd, *J* = 9.8, 4.9 Hz, 1H), 3.52 (dd, *J* = 9.8, 4.8 Hz, 1H), 3.37 (t, *J* = 6.6 Hz, 2H), 3.21 (t, *J* = 6.6 Hz, 2H), 2.50 (t, *J* = 6.6 Hz, 2H), 2.38 (t, *J* = 6.6 Hz, 2H), 2.27 (q, *J* = 7.6 Hz, 2H), 0.95 (t, *J* = 7.5 Hz, 3H), 0.81 (s, 3H), 0.70 (s, 3H) (Figure 2.10). ^{13}C NMR (126 MHz, D_2O) δ: 197.8, 177.8, 177.2, 154.6, 151.8, 148.9, 143.8, 121.6, 88.5, 85.8, 76.4, 76.1, 74.8, 66.5, 44.8, 42.1, 38.4, 29.8, 24.6, 21.6, 20.8, 9.8 (Figure 2.11).

Expression and Purification of 10-Deacetylbaccatin III Acetyltransferase (DBAT)

A glycerol stock of *E. coli* BL21(DE3) engineered to express the DBAT enzyme from the pCWori^{+}-pET28a-*dbat* plasmid containing the *dbat* gene was used to inoculate Lysogeny Broth (LB) (400 mL) containing kanamycin (50 μg/mL) and incubated at 37 °C overnight. This inoculum culture (50 mL) was added to fresh LB media (8 × 1 L) containing kanamycin (50 μg/mL). The cells were incubated at 37 °C until OD_{600} ≈ 0.6, IPTG (250 μM final concentration) was added, and the strains were incubated at 16 °C for 16 h. The cultures were centrifuged (2,100*g*) for 1 h at 4 °C to pellet the cells. The cells were resuspended in 100 mL of lysis buffer (50 mM sodium phosphate (pH 8.0), 300 mM NaCl, 10 mM imidazole, and 5% (v/v) glycerol,) and lysed by sonication (Misonix Sonicator (Danbury, CT): 10 s on, 20 s rest for 30 cycles) on ice. The cell debris was removed by centrifugation (1,500*g*) for 45 min at 4 °C, followed by high-speed centrifugation (25,000*g*) for 90 min at 2 °C to remove light membrane debris.

The supernatant was loaded onto a column containing nickel-nitrilotriacetic acid (Ni-NTA) resin (3 mL) and eluted by gravity flow. The column was washed with 50 mL of Wash 1 Buffer (300 mM NaCl, 50 mM sodium phosphate (pH 8.0), 10 mM imidazole, and 5% (v/v) glycerol) and 20 mL of Wash 2 Buffer (300 mM NaCl, 50 mM sodium phosphate (pH 8.0), 50 mM imidazole, and 5% (v/v) glycerol). Protein was eluted with Elution Buffer (300 mM NaCl, 50 mM sodium

phosphate (pH 8.0), 250 mM imidazole, and 5% (v/v) glycerol). Fractions containing enzymes of a molecular weight consistent with that of DBAT (~52 kDa) were combined and loaded onto a size-selective centrifugal filtration unit (30,000 NMWL, Millipore-Sigma, Burlington, MA). The quantity of DBAT (11 mg) was measured using a NanoDrop spectrophotometer, and the purity of the enzyme was assessed by SDS-PAGE and Coomassie Blue staining (Figure 2.7).

Screening DBAT In vitro Activity with 10-DAB, Cyclopropanecarbonyl CoA, and n-Propionyl CoA

A 1-mL suspension of 10-DAB (1 mM) in 50 mM NaH_2PO_4/Na_2HPO_4 buffer (pH 7.0) containing methanol (10 µL, as an organic solubilizer) was preincubated with DBAT (4 µg/mL) for 5 min. Cyclopropanecarbonyl CoA or propionyl CoA (1 mM final concentration) was added to the solution, and the assay was mixed at 31 °C on a rocking shaker for 4 h. The reaction was then extracted with EtOAc (2 × 1 mL). The organic extracts were combined, the solvent was removed under a stream of nitrogen, and the resulting residue was dissolved in acetonitrile (100 µL). An aliquot was analyzed by electrospray-ionization tandem mass spectrometry (LC/ESI-MS/MS) to provide preliminary diagnostic evidence and a monoisotopic mass calculation for 10-CPCDAB and 10-PDAB.

Kinetic Evaluation of DBAT for 10-DAB and Alkyl CoAs

The steady-state conditions for protein concentration and time were established for DBAT and an alkyl CoA separately incubated at low (0.05 mM) and high (1 mM) concentrations in 11 mL of Assay Buffer [50 mM NaH_2PO_4/Na_2HPO_4 buffer (pH 7.0)] containing DBAT (25 µg/mL) and 10-DAB (1 mM, at apparent saturation) at 31 °C on a rocking shaker. Aliquots (1 mL) were removed every 15 min up to 1h, then every 30 min up to 3 h, and lastly at 4, 6, and 10 h. At each time point, the reaction was stopped by adding EtOAc (500 µL), baccatin III (0.15 mM) was added as the internal standard to correct the loss of analyte during the isolation of the product. Each sample was

extracted with EtOAc (6 × 1 mL), the organic fractions were combined, and the solvent was removed under a stream of nitrogen. The resultant residue from each assay was separately resuspended in acetonitrile (100 µL) and quantified by LC/ESI-MS/MS. A stop time was established for the steady-state time range, and DBAT (25 µg/mL) and 10-DAB (1 mM) were incubated with varying concentrations of an acyl CoA (0.05 – 1 mM), respectively, in triplicate assays at 31 °C on a rocking shaker for 2 h. As described above, assay products were extracted from the reaction mixture and quantified by LC/ESI-MS/MS. The kinetic parameters (K_M and k_{cat}) were calculated by nonlinear regression with Origin Pro 9.0 software (Northampton, MA) using the Michaelis−Menten equation: $v_0 = k_{cat}[E_0][S]/(K_M + [S])$ (Figure 2.12).

Milligram-scale Production and Purification of the 10-CPCDAB and 10-PDAB

A suspension of 10-DAB (77 mg, 2 mM final concentration) in 50 mM NaH_2PO_4/Na_2HPO_4 buffer (pH 7.0) containing methanol (700 µL as an organic solubilizer) was incubated with DBAT (50 µg/mL, ~3mg total) and an acyl CoA thioester (~115 mg, 2 mM final concentration) in a total volume of 70 mL at 31 °C on a rocking shaker for 5 h. The reaction was extracted with EtOAc (3 × 50 mL). The EtOAc extracts were combined, and the solvent was removed under vacuum. The resultant residue was loaded on a silica gel flash column and eluted with 80% hexane: 20% EtOAc. The fractions containing pure 10-AcylDAB were combined, and the solvent evaporated under a vacuum. The purified 10-AcylDAB products were characterized by NMR, LC-MS/MS, and monotopic mass analyses.

NMR Data for 10-CPCDAB III (44 mg, 63% yield). ^{1}H NMR (500 MHz, $CDCl_3$) δ: 8.09 (dd, *J* = 8.4, 1.3 Hz, 2H), 7.61 (tt, *J* = 7.5, 1.3 Hz, 1H,), 7.46 (dd, *J* = 8.4, 7.5 Hz, 2H), 6.31 (s, 1H), 5.60 (d, *J* = 7.0 Hz, 1H), 4.99 (dd, *J* = 9.7, 2.1 Hz, 1H), 1H), 4.87 (m, 1H), 4.43 (dd, *J* = 9, 9 Hz 1H), 4.30 (d, *J* = 9 Hz 1H), 4.14 (d, *J* = 9 Hz 1H), 3.86 (d, *J* = 7.1 Hz, 1H), 2.56 (m, 1H), 2.29 (m, 2H), 2.27 (s, 3H), 2.02 (s, 3H), 1.86 (m, 1H), 1.68 (s, 3H), 1.58 (tt, *J* = 7.6, 4.6, Hz, 1H), 1.08 (s, 6H),

1.03 (dd, *J* = 5.3, 3.3 Hz, 2H), 0.91 (dd, *J* = 6.9, 4.6 Hz, 2H) (Figure 2.13). ^{13}C NMR (126 MHz, $CDCl_3$) δ: 204.25, 171.42, 170.74, 167.02, 146.61, 133.70, 131.58, 130.08, 129.29, 128.64, 84.46, 80.68, 79.03, 76.42, 76.27, 74.91, 72.25, 67.76, 58.59, 46.17, 42.65, 38.63, 35.58, 26.91, 22.56, 20.91, 15.60, 12.71, 9.46, 9.11 (Figure 2.14). LC/ESI-MS monoisotopic exact mass *m/z* 613.2635 $[M + H]^+$; calculated for $C_{33}H_{41}O_{11}$: 613.2649. (Figure 2.19).

NMR Data for 10-PDAB III (47 mg, 74% yield). ^{1}H NMR (500 MHz, $CDCl_3$) δ 8.09 (dd, *J* = 8.4, 1.3 Hz, 2H), 7.60 (tt, *J* = 7.5, 1.3 Hz, 1H), 7.45 (dd, *J* = 8.4, 7.5 Hz, 2H), 6.31 (s, 1H), 5.60 (d, *J* = 7.0 Hz, 1H), 4.98 (dd, *J* = 9.7, 2.1 Hz, 1H), 4.86 (m, 1H), 4.43 (dd, *J* = 9.0, 9.0 Hz, 1H), 4.30 (d, *J* = 9 Hz, 1H), 4.14 (d, *J* = 9 Hz 1H), 3.86 (d, *J* = 7.1 Hz, 1H), 2.56 (m, 1H), 2.34 (q, *J* = 7.6 Hz, 2H), 2.29 (m, 2H), 2.27 (s, 3H), 2.02 (s, 3H), 1.84 (m, 1H), 1.64 (s, 3H), 1.12 (t, *J* = 7.6 Hz, 3H), 1.08 (s, 6H) (Figure2.15). ^{13}C NMR (126 MHz, $CDCl_3$) δ: 204.22, 171.39, 170.90, 167.02, 146.60, 133.66, 131.49, 130.07, 129.29, 128.60, 84.49, 80.68, 79.06, 76.42, 76.30, 74.94, 72.16, 67.66, 58.51, 46.27, 42.62, 38.58, 35.57, 27.35, 26.90, 22.54, 20.89, 15.59, 9.45, 8.68 (Figure 2.16). LC/ESI-MS monoisotopic exact mass *m/z* 601.2635 $[M + H]^+$; calculated for $C_{33}H_{41}O_{11}$: 601.2649 (Figure 2.21).

Results and Discussion

Identifying Cyclopropanecarbonyl CoA as a Substrate of DBAT Catalysis

The substrate specificity and ability of the DBAT enzyme expressed in *E. coli* to use acetyl, propionyl, and butyryl CoA thioesters as substrates in vivo were described in an earlier study.[39] This earlier in vivo study highlighted feeding 10-DAB and small chain alkanoates to *E. coli* engineered to express the *dbat* gene. The whole-cell biocatalysis of the corresponding 10-AcylDAB compounds extracted from the bacteria growth medium was rationalized by the conversion of the alkanoates to their CoA thioesters by endogenous CoA ligases (for acetate (*acs*)

and propionate (*prpE*)) encoded on the bacterial genome and by coexpression of the butyryl CoA ligase (*atoAD*) engineered in an *E. coli* strain.[39]

We used the in vivo method in this study to screen the expressed DBAT for cyclopropanecarbonyl CoA specificity. We envisioned that the native *prpE* expressed from the *E. coli* genome might select for cyclopropanecarboxylate, which we felt was sterically similar to the natural propionate substrate, thus providing a resource of cyclopropanecarbonyl CoA. Bacterial cultures were fed 10-DAB and cyclopropanecarboxylic acid at the time of induction by IPTG. After 16 h, the baccatins extracted from the medium were surveyed by LC/ESI-MS selected-ion monitoring.

We observed selected ions consistent with baccatin III, 10-CPCDAB, and 10-PDAB (Figure 2.4A, B, C). In an earlier whole-cell biocatalysis feeding study with DBAT, baccatin III and 10-PDAB were made from reserves of acetyl CoA and n-propionyl CoA, respectively, in *E. coli.* A selected ion (*m/z* 630.26) was identified and tentatively assigned to the $[M + NH_4]^+$ for 10-CPCDAB in the LC/ESI-MS profile; this ion was absent in extracts from cell media in which cyclopropanecarboxylic acid was excluded (Figure 2.18). The presumed assembly of 10-CPCDAB in the cells suggested that cyclopropanecarbonate was converted to its corresponding acyl CoA by the bacterial ligase machinery. DBAT then transferred the cyclopropanecarbonyl group to 10-DAB to form 10-CPCDAB. These results encouraged us to synthesize cyclopropanecarbonyl and n-propionyl CoA thioesters at ~200 mg for mg-scale conversion of 10-DAB into precursors of SB-T-1214 and SB-T-12303.

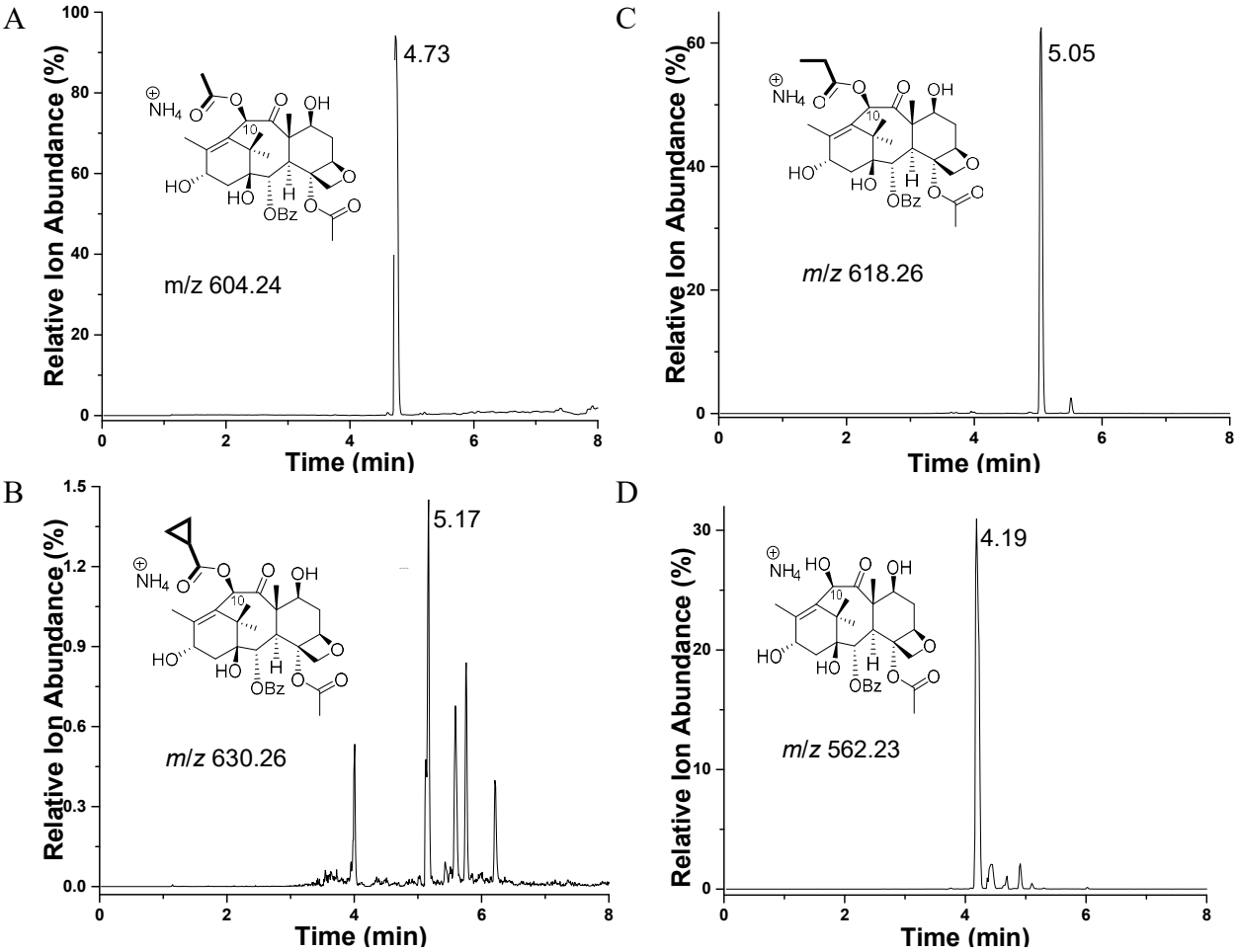

Figure 2.5: LC/ESI-MS selected-ion monitoring set at $[M + NH_4]^+$ for putative products. (A) baccatin III (4.73 min), (B) 10-CPCDAB (5.17 min), (C) 10-PDAB (5.05 min), and (D) the substrate 10-DAB (4.19 min) isolated from the Lysogeny Broth containing 10-DAB and cyclopropanecarboxylic acid in which E. coli transformed to express the dbat gene were grown as a whole-cell biocatalyst. The Y-axes are scaled according to the relative abundance of the ions for direct comparison. The data for the LC/ESI-MS selected-ion monitoring set at $[M + NH_4]^+$ for putative product 10-CPCDAB (m/z 630.26) isolated from the Lysogeny Broth containing 10-DAB without cyclopropanecarboxylic acid is in the Appendix A (Figure 2.18).

Preparative-Scale Biocatalysis of 10-CPCDAB AND 10-PDAB

A preparative-scale (8-L) culture of the bacteria engineered to express the *dbat* gene as an operationally soluble DBAT enzyme was grown, and the enzyme was isolated and purified. Portions of the concentrated DBAT enzyme were incubated with commercial 10-DAB and the synthesized acyl CoA cosubstrates to biocatalyze precursors of next-generation SB-T-taxanes. A previous study already informed that n-propionyl CoA was a substrate of DBAT. However, in this

study, we calculated the Michaelis-Menten parameters of DBAT for cyclopropanecarbonyl CoA (K_M = 0.15 M, k_{cat} = 0.83 s^{-1}) and n-propionyl CoA (K_M = 0.15 M, k_{cat} = 1.2 s^{-1}) substrates and used the values as a guide to make mg-quantities of the biocatalysis products for scale-up and to confirm their structures by NMR analysis.

NMR and LC/MS product validation. ^{1}H and ^{13}C NMR of the putative biocatalysis products 10-CPCDAB (44 mg) and 10-PDAB (47 mg) suggested that only the C10 hydroxyl was acylated by DBAT catalysis. This notion was supported by the chemical shifts of the protons and carbons bearing a hydroxyl group at C1 (3° hydroxyl), C7 (2° hydroxyl), or C13 (2° hydroxyl) staying virtually the same as those for the same positions in 10-DAB, deacylated at the C10 hydroxyl (Figure 2.5) and (Table 2.1). The diagnostic singlet observed at δ 6.31 for H10 of the putative 10-CPCDAB and 10-PDAB (Figure 2.13, and Figure 2.15) (and commercial baccatin III, see Figure 2.17) corresponds to C10 attached to an acyloxy functional group. By comparison, the H10 signal (δ 5.25) of 10-DAB, possessing only hydroxyl at C10, was relatively more shielded and upfield (Figure 2.5A) and (Table 2.1).

Up-field chemical shifts further confirmed the identity of the acyl groups of the putative 10-CPCDAB [two methylene (–CH_2–CH_2–, δ 1.03 and 0.91, each as a multiplet) and one methine (–CH–, δ 1.58, multiplet) protons of the cyclopropyl ring] (Figure 2.5C) and 10-PDAB [CH_3 (δ 1.12, triplet) and CH_2 (δ 2.34, quartet) protons of the alkanoyl side chain] (Figure 2.5D). The ^{13}C NMR chemical shifts for C10 of 10-CPCDAB and 10-PDAB (isochronous at δ 76.42) compared to that of 10-DAB (δ 75.03) further confirm the acylation regioselectivity catalyzed by DBAT at the C10 hydroxyl. Further product characterization included LC/ESI-MS/MS analysis to confirm that monoacylated products of the correct molecular weight were obtained ($[M + H]^+$ at *m*/*z* 613.26 for 10-CPCDAB and *m*/*z* 618.26 for 10-PDAB). The $[M + H]^+$ molecular ions of each

biosynthetically-derived product fragmented into a diagnostic ion at m/z 509 (M^+ − alkanoic acid at C10) and other distinguishing fragment ions (Figure 2.20 and Figure 2.21).

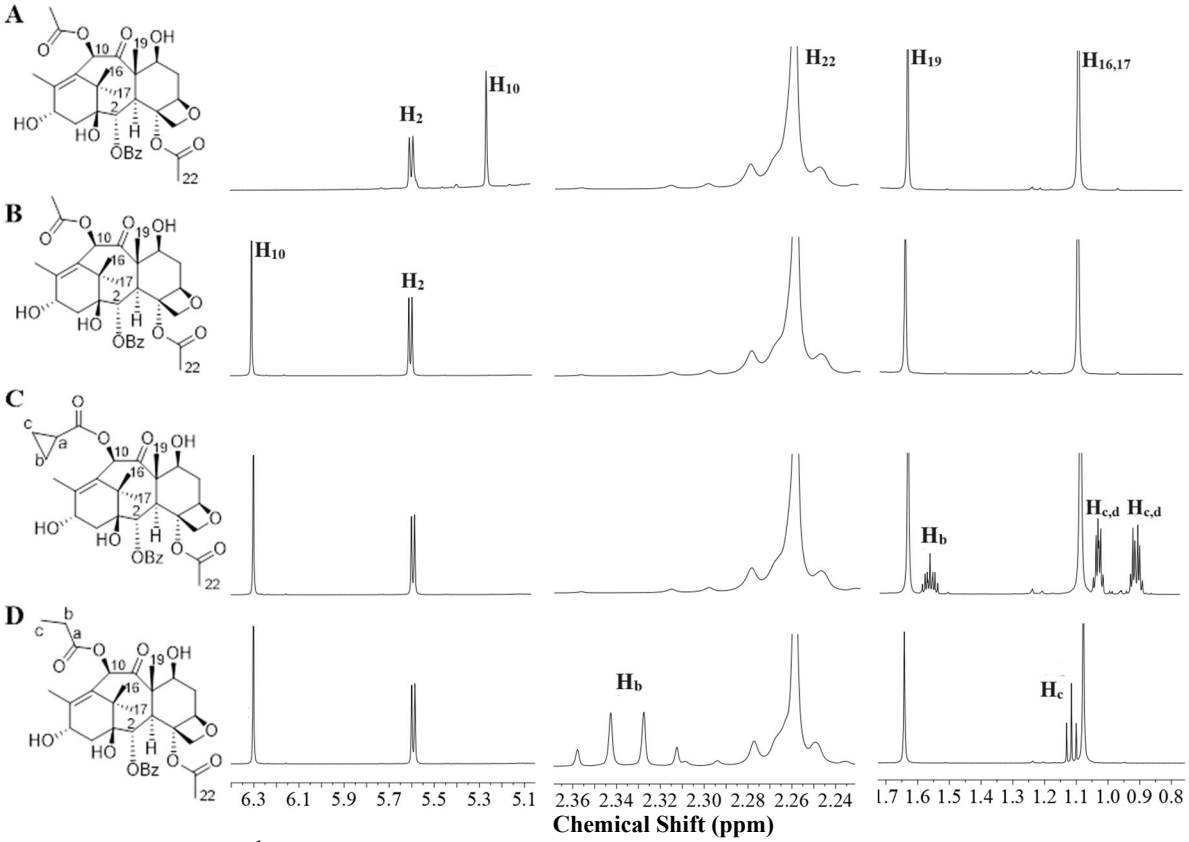

Figure 2.6: Partial ^{1}H NMR (500 MHz, $CDCl_3$) spectra of taxanes standards (A) 10-DAB and (B) Baccatin III and biocatalyzed (C) 10-CPCDAB and (D) 10-PDAB.

Table 2.1: 500 MHz ^{1}H-NMR data for 10-CPCDAB and 10-PDAB made biocatalytically.[a]

10-CPCDAB (Biocatalysis)			10-PDAB (Biocatalysis)		10-DAB (Commercial)	
Position	H: δ, mult (*J* in Hz)	C: δ	H: δ, mult (*J* in Hz)	C: δ	H: δ only	C: δ
1	—	79.03	—	79.06	—	78.81
2	5.60, d (7.0)	74.91	5.60, d, 7.0	74.94	5.64	74.72
3	3.86, d (7.1)	46.17	3.86, d, 7.1	46.27	3.92	46.91
4	—	80.68	—	80.68	—	80.70
5	4.99, dd (9.7, 2.1)	84.46	4.98, d, 9.7 / 2.1	84.49	4.98	84.12
6 (α / β)	1.86, m 2.56, m	35.58	1.84, m /	35.57	1.87 2.57	37.12
7	4.43, dd (9.0, 9.0)	72.25	4.43, dd (9.0, 9.0)	72.16	4.42	72.13
8	—	58.59	—	58.51	—	57.70
9	—	204.25	—	204.22	—	211.82
10	6.31, s	76.42	6.31, s	76.42	5.25	75.03
11	—	133.70	—	133.66	—	134.84
12	—	146.61	—	146.60	—	142.26
13	4.87, m	67.76	4.86, m	67.66	4.88	67.91
14	2.29, m	38.63	2.29, m	38.58	2.23	38.64
15	—	42.65	—	42.62	—	46.62
16 / 17	1.08, s	26.91 / 22.56	1.08, s	26.90 / 22.54	1.09	26.68 / 22.60
18	2.02, s	15.60	2.02, s	15.59	2.03	15.14
19	1.68, s	9.46	1.64, s	9.45	1.65	9.74
20(α / β)	4.14, d (9.0) 4.30, d (9.0)	76.27	4.14, d (9.0) 4.30, d (9.0)	76.30	4.16 4.32	76.59
21	—	170.74	—	170.90	—	170.72
22	2.27, s	20.91	2.27, s	20.89	2.29	19.69
BzO 23 - 29	*(o)*: 8.09, d (7.6) *(p)*: 7.62, t (7.6) *(m)*: 7.51, dd (7.6, 7.6)	(C=O): 167.02 *(o)*: 130.08 *(p)*: 131.58 *(m)*: 128.64 *(i)*: 129.29	*(o)*: 8.09, d (7.6) *(p)*: 7.62, t (7.6) *(m)*: 7.51, dd (7.6, 7.6)	(C=O): 167.02 *(o)*: 130.07 *(p)*: 131.49 *(m)*: 128.60 *ipso*: 129.29	*(o)*: 8.10 *(p)*: 7.64 *(m)*: 7.49	(C=O): 167.06 *(o)*: 130.09 *(p)*: 133.68 *(m)*: 128.64 *(i)*: 129.32
10-Acyl	Cyclopropanecarbonyl C*H*: 1.58, tt (7.6, 4.6) $HCH_{cis\ to\ C=O}$: 1.03, m $HCH_{trans\ to\ C=O}$: 0.91, m	Cyclopropanecarbonyl C*H*: 12.71; CH_2: 9.11; CH_2: 9.11 (C=O): 171.42	Propionyl CH_2: 2.34, q (7.2) CH_3: 1.12, t (7.2)	Propionyl CH_2: 27.35 CH_3: 8.68 (C=O): 171.39	N/A	N/A

[a] Samples were dissolved in $CDCl_3$, and analyzed at 300 K: δ in ppm, mult = multiplicity, *J* (coupling) in Hz. Abbreviations: s = singlet; d = doublet; dd = doublet of doublet; t = triplet; m = multiplet. *o = ortho, p = para, m = meta, i = ipso*; N/A: not applicable.

Conclusion

DBAT biocatalysis was found suitable as an alternative method for producing a ~40 mg scale of non-natural 10-AcylDAB compounds from a branchpoint natural product 10-DAB. This study describes the precursors of new-generation SB-T-taxanes with a cyclopropanecarbonyl or propionyl substitution at C10 of the taxane core catalyzed by DBAT. These precursors can serve as intermediates on biocatalytic or semisynthetic routes to construct the complete SB-T-taxanes, which have antiproliferative properties and adjuvant service against cancer cells resistant to commercial taxane drugs.[40]

While the synthesis of 10-AcylDAB compounds is considered a straightforward assembly,[41] we looked to deviate from the current chemical sector practices that typically follow a linear path to assemble compounds. At an industrial scale, production-chain chemicals often include highly reactive or toxic reagents that could potentially impact the surrounding workplace through accidental release.[42] It is estimated that many chemical synthesis practice generate waste, proportional with end-product complexity, at rates higher (projected at 5 to 50 times for specialty chemicals and 25 to 100 times for pharmaceuticals) than the target product.[43] We envision that the inclusion of enzyme catalysts gravitates toward the future of chemical processes that employ low toxicity renewable resources.

The biocatalytic construction of new-generation SB-T-taxanes in one pot is a system where a mixture of taxane acyltransferase enzymes, such as DBAT, a downstream 13-*O*-acyltransferase to install the isoserinyl side-chain, and *N*-acyltransferase to attach the *t*-Boc to the amino group of the isoserinyl group, are included. The intrinsic regioselectivities are hallmarks of the acyltransferase biocatalysts. The mixed-enzyme system lacks the start/stop (i.e., synthesis/isolation) steps and protecting group chemistries that could affect isolated yields. In addition, the one-pot system could potentially balance the chemical design scheme for making

taxane pharmaceuticals starting from a natural-product substrate isolated from renewable *Taxus* plants, biodegradable enzyme catalysts with reduced toxicity, and small molecule reactants resourced from new CO_2-reduction pathways that reduce petroleum-based chemicals.

REFERENCES

(1) How to Use a Chemotherapeutic Agent When Resistance to It Threatens the Patient. *PLOS Biol.* **2017**, *15*.

(2) Ashrafizadeh, M.; Mirzaei, S.; Hashemi, F.; Zarrabi, A.; Zabolian, A.; Saleki, H.; Sharifzadeh, S. O.; Soleymani, L.; Daneshi, S.; Hushmandi, K.; Khan, H.; Kumar, A. P.; Aref, A. R.; Samarghandian, S. New insight towards development of paclitaxel and docetaxel resistance in cancer cells: EMT as a novel molecular mechanism and therapeutic possibilities. *Biomed. pharmacother.* **2021**, *141*, 111824.

(3) Kesharwani, S. S.; Kaur, S.; Tummala, H.; Sangamwar, A. T. Overcoming multiple drug resistance in cancer using polymeric micelles. *Expert Opin. Drug Deliv.* **2018**, *15*, 1127-1142.

(4) Housman, G.; Byler, S.; Heerboth, S.; Lapinska, K.; Longacre, M.; Snyder, N.; Sarkar, S. Drug resistance in cancer: an overview. *Cancers* **2014**, *6*, 1769-1792.

(5) Kavallaris, M. Microtubules and resistance to tubulin-binding agents. *Nat. Rev. Cancer* **2010**, *10*, 194-204.

(6) Albrethsen, J.; Angeletti, R. H.; Horwitz, S. B.; Yang, C.-P. H. Proteomics of cancer cell lines resistant to microtubule-stabilizing agents. *Mol. Cancer Ther.* **2014**, *13*, 260-269.

(7) Bishop, J. F.; Dewar, J.; Toner, G. C.; Smith, J.; Tattersall, M. H.; Olver, I. N.; Ackland, S.; Kennedy, I.; Goldstein, D.; Gurney, H.; Walpole, E.; Levi, J.; Stephenson, J.; Canetta, R. Initial paclitaxel improves outcome compared with CMFP combination chemotherapy as front-line therapy in untreated metastatic breast cancer. *J. Clin. Oncol.* **1999**, *17*, 2355-2364.

(8) Tolaney, S. M.; Barry, W. T.; Dang, C. T.; Yardley, D. A.; Moy, B.; Marcom, P. K.; Albain, K. S.; Rugo, H. S.; Ellis, M.; Shapira, I.; Wolff, A. C.; Carey, L. A.; Overmoyer, B. A.; Partridge, A. H.; Guo, H.; Hudis, C. A.; Krop, I. E.; Burstein, H. J.; Winer, E. P. Adjuvant paclitaxel and trastuzumab for node-negative, HER2-positive breast cancer. *New Engl. J. Med.* **2015**, *372*, 134-141.

(9) Ozols, R. F.; Bundy, B. N.; Greer, B. E.; Fowler, J. M.; Clarke-Pearson, D.; Burger, R. A.; Mannel, R. S.; DeGeest, K.; Hartenbach, E. M.; Baergen, R. Phase III trial of carboplatin and paclitaxel compared with cisplatin and paclitaxel in patients with optimally resected stage III ovarian cancer: A gynecologic oncology group study. *J. Clin. Oncol.* **2003**, *21*, 3194-3200.

(10) Falchook, G.; Coleman, R. L.; Roszak, A.; Behbakht, K.; Matulonis, U.; Ray-Coquard, I.; Sawrycki, P.; Duska, L. R.; Tew, W.; Ghamande, S.; Lesoin, A.; Schwartz, P. E.; Buscema, J.; Fabbro, M.; Lortholary, A.; Goff, B.; Kurzrock, R.; Martin, L. P.; Gray, H. J.; Fu, S.; Sheldon-Waniga, E.; Lin, H. M.; Venkatakrishnan, K.; Zhou, X.; Leonard, E. J.; Schilder, R. J. Alisertib in combination with weekly paclitaxel in patients with advanced breast

cancer or recurrent ovarian cancer: A randomized clinical trial. *JAMA Oncol.* **2019**, *5*, e183773-e183773.

(11) Socinski, M. A. Cytotoxic chemotherapy in advanced non-small cell lung cancer: a review of standard treatment paradigms. *Clin. Cancer. Res.* **2004**, *10*, 4210s-4214s.

(12) Jiang, L.; Li, L.; He, X.; Yi, Q.; He, B.; Cao, J.; Pan, W.; Gu, Z. Overcoming drug-resistant lung cancer by paclitaxel loaded dual-functional liposomes with mitochondria targeting and pH-response. *Biomaterials* **2015**, *52*, 126-139.

(13) Woods, B. S.; Sideris, E.; Sydes, M. R.; Gannon, M. R.; Parmar, M. K. B.; Alzouebi, M.; Attard, G.; Birtle, A. J.; Brock, S.; Cathomas, R.; Chakraborti, P. R.; Cook, A.; Cross, W. R.; Dearnaley, D. P.; Gale, J.; Gibbs, S.; Graham, J. D.; Hughes, R.; Jones, R. J.; Laing, R.; Mason, M. D.; Matheson, D.; McLaren, D. B.; Millman, R.; O'Sullivan, J. M.; Parikh, O.; Parker, C. C.; Peedell, C.; Protheroe, A.; Ritchie, A. W. S.; Robinson, A.; Russell, J. M.; Simms, M. S.; Srihari, N. N.; Srinivasan, R.; Staffurth, J. N.; Sundar, S.; Thalmann, G. N.; Tolan, S.; Tran, A. T. H.; Tsang, D.; Wagstaff, J.; James, N. D.; Sculpher, M. J. Addition of docetaxel to first-line long-term hormone therapy in prostate cancer (STAMPEDE): Modelling to estimate long-term survival, quality-adjusted survival, and cost-effectiveness. *Eur. Urol. Oncol.* **2018**, *1*, 449-458.

(14) Singh, S. K.; Lillard, J. W.; Singh, R. Reversal of drug resistance by planetary ball milled (PBM) nanoparticle loaded with resveratrol and docetaxel in prostate cancer. *Cancer Lett.* **2018**, *427*, 49-62.

(15) Mita, A. C.; Figlin, R.; Mita, M. M. Cabazitaxel: More than a new taxane for metastatic castrate-resistant prostate cancer. *Clin. Cancer. Res.* **2012**, *18*, 6574-6579.

(16) Giannakakou, P.; Galletti, G.: Microtubules in Prostate Cancer. In *Precision Molecular Pathology of Prostate Cancer*; Robinson, B. D., Mosquera, J. M., Ro, J. Y., Divatia, M., Eds.; Springer International Publishing: Cham, **2018**; pp 439-453.

(17) Zasadil, L. M.; Andersen, K. A.; Yeum, D.; Rocque, G. B.; Wilke, L. G.; Tevaarwerk, A. J.; Raines, R. T.; Burkard, M. E.; Weaver, B. A. Cytotoxicity of paclitaxel in breast cancer is due to chromosome missegregation on multipolar spindles. *Sci. Transl. Med.* **2014**, *6*, 229ra243-229ra243.

(18) Sharom, F. J. The P-glycoprotein efflux pump: how does it transport drugs? *J. Membr. Biol.* **1997**, *160*, 161-175.

(19) Wang, C.; Wang, X.; Sun, Y.; Taouil, A. K.; Yan, S.; Botchkina, G. I.; Ojima, I. Design, synthesis and SAR study of 3rd-generation taxoids bearing 3-CH(3), 3-CF(3)O and 3-CHF(2)O groups at the C2-benzoate position. *Bioorg. Chem.* **2020**, *95*, 103523.

(20) Wang, C.; Chen, L.; Sun, Y.; Guo, W.; Taouil, A. K.; Ojima, I. Design, synthesis and SAR study of Fluorine-containing 3rd-generation taxoids. *Bioorg. Chem.* **2022**, *119*, 105578.

(21) Jelínek, M.; Balušíková, K.; Daniel, P.; Němcová-Fürstová, V.; Kirubakaran, P.; Jaček, M.; Wei, L.; Wang, X.; Vondrášek, J.; Ojima, I.; Kovář, J. Substituents at the C3′ and C3′N positions are critical for taxanes to overcome acquired resistance of cancer cells to paclitaxel. *Toxicol. Appl. Pharmacol.* **2018**, *347*, 79-91.

(22) Minderman, H.; Brooks, T. A.; O'Loughlin, K. L.; Ojima, I.; Bernacki, R. J.; Baer, M. R. Broad-spectrum modulation of ATP-binding cassette transport proteins by the taxane derivatives ortataxel (IDN-5109, BAY 59-8862) and tRA96023. *Cancer Chemother. Pharmacol.* **2004**, *53*, 363-369.

(23) Matesanz, R.; Trigili, C.; Rodríguez-Salarichs, J.; Zanardi, I.; Pera, B.; Nogales, A.; Fang, W.-S.; Jímenez-Barbero, J.; Canales, Á.; Barasoain, I.; Ojima, I.; Díaz, J. F. Taxanes with high potency inducing tubulin assembly overcome tumoural cell resistances. *Biorg. Med. Chem.* **2014**, *22*, 5078-5090.

(24) Yang, C. H.; Wang, C.; Ojima, I.; Horwitz, S. B. Taxol analogues exhibit differential effects on photoaffinity labelingof β-tubulin and the multidrug resistance associated P-glycoprotein. *J. Nat. Prod.* **2018**, *81*, 600-606.

(25) Ferlini, C.; Raspaglio, G.; Mozzetti, S.; Cicchillitti, L.; Filippetti, F.; Gallo, D.; Fattorusso, C.; Campiani, G.; Scambia, G. The seco-taxane IDN5390 is able to target class III β-tubulin and to overcome paclitaxel resistance. *Cancer Res.* **2005**, *65*, 2397-2405.

(26) Ojima, I.; Wang, X.; Jing, Y.; Wang, C. Quest for Efficacious Next-Generation Taxoid Anticancer Agents and Their Tumor-Targeted Delivery. *J. Nat. Prod.* **2018**, *81*, 703-721.

(27) Zheng, X.; Wang, C.; Xing, Y.; Chen, S.; Meng, T.; You, H.; Ojima, I.; Dong, Y. SB-T-121205, a next-generation taxane, enhances apoptosis and inhibits migration/invasion in MCF-7/PTX cells. *Int. J. Oncol.* **2017**, *50*, 893-902.

(28) Ojima, I.; Chen, J.; Sun, L.; Borella, C. P.; Wang, T.; Miller, M. L.; Lin, S.; Geng, X.; Kuznetsova, L.; Qu, C.; Gallager, D.; Zhao, X.; Zanardi, I.; Xia, S.; Horwitz, S. B.; Mallen-St Clair, J.; Guerriero, J. L.; Bar-Sagi, D.; Veith, J. M.; Pera, P.; Bernacki, R. J. Design, synthesis, and biological evaluation of new-generation taxoids. *J. Med. Chem.* **2008**, *51*, 3203-3221.

(29) Cheng, Z.; Li, N.; Cheng, J.; Hu, R.; Gao, G.; Cui, Y.; Gong, X.; Wang, L.; Hong, F. Signal pathway of hippocampal apoptosis and cognitive impairment of mice caused by cerium chloride. *Environ. Toxicol.* **2012**, *27*, 707-718.

(30) Cheng, J.; Li, N.; Cai, J.; Cheng, Z.; Hu, R.; Zhang, Q.; Wan, F.; Sun, Q.; Gui, S.; Sang, X.; Wang, L.; Hong, F. Organ histopathological changes and its function damage in mice following long-term exposure to lanthanides chloride. *Biol. Trace Elem. Res.* **2012**, *145*, 361-368.

(31) Cheng, J.; Cheng, Z.; Hu, R.; Cui, Y.; Cai, J.; Li, N.; Gui, S.; Sang, X.; Sun, Q.; Wang, L.; Hong, F. Immune dysfunction and liver damage of mice following exposure to lanthanoids.

Environ. Toxicol. **2014**, *29*, 64-73.

(32) Chen, K.; Zhang, S. Q.; Brandenberg, O. F.; Hong, X.; Arnold, F. H. Alternate Heme Ligation Steers Activity and Selectivity in Engineered Cytochrome P450-Catalyzed Carbene-Transfer Reactions. *J. Am. Chem. Soc.* **2018**, *140*, 16402-16407.

(33) Brandenberg, O. F.; Fasan, R.; Arnold, F. H. Exploiting and engineering hemoproteins for abiological carbene and nitrene transfer reactions. *Curr. Opin. Biotechnol.* **2017**, *47*, 102-111.

(34) Li, Y.; Li, S.; Thodey, K.; Trenchard, I.; Cravens, A.; Smolke, C. D. Complete biosynthesis of noscapine and halogenated alkaloids in yeast. *Proc. Natl. Acad. Sci. U.S.A.* **2018**, *115*, E3922-E3931.

(35) Yi, D.; Bayer, T.; Badenhorst, C. P. S.; Wu, S.; Doerr, M.; Hohne, M.; Bornscheuer, U. T. Recent trends in biocatalysis. *Chem. Soc. Rev.* **2021**, *50*, 8003-8049.

(36) Teufel, R.; Kaysser, L.; Villaume, M. T.; Diethelm, S.; Carbullido, M. K.; Baran, P. S.; Moore, B. S. One-pot enzymatic synthesis of merochlorin A and B. *Angew. Chem. Int. Ed.* **2014**, *53*, 11019-11022.

(37) Loncaric, C.; Merriweather, E.; Walker, K. D. Profiling a Taxol Pathway 10β-Acetyltransferase: Assessment of the Specificity and the Production of Baccatin III by In Vivo Acetylation in E. coli. *Chem. Biol.* **2006**, *13*, 309-317.

(38) Walker, K.; Croteau, R. Molecular cloning of a 10-deacetylbaccatin III-10-O-acetyl transferase cDNA from Taxus and functional expression in Escherichia coli. *Proc. Natl. Acad. Sci.* **2000**, *97*, 583-587.

(39) Loncaric, C.; Merriweather, E.; Walker, K. D. Profiling a Taxol pathway 10β-*O*-acetyltransferase: Assessment of the specificity and the production of baccatin III by *in vivo* acetylation in *E. coli*. *Chem. Biol.* **2006**, *13*, 1-9.

(40) Baloglu, E.; Hoch, J. M.; Chatterjee, S. K.; Ravindra, R.; Bane, S.; Kingston, D. G. I. Synthesis and biological evaluation of C-3'NH/C-10 and C-2/C-10 modified paclitaxel analogues. *Biorg. Med. Chem.* **2003**, *11*, 1557-1568.

(41) Appendino, G.; Belloro, E.; Del Grosso, E.; Minassi, A.; Bombardelli, E. Synthesis and evaluation of 14-nor-A-*seco*taxoids. *Eur. J. Org. Chem.* **2002**, *2002*, 277-283.

(42) Zimmerman, J. B.; Anastas, P. T.; Erythropel, H. C.; Leitner, W. Designing for a green chemistry future. *Science* **2020**, *367*, 397-400.

(43) Sheldon, R. A. The E factor 25 years on: the rise of green chemistry and sustainability. *Green Chemistry* **2017**, *19*, 18-43.

APPENDIX A: CHAPTER 2 SUPPLEMENTARY MATERIALS

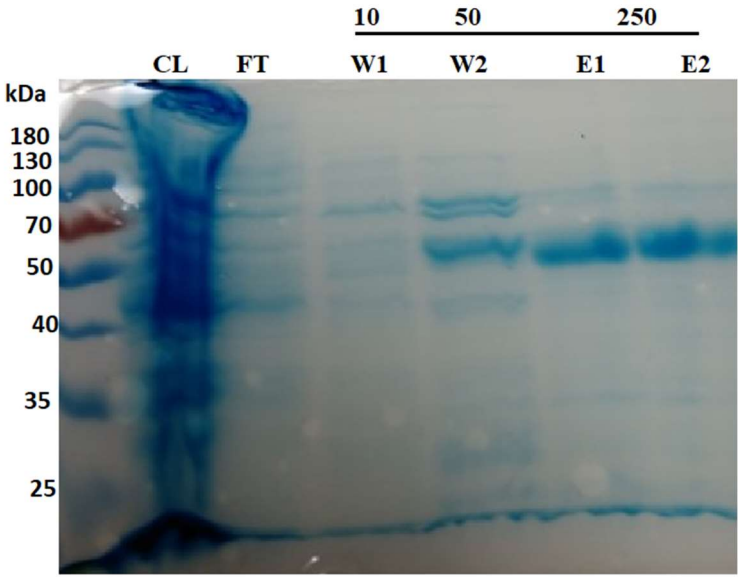

Figure 2.7: Coomassie Blue stained SDS-PAGE gel of aliquots from the fractions collected from Ni-NTA affinity exchange column used to purify the DBAT enzyme. Lanes represent protein contained in the crude lysate (**CL**); unbound flow-through (**FT**); Wash Buffer (**W1** and **W2**); and Elution Buffer (**E1** and **E2**) fractions. The numbers above the bar are the mM concentrations of imidazole in the respective buffers. Molecular weight references are in the leftmost lane.

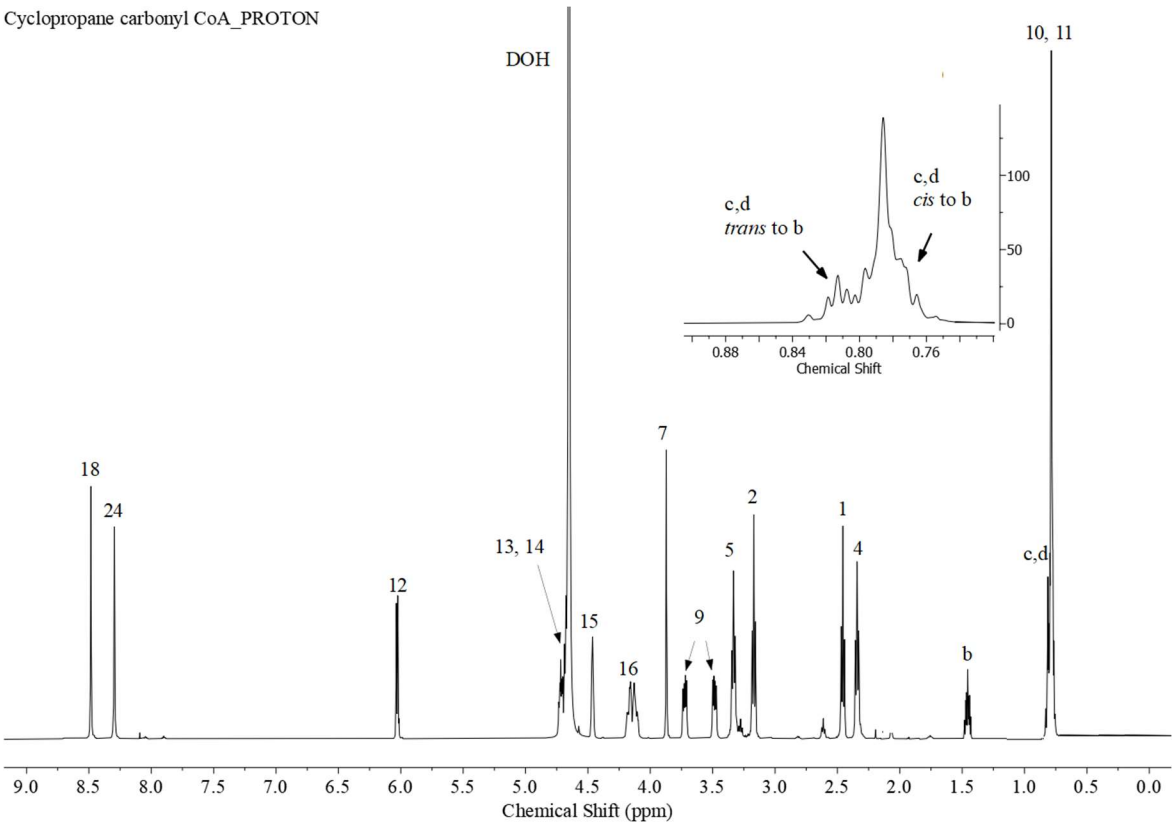

Figure 2.8: ^{1}H-NMR (500 MHz) of cyclopropanecarbonyl CoA.

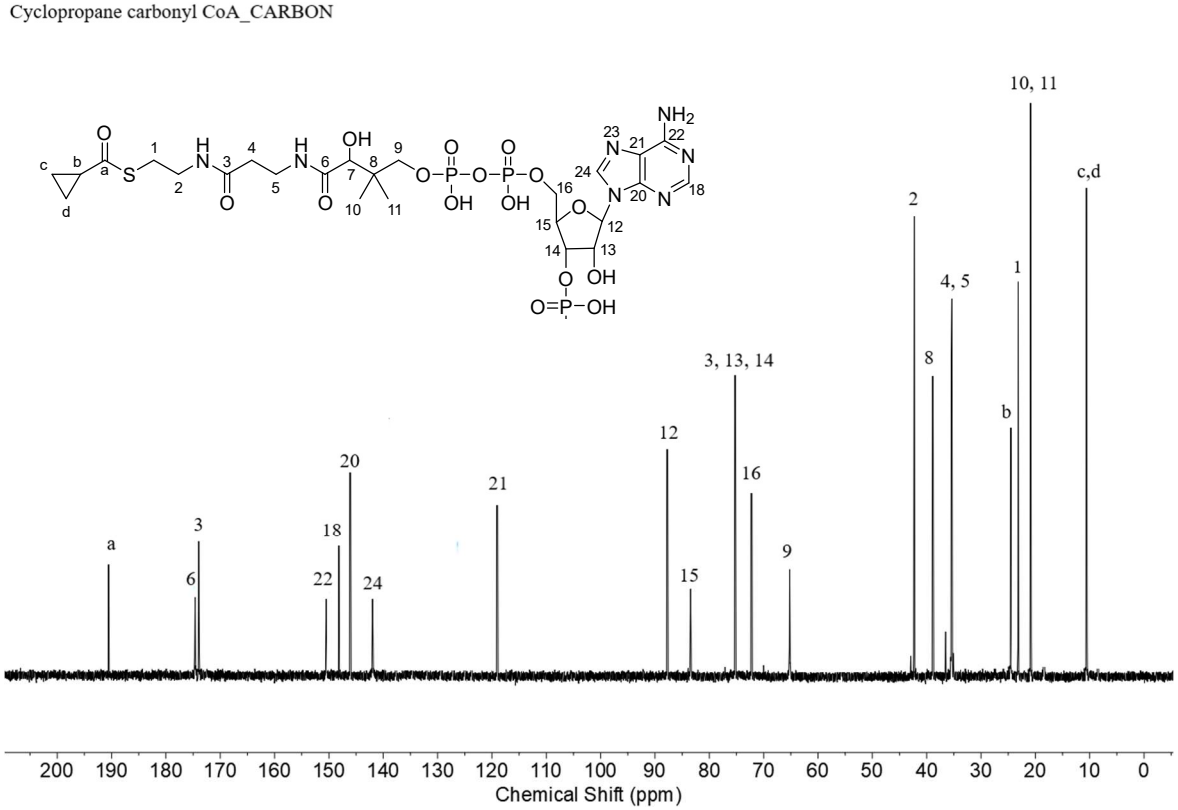

Figure 2.9: ^{13}C-NMR (126 MHz) of cyclopropanecarbonyl CoA.

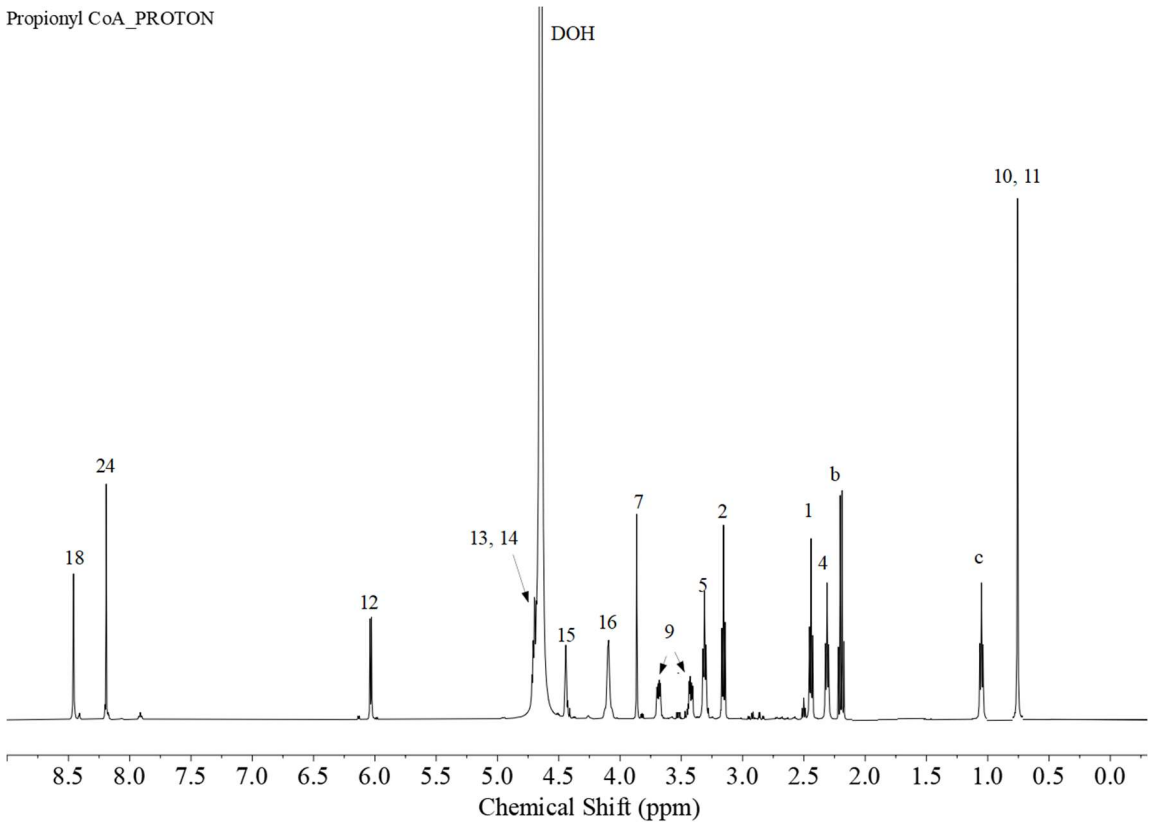

Figure 2.10: ^{1}H-NMR (500 MHz) of propionyl CoA.

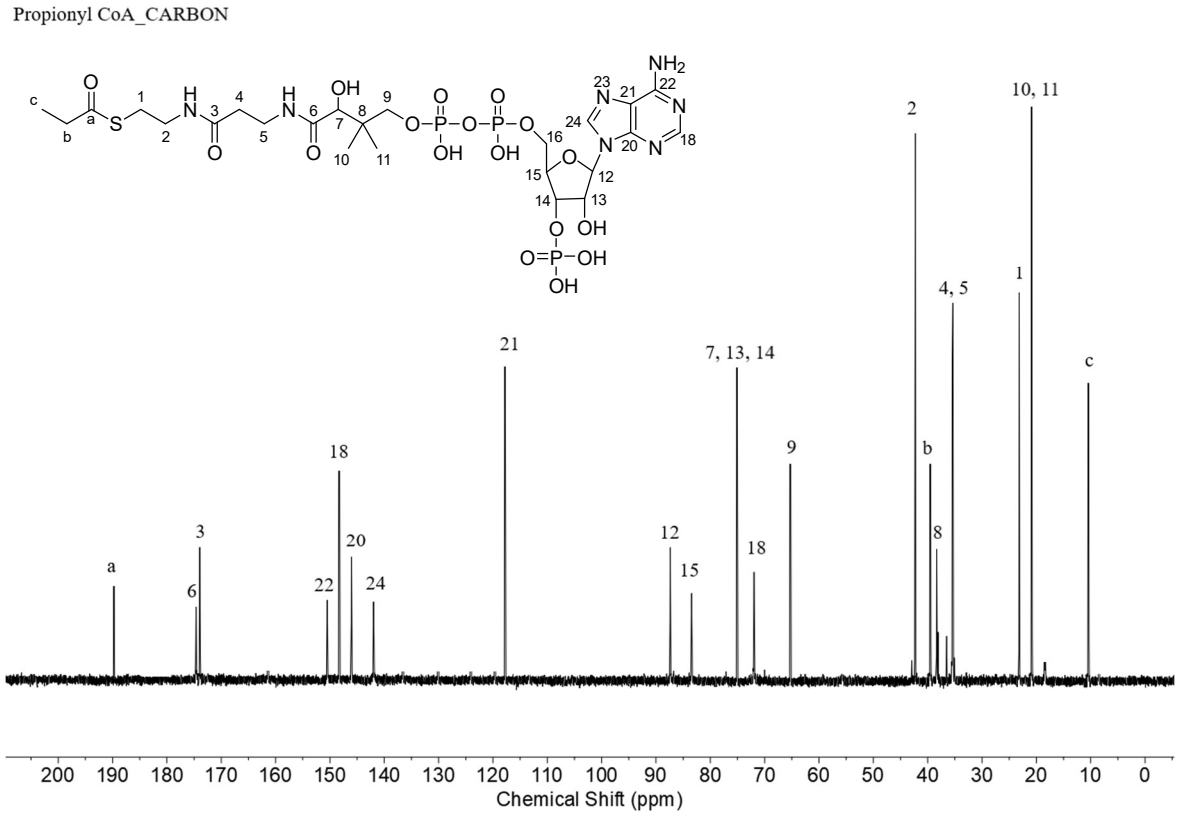

Figure 2.11: ^{13}C-NMR (126 MHz) of propionyl CoA.

A

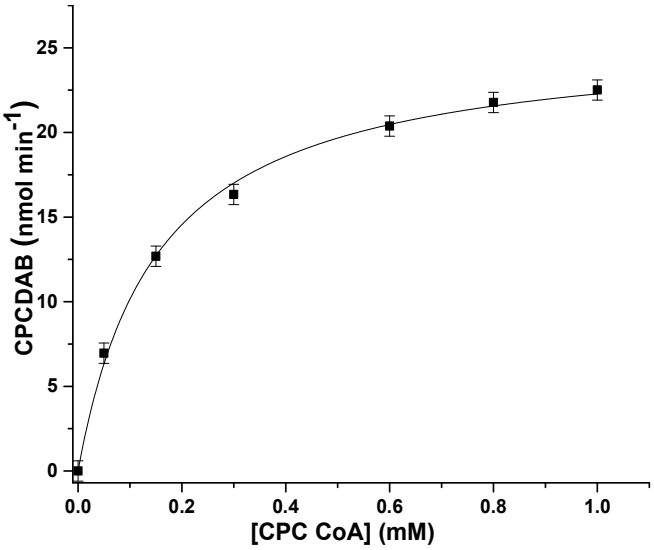

B

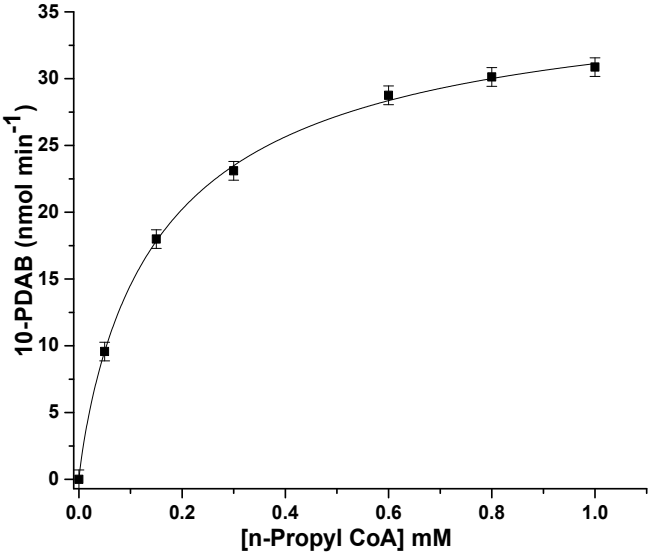

Figure 2.12: Nonlinear regression analysis of DBAT using the steady-state turnover rates of DBAT for varying acyl CoA concentrations to calculate the Michaelis parameters toward A) 10-CPCDAB (V_{max}= 25.7 nmol min^{-1}, K_M = 153 μM, k_{cat} = 50 min^{-1}) and B) 10-PDAB (V_{max}= 35.4 nmol min^{-1}, K_M = 145 μM, k_{cat} = 69 min^{-1}.

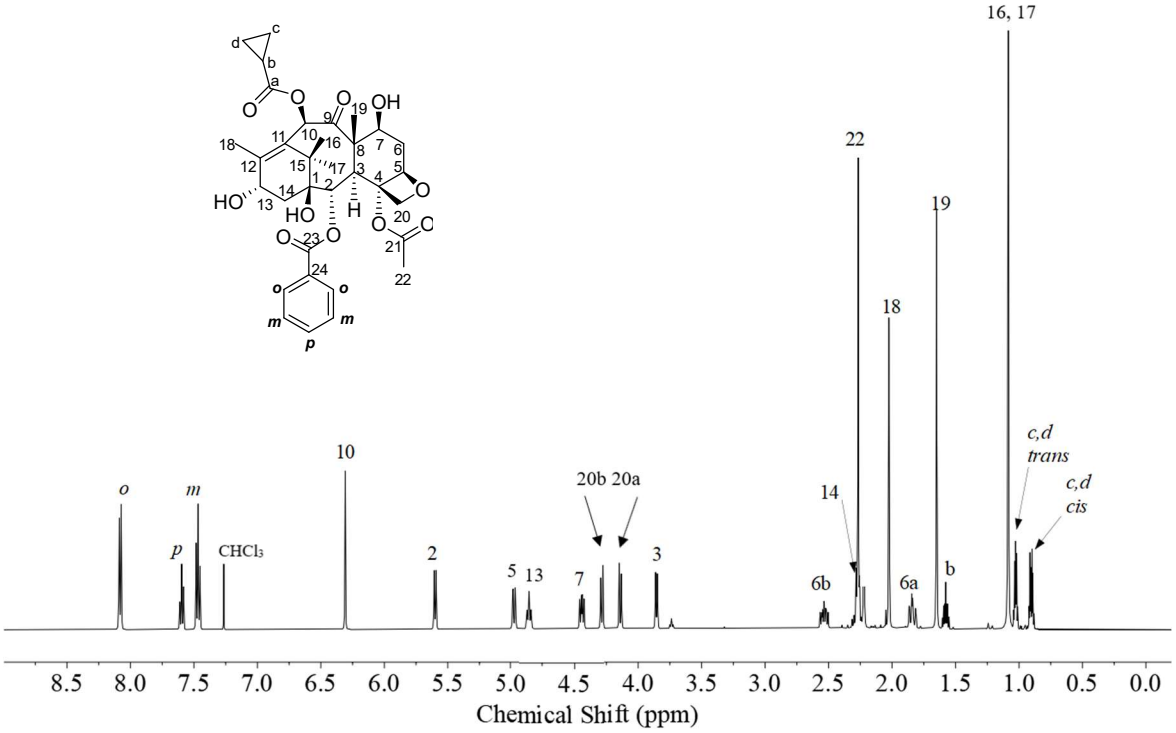

Figure 2.13: ^{1}H-NMR (500 MHz) of 10-CPCDAB.

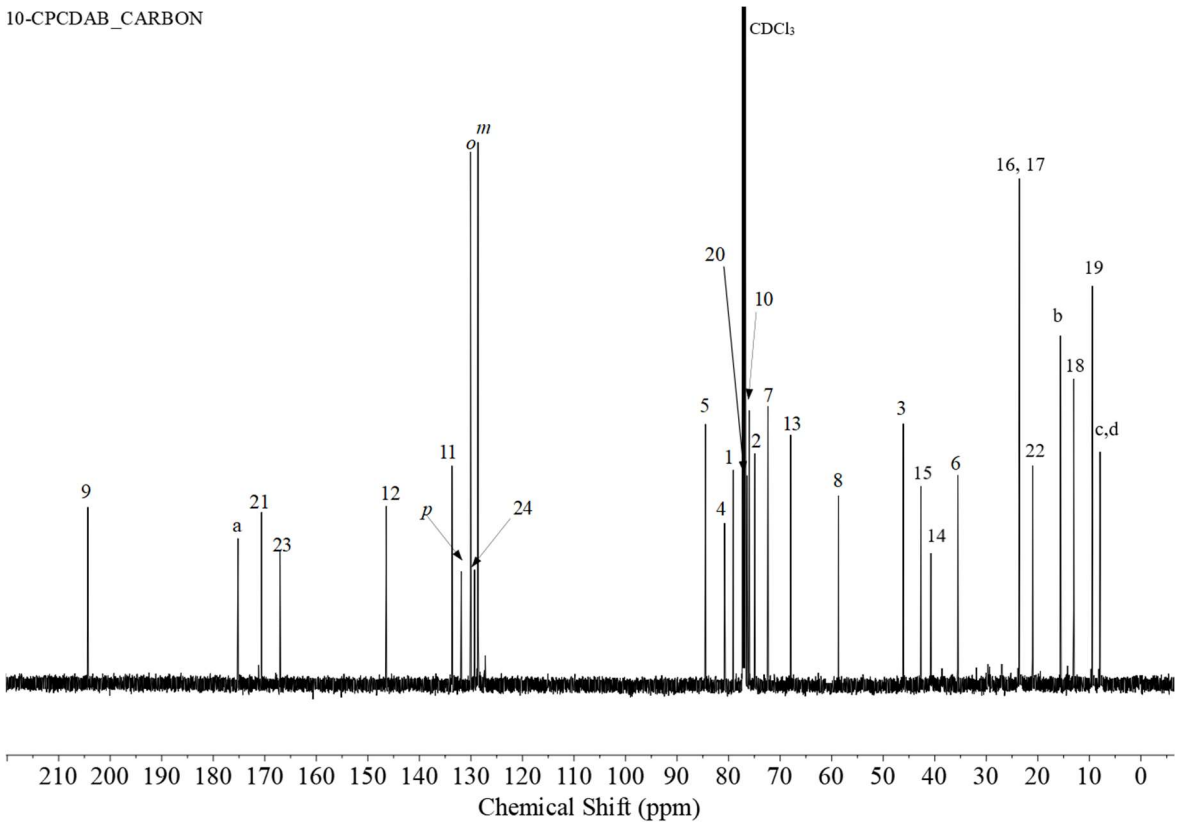

Figure 2.14: ^{13}C-NMR (126 MHz) of 10-CPCDAB.

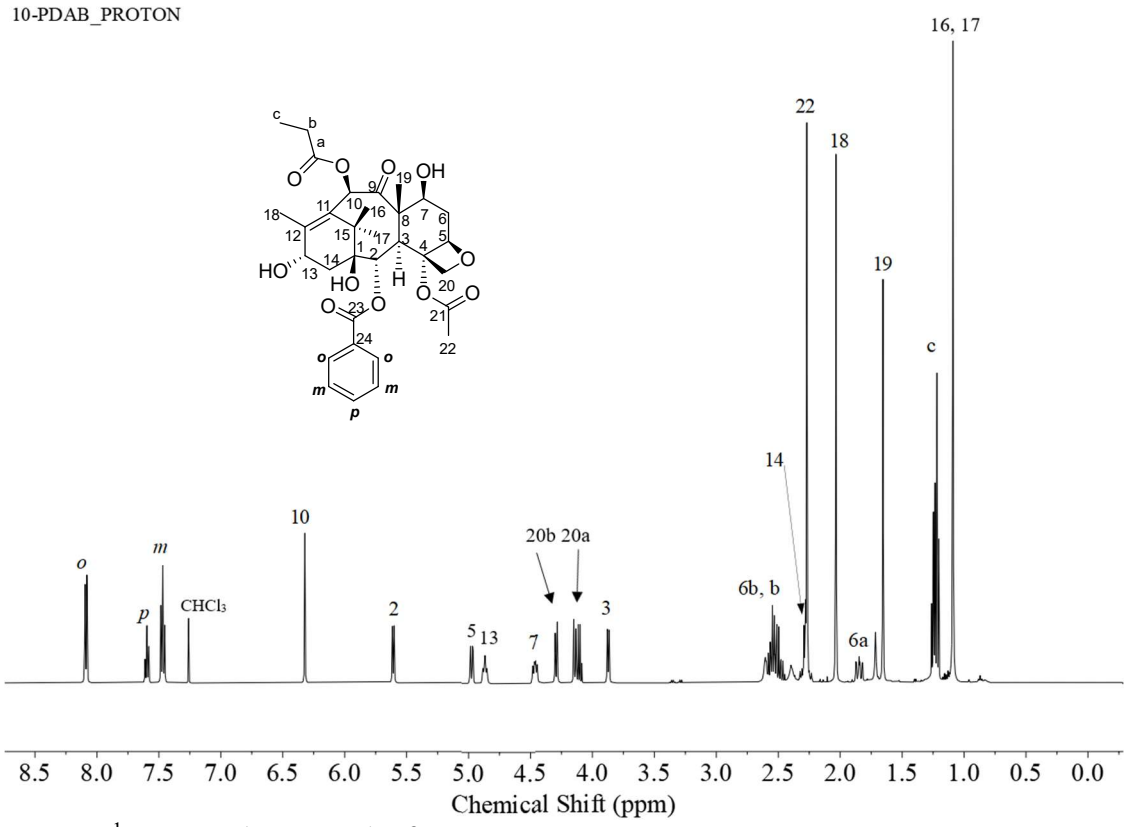

Figure 2.15: ^{1}H-NMR (500 MHz) of 10-PDAB.

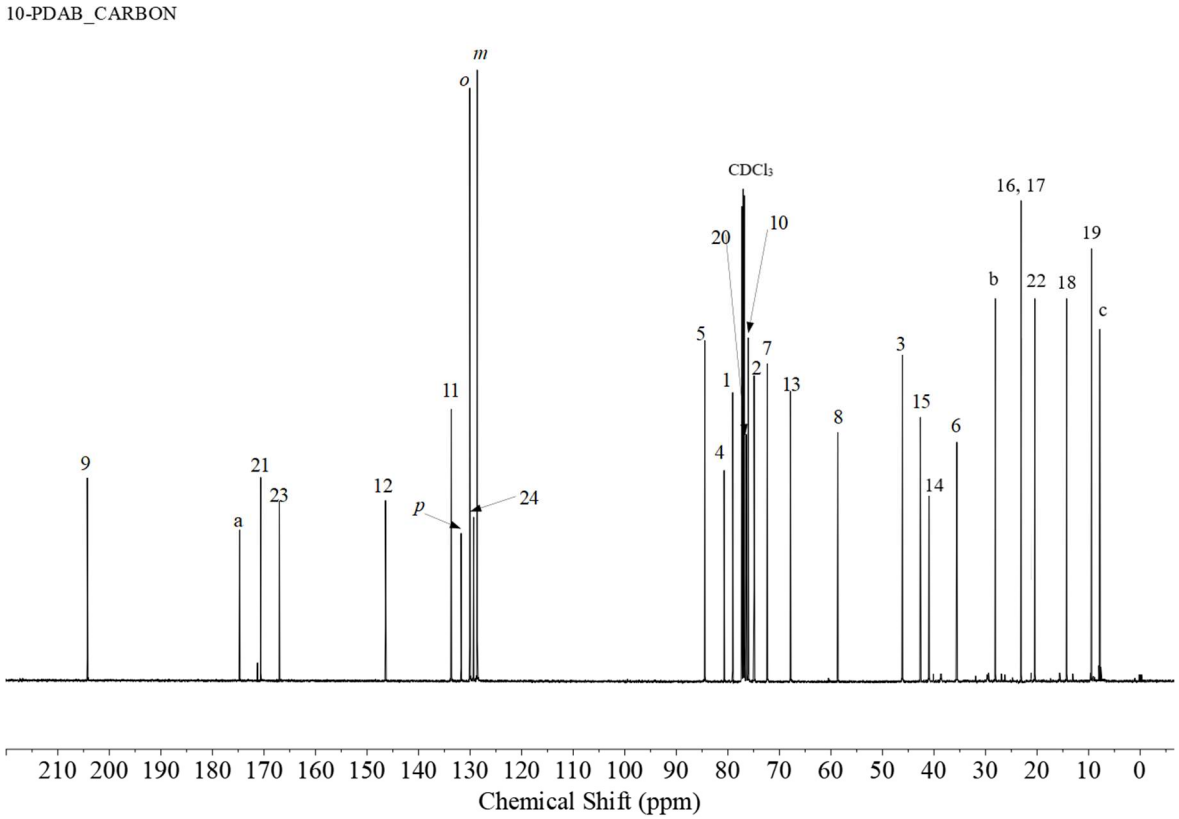

Figure 2.16: ^{13}C-NMR (126 MHz) of 10-PDAB.

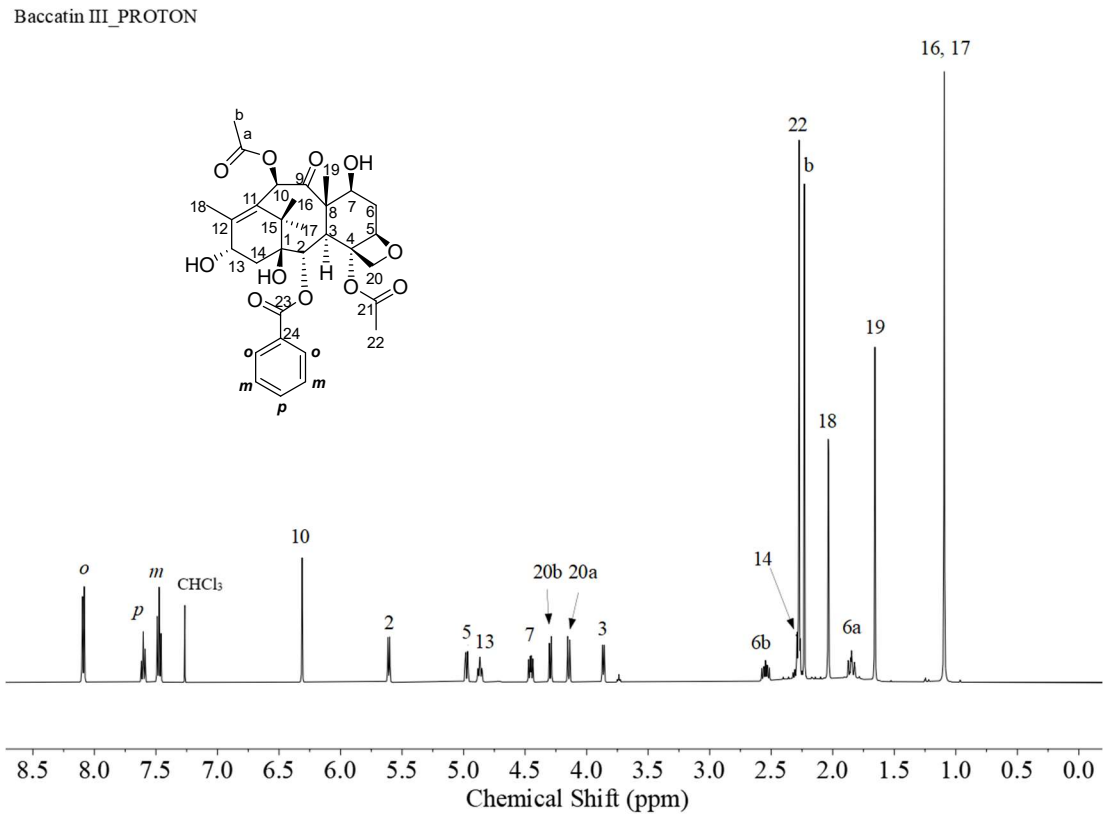

Figure 2.17: ^{1}H-NMR (500 MHz) of Baccatin III.

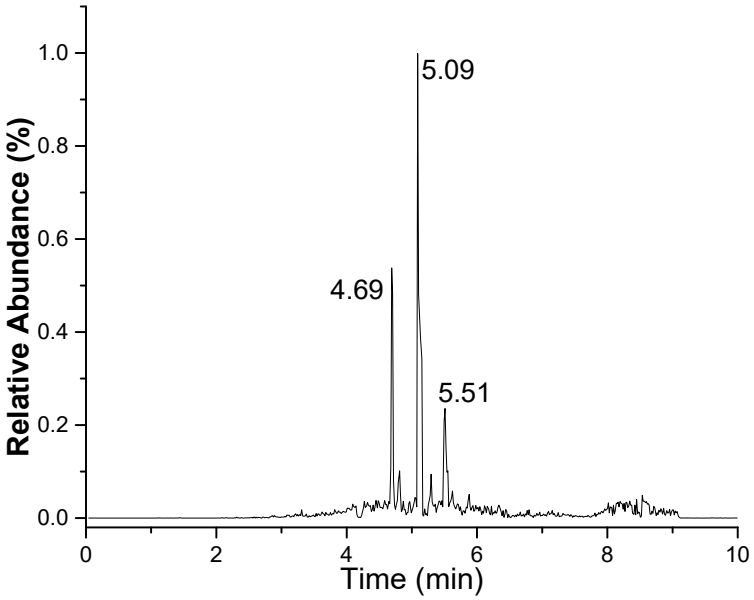

Figure 2.18: LC/ESI-MS selected-ion monitoring set at $[M + NH_4]^+$ for putative product 10-CPCDAB (m/z 630.26) isolated from the Lysogeny Broth containing 10-DAB <u>without</u> cyclopropanecarboxylic acid in which *E. coli* transformed to express the dbat gene were grown as a whole-cell biocatalyst.

A

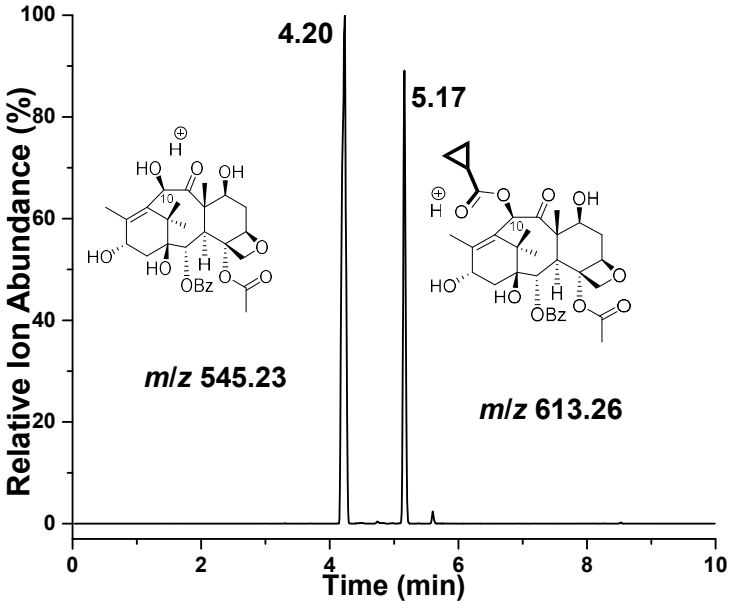

B

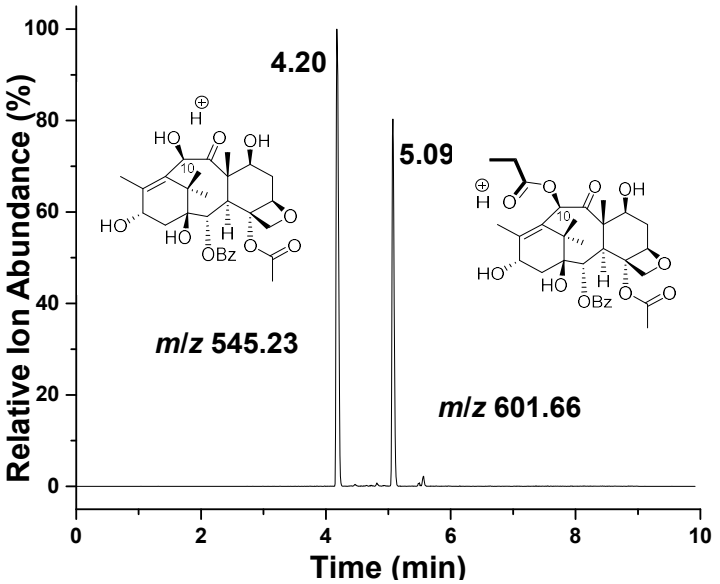

Figure 2.19: LC/ESI-MS (selected ion mode for m/z $[M + H]^+$) of the biocatalytic conversion of 10-DAB to (A) 10-CPCDAB and (B) 10-PDAB in the DBAT in vitro biocatalysis assay.

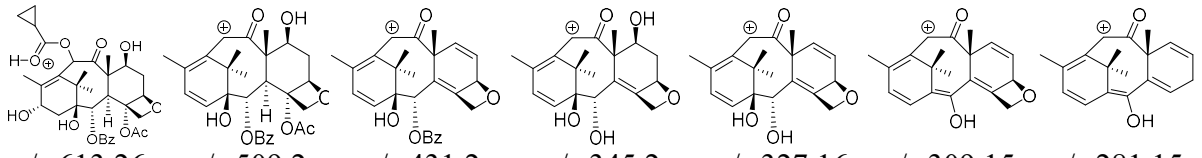

m/z 613.26 *m/z* 509.2 *m/z* 431.2 *m/z* 345.2 *m/z* 327.16 *m/z* 309.15 *m/z* 281.15

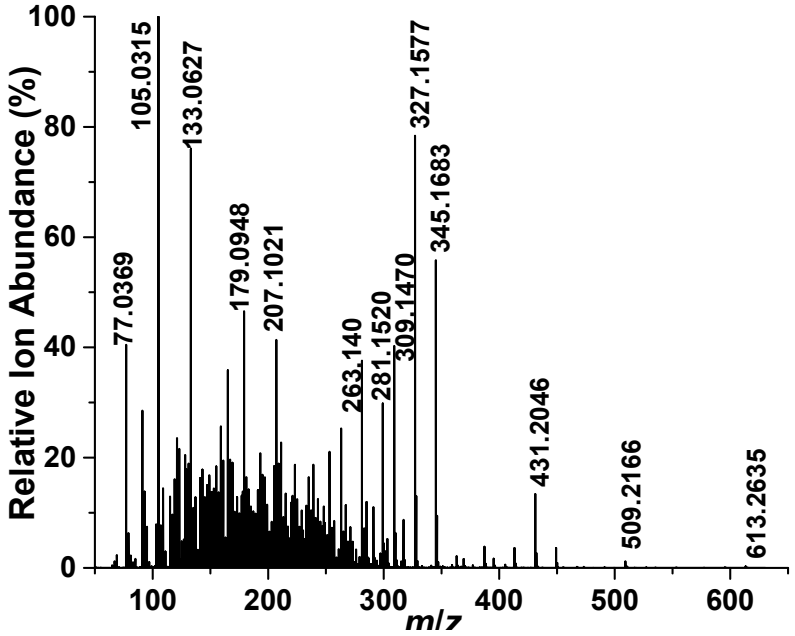

Figure 2.20: LC/ESI-MS/MS positive-ion mode of purified 10-CPCDAB made biocatalytic by DBAT, using 10-DAB and cyclopropane carbonyl CoA substrates. Magnification at between m/z 350 to m/z 75 with peak mass assignments and putative chemical transformations (above spectra).

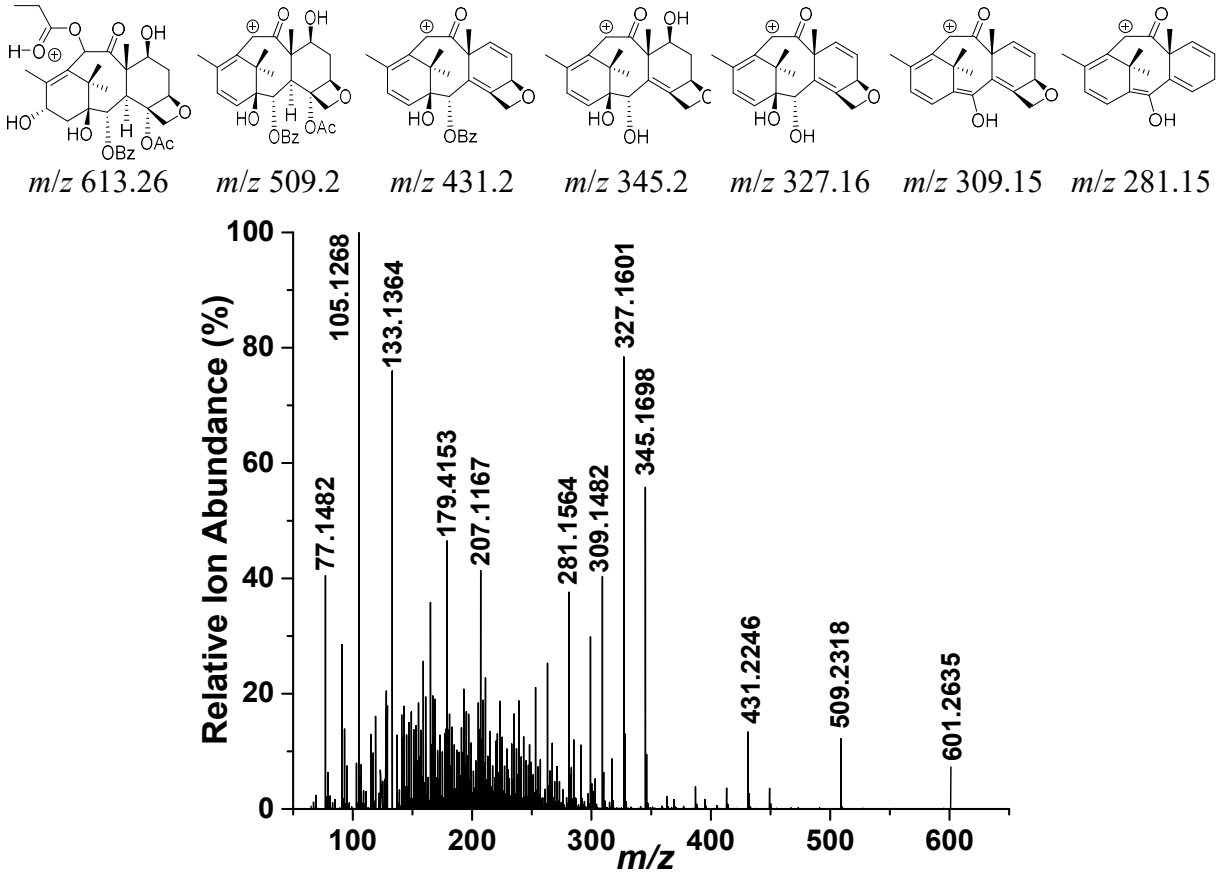

Figure 2.21: LC/ESI-MS/MS positive-ion mode of purified 10-PDAB made biocatalytic by DBAT, using 10-DAB and propionyl CoA substrates. Magnification at between m/z 350 to m/z 75 with peak mass assignments and putative chemical transformations (above spectra).

Chapter 3 is adapted from our published work in ChemCatChem

Al-Hilfi, A.; Li, Z.; Merz, K.M.; Nawarathne, I.N.; Walker, K.D. Biocatalytic and Regioselective Exchange of 2-*O*-Benzoyl for 2-*O*-(*m*-Substituted)Benzoyl Groups to Make Precursors of Next-Generation Paclitaxel Drugs. *ChemCatChem* **2024**, e202400186. (accepted)
https://doi.org/10.1002/cctc.202400186

CHAPTER 3: BIOCATALYTIC AND REGIOSELECTIVE EXCHANGE OF 2-*O*-BENZOYL FOR 2-*O*-(META-SUBSTITUTED)BENZOYL GROUPS TO MAKE PRECURSORS OF NEXT-GENERATION PACLITAXEL DRUGS

Introduction

Next-generation paclitaxel analogs containing 2-*O*-debenzoyl-2-*O*-(*m*-substituted)benzoyl analogs are effective against cancer cells resistant to existing chemotherapeutics.[1] These next-generation paclitaxel analogs are made from a decades-old, nine-step semisynthetic route starting from an abundant taxane natural product, for example, 10-deacetylbaccatin III (10-DAB, **3.1**) (Figure 3.1)[1,2] isolated from *Taxus* plants where paclitaxel (**3.12**) is made. The synthetic steps sometimes involve redundant protecting group chemistries and reductive ester cleavages to deacylate and selectively reacylate.[3,4] While these elegant synthetic approaches have been used unwaveringly to access these next-generation drug analogs, their continued application leaves a chemical footprint that potentially negatively affects the environment. Incorporating intrinsic chemo- and regioselective biocatalysts into these production streams could improve environmental sustainability under mild enzymatic reaction conditions.

Recent structure-activity relationship (SAR) studies dissected the mechanisms of new third-generation SB-Taxanes (developed at Stony Brook University, Stony Brook, NY). These studies showed that *m*-substituted aroyls at the C2 hydroxyl of the SB-Taxanes increase the cytotoxicity and potency against multiple-drug resistant (MDR)-cancer cell lines over the parent drug paclitaxel.[2,3,5] The SB-Taxanes containing *m*-substituted aroyl analogs have enhanced interaction with His229 in β-tubulin.[6] Most notable, C2 aroyl groups with *m*-fluoromethoxy (*m*-OCF_3 or *m*-$OCHF_2$) substituents improved the target-binding affinity and cytotoxicity of next-generation taxanes 7-fold over paclitaxel against drug-sensitive cancer cells and 3-fold over paclitaxel against drug-resistant cancer cells.[2,5]

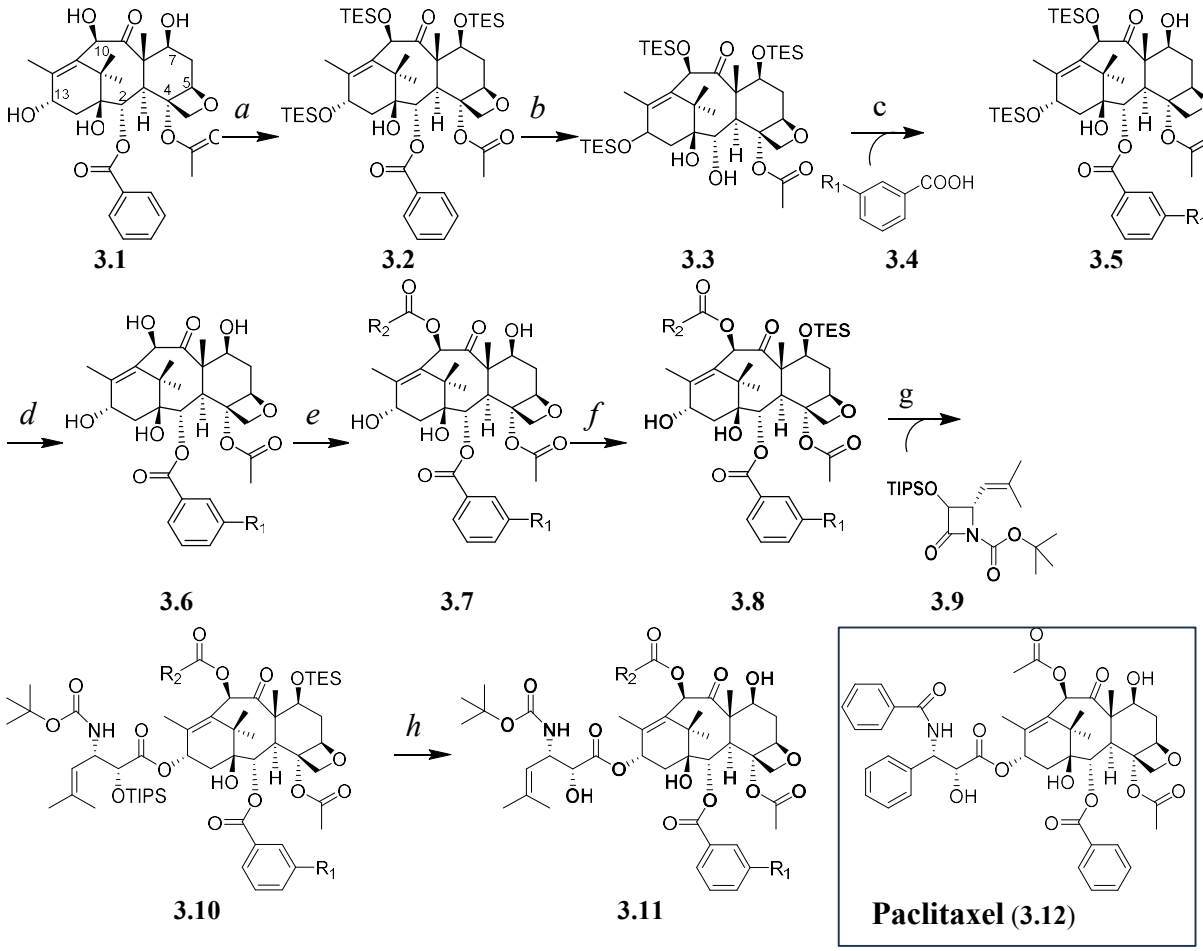

Figure 3.1: An example synthesis of the next-generation paclitaxel analogs. *Reagents and conditions*: (a) TES-Cl (20 equiv), imidazole (12 equiv), dry DMF, 0 °C to rt over 6 h; (b) Red-Al, dry THF, –10 °C, 20 min; (c) a m-benzoic acid analog (**4**) (8 equiv), DIC (8 equiv), DMAP (8 equiv), CH_2Cl_2, rt, 2-5 days; (d) HF/pyridine, pyridine/AcCN, 0 °C to rt, overnight; (e) acetic, propanoic, or cyclopropane carboxylic anhydride (10 equiv), $CeCl_3 \bullet 7H_2O$ (0.1 equiv), THF, rt, 20 h; (f) TES-Cl (3 equiv), imidazole (4 equiv), dry DMF, 0 °C to rt, over 45 min; (g) LiHMDS (1.5 equiv), dry THF, –40 °C, 2 h; (h) HF/pyridine, pyridine/AcCN, 0 °C to rt, overnight.

Installing *m*-substituted aroyl groups synthetically into SB-Taxanes necessitates removing the naturally occurring benzoyl moiety from the C2 hydroxyl (see Figure 3.1 for numbering) via reductive ester cleavage, for example, with Red-Al (sodium bis(2-methoxyethoxy) aluminum hydride) (see *step b* in Figure 3.1).[2,5,7] This reduction step requires silyl ether protection at the C7 hydroxyl of the 10-DAB reactant to prevent a retro-aldol ring fissure of the C-ring and racemization at C7 (**3.13**) (Figure 3.2A).[8] An advantage of Red-Al is that it is not pyrophoric and

does not ignite on contact with moist air, like the lithium aluminum hydride counterpart, and thus is a safer alternative reagent. However, several accounts report that the metal hydride reduction reagent stimulates an undesired intramolecular rearrangement where the newly made C2 alkoxide intermediate ring opens the adjacent oxetane ring and creates a new furan ring (**3.14**) (Figure 3.2B).[8-10] Red-Al can also cleave the C4 acyl group to afford an undesired triol (**3.15**) in quantitative yield (Figure 3.2C).[11-13] Furthermore, the aluminum salts produced in this reaction are considered toxic disposal agents and can cause conjunctivitis and fetal damage.[14,15]

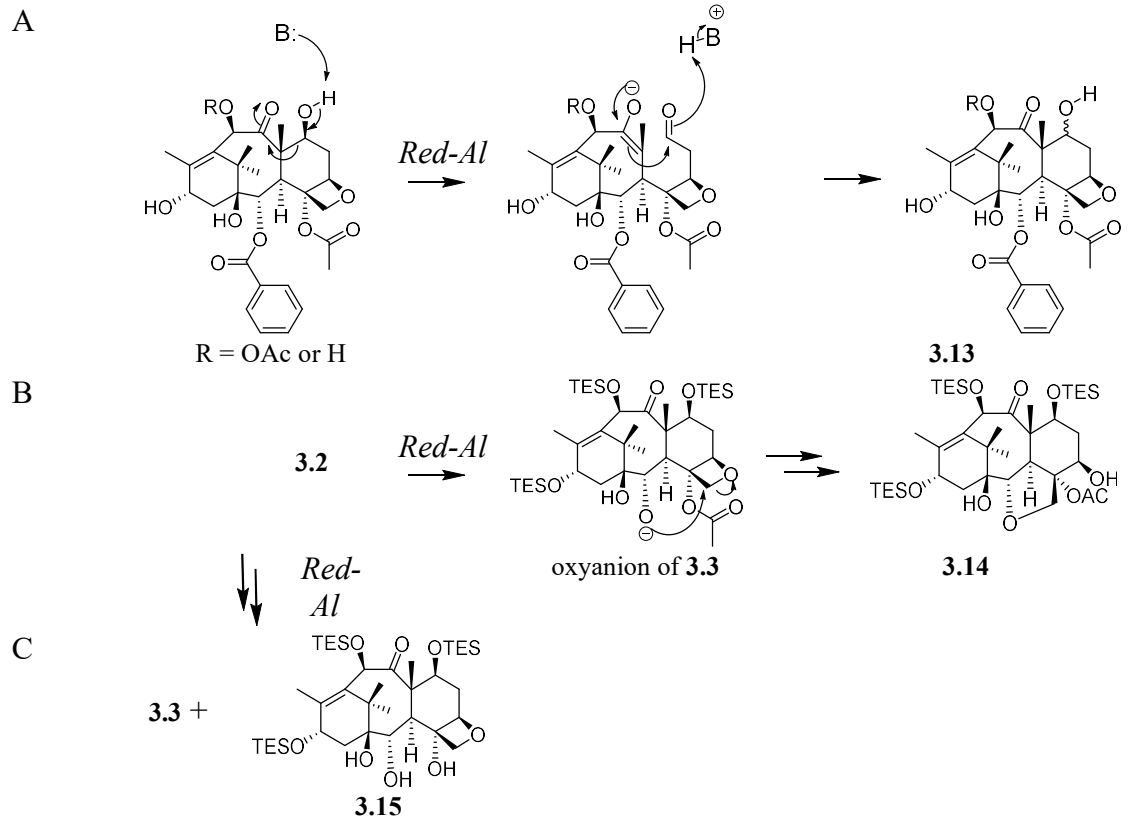

Figure 3.2: Proposed mechanisms for side reactions promoted by Red-Al. (A) Retro-aldol epimerization of 10-DAB or baccatin III under basic conditions; (B) intermolecular rearrangement; and (C) cleavage of the C2 and C4 acyl groups.

Biocatalysis continues to emerge as a promising technology for the assembly of fine chemicals.[16-20] This study uses a taxane benzoyltransferase (*m*TBT) instead of Red-Al to biocatalytically and regioselectively debenzoylate- (**3.22** – **3.24**) and rearoylate (**3.26** – **3.28**) the C2 hydroxyl of 13-oxobaccatin III scaffolds (without silyl ether protection) (Figure 3.3). The

kinetic parameters of the *m*TBT-catalyzed deacylation and reacylation for various *m*-aroyl donor cosubstrates and 13-oxo substrates were measured. The utility of this biocatalytic approach was made paramount after regio- and stereoselective hydride reduction of the 13-oxo intermediate to the native 13-β-hydroxyl gave access to a prerequisite intermediate used in the semisynthesis of several SB-Taxanes.

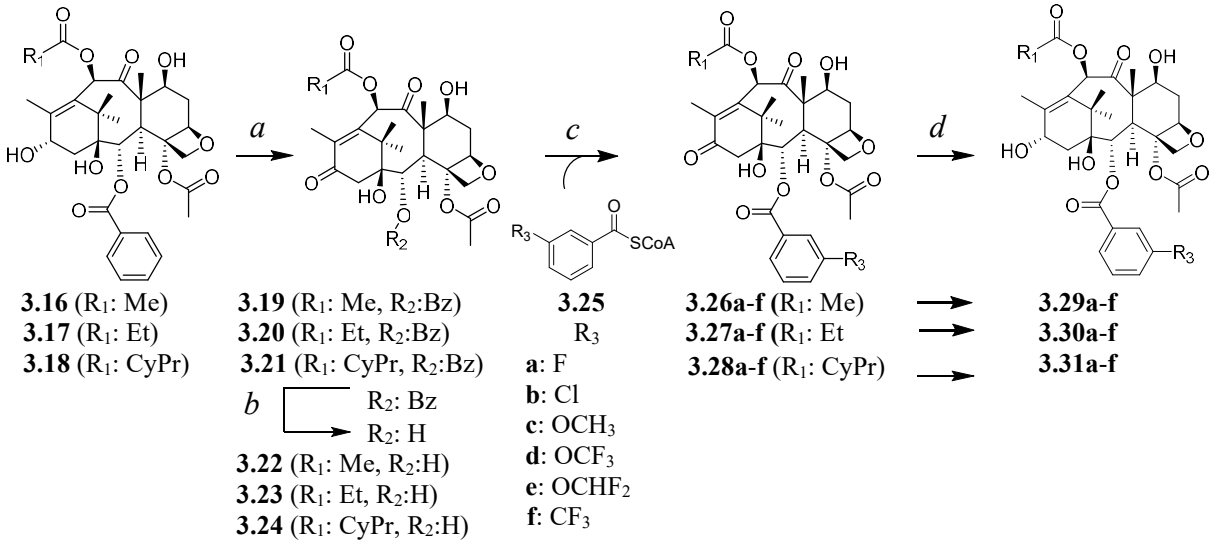

Figure 3.3: Biocatalysis of baccatin III analogs modified at C10 and C2 to make precursors of third generation taxoids. *Reagent and conditions*: (a) MnO_2, MeOH, rt, 8 h; (b) *m*TBT, CoA, 50 mM NaH_2PO_4/Na_2HPO_4 buffer (pH 7.4), 31 °C, 4 h; (c) *m*TBT, 50 mM NaH_2PO_4/Na_2HPO_4 buffer (pH 7.4), 31 °C, 4 h; (d) $NaBH_4$, (1:1) dry MeOH/dry THF, 0 °C to rt 7 h. CyPr: cyclopropyl.

Experimental

Chemicals and Reagents

Benzoic acid (98%), 3-methyl benzoic acid (98%), 3-methoxy benzoic acid (98%), 3-chlorobenzene acid (99%), 3-fluoro benzoic acid (97%), 3-(trifluoromethyl) benzoic acid (99%), 3-(trifluoromethoxy) benzoic acid (97%), 3-(difluoromethoxy) benzoic acid (97%), triethylsilyl chloride (97%), 4-(*N*,*N*-dimethylamino)pyridine (4-DMAP) (98%), acetic anhydride (98%), triethylamine (99%), hydrogen fluoride pyridine (97%), *tert*-butanol (≥99%) and reagents: methanol (>99.5%), hexane (>99.5%), and ethyl acetate (> 99.5%) were sourced from Sigma Aldrich (St. Louis, MO). Coenzyme A (CoA) (95%) was obtained from AmBeed (Arlington

Heights, IL). Nickel-affinity chromatography resin (HisPur™ Ni-NTA Resin) was purchased from Thermo Fisher Scientific (Waltham, MA). Isopropyl β-D-1-thiogalactopyranoside (IPTG), kanamycin, and phenylmethylsulfonyl fluoride (PMSF) were obtained from Gold Bio (St. Louis, MO). Taxanes (baccatin III (>98%), 10-deacetylbaccatin III (>98%), paclitaxel (>98%), and docetaxel (>98%) were bought from Natland International Corporation (Research Triangle Park, NC). C18 silica gel resin (carbon 23%, 40-63 μm) was purchased from Silicycle (Quebec City, Quebec, Canada).

Synthesis of 7-*O*-Acetylbaccatin III (3.32).[4,21,22]

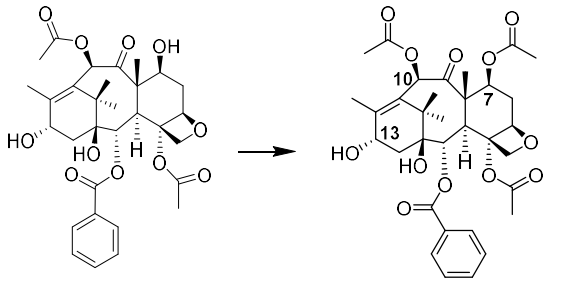

3.16 Baccatin III

3.32 7-*O*-acetylbaccatin III

Figure 3.4: Synthesis of 7-*O*-acetylbaccatin III. *Reagent and conditions*: 4-DMAP, TEA, THF, 23 °C.

To a stirred solution of baccatin III (3.16) (50 mg, 0.085 mmol) in dry THF (20 mL) at 23 °C under N_2 were added acetic anhydride (48 μL, 0.85 mmol, 10 equiv), 4-(*N*,*N*-dimethylamino)pyridine (4-DMAP) (53 mg, 0.43 mmol, 5 equiv), and triethylamine (12 μL, 0.085 mmol, 1 equiv). The reaction was monitored by TLC. After 8 h, the reaction was quenched with 10 mL of saturated aqueous solution of sodium bicarbonate and extracted with (2 × 30 mL) of ethyl acetate. The organic layer was dried over magnesium sulfate, filtered, and concentrated under a vacuum. The crude product was purified by silica-gel flash column chromatography using a linear gradient of EtOAc in hexane (30:70 to 60:40 (v/v) to give 7-*O*-acetylbaccatin III (**3.32**) (42 mg, 92% pure by ^{1}H NMR).

NMR Data for 7-*O*-acetylbaccatin III (**3.32**) (42 mg, 92% yield), ^{1}H NMR (500 MHz, $CDCl_3$) δ: 8.04 (m, 2H), 7.58 (m, 1H), 7.46 (dd, 2H, *J* = 8.4, 7.5 Hz), 6.22 (s, 1H), 5.61 (d, *J* = 7.0 Hz, 1H), 5.56 (dd, *J* = 9, 9 Hz 1H), 4.94 (dd, *J* = 9.7, 2.1 Hz, 1H), 4.82 (m, 1H), 4.28 (d, *J* = 9 Hz 1H), 4.11 (d, *J* = 9 Hz 1H), 3.95 (d, *J* = 7.1 Hz, 1H), 2.89 (m, 1H), 2.56 (m, 2H), 2.32 (s, 3H), 2.27 (s, 3H), 2.04 (s, 3H), 1.98 (s, 1H), 1.86 (m, 1H), 1.77 (s, 3H), 1.09 (s, 3H), 1.04 (s, 3H) (Figure 3.28). ^{13}C NMR (126 MHz, $CDCl_3$) δ: 202.51, 170.74, 169.09, 166.83, 145.13, 133.65, 131.21, 130.05, 129.32, 128.63, 83.92, 80.54, 78.52, 76.85, 75.87, 74.38, 71.69, 67.56, 56.03, 47.45, 42.72, 38.64, 33.28, 26.56, 22.51, 21.12, 20.79, 20.54, 15.19, 10.69 (3.29).

Synthesis of 13-*O*-Acetylbaccatin III (3.35)

The following methods are based on previously described procedures.[4,21,22]

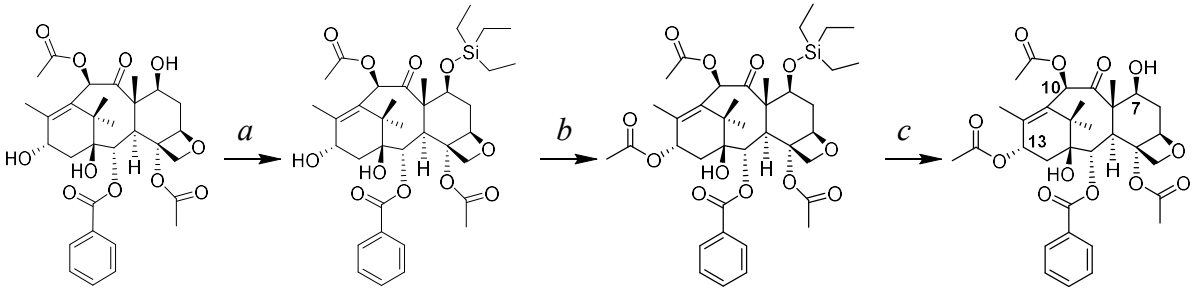

Figure 3.5: Synthesis of 13-*O*-acetylbaccatin III. *Reagent and conditions*: (a) DMF, TES-Cl, 45 °C, 5 h; (b) 4-DMAP, TEA, THF, 23 °C, 8 h; (c) HF/pyridine, pyridine/AcCN, 0 °C to rt, overnight.

Synthesis of 7-O-Triethylsilylbaccatin III (**3.33**). To a solution of baccatin III (**3.16**) (50 mg, 0.085 mmol) in 10 mL DMF was added imidazole (23 mg, 0.34 mmol, 4 equiv.) and triethylsilyl chloride (71 µL, 0.425 mmol, 5 equiv), and the mixture was stirred at 45 ºC for 5 h. The reaction was quenched with 20 mL of saturated aqueous ammonium chloride solution and extracted with (2 × 30 mL) of ethyl acetate. The organic layer was dried over magnesium sulfate, filtered, and concentrated under a vacuum. The crude product was purified by silica-gel flash column

chromatography using a linear gradient of EtOAc in hexane (30:70 to 50:50 (v/v) to give 7-*O*-triethylsilylbaccatin III (**3.33**).

NMR Data for 7-*O*-triethylsilylbaccatin III (**3.33**) (38 mg, 95% yield), ^{1}H NMR (500 MHz, $CDCl_3$) δ: 8.11 (d, *J* = 7.9 Hz, 2H), 7.60 (t, *J* = 7.4 Hz, 1H), 7.48 (t, *J* = 7.8 Hz, 2H), 6.46 (s, 1H), 5.63 (d, *J* = 7.1 Hz, 1H), 4.96 (d, *J* = 9.3 Hz, 1H), 4.83 (t, *J* = 8.4 Hz, 1H), 4.49 (dd, *J* = 10.6, 6.7 Hz, 1H), 4.31 (d, *J* = 8.4 Hz, 1H), 4.15 (d, *J* = 8.3 Hz, 1H), 3.88 (d, *J* = 7.1 Hz, 1H), 2.53 (ddd, *J* = 14.5, 9.7, 6.7 Hz, 1H), 2.27 (m, 2H), 2.29 (s, 3H), 2.19 (s, 3H), 1.83 (m, 1H), 1.68 (s, 3H), 1.19 (s, 3H), 1.04 (s, 3H), 0.93 (s, 3H), 0.91 (t, *J* = 5.2, Hz 9H), 0.59 (tt, *J* = 7.9, 3.6 Hz, 6H) (Figure 3.30). 13C NMR (126 MHz, CDCl3) δ: 202.21, 170.76, 169.39, 167.11, 143.95, 133.63, 132.68, 130.10, 129.37, 128.60, 84.22, 80.85, 78.73, 77.22, 75.78, 74.71, 72.35, 67.95, 58.65, 47.25, 42.77, 38.24, 37.23, 26.81, 22.69, 20.96, 20.08, 14.96, 9.95, 6.75, 5.27 (Figure 3.31).

Synthesis of 7-O-Triethylsilyl-13-O-acetylbaccatin III (**3.34**). To a solution of 7-*O*-triethylsilylbaccatin III (35 mg, 0.049 mmol) in 20 mL tetrahydrofuran (THF) were added acetic anhydride (27 μL, 0.49 mmol, 10 equiv.), 4-(*N*, *N*-dimethylamino)pyridine (4-DMAP) (30 mg, 0.245 mmol, 5 equiv.), and triethylamine (7 μL, 0.049 mmol, 1 equiv.) The mixture was stirred at room temperature for 8 h. The reaction was quenched with 10 mL of saturated aqueous sodium bicarbonate solution and extracted with (2 × 30 mL) of ethyl acetate. The organic layer was dried over magnesium sulfate, filtered, and concentrated under a vacuum. The crude product was purified by silica-gel flash column chromatography using a linear gradient of EtOAc in hexane (30:70 to 60:40 (v/v) 7-*O*-triethylsilyl-13-*O*-acetylbaccatin III (**3.34**).

NMR Data for 7-*O*-triethylsilyl-13-*O*-acetylbaccatin III (**3.34**) (32 mg, 96% yield) ^{1}H NMR (500 MHz, $CDCl_3$) δ: 8.08 (d, *J* = 7.8 Hz, 2H), 7.61 (t, *J* = 7.5 Hz, 1H), 7.48 (t, *J* = 7.8 Hz, 2H), 6.47 (s, 1H), 6.16 (t, *J* = 8.7 Hz, 1H), 5.68 (d, *J* = 7.0 Hz, 1H), 4.96 (d, *J* = 9.7 Hz, 1H), 4.48 (dd, *J* = 10.6, 6.6 Hz, 1H), 4.31 (d, *J* = 8.4 Hz, 1H), 4.16 (d, *J* = 8.4 Hz, 1H), 3.84 (d, *J* = 7.1 Hz, 1H),

2.57 (m, 1H), 2.34 (s, 3H), 2.27 (s, 3H), 2.04 (s, 3H), 1.85 (m, 1H), 1.68 (s, 3H), 1.24 (s, 3H), 1.18 (s, 3H), 0.93 (t, *J* = 7.9 Hz, 9H), 0.58 (qd, *J* = 7.8, 3.1 Hz, 6H) (Figure 3.32). 13C NMR (126 MHz, CDCl3) δ: 201.82, 170.21, 169.74, 169.25, 167.12, 140.71, 133.82, 133.54, 130.06, 129.25, 128.63, 84.17, 81.09, 78.92, 77.11, 75.18, 74.79, 72.27, 69.67, 58.52, 46.96, 43.12, 37.22, 35.43, 30.94, 26.51, 22.61, 21.26, 20.72, 14.55, 10.12, 6.76, 5.26 (Figure 3.33).

Synthesis of 13-O-Acetylbaccatin III (**3.35**). To a solution of 7-*O*-triethylsily13-*O*-acetylbaccatin III (**3.34**) (25 mg, 34 μmol) in 1.5 mL pyridine and 1.5 mL of acetonitrile was added 0.5 mL of HF/pyridine (70% as HF and 30% as pyridine) at 0 ºC. The reaction mixture was allowed to warm to room temperature and stirred overnight. The reaction was quenched with 10 mL of saturated aqueous solution of copper sulfate. The aqueous layer was extracted with (3 × 30 mL) of ethyl acetate. The combined organic layers were washed with 20 mL water and 15 mL brine, dried over magnesium sulfate, filtered, and concentrated under a vacuum. The crude product was purified by silica-gel flash column chromatography using a linear gradient of EtOAc in hexane (10:90 to 30:70 (v/v) to give 13-*O*-acetylbaccatin III (**3.35**).

NMR Data for 13-*O*-acetylbaccatin III (**3.35**) (21 mg, 92% yield) ^{1}H NMR (500 MHz, $CDCl_3$) δ: 8.10 (m, 2H), 7.62 (td, *J* = 7.5, 1.3 Hz, 1H), 7.53 (m, 2H), 7.27 (s, 1H), 6.31 (s, 1H), 6.22 (m, 1H), 5.67 (d, *J* = 7.1 Hz, 1H), 4.98 (d, *J* = 9.4 Hz, 1H), 4.48 (m, 1H), 4.32 (d, *J* = 8.6 Hz, 1H), 4.17 (d, *J* = 8.6 Hz, 1H), 3.83 (d, *J* = 7.1 Hz, 1H), 2.55 (ddd, *J* = 14.9, 9.8, 6.6 Hz, 1H), 2.34 (s, 3H), 2.32 (m, 2H), 2.25 (s, 3H), 2.22 (s, 3H), 1.91 (s, 3H), 1.84 (m, 1H), 1.68 (s, 3H), 1.26 (s, 3H), 1.14 (s, 3H) (Figure 3.34). 13C NMR (126 MHz, CDCl3) δ: 203.81, 171.34, 170.16, 169.76, 166.98, 143.01, 133.76, 132.71, 130.15, 129.16, 128.67, 84.39, 81.27, 79.32, 77.45, 75.72, 74,94, 72.21, 69.72, 58.59, 45.76, 43.13, 35.54, 29.71, 26.67, 22.34, 21.49, 20.87, 15.13, 9.48 (Figure 3.35).

General Procedure for Synthesis of (*m*-Substituted)Benzoyl CoA Thioesters (3.25a-f)

The following methods are based on previously described procedures.[23]

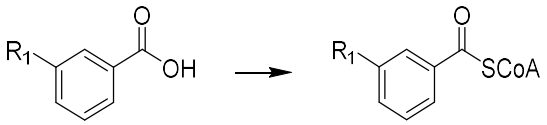

3.4 (a-f) **3.25 (a-f)**

Figure 3.6: Synthesis of (*meta*-substituted)benzoyl CoA thioester. R: (a: F), (b: Cl), (c: OCH_3), (d: OCF_3), (e: $OCHF_2$), (f: CF_3). *Reagents and conditions* are in the text below.

(*m*-Substituted)benzoyl CoA thioester analogs were synthesized in a 10 mL single-necked round-bottomed flask. Triethyl amine (10 µL, 72 µmol) was added to a solution of the (*m*-substituted)benzoic acid (**3.4a-f**) (60 µmol) in (5:2) (CH_2Cl_2/THF) (v/v, 4 mL) under N_2 gas. The mixture was stirred for 20 min at 25 °C, ethyl chloroformate (6.8 µL, 72 µmol) was added in one portion, and the reaction was stirred for 2 h at 25 °C. The solvents were evaporated under reduced pressure, and the residue was dissolved in 0.5 mL of *t*-BuOH. The sodium salt (66 µmol, 53 mg dissolved in 1 mL of 0.4 M $NaHCO_3$) of CoA was added to the solution, and the mixture was stirred for 1 h at 25 °C and quenched with the dropwise addition of 1 M HCl. The solvent was evaporated under vacuum, and the residue was purified by C18 silica gel column chromatography. The residue was dissolved in 5 mL distilled H_2O, loaded on a C18 silica column, washed with 100 % MeOH (25 mL), and pre-equilibrated with 25 mL distilled H2O. The sample was washed with 25 mL of distilled H_2O and eluted with 25 mL of 10% (v/v) MeOH in distilled H_2O. The fractions containing CoA thioesters, as assessed by C18 TLC, were combined, and the solvent evaporated. The remaining residue was extracted 4 times with diethyl ether (4 × 3 mL) to remove excess *t*-BuOH to yield products.

NMR Data for 3-Fluorobenzoyl CoA (**3.25a**) (78 mg, 92% yield) ^{1}H NMR (500 MHz, D_2O) δ: 8.39 (s, 1H), 8.10 (s, 1H), 7.74 (s, 1H), 7.64 (d, J = 5.3 Hz, 1H), 7.52 (d, J = 4.3 Hz, 1H), 7.42 (m, 1H), 6.00 (d, J = 6.2 Hz, 1H), 4.73 (m, 1H), 4.67 (d, J = 5.9 Hz, 1H), 4.43 (t, J = 2.7 Hz, 1H), 4.10 – 4.05 (m, 2H), 3.84 (s, 1H), 3.66 (dd, J = 9.8, 4.9 Hz, 1H), 3.39 (dd, J = 9.8, 4.8 Hz, 1H), 3.29 (t, J = 6.6 Hz, 2H), 3.14 (t, J = 6.6 Hz, 2H), 2.42 (t, J = 6.6 Hz, 2H), 2.29 (t, J = 6.6 Hz, 2H), 0.72 (s,

3H), 0.60 (s, 3H) (Figure 3.16). ^{13}C NMR (126 MHz, $CDCl_3$) δ: 191.51, 174.63, 173.96, 163.43, 150.72, 146.21, 142.85, 137.62, 131.27, 124.12, 120.79, 118.53, 112.85, 87.52, 84.41, 73.82, 72.38, 65.45, 42.23, 38.28, 34.95, 23.45, 20.78 (Figure 3.17).

NMR Data for 3-Chlorobenzoyl CoA (**3.25b**) (75 mg, 89% yield). ^{1}H NMR (500 MHz, Deuterium Oxide) δ: 8.62 (s, 1H), 8.32 (s, 1H), 7.95 (s, 1H), 7.84 (d, *J* = 4.6 Hz, 1H), 7.76 (d, *J* = 4.16 Hz, 1H), 7.59 (m, 1H), 6.26 (d, *J* = 5.32 Hz, 1H), 4.76 (m, 1H), 4.62 (d, *J* = 4.82 Hz, 1H), 4.46 (t, *J* = 2.5 Hz, 1H), 4.28 – 4.07 (m, 2H), 3.95 (s, 1H), 3.62 (dd, *J* = 8.4, 4.5 Hz, 1H), 3.42 (dd, *J* = 8.7, 4.6 Hz, 1H), 3.32 (t, *J* = 6.8 Hz, 2H), 3.13 (t, *J* = 6.5 Hz, 2H), 2.64 (t, *J* = 6.3 Hz, 2H), 2.35 (t, *J* = 6.5 Hz, 2H), 0.82 (s, 3H), 0.74 (s, 3H) (Figure 3.18). ^{13}C NMR (126 MHz, $CDCl_3$) δ: 192.37, 175.26, 174.57, 155.34, 148.27, 143.85, 137.62, 136.62, 135.62, 130.42, 129.62, 127.53, 119.21, 88.34, 85.12, 74.16, 73.74, 66.51, 43.63, 39.18, 35.17, 24.62, 21.15 (Figure 3.19).

NMR Data for 3-Methoxybenzoyl CoA (**3.25c**) (72 mg, 85% yield). ^{1}H NMR (500 MHz, Deuterium Oxide) δ: 8.55 (s, 1H), 8.35 (s, 1H), 7.74 (s, 1H), 7.64 (d, *J* = 5.3 Hz, 1H), 7.52 (d, *J* = 4.3 Hz, 1H), 7.42 (m, 1H), 6.00 (d, *J* = 6.2 Hz, 1H), 4.75 (m, 1H), 4.67 (d, *J* = 5.9 Hz, 1H), 4.43 (t, *J* = 2.7 Hz, 1H), 4.10 – 4.05 (m, 2H), 3.84 (s, 1H), 3.78 (s, 3H), 3.66 (dd, *J* = 9.8, 4.9 Hz, 1H), 3.39 (dd, *J* = 9.8, 4.8 Hz, 1H), 3.29 (t, *J* = 6.6 Hz, 2H), 3.14 (t, *J* = 6.6 Hz, 2H), 2.42 (t, *J* = 6.6 Hz, 2H), 2.29 (t, *J* = 6.6 Hz, 2H), 0.72 (s, 3H), 0.60 (s, 3H) (Figure 3.20). ^{13}C NMR (126 MHz, $CDCl_3$) δ: 192.62, 175.83, 174.15, 161.53, 152.62, 147.67, 145.21, 136.26, 129.68, 120.28, 117.53, 112.91, 86.72, 84.32, 75.23, 71.65, 65.29, 55.46, 43.62, 38.74, 35.59, 22.94, 20.82 (Figure 3.21).

NMR Data for 3-Trifluoromethoxybenzoyl CoA (**3.25d**) (75 mg, 89% yield). ^{1}H NMR (500 MHz, Deuterium Oxide) δ: 8.58 (s, 1H), 8.34 (s, 1H), 7.74 (s, 1H), 7.62 (d, *J* = 5.3 Hz, 1H), 7.51 (d, *J* = 4.3 Hz, 1H), 7.42 (m, 1H), 6.16 (d, *J* = 6.2 Hz, 1H), 4.73 (m, 1H), 4.67 (d, *J* = 5.9 Hz, 1H), 4.43 (t, *J* = 2.7 Hz, 1H), 4.10 – 4.05 (m, 2H), 3.84 (s, 1H), 3.66 (dd, *J* = 9.8, 4.9 Hz, 1H), 3.39 (dd, *J* = 9.8, 4.8 Hz, 1H), 3.29 (t, *J* = 6.6 Hz, 2H), 3.14 (t, *J* = 6.6 Hz, 2H), 2.42 (t, *J* = 6.6 Hz, 2H),

2.29 (t, *J* = 6.6 Hz, 2H), 0.72 (s, 3H), 0.60 (s, 3H) (Figure 3.22). ^{13}C NMR (126 MHz, $CDCl_3$) δ: 191.7, 175.24, 174.26, 161.51, 151.2, 146.85, 143.32, 136.68, 129.84, 129.52, 121.63, 120.54, 118.75, 88.41, 85.64, 73.86, 72.27, 66.18, 43.26, 39.14, 36.92, 24.59, 21.16 (Figure 3.23).

NMR Data for 3-Difluoromethoxybenzoyl CoA (3.25e) (74 mg, 88% yield). ^{1}H NMR (500 MHz, Deuterium Oxide) δ: 8.47 (s, 1H), 8.38 (s, 1H), 7.98 (s, 1H), 7.84 (d, *J* = 5.8 Hz, 1H), 7.78 (d, *J* = 4.7 Hz, 1H), 7.45 (s, 1H), 7.35 (m, 1H), 6.18 (d, *J* = 6.5 Hz, 1H), 4.76 (m, 1H), 4.64 (d, *J* = 5.2 Hz, 1H), 4.48 (t, *J* = 2.3 Hz, 1H), 4.10 – 4.05 (m, 2H), 3.86 (s, 1H), 3.67 (dd, *J* = 9.2, 4.5 Hz, 1H), 3.37 (dd, *J* = 9.2, 4.8 Hz, 1H), 3.31 (t, *J* = 6.5 Hz, 2H), 3.15 (t, *J* = 6.8 Hz, 2H), 2.47 (t, *J* = 6.4 Hz, 2H), 2.28 (t, *J* = 6.3 Hz, 2H), 0.82 (s, 3H), 0.73 (s, 3H) (Figure 3.24). ^{13}C NMR (126 MHz, $CDCl_3$) δ: 191.5, 175.72, 174.21, 167.52, 161.92, 152.79, 147.42, 145.86, 136.97, 129.19, 121.65, 119.54, 118.29, 86.35, 84.68, 74.58, 72.67, 65.27, 43.93, 39.47, 36.66, 23.13, 21.39 (Figure 3.25).

NMR Data for 3-Trifluoromethylbenzoyl CoA (3.25f) (68 mg, 81% yield). ^{1}H NMR (500 MHz, Deuterium Oxide) δ: 8.62 (s, 1H), 8.37 (s, 1H), 8.15 (s, 1H), 7.96 (d, *J*= 5.2 Hz, 1H), 7.89 (d, *J*= 4.3 Hz, 1H), 7.37 (m, 1H), 6.11 (d, *J* = 6.2 Hz, 1H), 4.72 (m, 1H), 4.67 (d, *J* = 5.9 Hz, 1H), 4.41 (t, *J* = 2.7 Hz, 1H), 4.10 – 4.05 (m, 2H), 3.84 (s, 1H), 3.66 (dd, *J* = 9.8, 4.9 Hz, 1H), 3.38 (dd, *J* = 9.8, 4.8 Hz, 1H), 3.29 (t, *J* = 6.6 Hz, 2H), 3.14 (t, *J* = 6.6 Hz, 2H), 2.42 (t, *J* = 6.6 Hz, 2H), 2.27 (t, *J* = 6.6 Hz, 2H), 0.72 (s, 3H), 0.63 (s, 3H) (Figure 3.26). ^{13}C NMR (126 MHz, $CDCl_3$) δ: 191.62, 176.21, 174.62, 154.53, 146.39, 143.51, 136.72, 131.76, 131.16, 130.75, 129.89, 125.95, 124.78, 119.92, 88.32, 85.86, 73.35, 65.53, 43.15, 38.47, 37.25, 25.14, 21.17 (Figure 3.27).

General procedure for the synthesis of 13-oxobaccatins (3.19 – 3.21)

The following method is based on a previously described procedure.[4,21]

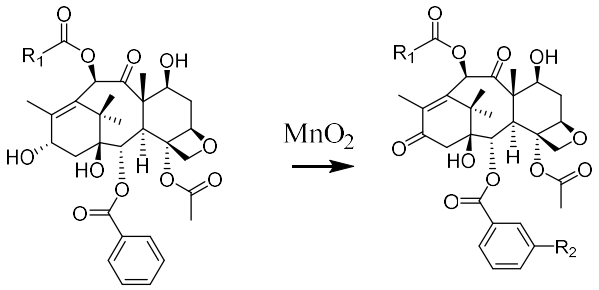

Figure 3.7: Synthesis of 13-oxotaxane analogs. *Reagents and conditions* are in the text below.

To separate solutions of (130 μmol) of baccatin III or each 10-acyl-10-deacetylbaccatin III analog (**3.16** – **3.18**) in 10 mL of dry CH_2Cl_2 was added activated MnO_2 powder (1 g), and the mixture was stirred at 25 °C under N_2 (g) for 8 h. The reaction was filtered, and the filtrate was diluted with EtOAc (25 mL) and quenched with H_2O (25 mL). The aqueous fraction was separated and extracted with EtOAc (2 × 25 mL). The combined organic fractions were washed with brine and H_2O and dried over anhydrous magnesium sulfate. The organic solvent was evaporated, and the crude product was purified by silica-gel flash column chromatography eluted with a linear gradient of EtOAc in hexanes (30:70 to 60:40 (v/v) to yield products of **3.19 – 3.21**.

NMR Data for 13-Oxobaccatin III (3.19) (74 mg, 97% yield). ^{1}H NMR (500 MHz, $CDCl_3$) δ: 8.05 (m, 2H), 7.63 (m, 1H), 7.49 (d, *J* = 6.3 Hz, 2H), 6.58 (s, 1H), 5.69 (d, *J* = 6.4 Hz, 1H), 4.93 (dd, *J* = 9.7, 1H), 4.47 (dd, *J* = 8.7 Hz, 1H), 4.32 (d, *J* = 8.5 Hz, 1H), 4.10 (d, *J* = 8.1 Hz, 1H), 3.90 (d, *J* = 6.8 Hz, 1H), 2.94 (d, *J* = 9.8 Hz, 1H), 2.67 (d, *J* = 9.8 Hz, 1H), 2.53 (m, 1H), 2.22 (s, 3H), 2.18 (s, 3H), 2.17 (s, 3H), 1.88 (m, 1H), 1.66 (s, 3H), 0.91 (s, 6H) (Figure 3.36). ^{13}C NMR (126 MHz, $CDCl_3$) δ: 200.24, 198.34, 170.13, 168.92, 166.86, 153.01, 140.26, 133.97, 130.05, 128.78, 128.74, 83.92, 80.52, 78.51, 76.04, 72.85, 72.26, 59.43, 46.21, 43.43, 42.42, 37.17, 21.72, 20.85, 13.53, 9.58 (Figure 3.37).

NMR Data for 13-oxo-10-PDAB (3.20) (76 mg, 97% yield). ^{1}H NMR (500 MHz, $CDCl_3$) δ: 8.04 (dd, *J* = 8.4, 1.4 Hz, 2H), 7.61 (tt, *J* = 7.0, 1.3 Hz, 1H), 7.54 (dd, *J* = 8.4, 7.5 Hz, 2H), 6.45 (s, 1H), 5.67 (d, *J* = 6.8 Hz, 1H), 4.93 (dd, *J* = 9.5, 1H), 4.44 (dd, *J* = 8.1 Hz, 1H), 4.30 (d, *J* = 8.2 Hz, 1H), 4.14 (d, *J* = 8.2 Hz, 1H), 3.90 (d, *J* = 6.7 Hz, 1H), 2.69 (d, *J* = 9.5 Hz, 1H), 2.67 (d, *J* = 9.4 Hz, 1H), 2.53 (m, 1H), 2.51 (m, 2H), 2.16 (s, 3H), 2.06 (s, 3H), 1.84 (m, *J* = 14.7, 10.9, 2.3 Hz, 1H), 1.65 (s, 3H), 1.12 (t, *J* = 7.6 Hz, 3H), 1.08 (s, 6H) (Figure 3.38). ^{13}C NMR (126 MHz, $CDCl_3$) δ: 202.03, 197.97, 174.08, 170.13, 166.78, 152.27, 141.62, 134.01, 130.04, 128.77, 128.73, 84.13, 80.51, 78.72, 76.35, 72.99, 72.07, 59.34, 45.33, 43.41, 42.47, 35.76, 27.53, 21.72, 18.73, 15.59, 9.45, 8.68 (Figure 3.39).

NMR Data for 13-oxo-10-CPCDAB (3.21) (75 mg, 95% yield). ^{1}H NMR (500 MHz, $CDCl_3$) δ: 8.04 (dd, *J* = 8.4, 1.3 Hz , 2H), 7.67 (tt, *J* = 7.5, 1.3 Hz,1H), 7.49 (td, *J* = 7.9, 1.5 Hz, 2H), 6.45 (s, 1H), 5.68 (d, *J* = 6.7 Hz, 1H), 4.95 (dd, *J* = 9.5 Hz, 1H), 4.45 (dd, *J* = 8.3 Hz, 1H), 4.32 (d, *J* = 8.8 Hz, 1H), 4.15 (d, *J* = 8.8 Hz, 1H), 3.91 (d, *J* = 6.8 Hz, 1H), 2.97 (d, *J* = 9.8 Hz, 1H), 2.70 (d, *J* = 9.3 Hz, 1H), 2.54 (m, 1H), 2.17 (s, 3H), 2.05 (s, 3H), 1.86 (m, 1H), 1.68 (s, 3H), 1.58 (tt, *J* = 7.6, 4.6, Hz, 1H), 1.08 (s, 6H), 1.03 (dd, *J* = 5.3, 3.3 Hz, 2H), 0.91 (dd, *J* = 6.9, 4.6 Hz, 2H) (Figure 3.40). ^{13}C NMR (126 MHz, $CDCl_3$) δ: 202.17, 197.97, 174.68, 170.14, 166.83, 152.23, 141.81, 134.05, 130.05, 128.76, 128.72, 84.17, 80.53, 78.79, 76.13, 72.99, 72.01, 59.38, 45.31, 43.42, 42.46, 35.70, 26.91, 22.56, 20.91, 15.60, 12.71, 9.46, 9.11 (Figure 3.41).

Expression and Purification of the Modified 2-*O*-Benzoyltransferase (*m*TBT)

A glycerol stock of *E. coli* BL21(DE3) bacterial cultures containing the modified-*tbt (mtbt)* gene[24] was used to inoculate Lysogeny Broth (LB) (400 mL) containing kanamycin (50 μg/mL) and incubated at 37 °C overnight. This inoculum culture (50 mL) was added to fresh LB media (8 × 1 L) containing kanamycin (50 μg/mL). The cells were incubated at 37 °C until $OD_{600} \approx 0.6$, IPTG (250 μM final concentration) was added, and the strains were incubated at 16 °C for 16 h.

The cultures were centrifuged (2,100*g*) for 1 h at 4 °C to pellet the cells. The cells were resuspended in 100 mL of lysis buffer (50 mM sodium phosphate (pH 8.0), 300 mM NaCl, 10 mM imidazole, and 5% (v/v) glycerol,) and lysed by sonication (Misonix Sonicator (Danbury, CT): 10 s on, 20 s rest for 30 cycles) on ice. The cell debris was removed by centrifugation (1,500*g*) for 45 min at 4 °C, followed by high-speed centrifugation (25,000*g*) for 90 min at 2 °C to remove light membrane debris. The supernatant was loaded onto a column containing nickel-nitrilotriacetic acid (Ni-NTA) resin (3 mL) and eluted by gravity flow. The column was washed with 50 mL of Wash 1 Buffer (300 mM NaCl, 50 mM sodium phosphate (pH 8.0), 10 mM imidazole, and 5% (v/v) glycerol) and 20 mL of Wash 2 Buffer (300 mM NaCl, 50 mM sodium phosphate (pH 8.0), 50 mM imidazole, and 5% (v/v) glycerol). The protein was eluted with Elution Buffer (300 mM NaCl, 50 mM sodium phosphate (pH 8.0), 250 mM imidazole, and 5% (v/v) glycerol).

Fractions containing enzymes of a molecular weight consistent with that of *m*TBT (~50 kDa) were combined and loaded onto a size-selective centrifugal filtration unit (30,000 NMWL, Millipore-Sigma, Burlington, MA). The quantity of *m*TBT (8 mg) was measured using a NanoDrop spectrophotometer, and the purity of the enzyme was assessed by SDS-PAGE and Coomassie Blue staining (Figure 3.15).

Assessing Productive Taxanes for the 2-*O*-Debenzoylation Reaction Catalyzed by *m*TBT

Taxanes bearing a 13-hydroxyl (baccatin III (**3.16**) and 7-*O*-acetylbaccatin III (**3.32**)), 13-oxo (13-oxobaccatin III (**3.19**), 13-oxo-10-*O*-propionyl-10-DAB (13-oxo-10-PDAB) (**3.20**), and 13-oxo-10-*O*-cyclopropane carbonyl-10-*O*-deacetylbaccatin III (13-oxo-10-CPCDAB) (**3.21**)), or 13-acyl (13-*O*-acetylbaccatin III (**3.35**), paclitaxel (**3.12**), and docetaxel (**3.37**)) (Figure 3.8) were screened in separate assays for activity against purified *m*TBT.

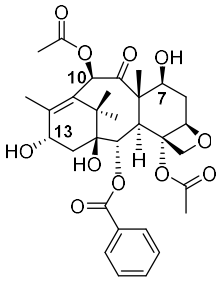

3.16
Baccatin III

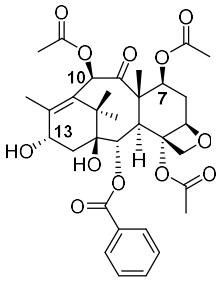

3.32
7-*O*-acetyl-baccatin III

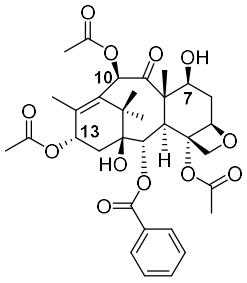

3.35
13-*O*-acetylbaccatin III

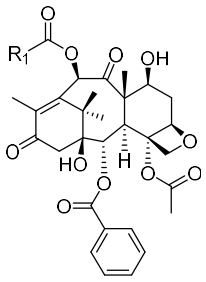

3.19 (R_1: Me)
3.20 (R_1: Et)
3.21 (R_1: CyPr)

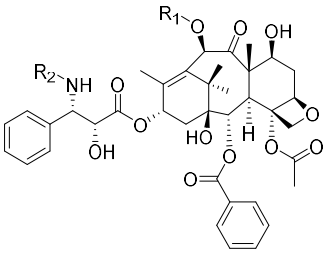

3.12
Paclitaxel (R_1: Acetyl; R_2: Bz)
3.37
Docetaxel (R_1: H; R_2: *t*-Boc)

Figure 3.8: Putative substrates used in an activity screen with *m*TBT.

A separate solution of each taxane (**3.16**, **3.19** – **3.21**, **3.32**, **3.35**, **3.12**, and **3.37**) (1 mM) in 2 mL of 50 mM NaH_2PO_4/Na_2HPO_4 buffer (pH 7.4) was incubated with *m*TBT (50 μg/mL). CoA (1 mM) was added to each solution, and the assays were mixed at 31 °C on a rocking shaker for 4 h. The reactions were stopped with EtOAc (2 × 1 mL); the EtOAc extracts were combined, and the solvent was removed under a N_2 (g) stream. The residue was dissolved in CH_3CN (100 μL), and an aliquot was analyzed by LC-MS/MS to monitor the production of a mass consistent with a 2-*O*-debenzoyl baccatin analog.

Kinetic Analysis of the 2-*O*-Debenzoylation Reaction Catalyzed by *m*TBT

The steady-state conditions for protein concentration and time were established for *m*TBT and productive 13-oxotaxanes (**3.19** – **3.21**) separately incubated at low (0.05 mM) and high (1 mM) concentrations in 10 mL of assay buffer [50 mM NaH_2PO_4/Na_2HPO_4 buffer (pH 7.4)] containing *m*TBT (250 μg/mL) and CoA (1 mM) at 31 °C on a rocking shaker. Aliquots (1 mL) were removed,

and the biosynthetic reaction was stopped by adding 500 µL of EtOAc at 10, 15, 30, and 45 min and 1, 2, 3, 5, 7, and 10 h. 7-*O*-acetyl-2-*O*-debenzoyl-baccatin III (**3.37**, see Figure 3.14) (0.15 mM) was added as the internal standard, and each sample was extracted with EtOAc (4 × 1 mL). The organic fractions were combined, and the solvent was removed under a N_2 (g) stream. The resultant residue from each assay was separately resuspended in CH_3CN (100 µL) and quantified by LC/ESI-MS/MS. A stop time was established for the steady-state time range, and *m*TBT (250 µg/mL) and CoA (1 mM) were incubated with varying concentrations of **3.19** – **3.21** (0.05 – 1 mM), respectively, in triplicate assays at 31 °C on a rocking shaker for 2 h. As before, the products were extracted from the reaction mixtures and quantified by LC/ESI-MS(/MS) (Figures 3.48 – 3.50). The kinetic parameters (K_M and k_{cat}) were calculated by nonlinear regression with Origin Pro 9.0 software (Northampton, MA) using the Michaelis−Menten equation: $v_0 = k_{cat}[E_0][S]/(K_M + [S])$.

Scale-Up of the 2-*O*-Debenzoylation Reaction Catalyzed by *m*TBT

A solution of *m*TBT (750 µg/mL, ~38 mg total) was incubated in 50 mL (25 test tubes, a 2 mL assay in each tube) of 50 mM NaH_2PO_4/Na_2HPO_4 assay buffer (pH 7.4) containing (2 mM) of a 13-oxotaxane analog (**3.19** – **3.21**) and (2 mM) of CoA. The mixture was stirred at 31 °C on a rocking shaker for 4 h. A second batch of *m*TBT enzyme (750 µg/mL) was added to each assay tube and incubated for another 4 h at 31 °C. The reactions were stopped by extracting with ethyl acetate (2 × 3 mL). The EtOAc fractions were combined, the solvent was removed under a stream of N_2 gas, and the residue was purified by silica-gel column chromatography to yield ≥94% pure product as determined by NMR (Figures 3.42 – 3.47). The purified residue was dissolved in CH_3CN (100 µL), and an aliquot was analyzed by LC-MS/MS for fragmentation analysis and monoisotopic mass calculation (Figure 3.54-3.56).

NMR Data for 2-*O*-Debenzoyl-13-oxobaccatin III (**3.22**) (27 mg, 62% yield). ^{1}H NMR (500 MHz, $CDCl_3$) δ: 6.37 (s, 1H), 4.93 (dd, *J* = 9.5, 1H), 4.67 (d, *J* = 9.1 Hz, 1H), 4.58 (d, *J* = 9.1 Hz, 1H), 4.41 (dd, *J* = 9 Hz, 1H), 3.98 (d, *J* = 4.1 Hz, 1H), 3.55 (d, *J* = 6.3 Hz, 1H), 2.86 (d, *J* = 9.8 Hz, 1H), 2.62 (d, *J* = 9.8 Hz, 1H), 2.53 (m, 1H), 2.25 (s, 3H), 2.02 (s, 3H), 2.01 (s, 3H), 1.85 (m, 1H), 1.63 (s, 3H), 1.21(s, 6H) (Figure 3.42). ^{13}C NMR (126 MHz, $CDCl_3$) δ: 201.03, 198.74, 169.99, 168.90, 153.07, 140.00, 83.75, 81.44, 77.55, 77.54, 77.22, 76.14, 72.57, 72.35, 59.53, 46.14, 43.06, 42.95, 32.74, 29.69, 21.06, 13.54, 9.75 (Figure 3.43). LC/ESI-MS monoisotopic exact mass *m/z* 481.2129 $[M + H]^+$; calculated for $C_{24}H_{33}O_{10}$: 481.2068.

NMR Data for 2-*O*-Debenzoyl-13-oxo-10-PDAB (**3.23**) (24 mg, 57% yield). ^{1}H NMR (500 MHz, $CDCl_3$) δ: 6.51 (s, 1H), 4.91 (dd, *J* = 9.5, 1H), 4.63 (d, *J* = 9.2 Hz, 1H), 4.56 (d, *J* = 9.0 Hz, 1H), 4.42 (dd, *J* = 9.1 Hz, 1H), 3.95 (d, *J* = 7.2 Hz, 1H), 3.54 (d, *J* = 6.5 Hz, 1H), 2.80 (d, *J* = 9.8 Hz, 1H), 2.64 (d, *J* = 9.8 Hz, 1H), 2.58 (m, 1H), 2.54 (m, 2H), 2.19 (s, 3H), 2.12 (s, 3H), 1.87 (m, 1H), 1.64 (s, 3H), 1.25 (t, *J* = 7.2 Hz, 3H), 1.18 (s, 6H) (Figure 3.44). ^{13}C NMR (126 MHz, $CDCl_3$) δ: 203.45, 202.95, 172.69, 169.08, 144.81, 134.26, 85.13, 81.76, 77.42, 76.28, 71.05, 67.84, 56.12, 53.57, 51.23, 47.36, 42.87, 38.65, 32.39, 25.41, 22.15, 16.43, 15.26, 10.85 (Figure 3.45). LC/ESI-MS monoisotopic exact mass *m/z* 495.2275 $[M + H]^+$; calculated for $C_{25}H_{35}O_{10}$: 495.2185.

NMR Data for 2-*O*-Debenzoyl-13-oxo-10-*O*-cyclopropane carbonyl-10-DAB (**3.24**) (21 mg, 52% yield). ^{1}H NMR (500 MHz, $CDCl_3$) δ: 6.37 (s, 1H), 4.94 (dd, *J* = 9.5, 1H), 4.67 (d, *J* = 9.2 Hz, 1H), 4.58 (d, *J* = 9.0 Hz, 1H), 4.41 (dd, *J* = 9 Hz, 1H), 3.96 (d, *J* = 6.7 Hz, 1H), 3.55 (d, *J* = 6.5 Hz, 1H), 2.84 (d, *J* = 9.4 Hz, 1H), 2.64 (d, *J* = 9.3 Hz, 1H), 2.55 (m, 1H), 2.23 (s, 3H), 2.16 (s, 3H), 1.84 (m, 1H), 1.62 (s, 3H), 1.58 (tt, *J* = 7.4, 4.2, Hz, 1H), 1.26 (dd, *J* = 5.3, 3.3 Hz, 2H), 1.21 (s, 6H), 1.18 (dd, *J* = 6.9, 4.6 Hz, 2H) (Figure 3.46). ^{13}C NMR (126 MHz, $CDCl_3$) δ: 201.04, 198.75, 169.95, 168.92, 153.07, 139.95, 83.75, 81.45, 78.62, 77.36, 76.14, 72.65, 59.53, 46.15,

43.06, 42.76, 32.75, 21.64, 20.82, 13.54, 9.75, 6.51 (Figure 3.47). LC/ESI-MS monoisotopic exact mass *m/z* 507.2353 $[M + H]^+$; calculated for $C_{26}H_{35}O_{10}$: 507.2276.

Characterization and Kinetic Analysis of the Aroylation Reaction Catalyzed by mTBT of the Aroylation Reaction Catalyzed by mTBT

A 2-debenzoyl-13-oxotaxane analog (**3.22**, **3.23**, and **3.24**) (1mM) in 1 mL of 50 mM NaH_2PO_4/Na_2HPO_4 buffer (pH 7.4) was incubated with *m*TBT (250 μg/mL) and (1 mM) of *m*-substituted benzoyl CoA thioesters **3.25a-f**. The assay was mixed at 31 °C on a rocking shaker for 4 h. The reaction was then stopped with ethyl acetate (2 × 1 mL). The EtOAc extracts were combined, and the solvent was removed under a stream of N_2 gas. The residue was then dissolved in CH_3CN (100 μL), and an aliquot was analyzed by LC-MS/MS for analogs **a-f** of **3.26**, **3.27**, and **3.28**. The steady-state conditions for protein concentration and time were established for *m*TBT and 2-debenzoyl-13-oxotaxane analogs (**3.22** – **3.24**) by separately incubating each substrate at low (0.05 mM) and high (1 mM) concentrations in 10 mL of assay buffer [50 mM NaH_2PO_4/Na_2HPO_4 buffer (pH 7.4)] containing *m*TBT (150 μg/mL) and *m*-substituted benzoyl CoA thioesters **3.25a-f** (1 mM) at 31 °C on a rocking shaker. Aliquots (1 mL) were removed, and the biosynthetic reaction was stopped by adding 500 μL of EtOAc at 10, 15, 30, and 45 min and 1, 2, 3, 5, 7, and 10 h. 13-oxobaccatin III (0.15 mM) was added as the internal standard, each sample was extracted with EtOAc (4 × 1 mL), the organic fractions were combined, and the solvent was removed under a stream of N_2 gas. The resultant residue from each assay was separately resuspended in CH_3CN (100 μL) and quantified by LC/ESI-MS/MS. Under steady-state conditions, *m*TBT (150 μg/mL) and CoA thioesters (**3.25a-f**, 1 mM) were incubated separately with varying concentrations of each 2-debenzoyl-13-oxotaxane analog (**3.22** – **3.24**) (0.05 – 1 mM), in triplicate assays at 31 °C on a rocking shaker for 3 h. As before, the assays were extracted with EtOAc, and the isolated products were quantified by LC/ESI-MS/MS. The kinetic parameters

(K_M and k_{cat}) were calculated by nonlinear regression with Origin Pro 9.0 software (Northampton, MA) using the Michaelis−Menten equation: $v_0 = k_{cat}[E_0][S]/(K_M + [S])$.

Scale-Up of the Aroylation Reaction Catalyzed by *m*TBT

*m*TBT (750 μg/mL) was incubated in 50 mL (25 test tubes, 2 mL assay in each tube) of 50 mM NaH_2PO_4/Na_2HPO_4 assay buffer (pH 7.4) containing (2 mM) of 2-debenzoyl-13-oxobaccatin analogs (**3.22-3.24**) and (2 mM) of *m*-substituted benzoyl CoA thioester **3.25a-f** at 31 °C on a rocking shaker for 4 h. A second batch of *m*TBT enzyme (750 μg/mL) was added to each assay tube and incubated for another 4 h at 31 °C. The reaction was then stopped with EtOAc (2 × 3 mL) to extract the taxane substrates from the assay. The EtOAc extracts were combined, the solvent was removed under a stream of N_2 gas, and the residue was purified by silica-gel column chromatography to yield ≥93% pure product, as determined by NMR (Figures 3.57 – 3.92). The purified residue was dissolved in CH_3CN (100 μL), and an aliquot was analyzed by LC-MS/MS for fragmentation analysis and monoisotopic mass calculation.

NMR Data for 2-*O*-Debenzoyl-2-*O*-(3-fluorobenzoyl)-13-oxobaccatin III (3.26a) (18 mg, 30% yield). ^{1}H NMR (500 MHz, $CDCl_3$) δ: 8.04 (d, *J* = 7.5, 1H), 7.91 (s, 1 H), 7.78 (d, *J* = 6.4 Hz, 1H), 7.50 (m, 1H), 6.56 (s, 1H), 5.68 (d, *J* = 6.3Hz, 1H), 4.97 (dd, *J* = 9.7, 1H), 4.48 (dd, *J* = 8.7 Hz, 1H), 4.34 (d, *J* = 8.5 Hz, 1H), 4.15 (d, *J* = 8.1 Hz, 1H), 3.92 (d, *J* = 6.8 Hz, 1H), 2.96 (d, *J* = 9.6 Hz, 1H), 2.66 (d, *J* = 9.6 Hz, 1H), 2.58 (m, 1H), 2.28 (s, 3H), 2.18 (s, 3H), 2.07 (s, 3H), 1. 89 (m, 1H), 1.67 (s, 3H), 1.24 (s, 6H) (Figure 3.57). ^{13}C NMR (126 MHz, $CDCl_3$) δ: 201.26, 198.54, 170.19, 166.92, 163.86, 161.62, 141.21, 134.26, 130.97, 129.35, 129.74, 128.64, 120.25. 117,82. 84.62, 80.72, 78.41, 76.14, 75.45, 72.26, 59.52, 45.32, 43.63, 35.72, 33.37, 21.82, 20.84, 18,71, 13.93, 9.13 (Figure 3.58). LC/ESI-MS monoisotopic exact mass *m/z* 603. 2215 $[M + H]^+$; calculated for $C_{31}H_{36}FO_{11}$: 603.2185.

NMR Data for 2-*O*-Debenzoyl-2-*O*-(3-chlorobenzoyl)-13-oxobaccatin III (3.26b) (16 mg, 26% yield). ^{1}H NMR (500 MHz, $CDCl_3$) δ: 8.07 (s, 1H), 7.97 (d, *J* = 7.3, 1H),7.62 (d, *J* = 6.4 Hz, 1H), 7.51 (m, 1H), 6.45 (s, 1H), 5.68 (d, *J* = 6.3 Hz, 1H), 4.96 (dd, *J* = 9.7, 1H), 4.48 (dd, *J* = 8.7 Hz, 1H), 4.31 (d, *J* = 8.5 Hz, 1H), 4.14 (d, *J* = 8.1 Hz, 1H), 3.91 (d, *J* = 6.8 Hz, 1H), 2.96 (d, *J* = 9.5 Hz, 1H), 2.65 (d, *J* = 9.6 Hz, 1H) 2.57 (m, 1H), 2.28 (s, 3H), 2.18 (s, 3H), 2.17 (s, 3H), 1. 87 (m, 1H), 1.67 (s, 3H), 1.26 (s, 6H) (Figure 3.59). ^{13}C NMR (126 MHz, $CDCl_3$) δ: 201.98, 197.97, 170.75, 170.17, 166.87, 141.75, 143.66, 134.12, 130.05, 129.35, 128.79, 84.62, 80.72, 78.41, 76.14, 75.45, 72.26, 59.52, 45.32, 43.63, 35.72, 33.37, 21.82, 20.84, 18,71, 13.93, 9.13 (Figure 3.60). LC/ESI-MS monoisotopic exact mass *m/z* 619. 2035 $[M + H]^+$; calculated for $C_{31}H_{36}ClO_{11}$: 619.1892.

NMR Data for 2-*O*-Debenzoyl-2-*O*-(3-methoxybenzoyl)-13-oxobaccatin III (3.26c) (12 mg, 20% yield). ^{1}H NMR (500 MHz, $CDCl_3$) δ: 8.08 (d, *J* = 7.5, 1H), 7.71 (s, 1 H), 7.64 (d, *J* = 6.4 Hz, 1H), 7.48 (m, 1H), 6.46 (s, 1H), 5.69 (d, *J* = 6.3 Hz, 1H), 4.95 (dd, *J* = 9.7, 1H), 4.47 (dd, *J* = 8.7 Hz, 1H), 4.34 (d, *J* = 8.5 Hz, 1H), 4.15 (d, *J* = 8.1 Hz, 1H), 3.92 (d, *J* = 6.8 Hz, 1H), 3.87 (s, 3H), 2.96 (d, *J* = 9.4 Hz, 1H), 2.66 (d, *J* = 9.6 Hz, 1H), 2.55 (m, 1H), 2.29 (s, 3H), 2.18 (s, 3H), 2.08 (s, 3H), 1. 92 (m, 1H), 1.67 (s, 3H), 1.23 (s, 6H) (Figure 3.61). ^{13}C NMR (126 MHz, $CDCl_3$) δ: 201.98, 197.94, 170.79,170,16, 166.85, 159.56, 141.74, 134.06, 130.24, 129.62, 122.64, 120.39, 114,32. 84.14, 80.72, 78.76. 76.55, 76.14, 73.15, 72.12, 59.32, 55,45, 45.31, 43.63, 35.75, 33.24, 21.82, 20.84, 18,71, 13.93, 9.13 (Figure 3.62). LC/ESI-MS monoisotopic exact mass *m/z* 615. 2532 $[M + H]^+$; calculated for $C_{32}H_{38}O_{12}$: 615.2491.

NMR Data for 2-*O*-Debenzoyl-2-*O*-(3-trifluoromethoxybenzoyl)-13-oxobaccatin III (3.26d) (14 mg, 21% yield). ^{1}H NMR (500 MHz, $CDCl_3$) δ: 8.06 (d, *J* = 7.3, 1H), 7.96 (s, 1H), 7.64 (d, *J* = 6.5 Hz, 1H), 7.48 (m, 1H), 6.46 (s, 1H), 5.69 (d, *J* = 6.3 Hz, 1H), 4.98 (dd, *J* = 9.7, 1H), 4.47

(dd, *J* = 8.7 Hz, 1H), 4.33 (d, *J* = 8.5 Hz, 1H), 4.16 (d, *J* = 8.1 Hz, 1H), 3.94 (d, *J* = 6.8 Hz, 1H), 2.96 (d, *J* = 9.6 Hz, 1H), 2.68 (d, *J* = 9.6 Hz, 1H), 2.55 (m, 1H), 2.29 (s, 3H), 2.16 (s, 3H), 2.08 (s, 3H), 1. 92 (m, 1H), 1.68 (s, 3H), 1.26 (s, 6H) (Figure 3.63). ^{13}C NMR (126 MHz, $CDCl_3$) δ: 202.08, 197.96, 174.19,170,26, 163.52, 161.56, 141.72, 134.12, 130.22, 129.53, 128.79, 125.96, 121,14.116.95, 84.15, 80.73, 77.76. 76.55, 76.14, 73.15, 72.14, 59.34, 45.31, 43.63, 35.75, 33.24, 21.83, 20.84, 18,72, 13.93, 9.14 (Figure 3.64). LC/ESI-MS monoisotopic exact mass *m/z* 670. 2368 $[M + H]^+$; calculated for $C_{32}H_{35}F_3O_{12}$: 670.2195.

NMR Data for 2-*O*-Debenzoyl-2-*O*-(3-difluoromethoxybenzoyl)-13-oxobaccatin III (**3.26e**) (17 mg, 27% yield). ^{1}H NMR (500 MHz, $CDCl_3$) δ: 8.35 (s, 1H), 8.05 (d, *J* = 7.4, 1H), 7.68 (d, *J* = 6.7 Hz, 1H), 7.36 (s, 1H), 7.46 (m, 1H), 6.47 (s, 1H), 5.64 (d, *J* = 6.3 Hz, 1H), 4.98 (dd, *J* = 9.7, 1H), 4.45 (dd, *J* = 8.7 Hz, 1H), 4.35 (d, *J* = 8.4 Hz, 1H), 4.16 (d, *J* = 8.1 Hz, 1H), 3.94 (d, *J* = 6.5 Hz, 1H), 2.97 (d, *J* = 9.2 Hz, 1H), 2.69 (d, *J* = 9.6 Hz, 1H), 2.57 (m, 1H), 2.28 (s, 3H), 2.17 (s, 3H), 2.08 (s, 3H), 1. 92 (m, 1H), 1.67 (s, 3H), 1.26 (s, 6H) (Figure 3.65). ^{13}C NMR (126 MHz, $CDCl_3$) δ: 201.96, 197.95, 170.85,170,35, 166.85, 162.28, 159.75, 141.75, 134.14, 130.25, 129.72, 122.68, 120.36, 117.96, 84.15, 80.78, 77.68. 76.58, 76.14, 73.18, 72.16, 58.32, 45.34, 43.63, 35.75, 34.24, 21.85, 20.84, 18,72, 13.87, 9.12 (Figure 3.66). LC/ESI-MS monoisotopic exact mass *m/z* 651. 2352 $[M + H]^+$; calculated for $C_{32}H_{37}F_2O_{12}$: 651.2185.

NMR Data for 2-*O*-Debenzoyl-2-*O*-(3-trifluoromethylbenzoyl)-13-oxobaccatin III (**3.26f**) (8 mg, 13% yield). ^{1}H NMR (500 MHz, $CDCl_3$) δ: 8.36 (s, 1H), 8.07 (d, *J* = 7.4, 1H), 7.62 (d, *J* = 6.7 Hz, 1H), 7.46 (m, 1H), 6.45 (s, 1H), 5.67 (d, *J* = 6.3 Hz, 1H), 4.96 (dd, *J* = 9.7, 1H), 4.48 (dd, *J* = 8.7 Hz, 1H), 4.34 (d, *J* = 8.4 Hz, 1H), 4.18 (d, *J* = 8.1 Hz, 1H), 3.95 (d, *J* = 6.5 Hz, 1H), 2.97 (d, *J* = 9.8 Hz, 1H), 2.69 (d, *J* = 9.6 Hz, 1H), 2.57 (m, 1H), 2.29 (s, 3H), 2.16 (s, 3H), 2.08 (s, 3H), 1. 92 (m, 1H), 1.67 (s, 3H), 1.26 (s, 6H) (Figure 3.67). ^{13}C NMR (126 MHz, $CDCl_3$) δ: 201.98,

197.98, 170.79,170,16, 166.87, 141.75, 134.14,133.34, 130.25, 129.72, 129.14, 128.78, 128.16, 127.96, 84.15, 80.73, 77.76. 76.55, 76.14, 73.15, 72.14, 58.32, 45.34, 43.63, 35.75, 34.24, 21.85, 20.84, 18,72, 13.93, 9.14 (Figure 3.68). LC/ESI-MS monoisotopic exact mass *m/z* 653. 2294 [M + H]$^+$; calculated for $C_{32}H_{35}F_3O_{11}$: 653.2128.

NMR Data for 2-*O*-Debenzoyl-2-*O*-(3-fluorobenzoyl)-13-oxo-10-PDAB (**3.27a**) (17 mg, 28% yield). ^{1}H NMR (500 MHz, $CDCl_3$) δ: 8.06 (d, *J* = 7.5, 1H), 7.89 (s, 1H), 7.79 (d, *J* = 6.2 Hz, 1H), 7.52 (m, 1H), 6.47 (s, 1H), 5.69 (d, *J* = 6.7 Hz, 1H), 4.96 (dd, *J* = 9.7, 1H), 4.48 (dd, *J* = 8.7 Hz, 1H), 4.36 (d, *J* = 8.22 Hz, 1H), 4.17 (d, *J* = 8.2 Hz, 1H), 3.94 (d, *J* = 6.4 Hz, 1H), 2.91 (d, *J* = 9.2 Hz, 1H), 2.69 (d, *J* = 9.6 Hz, 1H), 2.57 (m, 1H), 2.55 (m, 2H), 2.18 (s, 3H), 2.08 (s, 3H), 1. 86 (m, 1H), 1.69 (s, 3H), 1.27 (t, 3H), 1.23 (s, 6H) (Figure 3,69). ^{13}C NMR (126 MHz, $CDCl_3$) δ: 202.07, 197.95, 174.18, 170.189, 163.86, 161.53, 141.72, 134.45, 130.24, 129.72, 125.92, 128.64, 121.23. 116,86. 84.17, 80.51, 78.84, 76.54, 73.03, 72.12, 59.38, 45.34, 43.42, 35.74, 33.25, 27.54, 21.76, 18,73, 13.92, 9.88, 9.13 (Figure 3.70). LC/ESI-MS monoisotopic exact mass *m/z* 617. 2465 [M + H]$^+$; calculated for $C_{32}H_{38}FO_{11}$: 617.2376.

NMR Data for 2-*O*-Debenzoyl-2-*O*-(3-chlorobenzoyl)-13-oxo-10-PDAB (**3.27b**) (15 mg, 24% yield). ^{1}H NMR (500 MHz, $CDCl_3$) δ: 8.08 (s, 1H), 7.98 (d, , *J* = 7.6, 1H),7.64 (d, *J* = 6.2 Hz, 1H), 7.52 (m, 1H), 6.46 (s, 1H), 5.69 (d, *J* = 6.2 Hz, 1H), 4.96 (dd, *J* = 9.7, 1H), 4.48 (dd, *J* = 8.7 Hz, 1H), 4.32 (d, *J* = 8.2 Hz, 1H), 4.13 (d, *J* = 8.4 Hz, 1H), 3.95 (d, *J* = 6.4 Hz, 1H), 2.96 (d, *J* = 9.3 Hz, 1H), 2.69 (d, *J* = 9.6 Hz, 1H), 2.57 (m, 1H), 2.55 (m, 2H), 2.21 (s, 3H), 2.07 (s, 3H), 1. 87 (m, 1H), 1.67 (s, 3H), 1.29 (t, 3H), 1.26 (s, 6H) (Figure 3.71). ^{13}C NMR (126 MHz, $CDCl_3$) δ: 202.17, 197.98, 174.71, 169.95, 166.88, 152.25, 141.86, 134.68, 133.79, 130.68, 129.83, 128.29, 84.67, 80.76, 78.44, 77.56, 76.18, 73.65, 72.36, 59.57, 45.34, 43.63, 35.75, 33.38, 27.57, 21.82, 18.71,

13.93, 13.08, 9.87, 9.13 (Figure 3.72). LC/ESI-MS monoisotopic exact mass *m/z* 633. 2182 $[M + H]^+$; calculated for $C_{32}H_{38}ClO_{11}$: 633.2075.

NMR Data for 2-*O*-Debenzoyl-2-*O*-(3-methoxybenzoyl)-13-oxo-10-PDAB (3.27c) (11 mg, 18% yield). ^1H NMR (500 MHz, $CDCl_3$) δ: 8.07(d, *J* = 7.6, 1H), 7.69 (s, 1H), 7.61 (d, *J* = 6.7 Hz, 1H), 7.49 (m, 1H), 6.47 (s, 1H), 5.68 (d, *J* = 6.5 Hz, 1H), 4.96 (dd, *J* = 9.7, 1H), 4.48 (dd, *J* = 8.7 Hz, 1H), 4.32 (d, *J* = 8.4 Hz, 1H), 4.12 (d, *J* = 8.3 Hz, 1H), 3.91 (d, *J* = 6.4 Hz, 1H), 3.86 (s, 3H), 2.96 (d, *J* = 9.4 Hz, 1H), 2.67 (d, *J* = 9.6 Hz, 1H), 2.57 (m, 1H),), 2.55 (m, 2H), 2.29 (s, 3H), 2.08 (s, 3H), 1. 92 (m, 1H), 1.67 (s, 3H), 1.27 (t, 3H), 1.25 (s, 6H) (Figure 3.73). ^{13}C NMR (126 MHz, $CDCl_3$) δ: 202.18, 197.98, 174.69,170,17, 166.87, 159.58, 141.84, 134.15, 130.19, 129.75, 122.67, 120.42, 114,35. 84.19, 80.52, 78.81. 77.59, 76.27, 73.04, 72.09, 59.37, 55,46, 45.33, 43.41, 35.68, 33.31, 21.72, 18,71, 14.18, 13.93, 9.67, 9.13 (Figure 3.74). LC/ESI-MS monoisotopic exact mass *m/z* 629. 2684 $[M + H]^+$; calculated for $C_{33}H_{41}O_{12}$: 629.2562.

NMR Data for 2-*O*-Debenzoyl-2-*O*-(3-trifluoromethoxybenzoyl)-13-oxo-10-PDAB (3.27d) (15 mg, 25% yield). ^1H NMR (500 MHz, $CDCl_3$) δ: 8.07 (d, *J* = 7.8, 1H), 7.94 (s, 1H), 7.63 (d, *J* = 6.7 Hz, 1H), 7.49(m, 1H), 6.48 (s, 1H), 5.67 (d, *J* = 6.2 Hz, 1H), 4.96 (dd, *J* = 9.7, 1H), 4.48 (dd, *J* = 8.7 Hz, 1H), 4.34 (d, *J* = 8.6 Hz, 1H), 4.14 (d, *J* = 8.6 Hz, 1H), 3.93 (d, *J* = 6.5 Hz, 1H), 2.97 (d, *J* = 9.4 Hz, 1H), 2.69 (d, *J* = 9.6 Hz, 1H), 2.57 (m, 1H), 2.54 (m, 2H), 2.19 (s, 3H), 2.07 (s, 3H), 1. 89 (m, 1H), 1.66 (s, 3H), 1.27 (t, 3H), 1.24 (s, 6H) (Figure 3.75). ^{13}C NMR (126 MHz, $CDCl_3$) δ: 202.18, 198.07, 170.19,166,92, 163.53, 161.54, 141.81, 134.12, 130.08, 129.24, 128.81, 125.98, 121.08, 116.97, 84.24, 80.31, 78.82, 77.25. 76.17, 73.07, 72.09, 59.36, 45.35, 43.45, 35.71, 33.32, 21.73, 18.81, 13.95, 13.03, 9.68, 9.14 (Figure 3.76). LC/ESI-MS monoisotopic exact mass *m/z* 683. 2395 $[M + H]^+$; calculated for $C_{33}H_{38}F_3O_{12}$: 683.2236.

NMR Data for 2-*O*-Debenzoyl-2-*O*-(3-difluoromethoxybenzoyl)-13-oxo-10-PDAB (3.27e) (16 mg, 25% yield). ^{1}H NMR (500 MHz, $CDCl_3$) δ: 8.42 (s, 1H), 8.05 (d, *J* = 7.8, 1H), 7.64 (d, *J* = 6.7 Hz, 1H), 7.38 (s, 1H), 7.45 (m, 1H), 6.45 (s, 1H), 5.64 (d, *J* = 6.2 Hz, 1H), 4.96 (dd, *J* = 9.7, 1H), 4.48 (dd, *J* = 8.7 Hz, 1H), 4.35 (d, *J* = 8.7 Hz, 1H), 4.12 (d, *J* = 8.5 Hz, 1H), 3.93 (d, *J* = 6.7 Hz, 1H), 2.96 (d, *J* = 9.5 Hz, 1H), 2.69 (d, *J* = 9.6 Hz, 1H), 2.57 (m, 1H), 2.54 (m, 2H), 2.19 (s, 3H), 2.07 (s, 3H), 1. 85 (m, 1H), 1.67 (s, 3H), 1.28 (t, 3H), 1.25 (s, 6H) (Figure 3.77). ^{13}C NMR (126 MHz, $CDCl_3$) δ: 202.28, 197.97, 174.82, 170,43, 166.75, 152.53, 141.65, 133.35, 130.15, 129.68, 129.26, 128.79, 127.12, 84.35, 80.72, 78.83, 77.42, 76.14, 73.36, 72.12, 59.38, 45.31, 43.41, 35.57, 35.41, 33.32, 21.73, 18.55, 14.12, 13.17, 9.87, 9.18 (Figure 3.78). LC/ESI-MS monoisotopic exact mass *m/z* 665. 2426 $[M + H]^+$; calculated for $C_{33}H_{39}F_2O_{12}$: 665.235.

NMR Data for 2-*O*-Debenzoyl-2-*O*-(3-trifluoromethylbenzoyl)-13-oxo-10-PDAB (3.27f) (6 mg, 9% yield). ^{1}H NMR (500 MHz, $CDCl_3$) δ: 8.38 (s, 1H), 8.08 (d, *J* = 7.2, 1H), 7.64 (d, *J* = 6.4 Hz, 1H), 7.49 (m, 1H), 6.47 (s, 1H), 5.68 (d, *J* = 6.7 Hz, 1H), 4.96 (dd, *J* = 9.7, 1H), 4.48 (dd, *J* = 8.7 Hz, 1H), 4.32 (d, *J* = 8.6 Hz, 1H), 4.12 (d, *J* = 8.5 Hz, 1H), 3.93 (d, *J* = 6.7 Hz, 1H), 2.96 (d, *J* = 9.5 Hz, 1H), 2.69 (d, *J* = 9.6 Hz, 1H), 2.57 (m, 1H), 2.54 (m, 2H), 2.18 (s, 3H), 2.08 (s, 3H), 1. 87 (m, 1H), 1.66 (s, 3H), 1.29 (t, 3H), 1.24 (s, 6H) (Figure 3.79). ^{13}C NMR (126 MHz, $CDCl_3$) δ: 202.17, 197.87, 174.72, 170,23, 166.89, 152.23, 141.75, 133.35, 130.15, 129.68, 129.26, 128.79, 127.12, 84.25, 80.52, 78.83, 77.62, 76.14, 73.36, 72.12, 59.38, 45.31, 43.41, 35.66, 35.66, 33.32, 21.73, 18.85, 14.18, 13.17, 9.67, 9.18 (Figure 3.80). LC/ESI-MS monoisotopic exact mass *m/z* 667. 2487 $[M + H]^+$; calculated for $C_{33}H_{38}F_3O_{11}$: 667.2374.

NMR Data for 2-*O*-Debenzoyl-2-*O*-(3-fluorobenzoyl)-13-oxo-10-CPCDAB (3.28a) (15 mg, 25% yield). ^{1}H NMR (500 MHz, $CDCl_3$) δ: 8.08 (d, *J* = 7.4, 1H), 7.92 (s, 1H), 7.75 (d, *J* = 6.7 Hz, 1H), 7.47 (m, 1H), 6.45 (s, 1H), 5.68 (d, *J* = 6.2 Hz, 1H), 4.96 (dd, *J* = 9.7, 1H), 4.48 (dd, *J* = 8.7

Hz, 1H), 4.32 (d, *J* = 8.4 Hz, 1H), 4.16 (d, *J* = 8.2 Hz, 1H), 3.92 (d, *J* = 6.7 Hz, 1H), 2.96 (d, *J* = 9.7 Hz, 1H), 2.69 (d, *J* = 9.6 Hz, 1H), 2.57 (m, 1H), 2.17 (s, 3H), 2.04 (s, 3H), 1. 89 (m, 1H), 1.69 (s, 3H), 1.52 (t, *J* = 7.6, 4.6, Hz, 1H), 1.25 (s, 6H), 1.17 (dd, *J* = 5.4, 3.6 Hz, 2H), 1.05 (dd, *J* = 6.8, 4.7 Hz, 2H) (Figure 3.81). ^{13}C NMR (126 MHz, $CDCl_3$) δ: 202.18, 197.06, 170.29, 166.92, 163.53, 161.56, 141.81, 134.18, 130.16, 129.24, 128.81, 121.44. 117.86, 84.24, 80.36, 78.82, 77.68, 76.17, 73.18, 72.29, 59.36, 45.35, 43.45, 35.71, 33.35, 21.76, 18.73, 13.92, 13.03, 9.78, 9.11 (Figure 3.82). LC/ESI-MS monoisotopic exact mass *m/z* 629. 2454 $[M + H]^+$; calculated for $C_{33}H_{38}FO_{11}$: 629.2346.

NMR Data for 2-*O*-Debenzoyl-2-*O*-(3-chlorobenzoyl)-13-oxo-10-CPCDAB (3.28b) (13 mg, 20% yield). ^{1}H NMR (500 MHz, $CDCl_3$) δ: 8.09 (s, 1H), 7.95(d, , *J* = 7.4, 1H),7.66 (d, *J* = 6.8 Hz, 1H), 7.58 (m, 1H), 6.47 (s, 1H), 5.77 (d, *J* = 6.4 Hz, 1H), 4.96 (dd, *J* = 9.7, 1H), 4.48 (dd, *J* = 8.7 Hz, 1H), 4.37 (d, *J* = 8.7 Hz, 1H), 4.14 (d, *J* = 8.8 Hz, 1H), 3.92 (d, *J* = 6.8 Hz, 1H), 2.97 (d, *J* = 9.5 Hz, 1H), 2.69 (d, *J* = 9.6 Hz, 1H), 2.57 (m, 1H), 2.18 (s, 3H), 2.08 (s, 3H), 1. 84 (m, 1H), 1.58 (t, *J* = 7.6, 4.6, Hz, 1H), 1.26 (s, 6H), 1.15 (dd, *J* = 5.6, 3.4 Hz, 2H), 1.08 (dd, *J* = 6.8, 4.7 Hz, 2H) (Figure 3.83). ^{13}C NMR (126 MHz, $CDCl_3$) δ: 202.18, 197.58, 174.41, 170.18, 166.89, 152.38, 141.84, 134.64, 133.72, 130.22, 129.52, 129.85, 128.25, 84.49, 80.51, 78.81, 77.85, 76.14, 73.14, 72.18, 59.38, 45.31, 43.42, 35.86, 33.32, 21.73, 18.82, 14.19, 13.01, 9.67, 9.12 (Figure 3.84). LC/ESI-MS monoisotopic exact mass *m/z* 645. 2152 $[M + H]^+$; calculated for $C_{33}H_{38}ClO_{11}$: 645.2084.

NMR Data for 2-*O*-Debenzoyl-2-*O*-(3-methoxybenzoyl)-13-oxo-10-CPCDAB (3.28c) (10 mg, 15% yield). ^{1}H NMR (500 MHz, $CDCl_3$) δ: 8.08 (d, *J* = 7.8, 1H), 7.62 (s, 1H), 7.49 (d, *J* = 6.7 Hz, 1H), 7.38 (m, 1H), 6.45 (s, 1H), 5.96 (d, *J* = 6.3 Hz, 1H), 4.96 (dd, *J* = 9.7, 1H), 4.48 (dd, *J* = 8.7 Hz, 1H), 4.36 (d, *J* = 8.8 Hz, 1H), 4.15 (d, *J* = 8.5 Hz, 1H), 3.92 (d, *J* = 6.5 Hz, 1H), 3.85 (s, 3H),

2.97 (d, *J* = 9.4 Hz, 1H), 2.69 (d, *J* = 9.6 Hz, 1H), 2.57 (m, 1H), 2.17 (s, 3H), 2.07 (s, 3H), 1. 84 (m, 1H), 1.66 (s, 3H), 1.52 (t, *J* = 7.5, 4.6, Hz, 1H), 1.27 (s, 6H), 1.18 (dd, *J* = 5.8, 3.4 Hz, 2H), 1.07 (dd, *J* = 6.5, 4.8 Hz, 2H) (Figure 3.85). ^{13}C NMR (126 MHz, $CDCl_3$) δ: 202.16, 197.95, 174.75,170,35, 166.74, 159.49, 141.82, 134.17, 130.25, 129.62, 122.65, 120.48, 114.37, 84.15, 80.58, 78.81. 77.53, 76.36, 73.19, 72.28, 59.47, 55.45, 45.31, 43.46, 35.54, 33.37, 21.72, 18.71, 13.94, 13.12, 9.64, 9.18 (Figure 3.86). LC/ESI-MS monoisotopic exact mass *m/z* 641. 2665 $[M + H]^+$; calculated for $C_{34}H_{41}O_{12}$: 641.2548.

NMR Data for 2-*O*-Debenzoyl-2-*O*-(3-trifluoromethoxybenzoyl)-13-oxo-10-CPCDAB (3.28d) (12 mg, 18% yield). ^{1}H NMR (500 MHz, $CDCl_3$) δ: 8.06 (d, *J* = 7.4, 1H), 7.92 (s, 1H), 7.77 (d, *J* = 6.3 Hz, 1H), 7.45 (m, 1H), 6.43 (s, 1H), 5.69 (d, *J* = 6.5 Hz, 1H), 4.96 (dd, *J* = 9.7, 1H), 4.48 (dd, *J* = 8.7 Hz, 1H), 4.32 (d, *J* = 8.2 Hz, 1H), 4.12 (d, *J* = 8.5 Hz, 1H), 3.92 (d, *J* = 6.2 Hz, 1H), 2.96 (d, *J* = 9.7 Hz, 1H), 2.69 (d, *J* = 9.6 Hz, 1H), 2.57 (m, 1H), 2.17 (s, 3H), 2.08 (s, 3H), 1. 86 (m, 1H), 1.67 (s, 3H), 1.61 (t, *J* = 7.4, 4.2, Hz, 1H), 1.25 (s, 6H), 1.17 (dd, *J* = 5.8, 3.4 Hz, 2H), 1.06 (dd, *J* = 6.5, 4.8 Hz, 2H) (Figure 3.87). ^{13}C NMR (126 MHz, $CDCl_3$) δ: 202.17, 198.12, 170.28, 166,85, 163.42, 161.56, 141.75, 134.19, 130.16, 129.26, 128.86, 125.96, 120.87, 116.96, 84.28, 80.37, 78.81, 77.62. 76.39, 73.28, 72.38, 59.38, 45.31, 43.43, 35.62, 33.36, 21.75, 18.83, 13.96, 13.31, 9.48, 9.11 (Figure 3.88). LC/ESI-MS monoisotopic exact mass *m/z* 695. 2371 $[M + H]^+$; calculated for $C_{34}H_{38}F_3O_{12}$: 695.2267.

NMR Data for 2-*O*-Debenzoyl-2-*O*-(3-difluoromethoxybenzoyl)-13-oxo-10-CPCDAB (3.28e) (14 mg, 21% yield). ^{1}H NMR (500 MHz, $CDCl_3$) δ: 8.38 (s, 1H), 8.08 (d, *J* = 7.2, 1H), 7.66 (d, *J* = 6.5 Hz, 1H), 7.35 (s, 1H), 7.45 (m, 1H), 6.47 (s, 1H), 5.68 (d, *J* = 6.5 Hz, 1H), 4.96 (dd, *J* = 9.7, 1H), 4.48 (dd, *J* = 8.7 Hz, 1H), 4.38 (d, *J* = 8.9 Hz, 1H), 4.14 (d, *J* = 8.6 Hz, 1H), 3.97 (d, *J* = 6.8 Hz, 1H), 2.98 (d, *J* = 9.6 Hz, 1H), 2.69 (d, *J* = 9.6 Hz, 1H), 2.57 (m, 1H), 2.18 (s, 3H), 2.05 (s,

3H), 1.88 (m, 1H), 1.67 (s, 3H), 1.65 (t, *J* = 7.8, 4.5, Hz, 1H), 1.27 (s, 6H), 1.18 (dd, *J* = 5.7, 3.8 Hz, 2H), 1.08 (dd, *J* = 6.3, 4.5 Hz, 2H) (Figure 3.89). ^{13}C NMR (126 MHz, $CDCl_3$) δ: 202.15, 197.75, 174.57, 170,18, 166.49, 152.53, 141.42, 133.38, 130.14, 129.36, 129.28, 128.76, 127.45, 127.96, 84.28, 80.37, 78.81, 77.62. 76.39, 73.28, 72.38, 59.38, 45.54, 43.53, 35.62, 33.38, 21.75, 18.75, 13.84, 13.17, 9.77, 9.12 (Figure 3.90). LC/ESI-MS monoisotopic exact mass *m/z* 677. 2475 $[M + H]^+$; calculated for $C_{34}H_{39}F_2O_{12}$: 678.2346.

NMR Data for 2-*O*-Debenzoyl-2-*O*-(3-trifluoromethylbenzoyl)-13-oxo-10-CPCDAB (3.28f) (4 mg, 6% yield). ^{1}H NMR (500 MHz, $CDCl_3$) δ: 8.35 (s, 1H), 8.05 (d, *J* = 7.6, 1H), 7.62 (d, *J* = 6.8 Hz, 1H), 7.47 (m, 1H), 6.45 (s, 1H), 5.64 (d, *J* = 6.2 Hz, 1H), 4.96 (dd, *J* = 9.7, 1H), 4.48 (dd, *J* = 8.7 Hz, 1H), 4.35 (d, *J* = 8.2 Hz, 1H), 4.11 (d, *J* = 8.3 Hz, 1H), 3.91 (d, *J* = 6.3 Hz, 1H), 2.95 (d, *J* = 9.8 Hz, 1H), 2.69 (d, *J* = 9.6 Hz, 1H), 2.57 (m, 1H), 2.17 (s, 3H), 2.08 (s, 3H), 1.83 (m, 1H), 1.65 (s, 3H), 1.61 (t, *J* = 7.8, 4.5, Hz, 1H), 1.25 (s, 6H), 1.17 (dd, *J* = 5.3, 3.5 Hz, 2H), 1.03 (dd, *J* = 6.7, 4.2 Hz, 2H) (Figure 3.91). ^{13}C NMR (126 MHz, $CDCl_3$) δ: 202.18, 197.98, 174.65, 170,16, 166.45, 152.45, 141.35, 133.35, 130.04, 129.26, 129.23, 128.79, 127.15, 127.96, 84.28, 80.37, 78.81, 77.62. 76.39, 73.28, 72.38, 59.38, 45.31, 43.43, 35.62, 33.36, 21.75, 18.82, 13.95, 13.12, 9.67, 9.11 (Figure 3.92). LC/ESI-MS monoisotopic exact mass *m/z* 678. 2369 $[M + H]^+$; calculated for $C_{34}H_{38}F_3O_{11}$: 678.2285.

Reduction of 2-O-Debenzoyl-2-O-(m-Substituted)Benzoyl-13-Oxobaccatins to 3.29a-f, 3.30a-f, and 3.31a-f

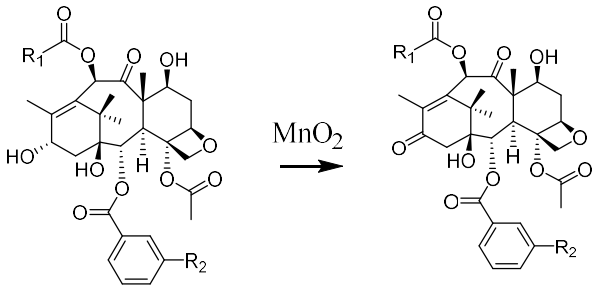

3.26a-f
3.27a-f
3.28a-f

3.29a-f
3.30a-f
3.31a-f

Figure 3.9: Reduction of (*meta*-substituted)benzoyl-13-oxo-taxane analogs. R: (a: F), (b: Cl), (c: OCH_3), (d: OCF_3), (e: $OCHF_2$), (f: CF_3). *Reagents and conditions* are in the text below.

The following method is based on a previously described procedure.[25] 2-*O*-Debenzoyl-2-*O*-(*m*-substituted)benzoyl-13-oxobaccatins **3.26a-f**, **3.27a-f**, and **3.28a-f** (0.084 mmol) were dissolved in 4 mL dry methanol and 1 mL dry THF and stirred at 0 °C for 5 min under N_2. Sodium borohydride ($NaBH_4$) (74 mg, 2 mmol) was added, and the reaction mixture was stirred for 2 h and then warmed to room temperature. The progress of the reaction was checked by TLC. After 5 h, the reaction was quenched with 10 mL of saturated aqueous solution of ammonium chloride and stirred for 5 min. The aqueous layer was extracted with (2 × 30 mL) EtOAc. The combined organic fractions were dried over anhydrous magnesium sulfate. The solution was filtered, the filtrate was concentrated under vacuum, and the crude product was purified by silica-gel flash column chromatography (60:40 (v/v), EtOAc/hexanes) to yield the pure product as determined by NMR and quantified by LC/ESI-MS/MS.

NMR Data for 2-*O*-Debenzoyl-2-*O*-(3-fluorobenzoyl)baccatin III (**3.29a**) (16 mg, 90% yield) ^{1}H NMR (500 MHz, $CDCl_3$) δ: 8.12 (d, *J* = 7.8 Hz, 1H), 7.93 (s, 1H), 7.79 (d, *J* = 6.5 Hz, 1H), 7.49 (m,1H), 6.34 (s, 1H), 5.63 (d, *J* = 7.5 Hz, 1H), 5.02 (dd, *J* = 9.7 Hz, 1H), 4.89 (m, 1H), 4.51 (dd, *J* = 9.9 Hz, 1H), 4.33 (d, *J* = 9 Hz, 1H), 4.18 (d, *J* = 9 Hz, 1H), 3.89 (d, *J* = 7.1 Hz, 1H), 2.58 (m,

1H), 2.29 (s, 3H), 2.06 (s, 3H), 1.88 (m, 1H), 1.68 (s, 3H), 1.12 (s, 6H) (Figure 3.93). ^{13}C NMR (126 MHz, $CDCl_3$) δ: 204.21, 171.42, 170.73, 167.08, 163.52, 146.49, 133.71, 130.09, 129.27, 128.65, 120.72, 117.09, 84.17, 79.09, 77.18, 76.25, 74.91, 72.31, 67.89, 58.65, 46.14, 42.68, 38.56, 35.57, 26.95, 22.59, 20.91, 15.63, 9.45 (Figure 3.94). LC/ESI-MS monoisotopic exact mass m/z 605.2354 $[M+H]^+$: calculated for $C_{31}H_{38}FO_{11}$: 605.2267.

NMR Data for 2-*O*-Debenzoyl-2-*O*-(3-chlorobenzoyl)baccatin III (**3.29b**) (13 mg, 88% yield). ^{1}H NMR (500 MHz, $CDCl_3$) δ: 8.09 (s, 1H), 7.98 (d, , *J* = 7.8, 1H),7.61 (d, *J* = 6.5 Hz, 1H), 7.46 (m, 1H), 6.32 (s, 1H), 5.65 (d, *J* = 7.6 Hz, 1H), 4.99 (dd, *J* = 9.4, 2.5 Hz, 1H), 4.87 (m, 1H), 4.48 (dd, *J* = 9.2 Hz 1H), 4.32 (d, *J* = 8.5 Hz 1H), 4.15 (d, *J* = 8.6 Hz 1H), 3.88 (d, *J* = 7.2 Hz, 1H), 2.56 (m, 1H), 2.30 (m, 2H), 2.24 (s, 3H), 2.05 (s, 3H), 1.86 (m, 1H), 1.67 (s, 3H), 1.11 (s, 6H) (Figure 3.95). ^{13}C NMR (126 MHz, $CDCl_3$) δ: 204.25, 174.25, 170.78, 167.09, 164.24, 146.28, 133.75, 131.86, 129.83, 129.28, 128.65, 128.28, 84.51, 80.78, 79.12, 77.36, 76.03, 74.92, 72.35, 67.94, 58.68, 46.16, 42.69, 38.56, 35.58, 27.62, 22.61, 20.97, 13.62, 9.47 (Figure 3.96). LC/ESI-MS monoisotopic exact mass *m/z* 621.2078 $[M + H]^+$; calculated for $C_{31}H_{38}ClO_{11}$: 621.1892.

NMR Data for 2-*O*-Debenzoyl-2-*O*-(3-methoxybenzoyl)baccatin III (**3.29c**) (10 mg, 84% yield). ^{1}H NMR (500 MHz, $CDCl_3$) δ: 8.11 (d, *J* = 7.6, 1H), 7.62 (s, 1H), 7.47 (d, *J* = 6.7 Hz, 1H), 7.36 (m, 1H), 6.31 (s, 1H), 5.62 (d, *J* = 7.8 Hz, 1H), 4.98 (dd, *J* = 9.5, 2.7 Hz, 1H), 4.89 (m, 1H), 4.46 (dd, *J* = 9.4 Hz 1H), 4.31 (d, *J* = 8.7 Hz 1H), 4.17 (d, *J* = 8.2 Hz 1H), 3.87 (d, *J* = 7.5 Hz, 1H), 2.57 (m, 1H), 2.31 (m, 2H), 2.29 (s, 3H), 2.11 (s, 3H), 1.87 (m, 1H), 1.68 (s, 3H), 1.12 (s, 6H) (Figure 3.97). ^{13}C NMR (126 MHz, $CDCl_3$) δ: 204.18, 171.38, 170.73, 167.07, 159.57, 146.43, 133.69, 129.51, 129.27, 122.64, 120.37, 114.34, 84.46, 80.75, 79.09, 77.82, 76.24, 74.90, 72.29, 67.91, 58.66, 55.45, 46.13, 42.67, 38.56, 35.58, 26.95, 22.58, 20.89, 15.62, 9.43 (Figure 3.98).

LC/ESI-MS monoisotopic exact mass *m/z* 617.2541 $[M + H]^+$; calculated for $C_{32}H_{41}O_{12}$: 617.2476.

NMR Data for 2-*O*-Debenzoyl-2-*O*-(3-trifluoromethoxybenzoyl)baccatin III (**3.29d**) (11 mg, 88% yield). ^1H NMR (500 MHz, $CDCl_3$) δ: 8.09 (d, *J* = 7.5, 1H), 7.93 (s, 1H), 7.59 (d, *J* = 6.7 Hz, 1H), 7.47 (m, 1H), 6.32 (s, 1H), 5.65 (d, *J* = 7.4 Hz, 1H), 4.95 (dd, *J* = 9.4, 2.8 Hz, 1H), 4.87 (m, 1H), 4.47 (dd, *J* = 9.2 Hz 1H), 4.31 (d, *J* = 8.5 Hz 1H), 4.16 (d, *J* = 8.5 Hz 1H), 3.84 (d, *J* = 7.4 Hz, 1H), 2.56 (m, 1H), 2.29 (m, 2H), 2.27 (s, 3H), 2.04 (s, 3H), 1.85 (m, 1H), 1.66 (s, 3H), 1.09 (s, 6H) (Figure 3.99). ^{13}C NMR (126 MHz, $CDCl_3$) δ: 204.21, 171.42, 170.75, 167.07, 163.52, 146.49, 133.71, 131.72, 130.09, 129.27, 128.64, 120.89, 117.09, 84.48, 80.74, 79.09, 77.61, 76.25, 74.91, 72.31, 67.89, 58.65, 46.14, 42.68, 38.58, 35.57, 26.95, 22.59, 21.08, 15.63, 9.5 (Figure 3.100). LC/ESI-MS monoisotopic exact mass *m/z* 671.2254 $[M + H]^+$; calculated for $C_{32}H_{38}F_3O_{12}$: 671.2168.

NMR Data for 2-*O*-Debenzoyl-2-*O*-(3-difluoromethoxybenzoyl)baccatin III (**3.29e**) (14 mg, 96% yield). ^1H NMR (500 MHz, $CDCl_3$) δ: 8.35 (s, 1H), 8.14 (d, *J* = 7.4, 1H), 7.61 (d, *J* = 6.2 Hz, 1H), 7.44 (m, 1H), 7.36 (s, 1H), 6.31 (s, 1H), 5.68 (d, *J* = 7.2 Hz, 1H), 4.94 (dd, *J* = 9.1, 2.8 Hz, 1H), 4.86 (m, 1H), 4.45 (dd, *J* = 9.2 Hz 1H), 4.34 (d, *J* = 8.5 Hz 1H), 4.15 (d, *J* = 8.5 Hz 1H), 3.85 (d, *J* = 7.3 Hz, 1H), 2.52 (m, 1H), 2.27 (m, 2H), 2.27 (s, 3H), 2.08 (s, 3H), 1.88 (m, 1H), 1.65 (s, 3H), 1.11 (s, 6H) (Figure 3.101). ^{13}C NMR (126 MHz, $CDCl_3$) δ: 204.19, 170.44, 170.81, 167.12, 146.47, 133.73, 133.25, 130.09, 129.26, 129.16, 128. 64, 128.15, 127.11, 84.48, 80.74, 79.09, 77.62, 76.27, 74.93, 72.32, 67.89, 58.65, 46.16, 42.68, 38.54, 35.56, 26.96, 22.58, 20.08, 15.65, 9.4 (Figure 3.102). LC/ESI-MS monoisotopic exact mass *m/z* 653. 2482 $[M + H]^+$; calculated for $C_{32}H_{39}F_2O_{12}$: 653.2318.

NMR Data for 2-*O*-Debenzoyl-2-*O*-(3-trifluoromethylbenzoyl)baccatin III (3.17f) (6 mg, 91% yield). ^{1}H NMR (500 MHz, $CDCl_3$) δ: 8.37 (s, 1H), 8.12 (d, *J* = 7.8, 1H), 7.63 (d, *J* = 6.5 Hz, 1H), 7.47 (m, 1H), 6.32 (s, 1H), 5.62 (d, *J* = 7.8 Hz, 1H), 4.99 (dd, *J* = 9.5, 2.4 Hz, 1H), 4.89 (m, 1H), 4.48 (dd, *J* = 9.5 Hz 1H), 4.31 (d, *J* = 8.7 Hz 1H), 4.17 (d, *J* = 8.7 Hz 1H), 3.89 (d, *J* = 7.5 Hz, 1H), 2.57 (m, 1H), 2.29 (m, 2H), 2.25 (s, 3H), 2.05 (s, 3H), 1.87 (m, 1H), 1.67 (s, 3H), 1.12 (s, 6H) (Figure 3.103). ^{13}C NMR (126 MHz, $CDCl_3$) δ: 204.19, 170.44, 170.81, 167.12, 146.47, 133.73, 133.25, 130.09, 129.26, 129.16, 128. 64, 128.15, 127.11, 84.48, 80.74, 79.09, 77.62, 76.27, 74.93, 72.32, 67.89, 58.65, 46.16, 42.68, 38.54, 35.56, 26.96, 22.58, 20.08, 15.65, 9.4 (Figure 3.104). LC/ESI-MS monoisotopic exact mass *m/z* 654. 2376 $[M + H]^+$; calculated for $C_{32}H_{38}F_3O_{11}$: 654.2268.

NMR Data for 2-*O*-Debenzoyl-2-*O*-(3-fluorobenzoyl)-10-PDAB (3.30a) (15 mg, 92% yield). ^{1}H NMR (500 MHz, $CDCl_3$) δ: 8.12 (d, *J* = 7.6, 1H), 7.91 (d, *J* = 6.5, 1H), 7.78 (s, 1H), 7.48 (m, 1H), 6.33 (s, 1H), 5.63 (d, *J* = 7.5 Hz, 1H), 4.97 (dd, *J* = 9.5, 2.4 Hz, 1H)), 4.87 (m, 1H), 4.47 (dd, *J* = 9.5 Hz 1H), 4.29 (d, *J* = 9.2 Hz 1H), 4.16 (d, *J* = 9.5 Hz 1H), 3.87 (d, *J* = 7.1 Hz, 1H), 2.57 (m, 1H), 2.54 (m, 2H), 2.28 (m, 2H), 2.04 (s, 3H), 1.86 (m, 1H), 1.66 (s, 3H), 1.12 (t, *J* = 7.6 Hz, 3H), 1.11 (s, 6H) (Figure 3.105). ^{13}C NMR (126 MHz, $CDCl_3$) δ: 204.25, 171.75, 170.77, 167.12, 163.52, 146.26, 133.72, 130.21, 129.27, 128.65, 120.98, 117.13, 84.51, 80.78, 79.12, 77.52, 76.03, 74.92, 72.34, 67.95, 58.68, 46.16, 42.68, 38.54, 35.59, 27.62, 22.61, 20.91, 15.62, 9.45, 9.05 (Figure 3.106). LC/ESI-MS monoisotopic exact mass *m/z* 619. 2578 $[M + H]^+$; calculated for $C_{32}H_{40}FO_{11}$: 619.2465.

NMR Data for 2-*O*-Debenzoyl-2-*O*-(3-chlorobenzoyl)-10-PDAB (3.30b) (11 mg, 90% yield). ^{1}H NMR (500 MHz, $CDCl_3$) δ: 8.11 (s, 1H), 7.96 (d, *J* = 7.8, 1H),7.61 (d, *J* = 6.5 Hz, 1H), 7.47 (m, 1H), 6.33 (s, 1H), 5.63 (d, *J* = 7.5 Hz, 1H), 4.98 (dd, *J* = 9.8, 2.5 Hz, 1H)), 4.87 (m, 1H), 4.47

(dd, *J* = 9.9 Hz, 1H), 4.29 (d, *J* = 9.2 Hz, 1H), 4.14 (d, *J* = 9.3 Hz, 1H), 3.89 (d, *J* = 7.5 Hz, 1H), 2.57 (m, 1H), 2.54 (m, 2H), 2.28 (m, 2H), 2.05 (s, 3H), 1.86 (m, 1H), 1.67 (s, 3H), 1.23 (t, *J* = 7.6 Hz, 3H), 1.11 (s, 6H) (Figure 3.107). ^{13}C NMR (126 MHz, $CDCl_3$) δ: 204.25, 174.73, 170.74, 167.09, 146.29, 133.75, 131.86, 130.22, 130.09, 129.28, 128.65, 128.28, 84.51, 80.78, 79.12, 77.52, 76.04, 74.92, 72.35, 67.94, 58.68, 46.16, 42.68, 38.56, 35.58, 27.62, 22.61, 20.92, 13.62, 9.45, 9.05 (Figure 3.108). LC/ESI-MS monoisotopic exact mass *m/z* 635. 2258 $[M + H]^+$; calculated for $C_{32}H_{40}ClO_{11}$: 635.2192.

NMR Data for 2-*O*-Debenzoyl-2-*O*-(3-methoxybenzoyl)-10-PDAB (**3.30c**) (9 mg, 88% yield). ^{1}H NMR (500 MHz, $CDCl_3$) δ: 8.11 (d, *J* = 7.8, 1H), 7.72 (d, *J* = 7.5, 1H), 7.49 (s, 1H), 7.37 (m, 1H), 6.34 (s, 1H), 5.64 (d, *J* = 7.5 Hz, 1H), 4.97 (dd, *J* = 9.8, 2.5 Hz, 1H), 4.89 (m, 1H), 4.51 (dd, *J* = 9, 5 Hz 1H), 4.32 (d, *J* = 9.4 Hz 1H), 4.15 (d, *J* = 9.5 Hz 1H), 3.87 (d, *J* = 7.6 Hz, 1H), 2.57 (m, 1H), 2.54 (m, 2H), 2.31 (m, 2H), 2.29 (s, 3H), 2.02 (s, 3H), 1.85 (m, 1H), 1.68 (s, 3H), 1.24 (t, *J* = 7.6 Hz, 3H), 1.12 (s, 6H) (Figure 3.109). ^{13}C NMR (126 MHz, $CDCl_3$) δ: 204.26, 174.74, 170.75, 167.09, 159.58, 146.31, 133.72, 129.53, 129.28, 122.65, 120.41, 114.35, 84.51, 80.78, 79.11, 77.36, 76.04, 74.92, 72.34, 67.93, 58.68, 55.47, 46.16, 42.68, 38.56, 35.58, 27.62, 22.65, 20.92, 15.62, 9.45, 9.05 (Figure 3.110). LC/ESI-MS monoisotopic exact mass *m/z* 631. 2774 $[M + H]^+$; calculated for $C_{33}H_{43}O_{12}$: 631.2684.

NMR Data for 2-*O*-Debenzoyl-2-*O*-(3-trifluoromethoxybenzoyl)-10-PDAB (**3.30d**) (12 mg, 92% yield). ^{1}H NMR (500 MHz, $CDCl_3$) δ: 8.09 (d, *J* = 7.5, 1H), 7.95 (s, 1H), 7.61 (d, *J* = 6.4 Hz, 1H), 7.48 (m, 1H), 6.34 (s, 1H), 5.62 (d, *J* = 7.4 Hz, 1H), 4.97 (dd, *J* = 9.5, 2.4 Hz, 1H), 4.88 (m, 1H), 4.46 (dd, *J* = 9.5 Hz, 1H), 4.30 (d, *J* = 9.2 Hz, 1H), 4.15 (d, *J* = 9 Hz 1H), 3.88 (d, *J* = 7.6 Hz, 1H), 2.57 (m, 1H), 2.54 (m, 2H), 2.29 (m, 2H), 2.29 (s, 3H), 2.05 (s, 3H), 1.84 (m, 1H), 1.64 (s, 3H), 1.23 (t, *J* = 7.6 Hz, 3H), 1.11 (s, 6H) (Figure 3.111). ^{13}C NMR (126 MHz, $CDCl_3$) δ: 204.27,

174.75, 170.77, 167.12, 163.52, 146.27, 133.72, 131.85, 130.21, 129.27, 128.65, 120.98, 117.13, 84.51, 80.78, 79.12, 77.42, 76.04, 74.92, 72.34, 67.95, 58.68, 46.16, 42.68, 38.59, 35.58, 27.62, 22.61, 20.91, 15.63, 9.45, 9.05 (Figure 3.112). LC/ESI-MS monoisotopic exact mass *m/z* 685. 2476 $[M + H]^+$; calculated for $C_{33}H_{40}F_3O_{12}$: 685.2362.

NMR Data for 2-*O*-Debenzoyl-2-*O*-(3-difluoromethoxybenzoyl)-10-PDAB (3.30e) (14 mg, 94% yield). ^{1}H NMR (500 MHz, $CDCl_3$) δ: 8.36 (s, 1H), 8.08 (d, *J* = 7.2, 1H), 7.61 (d, *J* = 6.5 Hz, 1H), 7.35 (s, 1H), 7.46 (m, 1H), 6.33 (s, 1H), 5.64 (d, *J* = 7.5 Hz, 1H), 4.96 (dd, *J* = 9.5, 2.4 Hz, 1H)), 4.86 (m, 1H), 4.47 (dd, *J* = 9.5 Hz 1H), 4.32 (d, *J* = 9.5 Hz, 1H), 4.17 (d, *J* = 9.5 Hz 1H), 3.84 (d, *J* = 7.5 Hz, 1H), 2.56 (m, 3H), 2.33 (m, 2H), 2.05 (s, 3H), 1.87 (m, 1H), 1.68 (s, 3H), 1.24 (t, *J* = 7.8 Hz, 3H), 1.08 (s, 6H) (Figure 3.113). ^{13}C NMR (126 MHz, $CDCl_3$) δ: 204.11, 171.54, 170.85, 167.15, 146.48, 133.77, 133.55, 131.75, 130.27, 129.65, 129.23, 128.64. 127.11, 84.51, 80.74, 79.14, 77.52, 76.26, 74.93, 72.32, 67.91, 58.65, 46.16, 42.68, 38.44, 35.76, 26.86, 22.48, 20.69, 15.67, 9.12, 9.06 (Figure 3.114). LC/ESI-MS monoisotopic exact mass *m/z* 667. 2587 $[M + H]^+$; calculated for $C_{33}H_{41}F_2O_{12}$: 667.2395.

NMR Data for 2-*O*-Debenzoyl-2-*O*-(3-trifluoromethylbenzoyl)-10-PDAB (3.30f) (4 mg, 90% yield). ^{1}H NMR (500 MHz, $CDCl_3$) δ: 8.35 (s, 1H), 8.11 (d, *J* = 7.5, 1H), 7.59 (d, *J* = 6.8 Hz, 1H), 7.47 (m, 1H), 6.33 (s, 1H), 5.65 (d, *J* = 7.6 Hz, 1H), 4.95 (dd, *J* = 9.7, 2.1 Hz, 1H)), 4.87 (m, 1H), 4.47 (dd, *J* = 9.5 Hz 1H), 4.32 (d, *J* = 9.2 Hz, 1H), 4.16 (d, *J* = 9.7 Hz 1H), 3.89 (d, *J* = 7.6 Hz, 1H), 2.57 (m, 1H), 2.54 (m, 2H), 2.31 (m, 2H), 2.04 (s, 3H), 1.86 (m, 1H), 1.66 (s, 3H), 1.21 (t, *J* = 7.8 Hz, 3H), 1.09 (s, 6H) (Figure 3.115). ^{13}C NMR (126 MHz, $CDCl_3$) δ: 204.19, 171.44, 170.81, 167.12, 146.47, 133.73, 133.35, 131.75, 130.27, 129.65, 129.23, 128.64. 127.11, 84.51, 80.74, 79.14, 77.52, 76.26, 74.93, 72.32, 67.91, 58.65, 46.16, 42.68, 38.54, 35.56, 26.96, 22.58, 20.89,

15.63, 9.4, 9.05 (Figure 3.116). LC/ESI-MS monoisotopic exact mass *m/z* 669. 2465 $[M + H]^+$; calculated for $C_{33}H_{40}F_3O_{11}$: 669.2346.

NMR Data for 2-*O*-Debenzoyl-2-*O*-(3-fluorobenzoyl)-10-CPCDAB (3.31a) (13 mg, 95% yield). ^1H NMR (500 MHz, $CDCl_3$) δ: 8.09 (d, *J* = 7.2, 1H), 7.93 (d, *J* = 6.4, 1H), 7.75 (s, 1H), 7.49 (m, 1H), 6.32 (s, 1H), 5.63 (d, *J* = 7.4 Hz, 1H), 4.98 (dd, *J* = 9.4, 2.5 Hz, 1H), 4.91 (m, 1H), 4.46 (dd, *J* = 9.6 Hz 1H), 4.32 (d, *J* = 9 Hz 1H), 4.16 (d, *J* = 9 Hz 1H), 3.89 (d, *J* = 7.4 Hz, 1H), 2.54 (m, 1H), 2.31 (m, 2H), 2.28 (s, 3H), 2.05 (s, 3H), 1.81 (m, 1H), 1.67 (s, 3H), 1.24 (t, *J* = 7.8, 4.7, Hz, 1H), 1.12 (s, 6H), 1.03 (dd, *J* = 5.6, 3.2 Hz, 2H), 0.95 (dd, *J* = 6.5, 4.7 Hz, 2H) (Figure 3.117). ^{13}C NMR (126 MHz, $CDCl_3$) δ: 204.35, 173.25, 170.73, 167.08, 163.51, 146.51, 133.69, 130.18, 129.28, 128.63, 120.71, 117.09, 84.52, 80.76, 79.14, 77.54, 76.03, 74.93, 72.34, 67.91, 58.65, 46.15, 42.67, 38.57, 35.52, 27.01, 22.58, 20.98, 15.64, 9.4, 9.18 (Figure 3.118). LC/ESI-MS monoisotopic exact mass *m/z* 631. 2586 $[M + H]^+$; calculated for $C_{33}H_{40}FO_{11}$: 631.2458.

NMR Data for 2-*O*-Debenzoyl-2-*O*-(3-chlorobenzoyl)-10-CPCDAB (3.31b) (10 mg, 86% yield). ^1H NMR (500 MHz, $CDCl_3$) δ: 8.08 (s, 1H), 7.94 (d, , *J* = 7.5, 1H),7.59 (d, *J* = 6.5 Hz, 1H), 7.48 (m, 1H), 6.31 (s, 1H), 5.61 (d, *J* = 7.5 Hz, 1H), 4.99 (dd, *J* = 9.6, 2.4 Hz, 1H), 4.87 (m, 1H), 4.46 (dd, *J* = 9.6 Hz, 1H), 4.31 (d, *J* = 9.2 Hz, 1H), 4.14 (d, *J* = 9.4 Hz 1H), 3.87 (d, *J* = 7.5 Hz, 1H), 2.55 (m, 1H), 2.27 (m, 2H), 2.27 (s, 3H), 2.03 (s, 3H), 1.84 (m, 1H), 1.65 (s, 3H), 1.28 (t, *J* = 7.2, 4.5, Hz, 1H), 1.07 (s, 6H), 1.07 (dd, *J* = 5.8, 3.4 Hz, 2H), 0.98 (dd, *J* = 6.5, 4.8 Hz, 2H) (Figure 3.119). ^{13}C NMR (126 MHz, $CDCl_3$) δ: 204.36, 175.23, 170.69, 167.04, 146.59, 133.67, 131.72, 130.07, 129.76, 129.29, 128.62, 128.22, 84.51, 80.72, 79.09, 77.51, 76.03, 74.93, 72.32, 67.85, 58.68, 46.14, 42.65, 38.61, 35.51, 26.98, 22.57, 21.06, 15.63, 9.41, 9.17 (Figure 3.120). LC/ESI-MS monoisotopic exact mass *m/z* 647. 2274 $[M + H]^+$; calculated for $C_{33}H_{40}ClO_{11}$: 647.2183.

NMR Data for 2-*O*-Debenzoyl-2-*O*-(3-methoxybenzoyl)-10-CPCDAB (3.31c) (8 mg, 92% yield). ^{1}H NMR (500 MHz, $CDCl_3$) δ: 8.08 (d, *J* = 7.4, 1H), 7.69 (s, 1H), 7.47 (d, *J* = 6.2 Hz, 1H), 7.31 (m, 1H), 6.31 (s, 1H), 5.59 (d, *J* = 7.6 Hz, 1H), 4.96 (dd, *J* = 9.4, 2.5 Hz, 1H), 4.85 (m, 1H), 4.45 (dd, *J* = 9.5 Hz, 1H), 4.28 (d, *J* = 9.3 Hz, 1H), 4.15 (d, *J* = 9.3 Hz, 1H), 3.86 (d, *J* = 7.8 Hz, 1H), 2.53 (m, 1H), 2.29 (m, 2H), 2.26 (s, 3H), 2.03 (s, 3H), 1.84 (m, 1H), 1.65 (s, 3H), 1.26 (t, *J* = 7.6, 4.6, Hz, 1H), 1.12 (s, 6H), 1.09 (dd, *J* = 5.8, 3.5 Hz, 2H), 0.98 (dd, *J* = 6.4, 4.8 Hz, 2H) (Figure 3.121). ^{13}C NMR (126 MHz, $CDCl_3$) δ: 204.26, 174.74, 170.75, 267.09, 259.58, 246.31, 133.71, 129.53, 129.26, 122.65, 120.41, 114.53, 84.51, 80.78, 79.11, 77.53, 76.36, 74.34, 72.34, 67.93, 58.68, 55.48, 46.16, 42.69, 38.56, 35.58, 27.61, 22.61, 20.92, 15.62, 9.45, 9.05 (Figure 3.122). LC/ESI-MS monoisotopic exact mass *m/z* 643. 2786 $[M + H]^+$; calculated for $C_{34}H_{43}O_{12}$: 631.2642.

NMR Data for 2-*O*-Debenzoyl-2-*O*-(3-trifluoromethoxybenzoyl)-10-CPCDAB (3.31d) (10 mg, 94% yield). ^{1}H NMR (500 MHz, $CDCl_3$) δ: 8.12 (d, *J* = 7.6, 1H), 7.91 (s, 1H), 7.79 (d, *J* = 6.8 Hz, 1H), 7.47 (m, 1H), 6.32 (s, 1H), 5.63 (d, *J* = 7.0 Hz, 1H), 4.98 (dd, *J* = 9.5, 2.4 Hz, 1H), 4.92 (m, 1H), 4.46 (dd, *J* = 9.5 Hz 1H), 4.32 (d, *J* = 9.2 Hz, 1H), 4.16 (d, *J* = 9.4 Hz, 1H), 3.87 (d, *J* = 7.4 Hz, 1H), 2.57 (m, 1H), 2.34 (m, 2H), 2.29 (s, 3H), 2.05 (s, 3H), 1.87 (m, 1H), 1.66 (s, 3H), 1.25 (t, *J* = 7.4, 4.7, Hz, 1H), 1.18 (s, 6H), 1.12 (dd, *J* = 5.4, 3.6 Hz, 2H), 0.95 (dd, *J* = 6.4, 4.8 Hz, 2H) (Figure 3.123). ^{13}C NMR (126 MHz, $CDCl_3$) δ: 204.35, 175.23, 170.74, 167.07, 163.51, 146.56, 133.69, 131.78, 130.12, 129.28, 128.64, 120.87, 117.08, 84.62, 80.75, 79.12, 77.51, 76.03, 74.94, 72.35, 67.91, 58.65, 46.15, 42.67, 38.57, 35.52, 27.12, 27.12, 22.58, 20.99, 15.64, 9.42, 9.18 (Figure 3.124). LC/ESI-MS monoisotopic exact mass *m/z* 697. 2453 $[M + H]^+$; calculated for $C_{34}H_{40}F_3O_{12}$: 697.2373.

NMR Data for 2-*O*-Debenzoyl-2-*O*-(3-difluoromethoxybenzoyl)-10-CPCDAB (3.31e) (12 mg, 92% yield). ^{1}H NMR (500 MHz, $CDCl_3$) δ: 8.35 (s, 1H), 8.16 (d, *J* = 7.5, 1H), 7.86 (d, *J* = 6.3 Hz, 1H), 7.35 (s, 1H), 7.46 (m, 1H), 6.32 (s, 1H), 5.64 (d, *J* = 7.2 Hz, 1H), 4.95 (dd, *J* = 9.4, 2.6 Hz, 1H), 4.84 (m, 1H), 4.49 (dd, *J* = 9.2 Hz, 1H), 4.37 (d, *J* = 9.4 Hz, 1H), 4.15 (d, *J* = 9.2 Hz, 1H), 3.85 (d, *J* = 7.4 Hz, 1H), 2.55 (m, 1H), 2.27 (m, 2H), 2.07 (s, 3H), 1.87 (m, 1H), 1.65 (s, 3H), 1.26 (t, *J* = 7.4, 4.5, Hz, 1H), 1.15 (s, 6H), 1.14 (dd, *J* = 5.4, 3.2 Hz, 2H), 0.98 (dd, *J* = 6.2, 4.5 Hz, 2H) (Figure 3.125).^{13}C NMR (126 MHz, $CDCl_3$) δ: 202.45, 175.25, 170.65, 167.17, 163.58, 146.45, 133.71, 133.34, 130.28, 129.54, 129.27, 128.68, 127.15, 84.57, 80.73, 79.16, 77.58, 76.32, 74.91, 72.32, 67.98, 58.65, 46.18, 42.65, 38.56, 35.58, 27.17, 22.53, 15.52, 13.08, 9.45, 9.14 (Figure 3.126). LC/ESI-MS monoisotopic exact mass *m/z* 679. 2564 $[M + H]^+$; calculated for $C_{34}H_{41}F_2O_{12}$: 679.2373.

NMR Data for 2-*O*-Debenzoyl-2-*O*-(3-trifluoromethylbenzoyl)-10-CPCDAB (3.31f) (3 mg, 89% yield). ^{1}H NMR (500 MHz, $CDCl_3$) δ: 8.38 (s, 1H), 8.12 (d, *J* = 7.4, 1H), 7.88 (d, *J* = 6.7 Hz, 1H), 7.49 (m, 1H), 6.32 (s, 1H), 5.63 (d, *J* = 7.6 Hz, 1H), 4.98 (dd, *J* = 9.3, 2.7 Hz, 1H), 4.88 (m, 1H), 4.48 (dd, *J* = 9.4 Hz, 1H), 4.32 (d, *J* = 9.3 Hz, 1H), 4.16 (d, *J* = 9.5 Hz, 1H), 3.89 (d, *J* = 7.1 Hz, 1H), 2.54 (m, 1H), 2.29 (m, 2H), 2.05 (s, 3H), 1.86 (m, 1H), 1.67 (s, 3H), 1.27 (t, *J* = 7.8, 4.2, Hz, 1H), 1.14 (s, 6H), 1.12 (dd, *J* = 5.8, 3.4 Hz, 2H), 0.97 (dd, *J* = 6.4, 4.7 Hz, 2H) (Figure 3.127). ^{13}C NMR (126 MHz, $CDCl_3$) δ: 202.43, 175.27, 170.79, 167.12, 163.54, 146.48, 133.72, 133.35, 130.26, 129.51, 129.23, 128.65, 127.11, 84.54, 80.77, 79.16, 77.56, 76.04, 74.95, 72.36, 67.94, 58.67, 46.16, 42.67, 38.54, 35.52, 27.15, 22.59, 15.56, 13.07, 9.43, 9.19 (Figure 3.128). LC/ESI-MS monoisotopic exact mass *m/z* 681. 2482 $[M + H]^+$; calculated for $C_{34}H_{40}F_3O_{11}$: 681.2371.

Molecular Modeling Analysis

Structure optimizations on baccatin III (**3.16**), 13-*O*-acetylbaccatin III (**3.35**), and 13-oxobaccatin III (**3.19**) were conducted using Gaussian 16 in a four-step pattern[26], starting from HF 3-21G* single point to HF 3-21G* optimization, then to B3LYP 3-21G*, and finally to B3LYP 6-31G*. Molecular dynamics (MD) simulations were performed using AMBER22.[27] The system was prepared in three steps. First, the antechamber, prepin, parmchk2 programs in AmberTools22 package[28] generated the charge and force constants. Minimization was done in five stages, gradually removing restrictions from the protein backbone to the side chain. Each step yields 10,000 steps of steepest descendent and 10,000 steps of conjugate gradient methods. A quick 9-ps *NPT* simulation was conducted to avoid the formation of bubbles during heating. Afterward, a 36-ns *NVT* heating was performed with the temperature increasing gradually from 0 to 300 K. Then another 20-ns simulation was performed to equilibrate the system in the *NPT* ensemble, and the last 2,000 frames were used for distance analysis. The PME method and PBC were used for the simulations, and the Langevin algorithm with a 2.0 ps^{-1} friction frequency coefficient was used for maintaining the temperature.[29] The Berendsen barostat method was used for pressure control with a relaxation time of 1.0 ps.[30] The time step was 1.0 fs, with the SHAKE function constraining the hydrogen atom bonds.[31]

Results and Discussion

Assessing the Productive Taxanes in the *m*TBT-Catalyzed Debenzoylation Reaction

Baccatin III (**3.16**), 7-*O*-acetylbaccatin III (**3.32**), 13-*O*-acetylbaccatin III (**3.35**), paclitaxel (**3.12**), 13-oxobaccatin III (**3.19**), 13-oxo-10-PDAB (**3.20**), docetaxel (**3.37**), paclitaxel (**3.12**), and 13-oxo-10-CPCDAB (**3.21**) were incubated separately with purified *m*TBT and CoA, and the putative products made biocatalytically were screened by LC/ESI-MS selected-ion monitoring.

Selected ions *m*/*z* 481.21, *m*/*z* 495.23, and *m*/*z* 507.23 were identified in the LC/ESI-MS profiles and putatively assigned to the $[M+H]^+$ ion for 2-*O*-debenzoyl-13-oxobaccatin III (**3.22**), 2-*O*-debenzoyl-13-oxo-10-PDAB (**3.23**), and 2-*O*-debenzoyl-13-oxo-10-CPCDA (**3.24**), respectively. 13-Acetyltaxane substrate (**3.35)** yielded a selected ion *m*/*z* 525.23 consistent with an $[M+H]^+$ ion for 13-*O*-acetyl-2-*O*-debenzoylbaccatin III but at a much lower relative abundance (0.0015%) compared to the $[M+H]^+$ ion abundance of the debenzoylated product derived from **3.19**, which was turned over fastest, based on relative ion abundance, by *m*TBT. Selected $[M+H]^+$ ions for products derived by the debenzoylation (loss of *m*/*z* 105) of 13-hydroxy substrates baccatin III (**3.16**) (*m*/*z* 587 – 105 = 482) and 7-*O*-acetylbaccatin III (**3.32**) (*m*/*z* 629 – 105 = 524) and 13-*O*-isoserinyl substrates paclitaxel (**3.12**) (*m*/*z* 854 – 105 = 749) and docetaxel (37) (*m*/*z* 808 – 105 = 703) were below the LC/MS detection limits. Thus, these substrates were considered non-productive, suggesting that a hydroxyl group or *N*-acyl-3-phenylisoserinyl at C13 prevented C2 debenzoylation by *m*TBT catalysis.

Kinetic Evaluation of *m*TBT for the 13-oxobaccatin III Substrates

The K_M and k_{cat} of the *m*TBT-catalyzed deacylation were calculated under steady-state conditions by incubating purified *m*TBT with varying concentrations of (13-oxobaccatin III (**3.19**), 13-oxo-10-PDAB (**3.20**), and 13-oxo-10-CPCDAB (**3.21**) and CoA in separate assays. The catalytic efficiency values among the three productive taxane substrates were similar (Table 3.1 and Figure 3.51-3.53) and were used to guide the scale-up (mg-laboratory scale) of the biocatalysis products and confirm their structures by NMR.

Laboratory Scale-Up. The NMR spectra of the purified biocatalysis products 2-*O*-debenzoyl-13-oxobaccatin III (**3.22**) (27 mg) showed that the C2 benzoyl group was removed by *m*TBT catalysis as evidenced by the absence of the signature aromatic proton chemical shifts between δ

7.4 and 8.2 (Figure 3.7). The ^{1}H NMR spectra of 2-*O*-debenzoyl-13-oxo-10-PDAB (**3.23**) (24 mg) and 2-*O*-debenzoyl-13-oxo-10-CPCDAB (**3.24**) (21 mg) were similar to that of **3.22** (Figures 3.44 – 3.47). The H2 chemical shift (δ 3.98) for **3.22** was shifted upfield relative to that for the 2-*O*-benzoyl analog **3.19** (δ 5.69) (Table 3.2 and Figures 3.42 – 3.45), which corroborated the debenzoylation. Also, the ^{1}H NMR showed that the C4 and C10 acetyl groups were retained in the debenzoylated products, suggesting that *m*TBT is highly regioselective for debenzoylation at C2 of the taxane core.

Authentic furano-13-acetyl-2-*O*-debenzoylbaccatin III (**3.36**) (Figure 3.14) was used as a standard to assess if the oxetane ring of the debenzoylated products catalyzed by *m*TBT rearranged to a furan.[32] The ^{1}H NMR chemical shifts for the oxetane protons (H20α/β) of the debenzoylated product **3.22** (δ 4.6 to 4.7) were shifted downfield relative to those for the 13-oxobaccatin III substrate **3.19** (δ 4.1 to 4.3) with nearly equal coupling constants (J ~ 9 Hz) (Table 3.2, Figure 3.7, and Figures 3.42 – 3.45). By comparison, the chemical shifts for H20α/β of authentic furan taxane **3.36** were upfield (δ 3.7 to 4.3) with larger coupling constants (J = 12 Hz) relative to those for **3.22**. Diagnostic ^{13}C NMR chemical shifts for C2 (δ ~72) and C20 (δ ~ 77) of the oxetane for **3.19** and **3.22** were nearly isochronous while those for **3.36** were significantly different (C2: δ ~ 71 and C20: δ ~ 85) (Table 3.2). The ^{1}H and ^{13}C NMR data suggest that the oxetane ring did not rearrange during *m*TBT biocatalysis.

Molecular Modeling Analysis of the *m*TBT-Catalyzed Debenzoylation Reaction

A homology model of the *m*TBT was constructed using AutoDock Vina,[33] and UCSF Chimera[34] to visualize and analyze all the binding poses. This model was based on the sequence homology and available structural data of hydroxycinnamoyltransferase (HCT) (PDB: 5KJT) within the BAHD family of acyltransferases.[35] Baccatin III (**3.16**), 13-acetylbaccatin III (**3.35**), and 13-

oxobaccatin III (**3.19**) were docked separately with the CoA cosubstrate in the active site of the *m*TBT model.

Table 3.1: Relative Kinetics of the *m*TBT Debenzoylation Reaction With 13- Oxobaccatin III Analogs and CoA.

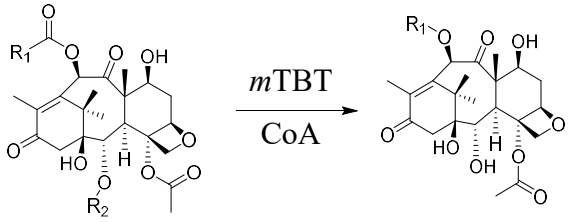

			R_1	Exact mass (Da)	$[M+H]^+$ (*m/z*)	k_{cat} (min^{-1})	K_M (μM)	k_{cat}/K_M (s^{-1} M^{-1})
3.19	→	**3.22**		480.20	481.21	14.7 ± 1.5	162 ± 12	1500
3.20	→	**3.23**		494.22	495.23	11.8 ± 2.4	141 ± 10	1400
3.21	→	**3.24**		506.22	507.23	9.3 ± 1.2	123 ± 9	1300

Table 3.2: Comparison of Diagnostic NMR Data on **3.19** and **3.22** Against **3.36**.

^1H and ^{13}C NMR Chemical Shifts (ppm), (*J* in Hz)			
	13-oxobaccatin III (**3.19**)	deBz-13-oxobaccatin III (**3.22**)	Furano-**3.36**
H-20β	4.32 (d, *J* = 8.5)	4.67 (d, *J* = 9.1)	4.34 (d, *J* = 12.0)
H-20α	4.10 (d, *J* = 8.1)	4.58 (d, *J* = 9.1)	3.66 (d, *J* = 12.0)
H-2	5.69 (d, *J* = 6.4)	3.98 (d, *J* = 4.1)	4.13 (d, *J* = 6.6)
C-20	76.04	77.22	71.03
C-2	72.85	72.35	85.78

Molecular dynamics simulations in this study conducted a thermodynamics analysis on a series of conformations accessible to flexible taxane molecules and CoA; each docked in *m*TBT. The intrinsic intramolecular stability of each cosubstrates conformer was calculated within the context of the proximate residues in the enzyme active site. These conformational snapshots aided in finding low-energy, catalytically competent structural conformations. The resolved structures showed **3.16**, **3.35**, and **3.19** were positioned close to the catalytic residues His160 and Trp360 (Figure 3.8), as suggested by the alignment of these conserved residues in the crystal structure of

the homologous HCT, co-crystallized with its hydroxycinnamoyl-CoA and shikimate substrates.[35]

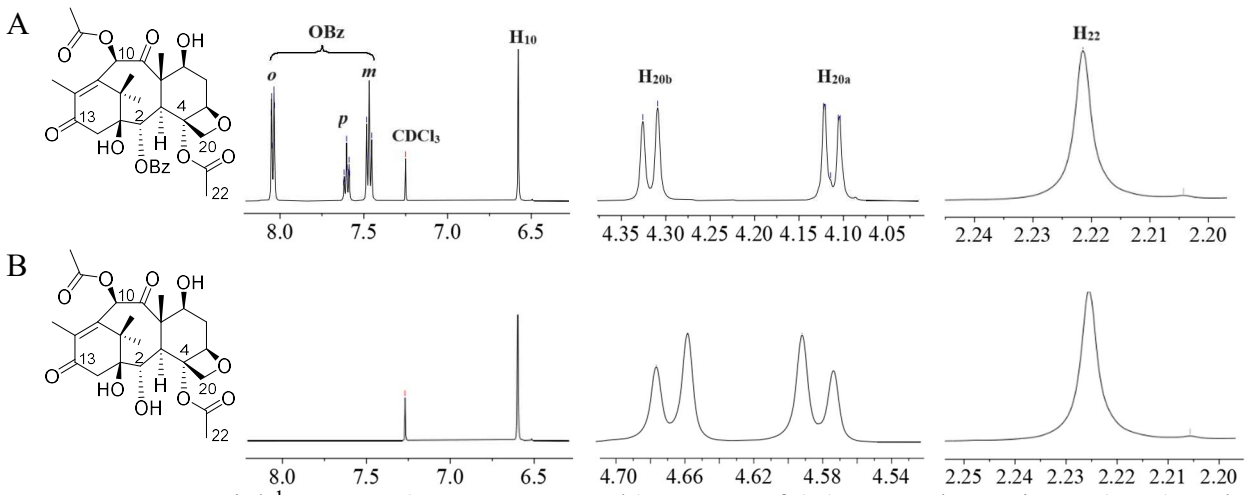

Figure 3.10: Partial ^{1}H NMR (500 MHz, $CDCl_3$) spectra of (A) 13-oxobaccatin III (**3.19**) and biocatalyzed (B) 2-*O*-debenzoyl-13-oxobaccatin III (**3.22**).

The assembly of the static snapshots from the molecular simulations revealed a dynamic equilibration model that highlighted the degrees of freedom between different conformations. Thus, the three baccatin III variants and their CoA cosubstrate in the modeled *m*TBT active site can be compared statically and dynamically. A static snapshot of the low-energy poses indicated that the endo configuration of the taxane A, B, and C rings of 13-oxobaccatin III (**3.19**) and the 13-acetylbaccatin III reside in more open conformations compared to that of baccatin III (the 13-hydroxy analog) (**3.16**) (Figure 3.11A, B, C).

Also, viewing a snapshot of the distances between the reactive thiol sulfur of CoA and the C2 benzoate ester carbon of the taxane substrates (Figure 3.8D, E, F) shows that the closest approach among the 2,000 simulation frames is 4.2 Å for the 13-oxobaccatin III (**3.19**), 5.6 Å. for 13-acetylbaccatin III (**3.35**), and 6.1 Å for baccatin III (**3.16**). We hypothesize that the more relaxed, open conformation of the 13-oxobaccatin III makes it more reactive, as seen experimentally.

This conformational flexibility, inferred by the Gaussian results, will place the CoA and 13-oxobaccatin III in catalytically competent orientations, where the CoA thiol can attack the π-

antibonding orbital of the benzoyl carbonyl at the proper angle (Figure 3.8D).[36,37] In contrast, baccatin III resides in a conformationally closed and rigid structure due to an H-bond between the 13-OH and the ester oxygen at C4 (Figure 3.8C, F). MD simulations orient this conformationally pinched structure in *m*TBT similar to 13-oxobaccatin III, but the intramolecular H-bond bridge causes the C2 benzoate to adopt a catalytically unproductive angle, precluding the CoA thiol approach (Figure 3.8F). Further, *m*TBT debenzoylated 13-acetylbaccatin III at 0.015% the rate of 13-oxobaccatin III under saturation conditions. The Gaussian results show that the C13 acetate removes the H-bond interactions with the C4 ester oxygen, as seen for baccatin III, enabling it to adopt an open conformation like 13-oxobaccatin III (Figure 3.8B).

However, the MD results show that the C13 acetate causes the taxane structure to adopt a slightly different binding orientation than the productive 13-oxobaccatin III benchmark substrate. We expect that the steric clash with the C4 and C13 acetates displaces the C2 benzoate carbonyl from ideal attack by CoA (Figure 3.8E). These results show that CoA can conceptually approach the C2 carbonyl of 13-oxobaccatin III better than that of 13-*O*-acetylbaccatin III and baccatin III for catalysis. When viewing the dynamic process of the taxane molecules over 2,000 simulation frames, the 13-oxobaccatin III has a longer residence time (~5 ns) than 13-acetylbaccatin III (~3 ns) and baccatin III (~1 ns) (Figure 3.154). The longer substrate dwell time reflects a higher likelihood of a productive reaction, consistent with the observed experimental turnover of the substrates.

Kinetic Evaluation of *m*TBT with 2-*O*-Debenzoyl-13-oxobaccatin III Substrates and Various (*m*-Substituted)Benzoyl CoA Thioesters

The K_M and k_{cat} values of the *m*TBT-catalyzed acylation reaction were calculated under steady-state conditions by incubating purified *m*TBT with various concentrations of 2-*O*-debenzoyl-13-oxotaxane substrates and (*m*-substituted)benzoyl CoA thioesters. The results showed that *m*TBT

had greater catalytic efficiencies (k_{cat}/K_M) for benzoyl CoA thioesters with 3-fluoro- (**3.25a**), 3-chloro- (**3.25b**), 3-(trifluoromethoxy)- (**3.25d**) and 3-(difluoromethoxy)- (**3.25e**) substituents than the 3-(methoxy)- (**3.25c**) and 3-trifluoromethylbenzoyl CoA (**3.25f**) analogs.

This trend was observed for each 2-*O*-debenzoyl-13-oxo-substrate (**3.22** – **3.24**), with *m*TBT turning over 10-*O*-acetylated **3.22** and 10-*O*-propanoylated **3.23** ~1.5-fold better than the 10-*O*-cyclopropane carbonylated **3.24** for each CoA substrate. The similar K_M values of *m*TBT for each taxane analog suggested that the different C10 substituents of **3.22** – **3.24** did not affect substrate binding. Thus, the differences in catalytic efficiency were principally governed by the 1.3 to 2-fold slower k_{cat} of *m*TBT for **3.24**, likely caused by the ring-constrained cyclopropyl side chain of **3.24** not allowing it to adopt a catalytically competent conformation for benzoylation (Table 3.3 and Figures 3.129 – 3.131).

Substituent electronics, according to the *m*-substituent constants (σ_{meta}) of the Hammett equation,[38] and steric effects likely combine to give different turnover rates. For example, the 3-fluoro and 3-chloro substituents have little steric impact, yet their inductive electron-withdrawing effect places a δ+ on the carbonyl group of the corresponding CoA thioesters. This inductive effect likely stabilizes the transition state of the benzoyl transfer reaction and accelerates its rate (Figure 3.9). Paradoxically, σ_{meta} for 3-trifluoromethyl is +0.43 and is deemed electronically similar to the 3-fluoro and 3-chloro (σ_{meta} both at +0.37),[38] suggesting that *m*TBT should turn over the corresponding CoA thioesters similarly. *m*TBT turned over 3-trifluoromethylbenzoyl CoA (**3.25f**) the poorest for each of the taxane substrates, suggesting that the increased sterics of the fluoro groups likely affected the catalytic conformation of the CoA substrate.

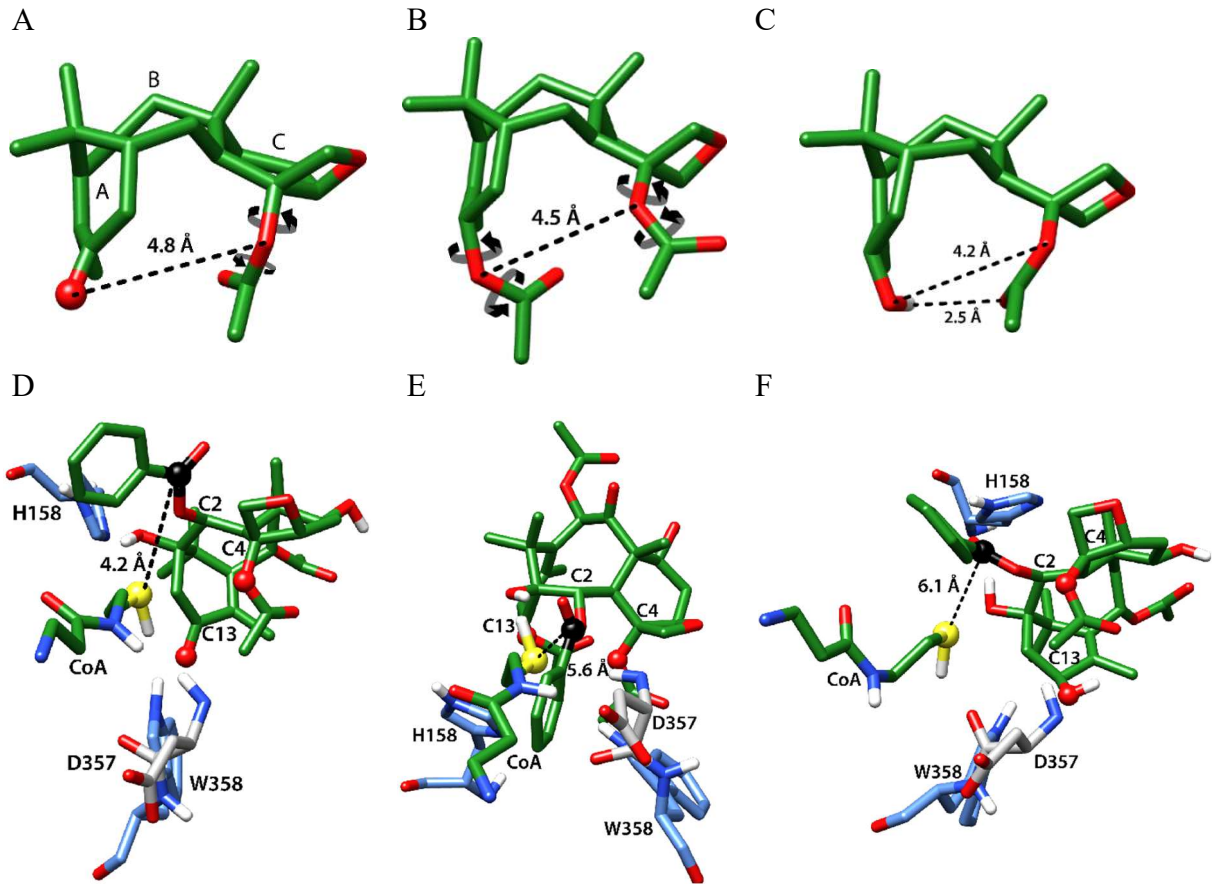

Figure 3.11: The resolved structures of 13-oxobaccatin III (**3.19**), 13-*O*-acetylbaccatin III (**3.35**), and baccatin III (**3.16**) within the *m*TBT active site resulted from MD simulations. The catalytic residues His158 and Trp358 are shown in relevant positions with the taxane and CoA (partial) substrates (green) (Figure 3.153 of the appendix). The carbon skeletons of the modeled (A) **3.19** (the A/B/C-rings are noted), (B) **3.35**, and (C) **3.16** highlight the intramolecular distance between the functional groups at C13 and C4. The other functional groups are removed for clarity, and the curved arrows show rotation about acetate σ-bonds. Snapshots of the taxanes with the shortest distance (dotted lines) between the C2 ester carbon (black ball)-CoA sulfur (yellow ball) in (D) **3.19** (322), (E) **3.35** (293), and (F) **3.16** (95) within the MD simulation; the numbers in parentheses indicate the frame number when the minimum distance was observed. The C13 and C4 oxygen atoms are designated as balls. Heteroatoms are colored by standard conventions.

In contrast, the σ_{meta} for the 3-(methoxy) of **3.25c** is +0.12, and this value is consistent with the slower turnover of **3.25c** by *m*TBT at saturation compared to **3.25a** and **3.25b**. The coplanar conformation of the **3.25c** methoxy (i.e., the ether oxygen electrons are conjugated with the aromatic π-electrons) may also create undesired steric interactions that affect turnover by *m*TBT.[39] While the σ_{meta} values are not reported for 3-(trifluoromethoxy)- (**3.25d**) and 3-(difluoromethoxy)- (**3.25e**), we estimate them to be electron-withdrawing with σ_{meta} values greater than reported for

OCH_3 at +0.12, and thus able to stabilize the transition state better (Figure 3.9). These estimates are consistent with the superior (~10-fold) turnover numbers for **3.25d** and **3.25e** compared to **3.25c**. The fluoromethoxy groups of **3.25d** and **3.25e** are sterically more demanding than the hydrogens of the methoxy group of **3.25c**, but they assume a lower energy orthogonal conformation to the aryl ring.[39,40] Though this conformational switch removes resonance stabilization with the π-electrons, the electron-withdrawing properties needed to stabilize the proposed transition state of the *m*TBT benzoylation reaction are retained.

Table 3.3: Relative Kinetics of *m*TBT with 2-*O*-Debenzoyl-13-oxotaxane Analogs and *m*-Substituted Benzoyl CoA Analogs.

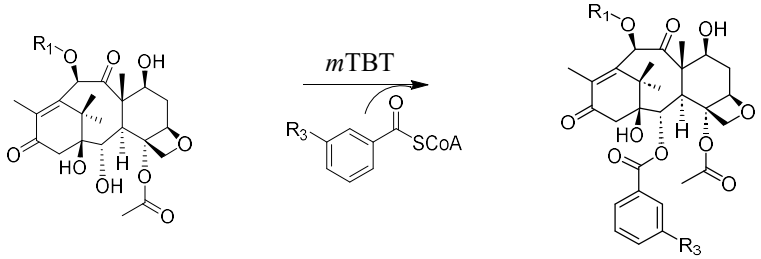

3.22, **3.23**, **3.24** **3.25** **3.26, 3.27, 3.28**

R_1	R_3	Exact mass (Da)	$[M+H]^+$ (*m*/*z*)	k_{cat} (min^{-1})	K_M (μM)	k_{cat}/K_M (s^{-1} M^{-1})
 **3.22→3.26**	**a**: F	602.22	603.23	13.6 ± 1.9	157 ± 15	1444
	b: Cl	618.19	619.20	10.8 ± 2.1	126 ± 12	1429
	c: OCH_3	614.24	615.25	1.6 ± 0.15	224 ± 19	119
	d: OCF_3	669.22	670.23	6.5 ± 1.1	144 ± 10	752
	e: $OCHF_2$	650.22	651.23	8.6 ± 2.2	108 ± 24	1327
	f: CF_3	652.21	653.22	0.4 ± 0.1	180 ± 21	37
 **3.23→3.27**	**a**: F	616.23	617.24	10.3 ± 2.2	164 ± 17	1047
	b: Cl	632.20	633.21	8.3 ± 1.3	146 ± 24	947
	c: OCH_3	628.25	629.26	0.8 ± 0.1	217 ± 12	61
	d: OCF_3	682.22	683.23	4.8 ± 1.6	151 ± 14	530
	e: $OCHF_2$	664.23	665.24	6.7 ± 1.1	115 ± 34	971
	f: CF_3	666.23	667.24	0.3 ± 0.1	195 ± 21	26
 **3.24→3.28**	**a**: F	628.23	629.24	8.3 ± 1.2	172 ± 16	804
	b: Cl	644.20	645.21	6.1 ± 1.3	137 ± 11	742
	c: OCH_3	640.25	641.26	0.5 ± 0.1	235 ± 12	35
	d: OCF_3	694.22	695.23	3.8 ± 0.5	162 ± 18	391
	e: $OCHF_2$	676.23	677.24	4.7 ± 0.8	120 ± 28	653
	f: CF_3	678.23	679.24	0.2 ± 0.1	176 ± 16	19

*m*TBT catalysis was highly selective for 2-*O*-debenzoylation of taxane substrates that were rebenzoylated by *m*TBT with non-natural *m*-substituted (F, Cl, OCH_3, OCF_3, and $OCHF_2$) benzoyl groups at C2. This biocatalytic approach described provides an alternative route to produce important intermediates to a new class of next-generation anticancer taxoids that reduces the use of environmentally toxic chemical reagents.

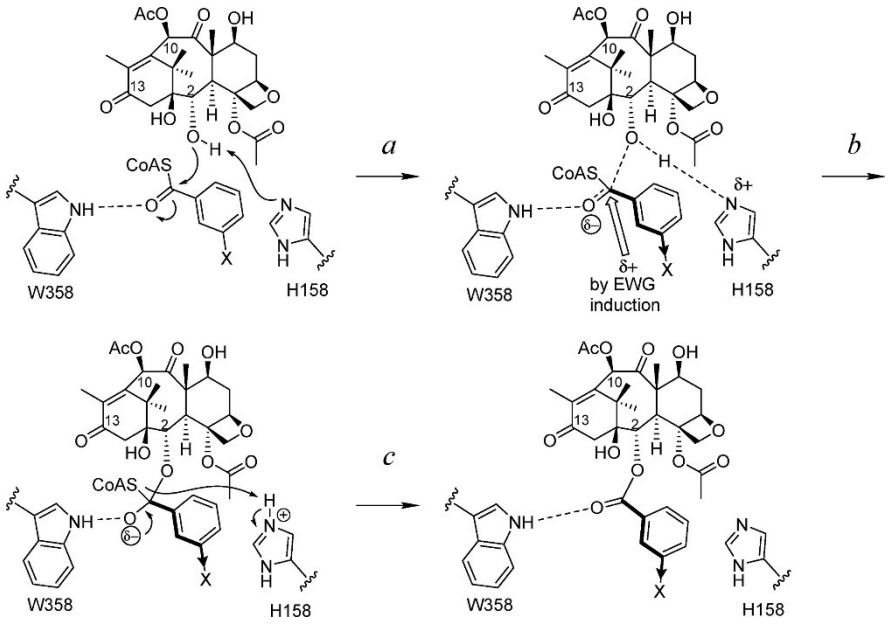

Figure 3.12: The proposed catalytic mechanism for the benzoyl transfer reaction catalyzed *m*TBT; this process is based on the homologous hydroxycinnamoyl transferase characterized by X-ray crystallography and biochemical analyses.[35] X is an electron-withdrawing group (EWG) m-substituent of the aryl CoA substrate. Catalytic residues W358 and His158 of *m*TBT are shown benzoylating the taxane substrate **3.22**.

Conclusion

*m*TBT catalysis was highly selective for 2-*O*-debenzoylation and 2-*O*-aroylation of 13-oxobaccatin III substrates with non-natural m-substituted (F, Cl, OCH_3, OCF_3, and $OCHF_2$) benzoyl groups. This biocatalytic approach provides an alternative route to produce important intermediates toward a new class of next-generation anticancer taxoids that reduces the use of environmentally toxic chemical reagents. Future studies will incorporate a permissive benzoyl

CoA ligase, used in previous studies,[41,42] to bypass synthesizing the thioesters and access the benzoylated taxanes in a coupled enzyme assay. In addition, the results of this biocatalytic study help narrow the location of the 2-*O*-benzoylation step on the overall paclitaxel biosynthetic pathway. Many purported genes on the biosynthetic pathway have been expressed and characterized, including *m*TBT,[43,44] which is proposed to function later the pathway. The pathway begins with the converting geranylgeranyl diphosphate (**3.39**) to taxa-4(5),11(12)-diene (**3.40**) followed by several hydroxylations/oxidations, *O*-acylations, oxetane formation, side chain assembly and attachment at C-13 to complete the sequence (Figure 3.10). *m*TBT is positioned on a step that benzoylates an advance 2-O-debenzoyl taxane (such as **3.54**), but the results of the present study suggest that **3.54**, with a 13-hydroxyl group, is likely not a productive substrate.

*m*TBT was initially characterized in an earlier study using a surrogate substrate 7,13-diacetyl-2-*O*-debenzoylbaccatin III (**3.55**),[45] which was not a logical precursor of the well-characterized downstream metabolites (10-DAB (**3.1**) or baccatin III (**3.16**)) that lack C7 and C13 acetates (Figure 5). The molecular dynamics and kinetics results of this study suggest that the 13-acetyl group of **3.56** slows the *m*TBT turnover rate due to unfavorable steric interactions between the substrate and the catalytic residues of *m*TBT. Converting the C13 functional group to a keto likely reduces these steric interactions so the substrate can adopt a catalytic competent orientation. Further, an earlier binding study on a Taxus 7β-hydroxylase with substituted taxoids[46] showed that the 2-*O*-acyltaxoids (**3.52** and **3.53**, Figure 3.10) bind relatively poorer to the hydroxylase compared to a 2-deoxytaxane, taxusin (**3.48**).

These data suggested that the 7β-hydroxylation occurs before C2 hydroxylation and 2-*O*-(acetyl/benzoyl)ation. Therefore, considering the data from the earlier study and the data described in this study, the 2-*O*-benzoylation step on the paclitaxel biosynthetic pathway is postulated to

occur after 2α- and 7β-hydroxylation yet before 13α-hydroxylation. Despite the presumed order of oxygenations based on a survey of known taxoids,[44,46] earlier biosynthetic analyses suggest that paclitaxel biosynthesis is not a linear pathway, and several branch points occur mid-pathway, potentially yielding multiple products (see Figure 3.10 at **3.42**, **3.44**, and **3.46**) that likely lead to other related taxoids that are not on the paclitaxel pathway.[46] The complexity of the oxygenation and acylation patterns seen in the taxoids is likely due to the permissivity of the enzymes that acylate and deacylate metabolites.[13,47] Therefore, apparent dead-end routes, such as multi-acetylated intermediates (**3.48**, **3.49**, and **3.51**), are encountered when arranging known taxane structures on a linear path to paclitaxel. Therefore, the interpretations of *in vitro* assays employing a limited set of available test substrate(s) and protein catalysts expressed from genes isolated from *Taxus* plants can be misleading.

The isolation and identification of an actual substrate(s) needed to characterize each mid-pathway step may remain elusive, mainly if the metabolite is at a low concentration in its natural resource or heterologous expression system. In addition, without these key substrates, it is not easy to know whether the cDNA encoding the enzymes has been identified.[48-50] While the position of the 2-*O*-benzoylation on the overall paclitaxel biosynthetic pathway cannot be precisely pinpointed, the described results help narrow the positioning. It is thus advantageous to continue biocatalytically testing and characterizing more taxane metabolites to understand the pathway organization and the regulation that will help craft the biotechnological production of more efficacious taxane analogs.

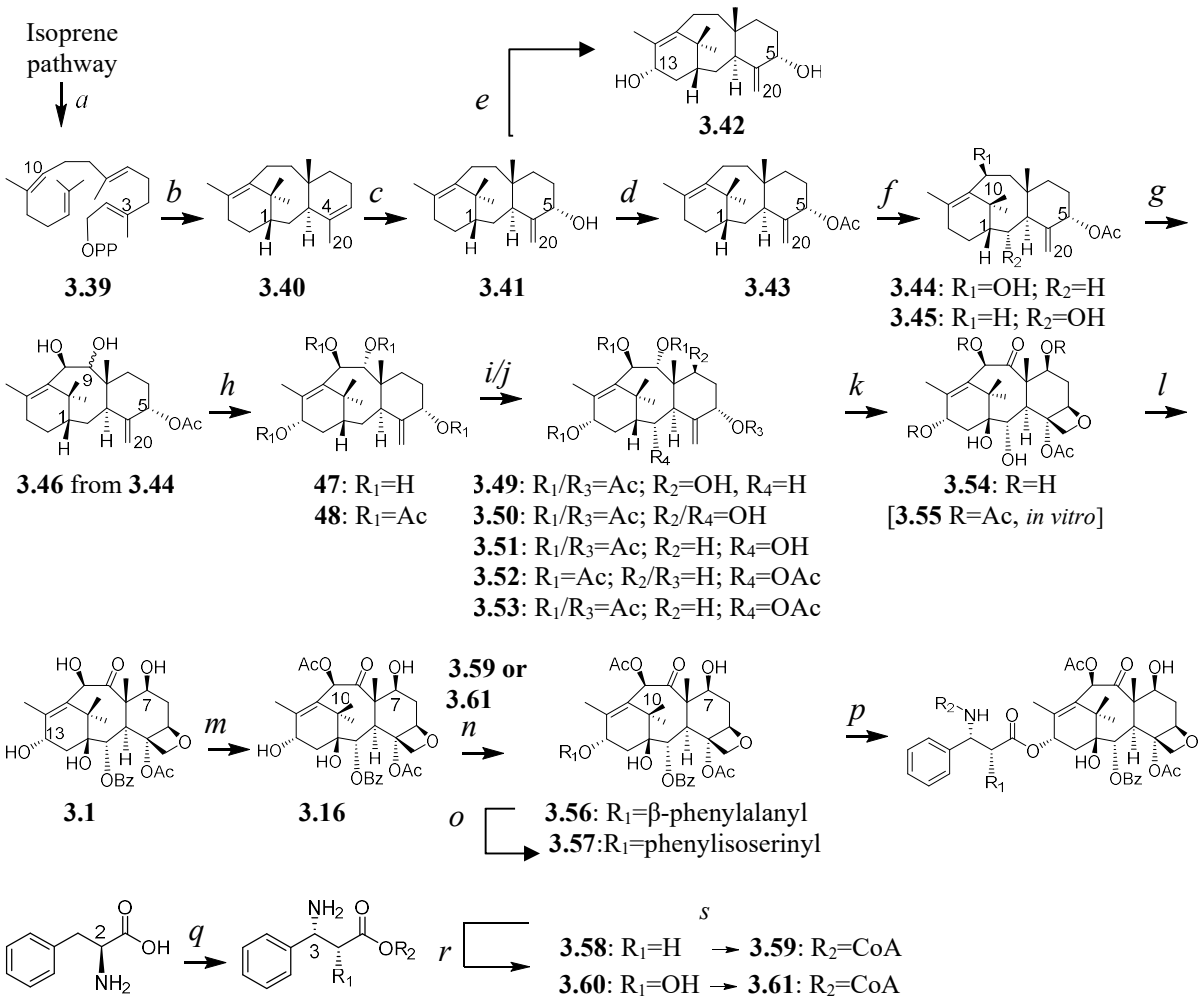

Figure 3.13: Proposed paclitaxel biosynthetic. Step a: geranylgeranyl diphosphate synthase; b: taxadiene synthase; c:taxadiene 5α-hydroxylase; d: taxa-4-(20),11(12)-diene-5α-ol-*O* acetyltransferase; e: taxane 13α-hydroxylase; f: taxane 10β-hydroxylase or taxane 2α-hydroxylase; g: taxane 9α/β-hydroxylase; h: taxane 13α-hydroxylase i: taxane 7β-hydroxylase; j: taxane 2α-hydroxylase; k: unknown sequence; l: 2-*O*-debenzoyl-7,13-*O*,*O*-diacetylbaccatin III-2α-*O*-benzoyltransferase (mTBT); m: 10-*O*-deacetylbaccatin III-10β-*O*-acetyltransferase n: baccatin III-13α-*O*-phenylpropanoyltransferase; o: unknown phenylpropanoyl hydroxylase (timing unknown); p:3'-*N*-benzoyltransferase; q: phenylalanine aminomutase; r: unknown phenylpropanoyl hydroxylase (timing unknown); s: unknown Taxus phenylpropanoyl CoA ligase. Geranylgeranyl diphosphate (**3.39**); Taxa-4(5),11(12)-diene (**3.40**); Taxa-4(20),11(12)-dien-5α-ol (**3.41**); Taxa-4(20),11(12)-dien-5α,13α-diol (**3.42**); Taxa-4(20),11(12)-dien-5α-yl-acetate (**3.43**); 5α-Acetoxytaxa-4(20),11(12)-dien-10β-ol (**3.44**); 5α-Acetoxytaxa-4(20),11(12)-dien-2α-ol (**3.45**); 5α-Acetoxytaxa-4(20),11(12)-dien-9α/β,10β-diol (**3.46**); taxusin tetraol; (**3.47**); Taxusin (**3.48**); 7β-Hydroxytaxusin (3.**49**); 2α-Hydroxytaxusin (**3.51**); 2α,7β-Dihydroxytaxusin (**3.50**); -Debenzoyl-10-deacetylbaccatin III (**3.54**); N-debenzoyl-2'-deoxypaclitaxel (3.**56**); N-debenzoyl-2'-deoxypaclitaxel (**3.57**); S-α-phenylalanine (**3.58**); R-β-phenylalanine (**3.60**); R-β-phenylalanyl CoA (**3.59**); (2S,3R)-phenylisoserinyl CoA (**3.61**).

REFERENCES

(1) Ojima, I.; Wang, X.; Jing, Y.; Wang, C. Quest for Efficacious Next-Generation Taxoid Anticancer Agents and Their Tumor-Targeted Delivery. *J. Nat. Prod.* **2018**, *81*, 703-721.

(2) Wang, C.; Wang, X.; Sun, Y.; Taouil, A. K.; Yan, S.; Botchkina, G. I.; Ojima, I. Design, synthesis and SAR study of 3rd-generation taxoids bearing 3-CH_3, 3-CF_3O and 3-CHF_2O groups at the C2-benzoate position. *Bioorg. Chem.* **2020**, *95*, 103523.

(3) Kuznetsova, L.; Sun, L.; Chen, J.; Zhao, X.; Seitz, J.; Das, M.; Li, Y.; Veith, J. M.; Pera, P.; Bernacki, R. J.; Xia, S.; Horwitz, S. B.; Ojima, I. Synthesis and biological evaluation of novel 3′-difluorovinyl taxoids. *J. Fluor. Chem.* **2012**, *143*, 177-188.

(4) Ojima, I.; Chen, J.; Sun, L.; Borella, C. P.; Wang, T.; Miller, M. L.; Lin, S.; Geng, X.; Kuznetsova, L.; Qu, C.; Gallager, D.; Zhao, X.; Zanardi, I.; Xia, S.; Horwitz, S. B.; Mallen-St. Clair, J.; Guerriero, J. L.; Bar-Sagi, D.; Veith, J. M.; Pera, P.; Bernacki, R. J. Design, Synthesis, and Biological Evaluation of New-Generation Taxoids. *J. Med. Chem.* **2008**, *51*, 3203-3221.

(5) Wang, C.; Chen, L.; Sun, Y.; Guo, W.; Taouil, A. K.; Ojima, I. Design, synthesis and SAR study of Fluorine-containing 3rd-generation taxoids. *Bioorg. Chem.* **2022**, *119*, 105578.

(6) Jayanetti, K.; Takemura, K.; Bendale, H.; Garg, A.; Ojima, I. Recent advances in the strategic incorporation of fluorine into new-generation taxoid anticancer agents. *J. Fluor. Chem.* **2023**, *267*, 110106.

(7) Wang, T.; Zhang, Y.; Wei, L.; Teng, Y. G.; Honda, T.; Ojima, I. Design, Synthesis, and Biological Evaluations of Asymmetric Bow-Tie PAMAM Dendrimer-Based Conjugates for Tumor-Targeted Drug Delivery. *ACS Omega.* **2018**, *3*, 3717-3736.

(8) Tian, J.; Stella, V. J. Degradation of paclitaxel and related compounds in aqueous solutions II: Nonepimerization degradation under neutral to basic pH conditions. *J. Pharm. Sci.* **2008**, *97*, 3100-3108.

(9) Kingston, D. G.; Chaudhary, A. G.; Chordia, M. D.; Gharpure, M.; Gunatilaka, A. A.; Higgs, P. I.; Rimoldi, J. M.; Samala, L.; Jagtap, P. G.; Giannakakou, P.; Jiang, Y. Q.; Lin, C. M.; Hamel, E.; Long, B. H.; Fairchild, C. R.; Johnston, K. A. Synthesis and biological evaluation of 2-acyl analogues of paclitaxel (Taxol). *J. Med. Chem.* **1998**, *41*, 3715-3726.

(10) Samaranayake, G.; Neidigh, K. A.; Kingston, D. G. Modified taxols, 8. Deacylation and reacylation of baccatin III. *J. Nat. Prod.* **1993**, *56*, 884-898.

(11) Chen, S.-H.; Kadow, J. F.; Farina, V.; Fairchild, C. R.; Johnston, K. A. First Syntheses of Novel Paclitaxel(Taxol) Analogs Modified at the C4-Position. *J. Org. Chem.* **1994**, *59*, 6156-6158.

(12) Chen, S.-H.; Farina, V.; Vyas, D. M.; Doyle, T. W.; Long, B. H.; Fairchild, C. Synthesis

and Biological Evaluation of C-13 Amide-Linked Paclitaxel (Taxol) Analogs. *J. Org. Chem.* **1996**, *61*, 2065-2070.

(13) Ondari, M. E.; Walker, K. D. The Taxol Pathway 10-*O*-Acetyltransferase Shows Regioselective Promiscuity with the Oxetane Hydroxyl of 4-Deacetyltaxanes. *J. Am. Chem. Soc.* **2008**, *130*, 17187-17194.

(14) Lokman, M.; Ashraf, E.; Kassab, R. B.; Abdel Moneim, A. E.; El-Yamany, N. A. Aluminum Chloride-Induced Reproductive Toxicity in Rats: the Protective Role of Zinc Oxide Nanoparticles. *Biol. Trace Elem. Res.* **2022**, *200*, 4035-4044.

(15) Liu, J.; Wang, Q.; Sun, X.; Yang, X.; Zhuang, C.; Xu, F.; Cao, Z.; Li, Y. The Toxicity of Aluminum Chloride on Kidney of Rats. *Biol. Trace Elem. Res.* **2016**, *173*, 339-344.

(16) Chen, K.; Zhang, S. Q.; Brandenberg, O. F.; Hong, X.; Arnold, F. H. Alternate Heme Ligation Steers Activity and Selectivity in Engineered Cytochrome P450-Catalyzed Carbene-Transfer Reactions. *J. Am. Chem. Soc.* **2018**, *140*, 16402-16407.

(17) Brandenberg, O. F.; Fasan, R.; Arnold, F. H. Exploiting and engineering hemoproteins for abiological carbene and nitrene transfer reactions. *Curr. Opin. Biotechnol.* **2017**, *47*, 102-111.

(18) Li, Y.; Li, S.; Thodey, K.; Trenchard, I.; Cravens, A.; Smolke, C. D. Complete biosynthesis of noscapine and halogenated alkaloids in yeast. *Proc. Natl. Acad. Sci. U.S.A.* **2018**, *115*, E3922-E3931.

(19) Yi, D.; Bayer, T.; Badenhorst, C. P. S.; Wu, S.; Doerr, M.; Hohne, M.; Bornscheuer, U. T. Recent trends in biocatalysis. *Chem. Soc. Rev.* **2021**, *50*, 8003-8049.

(20) Teufel, R.; Kaysser, L.; Villaume, M. T.; Diethelm, S.; Carbullido, M. K.; Baran, P. S.; Moore, B. S. One-pot enzymatic synthesis of merochlorin A and B. *Angew. Chem. Int. Ed.* **2014**, *53*, 11019-11022.

(21) Ojima, I.; Fumero-Oderda, C. L.; Kuduk, S. D.; Ma, Z.; Kirikae, F.; Kirikae, T. Structure–activity relationship study of taxoids for their ability to activate murine macrophages as well as inhibit the growth of macrophage-like cells. *Bioorg. Med. Chem.* **2003**, *11*, 2867-2888.

(22) Baloglu, E.; Kingston, D. G. I. A New Semisynthesis of Paclitaxel from Baccatin III. *J. Nat. Prod.* **1999**, *62*, 1068-1071.

(23) Nevarez, D. M.; Mengistu, Y. A.; Nawarathne, I. N.; Walker, K. D. An N-Aroyltransferase of the BAHD Superfamily Has Broad Aroyl CoA Specificity in Vitro with Analogues of N-Dearoylpaclitaxel. *J. Am. Chem. Soc.* **2009**, *131*, 5994-6002.

(24) Nawarathne, I. N.; Walker, K. D. Point Mutations (Q19P and N23K) Increase the

Operational Solubility of a 2α-*O*-Benzoyltransferase that Conveys Various Acyl Groups from CoA to a Taxane Acceptor. *J. Nat. Prod.* **2010**, *73*, 151-159.

(25) Taylor, G. F.; Thornton, S. S.; Tallent, C. R.; Kepler, J. A. Synthesis of [3″-3H]taxol and [13-3H]taxol1. *J. Labelled Comp. Radiopharm.* **1993**, *33*, 501-515.

(26) Frisch, M. J.; Trucks, G. W.; Schlegel, H. B.; Scuseria, G. E.; Robb, M. A.; Cheeseman, J. R.; Scalmani, G.; Barone, V.; Petersson, G. A.; Nakatsuji, H.; Li, X.; Caricato, M.; Marenich, A. V.; Bloino, J.; Janesko, B. G.; Gomperts, R.; Mennucci, B.; Hratchian, H. P.; Ortiz, J. V.; Izmaylov, A. F.; Sonnenberg, J. L.; Williams; Ding, F.; Lipparini, F.; Egidi, F.; Goings, J.; Peng, B.; Petrone, A.; Henderson, T.; Ranasinghe, D.; Zakrzewski, V. G.; Gao, J.; Rega, N.; Zheng, G.; Liang, W.; Hada, M.; Ehara, M.; Toyota, K.; Fukuda, R.; Hasegawa, J.; Ishida, M.; Nakajima, T.; Honda, Y.; Kitao, O.; Nakai, H.; Vreven, T.; Throssell, K.; Montgomery Jr., J. A.; Peralta, J. E.; Ogliaro, F.; Bearpark, M. J.; Heyd, J. J.; Brothers, E. N.; Kudin, K. N.; Staroverov, V. N.; Keith, T. A.; Kobayashi, R.; Normand, J.; Raghavachari, K.; Rendell, A. P.; Burant, J. C.; Iyengar, S. S.; Tomasi, J.; Cossi, M.; Millam, J. M.; Klene, M.; Adamo, C.; Cammi, R.; Ochterski, J. W.; Martin, R. L.; Morokuma, K.; Farkas, O.; Foresman, J. B.; Fox, D. J.: Gaussian 16 Rev. C.01. Wallingford, CT, **2016**.

(27) Case, D.; Aktulga, H. M.; Belfon, K.; Ben-Shalom, I.; Berryman, J.; Brozell, S.; Cerutti, D.; Cheatham, T.; Cisneros, G. A.; Cruzeiro, V.; Darden, T.; Duke, R.; Giambasu, G.; Gilson, M.; Gohlke, H.; Götz, A.; Harris, R.; Izadi, S.; Izmailov, S.; Kollman, P.: *Amber 2022*, **2022**.

(28) Wang, J.; Wang, W.; Kollman, P. A.; Case, D. A. Automatic atom type and bond type perception in molecular mechanical calculations. *J. Mol. Graph. Model.* **2006**, *25*, 247-260.

(29) Loncharich, R. J.; Brooks, B. R.; Pastor, R. W. Langevin dynamics of peptides: the frictional dependence of isomerization rates of N-acetylalanyl-N'-methylamide. *Biopolymers* **1992**, *32*, 523-535.

(30) Berendsen, H. J. C.; Postma, J. P. M.; van Gunsteren, W. F.; DiNola, A.; Haak, J. R. Molecular dynamics with coupling to an external bath. *J. Chem. Phys.* **1984**, *81*, 3684-3690.

(31) Miyamoto, S.; Kollman, P. A. Settle: An analytical version of the SHAKE and RATTLE algorithm for rigid water models. *J. Comput. Chem.* **1992**, *13*, 952-962.

(32) Farina, V.; Huang, S. The chemistry of taxanes: unexpected rearrangement of baccatin III during chemoselective debenzoylation with Bu3SnOMe/LiCl. *Tetrahedron Lett.* **1992**, *33*, 3979-3982.

(33) Trott, O.; Olson, A. J. AutoDock Vina: Improving the speed and accuracy of docking with a new scoring function, efficient optimization, and multithreading. *J. Comput. Chem.* **2010**,

31, 455-461.

(34) Pettersen, E. F.; Goddard, T. D.; Huang, C. C.; Couch, G. S.; Greenblatt, D. M.; Meng, E. C.; Ferrin, T. E. UCSF Chimera--a visualization system for exploratory research and analysis. *J. Comput. Chem.* **2004**, *25*, 1605-1612.

(35) Levsh, O.; Chiang, Y. C.; Tung, C. F.; Noel, J. P.; Wang, Y.; Weng, J.-K. Dynamic Conformational States Dictate Selectivity toward the Native Substrate in a Substrate-Permissive Acyltransferase. *Biochem.* **2016**, *55 45*, 6314-6326.

(36) B:urgi, H. B.; Dunitz, J. D.; Lehn, J. M.; Wipff, G. Stereochemistry of reaction paths at carbonyl centres. *Tetrahedron.* **1974**, *30*, 1563-1572.

(37) Fernández, I.; Bickelhaupt, F. M.; Svatunek, D. Unraveling the Bürgi-Dunitz Angle with Precision: The Power of a Two-Dimensional Energy Decomposition Analysis. *J. Chem. Theory Comput.* **2023**, *19*, 7300-7306.

(38) Flynn, G. L. Substituent constants for correlation analysis in chemistry and biology. By Corwin Hansch and Albert Leo. Wiley, 605 Third Ave., New York, NY 10016. 1979. 339 pp. 21 × 28 cm. Price $24.95. *J. Pharm. Sci.* **1980**, *69*, 1109-1109.

(39) Sap, J. B. I.; Meyer, C. F.; Straathof, N. J. W.; Iwumene, N.; Am Ende, C. W.; Trabanco, A. A.; Gouverneur, V. Late-stage difluoromethylation: concepts, developments and perspective. *Chem. Soc. Rev.* **2021**, *50*, 8214-8247.

(40) Zafrani, Y.; Yeffet, D.; Sod-Moriah, G.; Berliner, A.; Amir, D.; Marciano, D.; Gershonov, E.; Saphier, S. Difluoromethyl Bioisostere: Examining the "Lipophilic Hydrogen Bond Donor" Concept. *J. Med. Chem.* **2017**, *60*, 797-804.

(41) Long, R. M.; Lagisetti, C.; Coates, R. M.; Croteau, R. B. Specificity of the N-benzoyl transferase responsible for the last step of Taxol biosynthesis. *Arch. Biochem. Biophys.* **2008**, *477*, 384-389.

(42) Cragg, G. M.; Kingston, D. G. I.; Newman, D. J. *Anticancer Agents from Natural Products*; CRC, **2005**, p 89-122.

(43) Malik, S.; Cusido, R. M.; Mirjalili, M. H.; Moyano, E.; Palazón, J.; Bonfill, M. Production of the anticancer drug taxol in Taxus baccata suspension cultures: A review. *Process Biochem.* **2011**, *46*, 23-34.

(44) Heinig, U.; Jennewein, S. Taxol: A complex diterpenoid natural product with an evolutionarily obscure origin. *Afr. J. Biotechnol.* **2009**, *8*, 1370-1385.

(45) Baloglu, E.; Kingston, D. G. The taxane diterpenoids. *J. Nat. Prod.* **1999**, *62*, 1448-1472.

(46) Kingston, D. G.; Jagtap, P. G.; Yuan, H.; Samala, L. The chemistry of taxol and related

taxoids. *Fortschritte der Chemie organischer Naturstoffe = Progress in the chemistry of organic natural products. Progres dans la chimie des substances organiques naturelles* **2002**, *84*, 53-225.

(47) Chau, M.; Walker, K.; Long, R.; Croteau, R. Regioselectivity of taxoid-O-acetyltransferases: heterologous expression and characterization of a new taxadien-5α-ol-O-acetyltransferase. *Arch. Biochem. Biophys.* **2004**, *430*, 237-246.

(48) Hampel, D.; Mau, C. J.; Croteau, R. B. Taxol biosynthesis: Identification and characterization of two acetyl CoA:taxoid-O-acetyl transferases that divert pathway flux away from Taxol production. *Arch. Biochem. Biophys.* **2009**, *487*, 91-97.

(49) Chau, M.; Croteau, R. Molecular cloning and characterization of a cytochrome P450 taxoid 2α-hydroxylase involved in Taxol biosynthesis. *Arch. Biochem. Biophys.* **2004**, *427*, 48-57.

(50) Horiguchi, T.; Rithner, C. D.; Croteau, R.; Williams, R. M. Studies on Taxol® Biosynthesis. Preparation and Tritium Labeling of Biosynthetic intermediates by Deoxygenation of a Taxadiene Tetra-acetate Obtained from Japanese Yew. *J. Labelled Comp. Radiopharm.* **2008**, *51*, 325-328.

APPENDIX B: CHAPTER 3 SUPPLEMENTARY MATERIALS

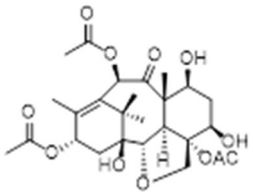

3.36
Furano-13-*O*-acetyl-2-*O*-debenzoylbaccatin III

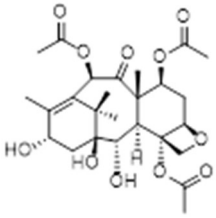

3.37
7-*O*-acetyl 2-*O*-debenzoyl-baccatin III

Figure 3.14: Structures of **3.36** and **3.37**, standards are used in the *m*TBT catalysis.These compounds were synthesized by Dr. Irosha N. Nawarathne (previous graduate student in Walker group, MSU).

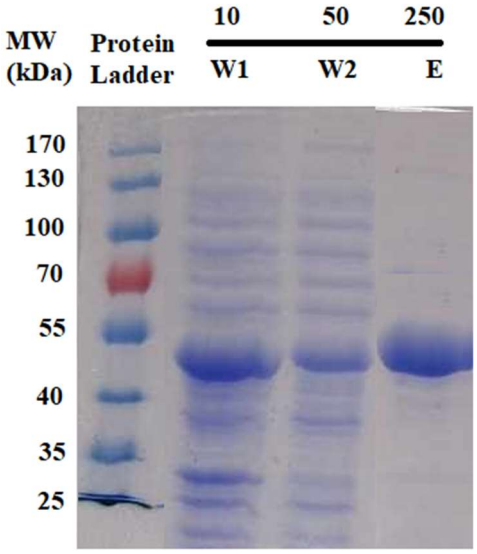

Figure 3.15: Coomassie Blue stained SDS-PAGE gel of aliquots from the fractions collected from Ni-NTA affinity exchange column used to purify the *m*TBT enzyme. Lanes represent protein contained in the Wash Buffer (**W1** and **W2**); and Elution Buffer (**E**) fractions. The numbers above the bar are the mM concentrations of imidazole in the respective buffers. Molecular weight references are in the leftmost lane.

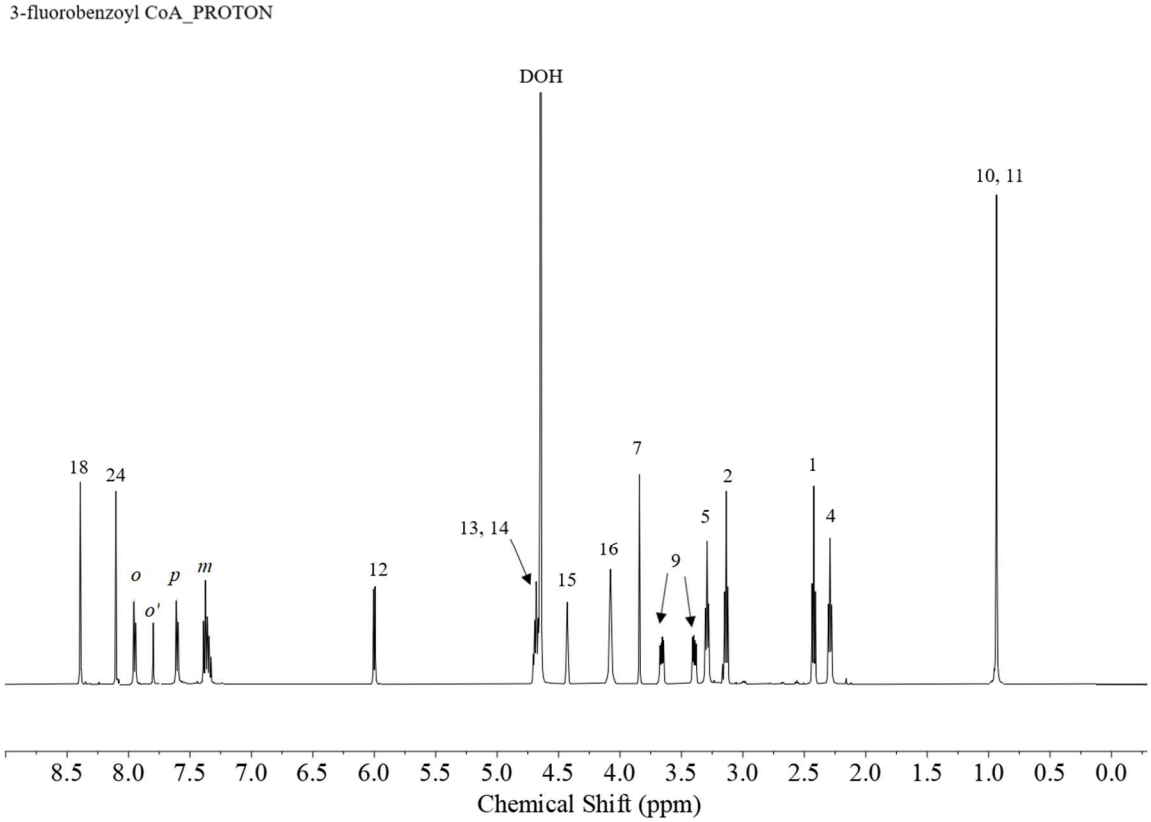

Figure 3.16: ^{1}H-NMR (500 MHz) of 3-F-benzoyl CoA.

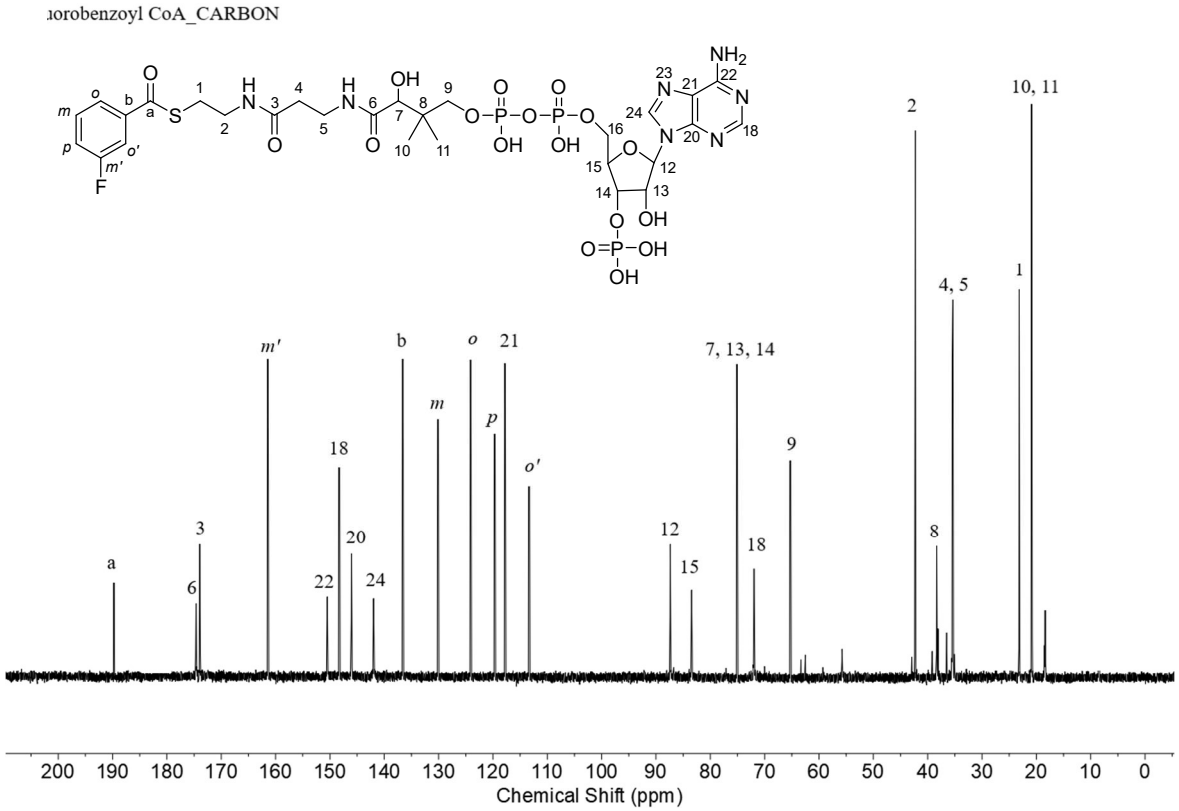

Figure 3.17: ^{13}C-NMR (126 MHz) of 3-F-benzoyl CoA.

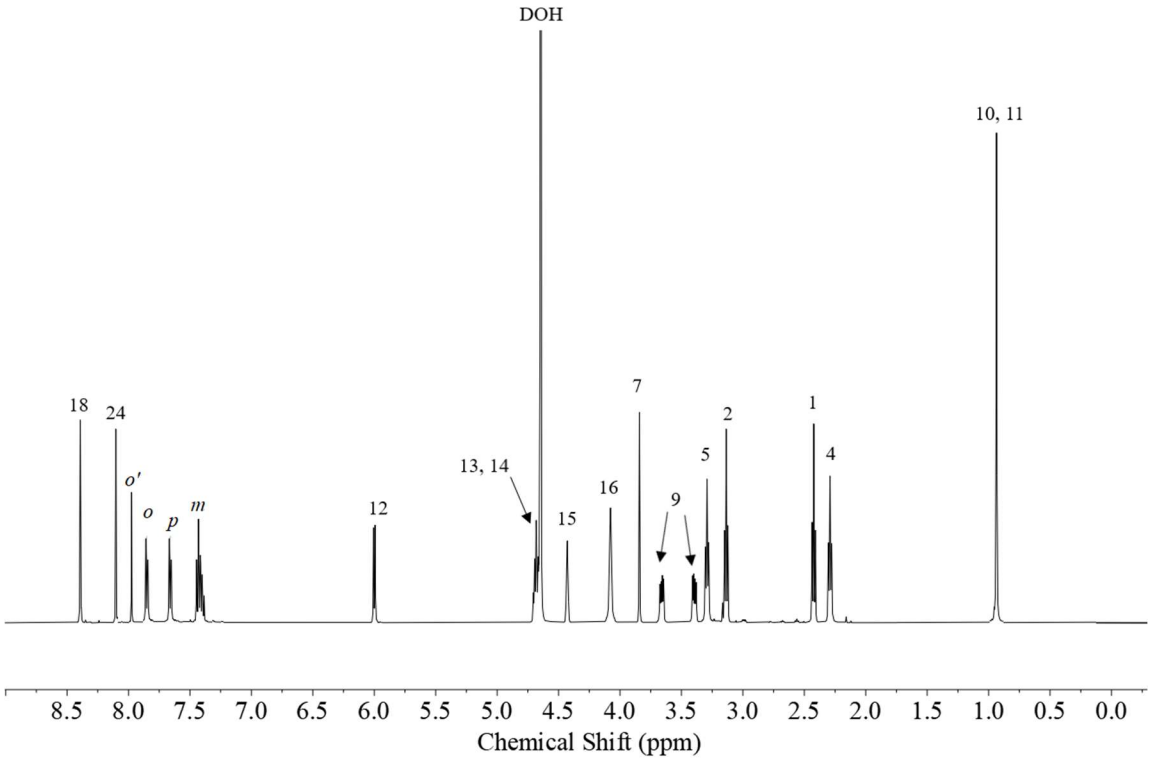

Figure 3.18: ^{1}H-NMR (500 MHz) of 3-Cl-benzoyl CoA.

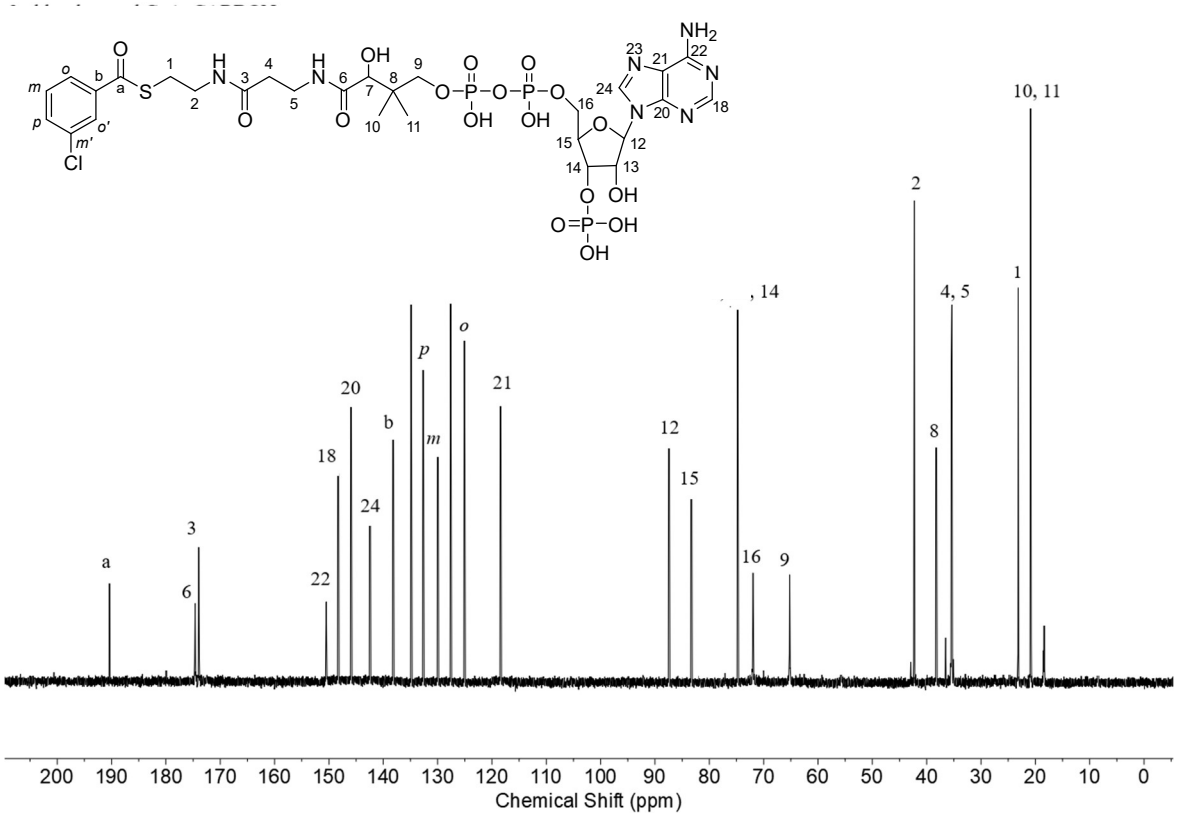

Figure 3.19: ^{13}C-NMR (126 MHz) of 3-Cl-benzoyl CoA.

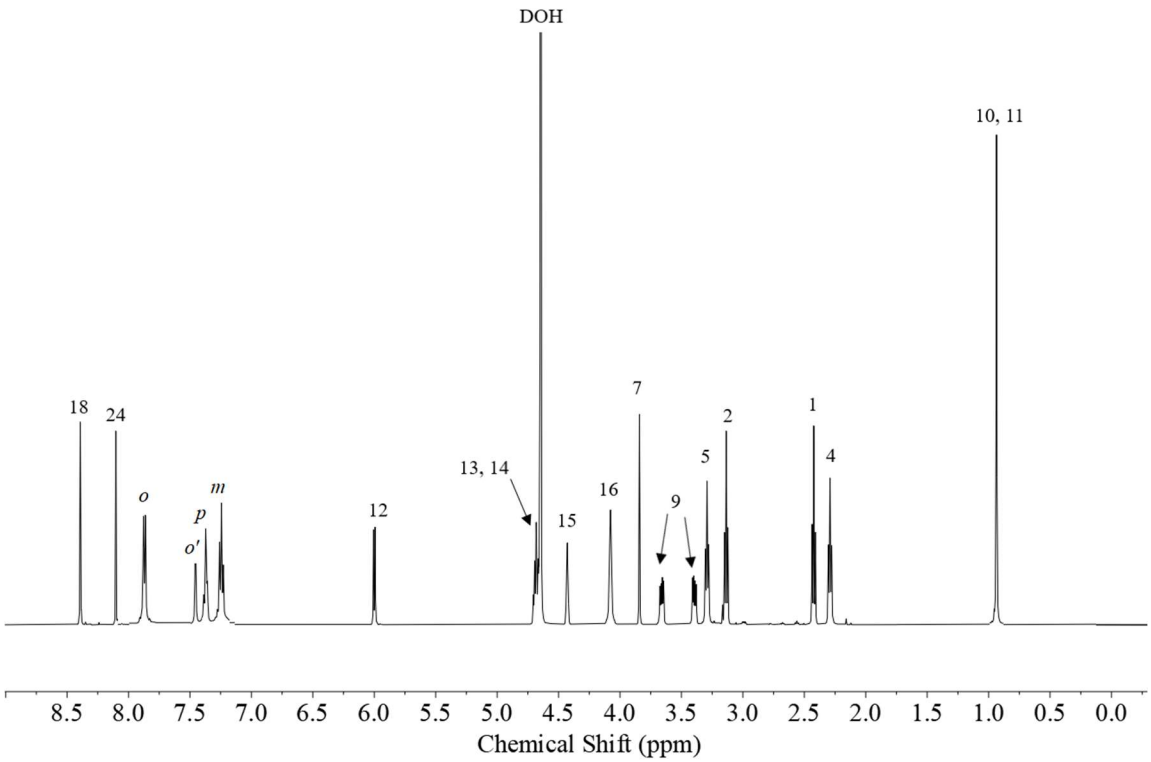

Figure 3.20: ^{1}H-NMR (500 MHz) of 3-(OCH_3)-benzoyl CoA.

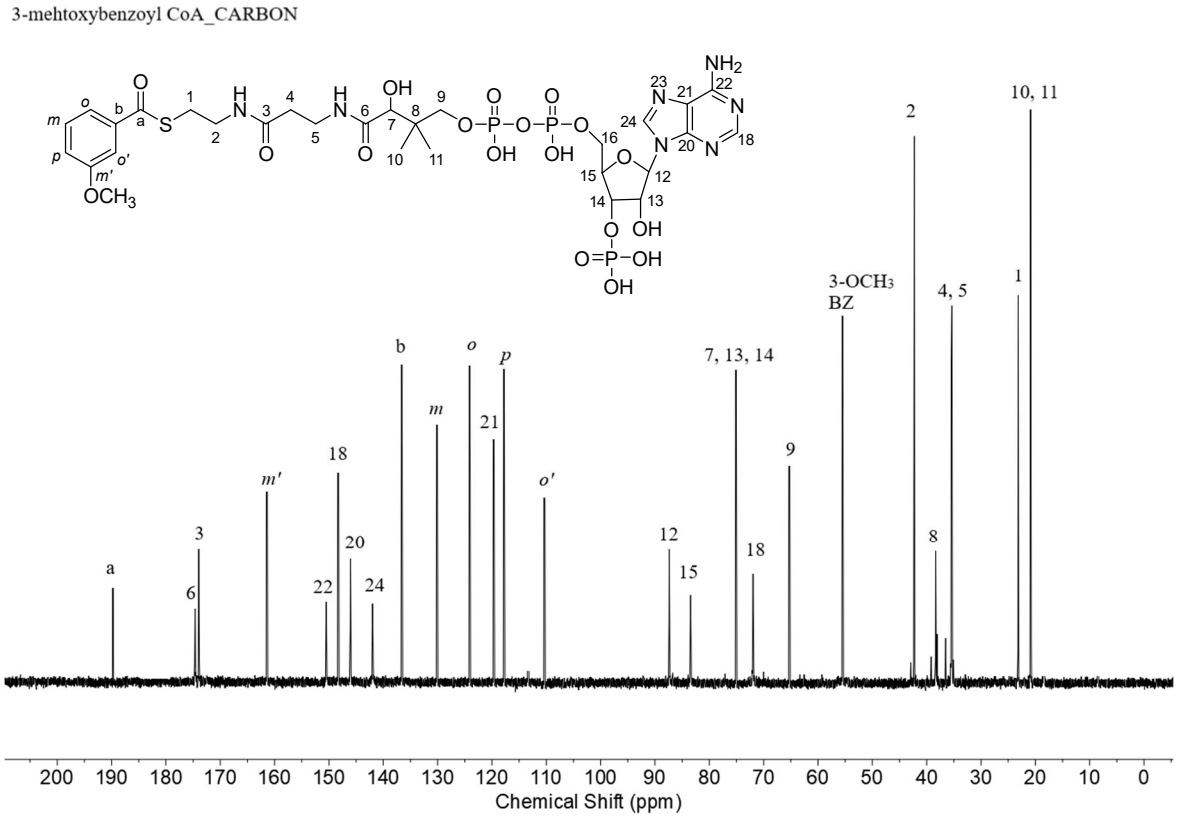

Figure 3.21: ^{13}C-NMR (126 MHz) of 3-(OCH_3)-benzoyl CoA.

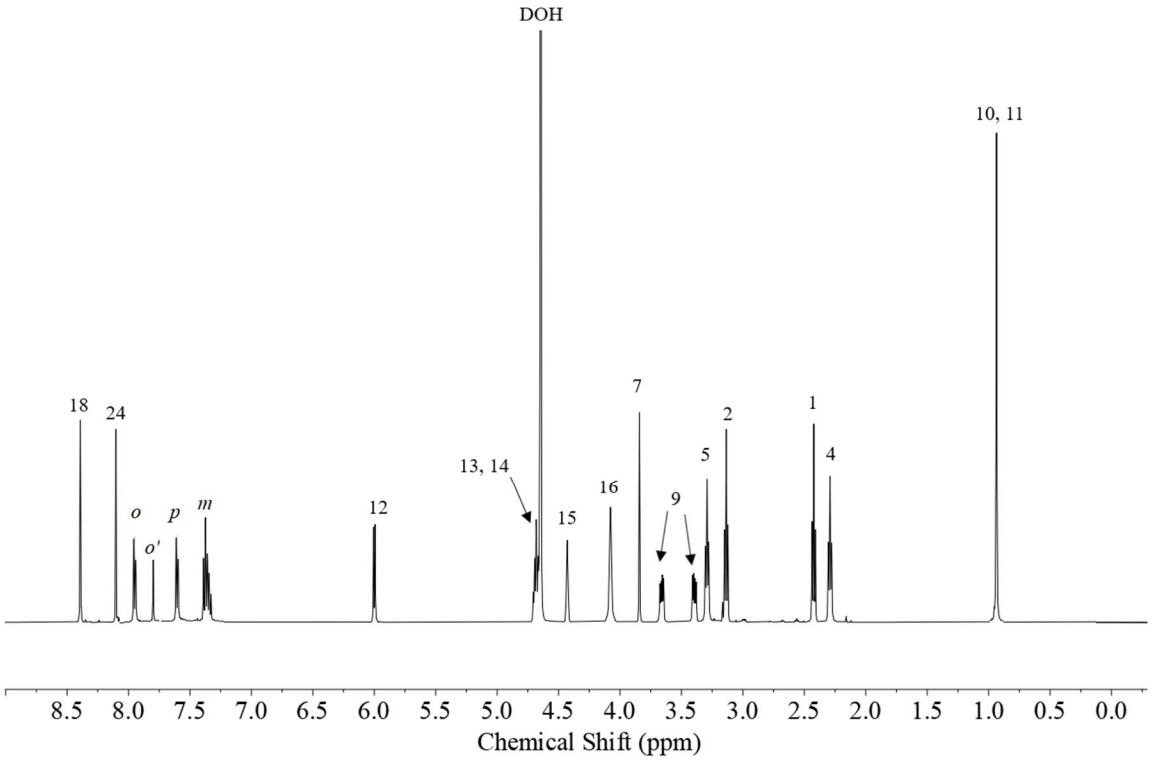

Figure 3.22: ^{1}H-NMR (500 MHz) of 3-(OCF_3)-benzoyl CoA.

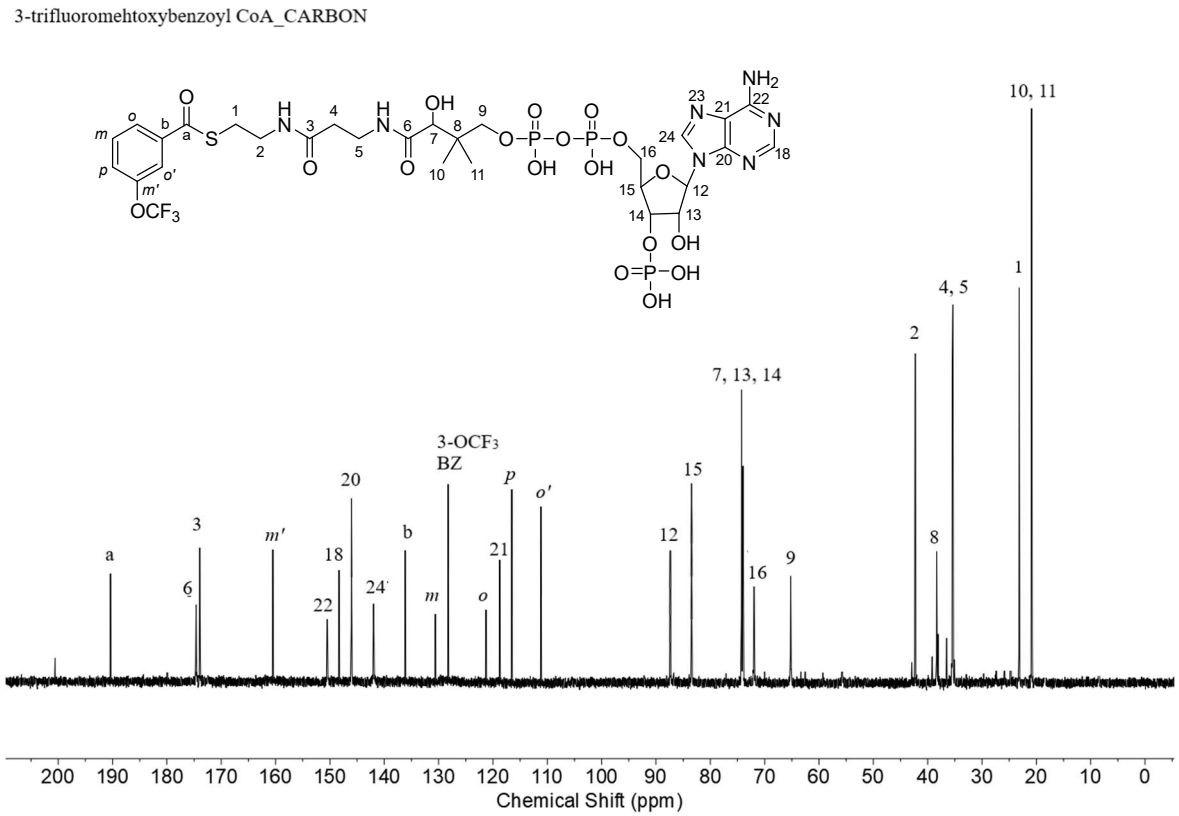

Figure 3.23: ^{13}C-NMR (126 MHz) of 3-(OCF_3)-benzoyl CoA.

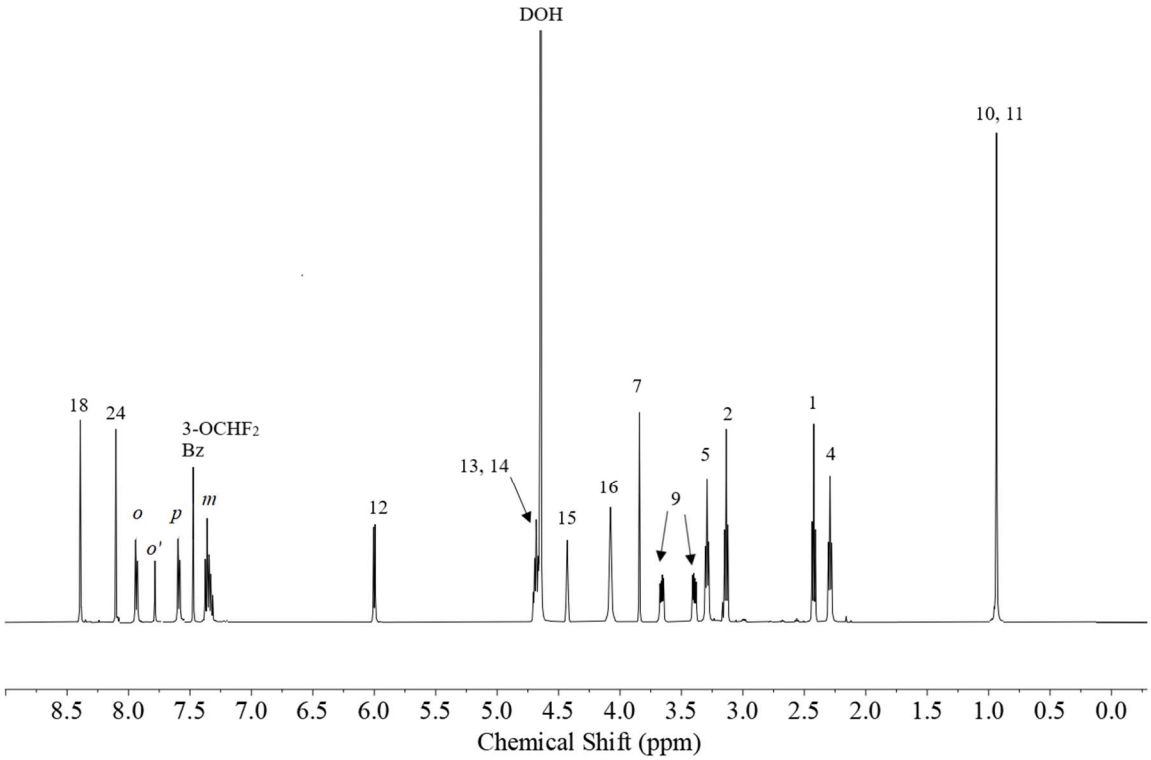

Figure 3.24: ^{1}H-NMR (500 MHz) of 3-($OCHF_2$)-benzoyl CoA.

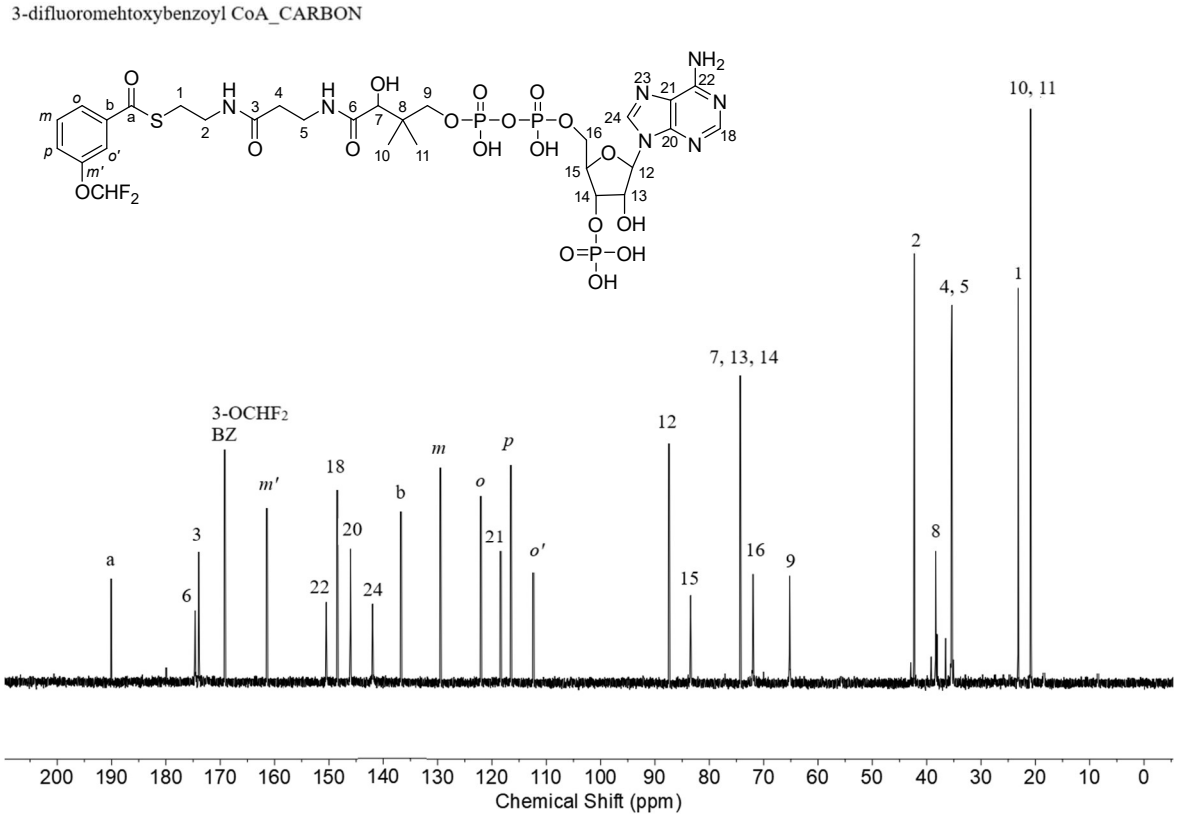

Figure 3.25: ^{13}C-NMR (126 MHz) of 3-($OCHF_2$)-benzoyl CoA.

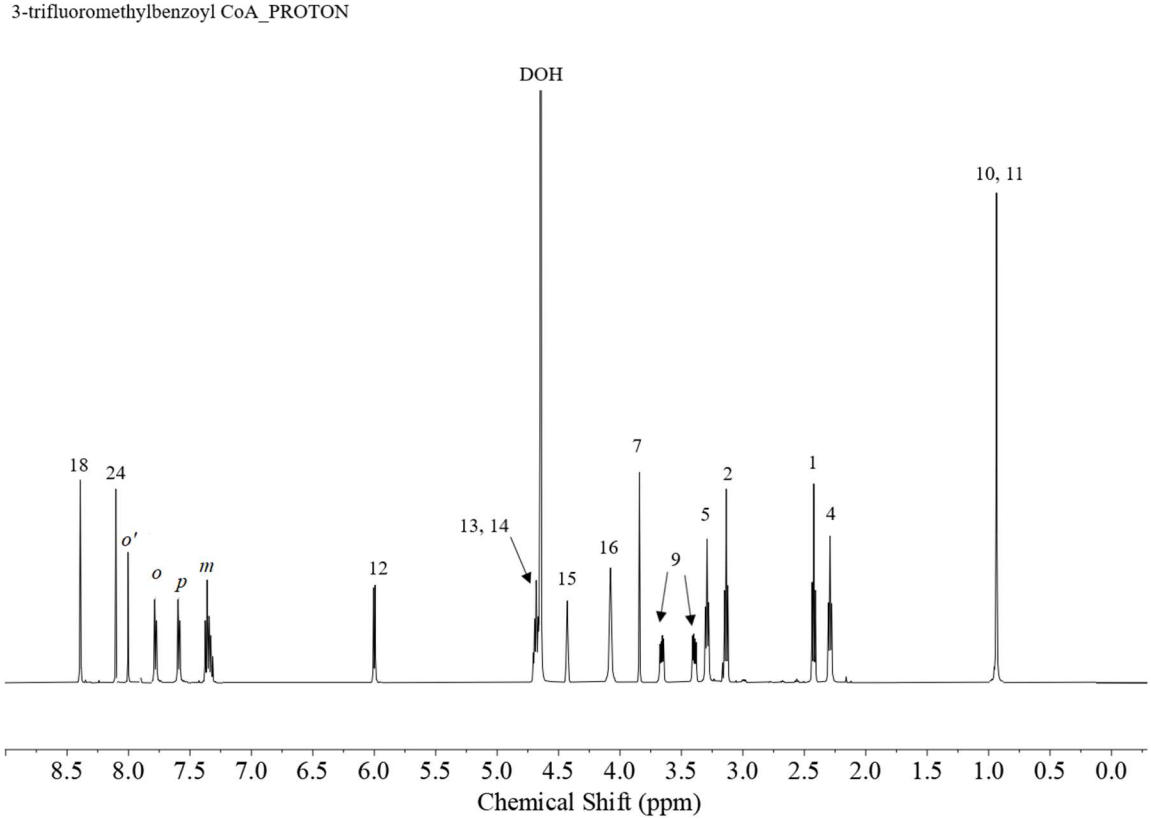

Figure 3.26: ^{1}H-NMR (500 MHz) of 3-(CF_3)-benzoyl CoA.

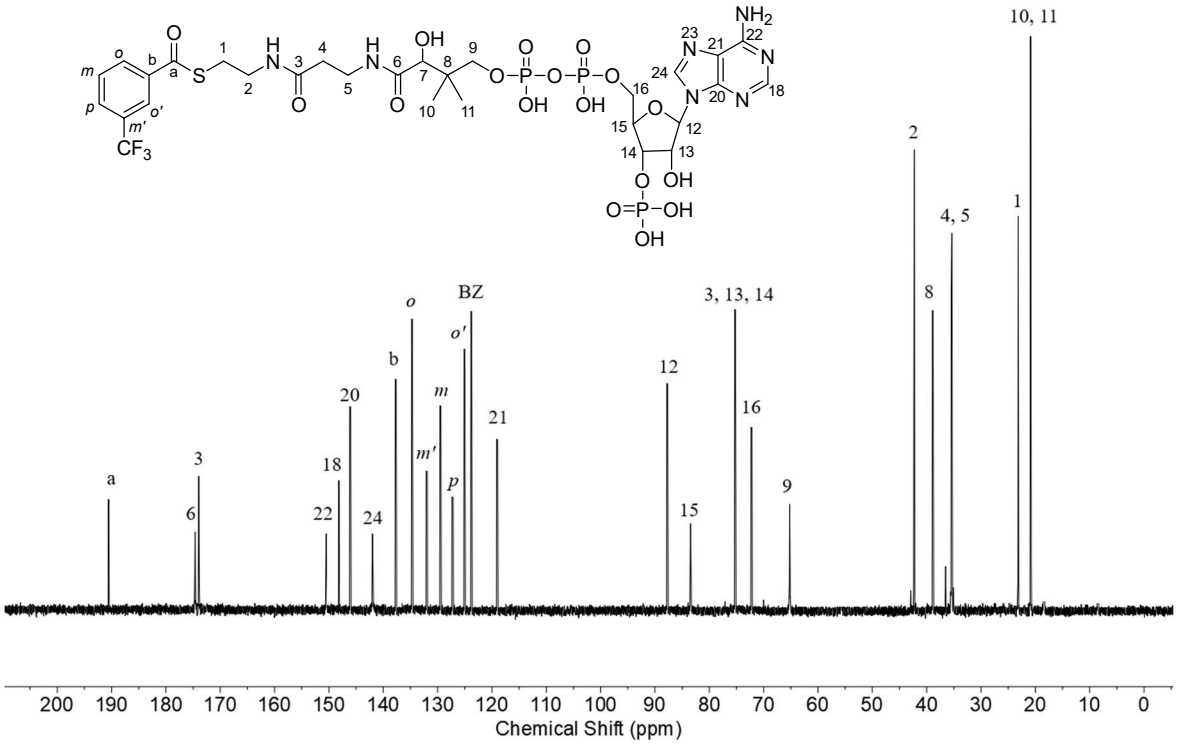

Figure 3.27: ^{13}C-NMR (126 MHz) of 3-(CF_3)-benzoyl CoA.

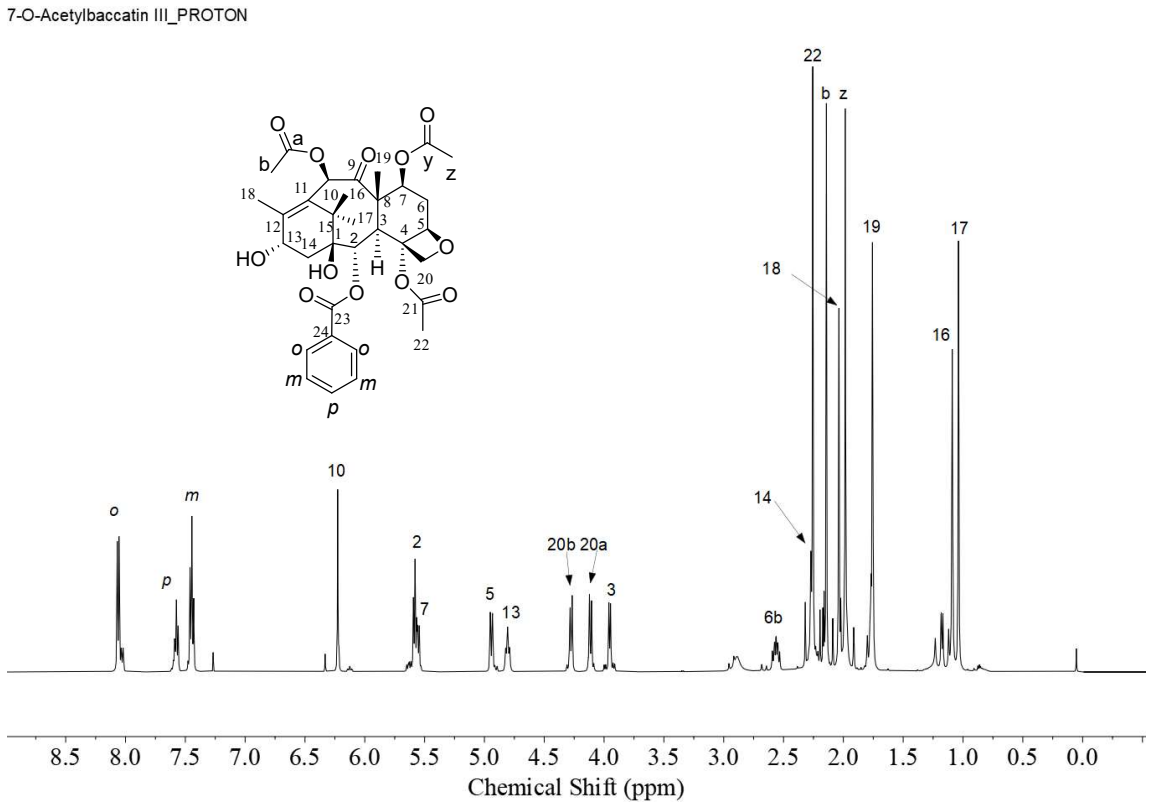

Figure 3.28: ^{1}H-NMR (500 MHz) of 7-*O*-acetylbaccatin III.

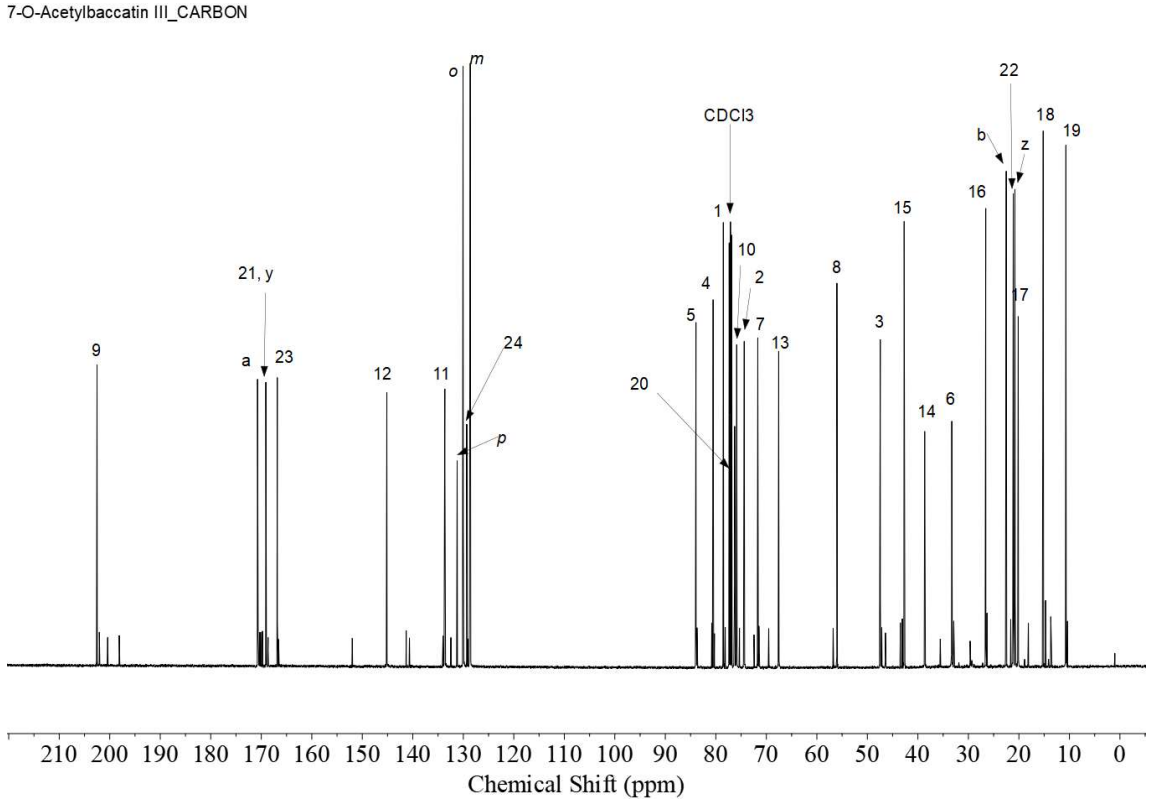

Figure 3.29: ^{13}C-NMR (126 MHz) of 7-*O*-acetylbaccatin III.

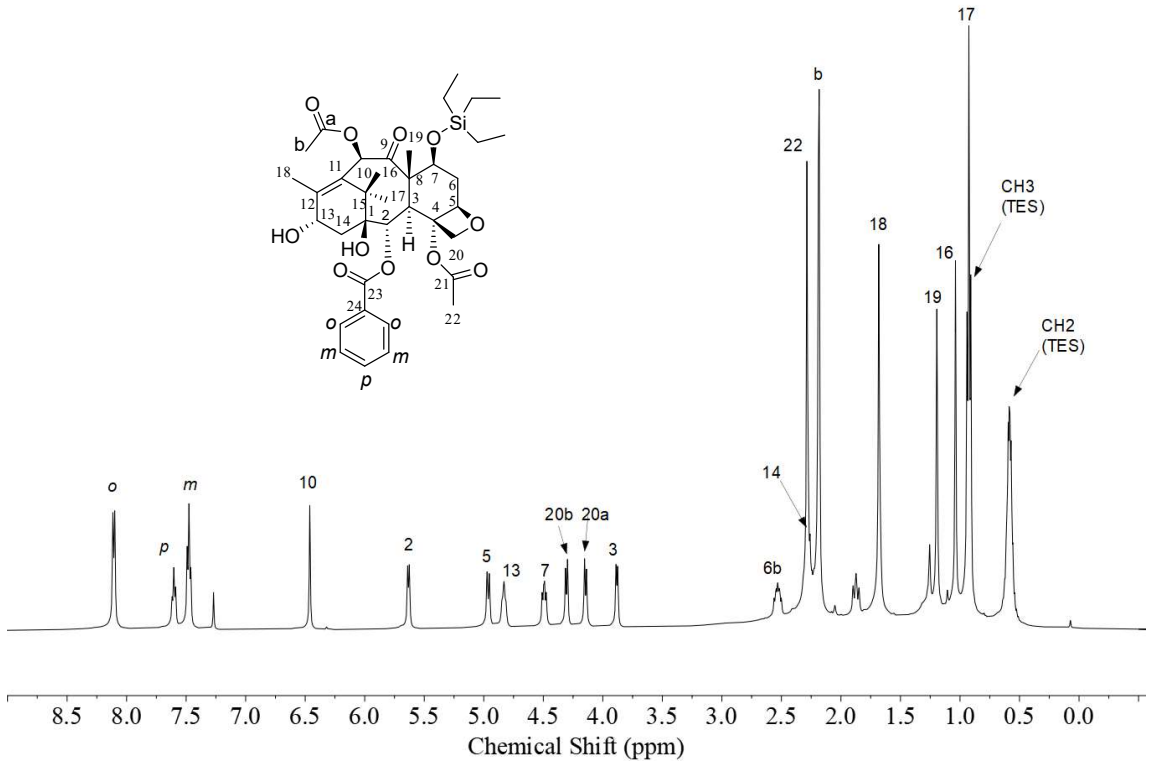

Figure 3.30: ^{1}H-NMR (500 MHz) of 7-*O*-triethylsilylbaccatin III.

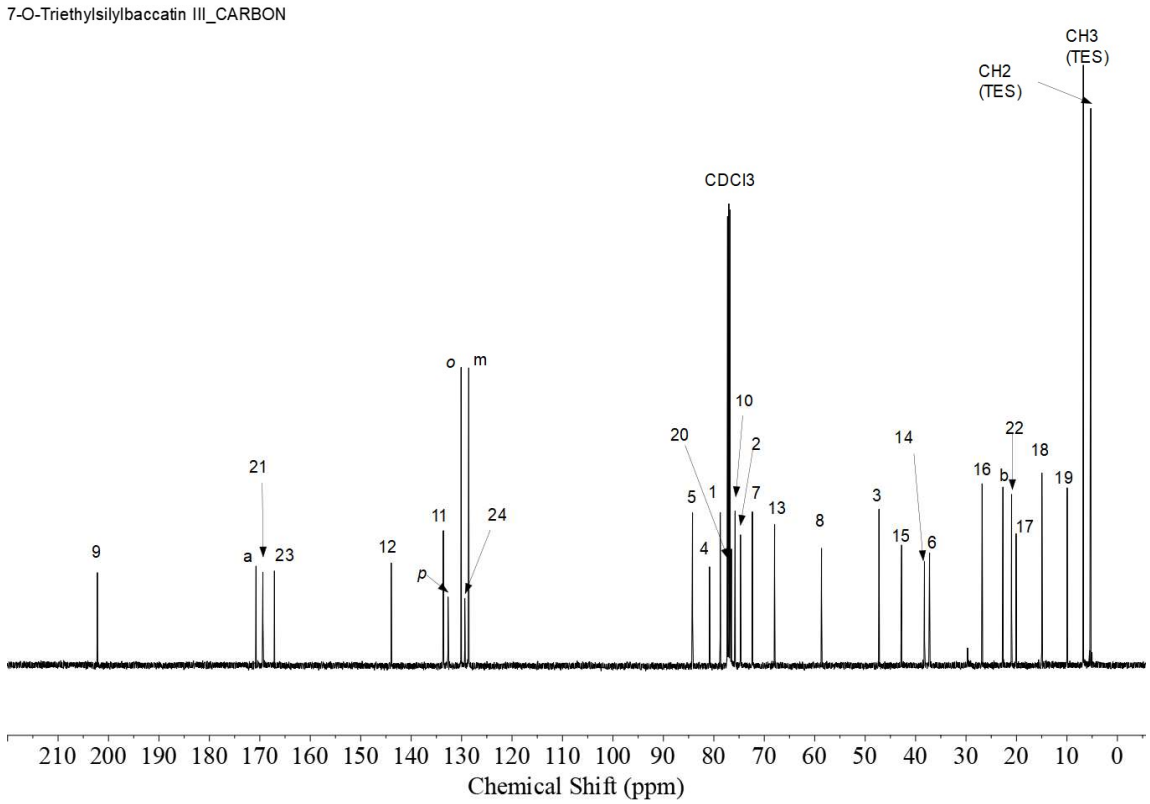

Figure 3.31:[13]C-NMR (126 MHz) of 7-*O*-triethylsilylbaccatin III.

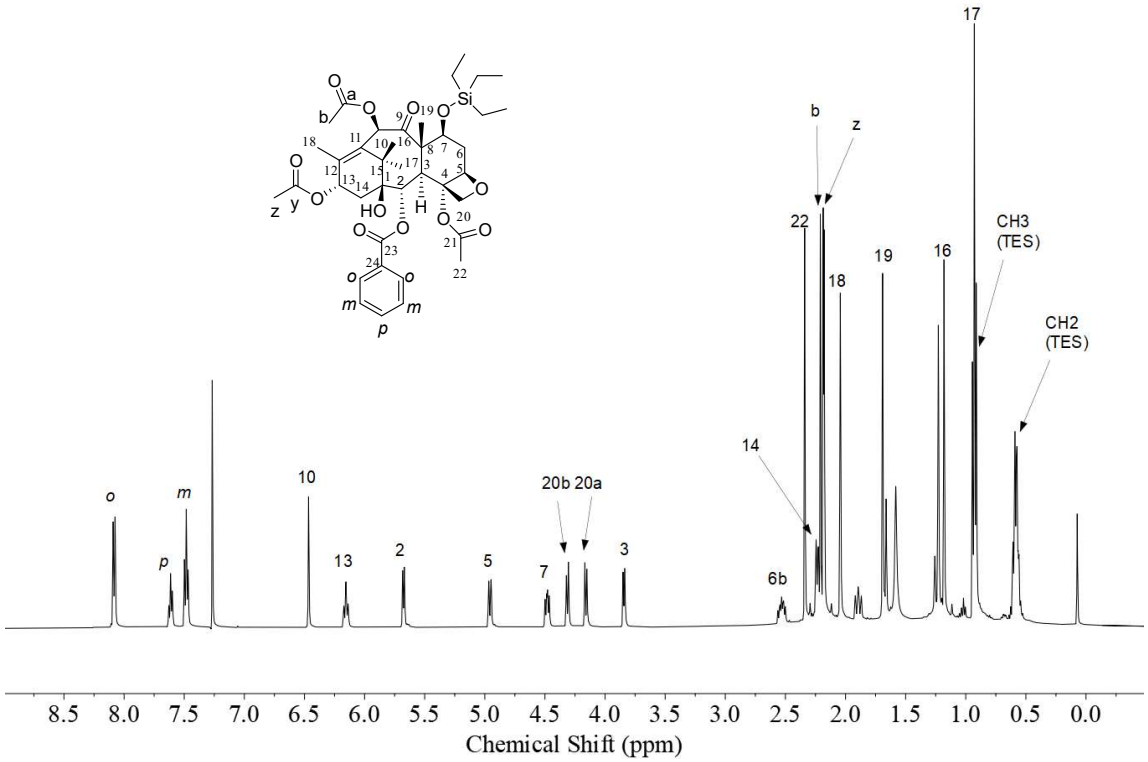

Figure 3.32: ^{1}H-NMR (500 MHz) of 7-*O*-triethylsilyl-13-acetylbaccatin III.

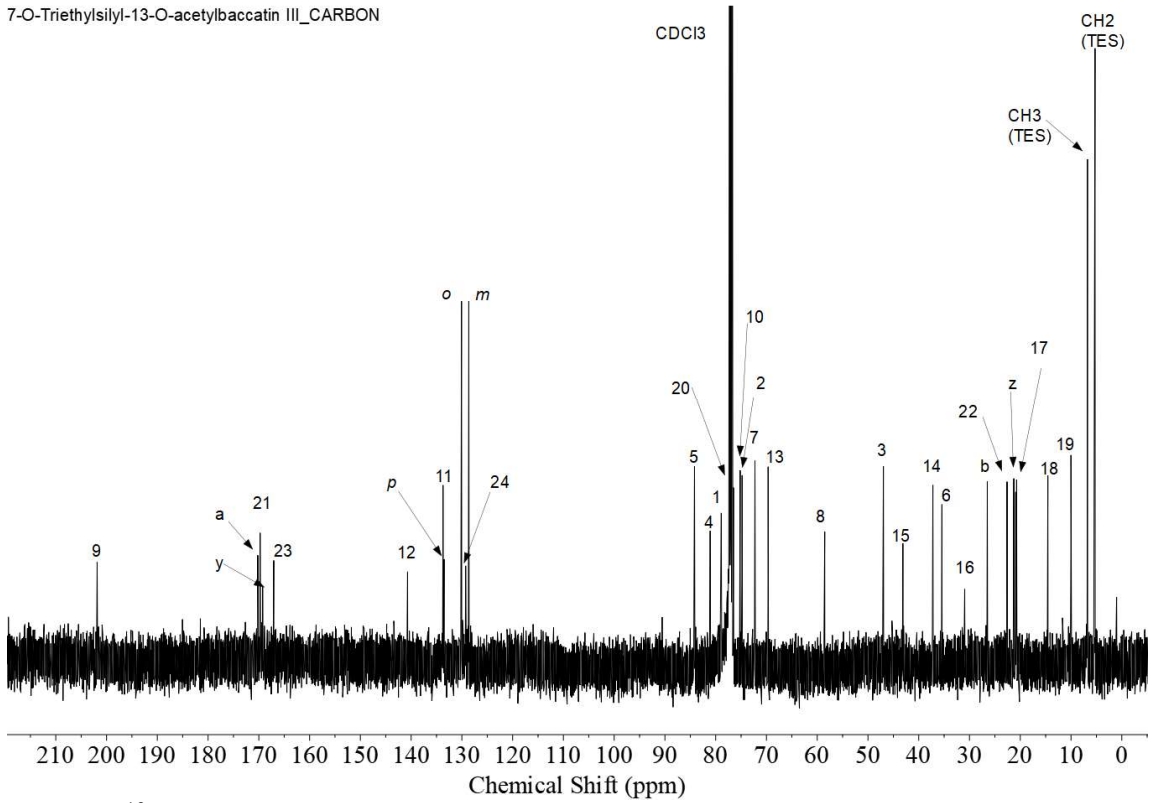

Figure 3.33: ^{13}C-NMR (126 MHz) of 7-*O*-triethylsilyl-13-acetylbaccatin III.

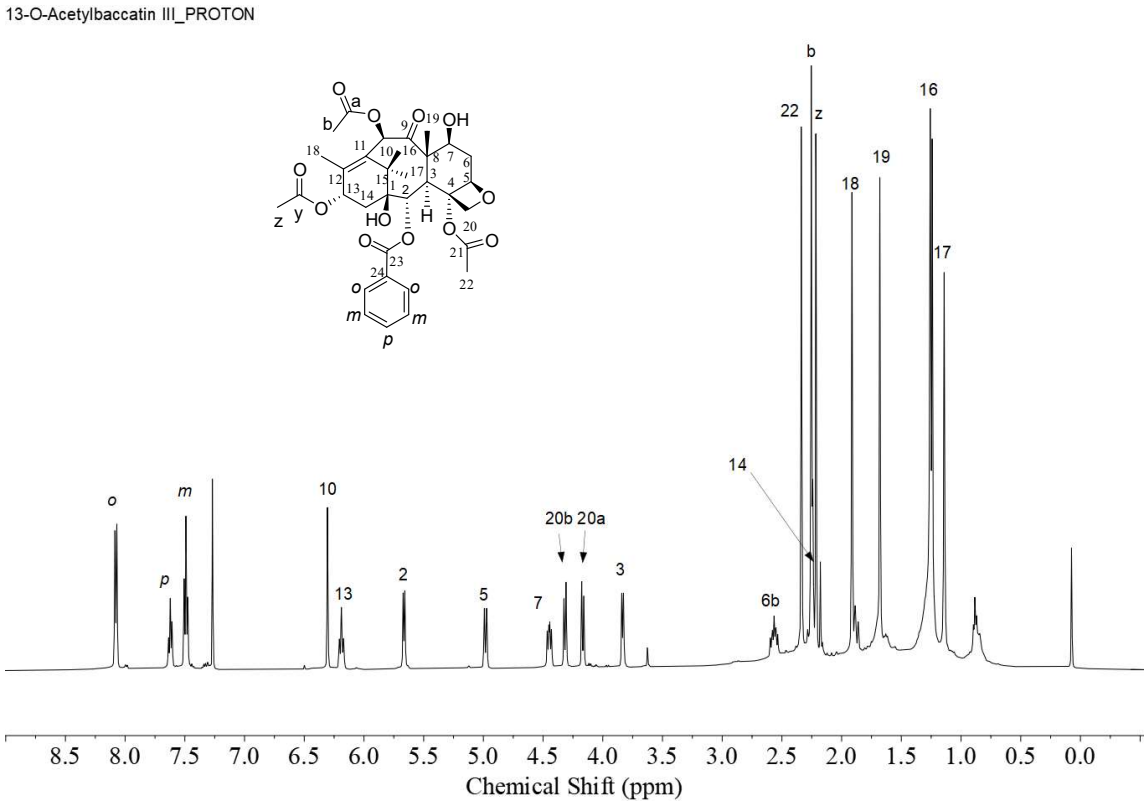

Figure 3.34: ^{1}H-NMR (500 MHz) of 13-acetylbaccatin III.

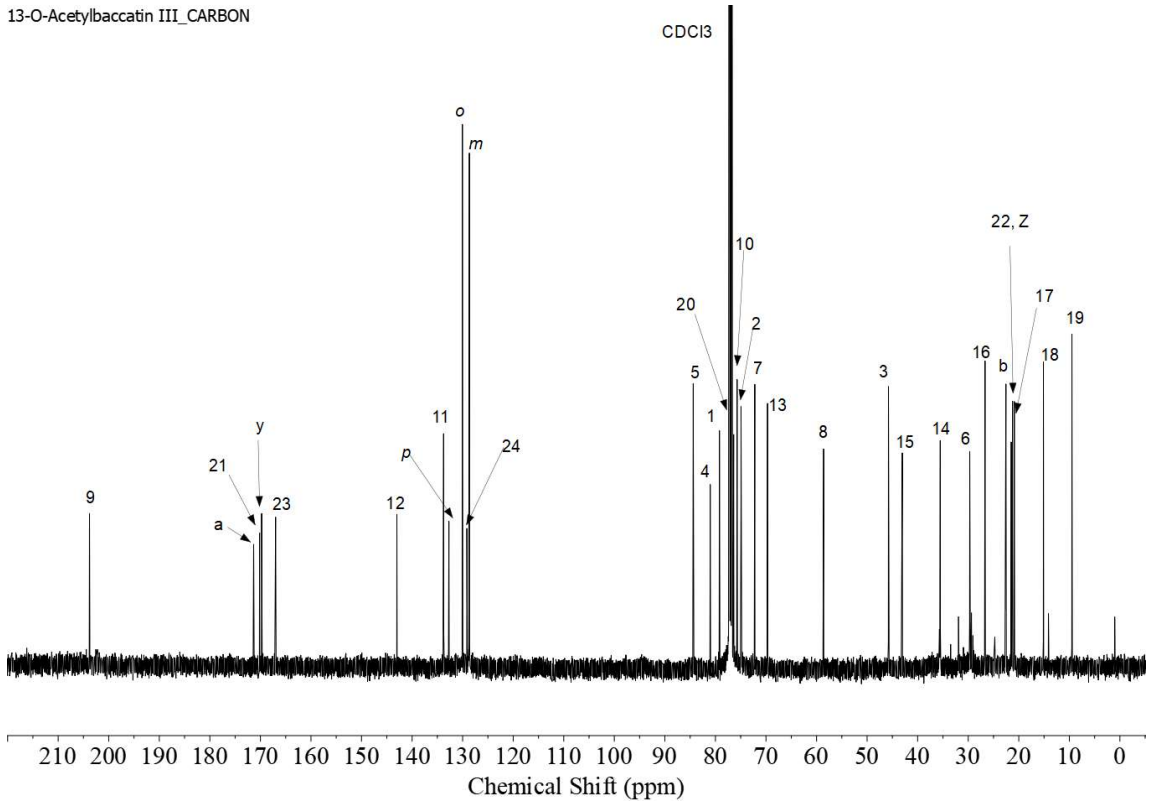

Figure 3.35: ^{13}C-NMR (126 MHz) of 13-acetylbaccatin III.

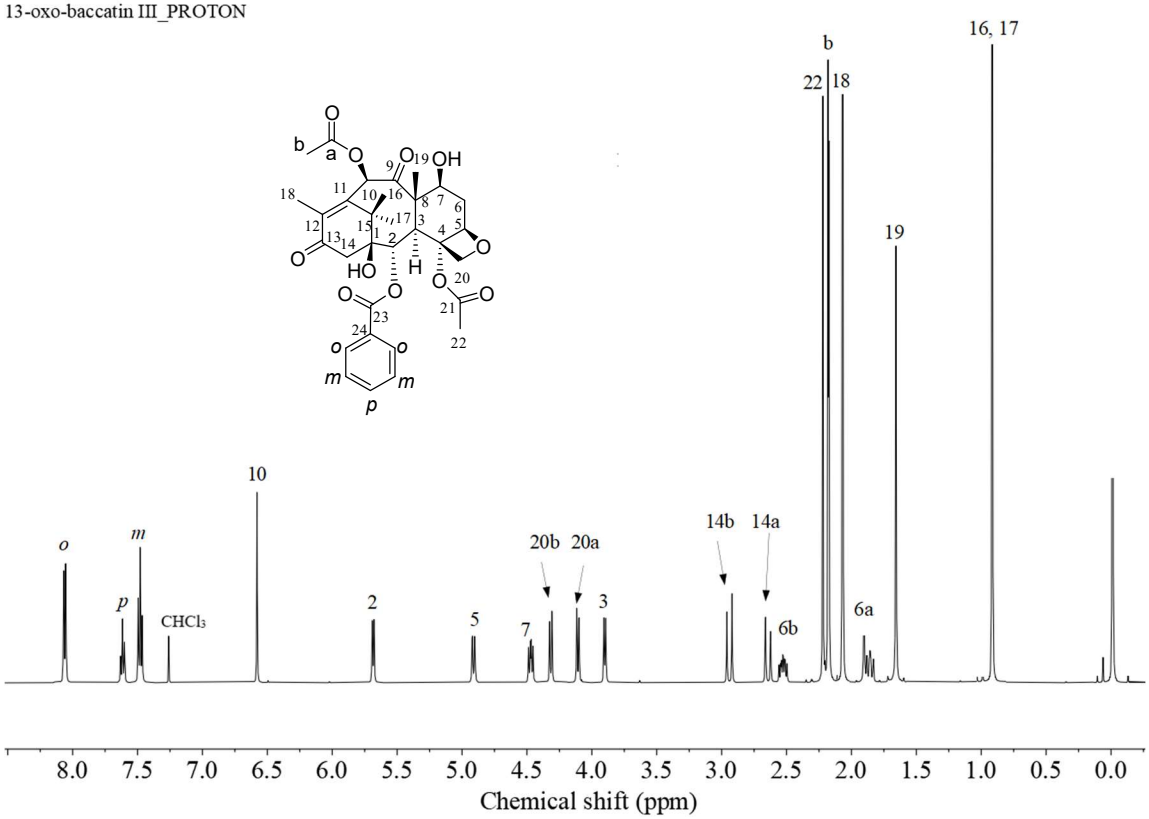

Figure 3.36: ^{1}H-NMR (500 MHz) of 13-oxo-baccatin III.

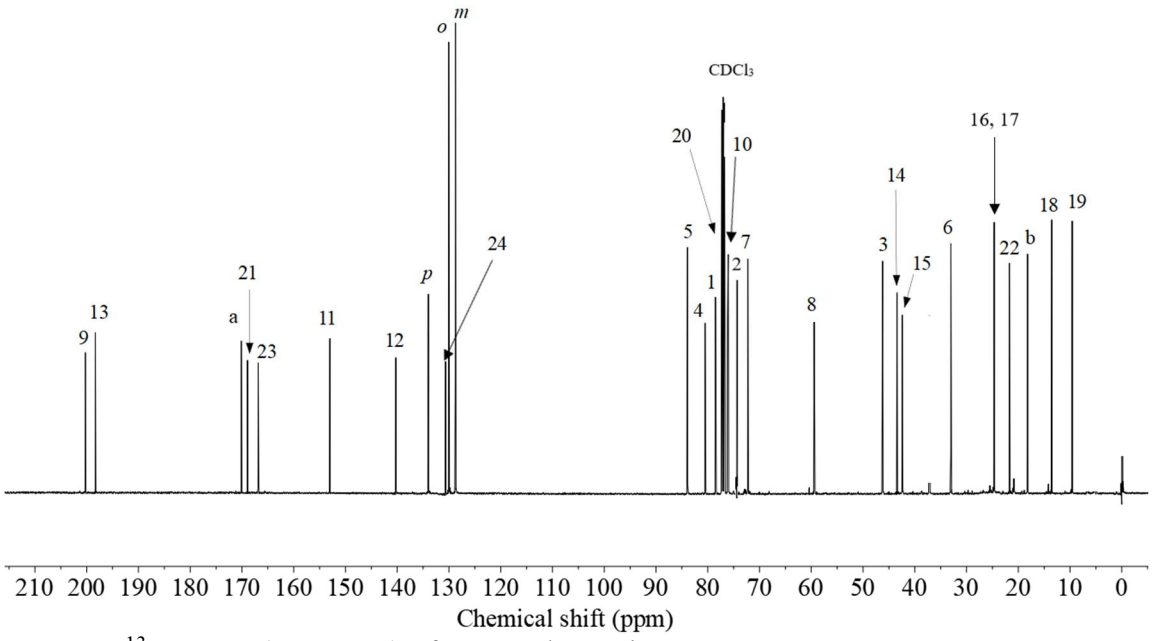

Figure 3.37: ^{13}C-NMR (126 MHz) of 13-oxo-baccatin III.

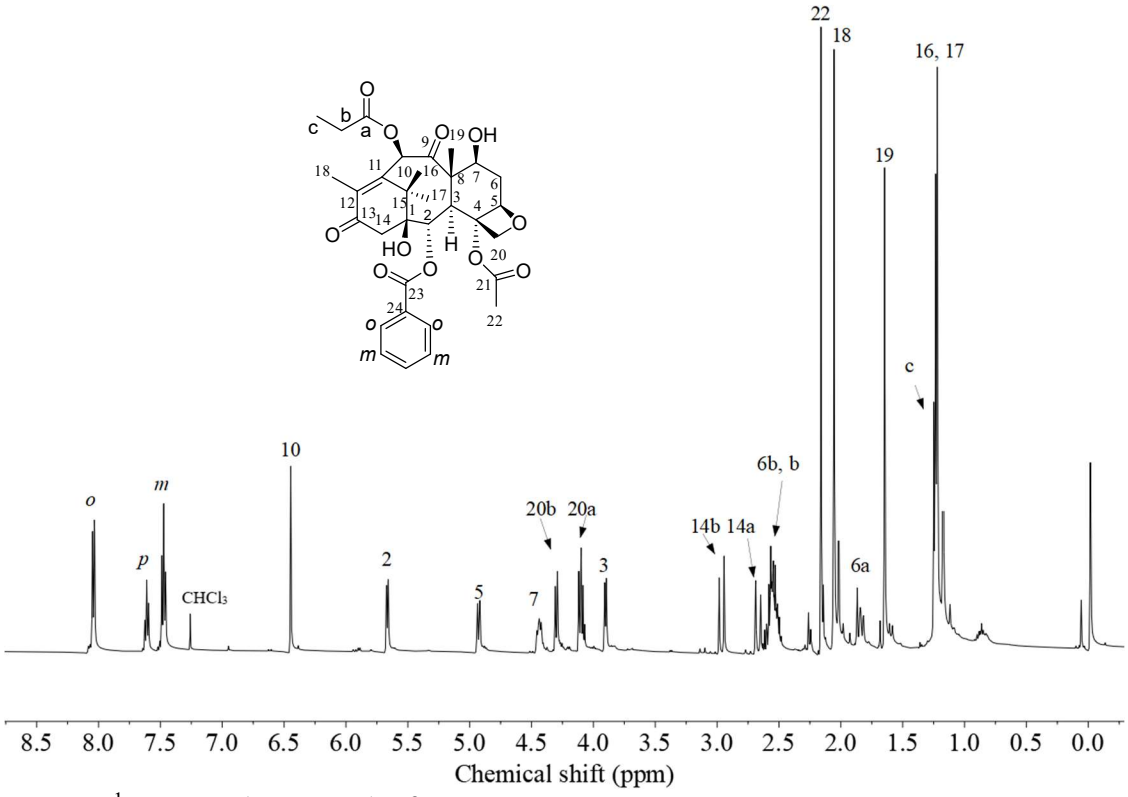

Figure 3.38: ^{1}H-NMR (500 MHz) of 13-oxo-10-PDAB.

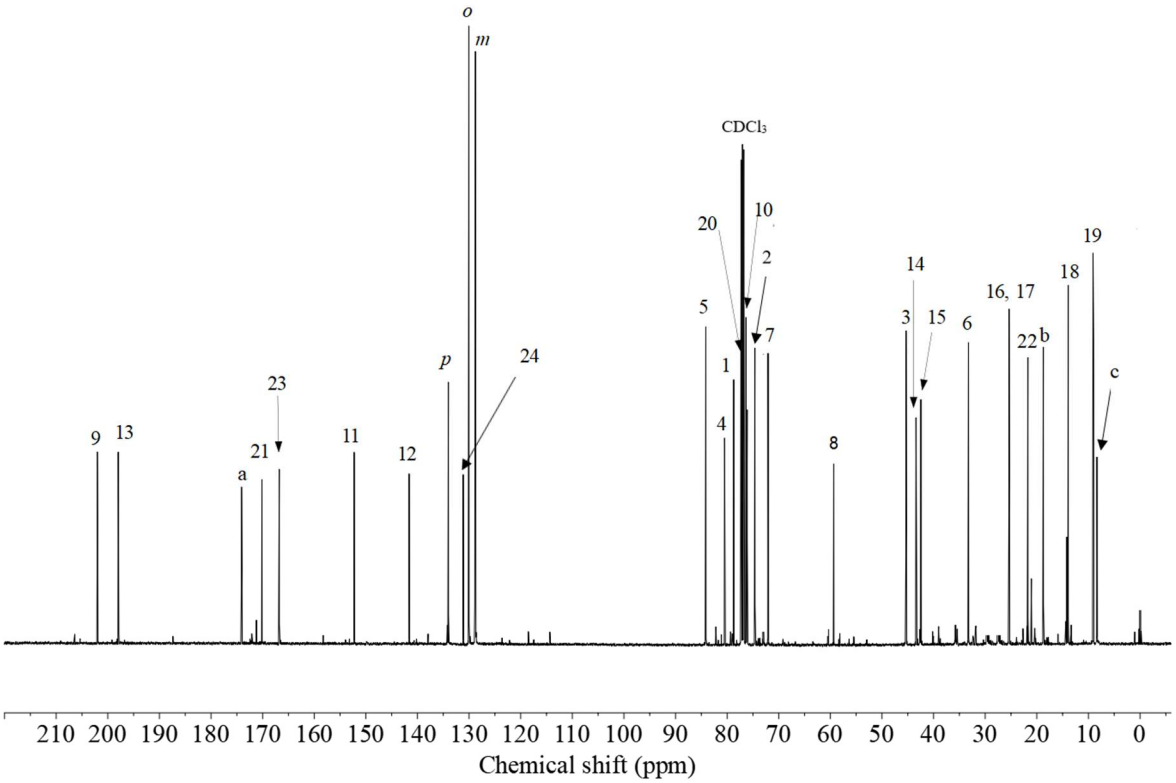

Figure 3.39: ^{13}C-NMR (126 MHz) of 13-oxo-10-PDAB.

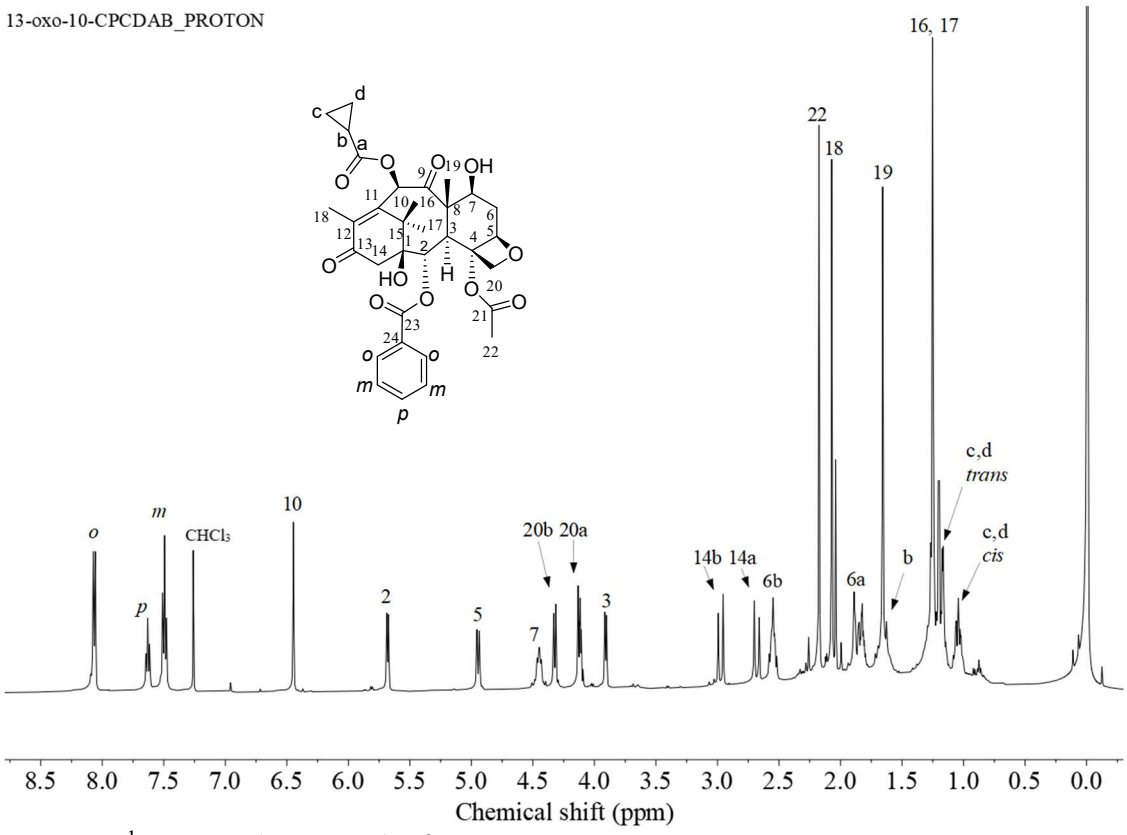

Figure 3.40: ^{1}H-NMR (500 MHz) of 13-oxo-10-CPCDAB.

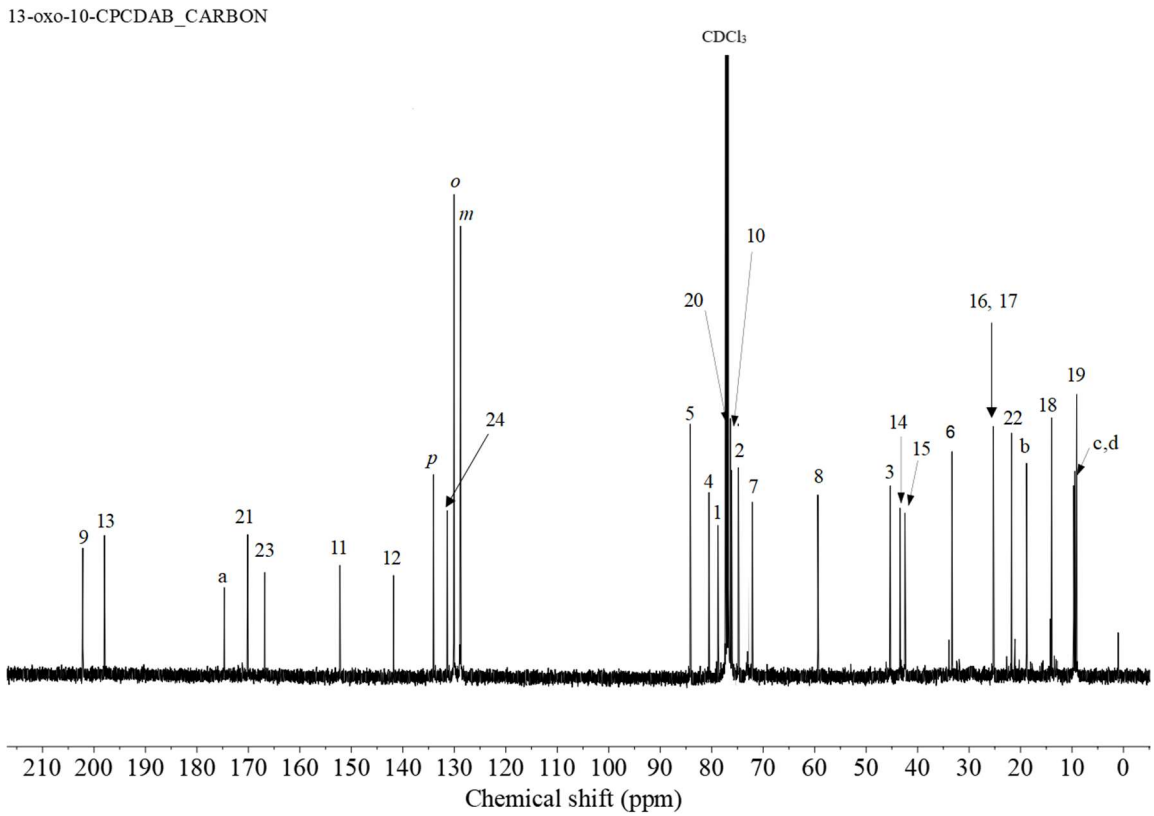

Figure 3.41: ^{13}C-NMR (126 MHz) of 13-oxo-10-CPCDAB.

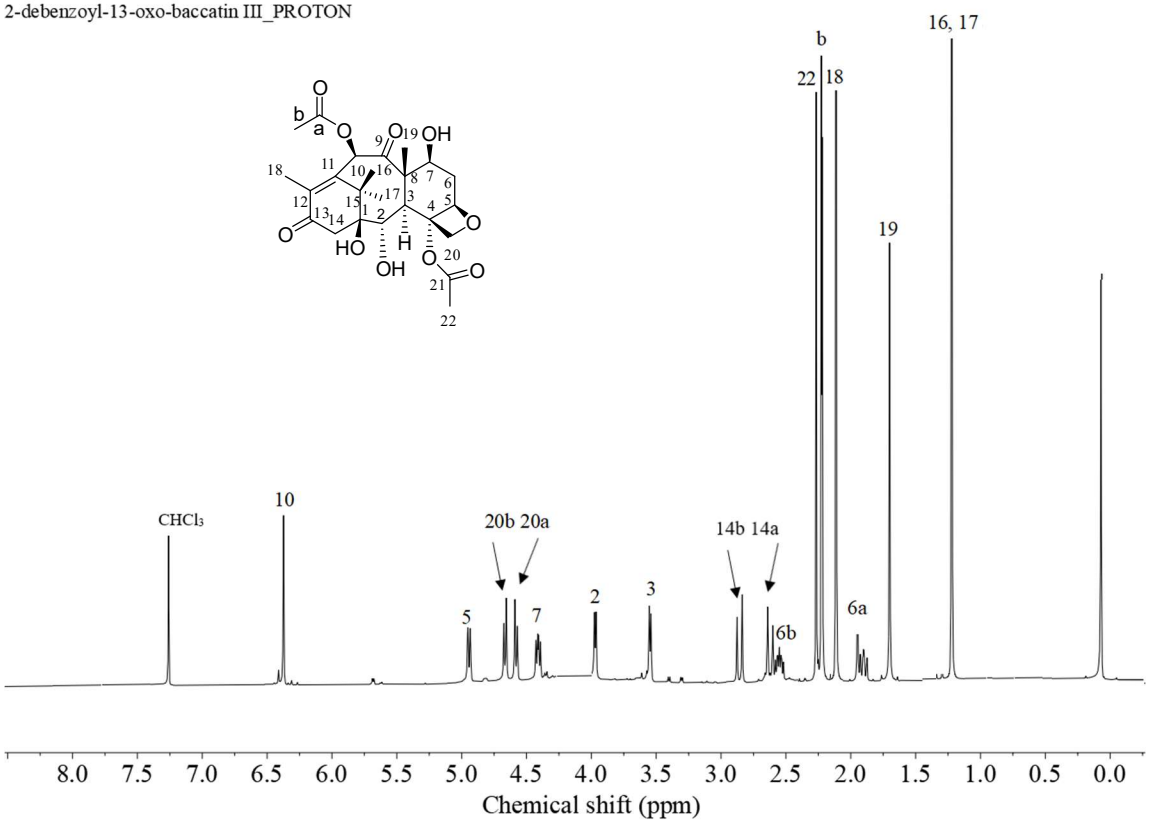

Figure 3.42: ^{1}H-NMR (500 MHz) of 2-DBz-13-oxo-baccatin III.

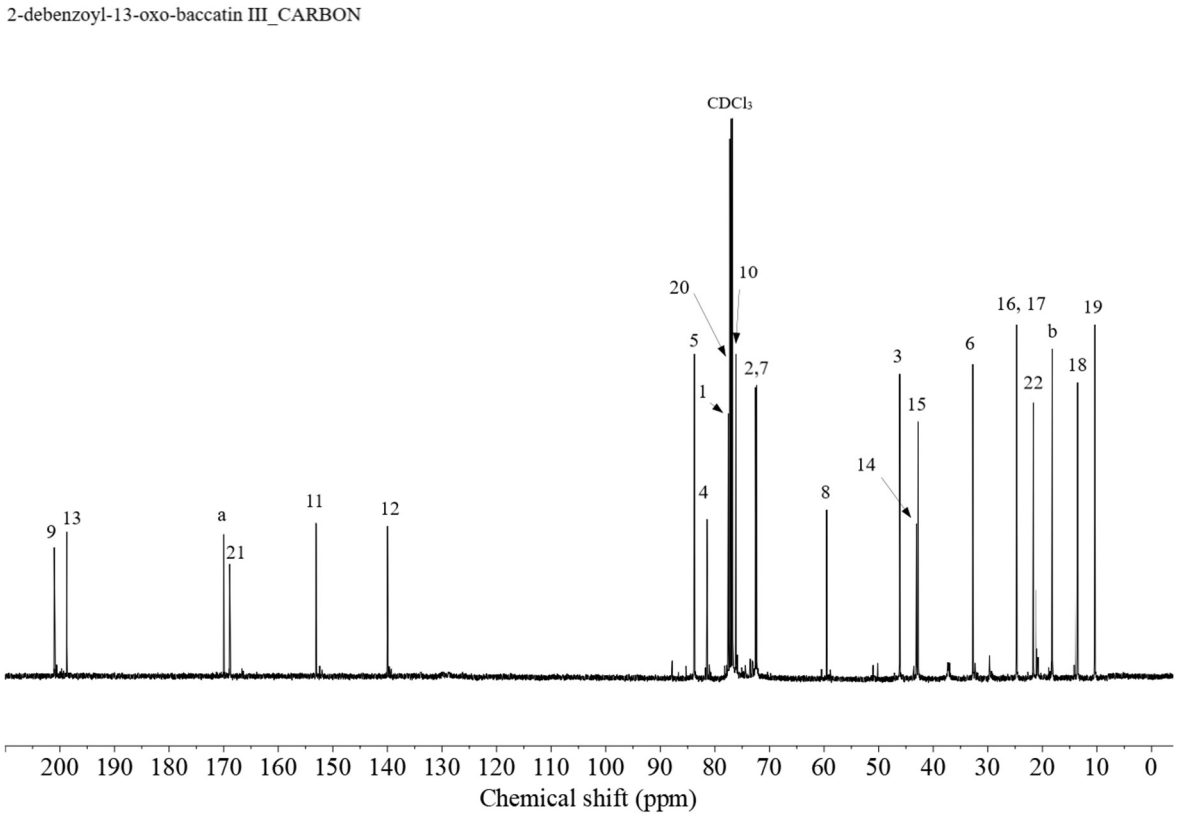

Figure 3.43: ^{13}C-NMR (126 MHz) of 2-DBz-13-oxo-baccatin III.

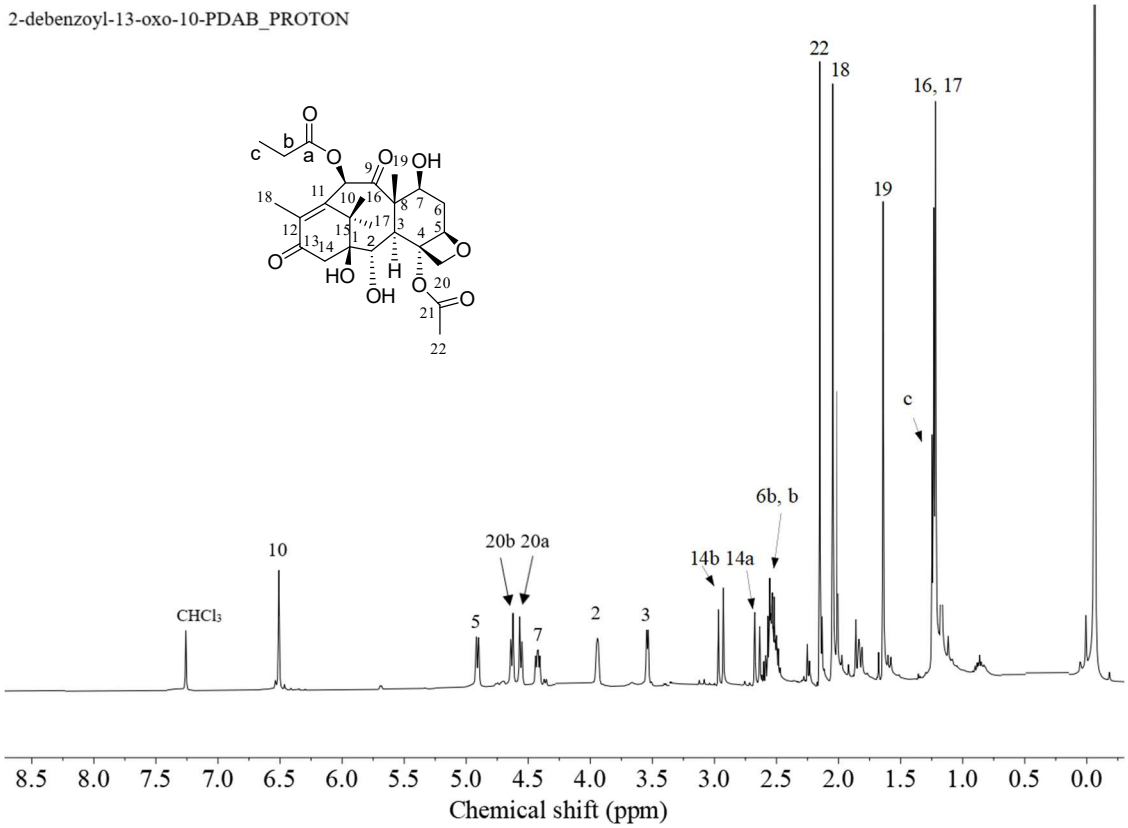

Figure 3.44: ^{1}H-NMR (500 MHz) of 2-DBz-13-oxo-10-PDAB.

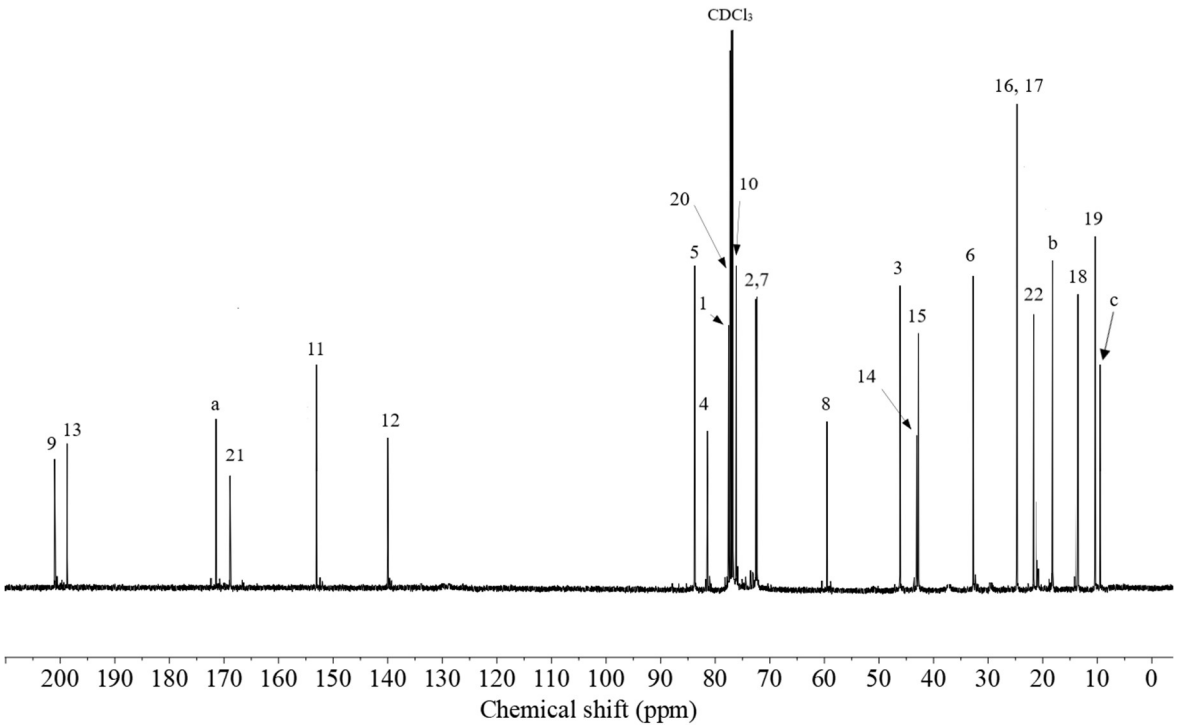

Figure 3.45: ^{13}C-NMR (126 MHz) of 2-DBz-13-oxo-10-PDAB.

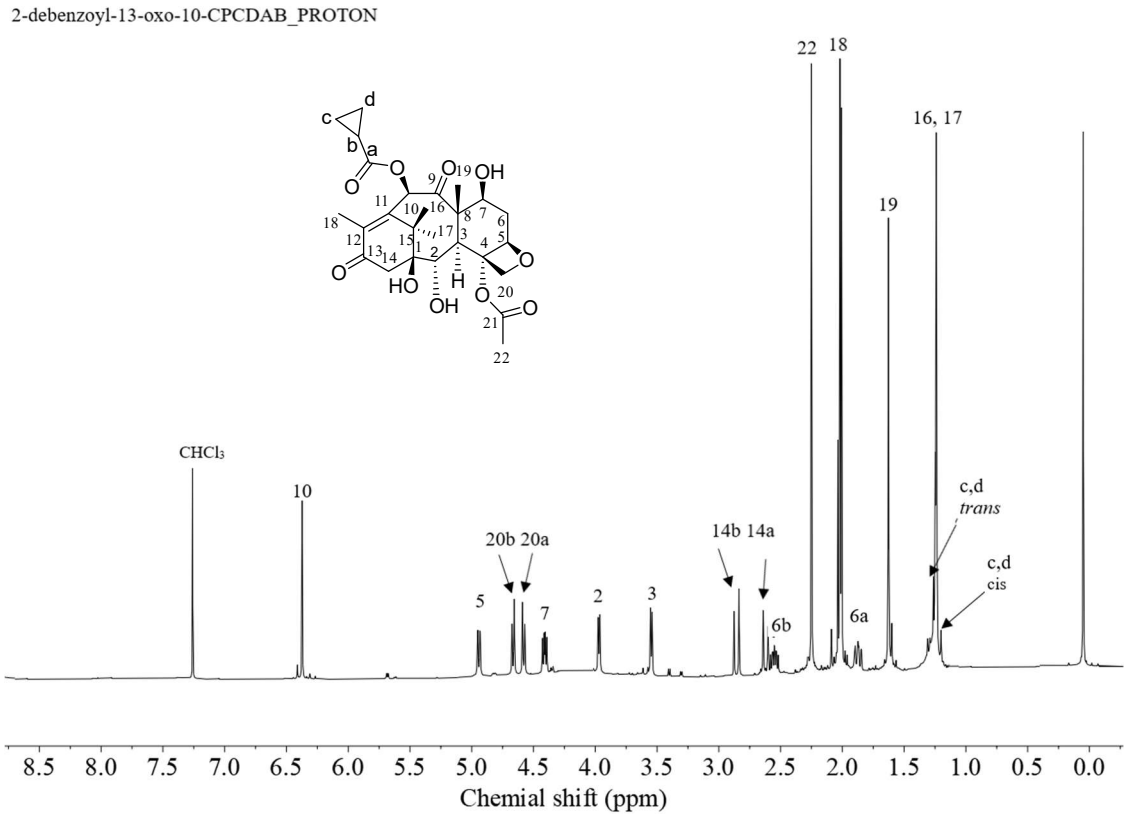

Figure 3.46: ^{1}H-NMR (500 MHz) of 2-DBz-13-oxo-10-CPCDAB.

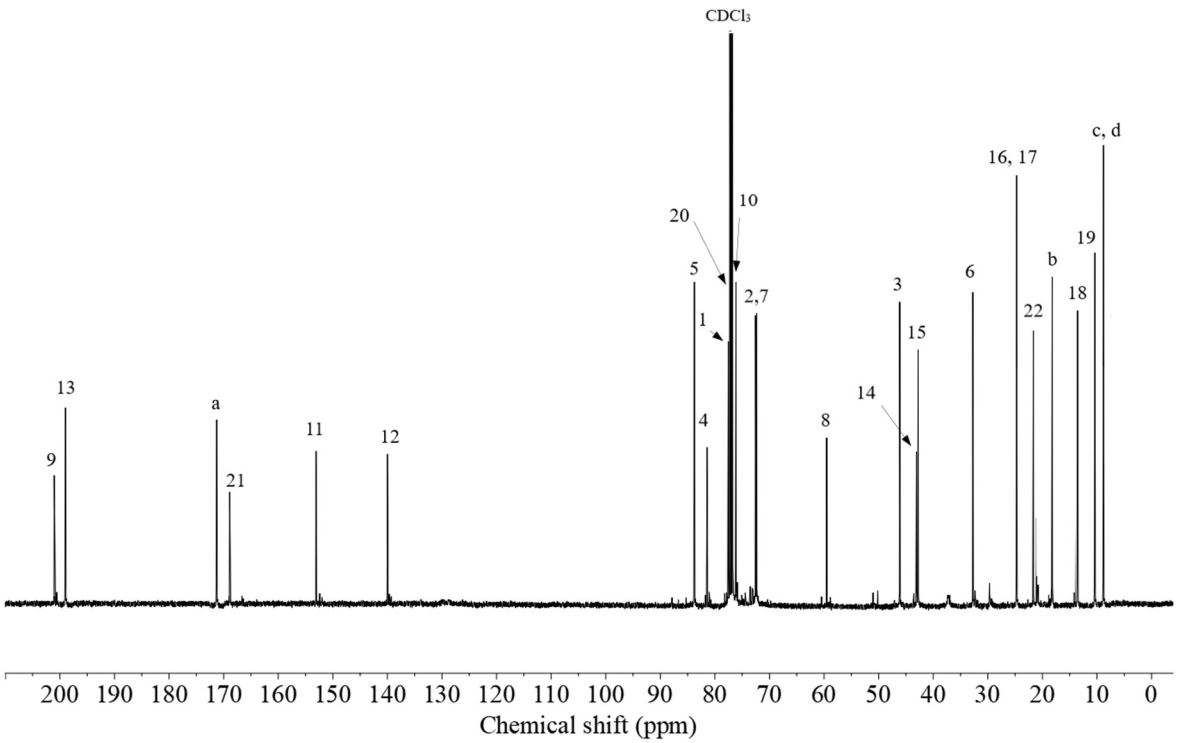

Figure 3.47: ^{13}C-NMR (126 MHz) of 2-DBz-13-oxo-10-CPCDAB.

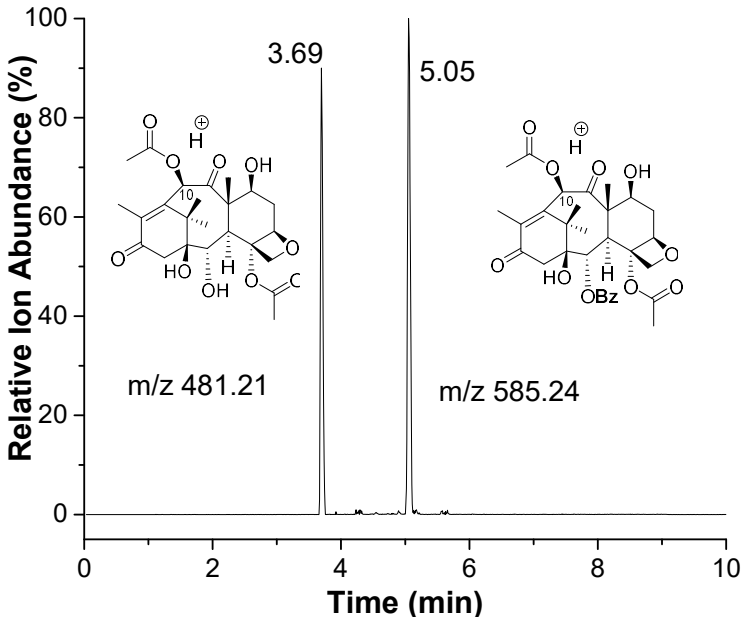

Figure 3.48: LC/ESI-MS (selected ion mode for m/z $[M + H]^+$) of the biocatalytic conversion of 13-oxo-baccatin III to 2-DBz-13-oxo-baccatin III in *m*TBT catalysis.

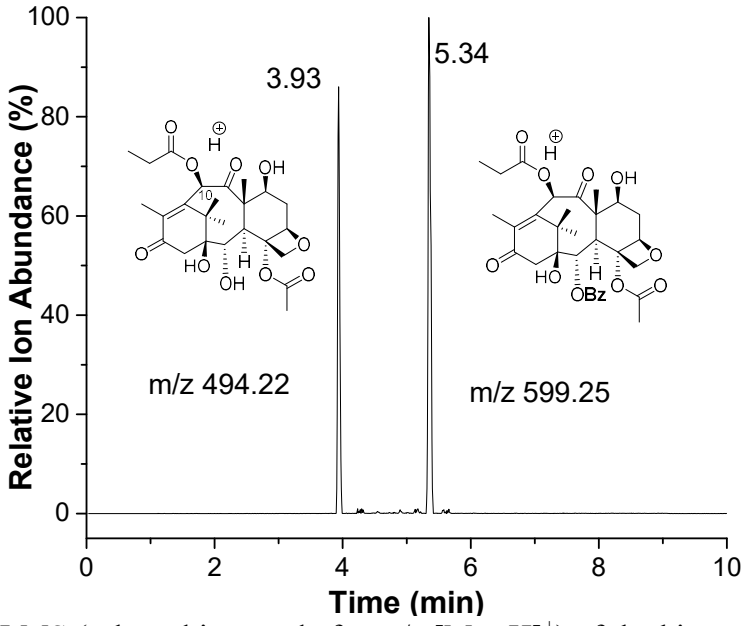

Figure 3.49: LC/ESI-MS (selected ion mode for m/z $[M + H]^+$) of the biocatalytic conversion of 13-oxo-10-PDAB to 2-DBz-13-oxo-10-PDAB in *m*TBT catalysis.

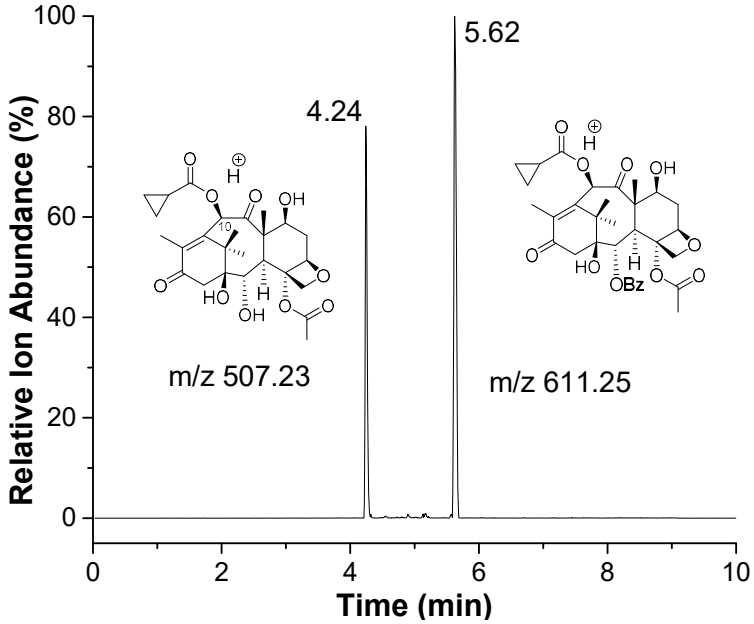

Figure 3.50: LC/ESI-MS (selected ion mode for m/z $[M + H]^+$) of the biocatalytic conversion of 13-oxo-10-CPCDAB to 2-DBz-13-oxo-10-CPCDAB in mTBT catalysis.

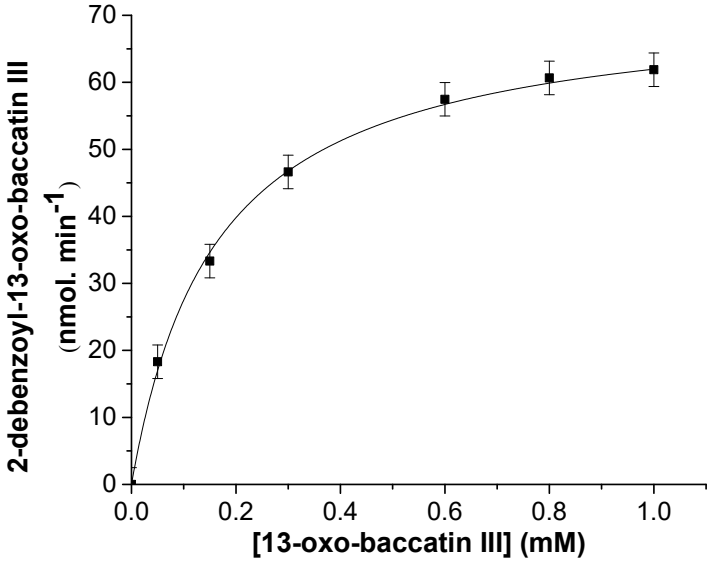

Figure 3.51: Michaelis-Menten kinetics for the turnover of 13-oxo-baccatin III to the 2-DBz-13-oxo-baccatin III.

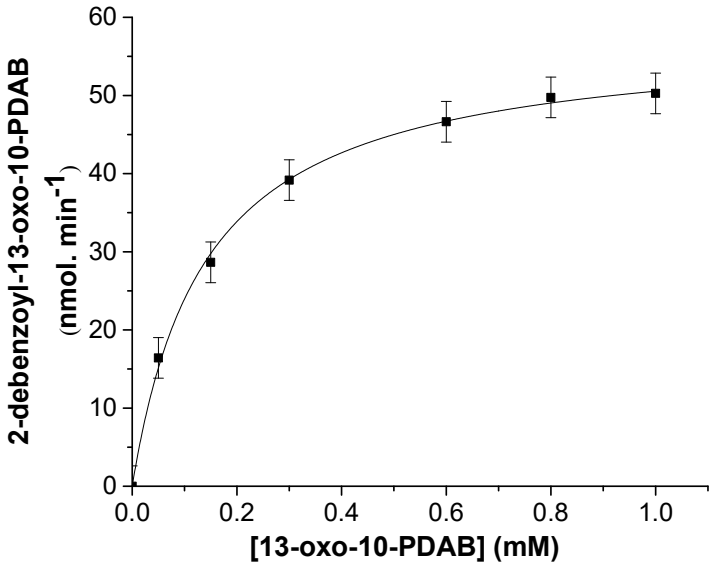

Figure 3.52: Michaelis-Menten kinetics for the turnover of 13-oxo-PDAB to the 2-DBz-13-oxo-10-PDAB.

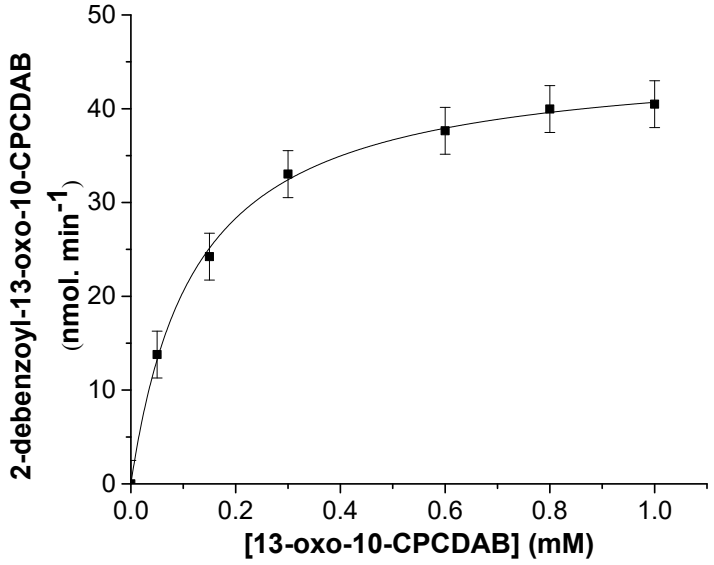

Figure 3.53: Michaelis-Menten kinetics for the turnover of 13-oxo-CPCDAB to the 2-DBz-13-oxo-10-CPCDAB.

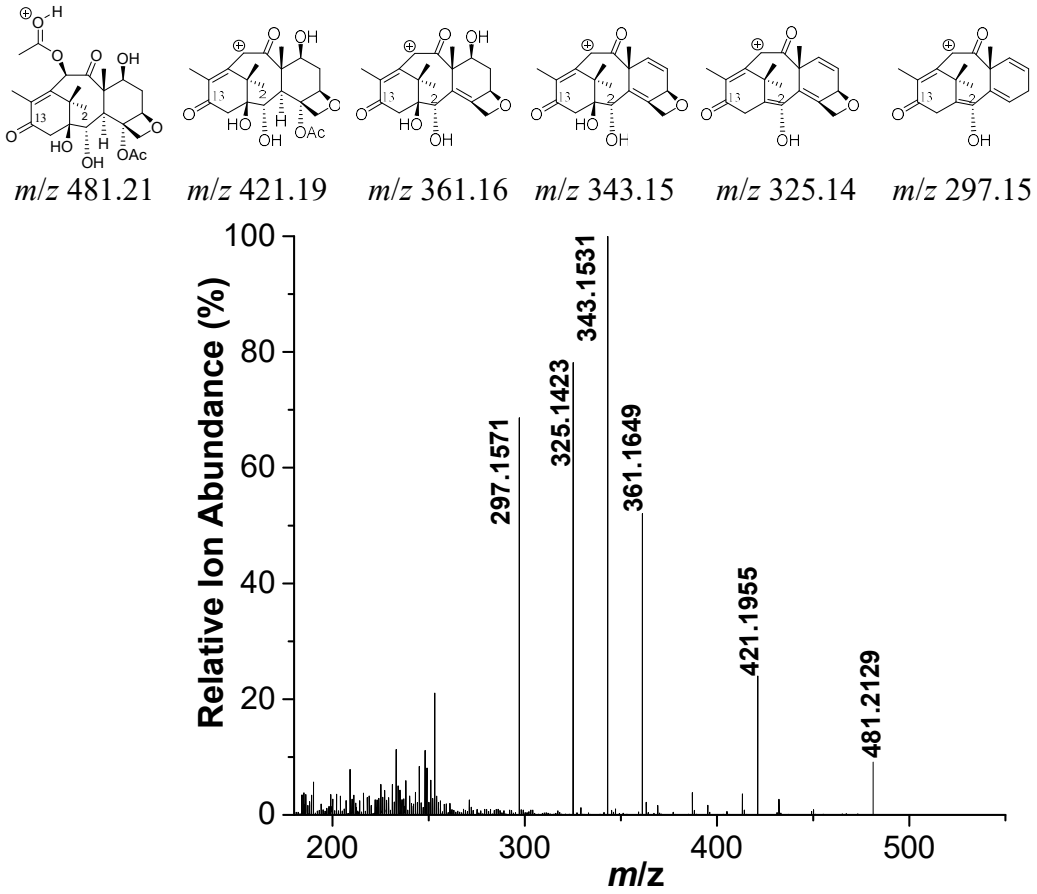

Figure 3.54: LC/ESI-MS/MS (positive-ion mode) of purified 2-DBz-13-oxo-baccatin III peak mass assignments and putative chemical transformations (above spectra).

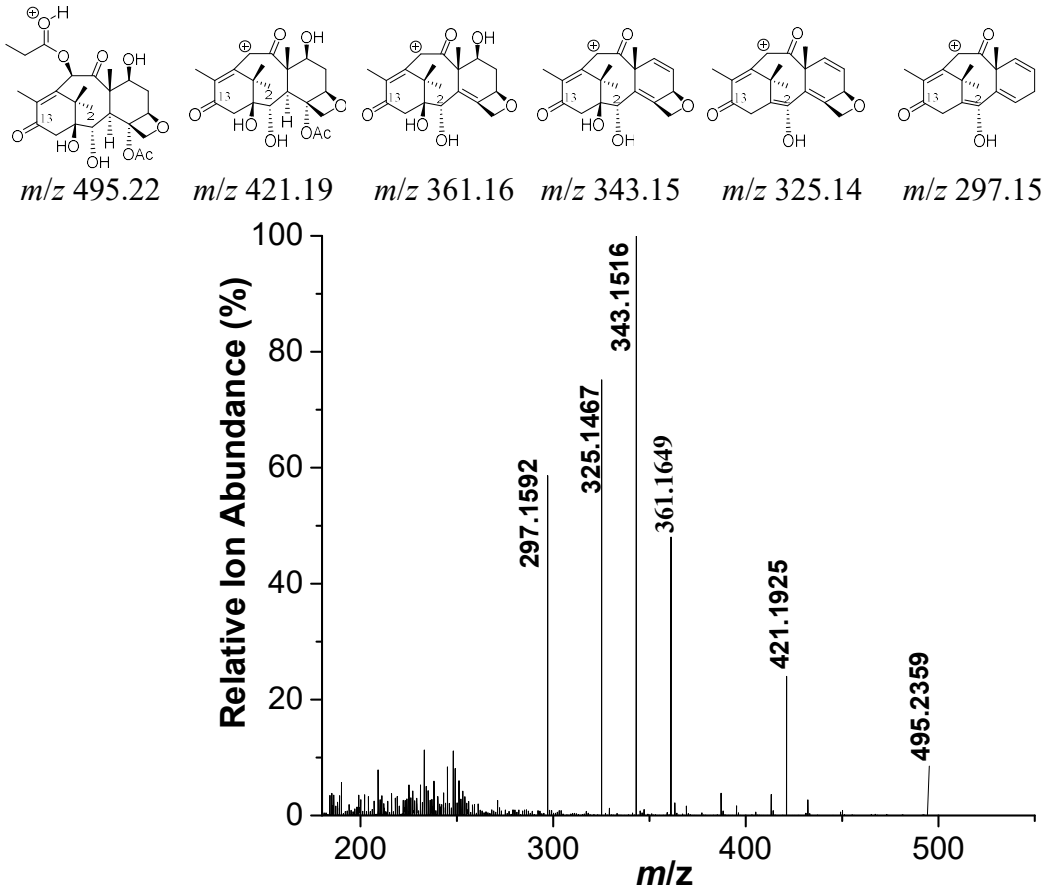

Figure 3.55: LC/ESI-MS/MS (positive-ion mode) of purified 2-DBz-13-oxo-10-PDAB with peak mass assignments and putative chemical transformations (above spectra).

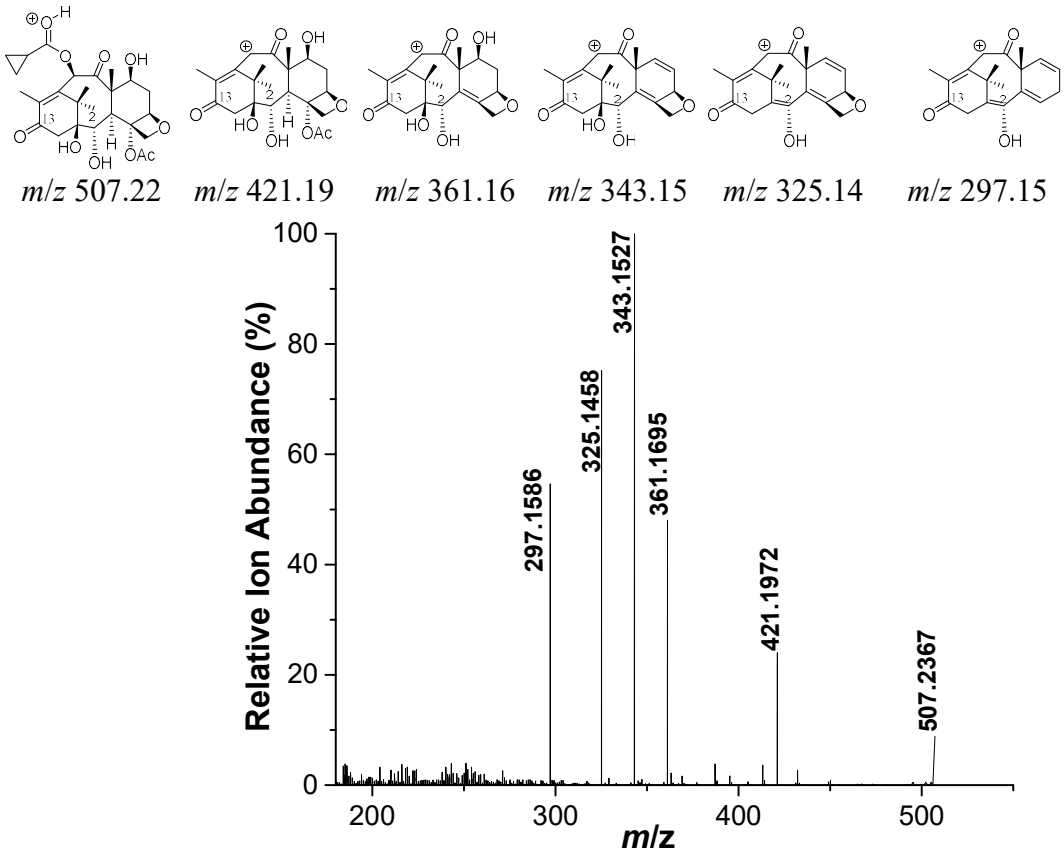

Figure 3.56: LC/ESI-MS/MS (positive-ion mode) of purified 2-DBz-13-oxo-10-CPCDAB with peak mass assignments and putative chemical transformations (above spectra).

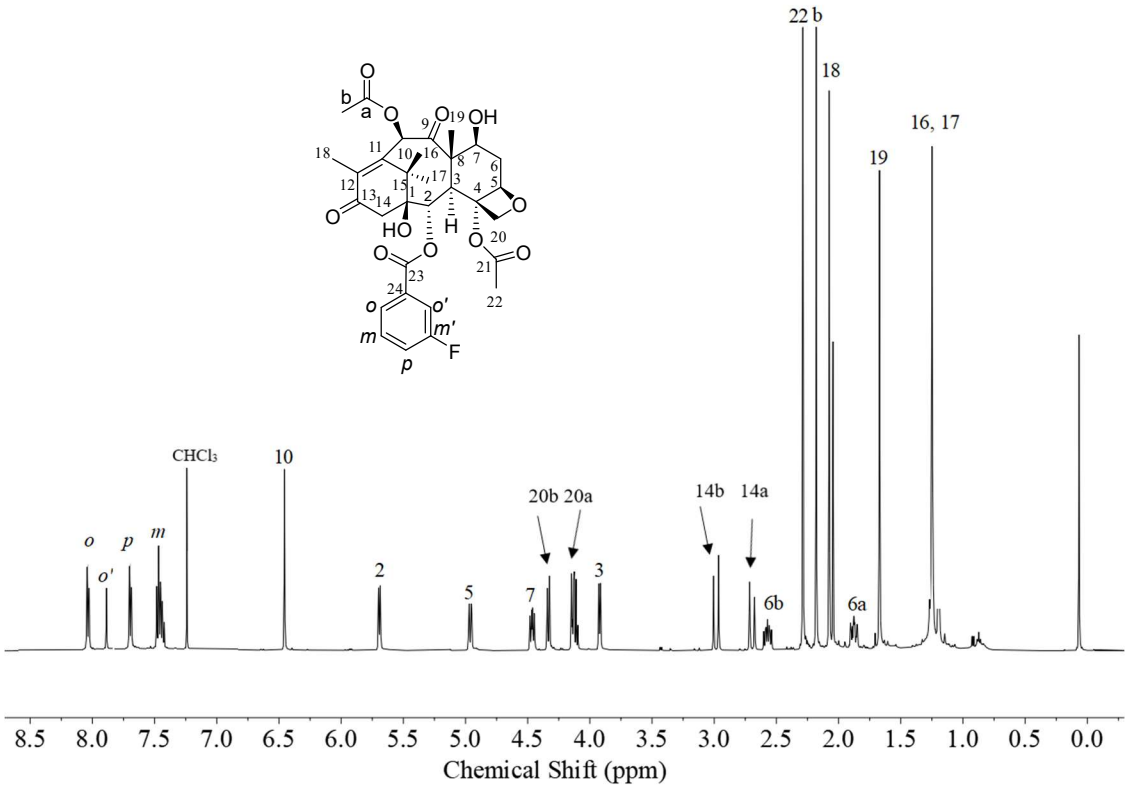

Figure 3.57: ^{1}H-NMR (500 MHz) of 2-DBz-2-(3-F)benzoyl-13-oxo-baccatin III.

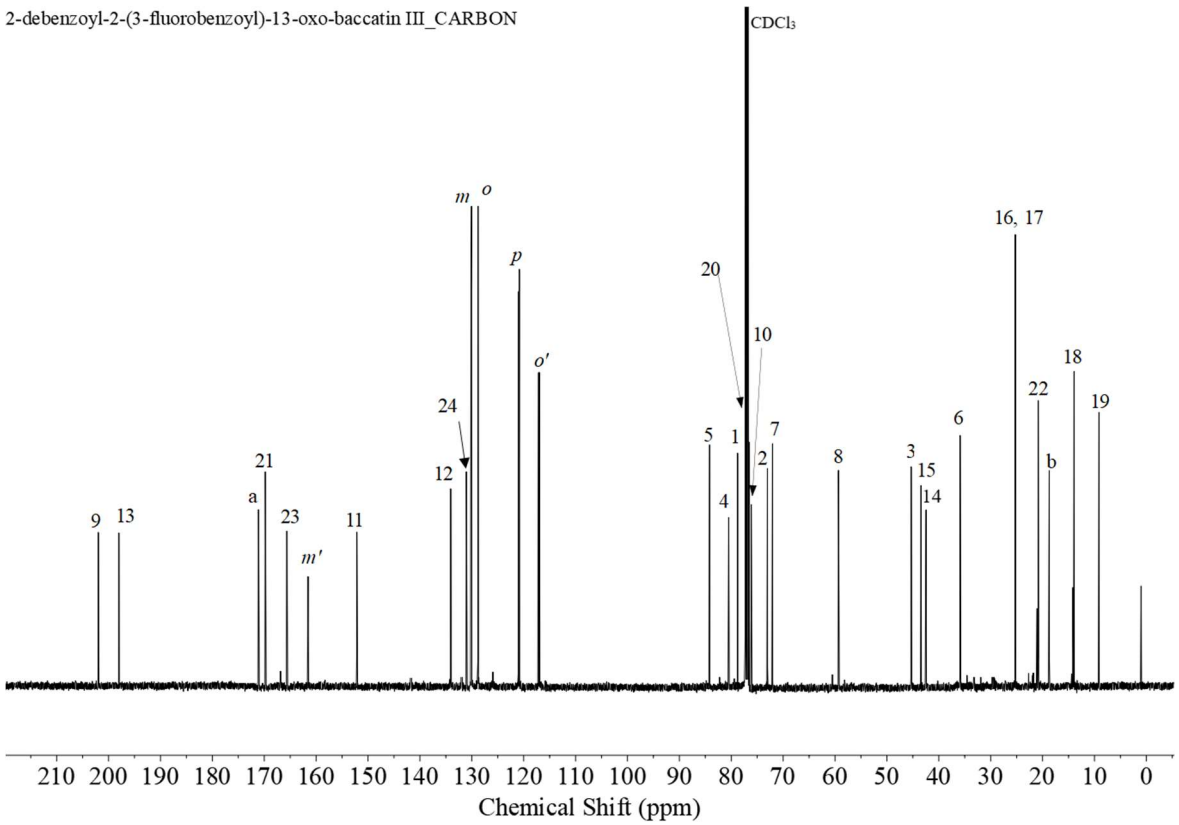

Figure 3.58: ^{13}C-NMR (126 MHz) of 2-DBz-2-(3-F)benzoyl-13-oxo-baccatin III.

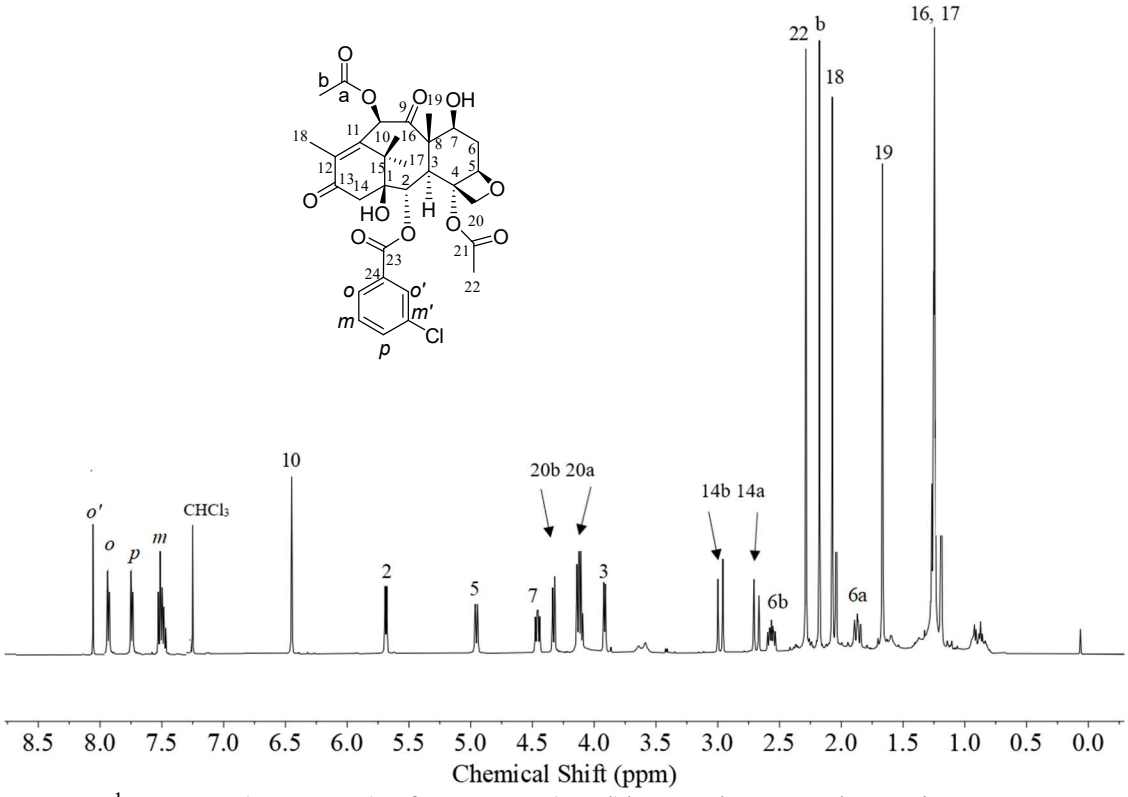

Figure 3.59: ^{1}H-NMR (500 MHz) of 2-DBz-2-(3-Cl)benzoyl-13-oxo-baccatin III.

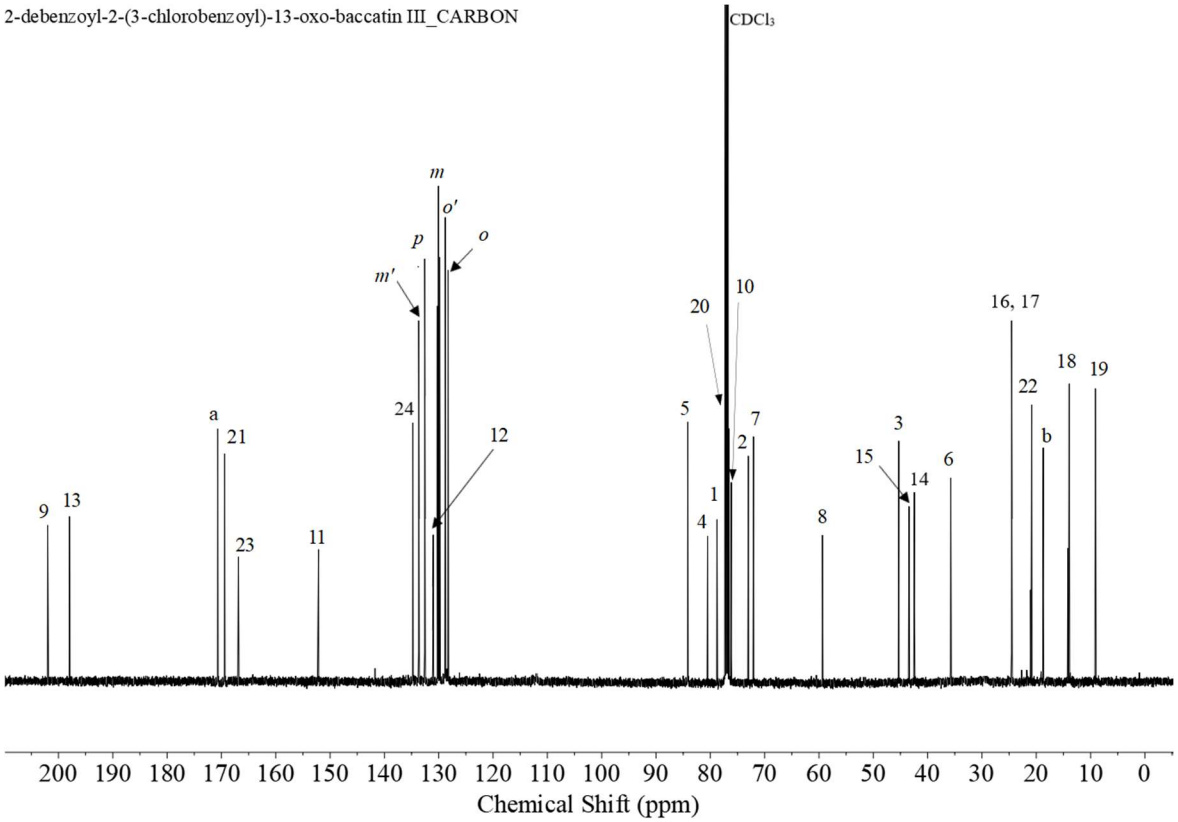

Figure 3.60: ^{13}C-NMR (126 MHz) of 2-DBz-2-(3-Cl)benzoyl-13-oxo-baccatin III.

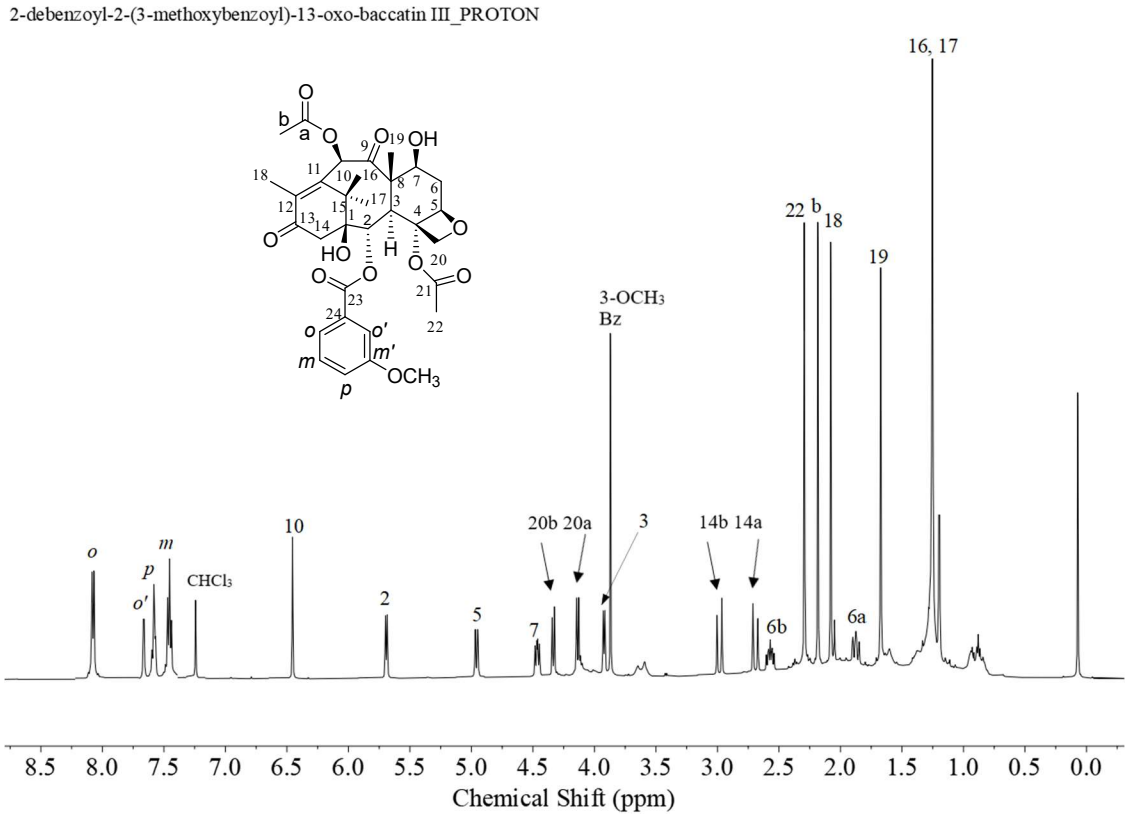

Figure 3.61: ^{1}H-NMR (500 MHz) of 2-DBz-2-(3-OCH_3)benzoyl-13-oxo-baccatin III.

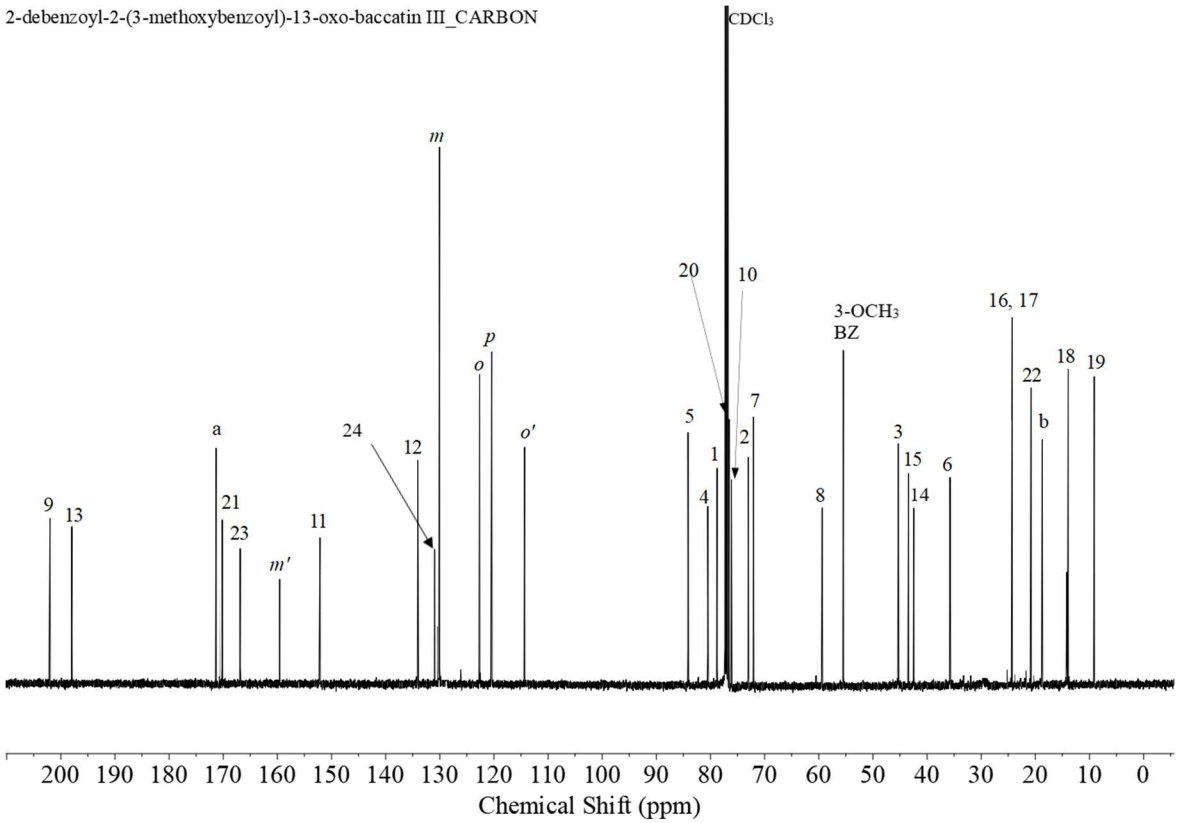

Figure 3.62: ^{13}C-NMR (126 MHz) of 2-DBz-2-(3-OCH$_3$)benzoyl-13-oxo-baccatin III.

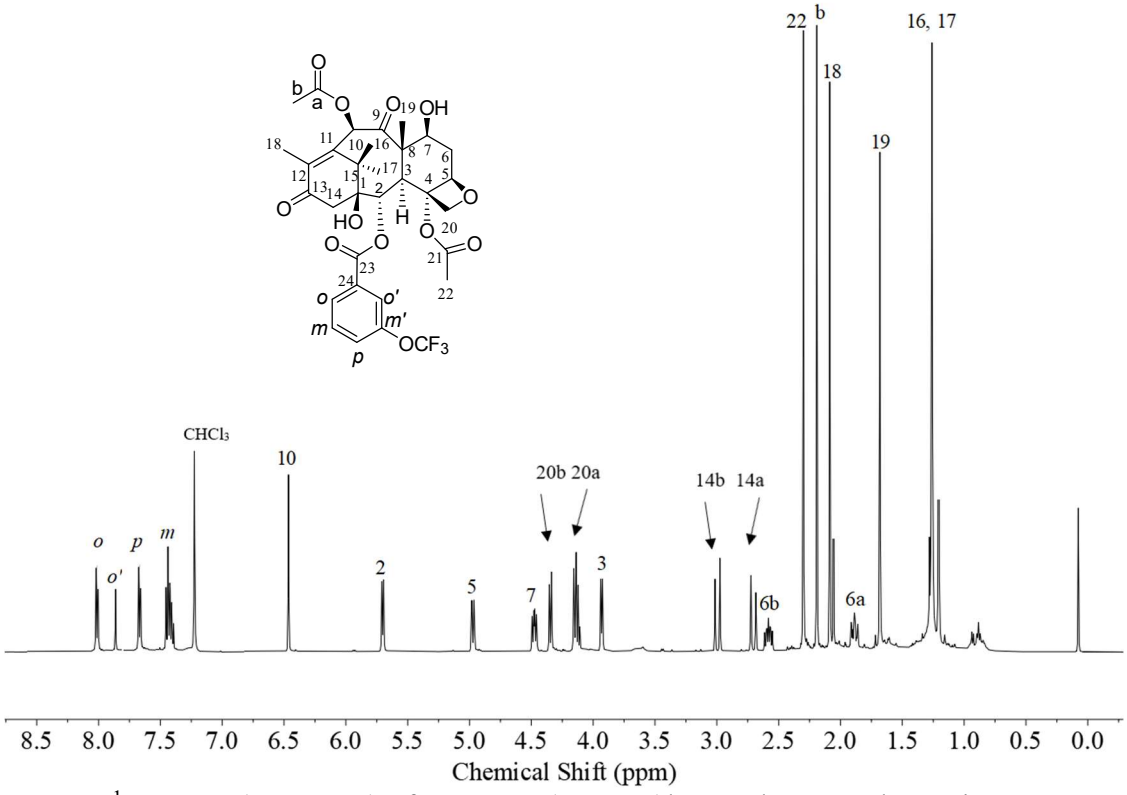

Figure 3.63: ^{1}H-NMR (500 MHz) of 2-DBz-2-(3-OCF_3)benzoyl-13-oxo-baccatin III.

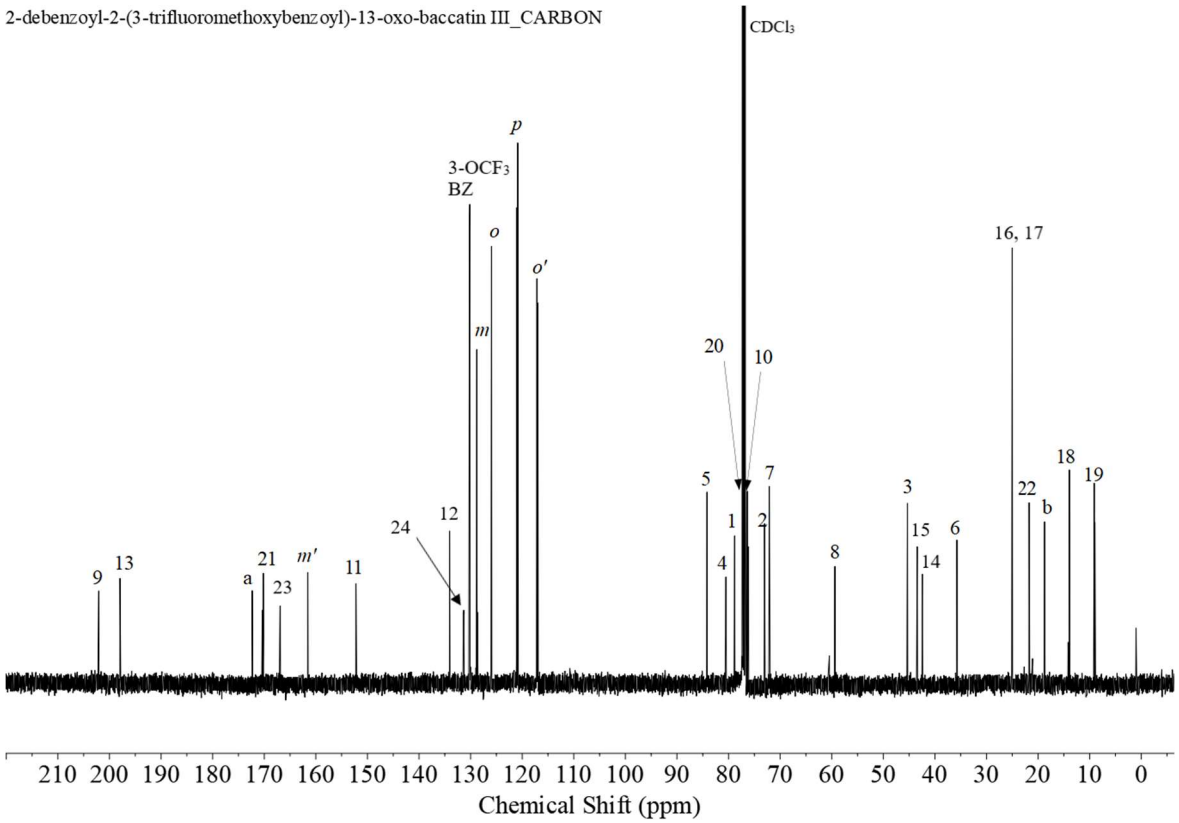

Figure 3.64: ^{13}C-NMR (126 MHz) of 2-DBz-2-(3-OCF_3)benzoyl-13-oxo-baccatin III.

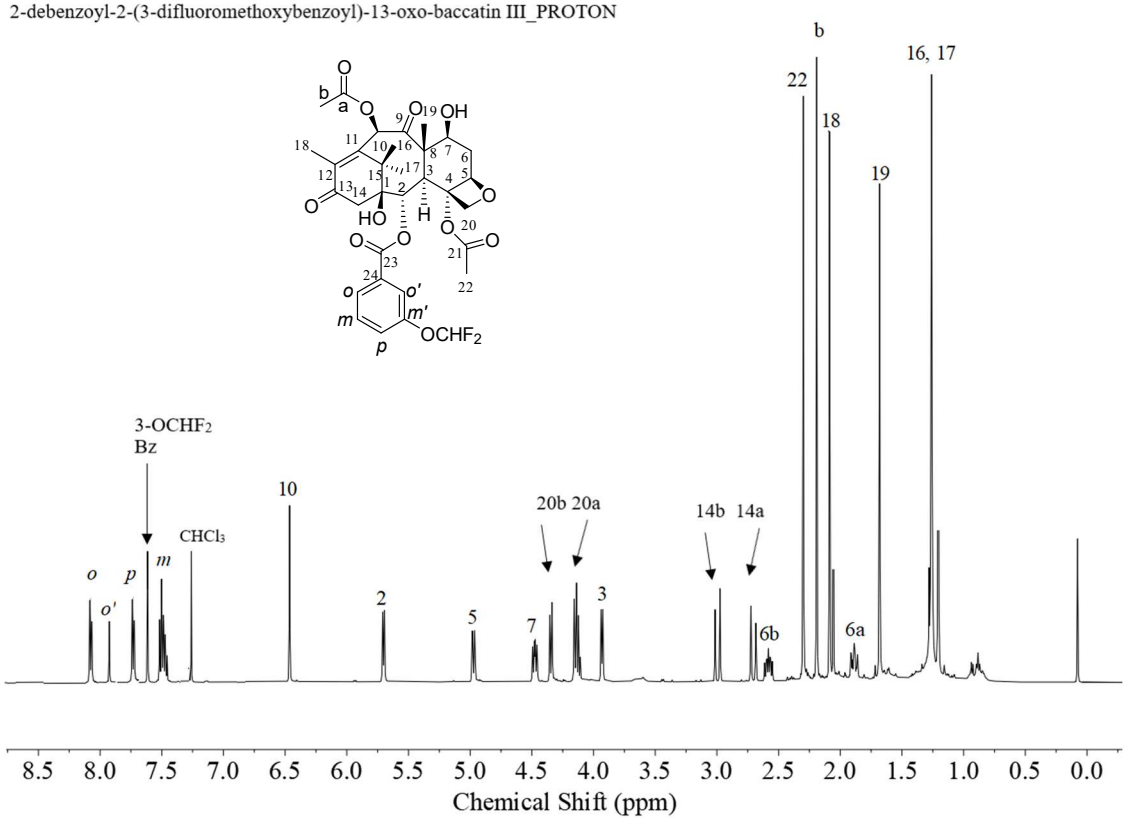

Figure 3.65: ^{1}H-NMR (500 MHz) of 2-DBz-2-(3-$OCHF_2$)benzoyl-13-oxo-baccatin III.

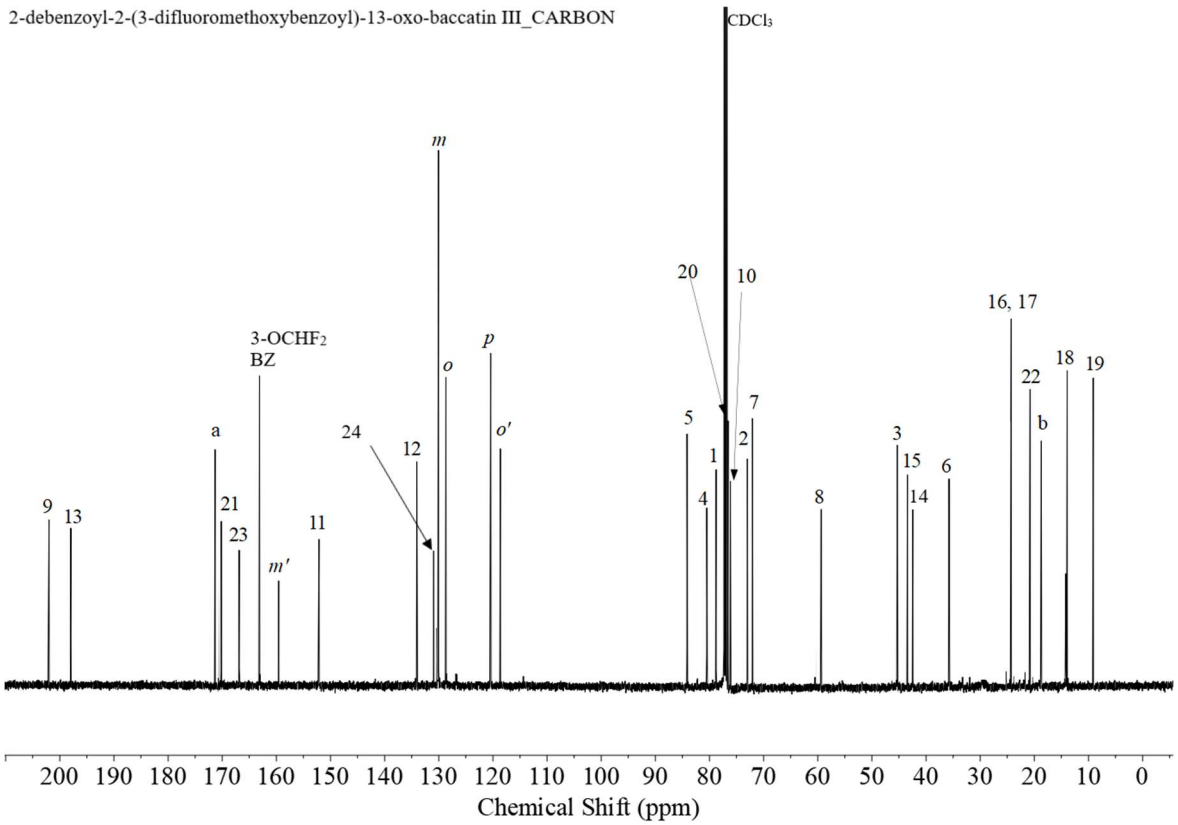

Figure 3.66: ^{13}C-NMR (126 MHz) of 2-DBz-2-(3-$OCHF_2$)benzoyl-13-oxo-baccatin III.

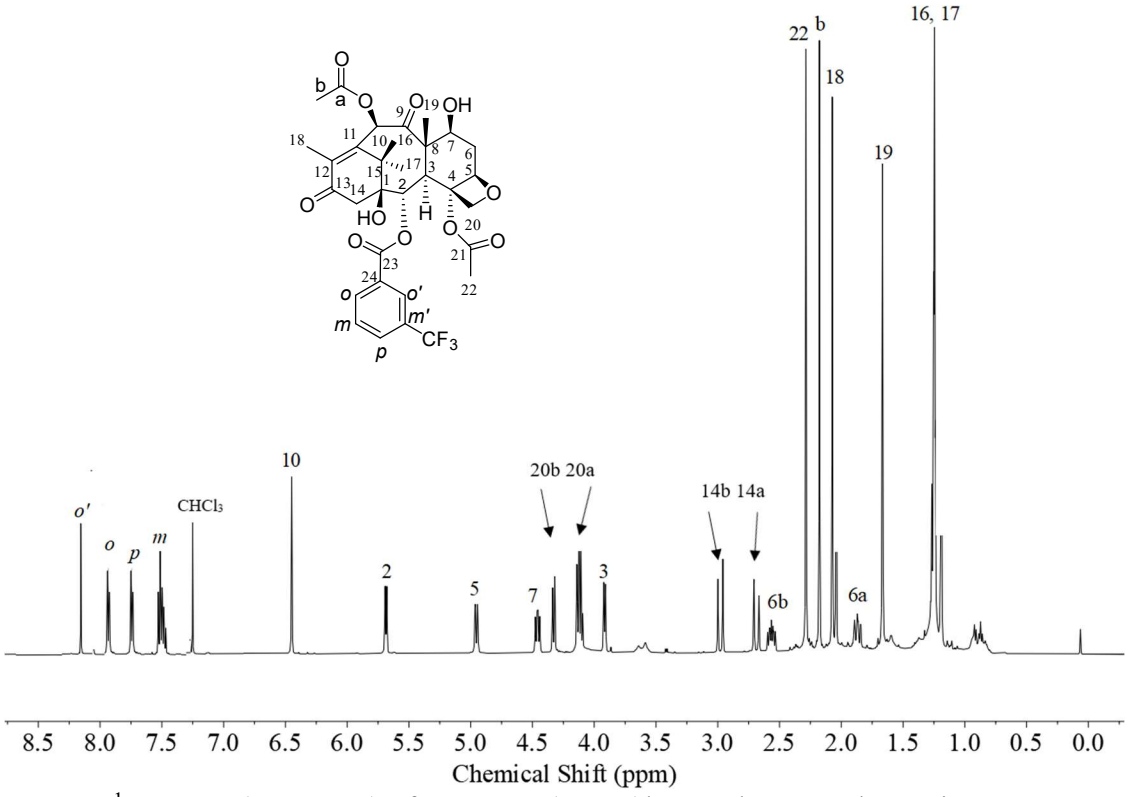

Figure 3.67: ^{1}H-NMR (500 MHz) of 2-DBz-2-(3-CF_3)benzoyl-13-oxo-baccatin III.

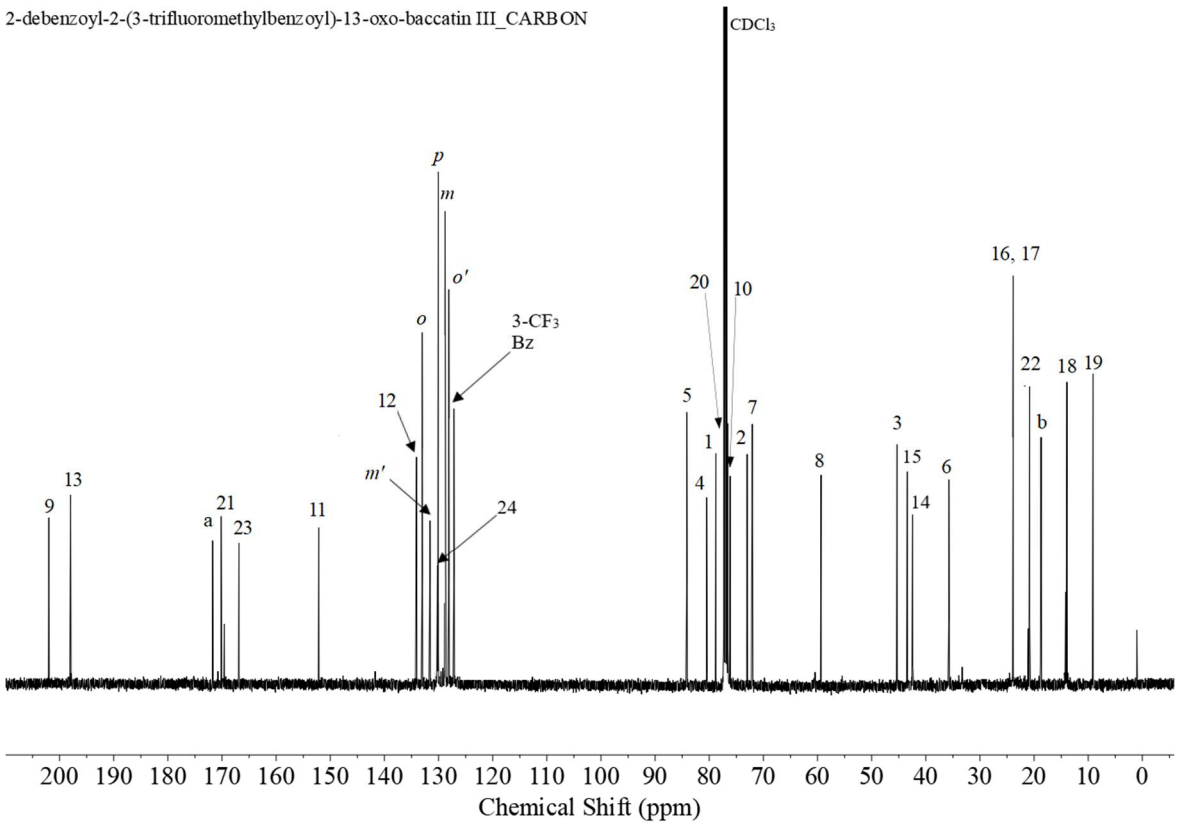

Figure 3.68: ^{13}C-NMR (126 MHz) of 2-DBz-2-(3-CF_3)benzoyl-13-oxo-baccatin III.

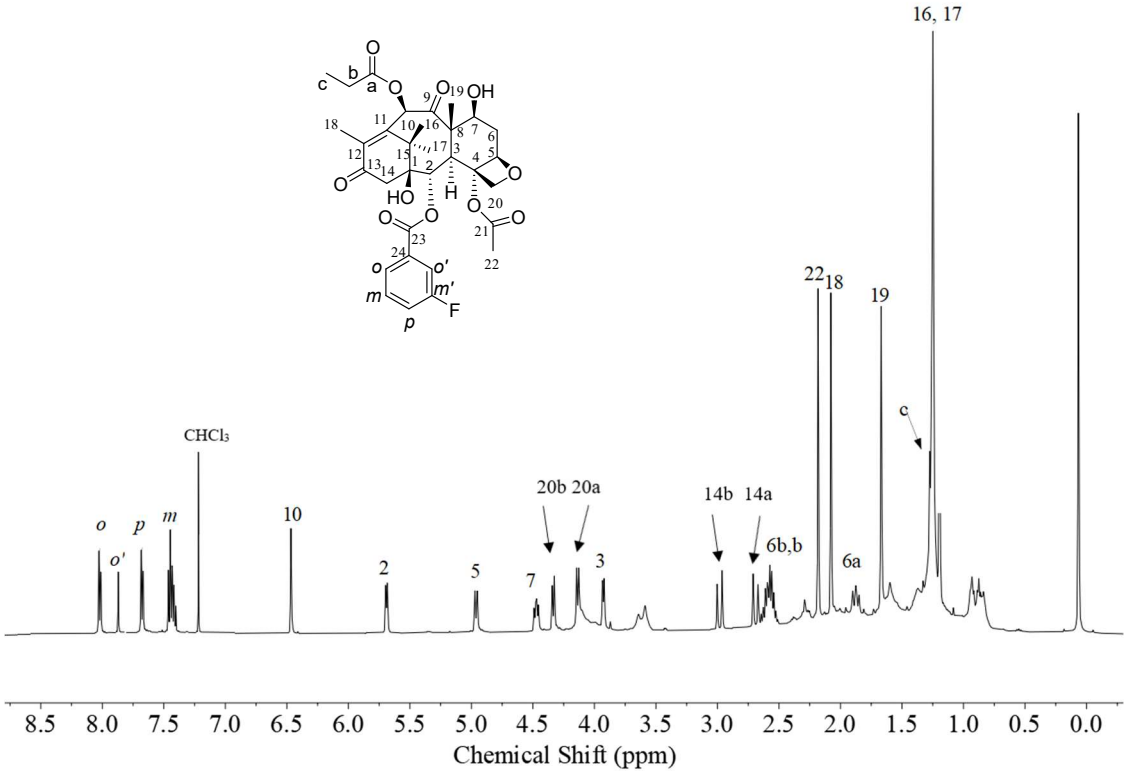

Figure 3.69: ^{1}H-NMR (500 MHz) of 2-DBz-2-(3-F)benzoyl-13-oxo-10-PDAB.

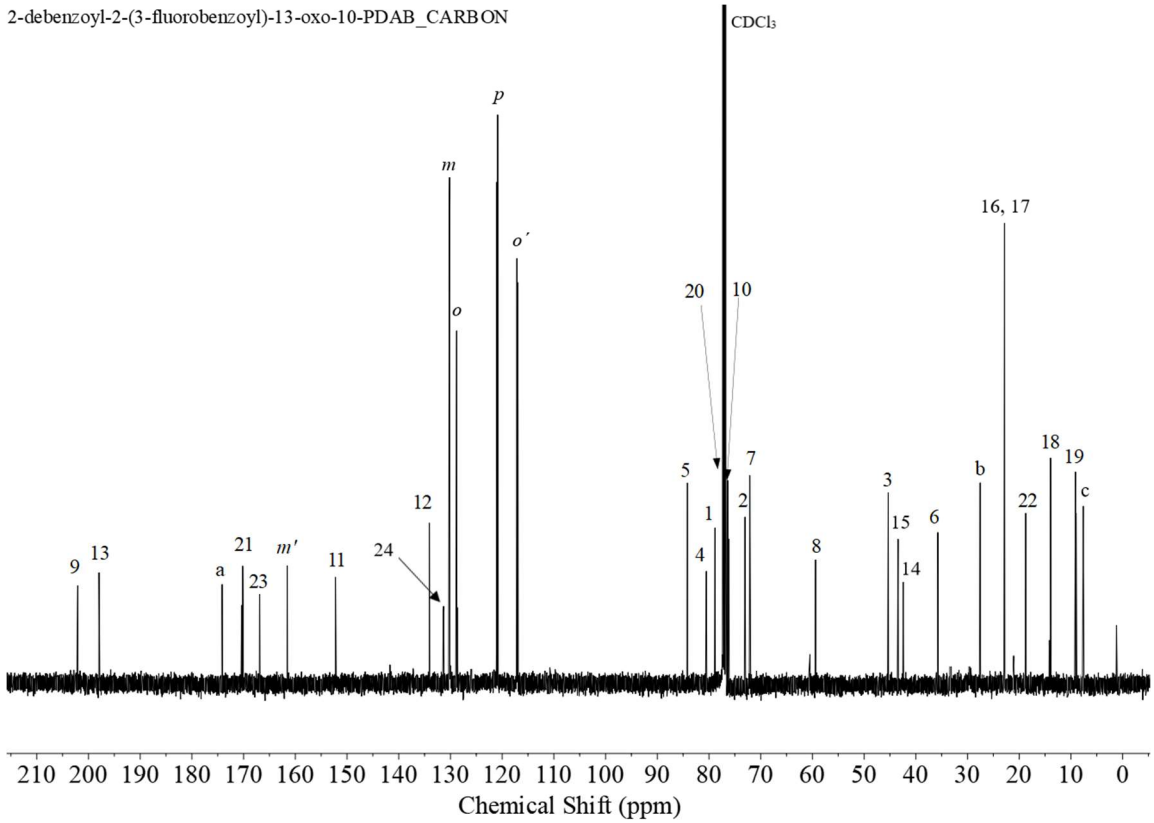

Figure 3.70: ^{13}C-NMR (126 MHz) of 2-DBz-2-(3-F)benzoyl-13-oxo-10-PDAB.

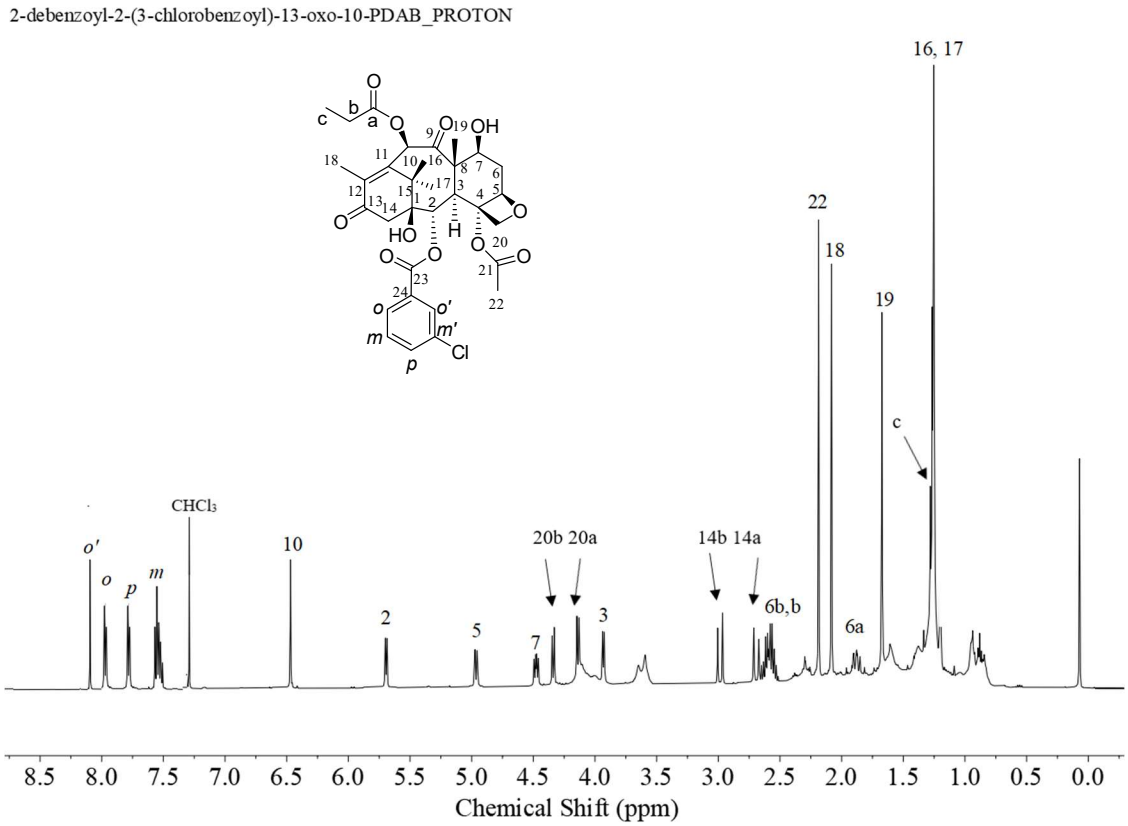

Figure 3.71: ^{1}H-NMR (500 MHz) of 2-DBz-2-(3-Cl)benzoyl-13-oxo-10-PDAB.

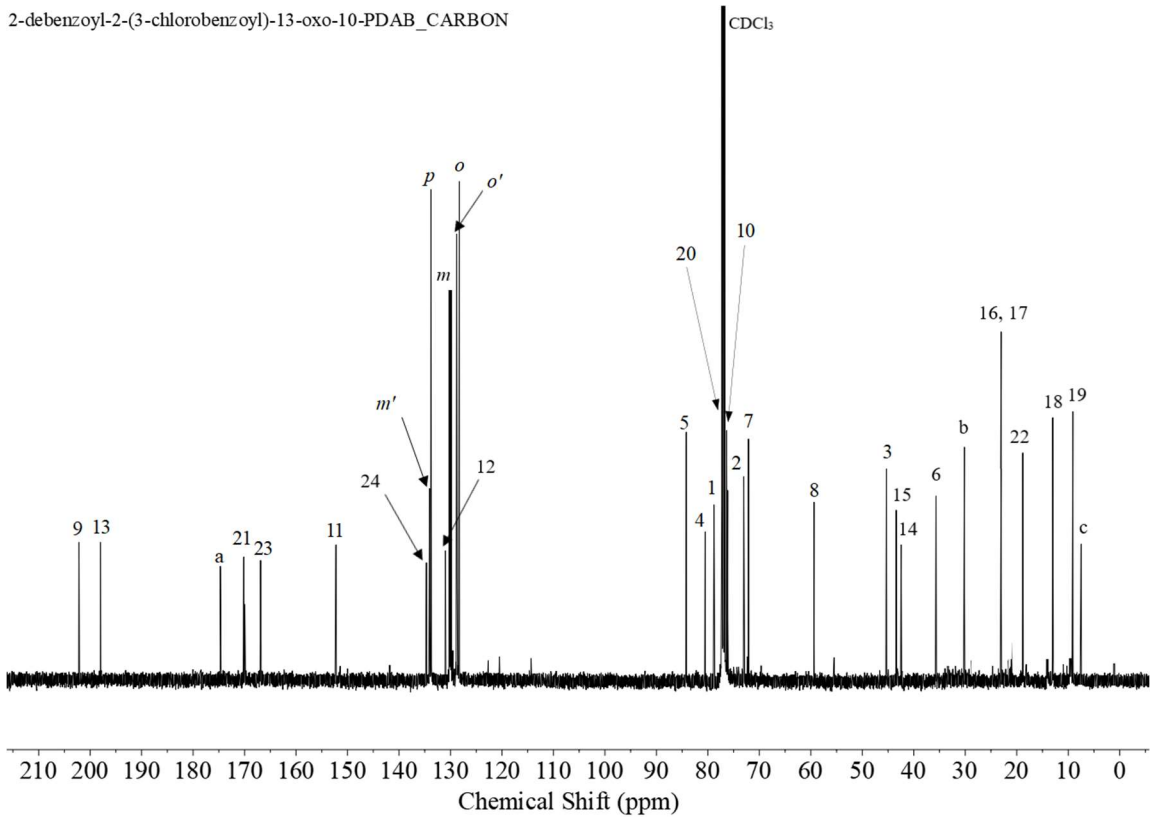

Figure 3.72: ^{13}C-NMR (126 MHz) of 2-DBz-2-(3-Cl)benzoyl-13-oxo-10-PDAB.

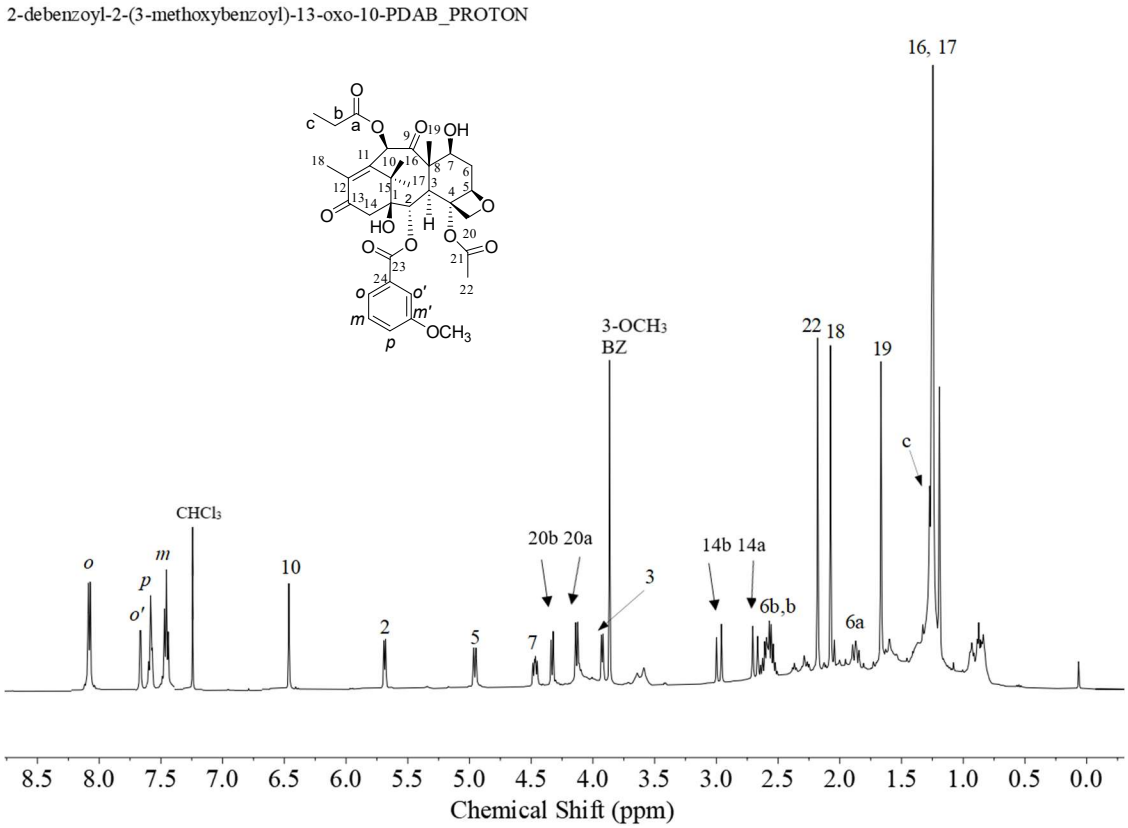

Figure 3.73: ^{1}H-NMR (500 MHz) of 2-DBz-2-(3-OCH_3)benzoyl-13-oxo-10-PDAB.

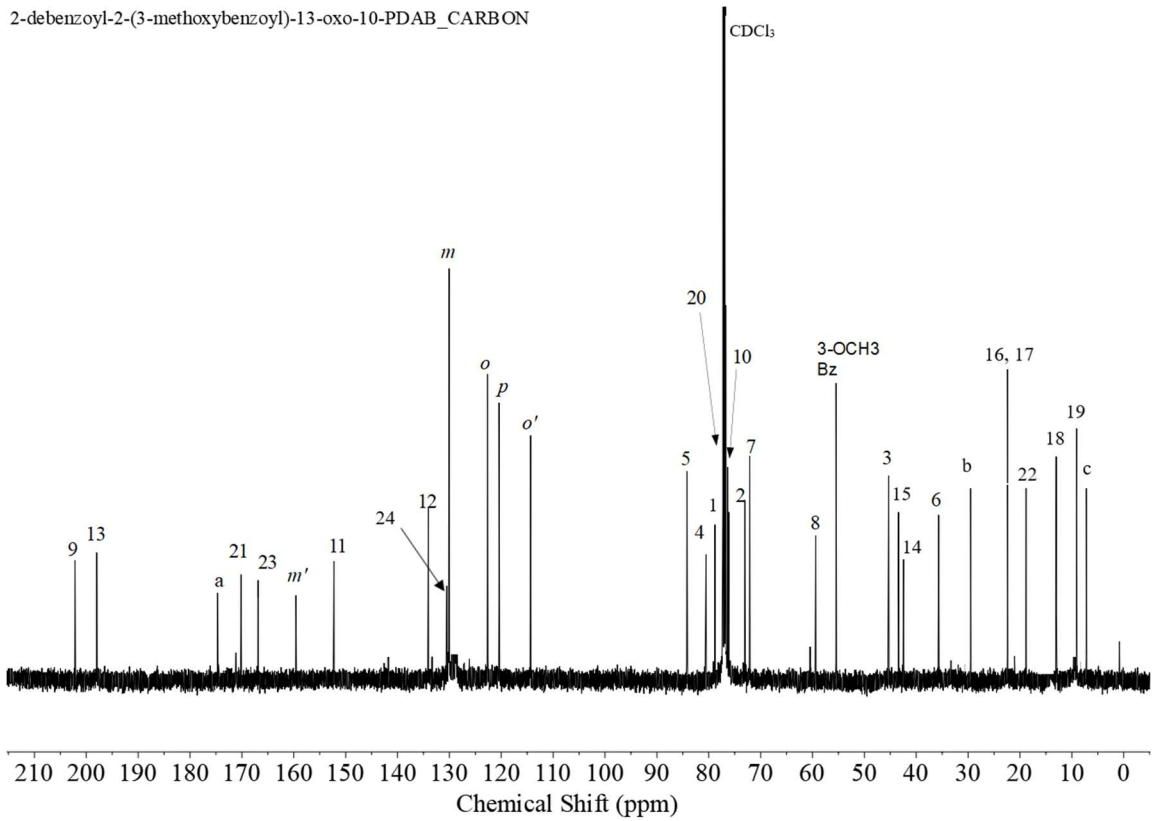

Figure 3.74: ^{13}C-NMR (126 MHz) of 2-DBz-2-(3-OCH_3)benzoyl-13-oxo-10-PDAB.

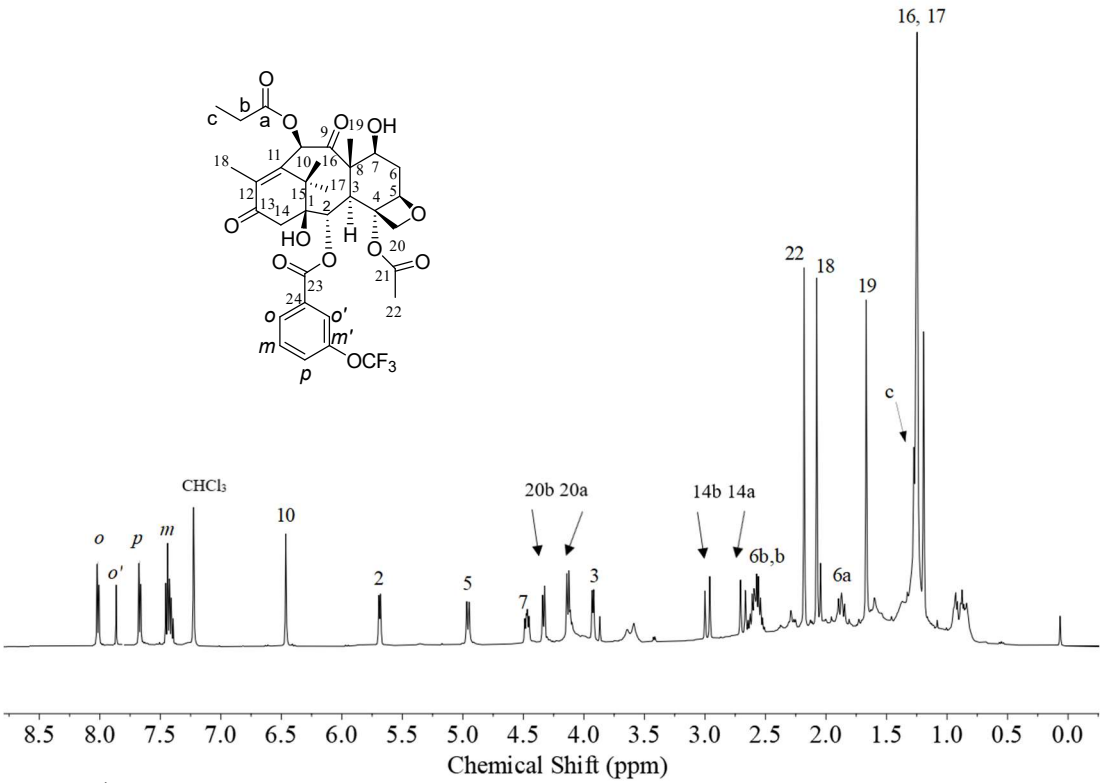

Figure 3.75: ^{1}H-NMR (500 MHz) of 2-DBz-2-(3-OCF_3)benzoyl-13-oxo-10-PDAB.

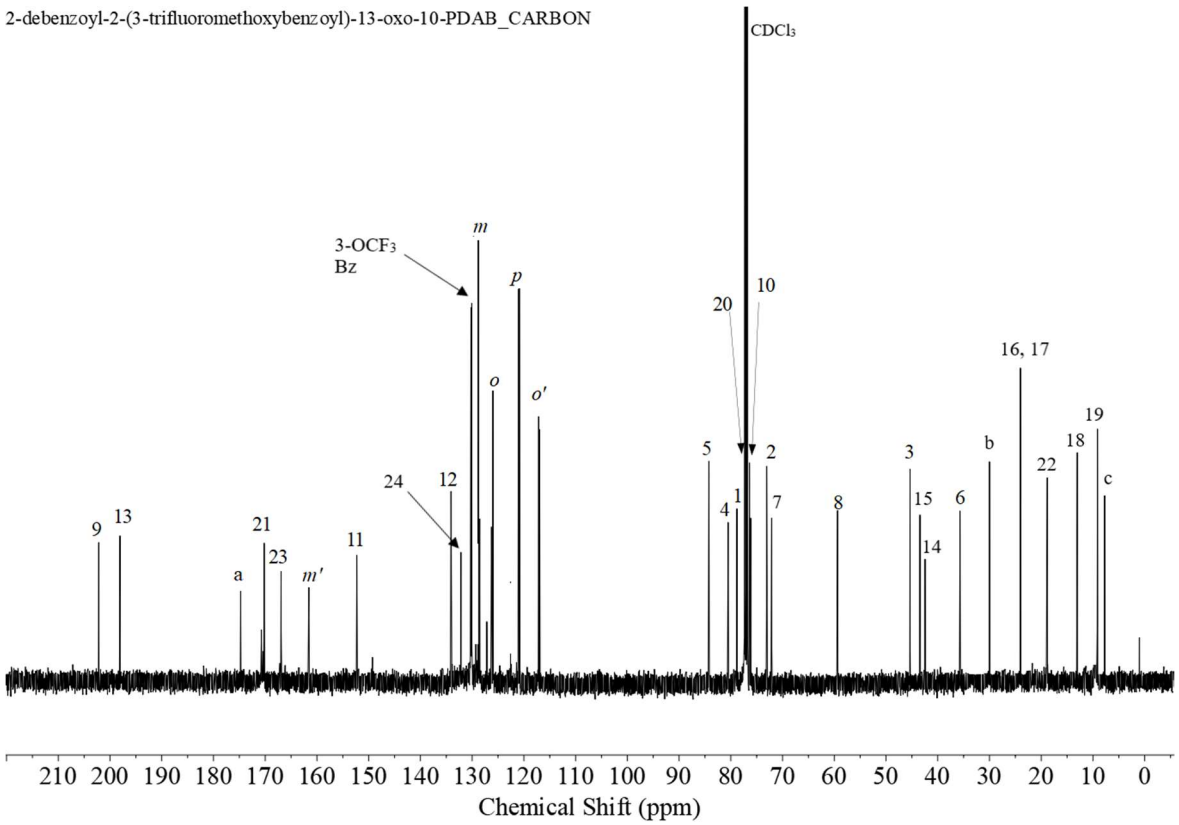

Figure 3.76: ^{13}C-NMR (126 MHz) of 2-DBz-2-(3-OCF_3)benzoyl-13-oxo-10-PDAB.

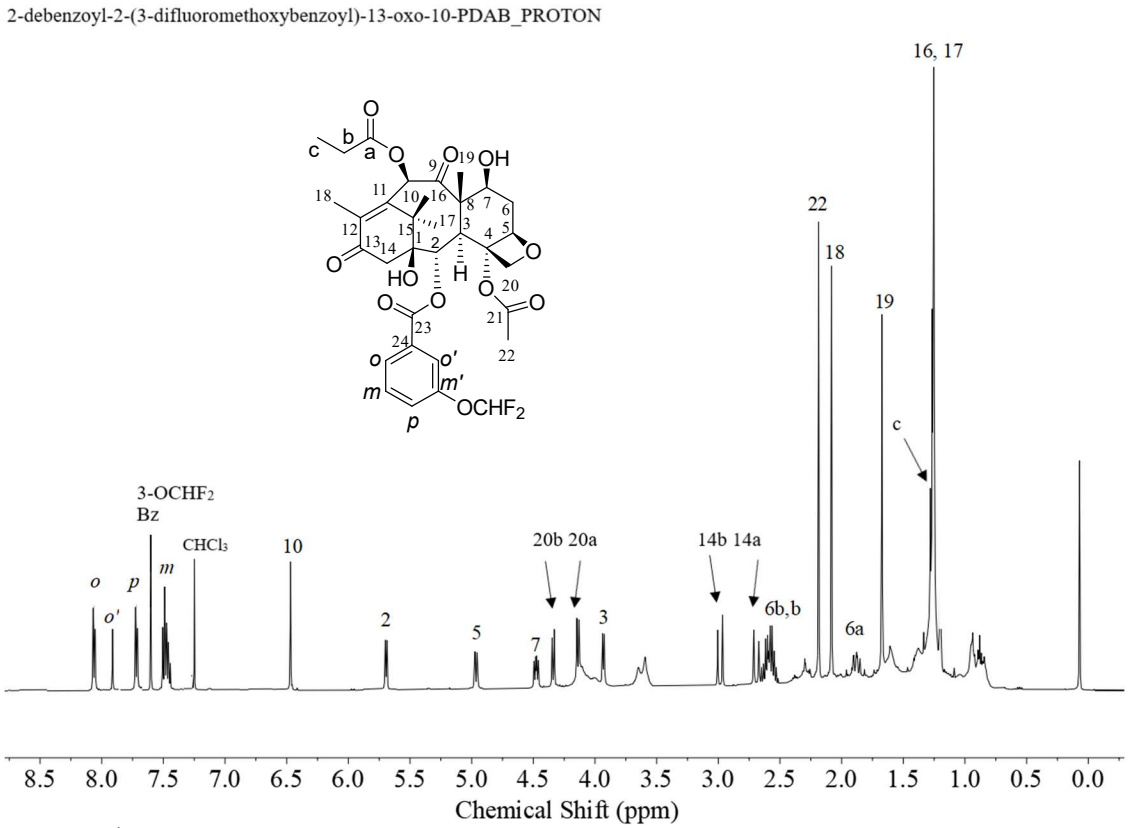

Figure 3.77: ^{1}H-NMR (500 MHz) of 2-DBz-2-(3-$OCHF_2$)benzoyl-13-oxo-10-PDAB.

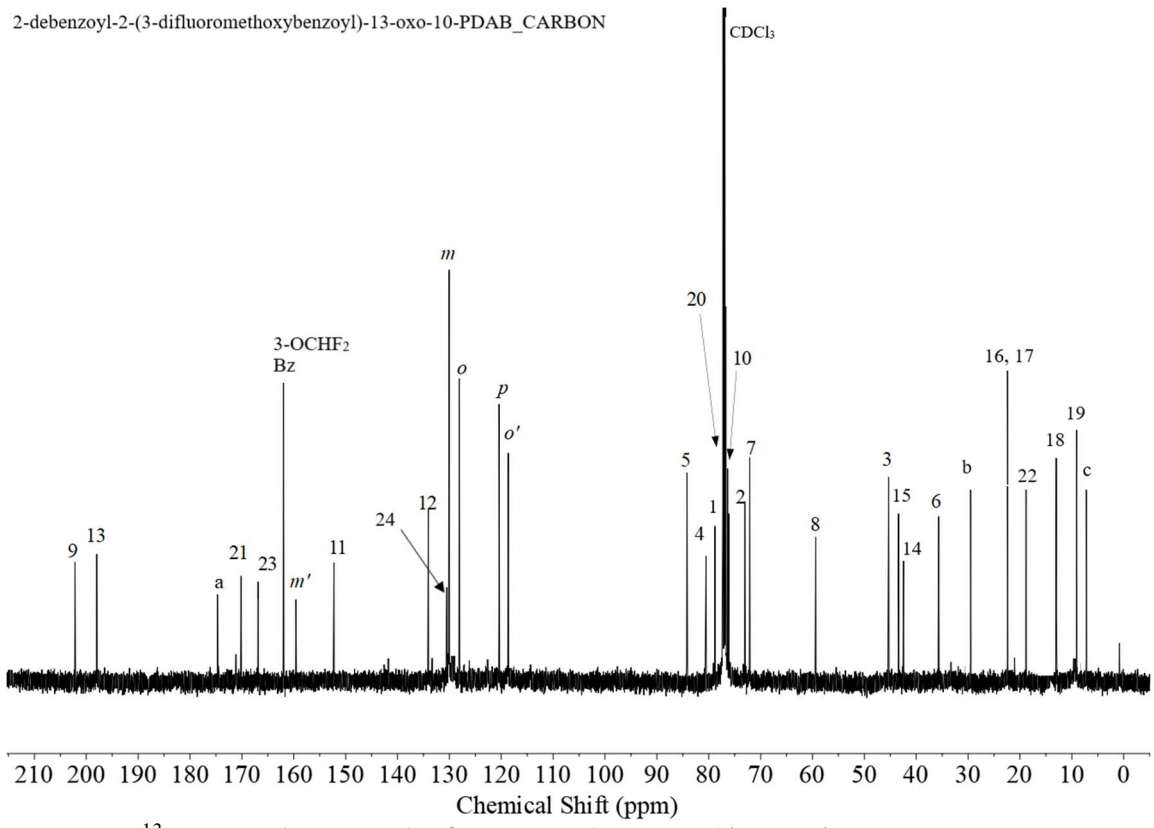

Figure 3.78: ^{13}C-NMR (126 MHz) of 2-DBz-2-(3-$OCHF_2$)benzoyl-13-oxo-10-PDAB.

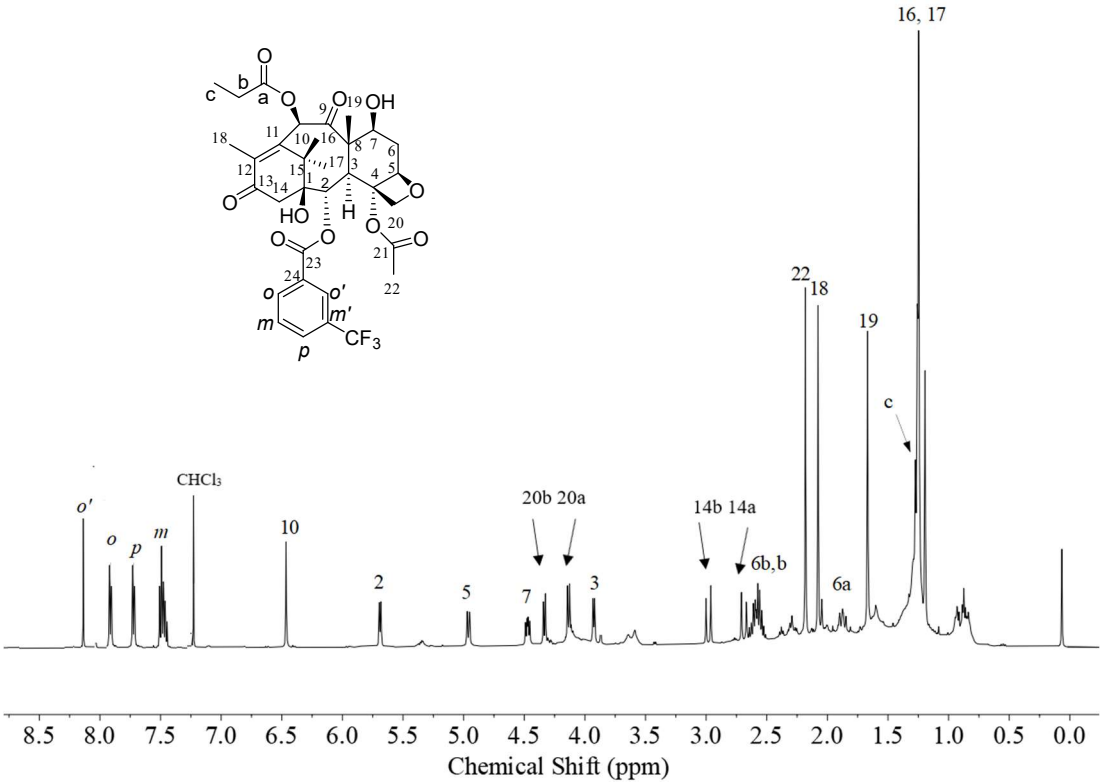

Figure 3.79: ^{1}H-NMR (500 MHz) of 2-DBz-2-(3-CF_3)benzoyl-13-oxo-10-PDAB.

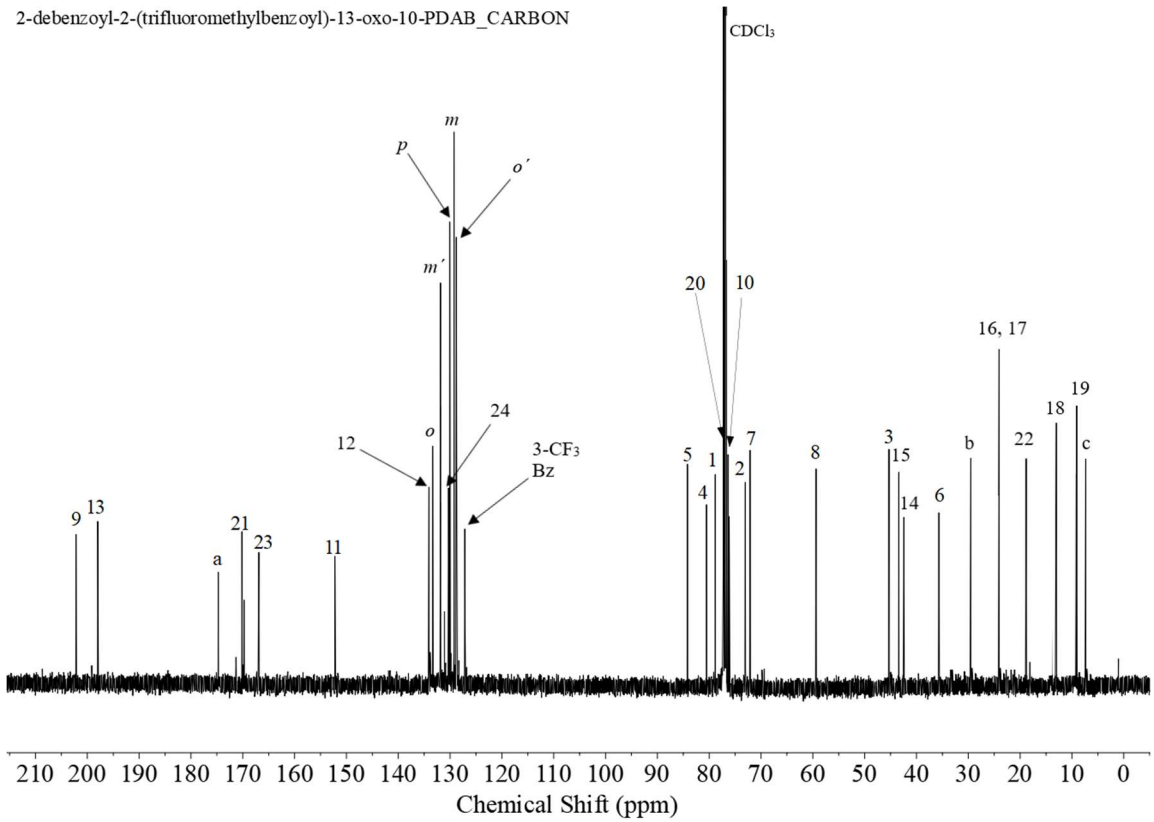

Figure 3.80: ^{13}C-NMR (126 MHz) of 2-DBz-2-(3-CF_3)benzoyl-13-oxo-10-PDAB.

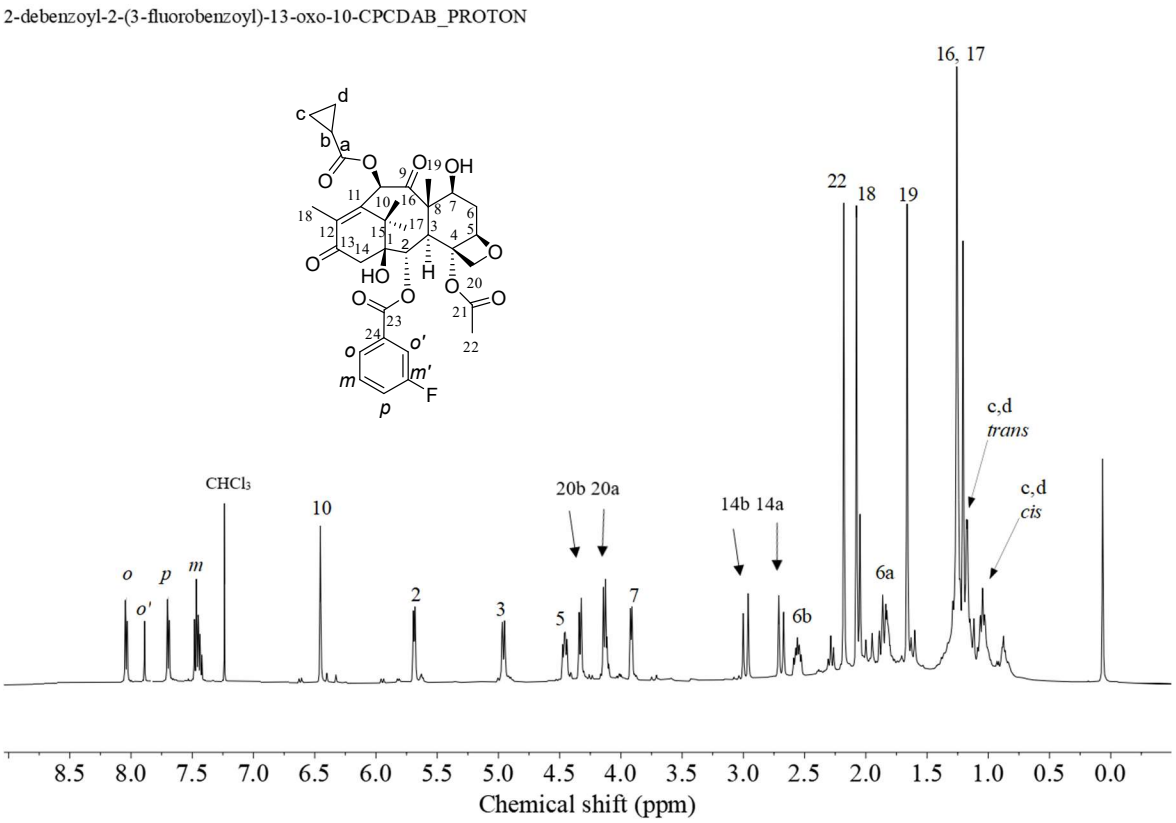

Figure 3.81: ^{1}H-NMR (500 MHz) of 2-DBz-2-(3-F)benzoyl-13-oxo-10-CPCDAB.

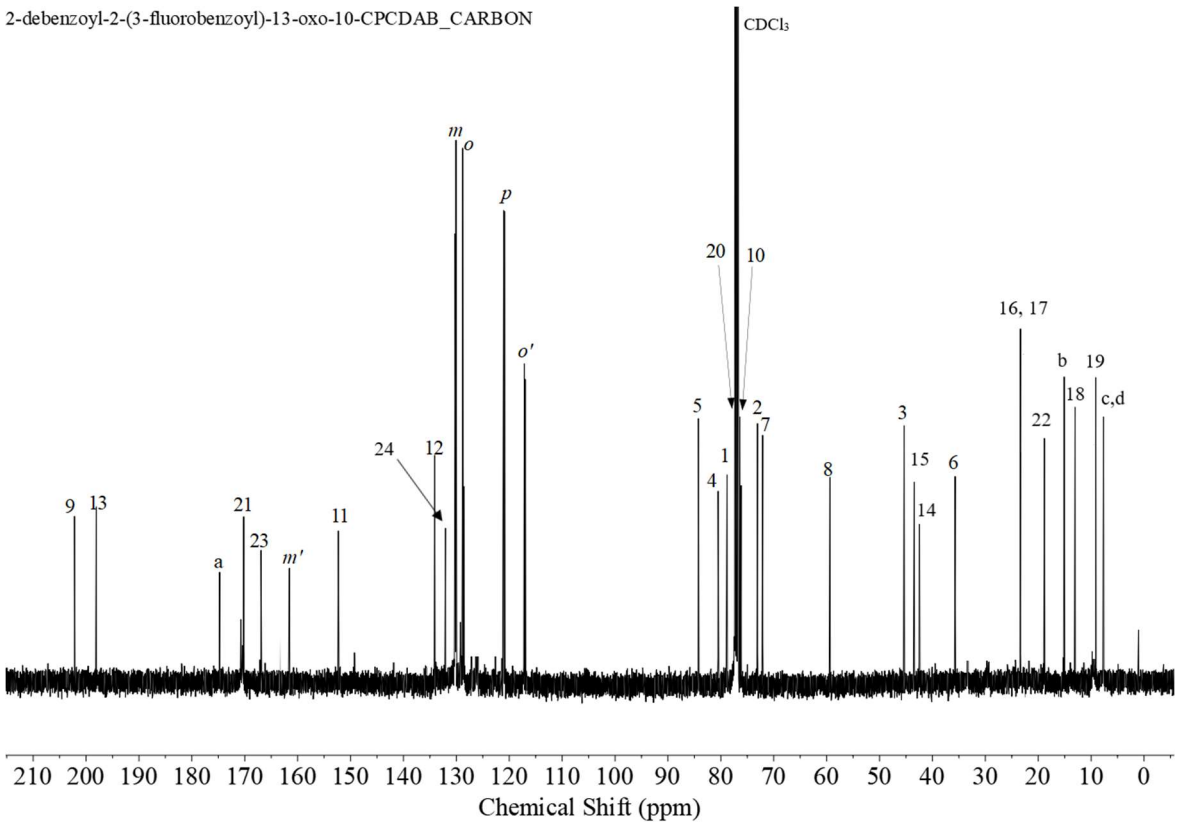

Figure 3.82: ^{13}C-NMR (126 MHz) of 2-DBz-2-(3-F)benzoyl-13-oxo-10-CPCDAB.

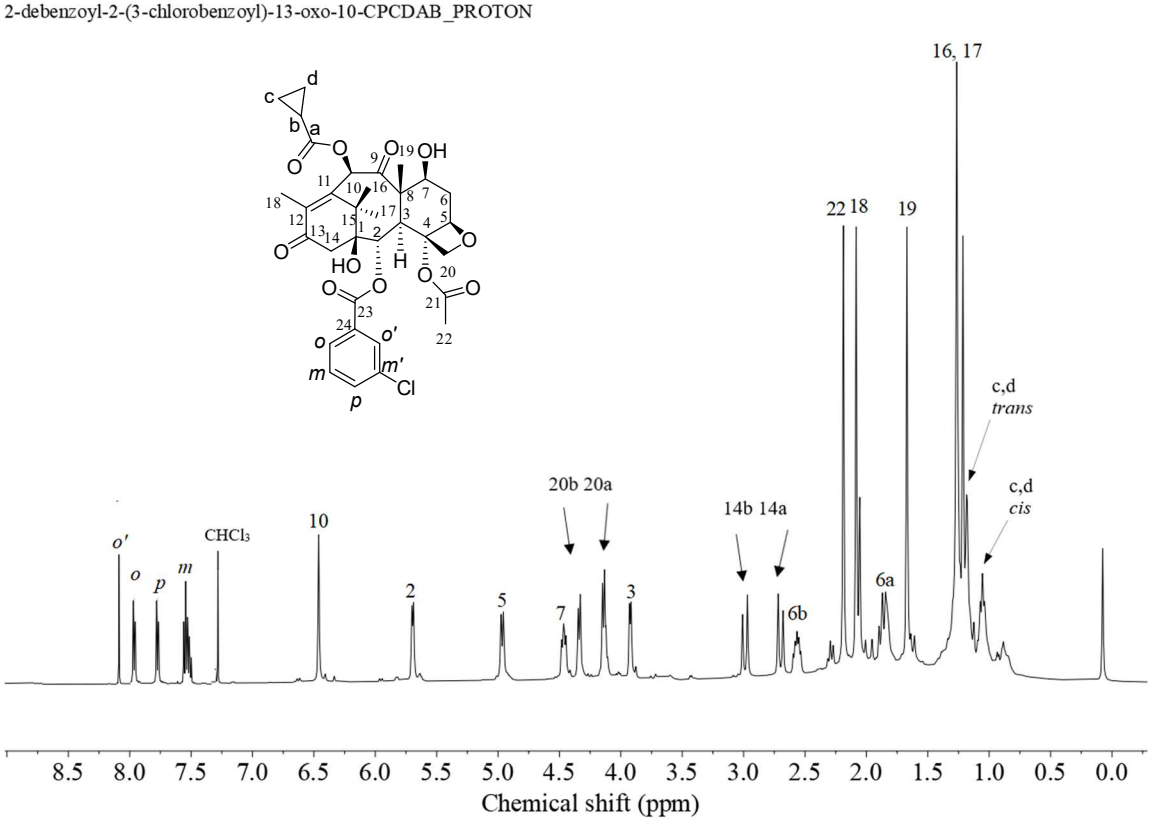

Figure 3.83: ^{1}H-NMR (500 MHz) of 2-DBz-2-(3-Cl)benzoyl-13-oxo-10-CPCDAB.

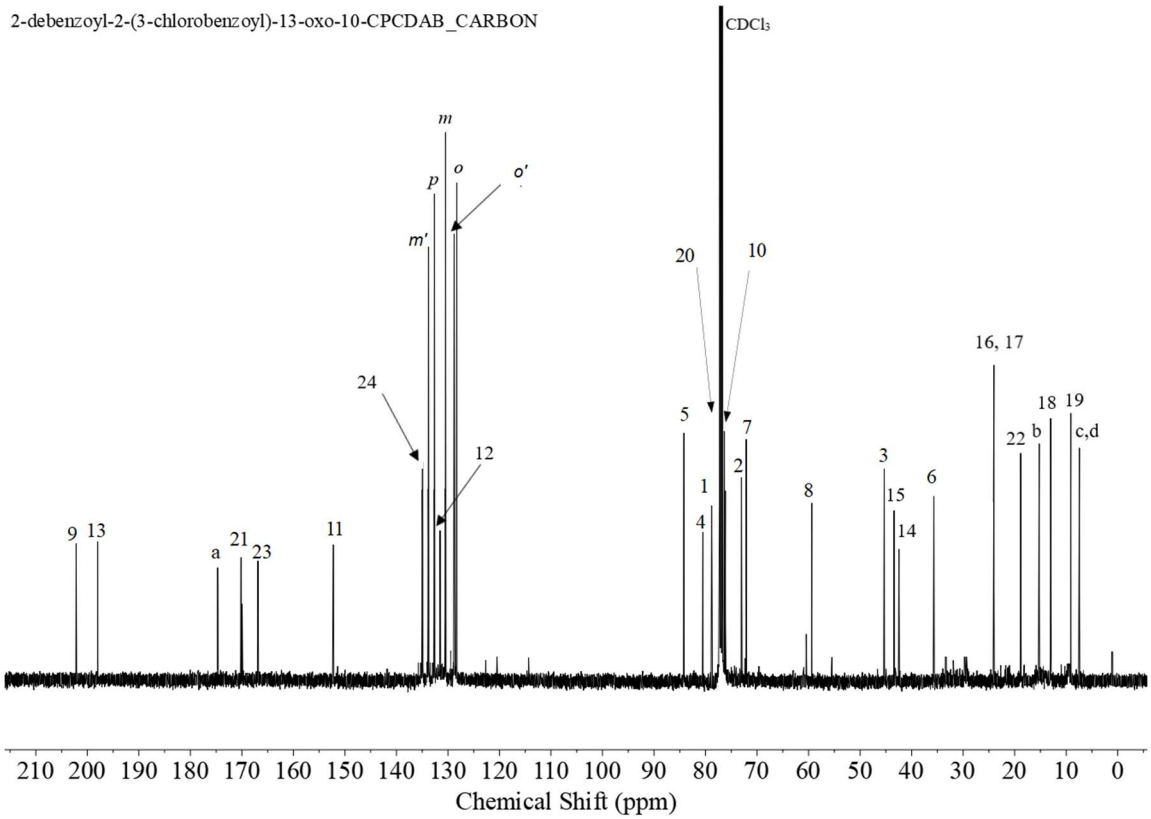

Figure 3.84: ^{13}C-NMR (126 MHz) of 2-DBz-2-(3-Cl)benzoyl-13-oxo-10-CPCDAB.

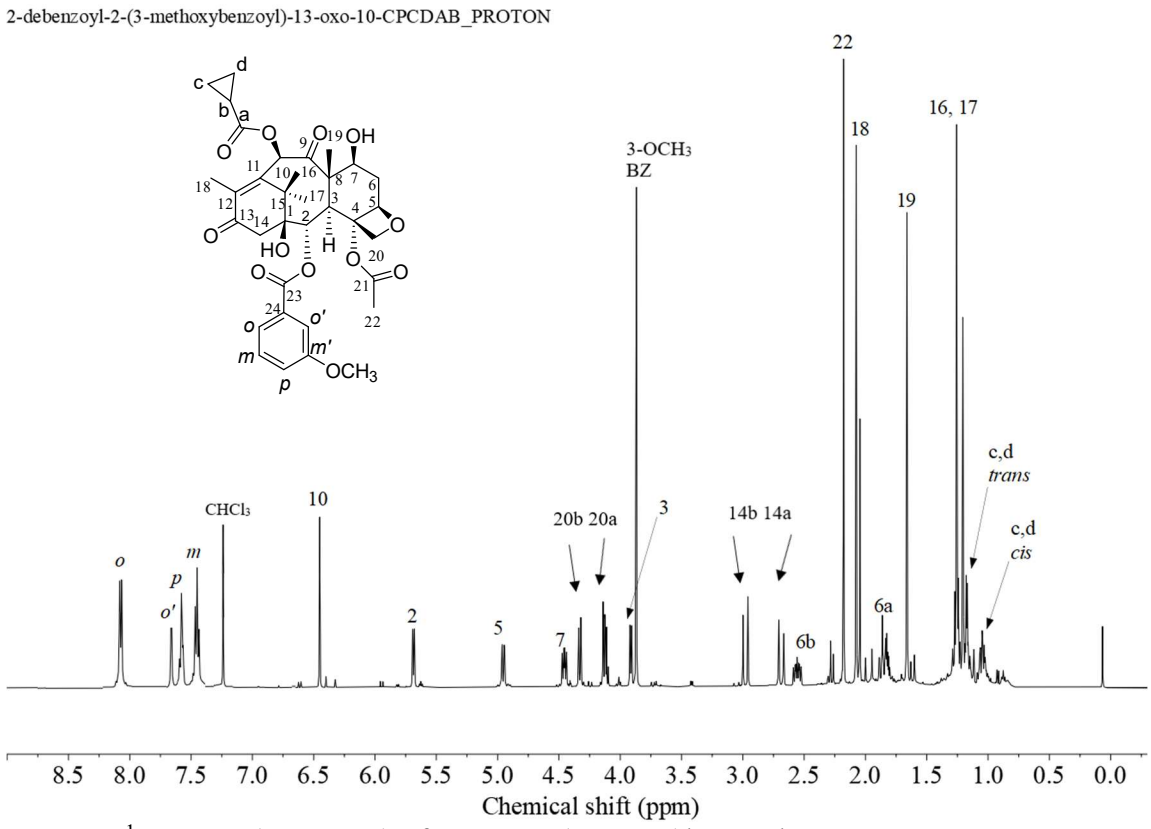

Figure 3.85: ^{1}H-NMR (500 MHz) of 2-DBz-2-(3-OCH_3)benzoyl-13-oxo-10-CPCDAB.

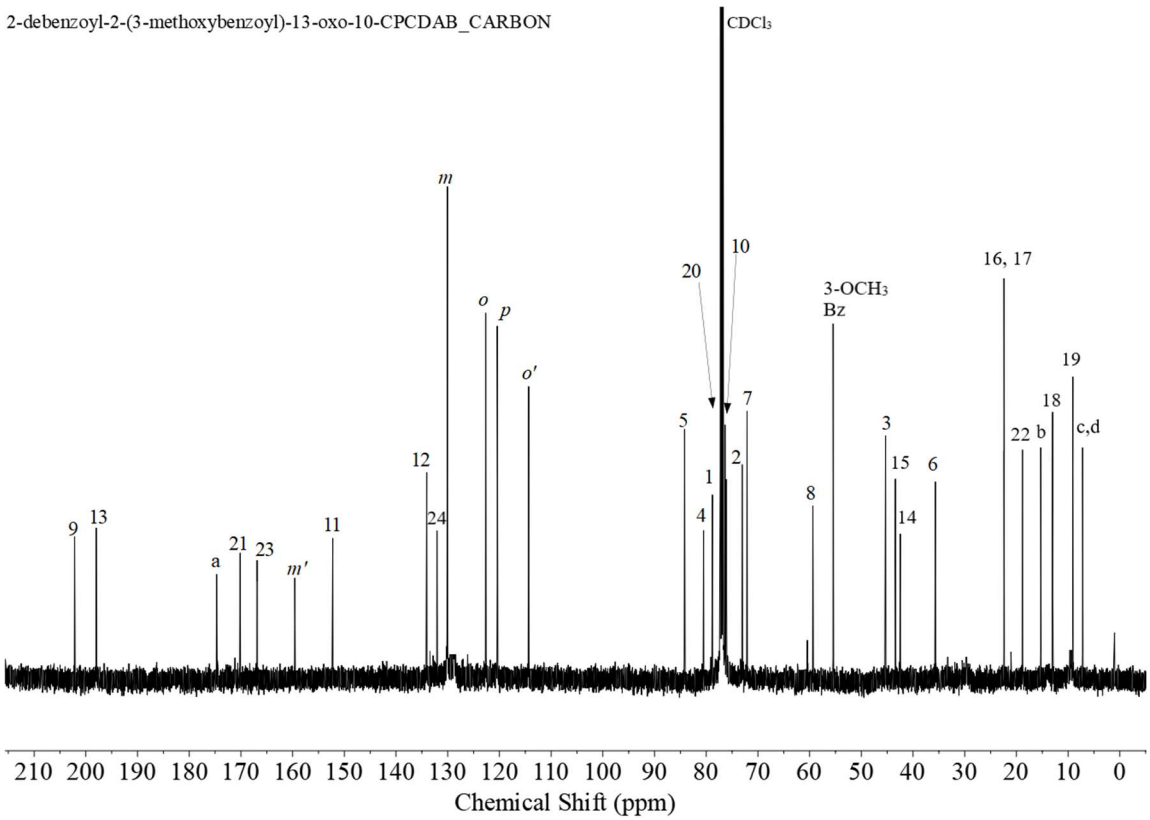

Figure 3.86: ^{13}C-NMR (126 MHz) of 2-DBz-2-(3- OCH_3)benzoyl-13-oxo-10-CPCDAB.

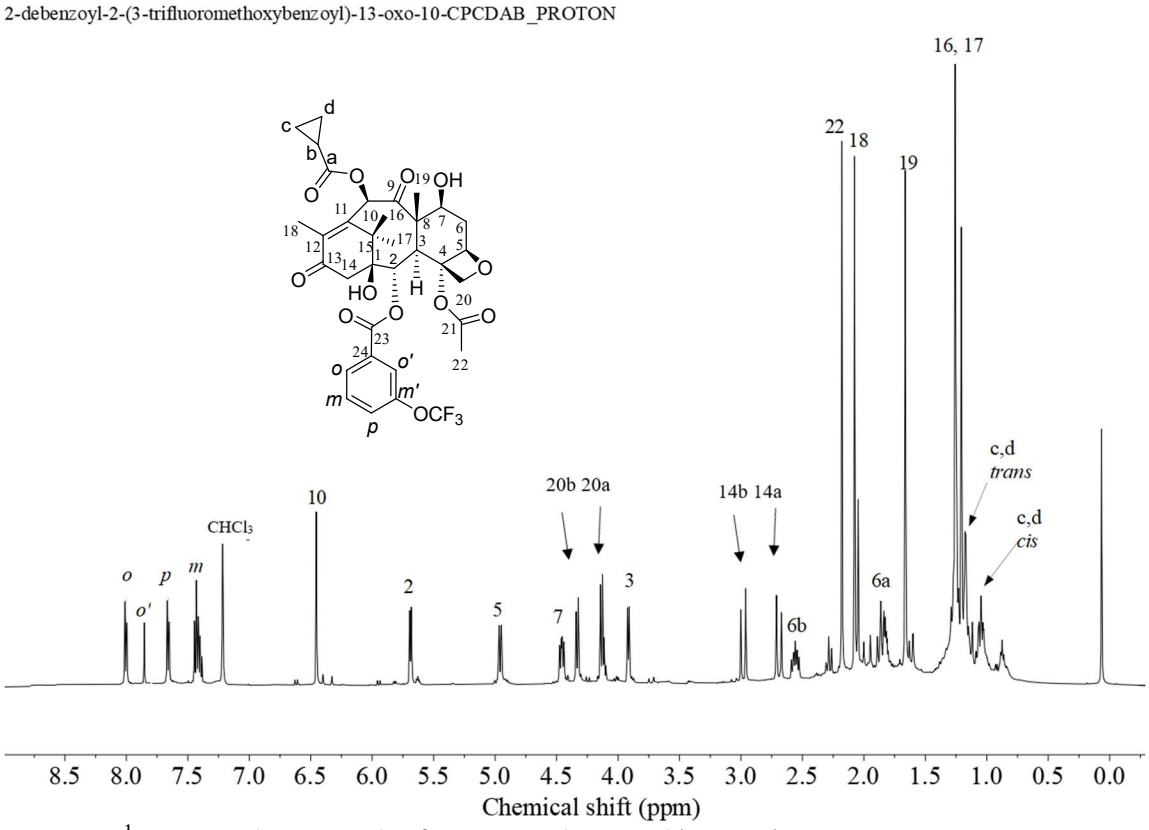

Figure 3.87: ^{1}H-NMR (500 MHz) of 2-DBz-2-(3-OCF_3)benzoyl-13-oxo-10-CPCDAB.

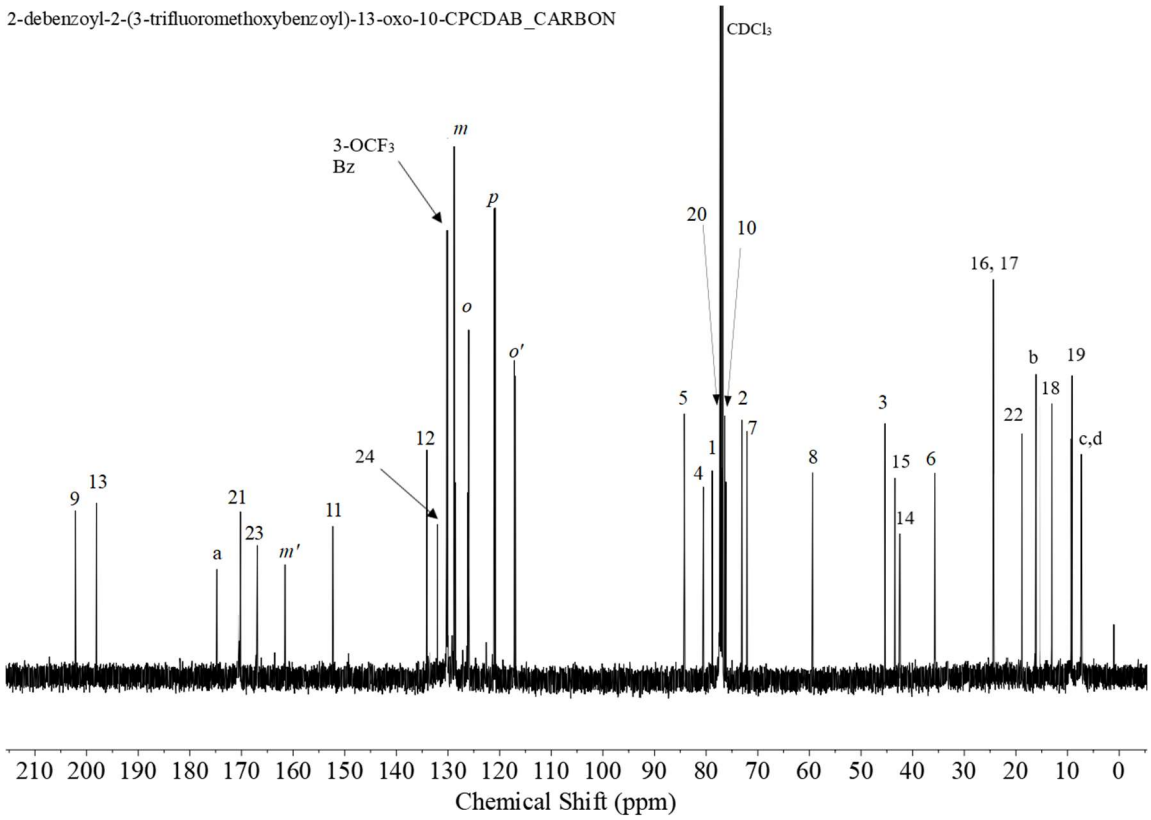

Figure 3.88: ^{13}C-NMR (126 MHz) of 2-DBz-2-(3- OCF_3)benzoyl-13-oxo-10-CPCDAB.

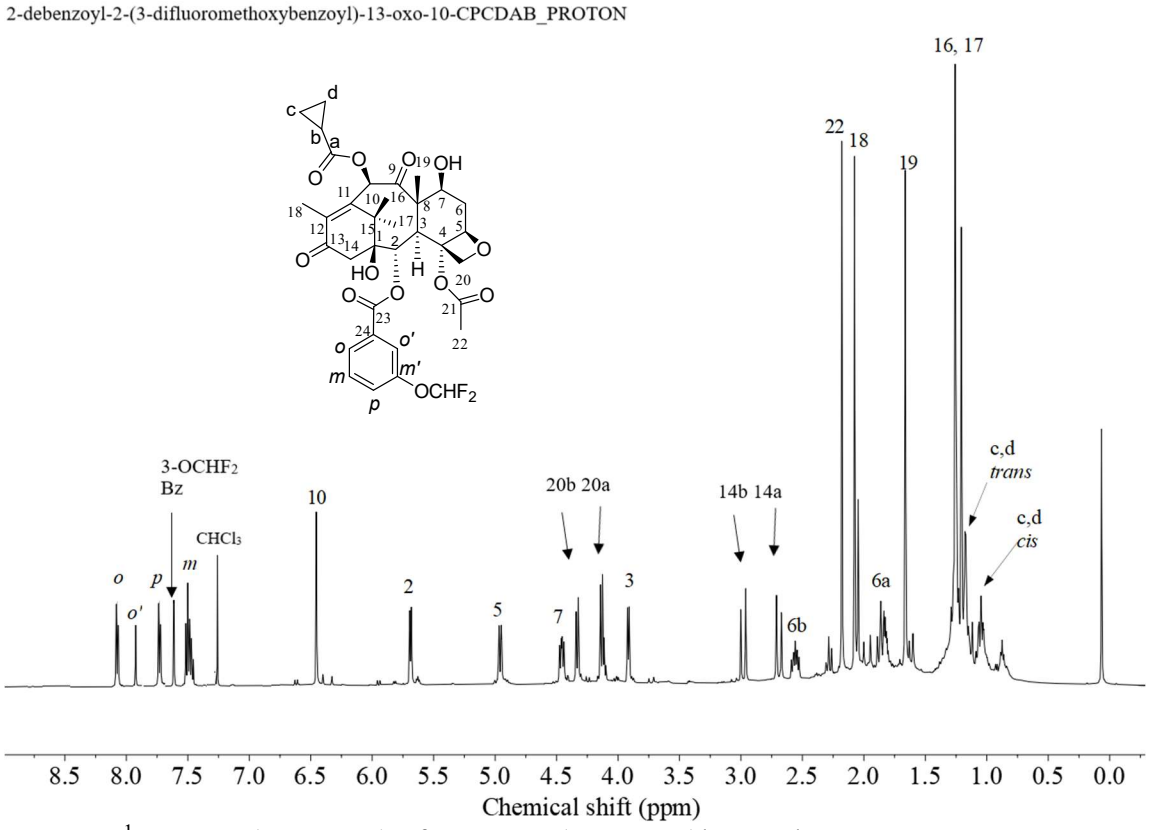

Figure 3.89: ^{1}H-NMR (500 MHz) of 2-DBz-2-(3-$OCHF_2$)benzoyl-13-oxo-10-CPCDAB.

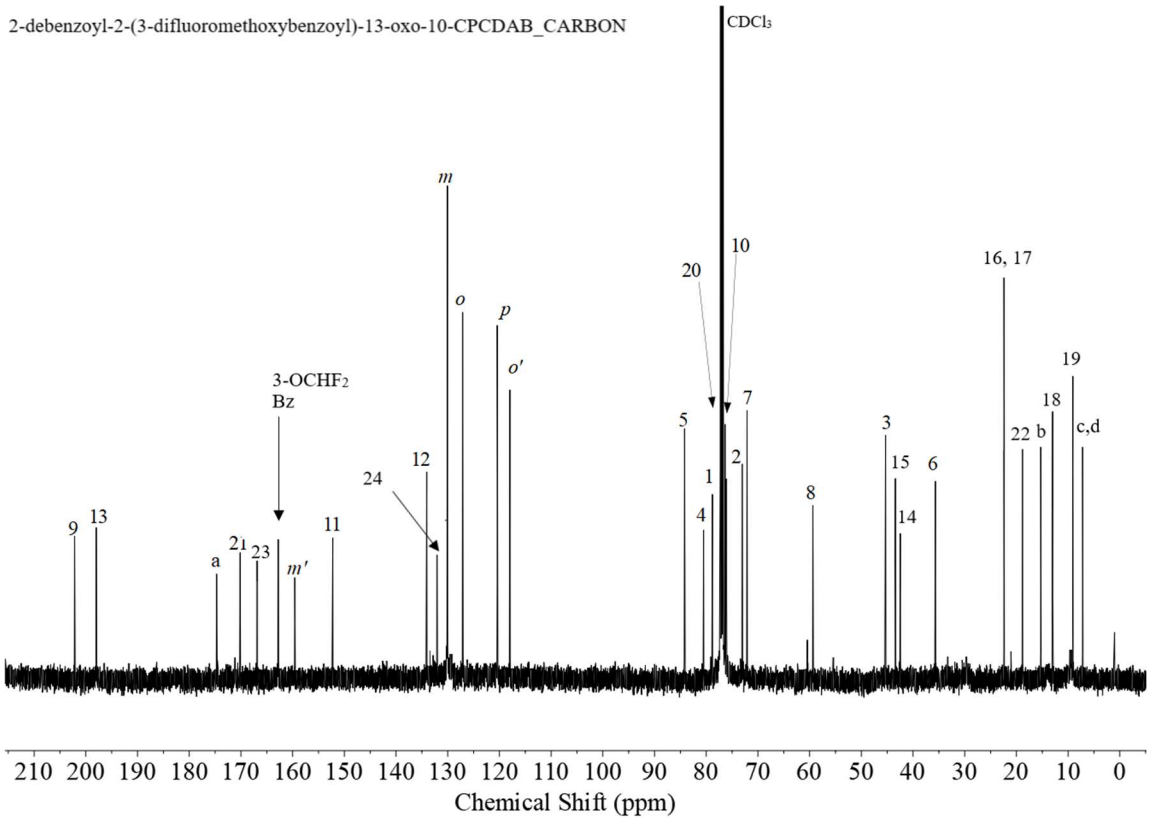

Figure 3.90: ^{13}C-NMR (126 MHz) of 2-DBz-2-(3- $OCHF_2$)benzoyl-13-oxo-10-CPCDAB.

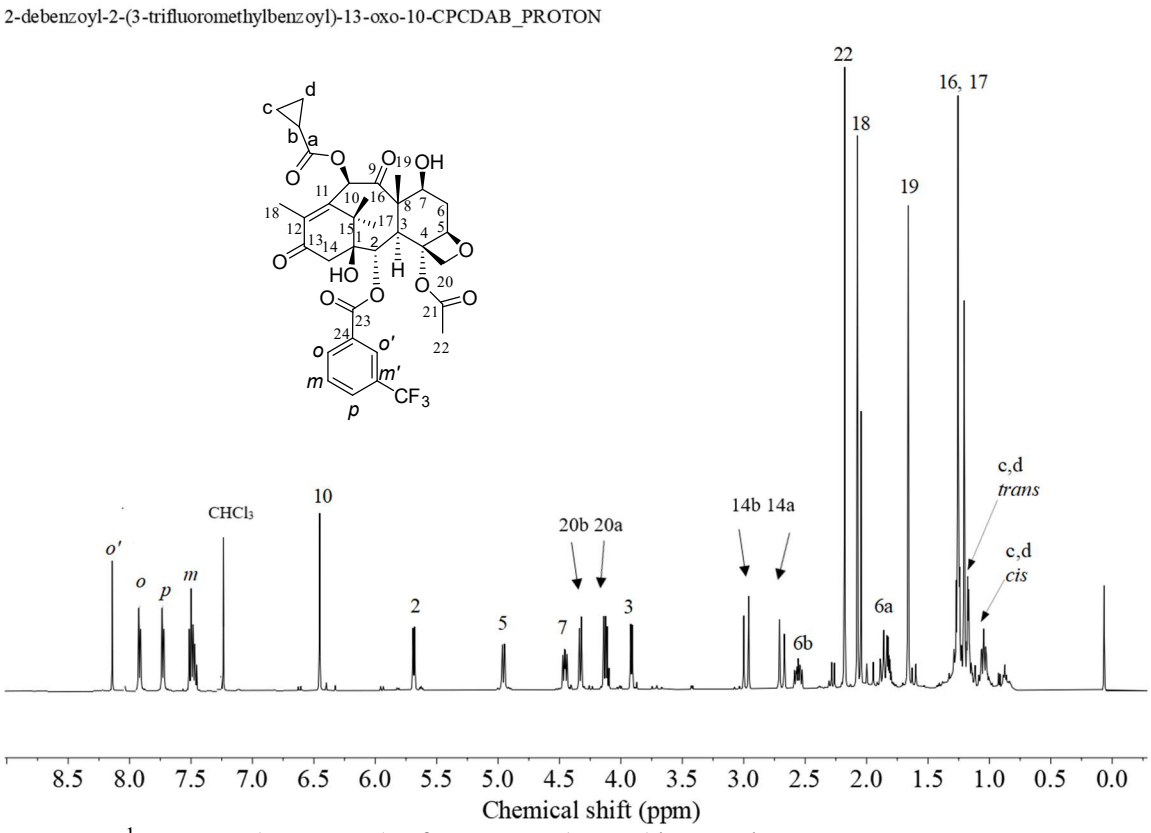

Figure 3.91: ^{1}H-NMR (500 MHz) of 2-DBz-2-(3-CF_3)benzoyl-13-oxo-10-CPCDAB.

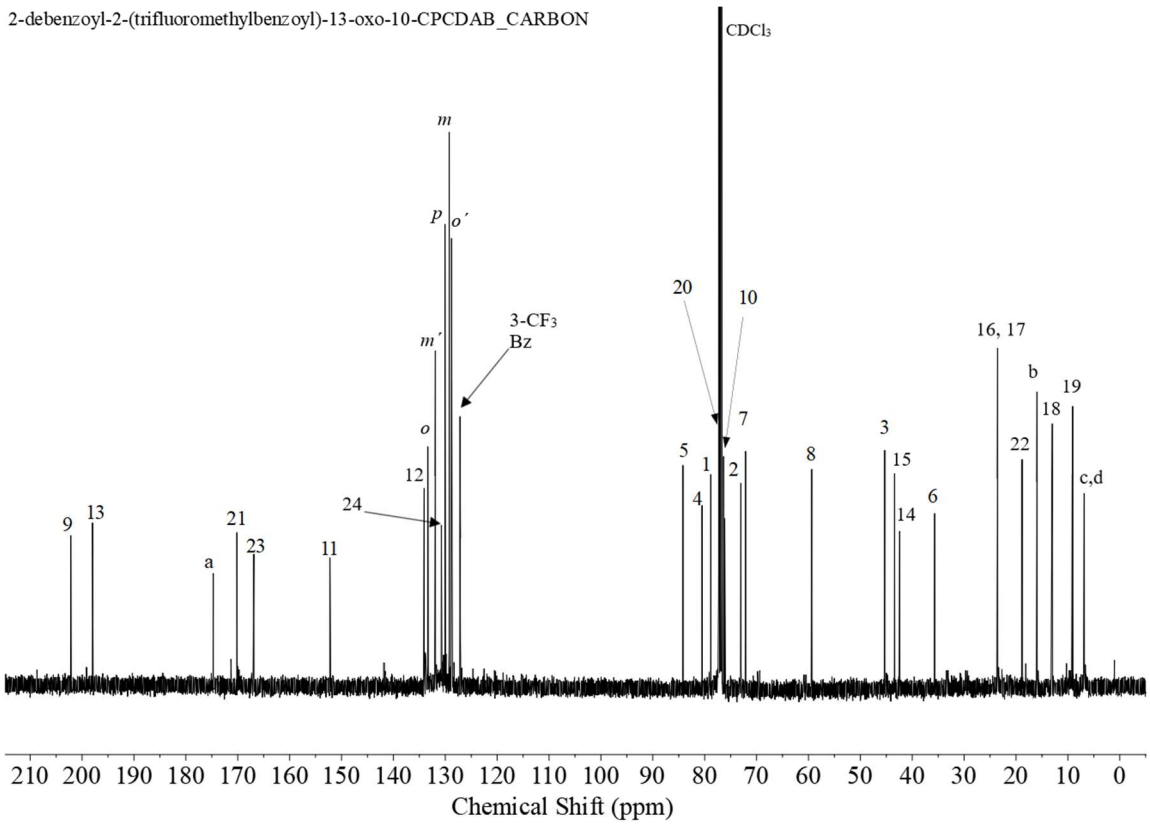

Figure 3.92: ^{13}C-NMR (126 MHz) of 2-DBz-2-(3-CF_3)benzoyl-13-oxo-10-CPCDAB.

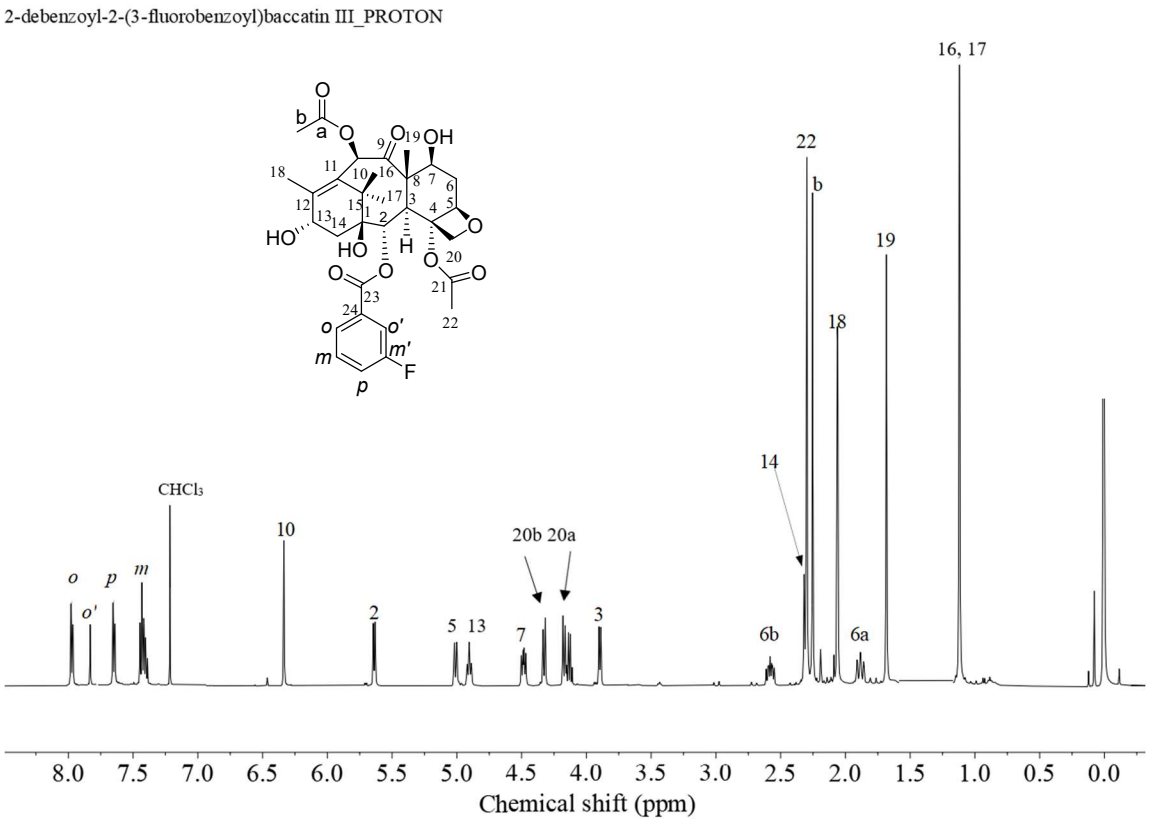

Figure 3.93: ^{1}H-NMR (500 MHz) of 2-DBz-2-(3-F)benzoylbaccatin III.

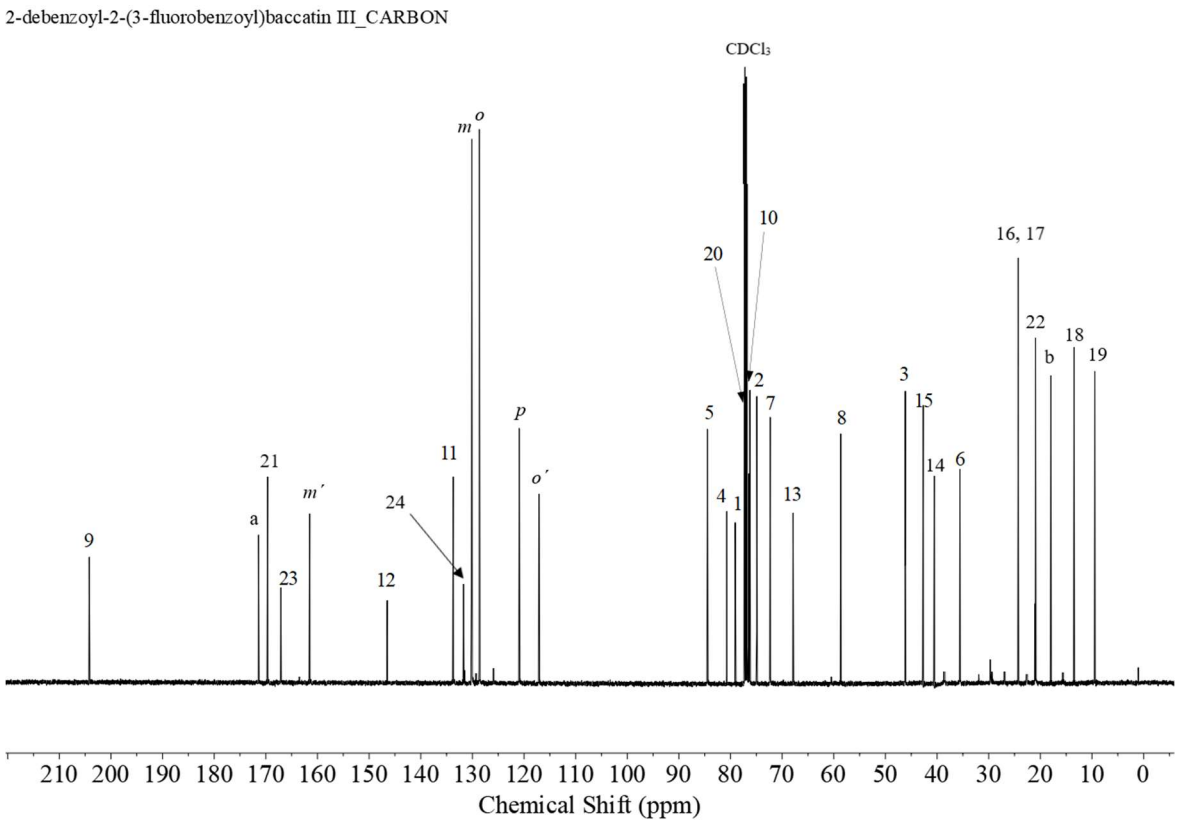

Figure 3.94: ^{13}C-NMR (126 MHz) of 2-DBz-2-(3-F)benzoylbaccatin III.

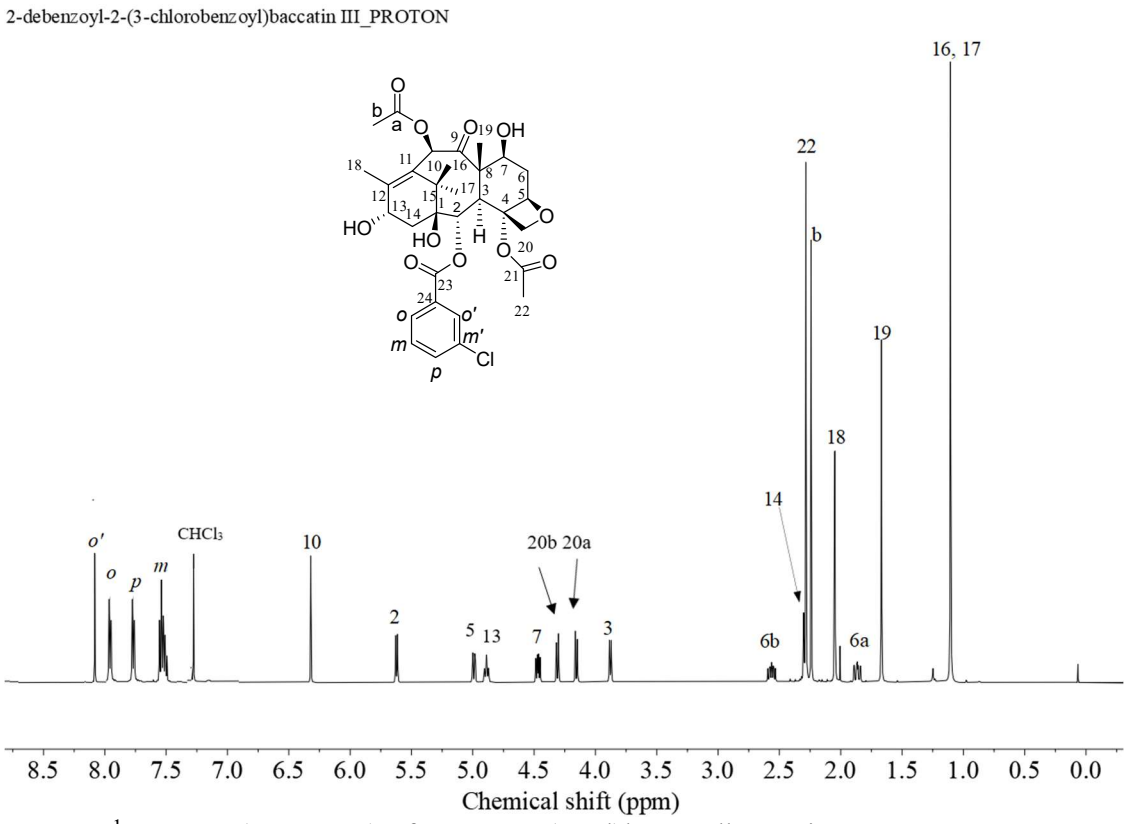

Figure 3.95: ^{1}H-NMR (500 MHz) of 2-DBz-2-(3-Cl)benzoylbaccatin III.

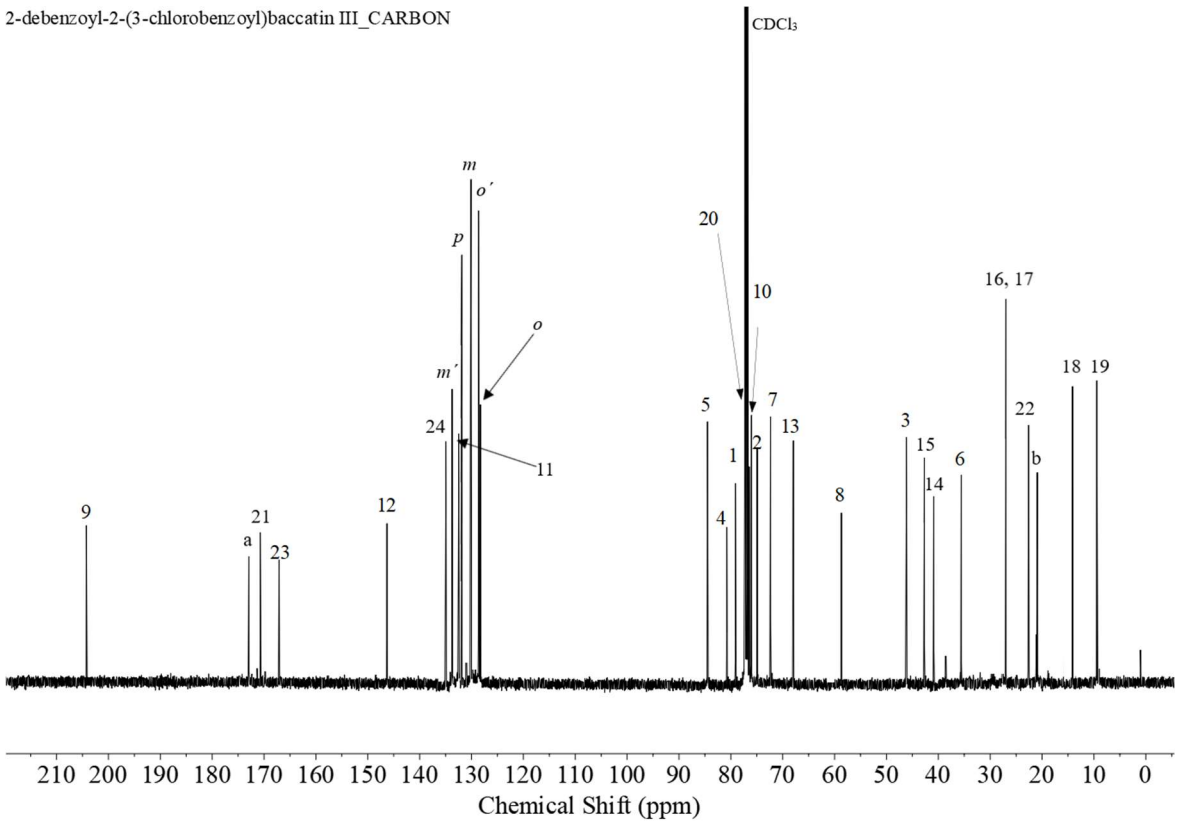

Figure 3.96: ^{13}C-NMR (126 MHz) of 2-DBz-2-(3-Cl)benzoylbaccatin III.

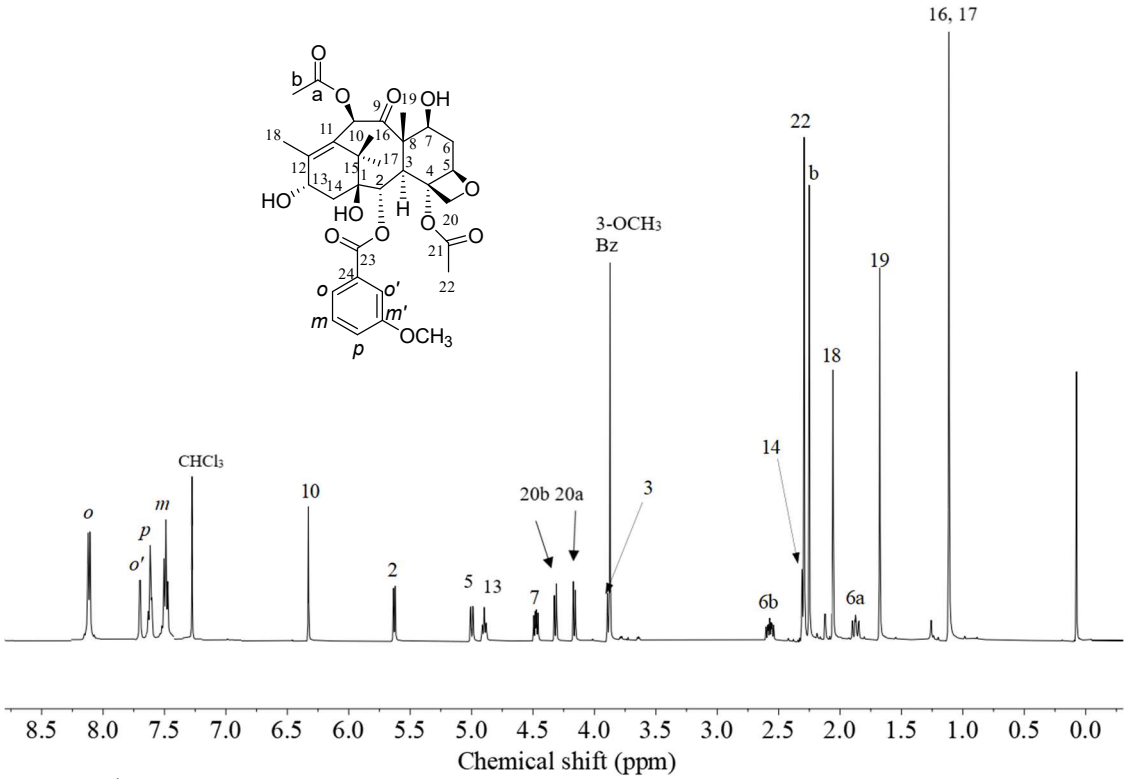

Figure 3.97: ^{1}H-NMR (500 MHz) of 2-DBz-2-(3-OCH_3)benzoylbaccatin III.

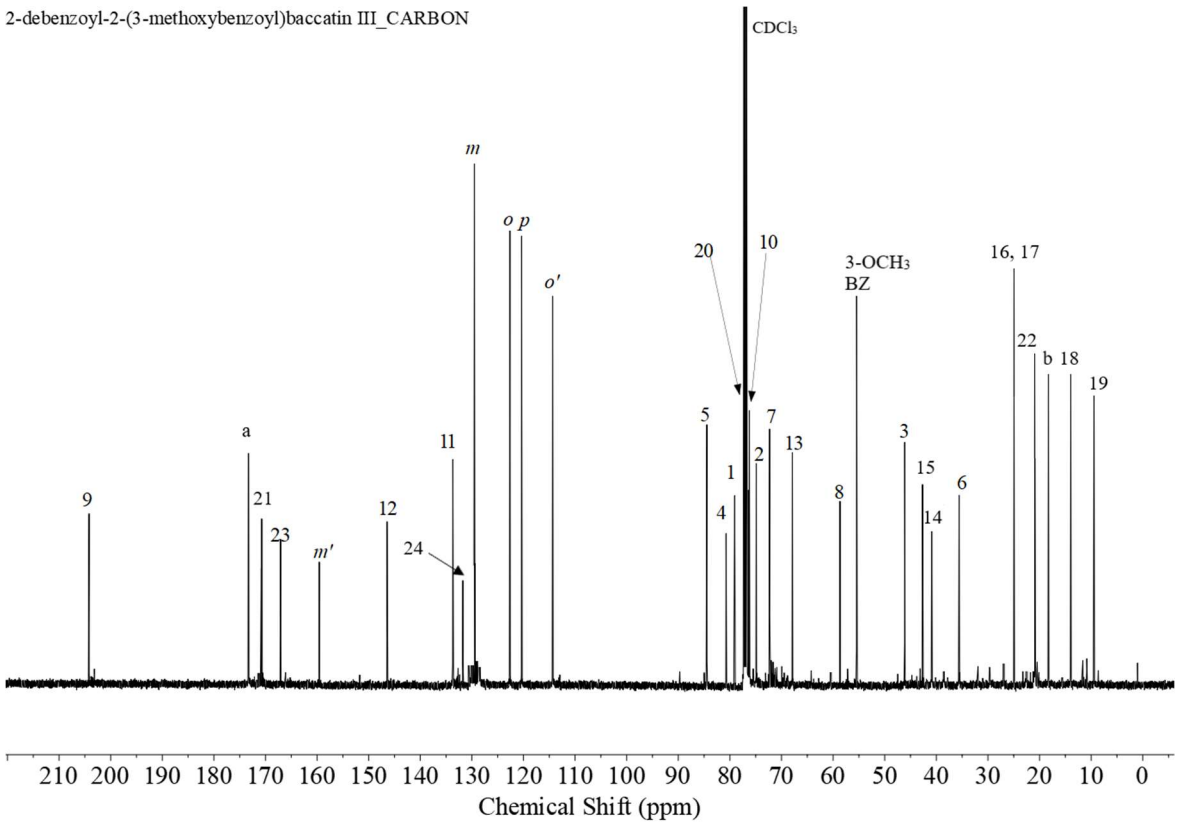

Figure 3.98: ^{13}C-NMR (126 MHz) of 2-DBz-2-(3-OCH_3)benzoylbaccatin III.

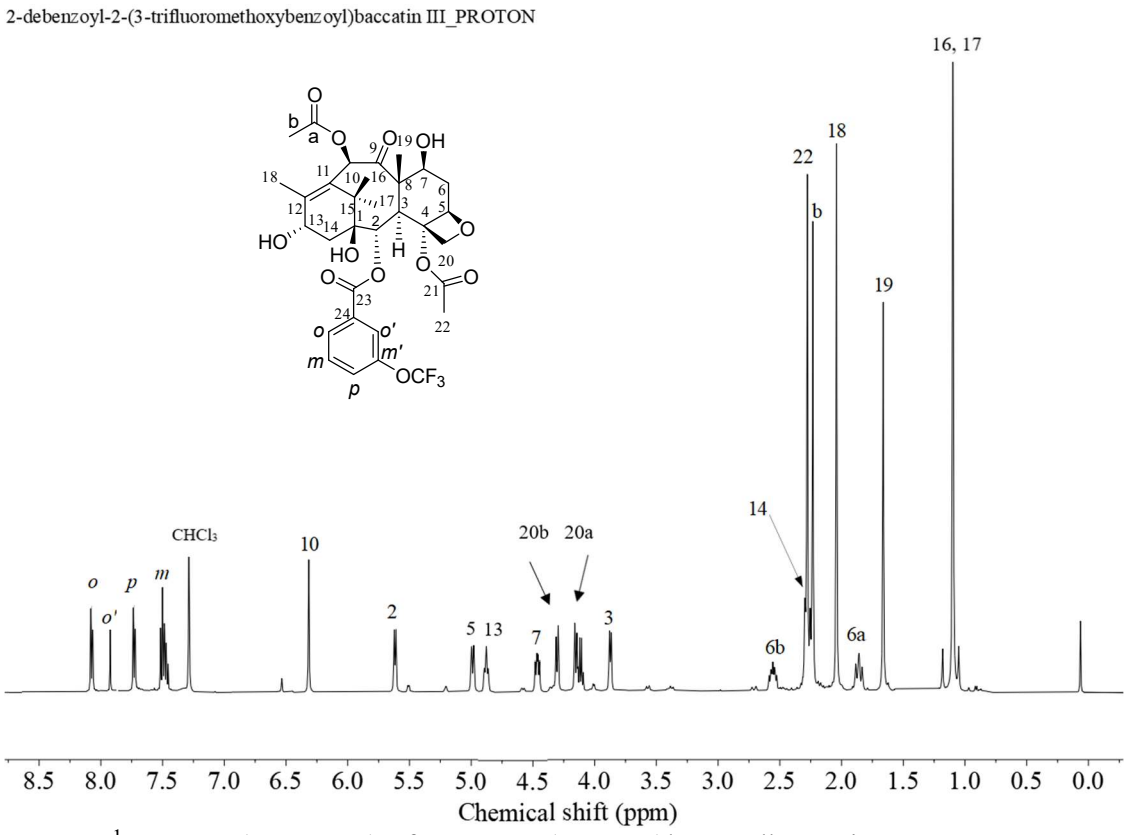

Figure 3.99: ^{1}H-NMR (500 MHz) of 2-DBz-2-(3-OCF_3)benzoylbaccatin III.

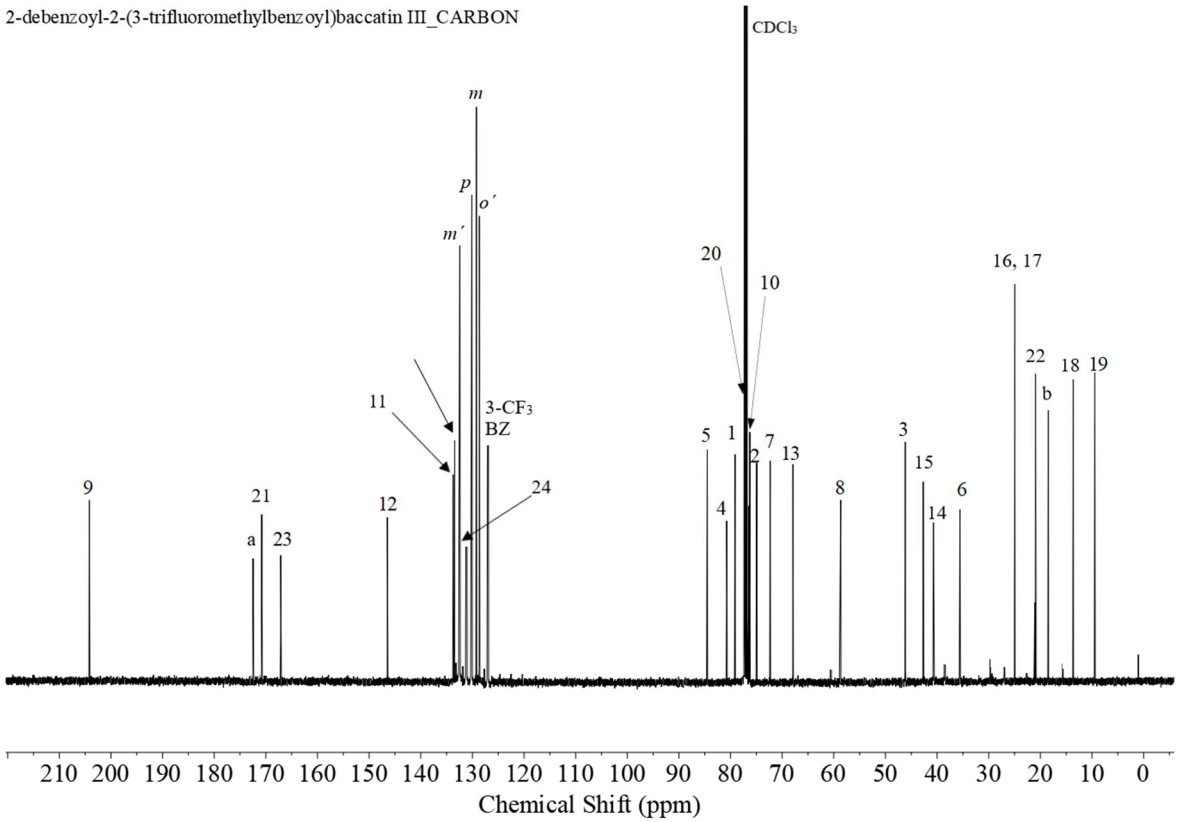

Figure 3.100: ^{13}C-NMR (126 MHz) of 2-DBz-2-(3-OCF_3)benzoylbaccatin III.

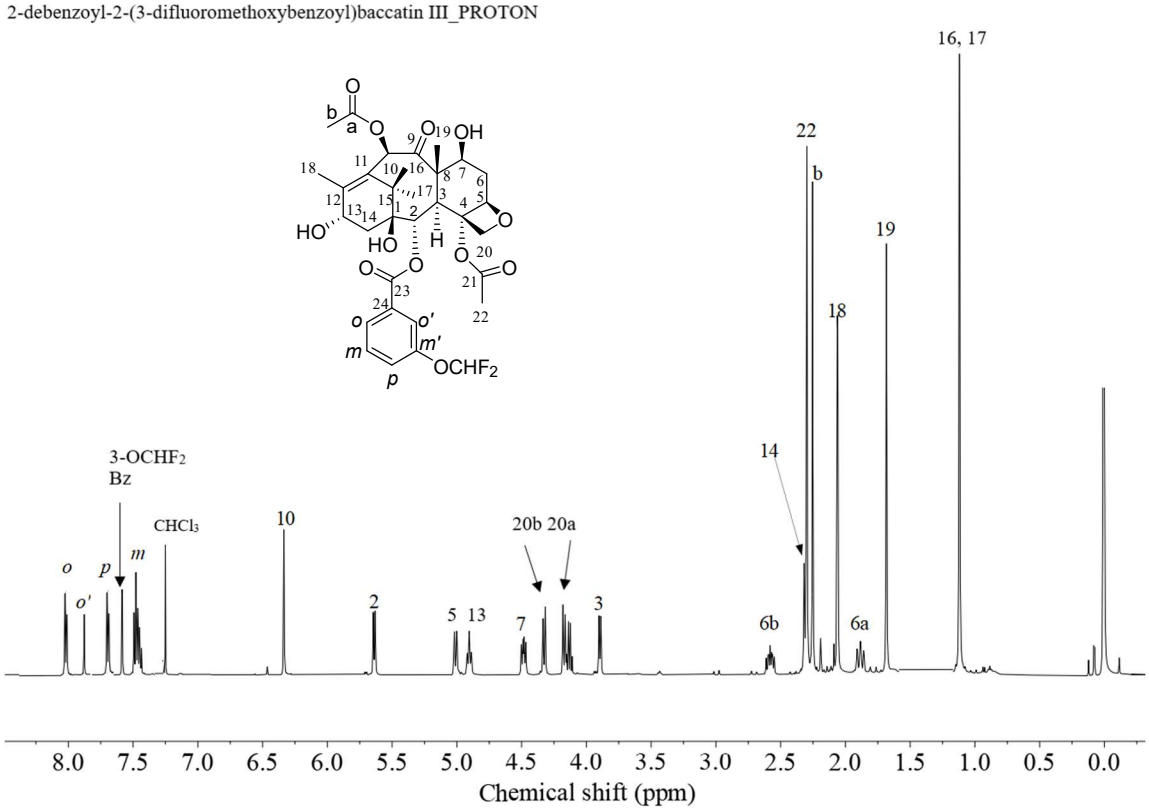

Figure 3.101: ^{1}H-NMR (500 MHz) of 2-DBz-2-(3-$OCHF_2$)benzoylbaccatin III.

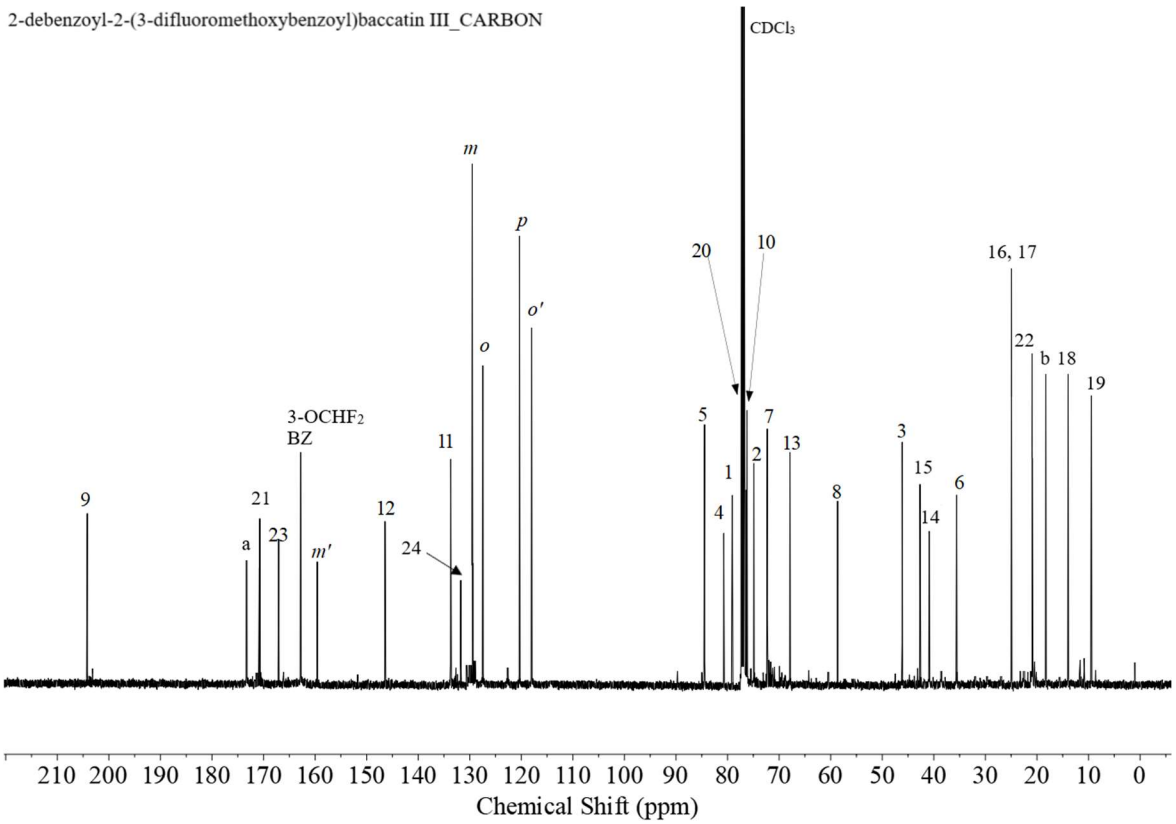

Figure 3.102: ^{13}C-NMR (126 MHz) of 2-DBz-2-(3-OCHF$_2$)benzoylbaccatin III.

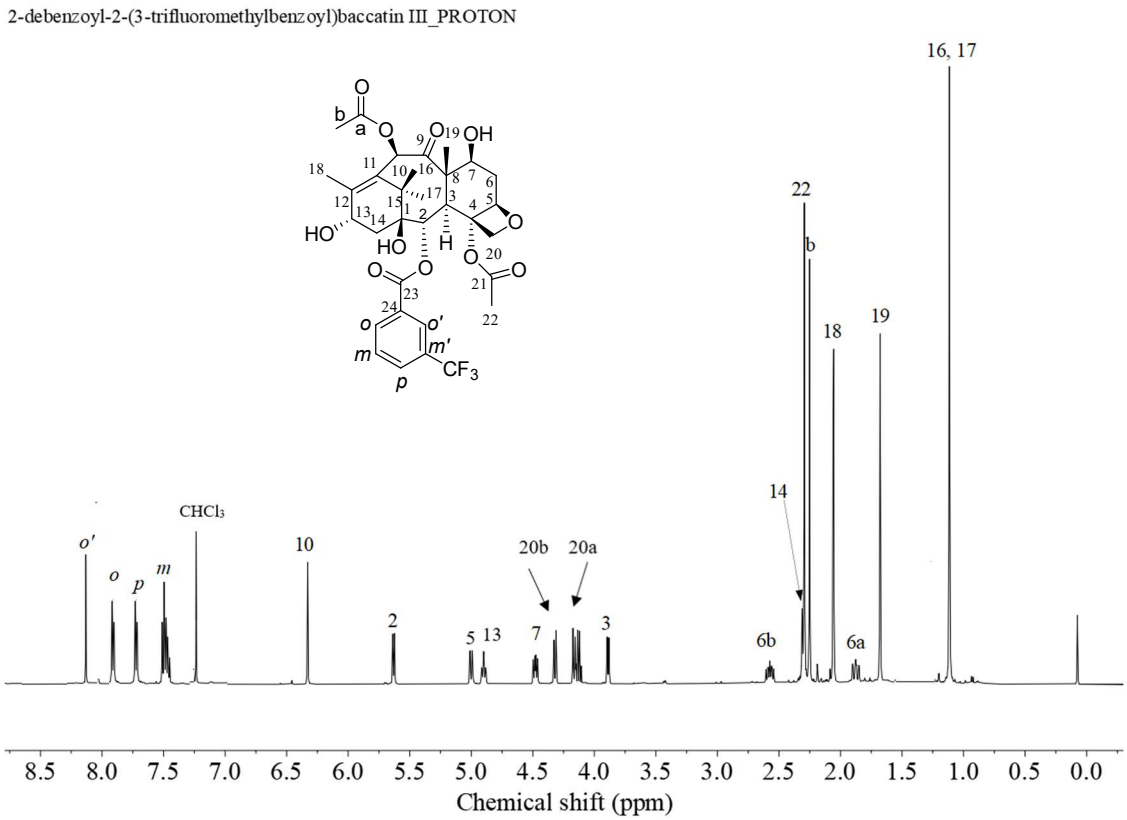

Figure 3.103: ^{1}H-NMR (500 MHz) of 2-DBz-2-(3-CF_3)benzoylbaccatin III.

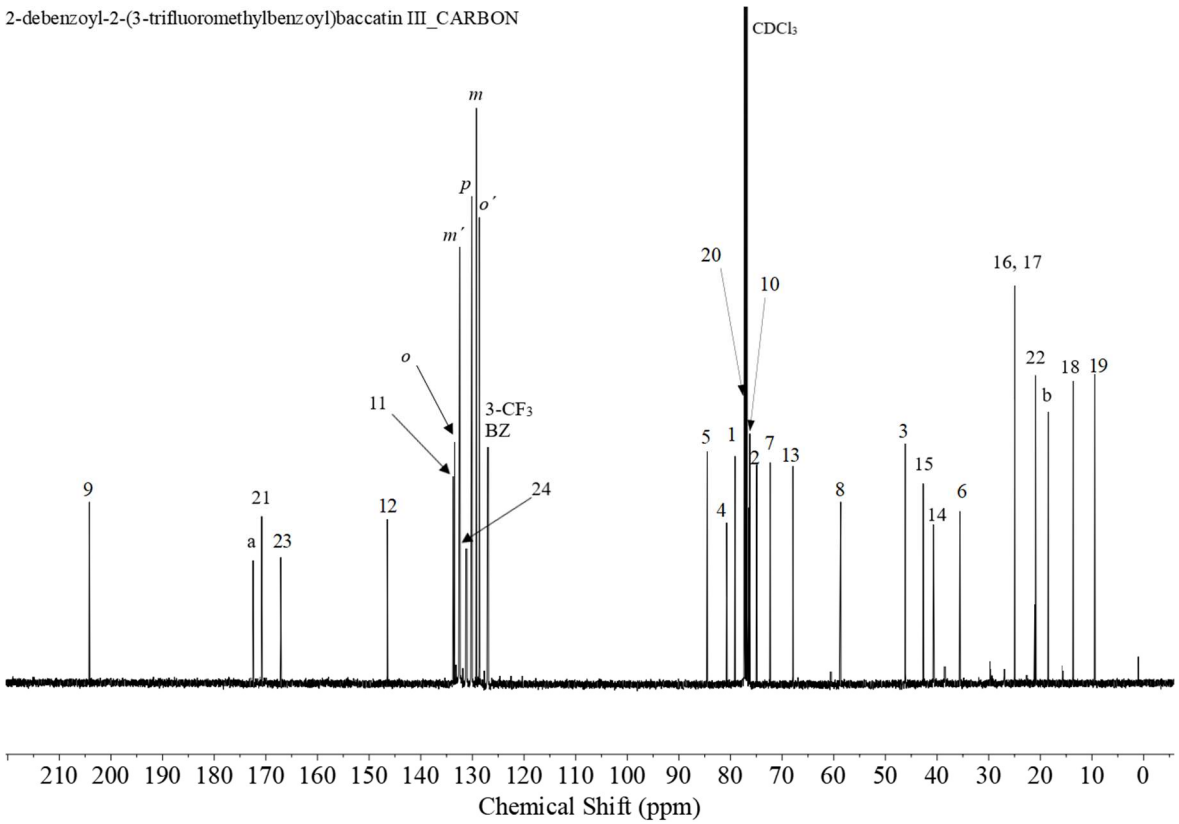

Figure 3.104: ^{13}C-NMR (126 MHz) of 2-DBz-2-(3-CF_3)benzoylbaccatin III.

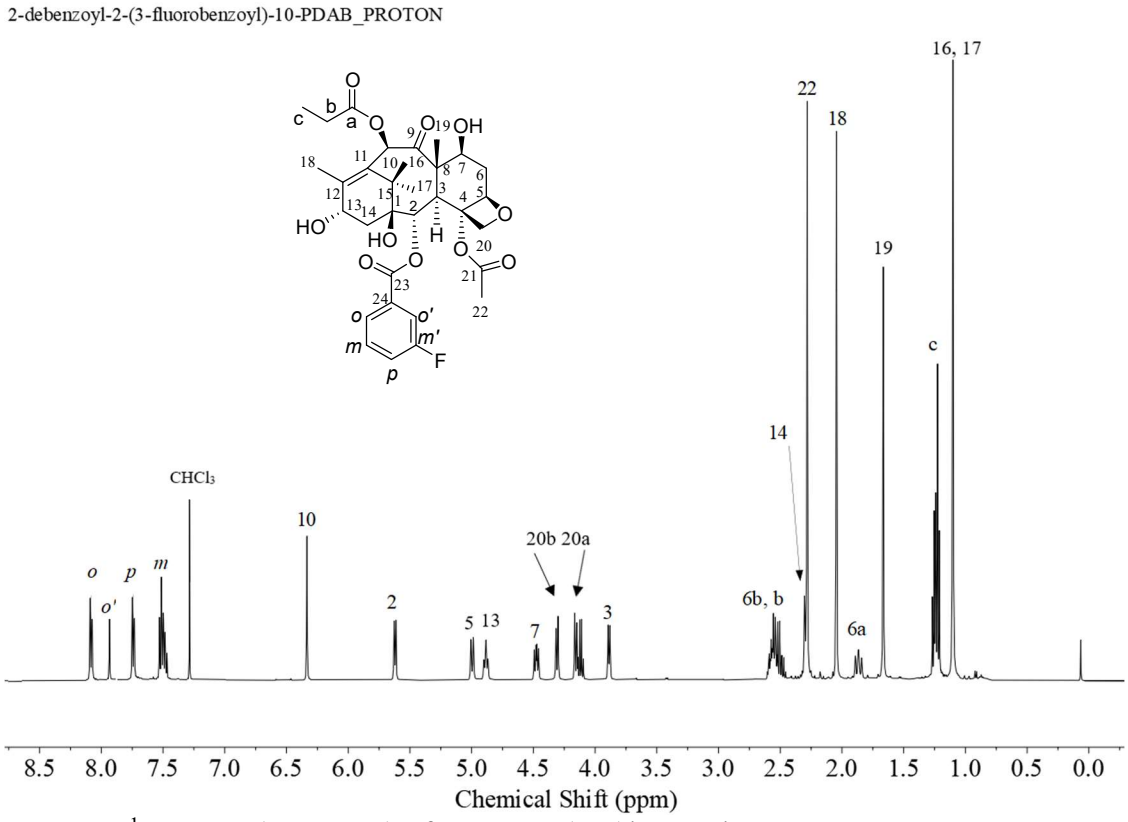

Figure 3.105: ^{1}H-NMR (500 MHz) of 2-DBz-2-(3-F)benzoyl-10-PDAB.

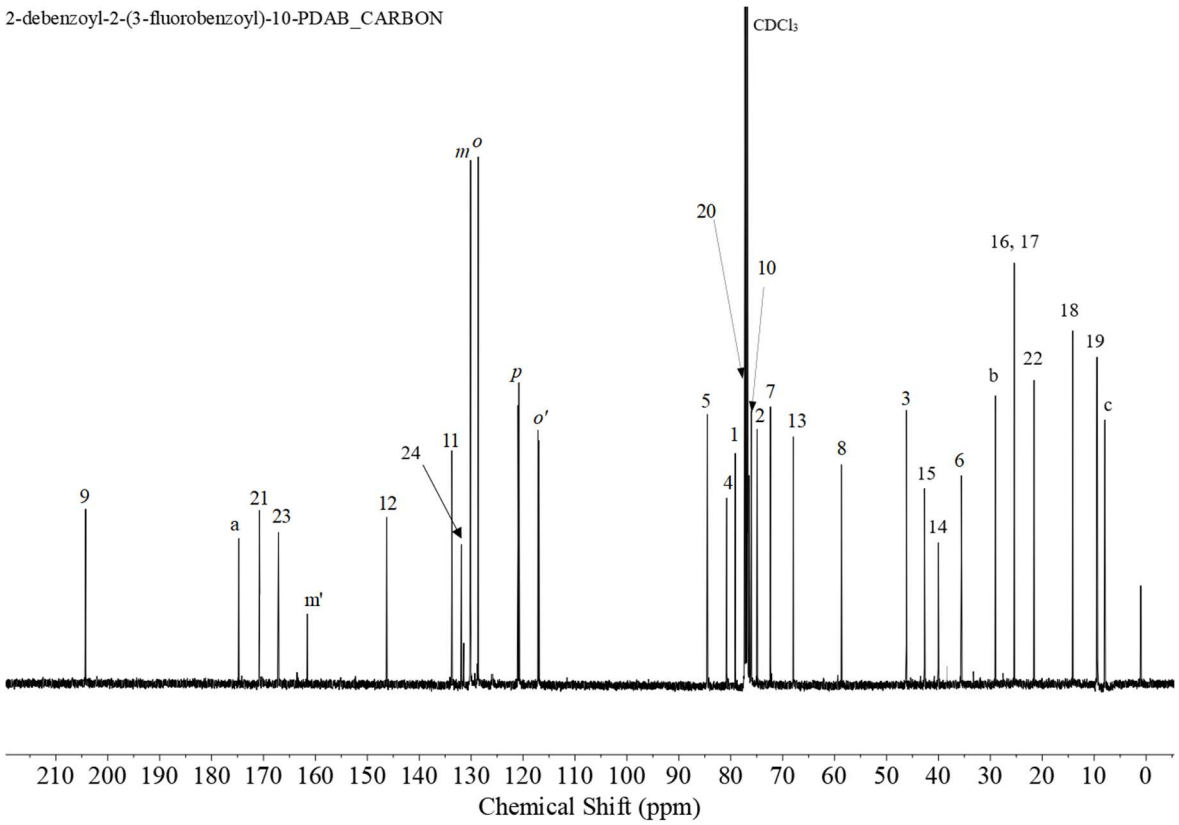

Figure 3.106: ^{13}C-NMR (126 MHz) of 2-DBz-2-(3-F)benzoyl-10-PDAB.

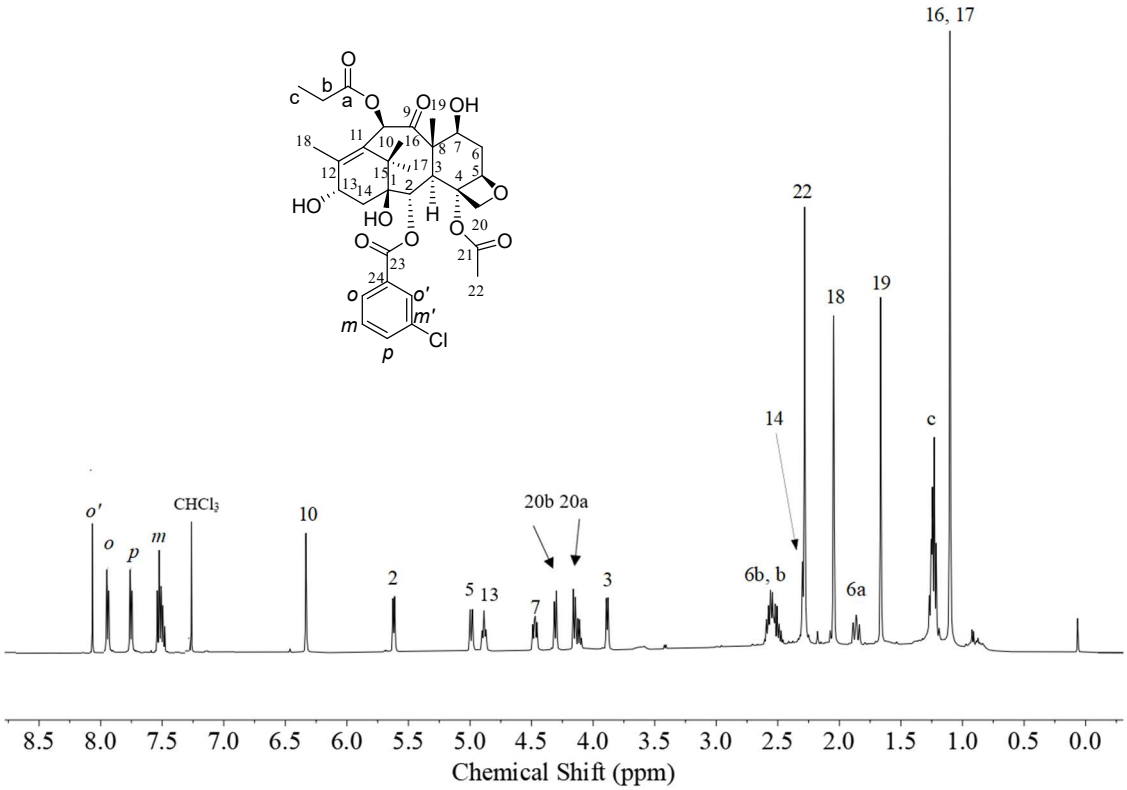

Figure 3.107: ^{1}H-NMR (500 MHz) of 2-DBz-2-(3-Cl)benzoyl-10-PDAB.

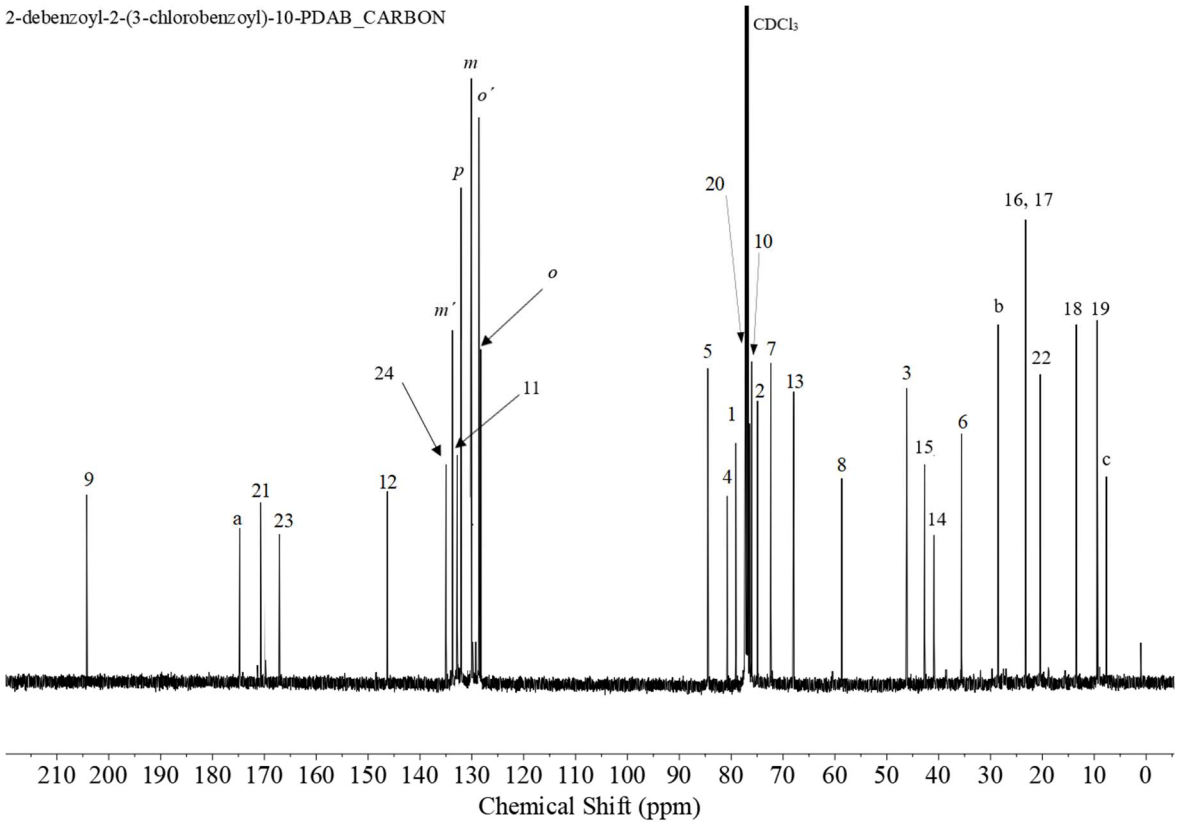

Figure 3.108: ^{13}C-NMR (126 MHz) of 2-DBz-2-(3-Cl)benzoyl-10-PDAB.

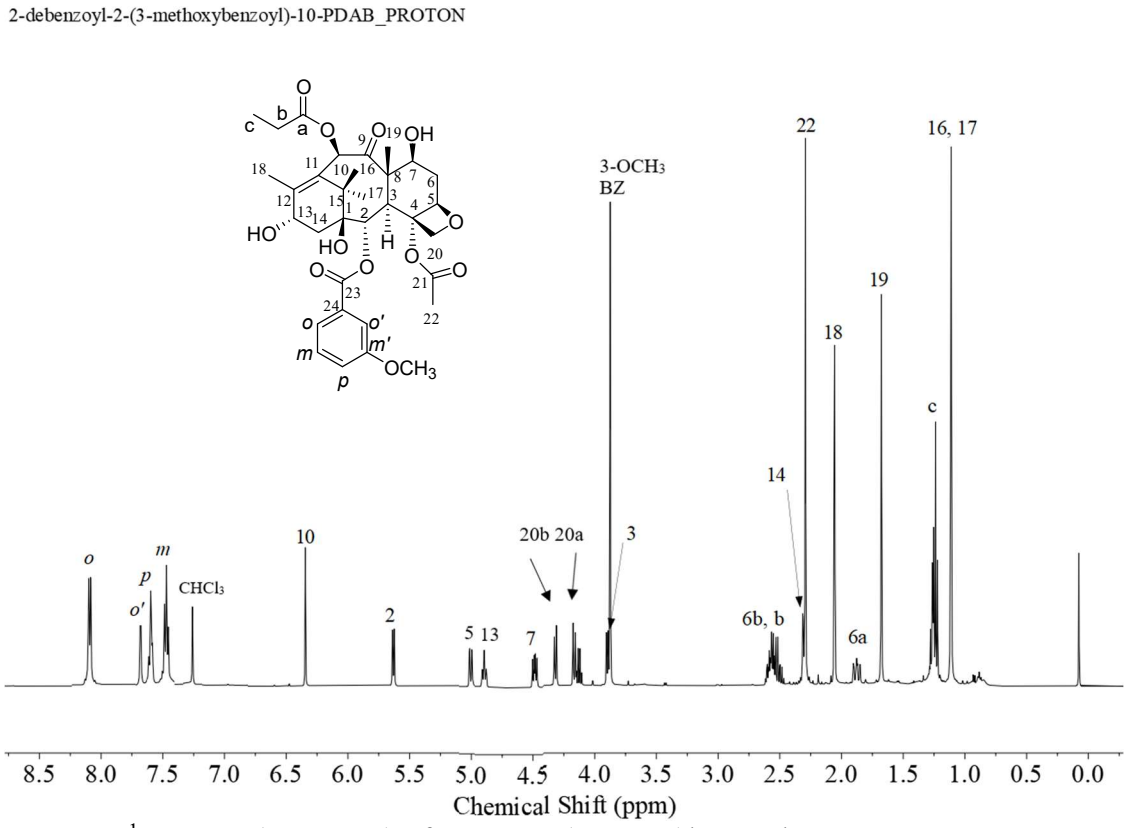

Figure 3.109: ^{1}H-NMR (500 MHz) of 2-DBz-2-(3-OCH_3)benzoyl-10-PDAB.

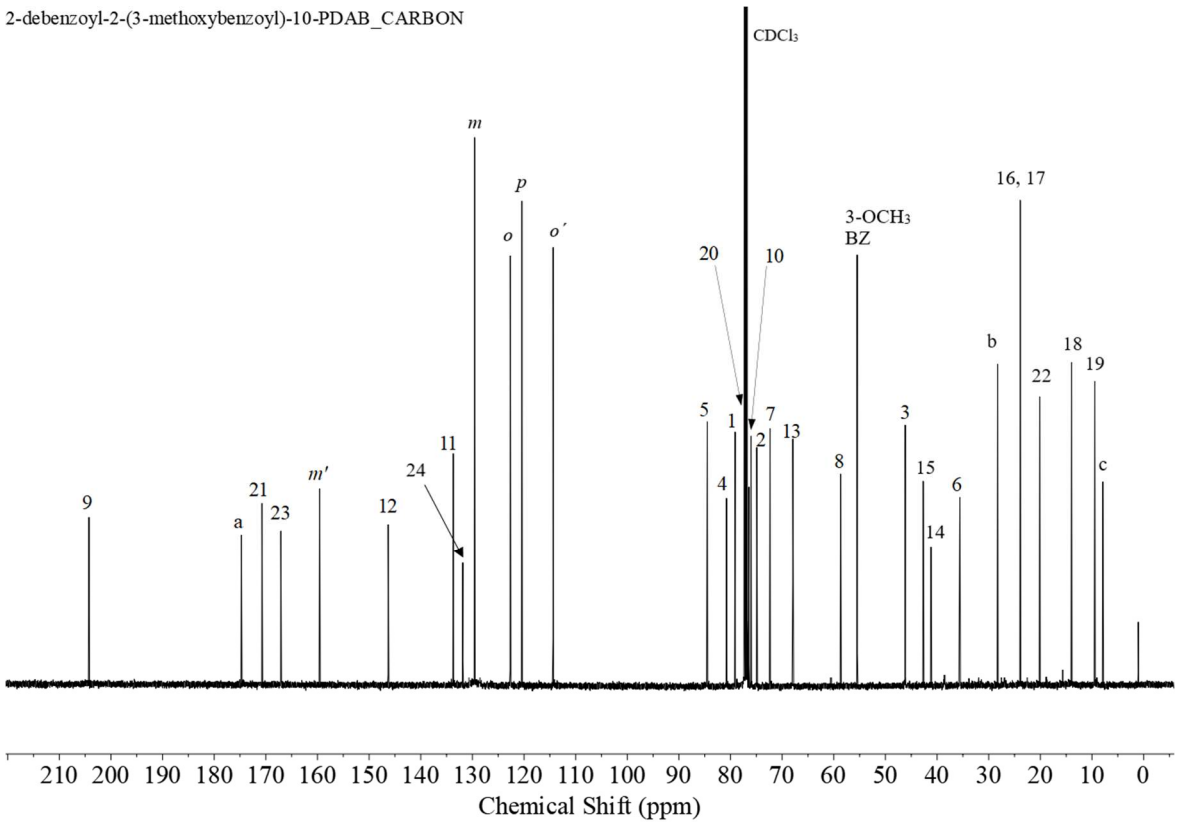

Figure 3.110: ^{13}C-NMR (126 MHz) of 2-DBz-2-(3-OCH_3)benzoyl-10-PDAB.

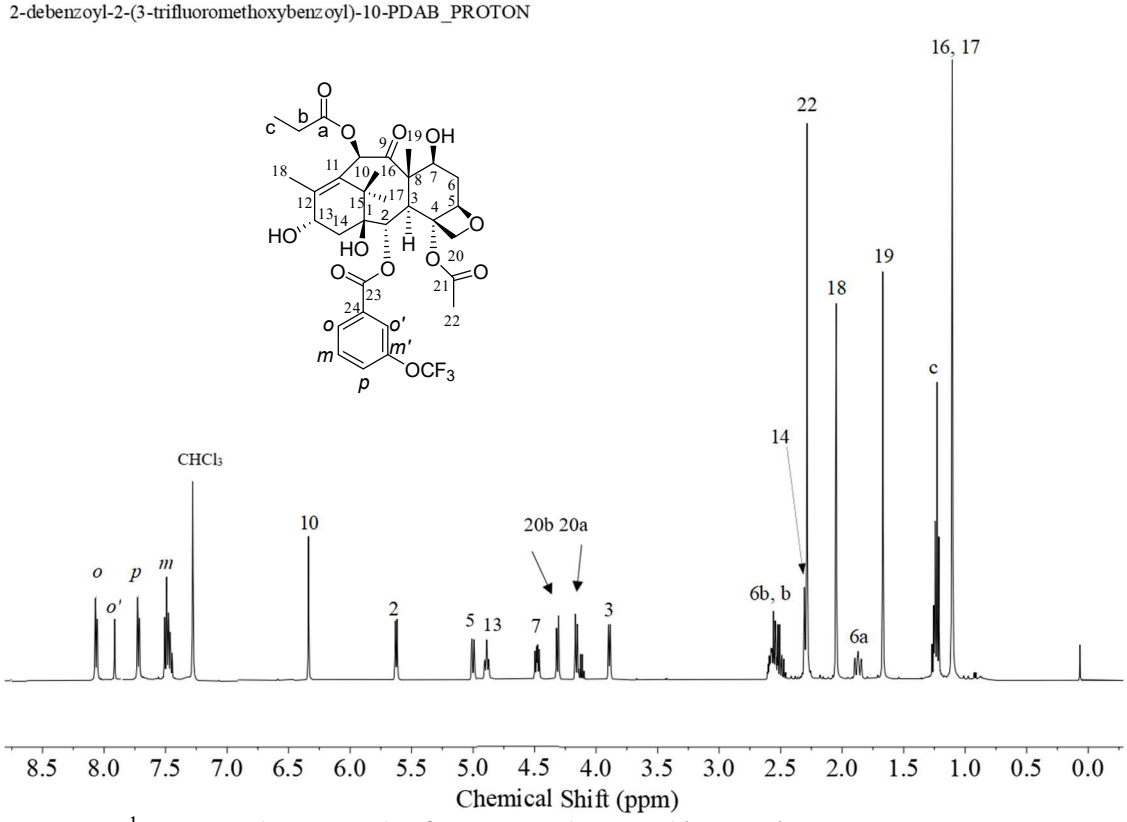

Figure 3.111: ^{1}H-NMR (500 MHz) of 2-DBz-2-(3-OCF_3)benzoyl-10-PDAB.

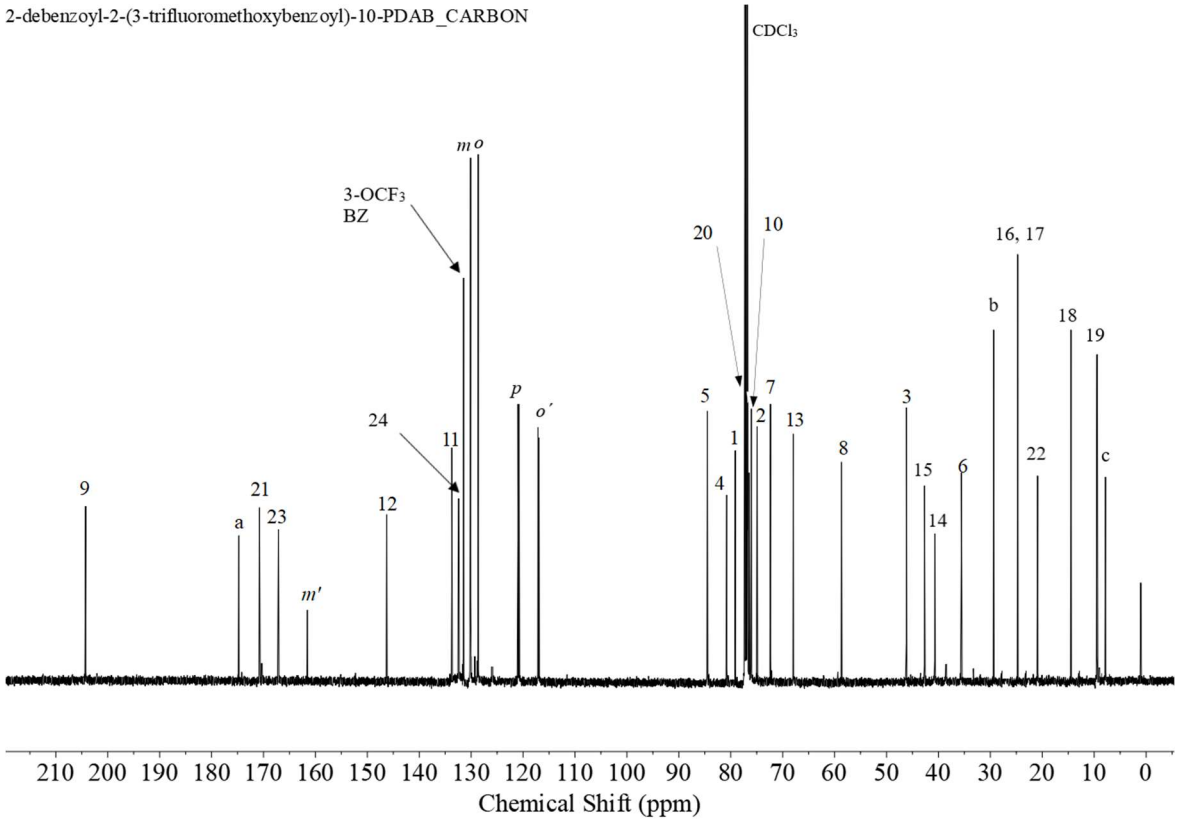

Figure 3.112: ^{13}C-NMR (126 MHz) of 2-DBz-2-(3-OCF_3)benzoyl-10-PDAB.

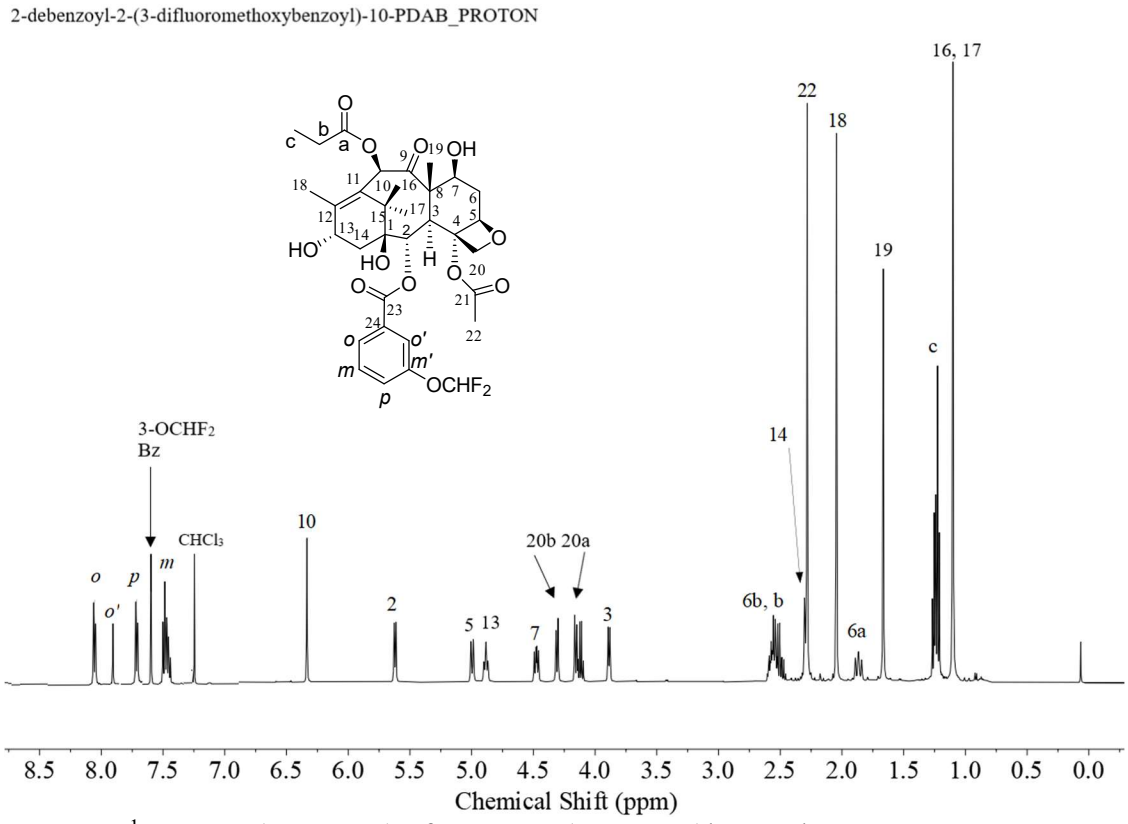

Figure 3.113: ^{1}H-NMR (500 MHz) of 2-DBz-2-(3-$OCHF_2$)benzoyl-10-PDAB.

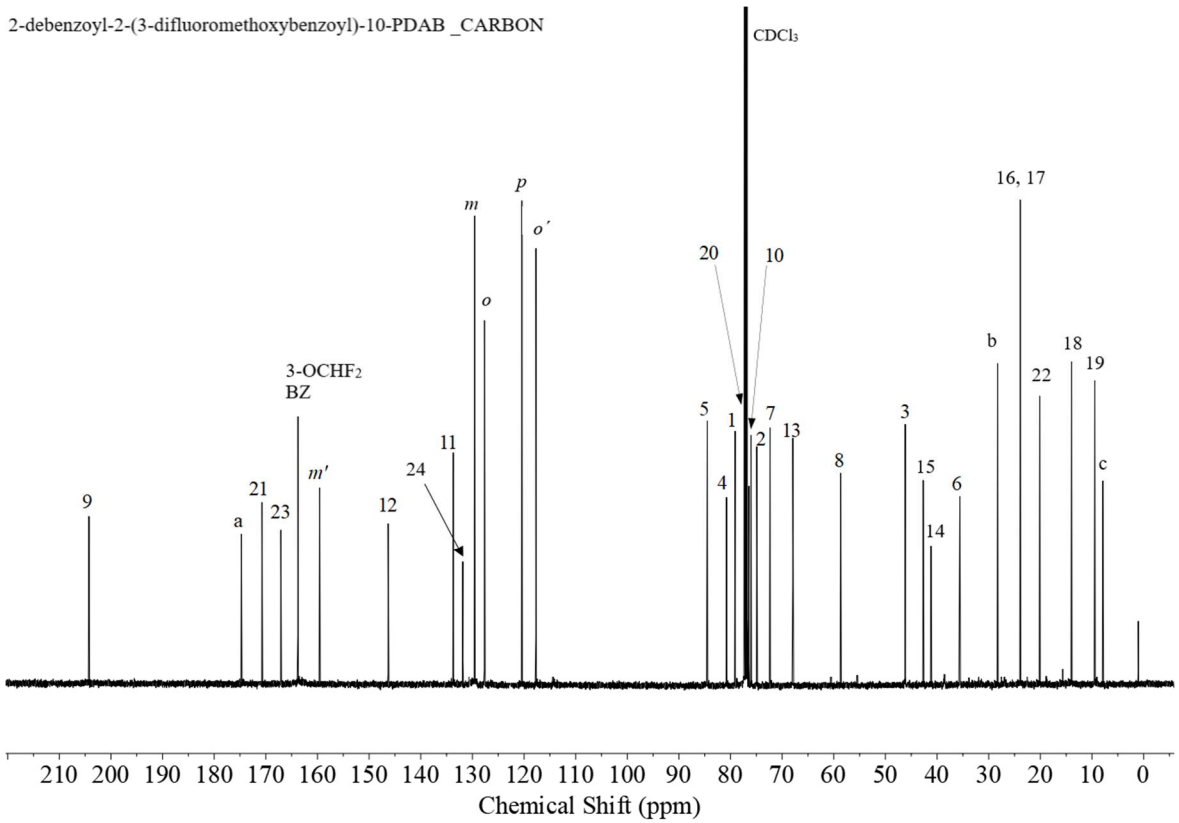

Figure 3.114: ^{13}C-NMR (126 MHz) of 2-DBz-2-(3-$OCHF_2$)benzoyl-10-PDAB.

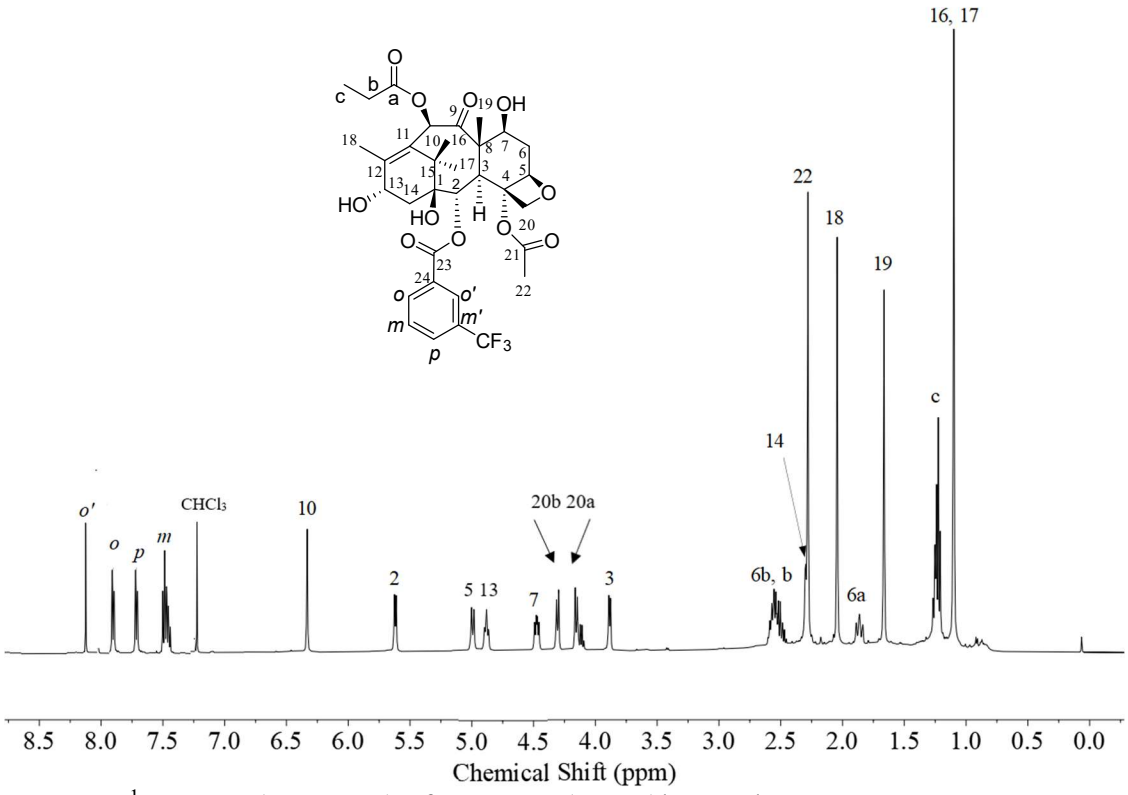

Figure 3.115: ^{1}H-NMR (500 MHz) of 2-DBz-2-(3-CF_3)benzoyl-10-PDAB.

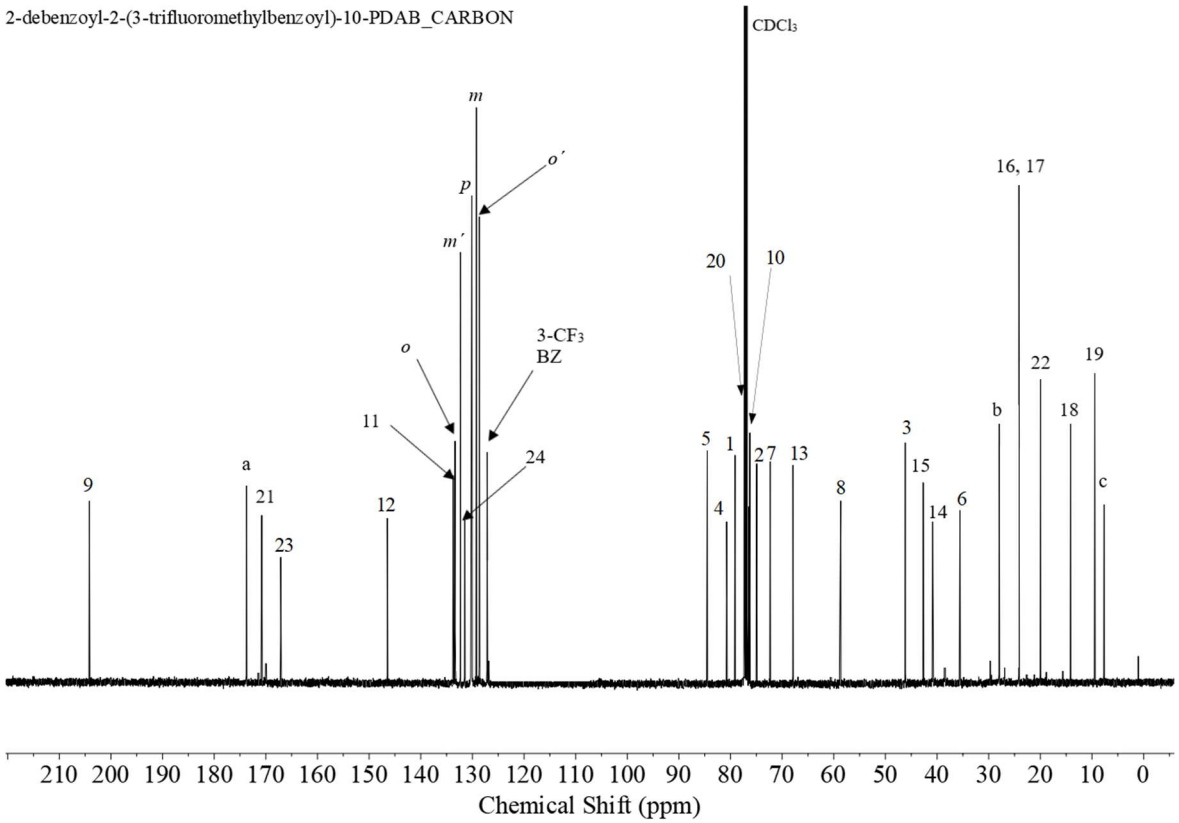

Figure 3.116: ^{13}C-NMR (126 MHz) of 2-DBz-2-(3-CF_3)benzoyl-10-PDAB.

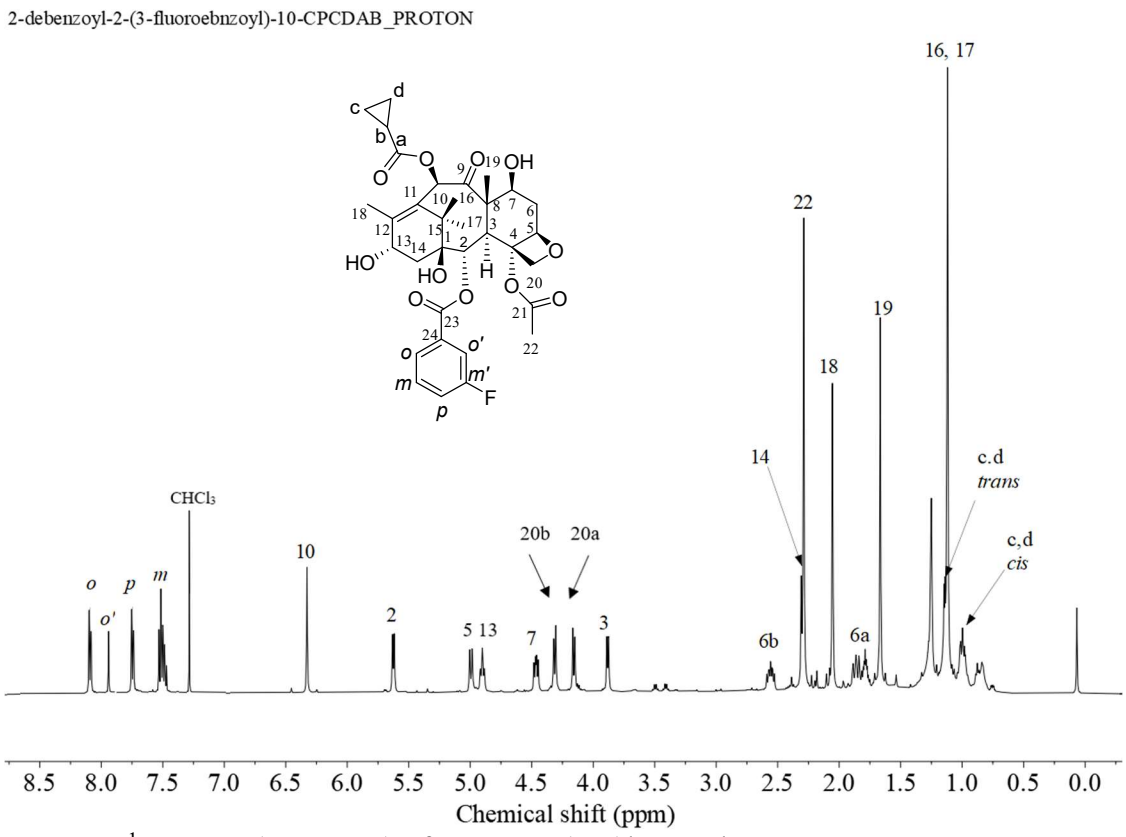

Figure 3.117: ^{1}H-NMR (500 MHz) of 2-DBz-2-(3-F)benzoyl-10-CPCDAB.

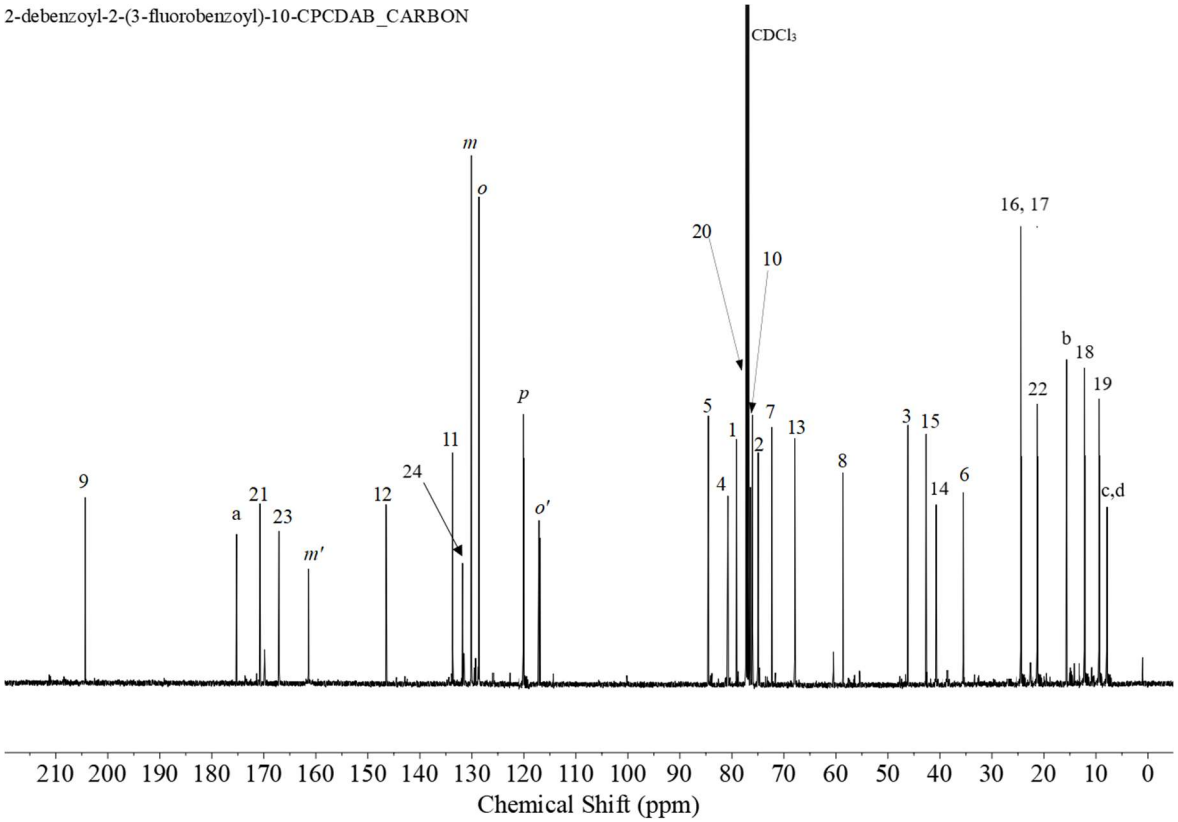

Figure 3.118: ^{13}C-NMR (126 MHz) of 2-DBz-2-(3-F)benzoyl-10-CPCDAB.

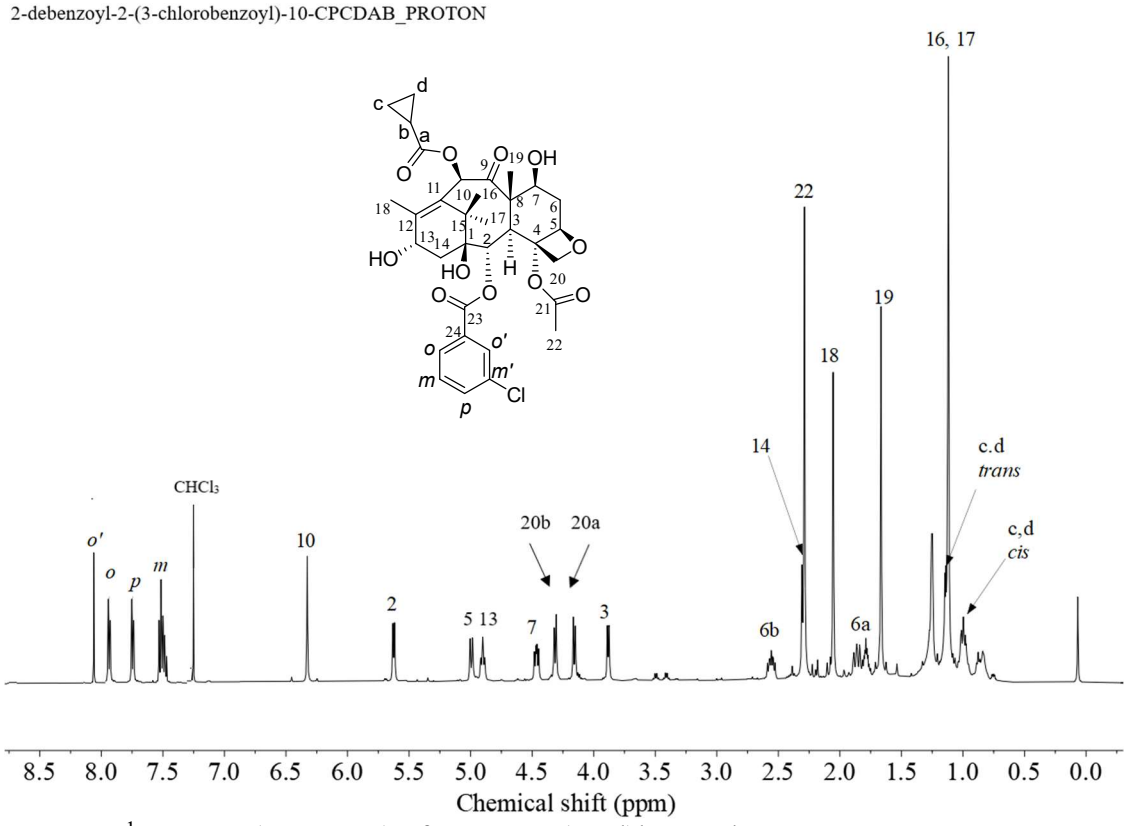

Figure 3.119: ^{1}H-NMR (500 MHz) of 2-DBz-2-(3-Cl)benzoyl-10-CPCDAB.

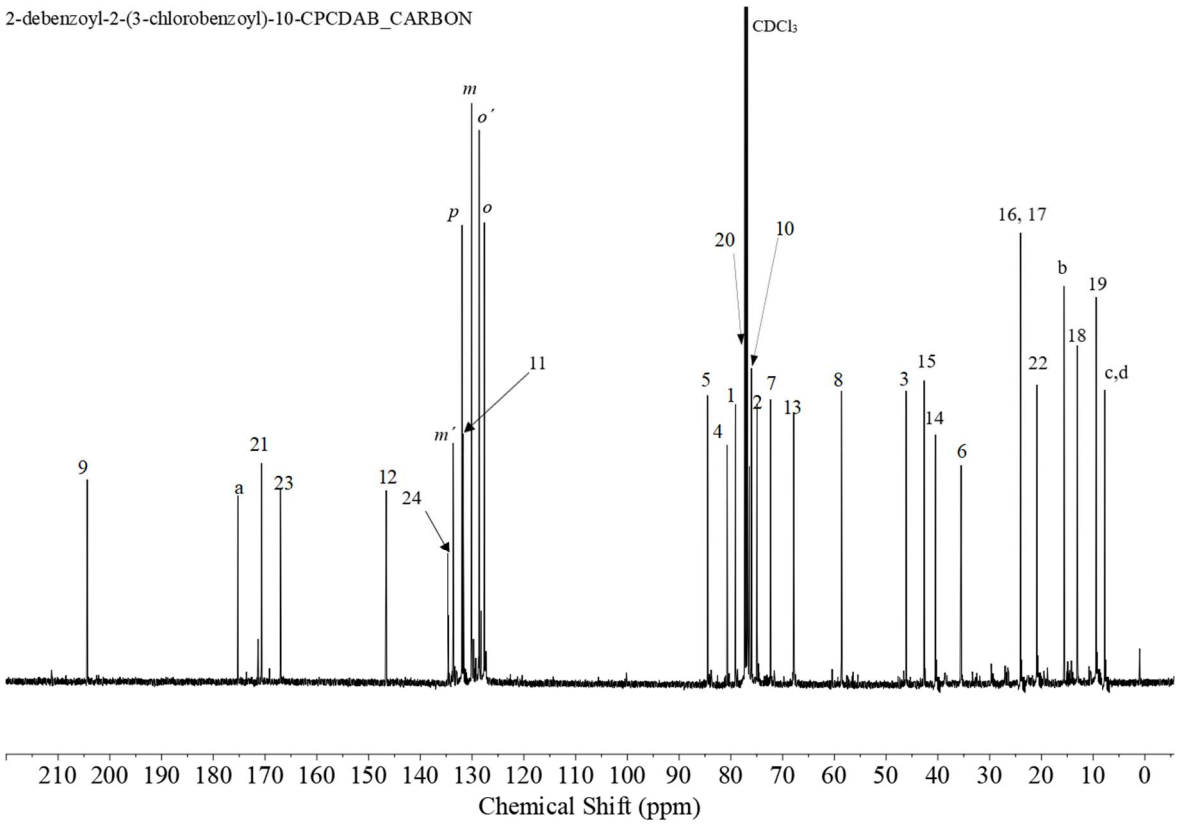

Figure 3.120: ^{13}C-NMR (126 MHz) of 2-DBz-2-(3-Cl)benzoyl-10-CPCDAB.

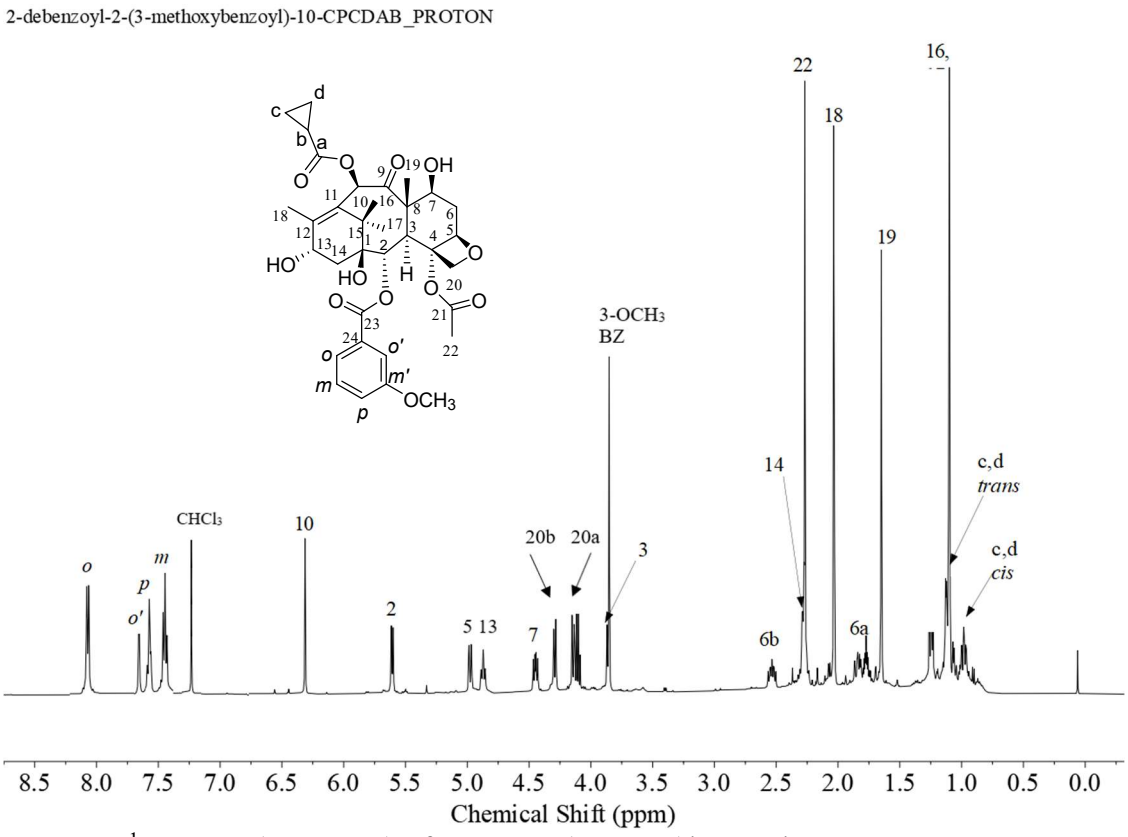

Figure 3.121: ^{1}H-NMR (500 MHz) of 2-DBz-2-(3-OCH_3)benzoyl-10-CPCDAB.

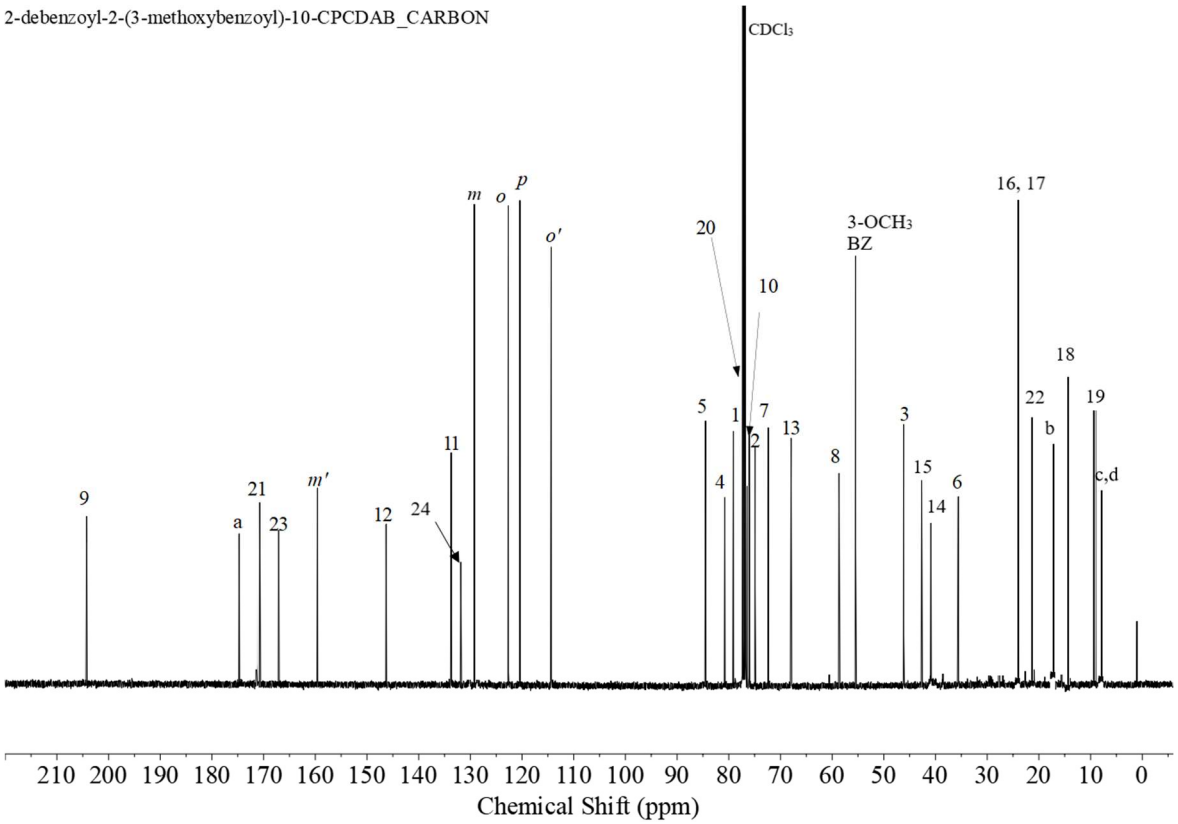

Figure 3.122: ^{13}C-NMR (126 MHz) of 2-DBz-2-(3-OCH_3)benzoyl-10-CPCDAB.

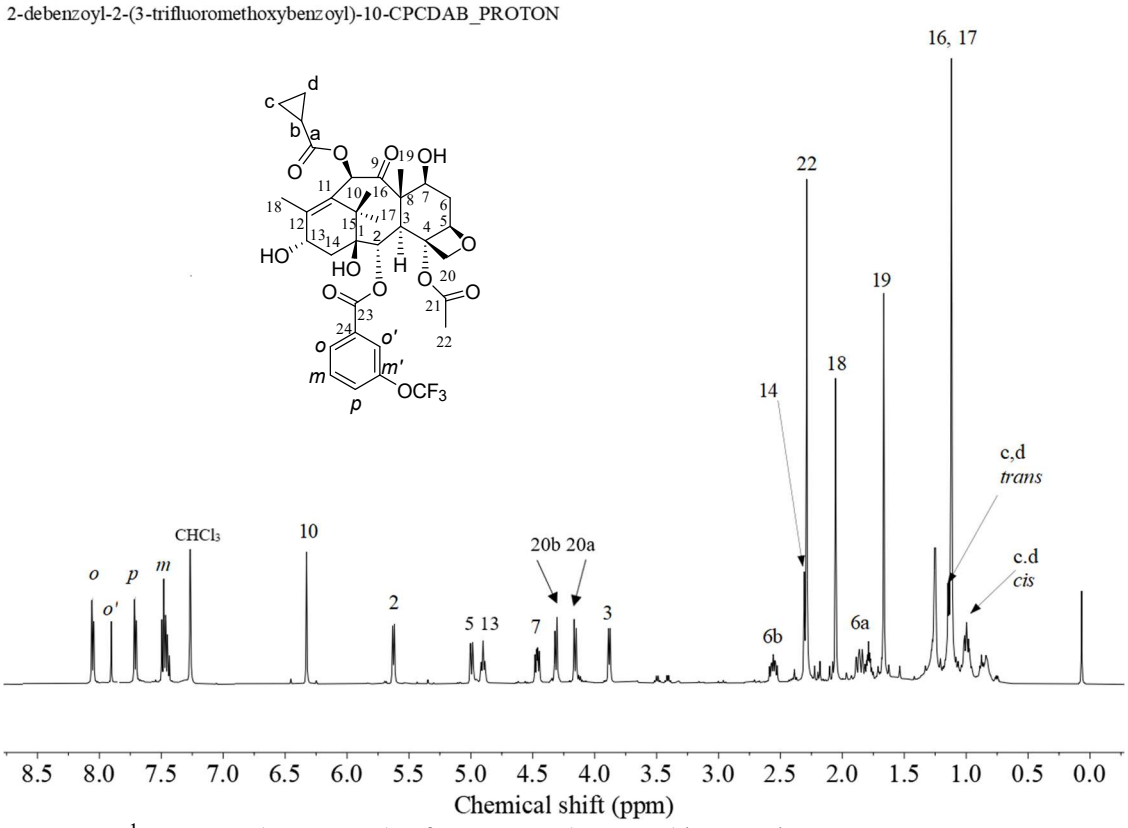

Figure 3.123: ^{1}H-NMR (500 MHz) of 2-DBz-2-(3-OCF_3)benzoyl-10-CPCDAB.

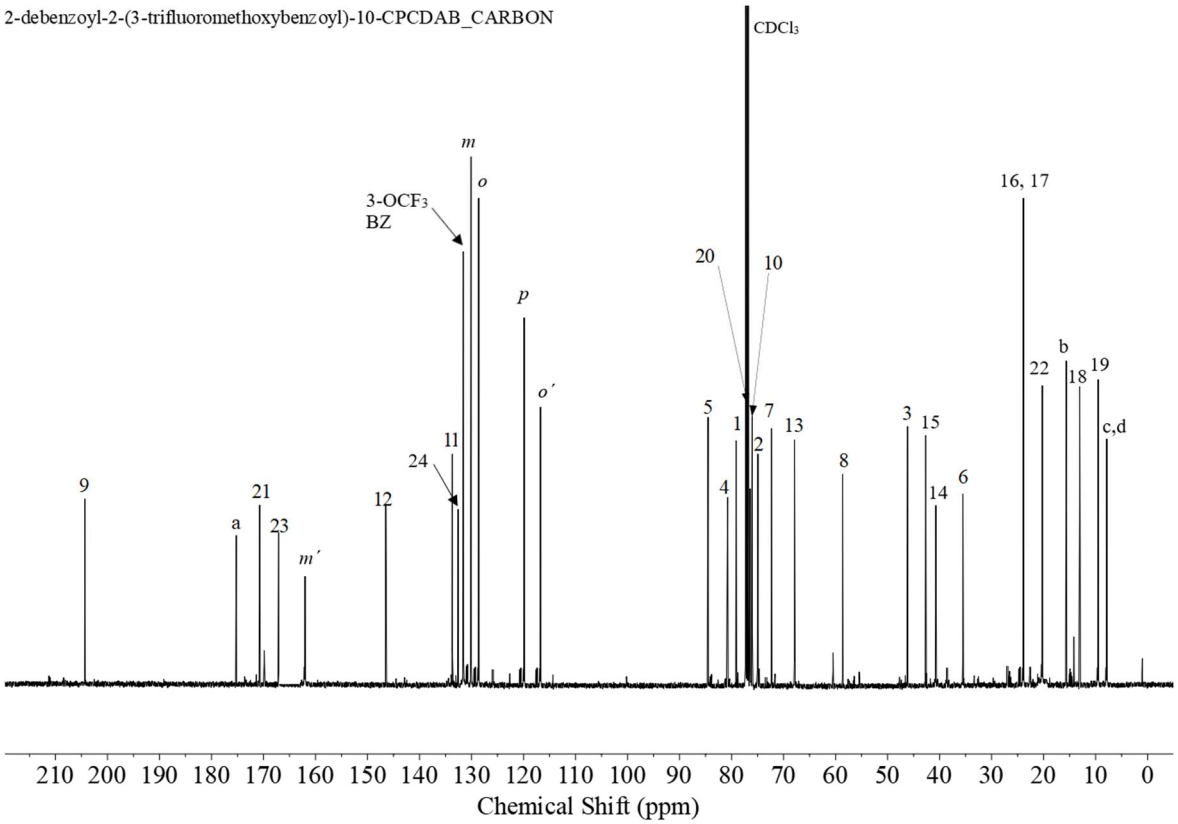

Figure 3.124: ^{13}C-NMR (126 MHz) of 2-DBz-2-(3-OCF_3)benzoyl-10-CPCDAB.

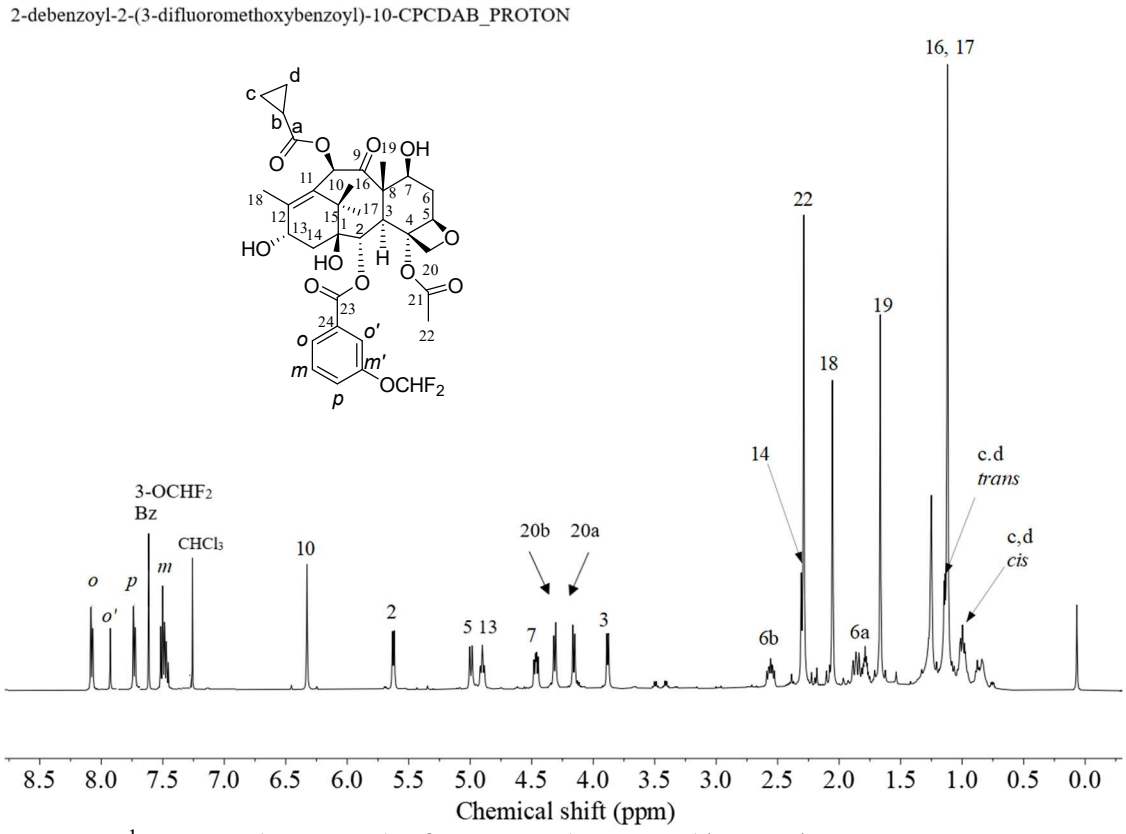

Figure 3.125: ^{1}H-NMR (500 MHz) of 2-DBz-2-(3-$OCHF_2$)benzoyl-10-CPCDAB.

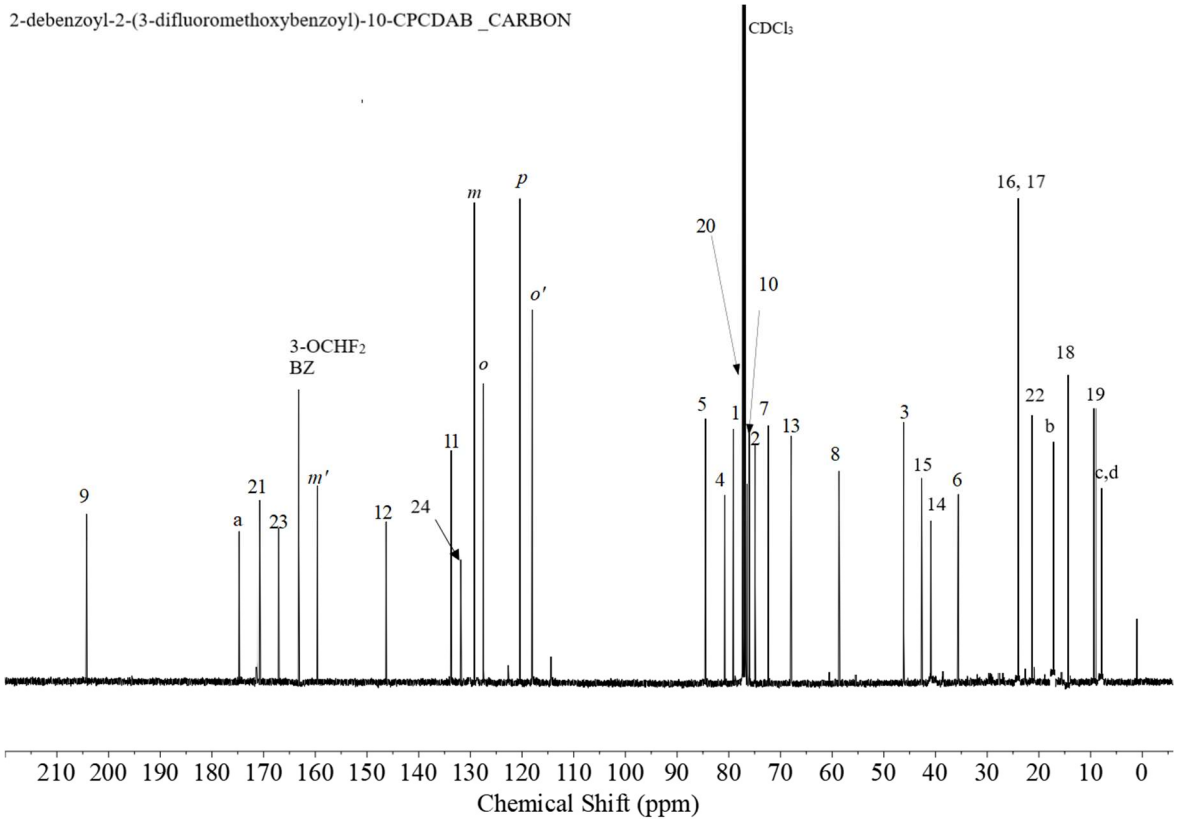

Figure 3.126: ^{13}C-NMR (126 MHz) of 2-DBz-2-(3-OCHF$_2$)benzoyl-10-CPCDAB.

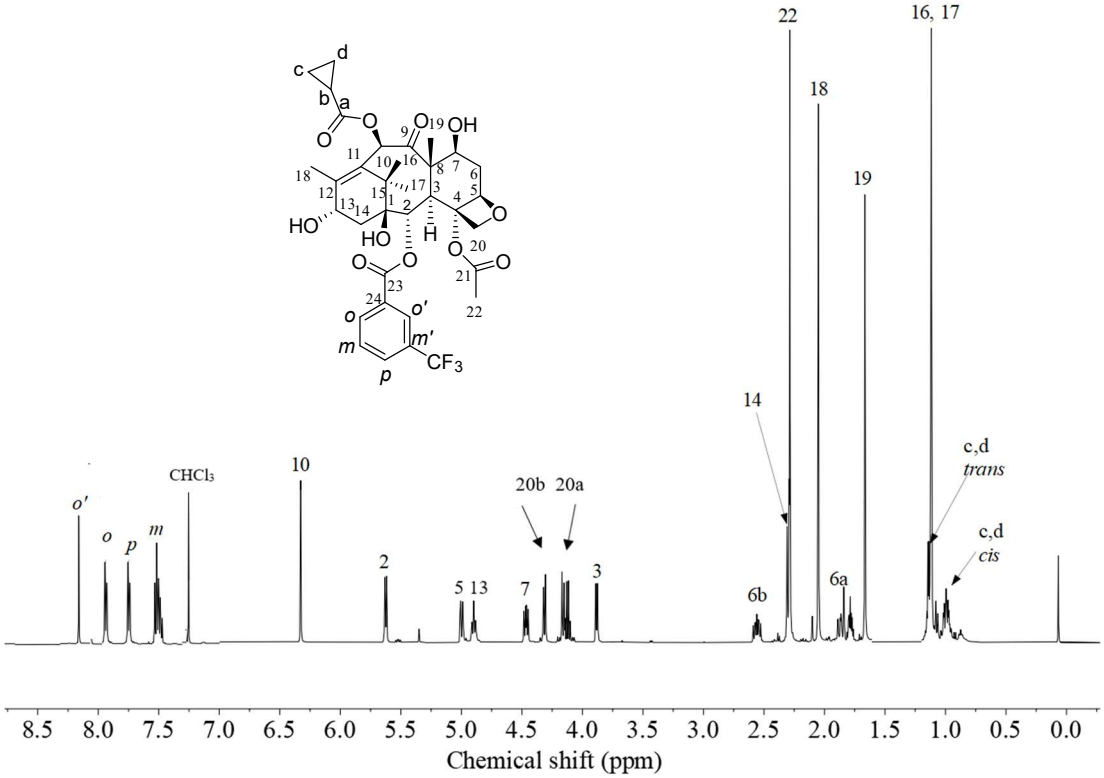

Figure 3.127: ^{1}H-NMR (500 MHz) of 2-DBz-2-(3-CF_3)benzoyl-10-CPCDAB.

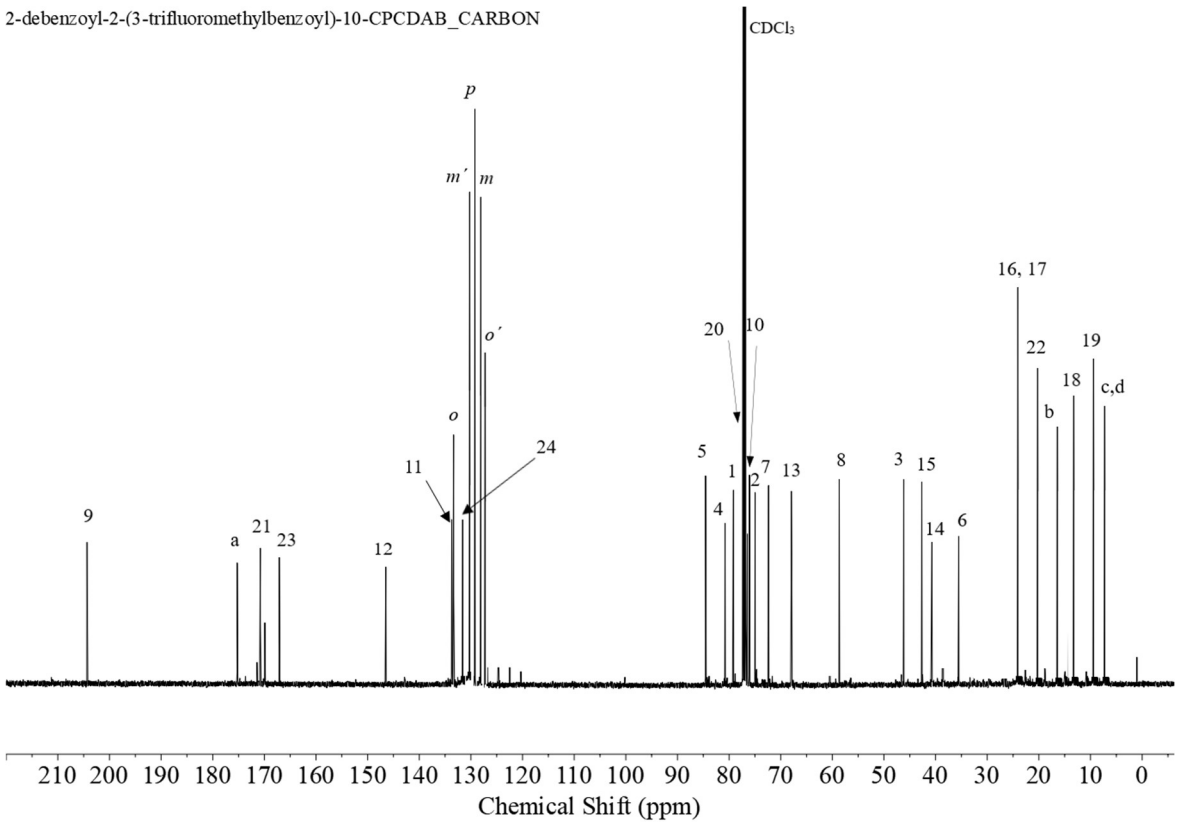

Figure 3.128: ^{13}C-NMR (126 MHz) of 2-DBz-2-(3-CF_3)benzoyl-10-CPCDAB.

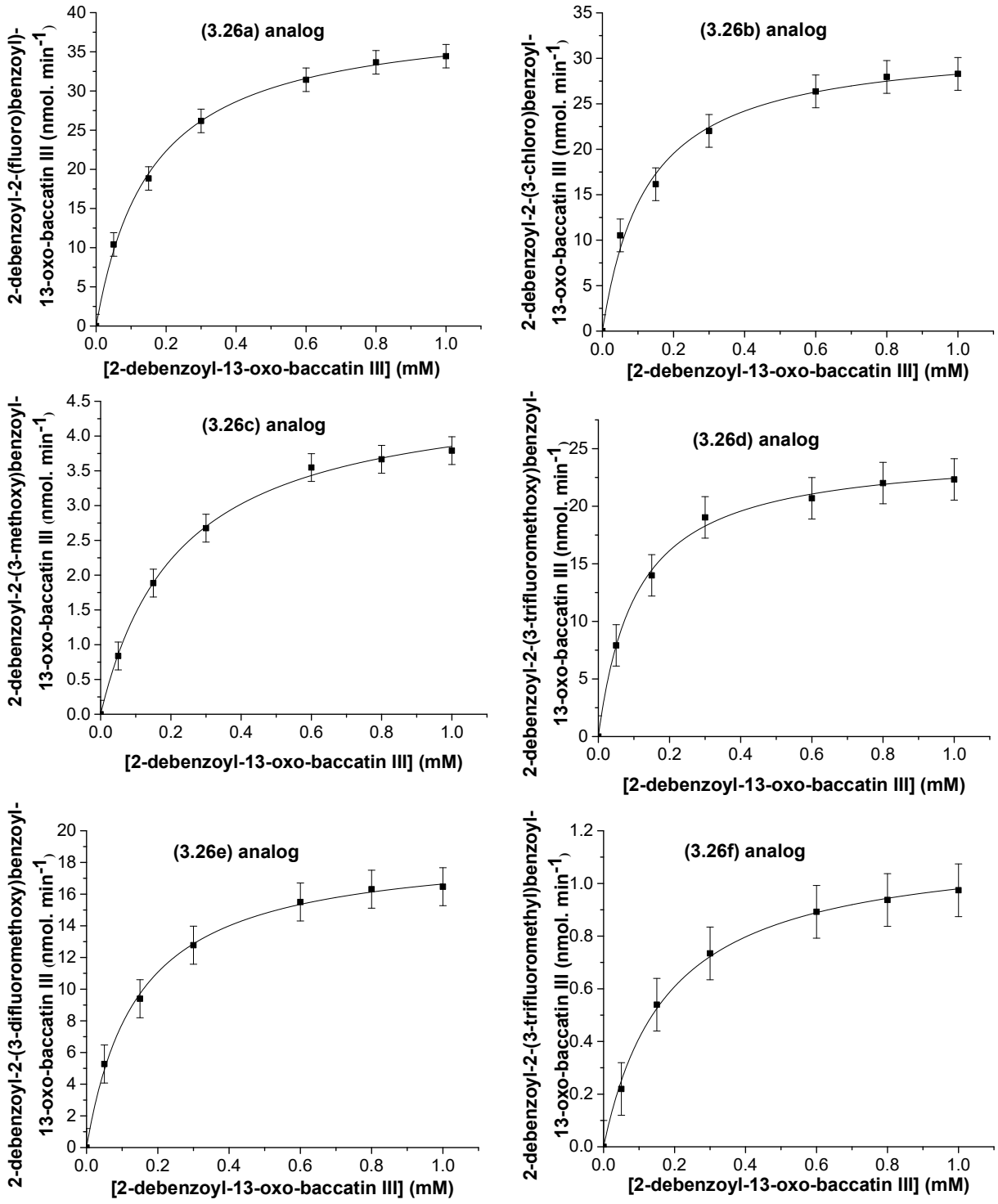

Figure 3.129: Michaelis-Menten kinetics for the turnover of 2-*O*-debenzoyl-13-oxo-baccatin III to the 2-*O*-debenzoyl-2-meta-substiuttedbenzoyl-13-oxo-baccatin III analogues **3.26** (**a**-**f**).

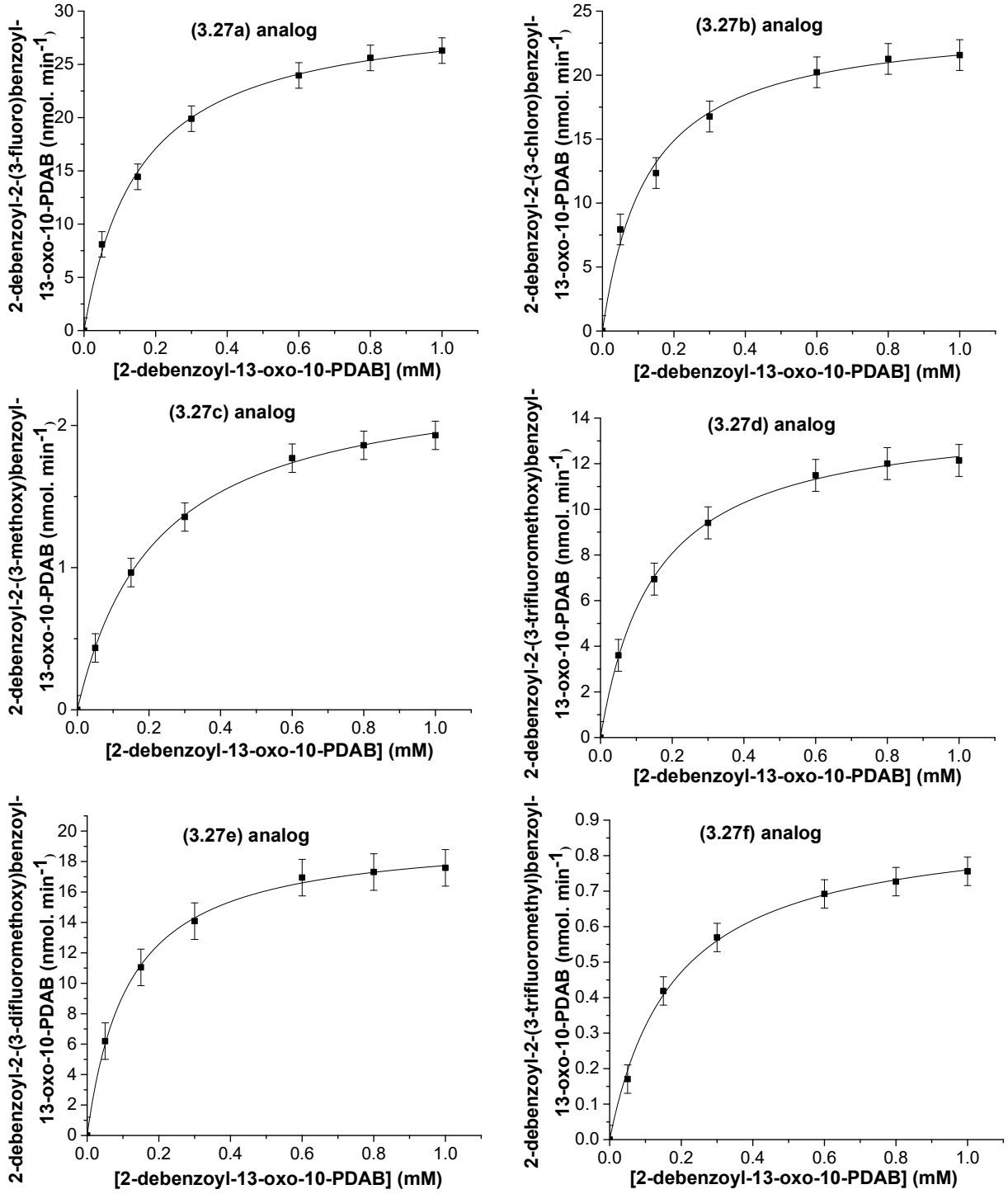

Figure 3.130: Michaelis-Menten kinetics for the turnover of 2-*O*-debenzoyl-13-oxo-10-PDAB to the 2-*O*-debenzoyl-2-meta-substiuttedbenzoyl-13-oxo-10-PDAB analogues **3.27** (**a**-**f**).

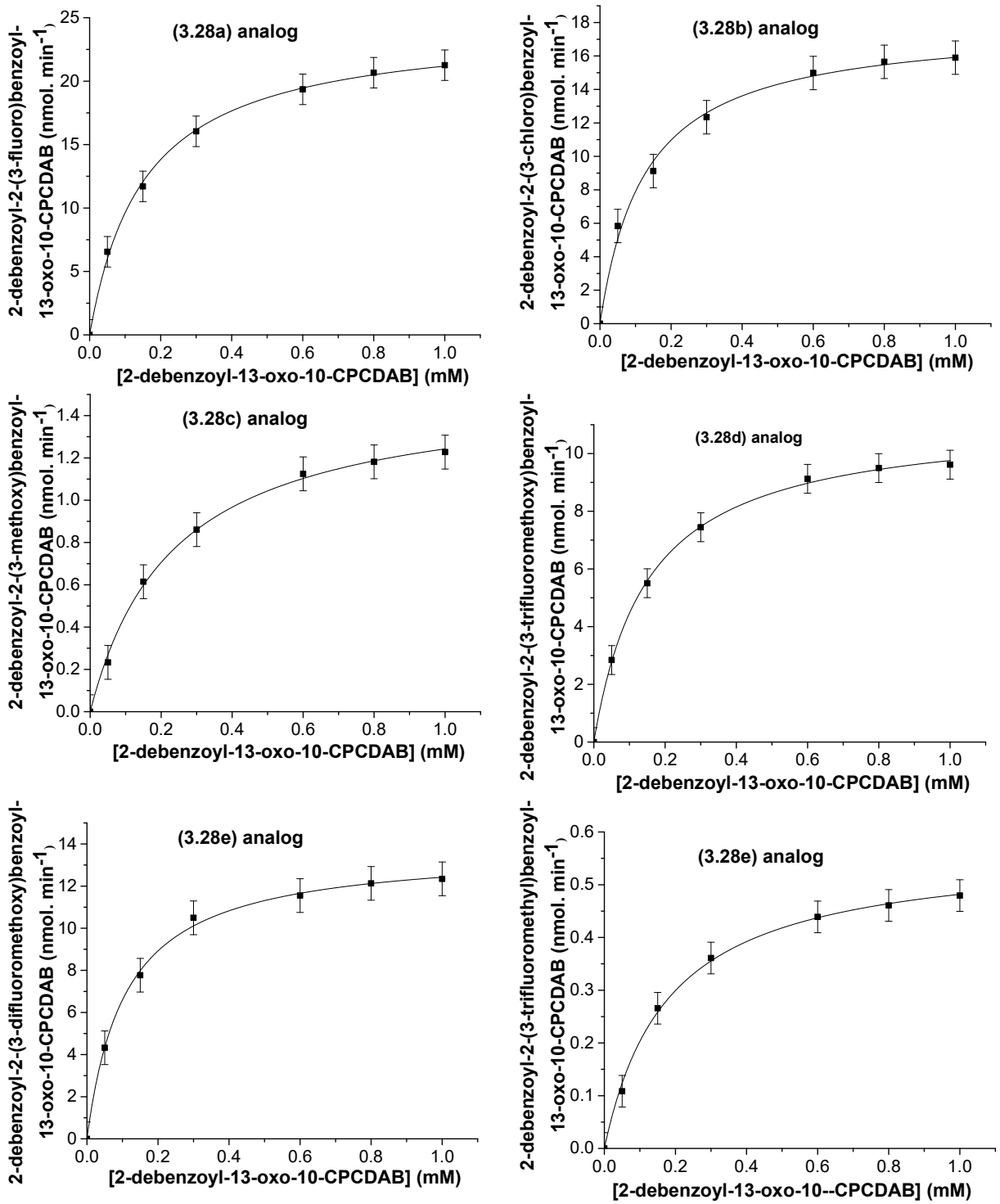

Figure 3.131: Michaelis-Menten kinetics for the turnover of 2-*O*-debenzoyl-13-oxo-10-CPCDAB to the 2-*O*-debenzoyl-2-*meta*-substiuttedbenzoyl-13-oxo-10-CPCDAB analogues **3.28** (**a**-**f**).

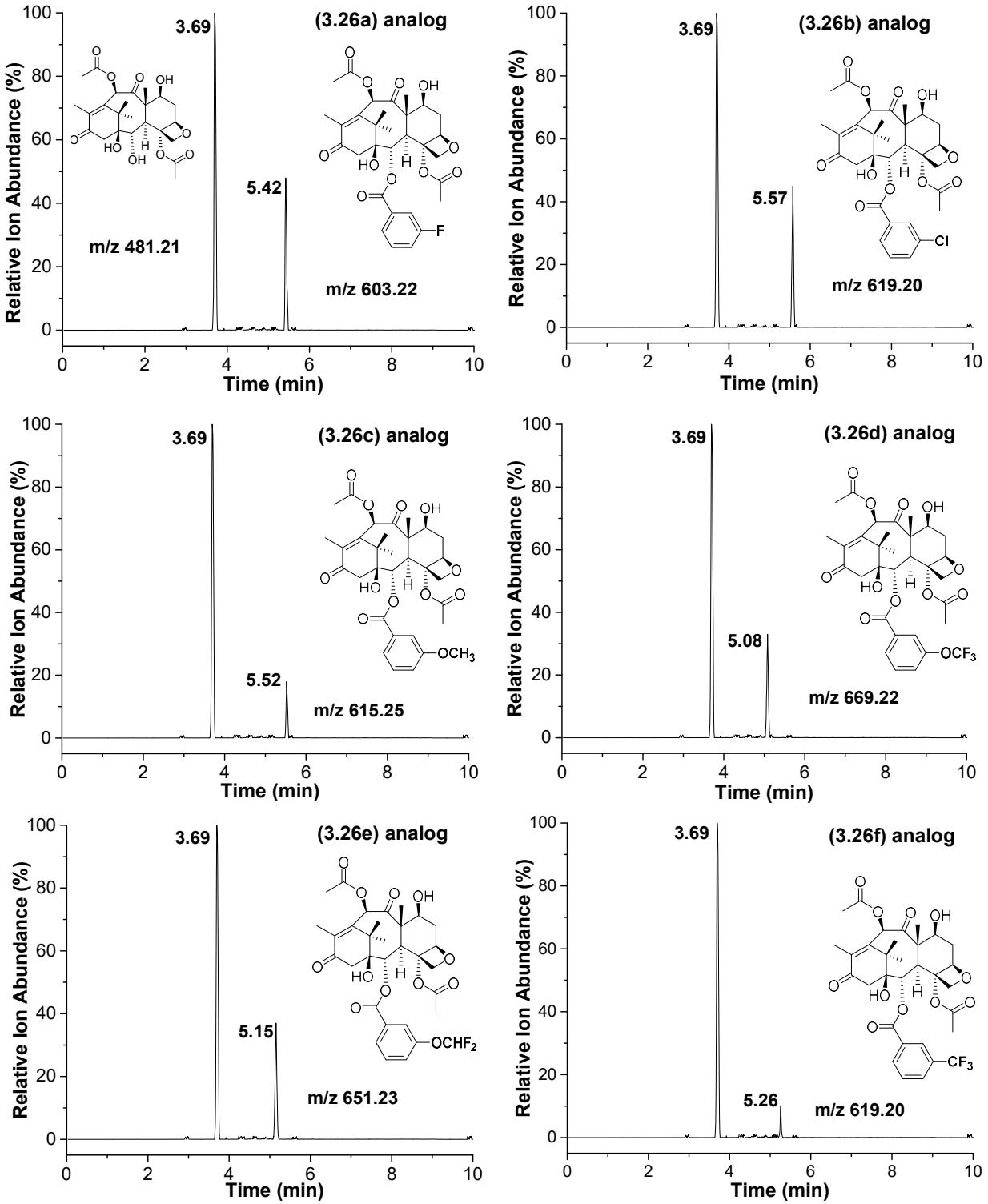

Figure 3.132: LC/ESI-MS (selected ion mode for m/z $[M + H]^+$) of the biocatalytic conversion of 2-*O*-debenzoyl-13-oxo-baccatin III to the 2-*O*-debenzoyl-2-*meta*-substiuttedbenzoyl-13-oxo-baccatin III analogues **3.26** (**a**-**f**).

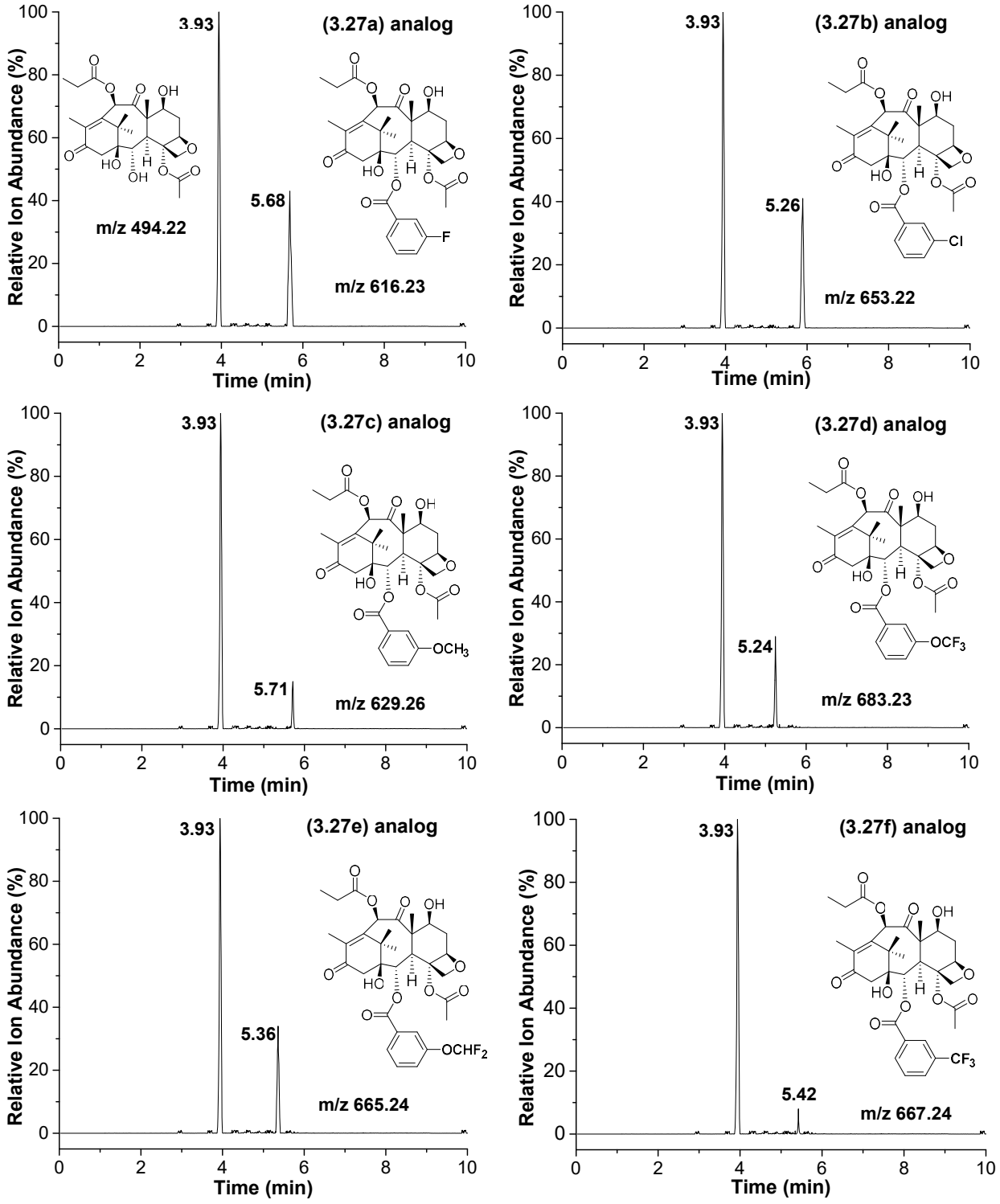

Figure 3.133: LC/ESI-MS (selected ion mode for m/z $[M + H]^+$) of the biocatalytic conversion of 2-*O*-debenzoyl-13-oxo-10-PDAB to the 2-*O*-debenzoyl-2-*meta*-substiuttedbenzoyl-13-oxo-10-PDAB analogues **3.27** (**a**-**f**).

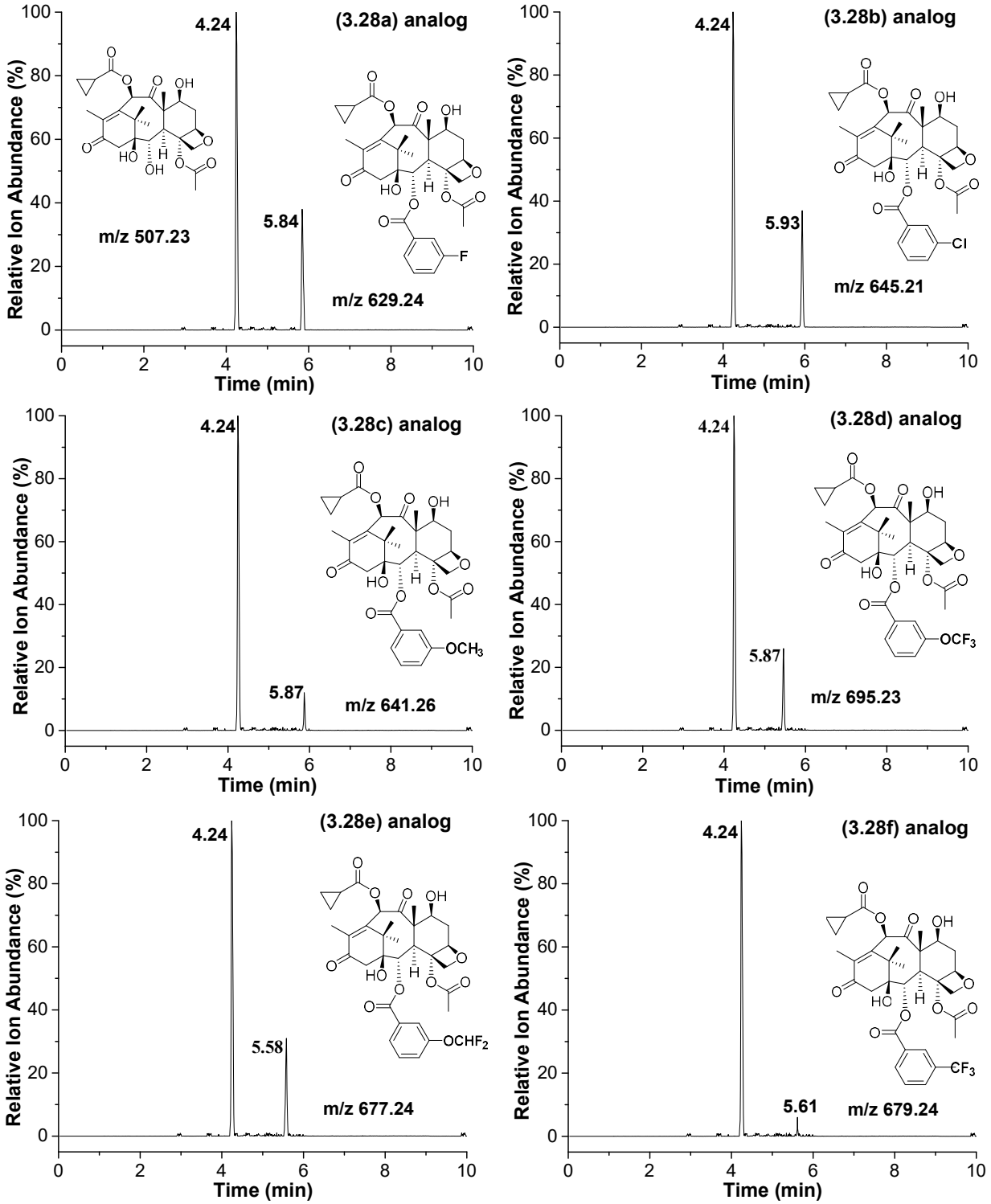

Figure 3.134: LC/ESI-MS (selected ion mode for m/z $[M + H]^+$) of the biocatalytic conversion of 2-*O*-debenzoyl-13-oxo-10-CPDCAB to the 2-*O*-debenzoyl-2-*meta*-substiuttedbenzoyl-13-oxo-10-CPCDAB analogues **3.28** (**a**-**f**).

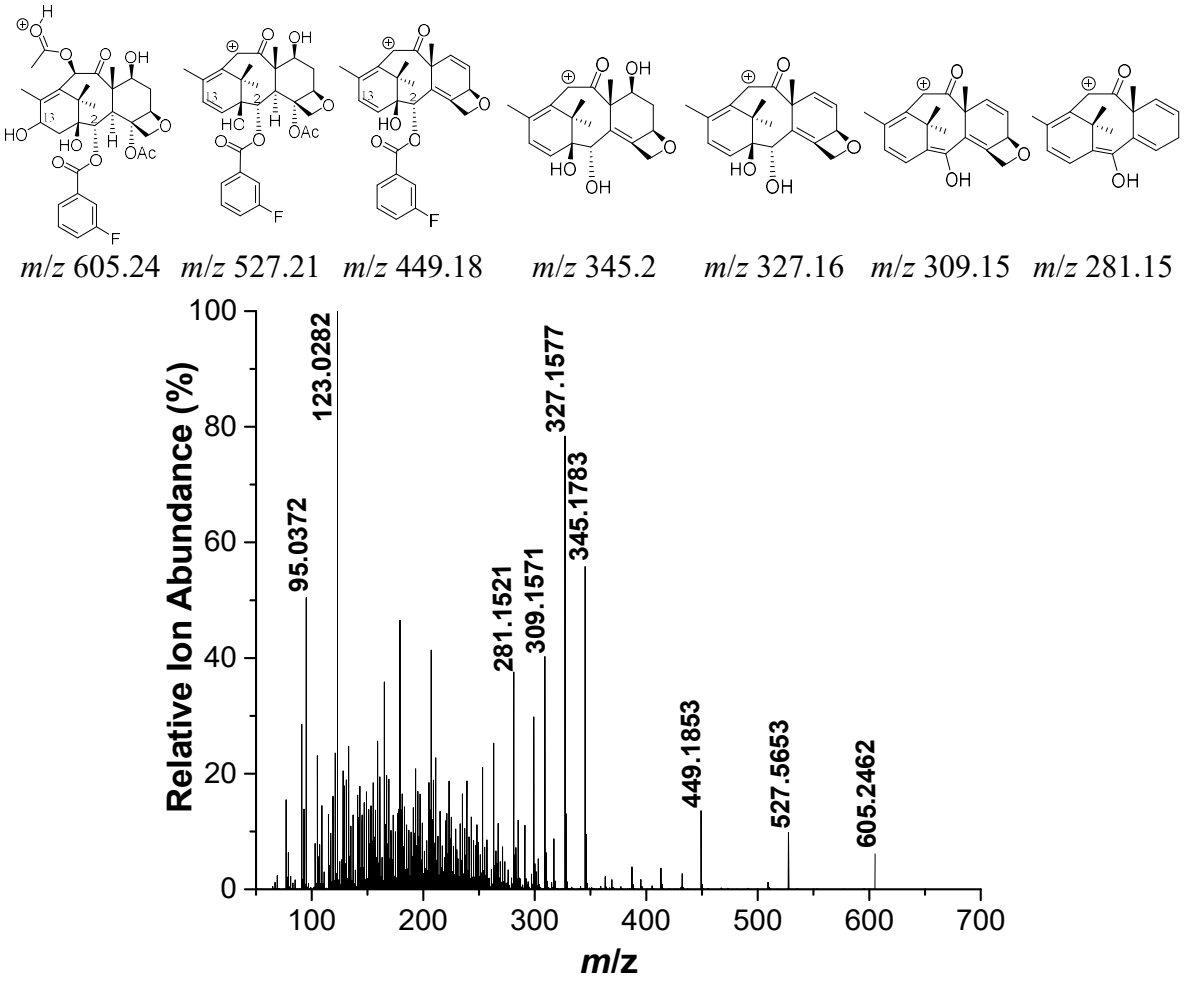

Figure 3.135: LC/ESI-MS/MS (positive-ion mode) of purified 2-DBz-2-(3-fluoro) benzoyl baccatin III with peak mass assignments and putative chemical transformations (above spectra).

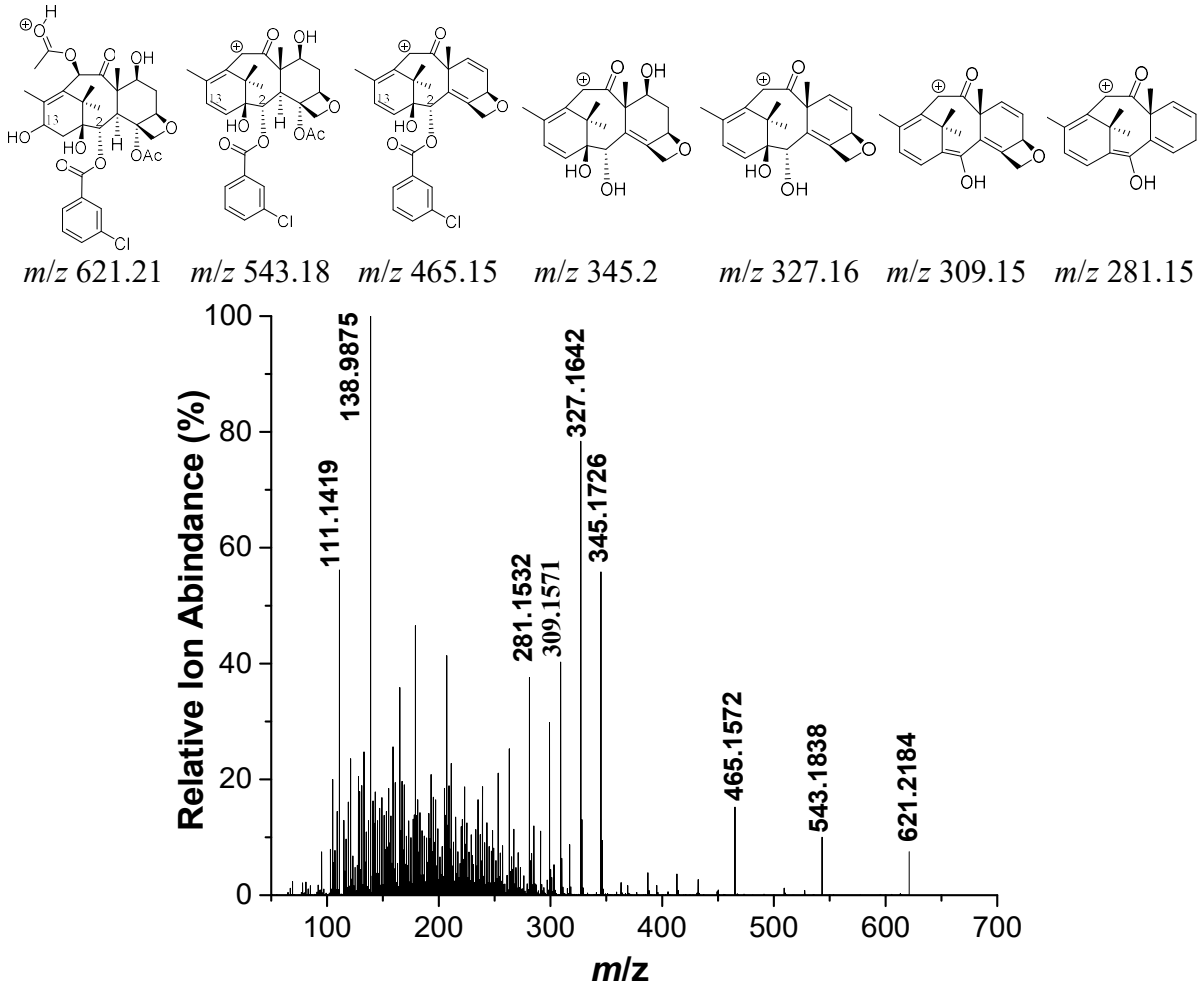

Figure 3.136: LC/ESI-MS/MS (positive-ion mode) of purified 2-DBz-2-(3-chloro) benzoyl baccatin III with peak mass assignments and putative chemical transformations (above spectra).

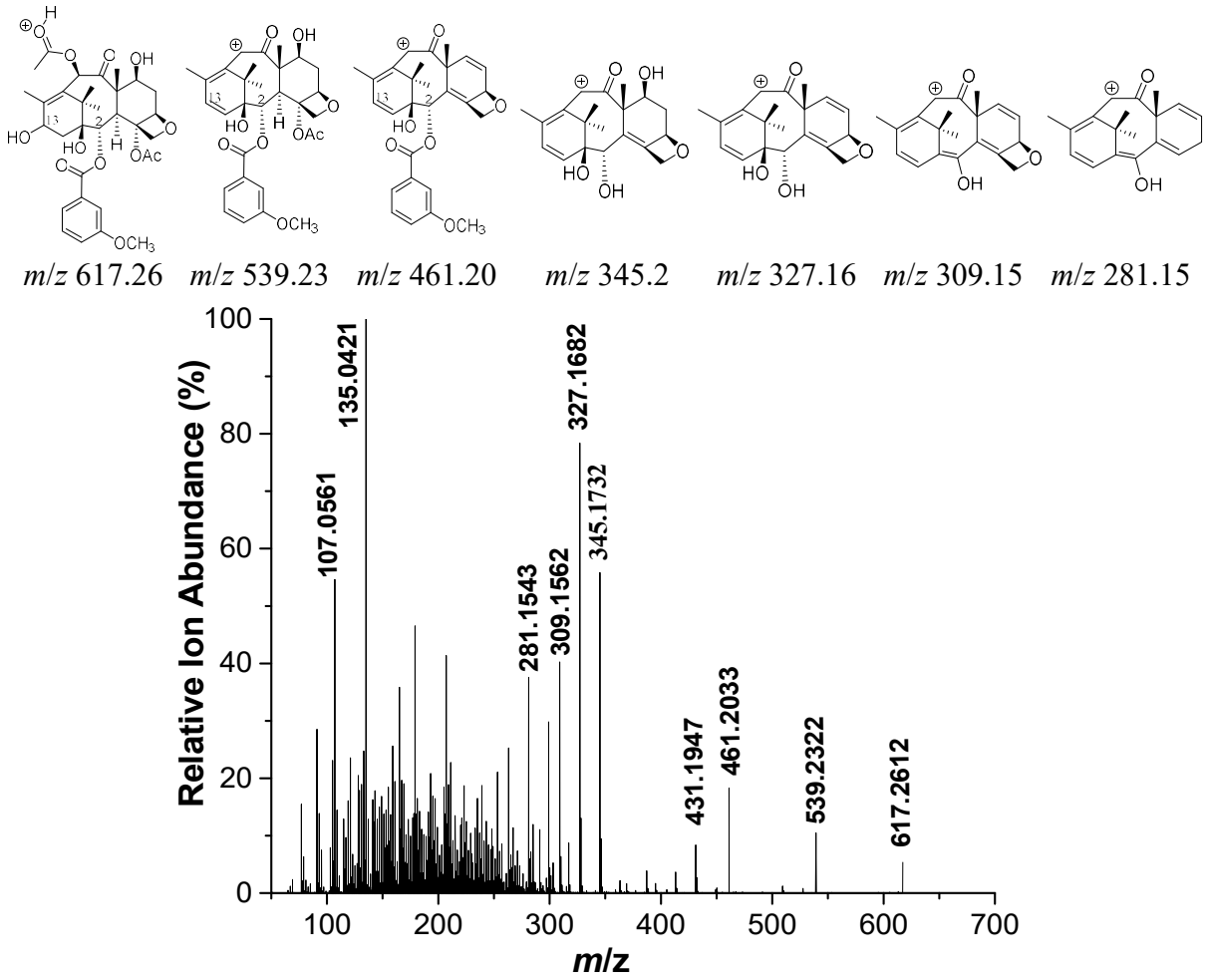

Figure3.137: LC/ESI-MS/MS (positive-ion mode) of purified 2-DBz-2-(3-methoxy) benzoyl baccatin III with peak mass assignments and putative chemical transformations (above spectra).

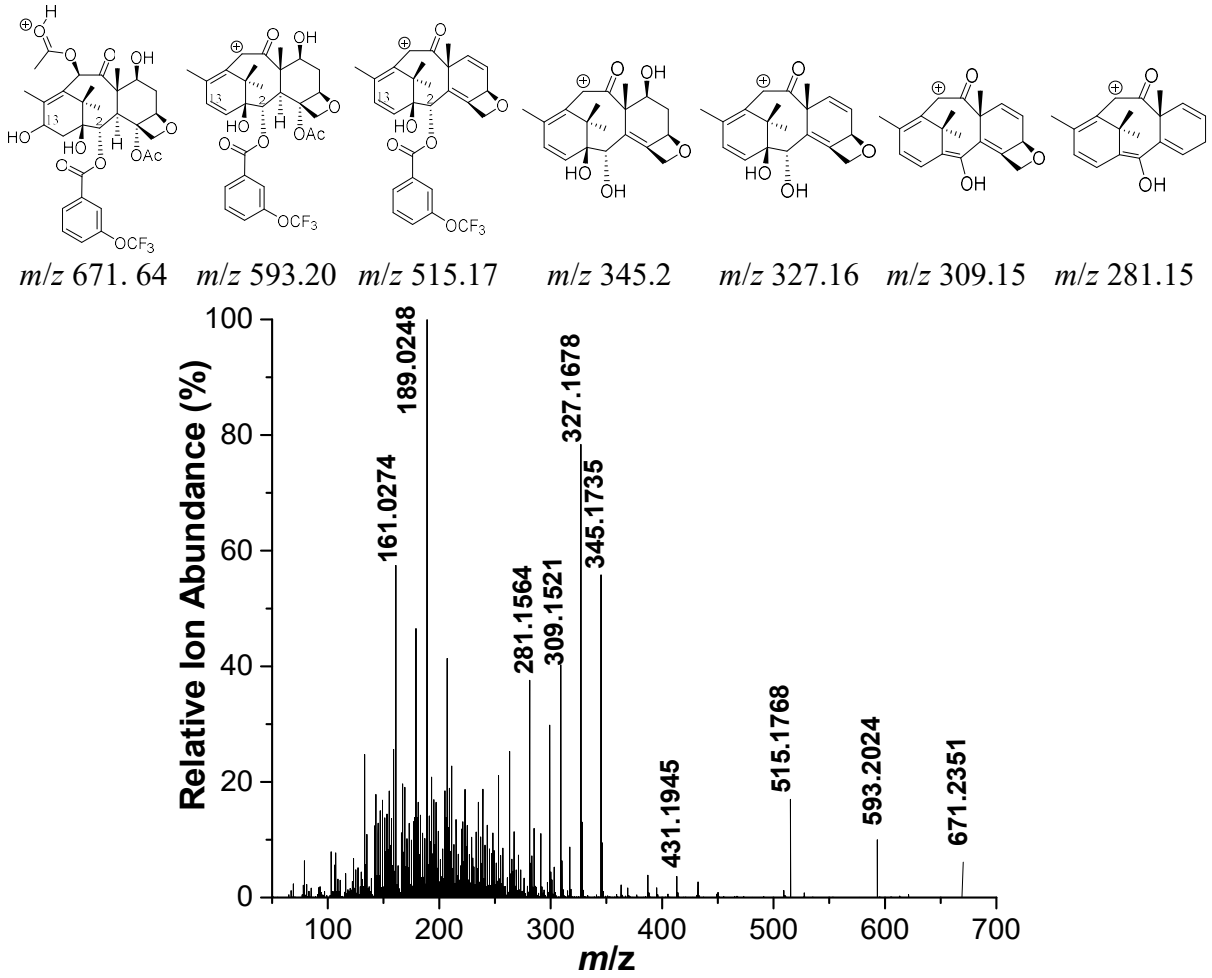

Figure 3.138: LC/ESI-MS/MS (positive-ion mode) of purified 2-DBz-2-(3-trifluoromethoxy) benzoyl baccatin III with peak mass assignments and putative chemical transformations (above spectra).

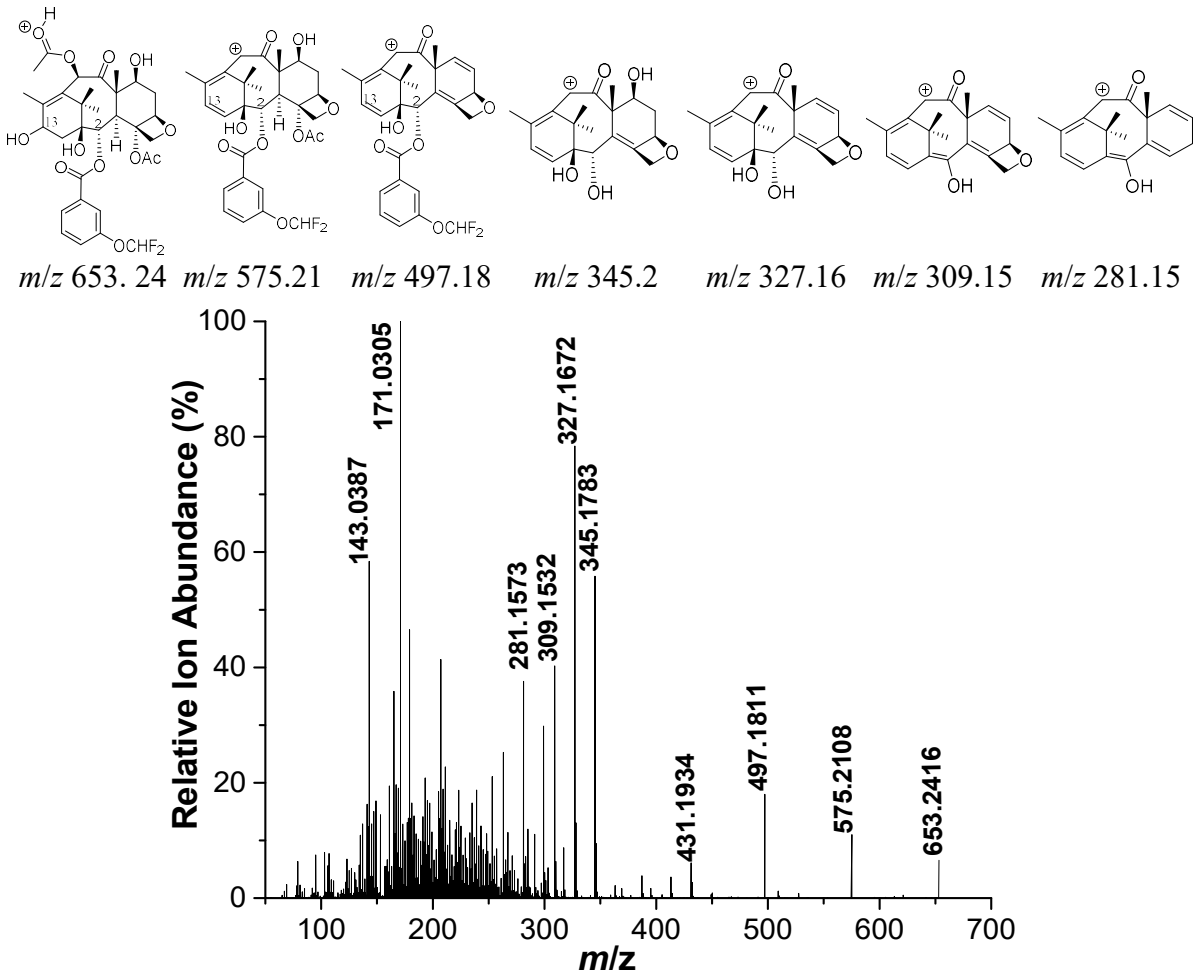

Figure 3.139: LC/ESI-MS/MS (positive-ion mode) of purified 2-DBz-2-(3-difluoromethoxy) benzoyl baccatin III with peak mass assignments and putative chemical transformations (above spectra).

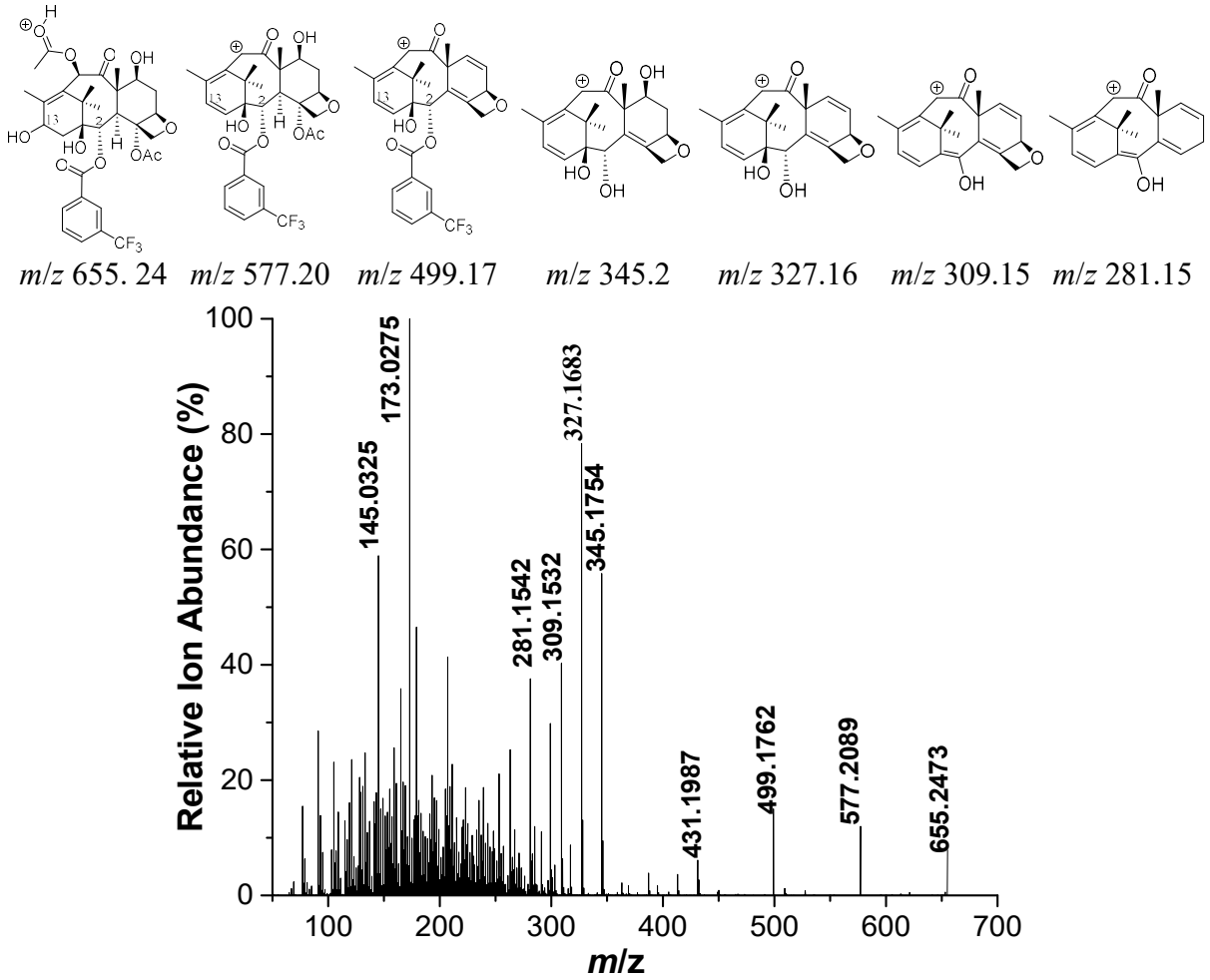

Figure 3.140: LC/ESI-MS/MS (positive-ion mode) of purified 2-DBz-2-(3-trifluoromethyl) benzoyl baccatin III with peak mass assignments and putative chemical transformations (above spectra).

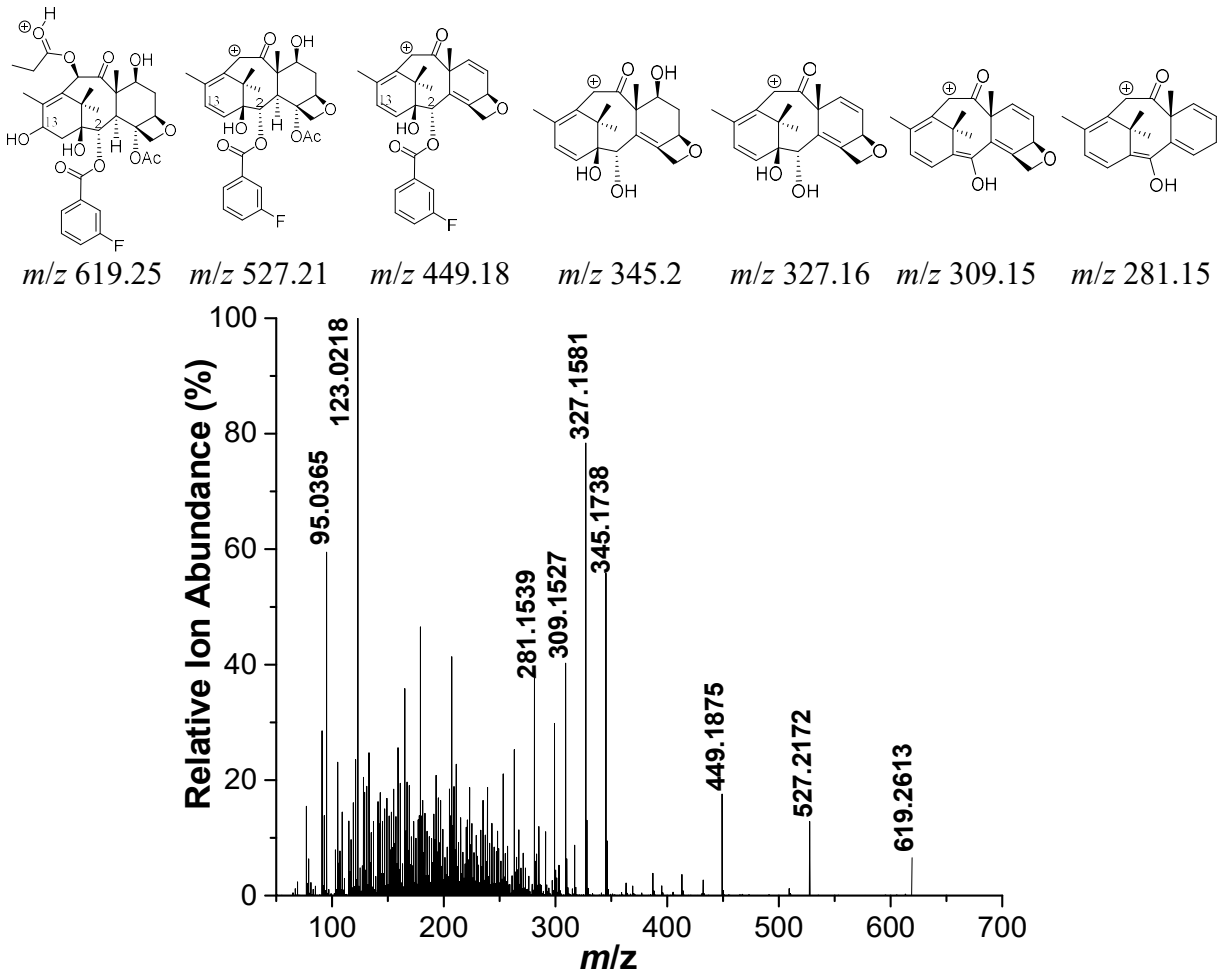

Figure 3.141: LC/ESI-MS/MS (positive-ion mode) of purified 2-DBz-2-(3-fluoro) benzoyl-10-PDAB with peak mass assignments and putative chemical transformations (above spectra).

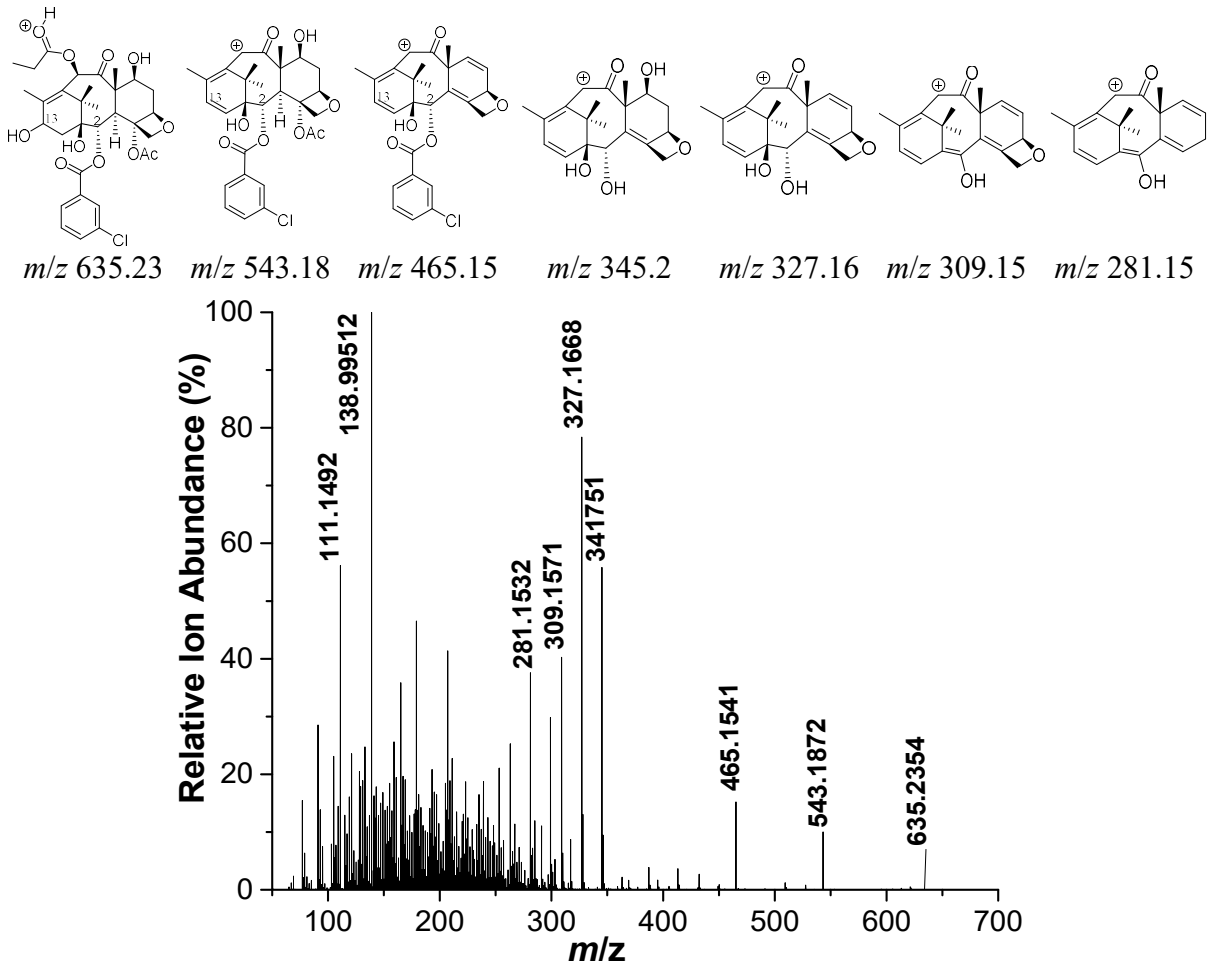

Figure 3.142: LC/ESI-MS/MS (positive-ion mode) of purified 2-DBz-2-(3-chloro) benzoyl-10-PDAB with peak mass assignments and putative chemical transformations (above spectra).

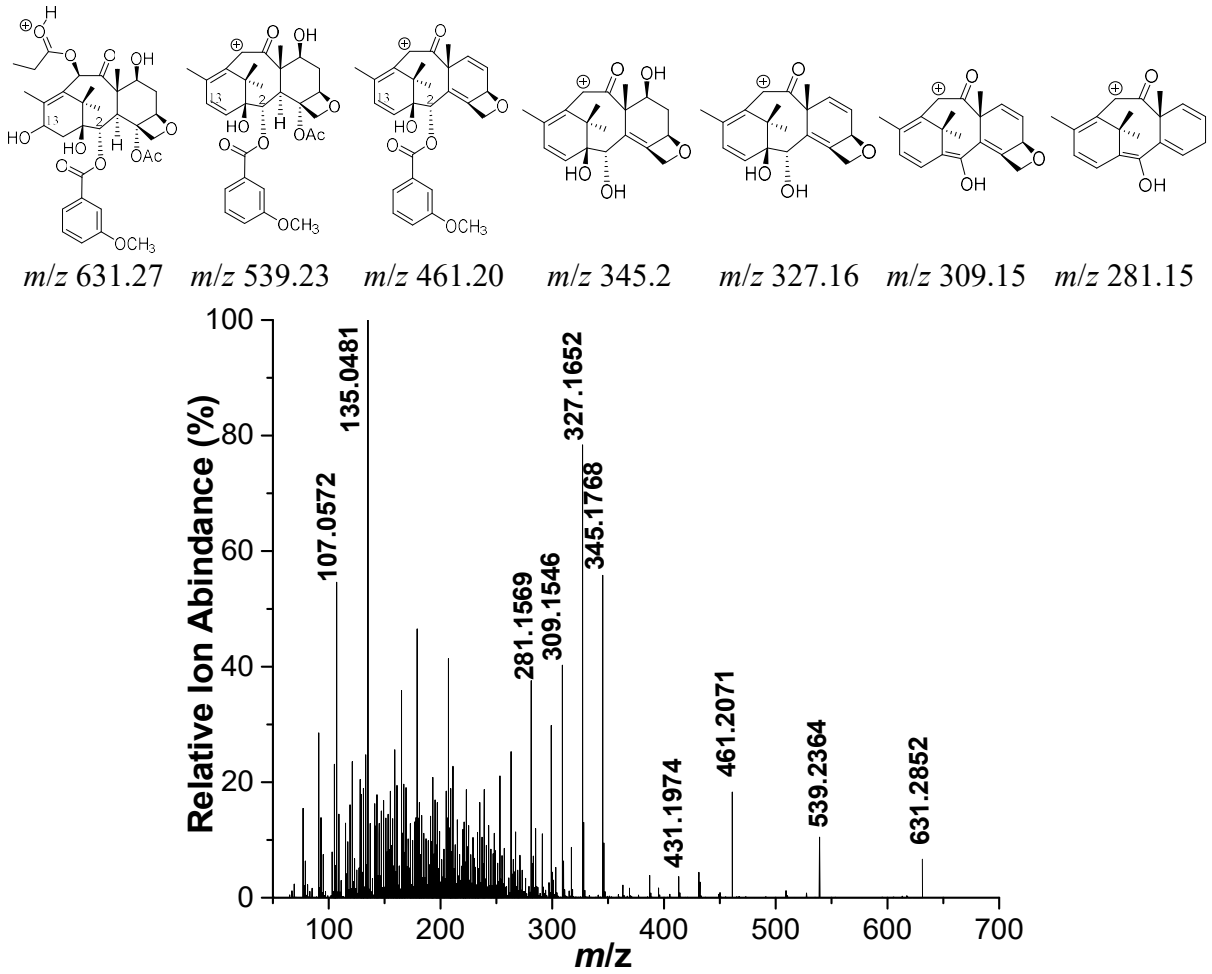

Figure 3.143: LC/ESI-MS/MS (positive-ion mode) of purified 2-DBz-2-(3-methoxy) benzoyl-10-PDAB with peak mass assignments and putative chemical transformations (above spectra).

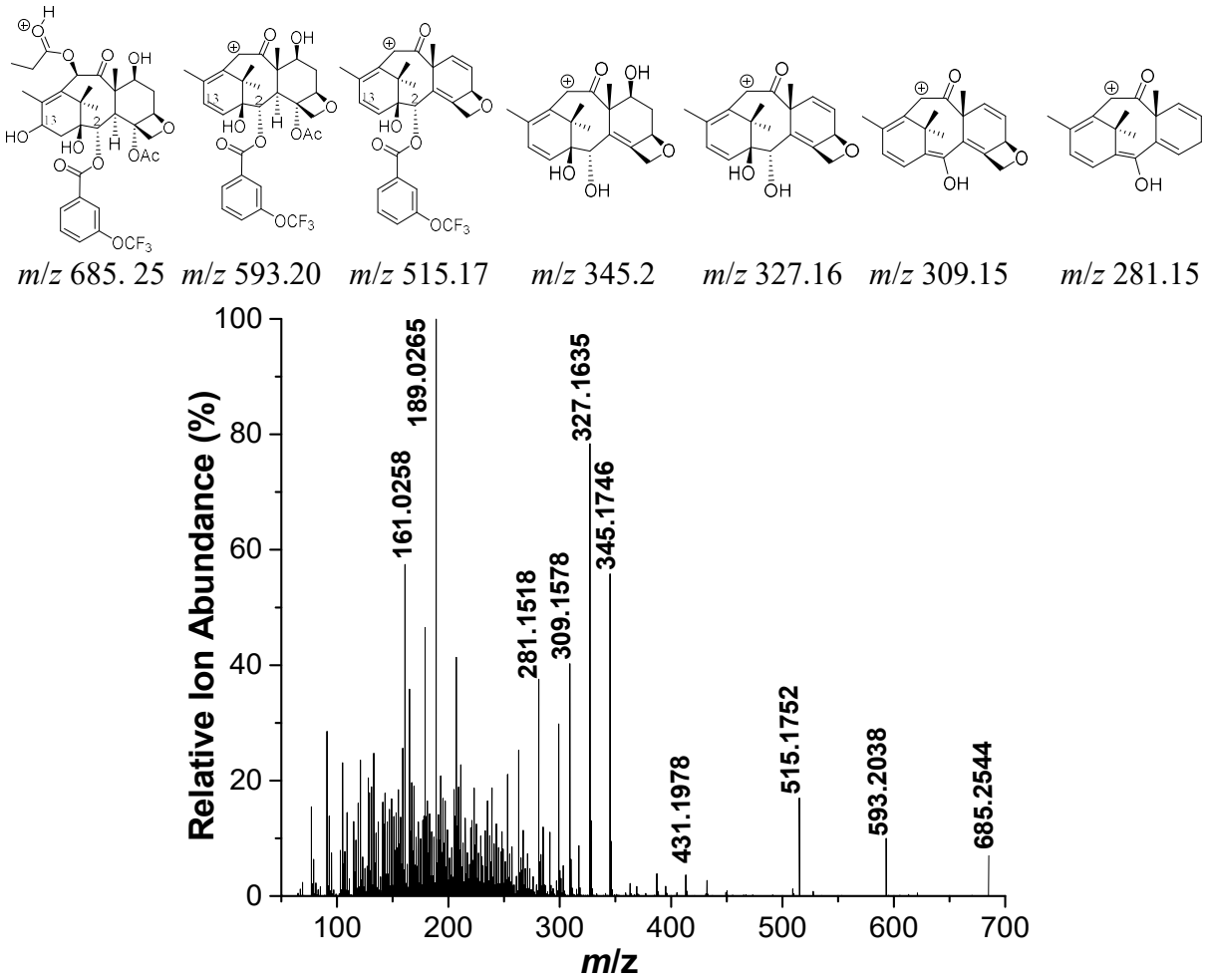

Figure 3.144: LC/ESI-MS/MS (positive-ion mode) of purified 2-DBz-2-(3-trifluoromethoxy) benzoyl-10-PDAB with peak mass assignments and putative chemical transformations (above spectra).

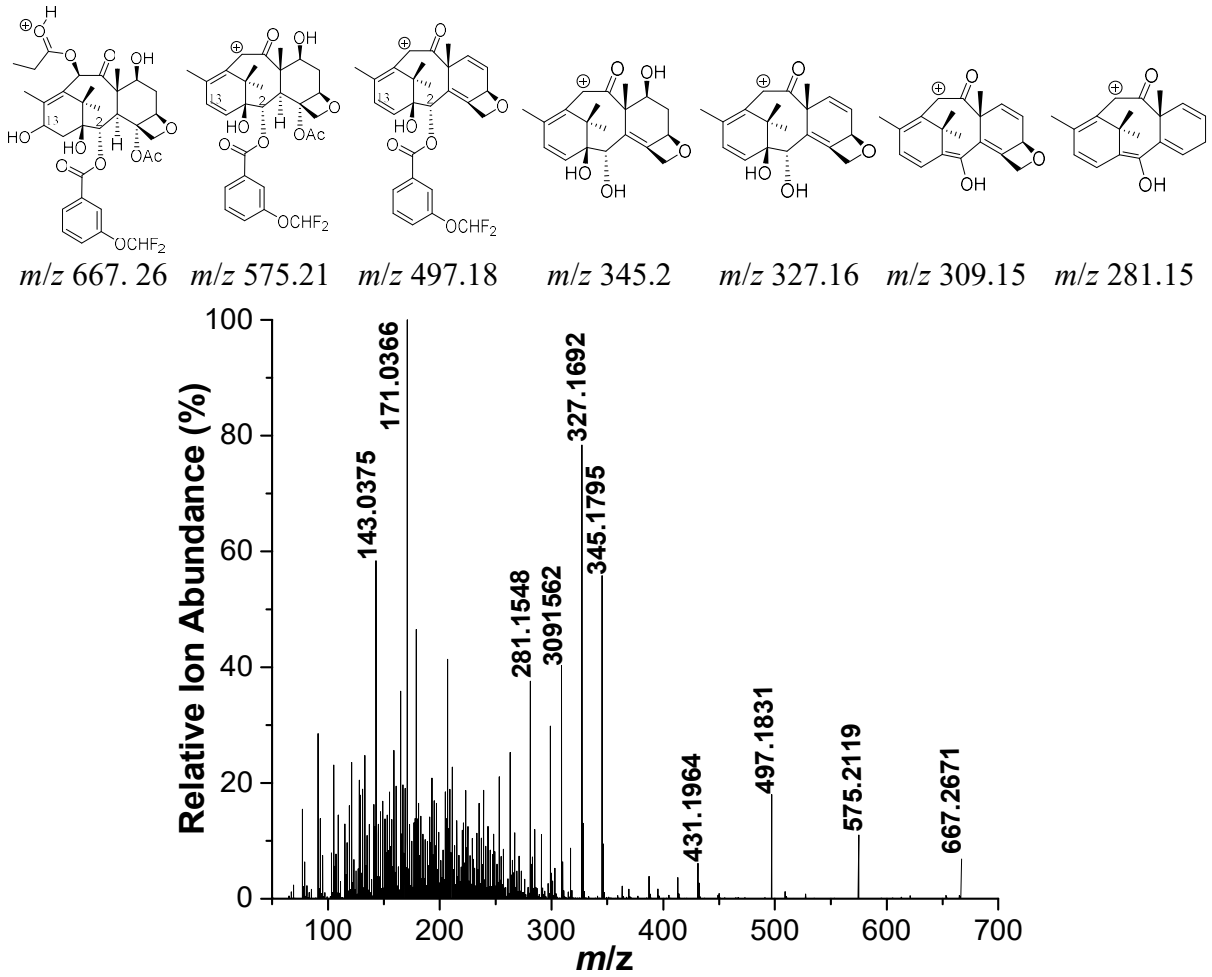

Figure 3.145: LC/ESI-MS/MS (positive-ion mode) of purified 2-DBz-2-(3-difluoromethoxy) benzoyl-10-PDAB with peak mass assignments and putative chemical transformations (above spectra).

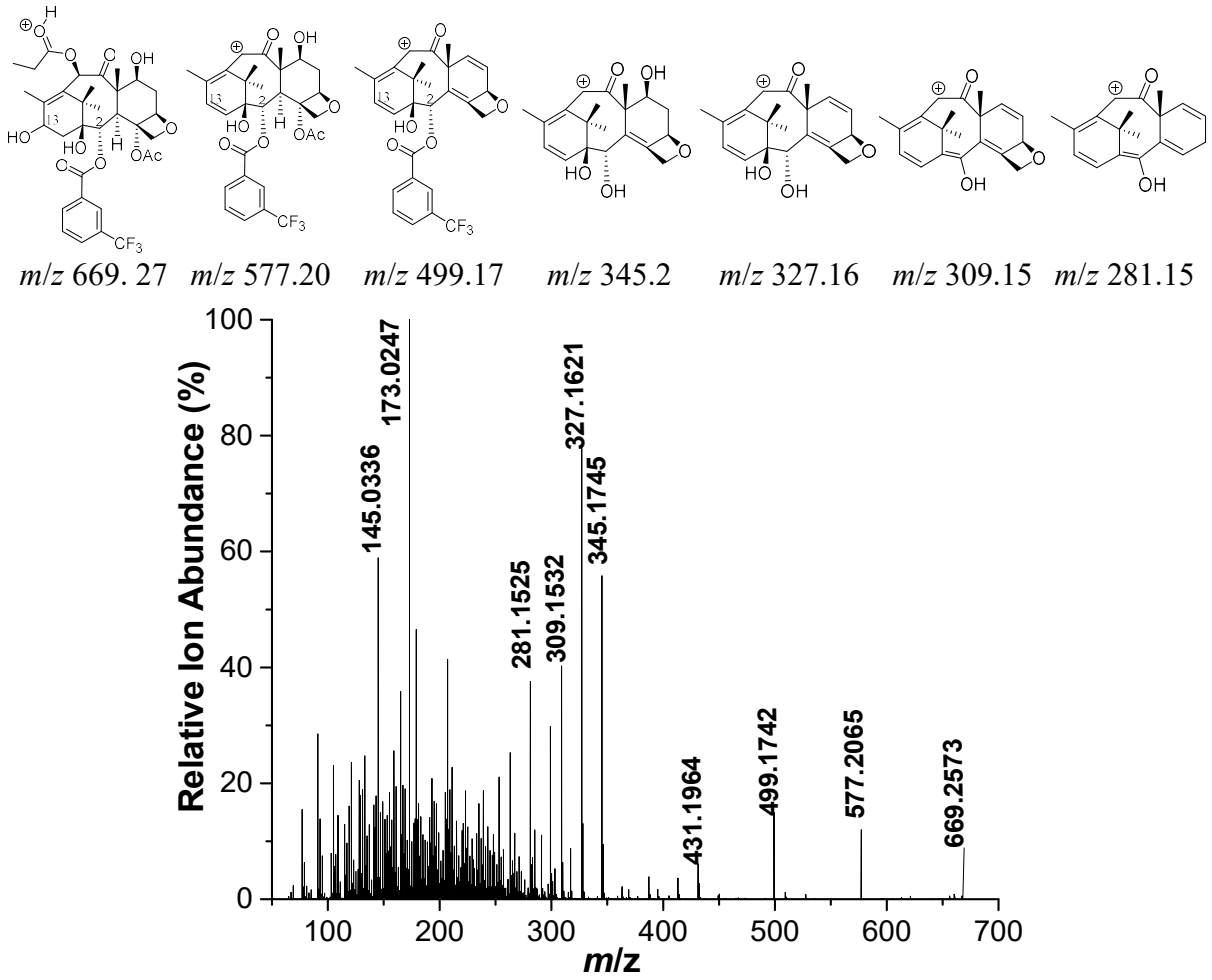

Figure 3.146: LC/ESI-MS/MS (positive-ion mode) of purified 2-DBz-2-(3-trifluoromethyl) benzoyl-10-PDAB with peak mass assignments and putative chemical transformations (above spectra).

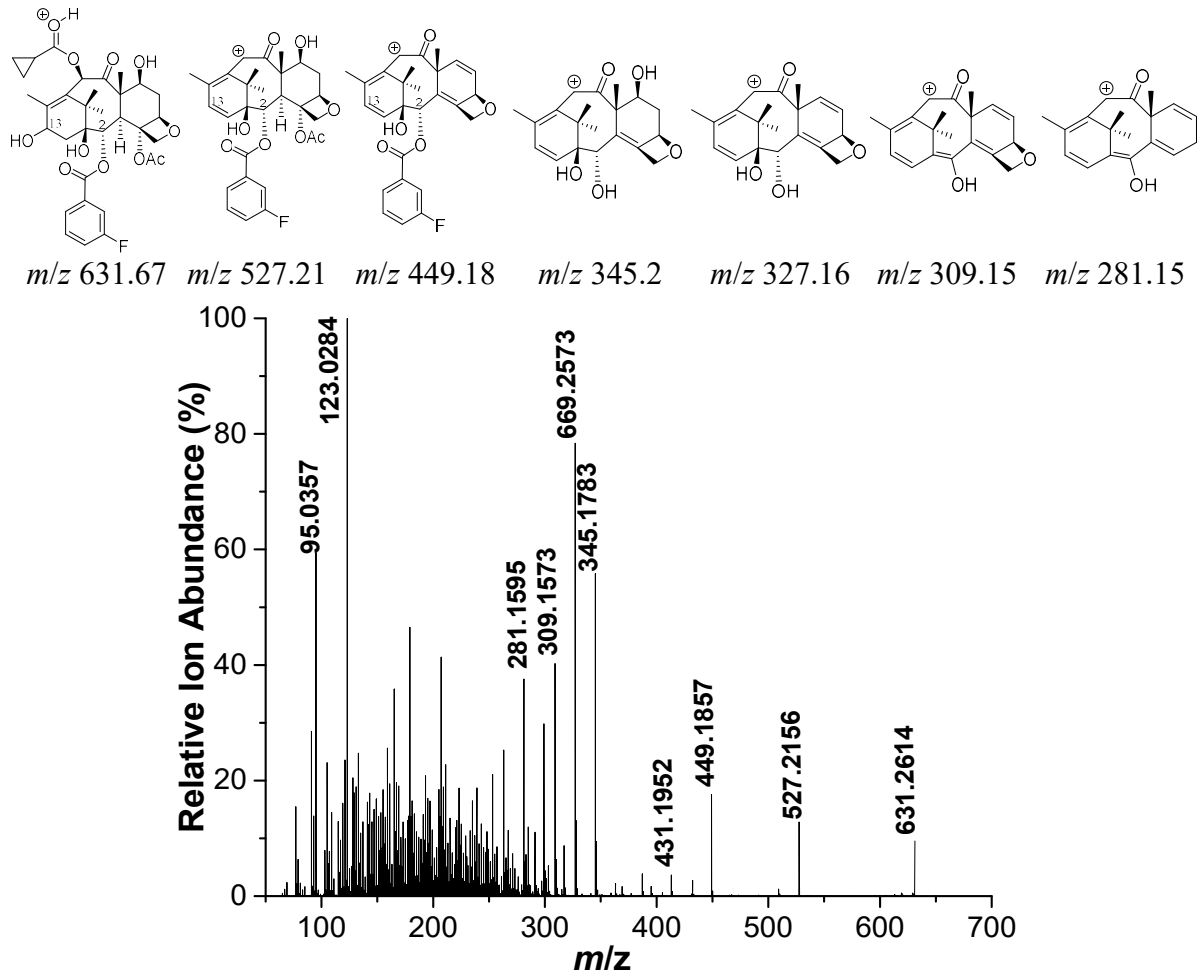

Figure 3.147: LC/ESI-MS/MS (positive-ion mode) of purified 2-DBz-2-(3-fluoro) benzoyl-10-CPCDAB with peak mass assignments and putative chemical transformations (above spectra).

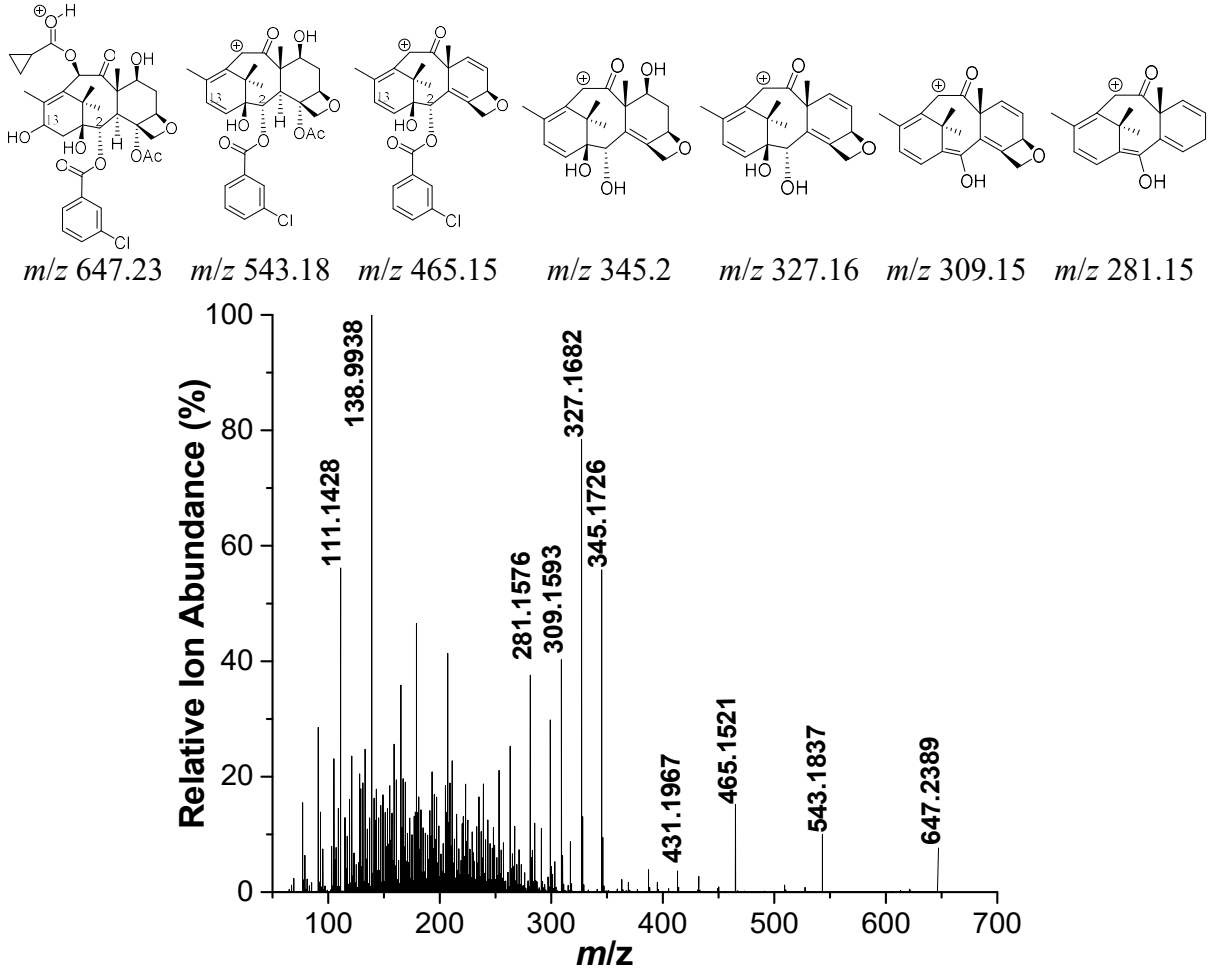

Figure 3.148: LC/ESI-MS/MS (positive-ion mode) of purified 2-DBz-2-(3-chloro) benzoyl-10-CPCDAB with peak mass assignments and putative chemical transformations (above spectra).

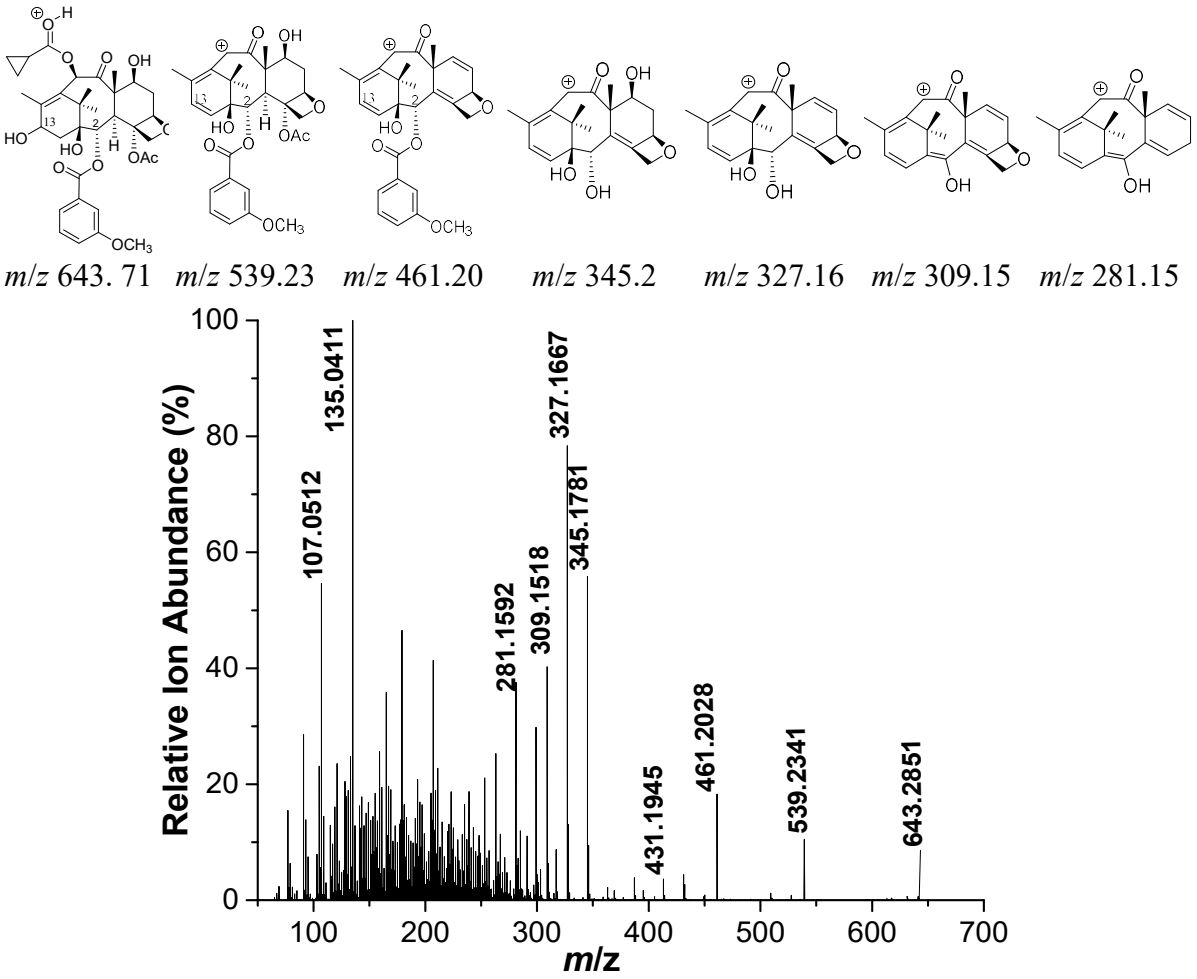

Figure 3.149: LC/ESI-MS/MS (positive-ion mode) of purified 2-DBz-2-(3-methoxy) benzoyl-10-CPCDAB with peak mass assignments and putative chemical transformations (above spectra).

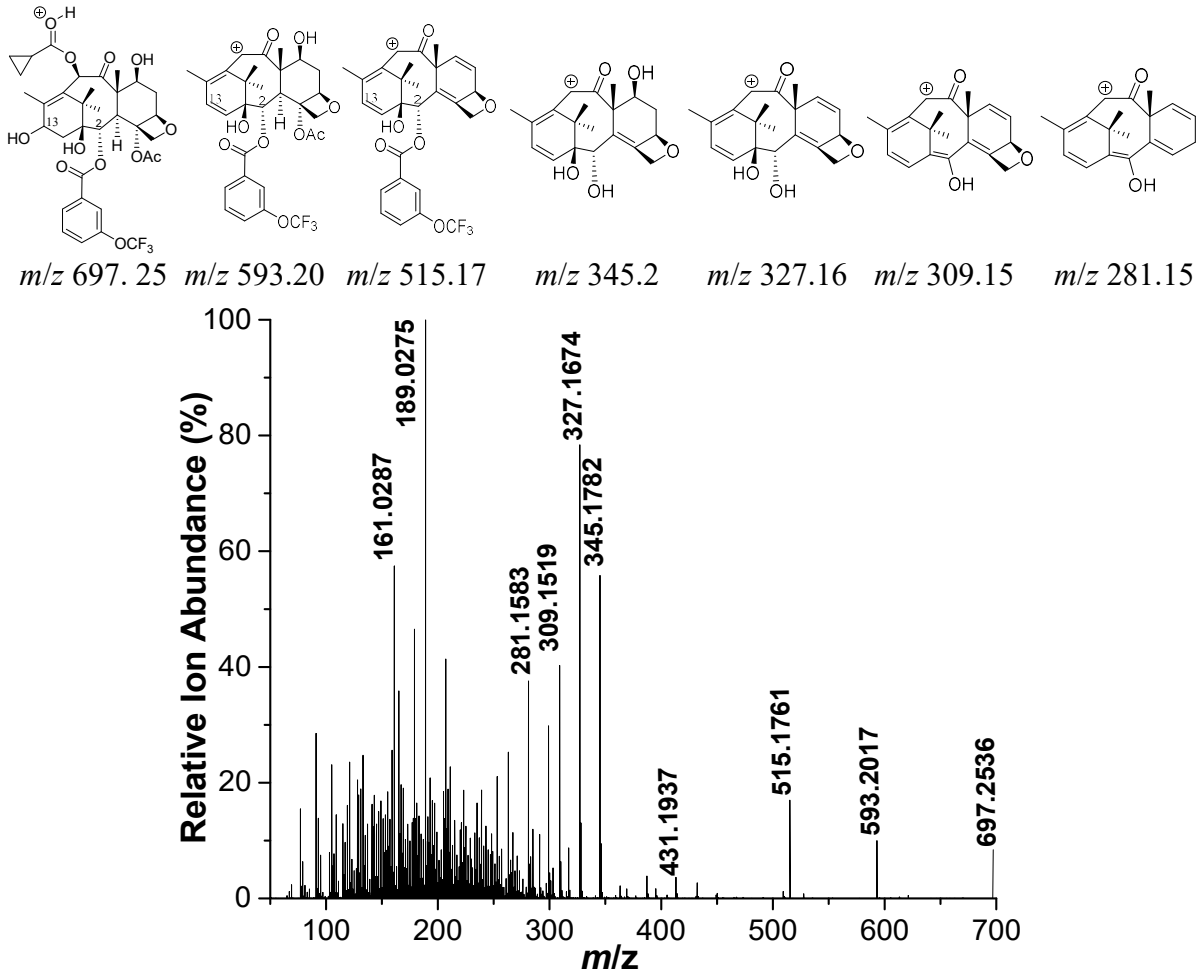

Figure 3.150: LC/ESI-MS/MS (positive-ion mode) of purified 2-DBz-2-(3-trifluoromethoxy) benzoyl-10-CPCDAB with peak mass assignments and putative chemical transformations (above spectra).

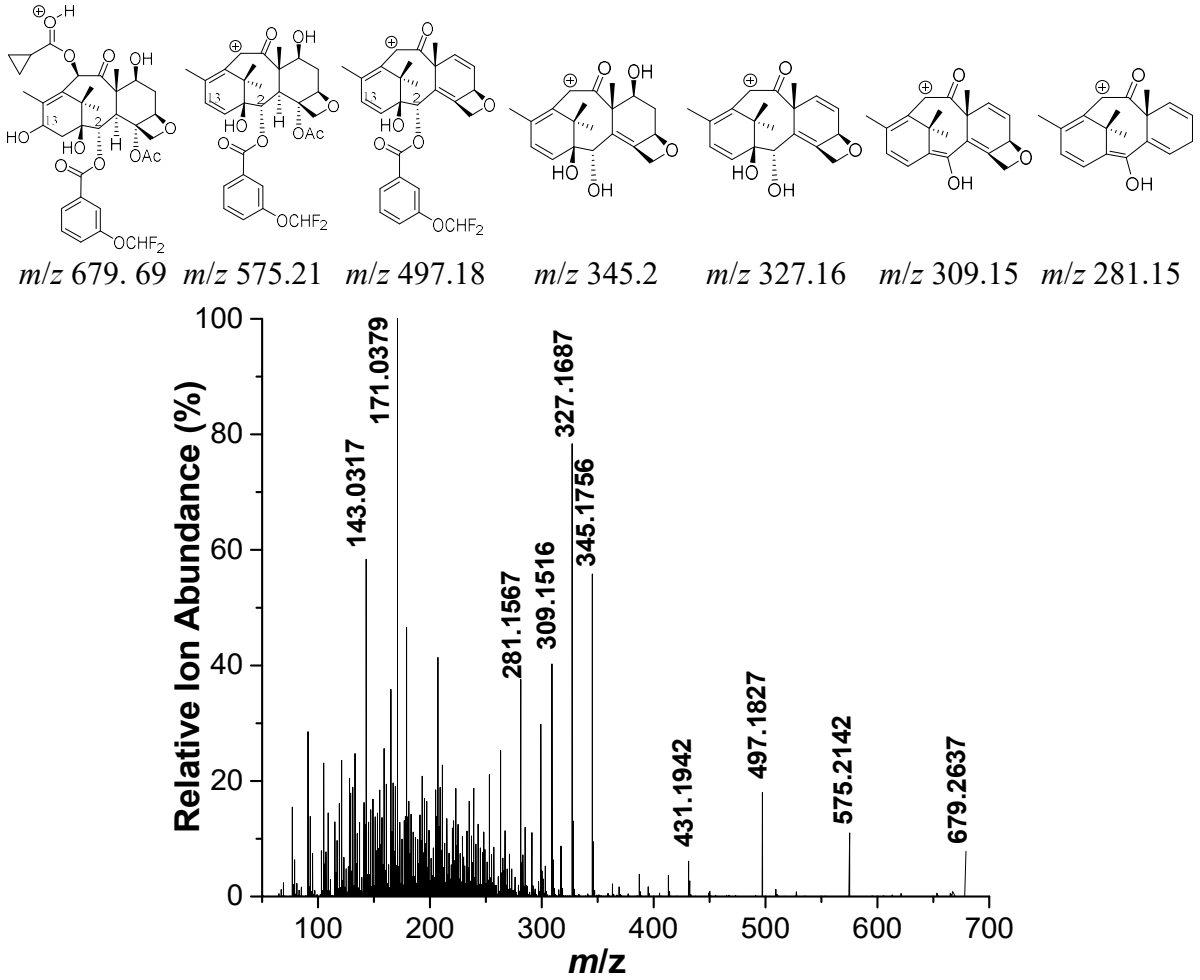

Figure 3.151: LC/ESI-MS/MS (positive-ion mode) of purified 2-DBz-2-(3-difluoromethoxy) benzoyl-10-CPCDAB with peak mass assignments and putative chemical transformations (above spectra).

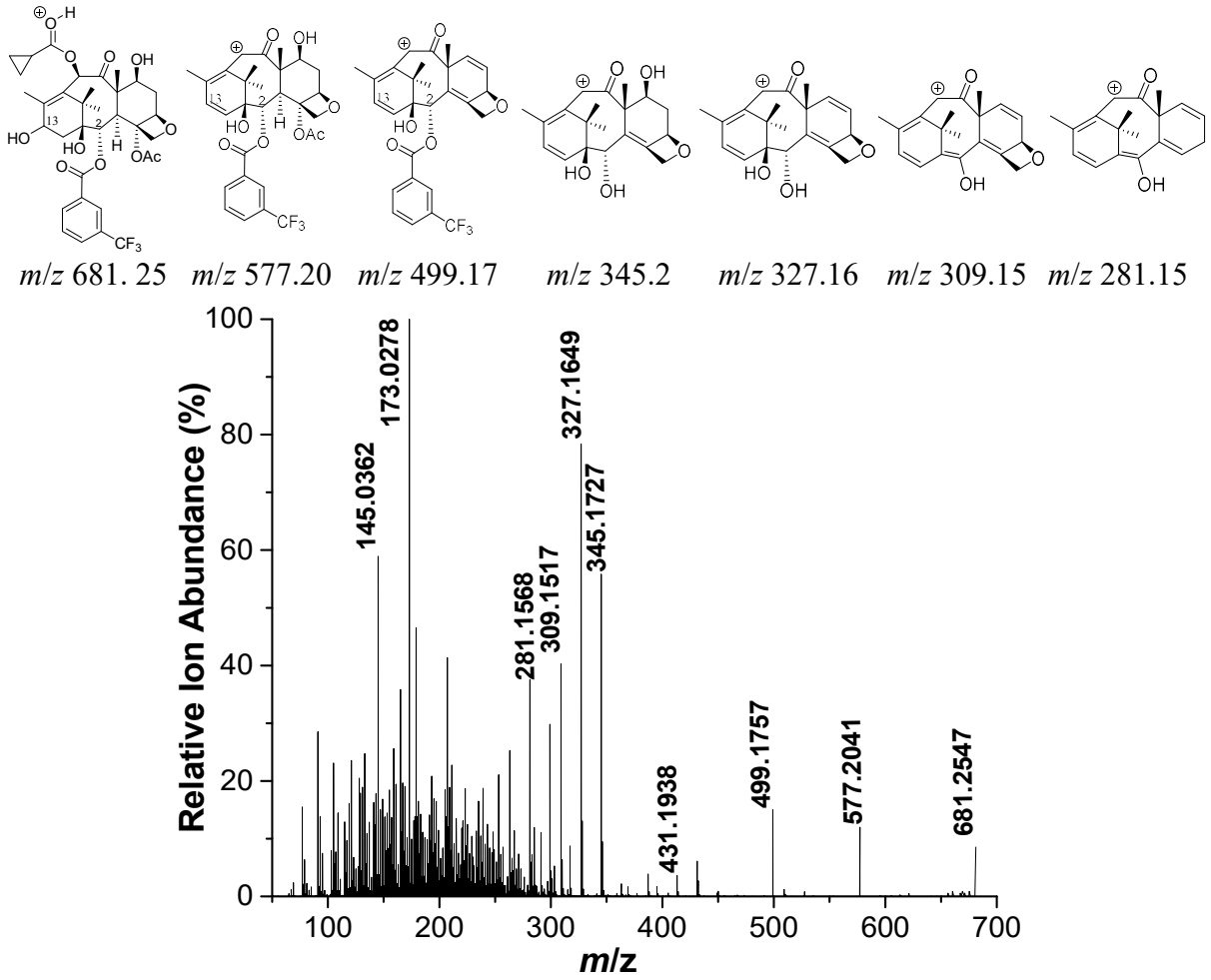

Figure 3.152: LC/ESI-MS/MS (positive-ion mode) of purified 2-DBz-2-(3-trifluoromethyl) benzoyl-10-CPCDAB with peak mass assignments and putative chemical transformations (above spectra).

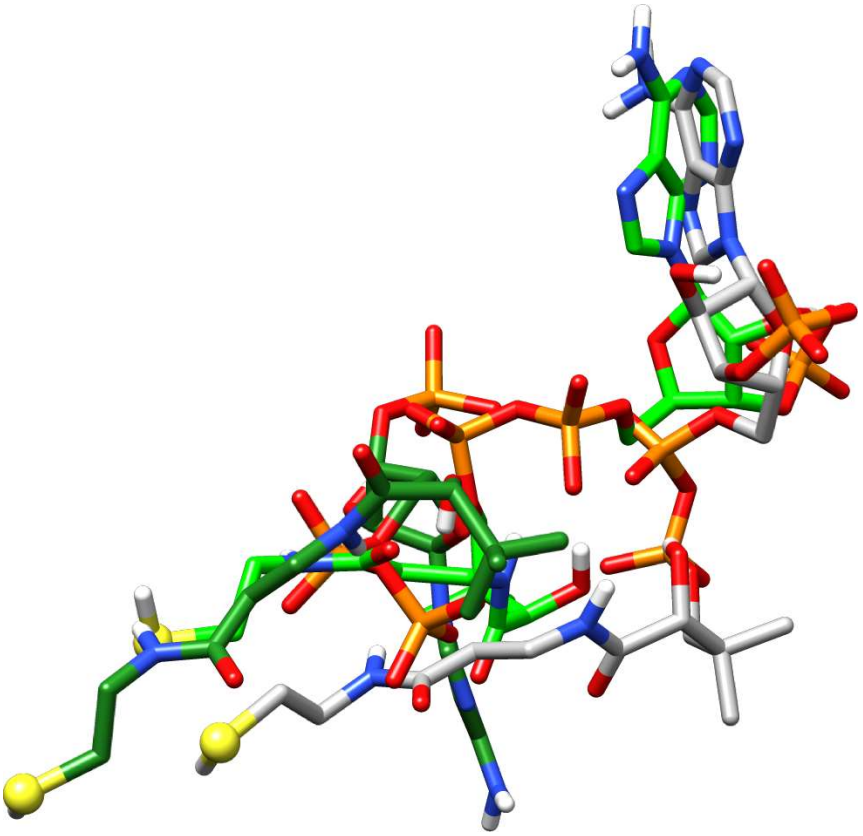

Figure 3.153: Complete structures of CoA substrates docked with 13-oxobaccatin III (dark green), 13-O-acetylbaccatin III (light green), and baccatin III (light gray) in the mTBT active site modeled by MD simulations. Heteroatoms are colored by standard conventions.

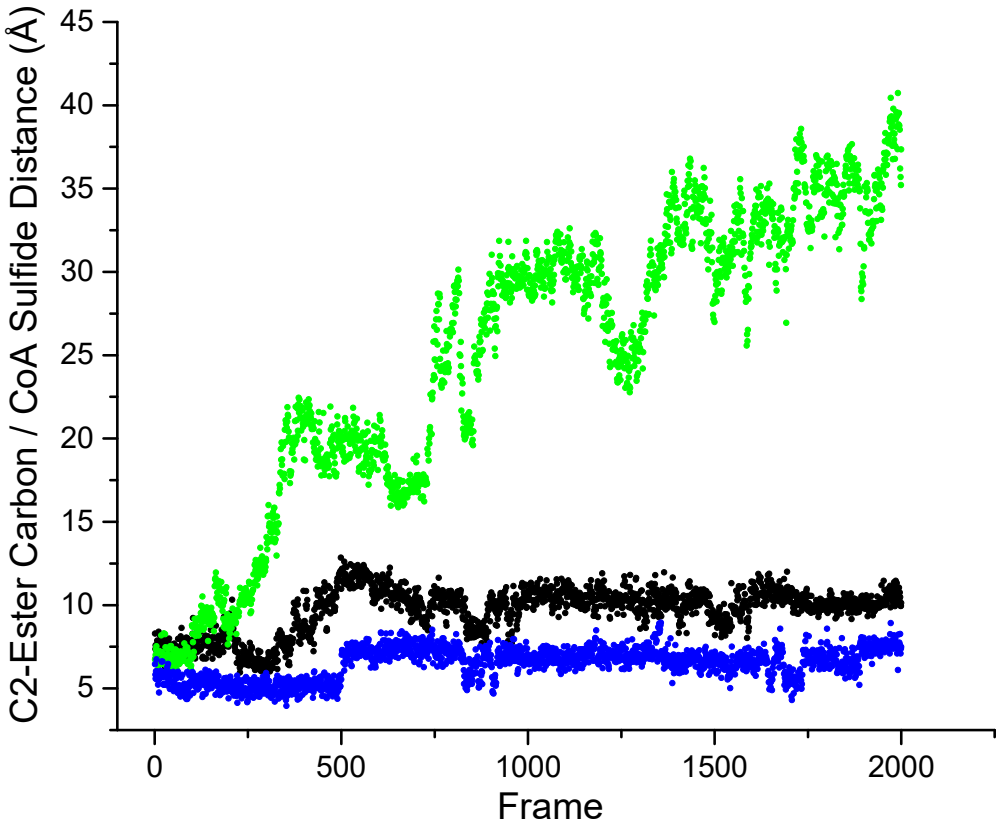

Figure 3.154: Molecular dynamics simulations over 2,000 frames (10 ps per frame, totaling 20 ns) estimate the intermolecular distance between the 2-O-ester carbon (of 13-oxobaccatin III (**3.19**) (blue dots), baccatin III (**3.16**) (black dots), 13-O-acetylbaccatin III (**3.35**) (green dots)) and the CoA sulfide for each frame.

CHAPTER 4: THE ROLE OF MAGNESSIUM ION IN UNDERSTANDING THE *TAXUS* BAPT CATALYSIS. INSPIRATION TO REPROPOSED BAHD ACYLTRANSFERASE MECHANISMS

Introduction

Acyltransferases play crucial roles in modifying the characteristics of plant metabolites such as improving the polarity, volatility, solubility, chemical stability, and biological activity.[1,2] These enzymes also contribute to the diversity of ester- and amide-containing natural products.[2] In contrast, five *Taxus* acyltransferases have been identified, characterized, and are involved in paclitaxel biosynthesis.[3-9] *Taxus* acyltransferases belong to a large superfamily of plant-derived acyltransferases (designated BAHD).[2] BAHD family of acyltransferases is named after the first four biochemically characterized enzymes of this superfamily (BEAT, AHCT, HCBT, and DAT).[2] Enzymes in this family utilize acyl-coenzyme A as acyl donor substrate and the amino or hydroxy group acceptors as cosubstrates.[1,2] Members of the BAHD acyltransferase family typically share conserved amino acid motifs such as HXXXD and DFGWG motifs.[10-12] The HXXXD is the catalytic motif, (H) identifies as the catalytic residue, and (D) plays an important structural role.[11] The DFGWG motif is necessary for catalysis and acts as a structural function by allowing the substrate access to the catalysis channel.[11] Previous site-direct mutagenesis on BAHD acetyltransferase, vinorine synthase show that mutating the catalytic His_{160} to alanine lead to loss of the catalytic activity.[13] This suggested that His_{160} in the HXXXD motif is very important for the vinorine synthase catalysis.[11] In the mechanism of the vinorine synthase catalysis, His_{160} is proposed to serve as basic residue as base that deprotonates the hydroxy group of acyl accepter substrate. The resulting nucleophile attacks the carbonyl carbon of the acyl-CoA donor substrate forming an oxyanion tetrahedral intermediate. In the final step of the catalytic cycle, the CoASH is released from the intermediate to produce the ester product (Figure 4.1).[11]

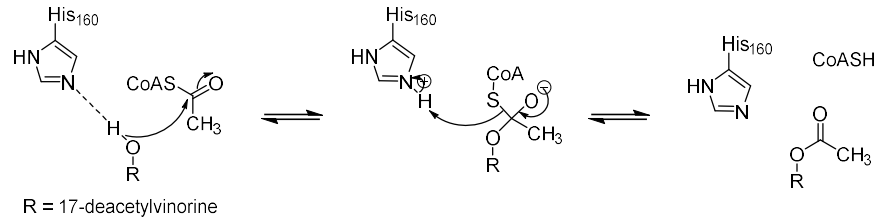

Figure 4.1: The proposed catalytic mechanism of vinorine synthase involves His_{160} as a general base.

However, *Taxus* baccatin III:3-amino-3-phenylpropanoyltransferase (BAPT) sequence has a unique catalytic motif containing a natural (GXXXD).[9] Earlier studies proposed that the mechanism of BAPT utilizes the free amine of the β-amino-3- phenylpropanoyl CoA thioester (Figure 4.2).[9] Based on our substrates specificity, Gaussian structure optimizations, and molecular dynamics (MD) simulation studies of *Taxus m*TBT catalysis, we gain a greater detail of understanding the molecular interactions of *m*TBT with taxane analogs. Our previous Gaussian structure optimization studies show that when taxane C13 has a hydroxyl group connected to it, it tends to form an intermolecular hydrogen bond with the oxygen connected to C4 OAc (Figure 4.3A). Other studies on how metal ions such as Mg^{2+}, Ca^{2+}, and Ba^{2+} can disassemble the intermolecular hydrogen bonding show that introducing metal cations effectively disrupt the intermolecular hydrogen bond.[14,15] These findings inspire us to interrupt the hydrogen bonding between C13 (OH) and C21 (OAc) of taxane analogs by using metal ions such as Mg^{2+} so C13(OH) will be free and ready after deprotonation for nucleophilic attack on the carbonyl carbon of acyl-CoA accepter in the BAPT catalysis. Herein, we propose that BAPT catalysis is stimulated by Mg^{+2} ions by preparing the baccatin III substrate for nucleophilic attack by liberating the C13-OH from its intramolecular H-bond neighbor. Accelerated molecular dynamics analysis suggests that the divalent metal cofactor interrupts the intramolecular H-bonding but also serves also organizes the acids active site residues (Figure 4.3B). To test this hypothesis, we used phenylisoserine CoA native substrate and isobutenylisoerine nonnative substrate to couple with taxane analogs by BAPT

catalysis (Figure 4.4).

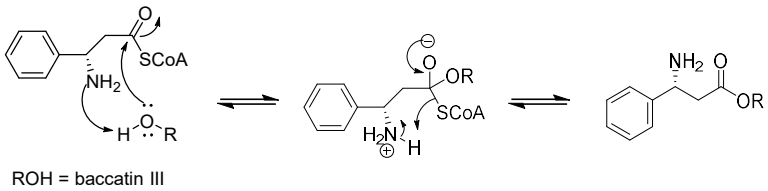

Figure 4.2: Previous substrate-assisted mechanism for BAPT catalysis.

A

B

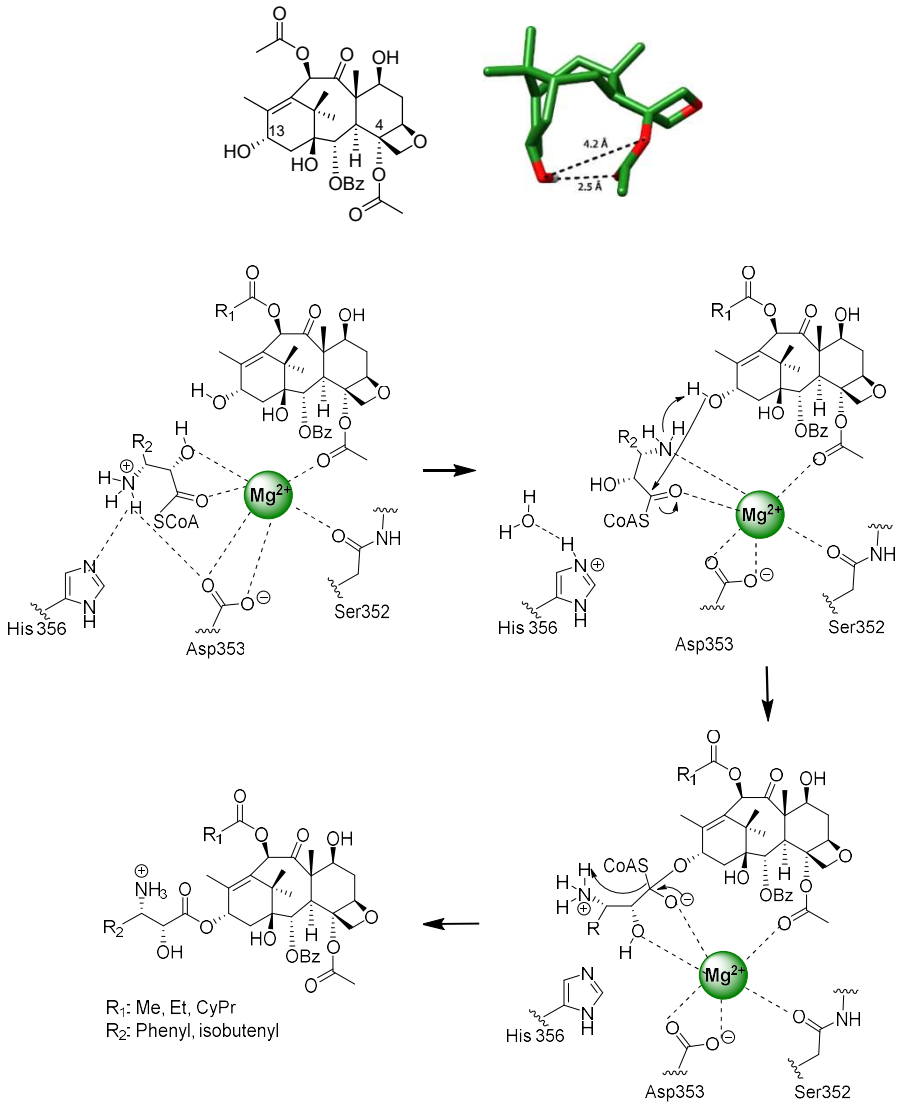

Figure 4.3: Proposed BAPT mechanism catalysis. (A) baccatin III structure and (B) the role of Mg ions as cofactor in BAPT catalysis.

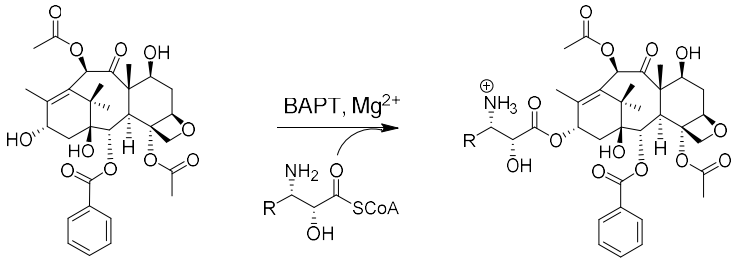

Figure 4.4: Testing the role of Mg^{2+} in the BAPT catalysis.

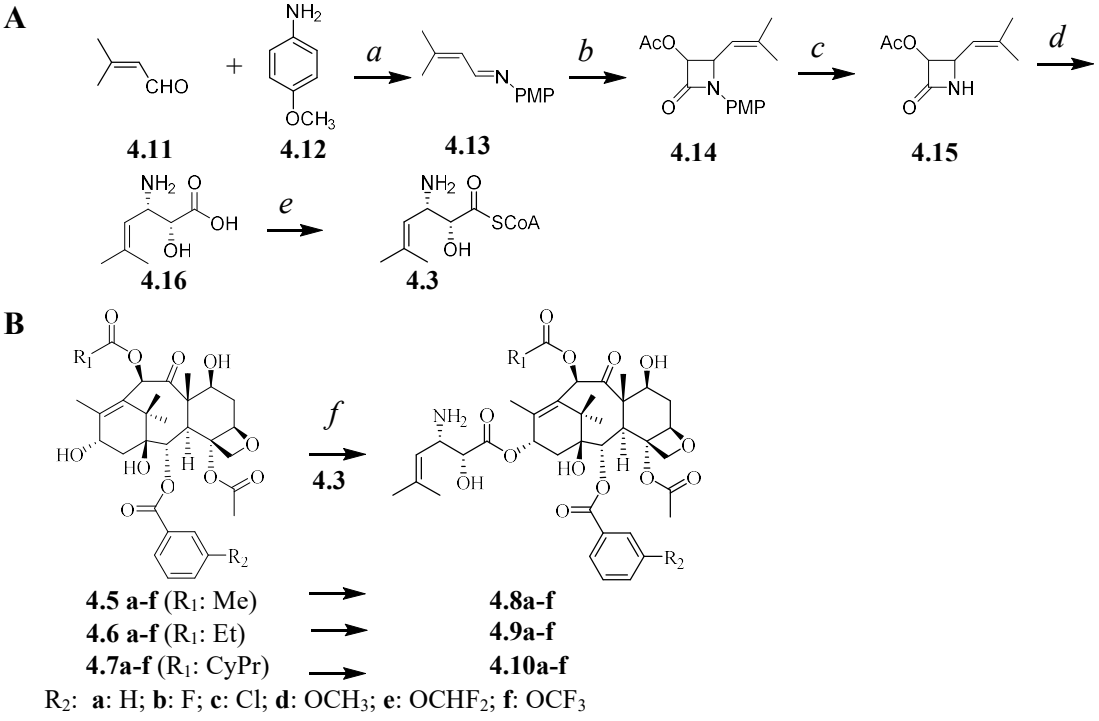

Figure 4.5: (A) proposed semi-biocatalysis of (2*R*, 3*S*)-isobutenylisoserinyl CoA. (B) proposed biocatalysis coupling between isosernyl CoA and taxane analogs. *Reagent and conditions*: (a) CH_2Cl_2, r.t., 8 h; (b) acetoxyacetyl chloride, TEA, CH_2Cl_2, 0 °C; 6 h; (c) CAN, CH_3CN, H_2O, 0 °C-r.t., 8 h; (d) immobilized CAL-B, H_2O, iPr_2O, r.t.; (e) PheAT, CoA, ATP, $MgCl_2$•($6H_2O$); (f) BAPT, $MgCl_2$•($6H_2O$).

We believe that understanding the role of Mg^{2+} ion in the *Taxus* BAPT acyltransferase catalysis in greater detail is vital not only to produce the next-generation paclitaxel analogs (Figure 4.5) but also to add another information of understanding and may help to repropose the mechanism of the BAHD acytransferase members.

Experimental

Chemicals and Reagents

3-methylbut-2-enal (97%), *p*-Anisidine (99%), and Acetoxy acetyl chloride (97%), *tert*-butanol (≥99%) were purchased from Sigma Aldrich (St. Louis, MO). Ceric Ammonium Nitrate (99%) was purchased from Fisher Scientific Company (Fair Lawn, New Jersey). Coenzyme A (95%) was obtained from AmBeed (Arlington Hts, IL). Nickel-affinity chromatography resin (HisPur™ Ni-NTA Resin) was purchased from Thermo Fisher Scientific (Waltham, MA). ATP, DTT, Isopropyl β-D-1-thiogalactopyranoside (IPTG), kanamycin, and phenylmethylsulfonyl fluoride (PMSF) were purchased from Gold Bio (St. Louis, MO). Immobilized CAL-B (lipase B from Candida antarctica) on the acrylic resin (L4777) was purchased from Sigma Aldrich (St. Louis, MO). Taxanes (baccatin III (>98%) and 10-deacetyl baccatin III (>98%) were purchased from Natland International Corporation (Research Triangle Park, NC). Additional reagents: TEA (100%) (J. T. Baker, Center Valley, PA), methanol (>99.5%), hexane (>99.5%), and ethyl acetate (> 99.5%), Diisopropyl ether (≥98.5%) were sourced from Sigma Aldrich, St. Louis, MO. C18 silica gel resin (carbon 23%, 40-63 μm) was purchased from Silicycle, Quebec City, Quebec, Canada.

Synthesis of *N*-(*p*-methoxy phenyl)-3-acetoxy-4-(2-methyl-1-propen-1-yl) azetidin-2-one (4.14)

In a 25 mL single-necked round-bottomed flask, 3-methylbut-2-enal (**4.11**) (0.4 g, 4.8 mmol, 1 equiv) and *p*-methoxyaniline (**4.12**) (1.48 g, 12 mmol, 2.5 equiv) was added and dissolved in 15

mL dichloromethane. Oven-dried molecular sieves (~1.5 g) were added to remove water formed during the reaction. The reaction was stirred at room temperature for 16 h. The molecular sieves were removed by filtration, and the filtrate was transferred to a clean, oven-dried round-bottomed flask, which was then sealed using a rubber septum. To this crude imine mixture, triethylamine was added (2.1 mL, 14.4 mmol, 3 equiv) and stirred at 0 °C. Acetoxyacetyl chloride (1 mL, 9.3 mmol, 2 equiv) was separately dissolved in dichloromethane, and the solution was added slowly to the reaction mixture. The reaction was stirred at 0 °C for an additional 5 min, then warmed up to room temperature and stirred for 5 h. The solution was washed successively with 5% (w/v) $NaHCO_3$ (15 mL), 5% v/v HCl (15 mL), and water (3 × 15 mL). The organic fraction was dried ($MgSO_4$) and concentrated under a vacuum. The crude mixture was purified by silica gel column chromatography (1:4 EtOAc/hexane, *v*/*v*) to yield a pure product as determined by NMR.

NMR Data for N-(p-methoxy phenyl)-3-acetoxy-4-(2-methyl-1-propen-1-yl) azetidin-2-one (4.14) (350 mg, 87% yield), ^{1}H NMR (500 MHz, $CDCl_3$) δ: 7.28 (d, J = 5.4 Hz, 2H), 6.82 (d, J = 5.1 Hz 2H), 5.71 (d, J = 4.9 Hz, 1H), 5.06 (d, J = 4.2 Hz, 1H), 4.88 (dd, J = 9.4, 9.1 Hz, 1H), 3.70 (s, 3H), 2.05 (s, 3H), 1.75 (s, 3H), 1.72 (s. 3H) (Figure 4.12). ^{13}C NMR (126 MHz, $CDCl_3$) δ: 169.35, 161.22, 156.36, 141.95, 130.65, 118.42, 117.49, 114.01, 75.94, 56.35, 55.04, 25.78, 20.37, 18.35 (Figure 4.13).

Synthesis of 3-acetoxy-4-(2-methyl-1-propen-1-yl) azetidine-2-one (4.15)

In a 50 mL single-necked round-bottomed flask, *N*-(*p*-methoxy phenyl)-3-acetoxy-4-(2-methyl-1-propen-1-yl) azetidine-2-one (4.14) (0.25 g, 0.86 mmol, 1 equiv) was added and dissolved in 14 mL CH_3CN and solution was cool down at 0 °C for 10 min. Ceric ammonium nitrate [$(NH4)_2Ce(NO_3)_6$)] (2.58 g, 1.41 mmol, 3 equiv), dissolved in 16 mL water, was added dropwise to the solution. The mixture was stirred at 0 °C until the starting material disappeared by TLC analysis and then diluted with water (20 mL). The mixture was then extracted with EtOAc (3

× 20 mL). The organic layer was washed with 5% (*w*/*v*) $NaHCO_3$ (15 mL), and the aqueous extracts were washed with EtOAc (20 mL). The combined organic extracts were washed sequentially with 10% (*w*/*v*) Na_2SO_3 (15 mL), 5% (*w*/*v*) $NaHCO_3$ (15 mL), and brine (15 mL). The combined extracts were dried over $MgSO_4$ and concentrated under a vacuum. The mixture was purified by silica gel column chromatography (1:3 EtOAc/ hexane, *v*/*v*) to yield a pure product as determined by NMR.

NMR Data for 3-acetoxy-4-(2-methyl-1-propen-1-yl) azetidine-2-one (4.15) (210 mg, 84% yield), ^{1}H NMR (500 MHz, $CDCl_3$) δ: 5.65 (d, *J* = 4.7 Hz, 1H), 5.06 (d, *J* = 4.5 Hz, 1H,), 4.56 (dd, *J* = 9.1, 9.2 Hz, 1H), 2.11 (s, 3H), 1.69 (s, 3H), 1.61 (s. 3H) (Figure 4.14). ^{13}C NMR (126 MHz, $CDCl_3$) δ: 169.46, 166.36, 141.43, 118.88, 77.68, 52.49, 25.91, 18.26, 17.54 (Figure 4.15).

Biosynthesis of (2*R*,3*S*)-3-amino-2-hydroxy-5-methylhex-4-enoic acid (4.16)

In a 50 mL single-necked round-bottomed flask, 3-acetoxy-4-(2-methyl-1-propen-1-yl) azetidine-2-one (**4.16**) (100 mg, 0.55 mmol) was added and dissolved in 30 mL diisopropyl ether. Immobilized CAL-B (1.5 g, 50 mg /mL), and H_2O (2 mL) were added, and the mixture was stirred at 60 °C for 72 h. The precipitated reaction was filtered to remove the enzyme and the filtrate was washed with water (3 × 15 mL). The water layers were collected, flash-frozen in liquid nitrogen, and lyophilized. The residue was dissolved in acetonitrile (100 μL), and an aliquot was analyzed by LC/ESI-MS to assess the production of the (2*R*,3*S*)-3-amino-2-hydroxy-5-methylhex-4-enoic acid (**4.16**) (Figure 4.18). The resultant crude residue was loaded onto a C18 reverse phase silica gel (SiliCycle, Quebec City, Canada) column (diameter: 1.2 mm, height: 32 cm) and eluted with 10% acetonitrile in water. The fractions containing the product were collected, flash-frozen, and lyophilized to yield a pure product as determined by NMR.

NMR Data for (2*R*,3*S*)-3-amino-2-hydroxy-5-methylhex-4-enoic acid (**4.16**) (47 mg, 45% yield), ^{1}H NMR (500 MHz, $CDCl_3$) δ: 5.43 (d, *J* = 4.7 Hz, 1H), 5.11 (d, *J* = 4.8, 1H), 4.56 (dd, *J*

= 4.7, 4.6 Hz, 1H), 1.78 (s, 3H), 1.69 (s, 3H) (Figure 4.16). ^{13}C NMR (126 MHz, $CDCl_3$) δ: 169.46, 137.36, 129.48, 75.88, 77.68, 47.12, 22.91, 18.56, 17.14 (Figure 4.17). LC/ESI-MS monoisotopic exact mass m/z 160.0928 $[M + H]^+$; calculated for $C_7H_{14}NO_3$: 160.0973.

Expression and Purification of the PheAT Enzyme

A glycerol stock of *E. coli* BL21 (DE3) engineered with KDW- pET28a-phe-at plasmid encoding the *pheat* gene for expression of the PheAT enzyme was used to inoculate 250 mL of Lysogeny Broth (LB) containing kanamycin (50 μg/ mL). The seed culture was incubated at 37 °C overnight, and 25 mL of the inoculum cultures were added to each of ten 1-L LB media containing kanamycin (50 μg/mL). The cells were incubated at 37 °C until OD_{600} = 0.6, then IPTG (250 μM final concentration) was added, and the strains were incubated at 16 °C. After 16 h, the cultures were centrifuged (2100*g*) for 1 h at 4 °C to pellet the cells. The cells were resuspended in 100 mL of lysis buffer (50 mM sodium phosphate (pH 8.0), 300 mM NaCl, 10 mM imidazole, and 5% (v/v) glycerol,) and lysed by sonication (Misonix Sonicator; Danbury, CT): 10 s on, 20 s rest for 30 cycles) on ice. The cell debris was removed by centrifugation (1500*g*) for 45 min at 4 °C followed by high-speed centrifugation (25000*g*) for 90 min at 2 °C to remove light membrane debris. The supernatant was loaded onto a column containing 3 mL of nickel-nitrilotriacetic acid (Ni-NTA) resin and eluted by gravity flow. The column was washed with 50 mL of Wash 1 Buffer (300 mM NaCl, 50 mM sodium phosphate (pH 8.0), 10 mM imidazole, and 5% (v/v) glycerol) and 20 mL of Wash 2 Buffer (300 mM NaCl, 50 mM sodium phosphate (pH 8.0), 50 mM imidazole, and 5% (v/v) glycerol). Protein was eluted with Elution Buffer (300 mM NaCl, 50 mM sodium phosphate (pH 8.0), 250 mM Imidazole, and 5% (v/v) glycerol). Each eluted fraction was analyzed by SDS-PAGE to establish the presence and purity of the protein. Fractions containing enzymes of molecular weight similar to that of PheAT (~70 kDa) were combined and loaded onto a size-selective centrifugal filtration unit (30 000 NMWL, Millipore Sigma, Burlington, MA). The

quantity of PheAT (12 mg) was measured using a Nanodrop spectrophotometer, and the purity was assessed by SDS-PAGE with Coomassie Blue staining (Figure 4.11).

Screening PheAT Activity with (2*R*,3*S*)-3-amino-2-hydroxy-5-methylhex-4-enoic acid and CoA (4.16)

A solution of (2*R*,3*S*)-3-amino-2-hydroxy-5-methylhex-4-enoic acid (**4.16**) (1 mM) in 50 mM NaH_2PO_4/Na_2HPO_4 buffer (pH 8) (1 mL) was incubated with purified PheAT (25 μg/mL). CoA (1mM), ATP (1mM), and $MgCl_2•(6H_2O)$ (5 mg) were added to the solution, and the assay mixture was incubated at 31 °C on a rocking shaker for 4 h. The reaction was stopped by the addition of 8.8% formic acid to pH 4 to precipitate PheAT. The precipitated reaction was centrifuged at 5000g for 10 min. The supernatant was collected, and the pellet was washed with water (pH 4 with formic acid) and centrifuged. Supernatants were combined and filtered through a Millipore Amicon Ultra 30 kDa concentrator to remove trace protein. The flow-through was collected, flash-frozen in liquid nitrogen, and lyophilized. The residue was dissolved in acetonitrile (100 μL), and an aliquot was analyzed by LC/ESI-MS to assess the production of the (2*R*,3*S*)-3-amino-2-hydroxy-5-methylhex-4-enoyl CoA (**4.3**) (Figure 4.19).

Kinetics Evaluation of PheAT catalysis with the (2*R*,3*S*)-3-amino-2-hydroxy-5-methylhex-4-enoic acid (4.16)

The steady-state conditions for protein concentration and time were established for PheAT and (2*R*,3*S*)-3-amino-2-hydroxy-5-methylhex-4-enoic acid (**4.16**) separately incubated at low (0.05 mM) and high (1 mM) concentrations in 10 mL of assay buffer [50 mM NaH_2PO_4/Na_2HPO_4 buffer (pH 8) containing PheAT (150 μg/mL) and CoA (1 mM), ATP (1 mM), and $MgCl_2•(6H_2O)$ (100 mg) at 31 °C on a rocking shaker. Aliquots (1 mL) were removed, and the biosynthetic reaction was stopped by the addition of addition of 8.8% formic acid at 10, 15, 30, and 45 min and at 1, 2, 3, 5, 7, and 10 h. (2*R*,3*S*)-phenylisoserinyl CoA (0.15 mM) was added as the internal standard to correct the loss of analyte during the isolation of the product. Each sample was flash-frozen in

liquid nitrogen and lyophilized. The resultant residue from each assay was separately resuspended in acetonitrile (100 µL) and quantified by LC/ESI-MS/MS. A stop time was established for the steady-state time range, and PheAT (150 µg/mL) and CoA (1 mM), ATP (1 mM), and $MgCl_2$•($6H_2O$) (100 mg) were incubated with varying concentrations of (2*R*,3*S*)-3-amino-2-hydroxy-5-methylhex-4-enoic acid (**4.16**) (0.05 – 1 mM), respectively, in triplicate assays at 31 °C on a rocking shaker for 3 h. As described above, assay products were extracted from the reaction mixture and quantified by LC/ESI-MS/MS. The kinetic parameters (K_M and k_{cat}) were calculated by nonlinear regression with Origin Pro 9.0 software (Northampton, MA) using the Michaelis−Menten equation: $v_0 = k_{cat}[E_0][S]/(K_M + [S])$ (Figure 4.22).

Scale-Up the production of (2*R*,3*S*)-3-amino-2-hydroxy-5-methylhex-4-enoyl CoA (4.3)

A large-scale preparative PheAT enzymatic assay was carried out by adding a concentrated solution of PheAT (20 mL of 360 µg/mL) in 50 mM NaH_2PO_4/Na_2HPO_4 (pH 8) (10 test tubes, 2 mL assay in each tube). (2*R*,3*S*)-3-amino-2-hydroxy-5-methylhex-4-enoic acid (**4.16**) (0.31 mmol, 50 mg), $MgCl_2$•($6H_2O$) (20 mg) were dissolved in the PheAT solution. Separately, ATP (0.31 mmol) and CoA (0.31 mmol) were dissolved in 1 mL each of 50 mM phosphate buffer (pH 8). The ATP and CoA solutions were then added to the PheAT solution, and the mixture was incubated for 4 h at 31 °C on a rocking shaker. A second batch of PheAT enzyme (360 µg/mL) was added to each assay tube and incubated for another 4 h at 31 °C. The reaction was stopped by the addition of 8.8% formic acid to pH 4 to precipitate PheAT. The precipitated reaction was centrifuged at 5000g for 10 min. The supernatant was collected, and the pellet was washed with water (pH 4 with formic acid) and centrifuged. Supernatants were combined and filtered through a Millipore Amicon Ultra 30 kDa concentrator to remove trace protein. The flow-through was collected, flash-frozen in liquid nitrogen, and lyophilized. The lyophilized crude product was then dissolved in 2 mL of ultrapure water (pH 4), for preparative HPLC purification.

Purification of (2*R*,3*S*)-3-amino-2-hydroxy-5-methylhex-4-enoyl CoA (4.3)

100 µL of the filtered, lyophilized (2*R*,3*S*)-3-amino-2-hydroxy-5-methylhex-4-enoyl CoA crude mixture was loaded onto a preparative C18 column (Atlantis C18 OBD, 5 µm, 19 mm × 150 mm). The column was eluted at 5 mL/min with 5% solvent B (100% acetonitrile) and 95% solvent A (0.1% trifluoroacetic acid in water) with a 5 min hold, a linear gradient to 30% solvent B over 15 min, then increased to 100% solvent B over 4 min, and finally lowered to 5% solvent B over 5 min. Peak fractions were collected, flash-frozen, and lyophilized to yield a pure product as determined by NMR (Figures 4.20 and 4.21). The purified residue was dissolved in acetonitrile (100 µL), and an aliquot was analyzed by LC-MS/MS for fragmentation analysis and monoisotopic mass calculation (Figure 4.24).

NMR Data for (2*R*,3*S*)-3-amino-2-hydroxy-5-methylhex-4-enoyl CoA (4.3) (23 mg, 46% yield), ^{1}H NMR (500 MHz, $CDCl_3$) δ: 8.39 (s, 1H), 8.11 (s, 1H), 6.04 (d, *J* = 6.2 Hz, 1H), 5.12 (d, *J* = 4.5 Hz, 1H), 4.83 (d, *J* = 4.6, 1H), 4.72 (m, 1H), 4.68 (d, *J* = 5.9 Hz, 1H), 4.47 (t, *J* = 2.7 Hz, 1H), 4.21 (dd, *J* = 4.7, 4.6 Hz, 1H), 4.11 (m, 2H), 3.84 (s, 1H), 3.73 (dd, J = 4.8, 4.6 Hz, 1H), 3.38 (dd, *J* = 4.8, 4.5 Hz, 1H), 3.31 (t, *J* = 6.6 Hz, 2H), 3.17 (t, *J* = 6.6 Hz, 2H), 2.46 (t, *J* = 6.6 Hz, 2H), 2.34 (t, *J* = 6.6 Hz, 2H), 1.82 (s, 3H), 1.69 (s, 3H), 0.86 (s, 6H) (Figure 4.20). ^{13}C NMR (126 MHz, $CDCl_3$) δ: 198.5, 178.9, 178.6, 152.1, 147.8, 147.6, 141.2, 138.11, 127.84, 117.83, 96.12, 87.52, 81.62. 75.36, 73.45, 64.82, 48.21, 41.23, 37.64, 34.72, 29.95, 21.65, 18.52, 16.42 (Figure 4.21). LC/ESI-MS monoisotopic exact mass m/z 907.1842 $[M - H]^{-1}$; calculated for $C_{28}H_{46}N_8O_{18}P_3S$: 907.1864.

Expression and Purification of the BAPT Enzyme

A glycerol stock of *E. coli* BL21(DE3) engineered to express the BAPT enzyme from the *bapt*-pET28a-*bapt* plasmid containing the *bapt* gene was used to inoculate Lysogeny Broth (LB) (400 mL) containing kanamycin (50 µg/mL) and incubated at 37 °C overnight. This inoculum culture

(50 mL) was added to fresh LB media (8 × 1 L) containing kanamycin (50 μg/mL). The cells were incubated at 37 °C until $OD_{600} \approx 0.6$, IPTG (250 μM final concentration) was added, and the strains were incubated at 16 °C for 16 h. The cultures were centrifuged (2,100*g*) for 1 h at 4 °C to pellet the cells. The cells were resuspended in 100 mL of lysis buffer (50 mM sodium phosphate (pH 8.0), 300 mM NaCl, 10 mM imidazole, and 5% (v/v) glycerol,) and lysed by sonication (Misonix Sonicator (Danbury, CT): 10 s on, 20 s rest for 30 cycles) on ice. The cell debris was removed by centrifugation (1,500*g*) for 45 min at 4 °C, followed by high-speed centrifugation (25,000*g*) for 90 min at 2 °C to remove light membrane debris. The supernatant was loaded onto a column containing nickel-nitrilotriacetic acid (Ni-NTA) resin (3 mL) and eluted by gravity flow. The column was washed with 50 mL of Wash 1 Buffer (300 mM NaCl, 50 mM sodium phosphate (pH 8.0), 10 mM imidazole, and 5% (v/v) glycerol) and 20 mL of Wash 2 Buffer (300 mM NaCl, 50 mM sodium phosphate (pH 8.0), 50 mM imidazole, and 5% (v/v) glycerol). Protein was eluted with Elution Buffer (300 mM NaCl, 50 mM sodium phosphate (pH 8.0), 250 mM imidazole, and 5% (v/v) glycerol). Fractions containing enzymes of a molecular weight consistent with that of BAPT (~51 kDa) were combined and loaded onto a size-selective centrifugal filtration unit (30,000 NMWL, Millipore-Sigma, Burlington, MA). The quantity of BAPT (8 mg) was measured using a NanoDrop spectrophotometer, and the purity of the enzyme was assessed by SDS-PAGE and Coomassie Blue staining (Figure 4.23).

Screening BAPT Activity with Isoserinyl CoA analogs and Baccatin III

A solution of baccatin III (**4.1**) (1mM), purified BAPT (25 μg/mL), synthetic (2*R*,3*S*)-phenylisoserinyl CoA (**4.2**) (see structure, Figure 4.9) (1mM), bio-synthetic (2*R*,3*S*)-3-amino-2-hydroxy-5-methylhex-4-enoyl CoA (**4.3**) in 50 mM NaH_2PO_4/Na_2HPO_4 buffer (pH 7.4) (1 mL) were incubated separately with $MgCl_2.(6H_2O)$ (4 mg), and without the addition of $MgCl_2.(6H_2O)$. The assays were mixed at 31 °C on a rocking shaker for 4 h. The reaction was then stopped with

ethyl acetate (3 × 1 mL). The EtOAc extracts were combined, and the solvent was removed under a stream of nitrogen gas. The residue was dissolved in acetonitrile (100 µL), and an aliquot was analyzed by LC/ESI-MS to assess the production of the 3′-*N*-debenzoyl-paclitaxel (Figure 4.25), and 3′-*N*-de(*tert*-butoxycarbonyl)-SB-T-1212 (Figure 4.26).

Kinetics Evaluation of BAPT catalysis with (2*R*,3*S*)-3-amino-2-hydroxy-5-methylhex-4-enoyl CoA (4.3) and taxanes ((4.5, 4.6, and 4.7)(a-f))

The steady-state conditions for protein concentration and time were established for BAPT and (2*R*,3*S*)-3-amino-2-hydroxy-5-methylhex-4-enoyl CoA (**4.3**) separately incubated at low (0.05 mM) and high (1 mM) concentrations in 10 mL of assay buffer [50 mM NaH_2PO_4/Na_2HPO_4 buffer (pH 8)] containing BAPT (250 µg/mL), taxane analogs (**4.5**, **4.6**, and **4.7**) (1 mM), and $MgCl_2.(6H_2O)$ (40 mg) at 31 °C on a rocking shaker. Aliquots (1 mL) were removed, and the biosynthetic reaction was stopped by adding 500 µL of EtOAc at 10, 15, 30, and 45 min and 1, 2, 3, 5, 7, and 10 h. Docetaxel (**4.17**) (see structure, Figure 4.10) (0.15 mM) was added as the internal standard to correct the loss of analyte during the isolation of the product. Each sample was extracted with EtOAc (4 × 1 mL), the organic fractions were combined, and the solvent was removed under a stream of nitrogen. The resultant residue from each assay was separately resuspended in acetonitrile (100 µL) and quantified by LC/ESI-MS/MS.A stop time was established for the steady-state time range, and BAPT (250 µg/mL), taxane analogs (1 mM), and $MgCl_2$•$(6H_2O)$ (40 mg) were incubated with varying concentrations of (2*R*,3*S*)-3-amino-2-hydroxy-5-methylhex-4-enoyl CoA (**4.3**) (0.05 – 1 mM), respectively, in triplicate assays at 31 °C on a rocking shaker for 2 h. As described above, assay products were extracted from the reaction mixture and quantified by LC/ESI-MS/MS. The kinetic parameters (K_M and k_{cat}) were calculated by nonlinear regression with Origin Pro 9.0 software (Northampton, MA) using the Michaelis−Menten equation: $v_0 = k_{cat}[E_0][S]/(K_M + [S])$ (Figure 4.63-4.65).

Scale-Up the production of 3´-*N*-de(*tert*-butoxycarbonyl)-SB-T-12 analogs ((4.8, 4.9, and 4.10)(a-f))

A concentrated solution of BAPT (30 mL of 250 µg/mL) was incubated in 50 mM NaH_2PO_4/Na_2HPO_4 assay buffer (pH 7.4) (15 test tubes, 2 mL assay in each tube) containing (2 mM) of taxane analogs ((**4.5**, **4.6**, and **4.7**)(**a-f**)) and (2 mM) of (2*R*,3*S*)-3-amino-2-hydroxy-5-methylhex-4-enoyl CoA (**4.3**), and $MgCl_2.(6H_2O)$ (80 mg) at 31 °C on a rocking shaker for 4 h. A second batch of BAPT enzyme (250 µg/mL) was added to each assay tube and incubated for another 4 h at 31 °C. The reaction was then stopped with ethyl acetate (2 × 3 mL) to extract the taxane substrates from the assay. The EtOAc extracts were combined, and the solvent was removed under a stream of nitrogen and the residue was purified by silica gel column chromatography to yield a pure product, as determined by NMR (Figure 4.27-4.62). The purified residue was dissolved in acetonitrile (100 µL), and an aliquot was analyzed by LC-MS/MS for fragmentation analysis and monoisotopic mass calculation.

NMR Data for 3´-*N*-de(*tert*-butoxycarbonyl)-SB-T-1212 (4.8a) (18 mg, 42% yield), ^{1}H NMR (500 MHz, $CDCl_3$) δ: 8.10 (d, *J* = 8.4 Hz, 2H), 7.61 (dd, *J* = 7.4, 7.3 Hz, 1H), 7.46 (dd, *J* = 8.4, 7.5 Hz, 2H), 6.32 (s, 1H), 6.19 (t, *J* = 8.7 Hz, 1H), 5.61 (d, *J* = 7.1 Hz, 1H), 5.43 (d, *J* = 4.5 Hz, 1H), 5.11 (d, *J* = 4.7, 1H), 4.98 (d, *J* = 9.7, 1H), 4.62 (dd, *J* = 4.7, 4.5 Hz, 1H), 4.46 (dd , *J* = 9, 9 Hz, 1H), 4.30 (d, *J* = 9 Hz, 1H), 4.15 (d, *J* = 9 Hz, 1H), 3.85 (d, *J* = 7.1 Hz, 1H), 2.55 (m, 1H), 2.32 (q, *J* = 7.6 Hz, 2H), 2.28 (s, 3H), 2.24, (s, 3H), 2.11 (s, 3H), 2.06 (s, 3H), 1.87 (m, 1H), 1.76 (s, 3H), 1.66 (s, 3H), 1.13 (s, 6H) (Figure 4.27). ^{13}C NMR (126 MHz, $CDCl_3$) δ: 204.18, 171.36, 170.66, 167.14, 165.78, 146.46, 140.82, 133.69, 131.75, 130.12, 129.31, 128.63, 118.76, 84.43, 80.73, 79.07, 77.81, 77.12, 76.23, 74.89, 72.32, 67.92, 58.68, 52.54, 46.12, 42.69, 38.57, 35.59, 26.95, 26.01, 22.59, 20.92, 18.24, 15.62, 8.43 (Figure 4.28). LC/ESI-MS monoisotopic exact mass m/z 728.3194 $[M + H]^+$; calculated for $C_{38}H_{50}NO_{13}$: 728.3282.

NMR Data for 2-debenzoyl-2-(3-fluorobenzoyl)-3´-*N*-de(*tert*-butoxycarbonyl)-SB-T-1212 (4.8b) (15 mg, 33% yield), ^{1}H NMR (500 MHz, $CDCl_3$) δ: 8.11 (d, *J* = 7.4 Hz, 1H), 7.86 (s, 1H) 7.75 (d, *J* = 7.0 Hz, 1H), 7.49 (dd, *J* = 8.4, 7.5 Hz, 1H), 6.32 (s, 1H), 6.19 (t, *J* = 8.5 Hz, 1H), 5.62 (d, *J* = 7.1 Hz, 1H), 5.42 (d, *J* = 4.5 Hz, 1H), 5.13 (d, *J* = 4.6 Hz, 1H), 4.98 (d, *J* = 9.7 Hz, 1H), 4.64 (dd, *J* = 4.7, 4.5 Hz, 1H), 4.47 (dd, *J* = 9, 9Hz, 1H), 4.30 (d, *J* = 9 Hz, 1H), 4.14 (d, *J* = 9 Hz, 1H), 3.89 (d, *J* = 7.1 Hz, 1H), 2.56 (m, 1H), 2.31 (q, *J* = 7.6 Hz, 2H), 2.29 (s, 3H), 2.25, (s, 3H), 2.11 (s, 3H), 2.05 (s, 3H), 1.87 (m, 1H), 1.76 (s, 3H), 1.67 (s, 3H), 1.11 (s, 6H) (Figure 4.29). ^{13}C NMR (126 MHz, $CDCl_3$) δ: 204.17, 171.38, 170.73, 168.08, 163.52, 146.44, 140.91, 133.71, 130.19, 129.28, 128.64, 125.91, 120.87, 118.67, 84.47, 80.76, 79.09, 77.73, 77.16, 76.24, 74.91, 72.32, 67.92, 58.68, 52.69, 46.13, 42.68, 38.55, 35.57, 26.96, 26.08, 22.64, 20.94, 18.25, 15.64, 8.46 (Figure 4.30). LC/ESI-MS monoisotopic exact mass *m/z* 746.3094 $[M + H]^+$; calculated for $C_{38}H_{49}FNO_{13}$: 746.3187.

NMR Data for 2-debenzoyl-2-(3-chlorobenzoyl)-3´-*N*-de(*tert*-butoxycarbonyl)-SB-T-1212 (4.8c) (12 mg, 27% yield), ^{1}H NMR (500 MHz, $CDCl_3$) δ: 8.12 (s, 1H), 7.89 (d, *J* = 7.4 Hz, 1H), 7.77 (d, *J* = 7.2 Hz, 1H), 7.49 (dd, *J* = 8.5, 7.4 Hz, 1H), 6.32 (s, 1H), 6.19 (t, *J* = 8.5 Hz, 1H), 5.62 (d, *J* = 7.1 Hz, 1H), 5.42 (d, *J* = 4.5 Hz, 1H), 5.13 (d, *J* = 4.6 Hz, 1H), 4.98 (d, *J* = 9.7 Hz, 1H), 4.64 (dd, *J* = 4.7, 4.5 Hz, 1H), 4.47 (dd, *J* = 9, 9Hz, 1H), 4.30 (d, *J* = 9 Hz, 1H), 4.14 (d, *J* = 9 Hz, 1H), 3.89 (d, *J* = 7.1 Hz, 1H), 2.56 (m, 1H), 2.31 (q, *J* = 7.6 Hz, 2H), 2.29 (s, 3H), 2.25, (s, 3H), 2.11 (s, 3H), 2.05 (s, 3H), 1.87 (m, 1H), 1.76 (s, 3H), 1.67 (s, 3H), 1.11 (s, 6H) (Figure 4.31). ^{13}C NMR (126 MHz, $CDCl_3$) δ: 204.15, 171.35, 170.72, 168.09, 165.12, 146.43, 140.91, 135.12, 134.28, 131.62, 130.28, 129.82, 129.76, 127.65, 126.84, 84.47, 80.76, 79.09, 77.73, 77.16, 76.24, 74.91, 72.32, 71.92, 58.68, 53.69, 46.13, 42.68, 39.55, 35.57, 26.96, 24.08, 21.64, 20.94, 17.25, 15.64, 8.44 (Figure 4.32). LC/ESI-MS monoisotopic exact mass *m/z* 762.2786 $[M + H]^+$; calculated for $C_{38}H_{49}FNO_{13}$: 762.2892.

NMR Data for 2-debenzoyl-2-(3-methoxybenzoyl)-3´-*N*-de(*tert*-butoxycarbonyl)-SB-T-1212 (4.8d) (6 mg, 13% yield), ^{1}H NMR (500 MHz, $CDCl_3$) δ: 8.09 (d, *J* = 7.4 Hz, 1H), 7.67 (s, 1H) 7.59 (d, *J* = 7.0 Hz, 1H), 7.47 (dd, *J* = 8.4, 7.5 Hz, 1H), 6.32 (s, 1H), 6.19 (t, *J* = 8.5 Hz, 1H), 5.62 (d, *J* = 7.1 Hz, 1H), 5.42 (d, *J* = 4.5 Hz, 1H), 5.13 (d, *J* = 4.6 Hz, 1H), 4.98 (d, *J* = 9.7 Hz, 1H), 4.64 (dd, *J* = 4.7, 4.5 Hz, 1H), 4.47 (dd, *J* = 9, 9Hz, 1H), 4.30 (d, *J* = 9 Hz, 1H), 4.14 (d, *J* = 9 Hz, 1H), 3.89 (d, *J* = 7.1 Hz, 1H), 3.86 (s, 3H), 2.56 (m, 1H), 2.31 (q, *J* = 7.6 Hz, 2H), 2.29 (s, 3H), 2.25, (s, 3H), 2.11 (s, 3H), 2.05 (s, 3H), 1.87 (m, 1H), 1.76 (s, 3H), 1.67 (s, 3H), 1.11 (s, 6H) (Figure 4.33). ^{13}C NMR (126 MHz, $CDCl_3$) δ: 203.42, 171.35, 170.71, 168.16, 165.14, 158.62, 146.47, 140.93, 131.62, 130.42, 129.76, 128.64, 121.57, 117.84, 114. 63, 84.47, 80.76, 79.09, 77.73, 77.16, 76.24, 74.91, 72.32, 71.92, 58.68, 55.8, 53.69, 46.13, 42.68, 39.55, 35.57, 26.96, 24.08, 21.64, 20.94, 17.25, 15.64, 8.44 (Figure 4.34).LC/ESI-MS monoisotopic exact mass *m/z* 758.3293 $[M + H]^+$; calculated for $C_{39}H_{52}NO_{14}$: 758.3387.

NMR Data for 2-debenzoyl-2-(3-difluoromethoxybenzoyl)-3´-*N*-de(*tert*-butoxycarbonyl)-SB-T-1212 (4.8e) (14 mg, 30% yield), ^{1}H NMR (500 MHz, $CDCl_3$) δ: 8.12 (d, *J* = 7.4 Hz, 1H), 7.85 (s, 1H), 7.71 (d, *J* = 7.1Hz, 1H), 7.64 (s, 1H), 7.48 (dd, *J* = 8.4, 7.5 Hz, 1H), 6.32 (s, 1H), 6.19 (t, *J* = 8.5 Hz, 1H), 5.62 (d, *J* = 7.1 Hz, 1H), 5.42 (d, *J* = 4.5 Hz, 1H), 5.13 (d, *J* = 4.6 Hz, 1H), 4.98 (d, *J* = 9.7 Hz, 1H), 4.64 (dd, *J* = 4.7, 4.5 Hz, 1H), 4.47 (dd, *J* = 9, 9Hz, 1H), 4.30 (d, *J* = 9 Hz, 1H), 4.14 (d, *J* = 9 Hz, 1H), 3.89 (d, *J* = 7.1 Hz, 1H), 2.56 (m, 1H), 2.31 (q, *J* = 7.6 Hz, 2H), 2.29 (s, 3H), 2.25, (s, 3H), 2.12 (s, 3H), 2.06 (s, 3H), 1.88 (m, 1H), 1.76 (s, 3H), 1.68 (s, 3H), 1.12 (s, 6H) (Figure 4.35). ^{13}C NMR (126 MHz, $CDCl_3$) δ: 205.28, 171.42, 170.65, 169.32, 167.46, 164.81, 147.35, 141.23, 132.82, 131.36, 129.52, 128.41, 127.91, 118.65, 116.72, 84.47, 80.76, 79.09, 77.73, 77.16, 76.24, 74.91, 72.32, 67.92, 58.68, 52.69, 46.13, 42.68, 38.55, 35.57, 26.96, 26.08, 22.64, 20.94, 18.25, 15.64, 8.47 (Figure 4.36). LC/ESI-MS monoisotopic exact mass *m/z* 794.3096 $[M + H]^+$; calculated for $C_{39}H_{50}F_2NO_{14}$: 794.3199.

NMR Data for 2-debenzoyl-2-(3-trifluoromethoxybenzoyl)-3´-*N*-de(*tert*-butoxycarbonyl)-SB-T-1212 (4.8f) (10 mg, 20% yield), ^{1}H NMR (500 MHz, $CDCl_3$) δ: 8.09 (d, *J* = 7.5 Hz, 1H), 7.87 (s, 1H) 7.68 (d, *J* = 7.2 Hz, 1H), 7.45 (dd, *J* = 8.2, 7.8 Hz, 1H), 6.32 (s, 1H), 6.19 (t, *J* = 8.4 Hz, 1H), 5.63 (d, *J* = 7.1 Hz, 1H), 5.42 (d, *J* = 4.5 Hz, 1H), 5.13 (d, *J* = 4.6 Hz, 1H), 4.98 (d, *J* = 9.7 Hz, 1H), 4.64 (dd, *J* = 4.7, 4.5 Hz, 1H), 4.47 (dd, *J* = 9, 9Hz, 1H), 4.30 (d, *J* = 9 Hz, 1H), 4.14 (d, *J* = 9 Hz, 1H), 3.89 (d, *J* = 7.1 Hz, 1H), 2.56 (m, 1H), 2.31 (q, *J* = 7.6 Hz, 2H), 2.29 (s, 3H), 2.25, (s, 3H), 2.12 (s, 3H), 2.06 (s, 3H), 1.87 (m, 1H), 1.78 (s, 3H), 1.66 (s, 3H), 1.12(s, 6H) (Figure 4.37). ^{13}C NMR (126 MHz, $CDCl_3$) δ: 204.27, 171.31, 170.82, 169.12, 167.35, 165.11, 146.62, 141.11, 132.18, 130.47, 129.12, 127.75, 127.72, 126.36, 121.68, 117.55, 84.47, 80.76, 79.09, 77.73, 77.16, 76.24, 74.91, 72.32, 71.92, 58.68, 53.69, 46.13, 42.68, 39.55, 35.57, 26.96, 24.08, 21.64, 20.94, 17.25, 15.64, 8.44 (Figure 4.38). LC/ESI-MS monoisotopic exact mass *m/z* 812.3085 $[M + H]^+$; calculated for $C_{39}H_{49}F_2NO_{14}$: 812.3105.

NMR Data for 3´-*N*-de(*tert*-butoxycarbonyl)-SB-T-1213 (4.9a) (14 mg, 31% yield), ^{1}H NMR (500 MHz, $CDCl_3$) δ: 8.08 (d, *J* = 8.4 Hz, 2H), 7.62 (dd, *J* = 7.4, 7.3 Hz, 1H), 7.46 (dd, *J* = 8.4, 7.5 Hz, 2H), 6.31 (s, 1H), 6.19 (t, *J* = 8.7 Hz, 1H), 5.61 (d, *J* = 7.1 Hz, 1H), 5.42 (d, *J* = 4.5 Hz, 1H), 5.11 (d, *J* = 4.7, 1H), 4.98 (d, *J* = 9.7, 1H), 4.62 (dd, *J* = 4.7, 4.5 Hz, 1H), 4.46 (dd , *J* = 9, 9 Hz, 1H), 4.30 (d, *J* = 9 Hz, 1H), 4.15 (d, *J* = 9 Hz, 1H), 3.85 (d, *J* = 7.1 Hz, 1H), 2.54 (m, 1H), 2.53 (q, *J* = 8.2 Hz, 2H), 2.30 (q, *J* = 7.6 Hz, 2H), 2.28 (s, 3H), 2.09 (s, 3H), 2.03 (s, 3H), 1.85 (m, 1H), 1.75 (s, 3H), 1.64 (s, 3H), 1.23 (t, *J* = 7.6 Hz, 3H), 1.09 (s, 6H) (Figure 4.39). ^{13}C NMR (126 MHz, $CDCl_3$) δ: 204.28, 174.68, 172.85, 168.23, 166.89, 147.45, 142.78, 134.66, 132.76, 130.98, 129.32, 128.64, 118.76, 84.46, 81.75, 79.65, 77.68, 76.53, 76.14, 74.91, 72.43, 67.85, 58.66, 53.69, 46.26, 42.76, 38.96, 35.62, 26.92, 22.58, 20.73, 18.95, 15.91, 8.45, 8.25 (Figure 4.40). LC/ESI-MS monoisotopic exact mass *m/z* 742.3378 $[M + H]^+$; calculated for $C_{39}H_{52}NO_{13}$: 742.3439.

NMR Data for 2-debenzoyl-2-(3-fluorobenzoyl)-3′-*N*-de(*tert*-butoxycarbonyl)-SB-T-1213 (4.9b) (12 mg, 27% yield), ^{1}H NMR (500 MHz, $CDCl_3$) δ: 8.11 (d, *J* = 7.4 Hz, 1H), 7.86 (s, 1H) 7.75 (d, *J* = 7.0 Hz, 1H), 7.49 (dd, *J* = 8.4, 7.5 Hz, 1H), 6.32 (s, 1H), 6.18 (t, *J* = 8.5 Hz, 1H), 5.62 (d, *J* = 7.1 Hz, 1H), 5.42 (d, *J* = 4.5 Hz, 1H), 5.13 (d, *J* = 4.6 Hz, 1H), 4.98 (d, *J* = 9.7 Hz, 1H), 4.64 (dd, *J* = 4.7, 4.5 Hz, 1H), 4.47 (dd, *J* = 9, 9Hz, 1H), 4.30 (d, *J* = 9 Hz, 1H), 4.14 (d, *J* = 9 Hz, 1H), 3.89 (d, *J* = 7.1 Hz, 1H), 2.56 (m, 1H), 2.54 (q, *J* = 8.2 Hz, 2H), 2.31 (q, *J* = 7.6 Hz, 2H), 2.29 (s, 3H), 2.10 (s, 3H), 2.05 (s, 3H), 1.87 (m, 1H), 1.77 (s, 3H), 1.67 (s, 3H), 1.25 (t, *J* = 7.6 Hz, 3H), 1.11 (s, 6H) (Figure 4.41). ^{13}C NMR (126 MHz, $CDCl_3$) δ: 204.26, 174.71, 171,98, 168.91, 167.25, 163.52, 147.56, 142.92, 134.88, 130.46, 129.96, 128.64, 125.85, 120.78, 118.67, 84.89, 81.78, 79.82, 77.85, 76.92, 76.34, 74.95, 72.46, 67.89, 58.78, 63.92, 46.67, 42.82, 39.14, 35.91, 27.46, 67.89, 58.78, 53.92, 46.67, 42.82, 39.14, 35.91, 27.95, 27.17, 22.92, 20.81, 19.18, 16.21, 8.55, 8.37 (Figure 4.42). LC/ESI-MS monoisotopic exact mass *m/z* 760.3284 $[M + H]^+$; calculated for $C_{39}H_{51}FNO_{13}$: 760.3345.

NMR Data for 2-debenzoyl-2-(3-chlorobenzoyl)-3′-*N*-de(*tert*-butoxycarbonyl)-SB-T-1213 (4.9c) (11 mg, 23% yield), ^{1}H NMR (500 MHz, $CDCl_3$) δ: 8.12 (s, 1H), 7.89 (d, *J* = 7.4 Hz, 1H), 7.77 (d, *J* = 7.2 Hz, 1H), 7.49 (dd, *J* = 8.5, 7.4 Hz, 1H), 6.32 (s, 1H), 6.19 (t, *J* = 8.5 Hz, 1H), 5.62 (d, *J* = 7.1 Hz, 1H), 5.42 (d, *J* = 4.5 Hz, 1H), 5.13 (d, J = 4.6 Hz, 1H), 4.98 (d, *J* = 9.7 Hz, 1H), 4.64 (dd, *J* = 4.7, 4.5 Hz, 1H), 4.47 (dd, *J* = 9, 9Hz, 1H), 4.30 (d, *J* = 9 Hz, 1H), 4.14 (d, *J* = 9 Hz, 1H), 3.89 (d, *J* = 7.1 Hz, 1H), 2.56 (m, 1H), 2.54 (q, *J* = 8.2 Hz, 2H), 2.31 (q, *J* = 7.6 Hz, 2H), 2.29 (s, 3H), 2.10 (s, 3H), 2.05 (s, 3H), 1.87 (m, 1H), 1.77 (s, 3H), 1.67 (s, 3H), 1.25 (t, *J* = 7.6 Hz, 3H), 1.11 (s, 6H) (Figure 4.43). ^{13}C NMR (126 MHz, $CDCl_3$) δ: 205.26, 174.71, 171,98, 168.91, 167.25, 146.43, 140.91, 135.12, 134.28, 131.62, 130.28, 129.82, 129.76, 127.65, 126.84, 84.89, 81.78, 79.82, 77.85, 76.92, 76.34, 74.95, 72.46, 67.89, 58.78, 63.92, 46.67, 42.82, 39.14, 35.91, 27.46, 67.89, 58.78, 53.92, 46.67, 42.82, 39.14, 35.91, 27.95, 27.17, 22.92, 20.81, 19.18, 16.21,

8.55, 8.37 (Figure 4.44). LC/ESI-MS monoisotopic exact mass *m/z* 776.2969 $[M + H]^+$; calculated for $C_{39}H_{51}ClNO_{13}$: 776.3049.

2-debenzoyl-2-(3-methoxybenzoyl)-3´-*N*-de(*tert*-butoxycarbonyl)-SB-T-1213 (4.9d) (4 mg, 9% yield), ^{1}H NMR (500 MHz, $CDCl_3$) δ: 8.08 (d, *J* = 7.4 Hz, 1H), 7.65 (s, 1H) 7.56 (d, *J* = 7.0 Hz, 1H), 7.47 (dd, *J* = 8.4, 7.5 Hz, 1H), 6.32 (s, 1H), 6.18 (t, *J* = 8.5 Hz, 1H), 5.62 (d, *J* = 7.1 Hz, 1H), 5.42 (d, *J* = 4.5 Hz, 1H), 5.13 (d, *J* = 4.6 Hz, 1H), 4.98 (d, *J* = 9.7 Hz, 1H), 4.64 (dd, *J* = 4.7, 4.5 Hz, 1H), 4.47 (dd, *J* = 9, 9Hz, 1H), 4.30 (d, *J* = 9 Hz, 1H), 4.14 (d, *J* = 9 Hz, 1H), 3.89 (d, *J* = 7.1 Hz, 1H), 3.86 (s, 3H), 2.54 (m, 1H), 2.52 (q, *J* = 8.2 Hz, 2H), 2.30 (q, *J* = 7.6 Hz, 2H), 2.27 (s, 3H), 2.10 (s, 3H), 2.04 (s, 3H), 1.86 (m, 1H), 1.76 (s, 3H), 1.66 (s, 3H), 1.23 (t, *J* = 7.6 Hz, 3H), 1.10 (s, 6H) (Figure 4.45). ^{13}C NMR (126 MHz, $CDCl_3$) δ: 204.26, 174.72, 171.96, 168.78, 166.78, 159.56, 147.33, 141.52, 133.67, 130.49, 129.49, 128.63, 122.59, 120.27, 114.32, 84.78, 81.76, 79.53, 77.84, 76.91, 76.32, 74.91, 72.33, 67.86, 58.67, 55.45, 52.64, 46.62, 42.78, 38.86, 35.84, 27.92, 26.95, 22.89, 20.79, 18.93, 15.96, 8.67, 8.48 (Figure 4.46). LC/ESI-MS monoisotopic exact mass *m/z* 772.3482 $[M + H]^+$; calculated for $C_{40}H_{54}NO_{14}$: 772.3544.

2-debenzoyl-2-(3-difluoromethylbenzoyl)-3´-*N*-de(*tert*-butoxycarbonyl)-SB-T-1213 (4.9e) (11 mg, 23% yield), ^{1}H NMR (500 MHz, $CDCl_3$) δ: 8.12 (d, *J* = 7.4 Hz, 1H), 7.85 (s, 1H) 7.71 (d, *J* = 7.1Hz, 1H), 7.64 (s, 1H), 7.48 (dd, *J* = 8.4, 7.5 Hz, 1H), 6.32 (s, 1H), 6.19 (t, *J* = 8.5 Hz, 1H), 5.62 (d, *J* = 7.1 Hz, 1H), 5.42 (d, *J* = 4.5 Hz, 1H), 5.13 (d, *J* = 4.6 Hz, 1H), 4.98 (d, *J* = 9.7 Hz, 1H), 4.64 (dd, *J* = 4.7, 4.5 Hz, 1H), 4.47 (dd, *J* = 9, 9Hz, 1H), 4.30 (d, *J* = 9 Hz, 1H), 4.14 (d, *J* = 9 Hz, 1H), 3.89 (d, *J* = 7.1 Hz, 1H), 2.54 (m, 1H), 2.52 (q, *J* = 8.2 Hz, 2H), 2.30 (q, *J* = 7.6 Hz, 2H), 2.27 (s, 3H), 2.10 (s, 3H), 2.04 (s, 3H), 1.86 (m, 1H), 1.76 (s, 3H), 1.66 (s, 3H), 1.23 (t, *J* = 7.6 Hz, 3H), 1.11 (s, 6H) (Figure 4.47). ^{13}C NMR (126 MHz, $CDCl_3$) δ: 206.28, 171.45, 170.65, 169.32, 167.46, 164.81, 147.35, 141.23, 132.82, 131.36, 129.52, 128.41, 127.91, 118.65, 116.72, 84.46, 81.75, 79.65, 77.68, 76.53, 76.14, 74.91, 72.43, 67.85, 58.68, 53.69, 46.27, 42.76, 38.96,

35.62, 26.93, 22.56, 20.73, 18.95, 15.92, 8.46, 8.27 (Figure 4.48). LC/ESI-MS monoisotopic exact mass *m/z* 808.3298 $[M + H]^+$; calculated for $C_{40}H_{52}F_2NO_{14}$: 808.3356.

NMR Data for 2-debenzoyl-2-(3-trifluoromethylbenzoyl)-3´-*N*-de(*tert*-butoxycarbonyl)-SB-T-1213 (4.9f) (8 mg, 17% yield), ^{1}H NMR (500 MHz, $CDCl_3$) δ: 8.09 (d, *J* = 7.5 Hz, 1H), 7.87 (s, 1H) 7.68 (d, *J* = 7.2 Hz, 1H), 7.45 (dd, *J* = 8.2, 7.8 Hz, 1H), 6.32 (s, 1H), 6.19 (t, *J* = 8.5 Hz, 1H), 5.63 (d, *J* = 7.1 Hz, 1H), 5.42 (d, *J* = 4.5 Hz, 1H), 5.13 (d, *J* = 4.6 Hz, 1H), 4.98 (d, *J* = 9.7 Hz, 1H), 4.64 (dd, *J* = 4.7, 4.5 Hz, 1H), 4.47 (dd, *J* = 9, 9Hz, 1H), 4.30 (d, *J* = 9 Hz, 1H), 4.14 (d, *J* = 9 Hz, 1H), 3.89 (d, *J* = 7.1 Hz, 1H), 2.56 (m, 1H), 2.54 (q, *J* = 8.2 Hz, 2H), 2.31 (q, *J* = 7.6 Hz, 2H), 2.29 (s, 3H), 2.11 (s, 3H), 2.05 (s, 3H), 1.88 (m, 1H), 1.78 (s, 3H), 1.68 (s, 3H), 1.25 (t, *J* = 7.6 Hz, 3H), 1.11 (s, 6H) (Figure 4.49). ^{13}C NMR (126 MHz, $CDCl_3$) δ: 204.27, 171.31, 170.82, 169.12, 167.35, 165.11, 146.62, 141.11, 132.18, 130.47, 129.12, 127.75, 127.72, 126.46, 122.68, 118.55, 84.49, 80.77, 79.10, 77.73, 77.32, 76.05, 74.92, 72.34, 67.91, 58.67, 52.69, 46.17, 42.68, 38.57, 35.59, 26.96, 26.01, 22.60, 20.34, 18.24, 15.61, 8.46, 8.35 (Figure 4.50). LC/ESI-MS monoisotopic exact mass *m/z* 826.3195 $[M + H]^+$; calculated for $C_{40}H_{51}F_3NO_{14}$: 826.3262.

NMR Data for 3´-*N*-de(*tert*-butoxycarbonyl)-SB-T-1214 (4.10a) (12 mg, 27% yield), ^{1}H NMR (500 MHz, $CDCl_3$) δ: 8.11 (d, *J* = 8.4 Hz, 2H), 7.67 (dd, *J* = 7.4, 7.3 Hz, 1H), 7.46 (dd, *J* = 8.4, 7.5 Hz, 2H), 6.31 (s, 1H), 6.19 (t, *J* = 8.7 Hz, 1H), 5.61 (d, *J* = 7.1 Hz, 1H), 5.42 (d, *J* = 4.5 Hz, 1H), 5.11 (d, *J* = 4.7, 1H), 4.98 (d, *J* = 9.7, 1H), 4.62 (dd, *J* = 4.7, 4.5 Hz, 1H), 4.46 (dd , *J* = 9, 9 Hz, 1H), 4.30 (d, *J* = 9 Hz, 1H), 4.15 (d, *J* = 9 Hz, 1H), 3.85 (d, *J* = 7.1 Hz, 1H), 2.55 (m, 1H), 2.29 (q, *J* = 7.6 Hz, 2H), 2.26 (s, 3H), 2.07 (s, 3H), 2.03 (s, 3H), 1.84 (m, 1H), 1.75 (s, 3H), 1.66 (s, 3H), 1.24 (tt, *J* = 7.6, 4.6 Hz, 1H), 1.13 (dd, *J* = 5.3, 3.3 Hz, 2H), 1.11 (s, 6H), 1.01 (dd, *J* = 6.9, 4.6 Hz, 2H) (Figure 4.51). ^{13}C NMR (126 MHz, CDCl3) δ: 204.35, 175.17, 171.62, 168.83, 167.31, 148.13, 143.89, 135.43, 133.27, 131.52, 130.17, 129.52, 119.32, 84.39, 81.73, 79.82, 78.56, 77.31, 76.86, 74.27, 72.51, 67.72, 58.76, 53.12, 46.65, 42.46, 39.28, 35.11, 27.24, 22.62,

20.43, 18.62, 13.27, 8.41, 8.32 (Figure 4.52). LC/ESI-MS monoisotopic exact mass m/z 754.3383 $[M + H]^+$; calculated for $C_{40}H_{52}NO_{13}$: 754.3438.

NMR Data for 2-debenzoyl-2-(3-fluorobenzoyl)-3′-*N*-de(*tert*-butoxycarbonyl)-SB-T-1214 (4.10b) (11 mg, 23% yield), ^{1}H NMR (500 MHz, $CDCl_3$) δ: : 8.09 (d, *J* = 7.4 Hz, 1H), 7.86 (s, 1H) 7.76 (d, *J* = 7.0 Hz, 1H), 7.49 (dd, *J* = 8.4, 7.5 Hz, 1H), 6.32 (s, 1H), 6.19 (t, *J* = 8.5 Hz, 1H), 5.62 (d, *J* = 7.1 Hz, 1H), 5.42 (d, *J* = 4.5 Hz, 1H), 5.13 (d, *J* = 4.6 Hz, 1H), 4.98 (d, *J* = 9.7 Hz, 1H), 4.64 (dd, *J* = 4.7, 4.5 Hz, 1H), 4.47 (dd, *J* = 9, 9Hz, 1H), 4.30 (d, *J* = 9 Hz, 1H), 4.14 (d, *J* = 9 Hz, 1H), 3.89 (d, *J* = 7.1 Hz, 1H), 2.55 (m, 1H), 2.31 (q, *J* = 7.6 Hz, 2H), 2.28 (s, 3H), 2.10 (s, 3H), 2.05 (s, 3H), 1.85 (m, 1H), 1.77 (s, 3H), 1.68 (s, 3H), 1.25 (tt, *J* = 7.6, 4.6 Hz, 1H), 1.14 (dd, *J* = 5.3, 3.3 Hz, 2H), 1.11 (s, 6H), 0.99 (dd, *J* = 6.9, 4.6 Hz, 2H) (Figure 4.53). ^{13}C NMR (126 MHz, CDCl3) δ: 205.26, 176.71, 171,68, 168.86, 167.25, 163.52, 147.56, 142.92, 134.88, 130.46, 129.96, 128.64, 125.85, 121.78, 116.67, 84.51, 81.79, 79.81, 77.37, 76.31, 74.93, 72.34, 67.92, 58.67, 53.79, 46.67, 42.76, 39.28, 35.93, 27.21, 26.92, 22.88, 20.76, 18.65, 13.61, 8.47, 8.36 (Figure 4.54). LC/ESI-MS monoisotopic exact mass *m/z* 772.3294 $[M + H]^+$; calculated for $C_{40}H_{51}FNO_{13}$: 772.3345.

NMR Data for 2-debenzoyl-2-(3-chlorobenzoyl)-3′-*N*-de(*tert*-butoxycarbonyl)-SB-T-1214 (4.10c) (9 mg, 18% yield), ^{1}H NMR (500 MHz, $CDCl_3$) δ: 8.12 (s, 1H), 7.89 (d, *J* = 7.4 Hz, 1H), 7.77 (d, *J* = 7.2 Hz, 1H), 7.49 (dd, *J* = 8.5, 7.4 Hz, 1H), 6.32 (s, 1H), 6.19 (t, *J* = 8.5 Hz, 1H), 5.62 (d, *J* = 7.1 Hz, 1H), 5.42 (d, J = 4.5 Hz, 1H), 5.13 (d, J = 4.6 Hz, 1H), 4.98 (d, *J* = 9.7 Hz, 1H), 4.64 (dd, *J* = 4.7, 4.5 Hz, 1H), 4.47 (dd, *J* = 9, 9Hz, 1H), 4.30 (d, *J* = 9 Hz, 1H), 4.14 (d, *J* = 9 Hz, 1H), 3.89 (d, *J* = 7.1 Hz, 1H), 2.55 (m, 1H), 2.31 (q, *J* = 7.6 Hz, 2H), 2.28 (s, 3H), 2.10 (s, 3H), 2.05 (s, 3H), 1.85 (m, 1H), 1.77 (s, 3H), 1.68 (s, 3H), 1.25 (tt, *J* = 7.6, 4.6 Hz, 1H), 1.14 (dd, *J* = 5.3, 3.3 Hz, 2H), 1.11 (s, 6H), 0.99 (dd, *J* = 6.9, 4.6 Hz, 2H) (Figure 4.55). ^{13}C NMR (126 MHz, $CDCl_3$) δ: 205.26, 174.71, 171,98, 168.91, 167.25, 146.43, 140.91, 135.12, 134.28, 131.62, 130.28,

129.82, 129.76, 127.65, 126.84, 84.51, 81.79, 79.81, 77.37, 76.31, 74.93, 72.34, 67.92, 58.67, 53.79, 46.67, 42.76, 39.28, 35.93, 27.21, 26.92, 22.88, 20.76, 18.65, 13.61, 8.45, 8.37 (Figure 4.56). LC/ESI-MS monoisotopic exact mass *m/z* 788.2986 $[M + H]^+$; calculated for $C_{40}H_{51}ClNO_{13}$: 788.3049.

NMR Data for 2-debenzoyl-2-(3-methoxybenzoyl)-3´-*N*-de(*tert*-butoxycarbonyl)-SB-T-1214 (4.10d) (3 mg, 6% yield), ^1H NMR (500 MHz, $CDCl_3$) δ: 8.07 (d, *J* = 7.4 Hz, 1H), 7.68 (s, 1H) 7.57 (d, *J* = 7.2 Hz, 1H), 7.48 (dd, *J* = 8.5, 7.8 Hz, 1H), 6.32 (s, 1H), 6.18 (t, *J* = 8.5 Hz, 1H), 5.63 (d, *J* = 7.1 Hz, 1H), 5.45 (d, *J* = 4.5 Hz, 1H), 5.12 (d, *J* = 4.6 Hz, 1H), 4.98 (d, *J* = 9.7 Hz, 1H), 4.64 (dd, *J* = 4.7, 4.5 Hz, 1H), 4.47 (dd, *J* = 9, 9Hz, 1H), 4.30 (d, *J* = 9 Hz, 1H), 4.14 (d, *J* = 9 Hz, 1H), 3.89 (d, *J* = 7.1 Hz, 1H), 3.86 (s, 3H), 2.54 (m, 1H), 2.30 (q, *J* = 7.6 Hz, 2H), 2.27 (s, 3H), 2.10 (s, 3H), 2.04 (s, 3H), 1.84 (m, 1H), 1.75 (s, 3H), 1.66 (s, 3H), 1.24 (tt, *J* = 7.6, 4.6 Hz, 1H), 1.14 (dd, *J* = 5.3, 3.3 Hz, 2H), 1.11 (s, 6H), 0.99 (dd, *J* = 6.9, 4.6 Hz, 2H) (Figure 4.57). ^{13}C NMR (126 MHz, CDCl3) δ: 204.35, 175.21, 171.14, 167.59, 166.16, 159.52, 146.17, 141.46, 133.48, 130.83, 129.46, 128.35, 122.33, 118.72, 114.25, 84.28, 81.14, 79.35, 77.31, 76.75, 76.15, 74.59, 72.24, 67.78, 58.56, 55.12, 52.35, 46.15, 42.67, 38.58, 35.54, 27.15, 26.55, 22.57, 20.34, 15.63, 13.62, 8.41, 8.36 (Figure 4.58). LC/ESI-MS monoisotopic exact mass *m/z* 784.3491 $[M + H]^+$; calculated for $C_{41}H_{54}NO_{14}$: 784.3544.

NMR Data for 2-debenzoyl-2-(3-difluoromethylbenzoyl)-3´-*N*-de(*tert*-butoxycarbonyl)-SB-T-1214 (4.10e) (8 mg, 17% yield), ^1H NMR (500 MHz, CDCl3) δ: 8.11 (d, *J* = 7.4 Hz, 1H), 7.84 (s, 1H), 7.74 (d, *J* = 7.1Hz, 1H), 7.65 (s, 1H), 7.48 (dd, *J* = 8.4, 7.5 Hz, 1H), 6.32 (s, 1H), 6.19 (t, *J* = 8.5 Hz, 1H), 5.62 (d, *J* = 7.1 Hz, 1H), 5.42 (d, *J* = 4.5 Hz, 1H), 5.13 (d, *J* = 4.6 Hz, 1H), 4.98 (d, *J* = 9.7 Hz, 1H), 4.64 (dd, *J* = 4.7, 4.5 Hz, 1H), 4.47 (dd, *J* = 9, 9Hz, 1H), 4.30 (d, *J* = 9 Hz, 1H), 4.14 (d, *J* = 9 Hz, 1H), 3.89 (d, *J* = 7.1 Hz, 1H), 2.55 (m, 1H), 2.29 (q, *J* = 7.6 Hz, 2H), 2.26 (s, 3H), 2.07 (s, 3H), 2.03 (s, 3H), 1.84 (m, 1H), 1.75 (s, 3H), 1.66 (s, 3H), 1.24 (tt, *J* = 7.6, 4.6

Hz, 1H), 1.13 (dd, *J* = 5.3, 3.3 Hz, 2H), 1.11 (s, 6H), 1.01 (dd, *J* = 6.9, 4.6 Hz, 2H) (Figure 4.59). ^{13}C NMR (126 MHz, $CDCl_3$) δ: 206.28, 171.45, 170.65, 169.32, 167.46, 164.81, 147.35, 141.23, 132.82, 131.36, 129.52, 128.41, 127.91, 118.65, 116.72, 84.28, 81.14, 79.35, 77.31, 76.75, 76.15, 74.59, 72.24, 67.78, 58.56, 55.12, 52.35, 46.15, 42.67, 38.58, 35.54, 27.15, 26.55, 22.57, 20.34, 15.63, 13.62, 8.41, 8.36 (Figure 4.60). LC/ESI-MS monoisotopic exact mass m/z 820.3296 [M + H] +; calculated for $C_{41}H_{52}F_2NO_{14}$: 820.3356.

NMR Data for 2-debenzoyl-2-(3-trifluoromethoxybenzoyl)-3′-*N*-de(*tert*-butoxycarbonyl)-SB-T-1214 (7 mg, 13% yield), ^{1}H NMR (500 MHz, $CDCl_3$) δ: 8: 8.09 (d, *J* = 7.5 Hz, 1H), 7.87 (s, 1H) 7.68 (d, *J* = 7.2 Hz, 1H), 7.45 (dd, *J* = 8.2, 7.8 Hz, 1H), 6.32 (s, 1H), 6.19 (t, *J* = 8.5 Hz, 1H), 5.63 (d, *J* = 7.1 Hz, 1H), 5.42 (d, *J* = 4.5 Hz, 1H), 5.13 (d, *J* = 4.6 Hz, 1H), 4.98 (d, *J* = 9.7 Hz, 1H), 4.64 (dd, *J* = 4.7, 4.5 Hz, 1H), 4.47 (dd, *J* = 9, 9Hz, 1H), 4.30 (d, *J* = 9 Hz, 1H), 4.14 (d, *J* = 9 Hz, 1H), 3.89 (d, *J* = 7.1 Hz, 1H), 2.56 (m, 1H), 2.30 (q, *J* = 7.6 Hz, 2H), 2.29 (s, 3H), 2.11 (s, 3H), 2.06 (s, 3H), 1.86 (m, 1H), 1.76 (s, 3H), 1.68 (s, 3H), 1.25 (tt, *J* = 7.6, 4.6 Hz, 1H), 1.15 (dd, *J* = 5.3, 3.3 Hz, 2H), 1.12 (s, 6H), 1.00 (dd, *J* = 6.9, 4.6 Hz, 2H) (Figure 4.61). ^{13}C NMR (126 MHz, $CDCl_3$) δ: 204.36, 175.35, 171.72, 169.11, 167.65, 166.63, 146.47, 141.81, 133.68, 131.83, 130.88, 129.31, 128.46, 122.54, 118.84, 84.48, 81.72, 79.75, 77.32, 76.81, 76.28, 74.91, 72.31, 67.87, 58.61, 53.67, 46.62, 42.67, 38.75, 35.54, 27.12, 26.85, 22.58, 20.33, 18.23, 13.58, 8.41, 8.35 (Figure 4.62). LC/ESI-MS monoisotopic exact mass *m/z* 838.3184 [M + H] $^+$; calculated for $C_{41}H_{51}F_3NO_{14}$: 838.3262.

Molecular modeling analysis

Structure optimizations on baccatin III and (2*R*,3*S*)-isoserninyl-CoA were conducted using Gaussian 16 in a four-step pattern,[16] starting from HF 3-21G* single point to HF 3-21G* optimization, then to B3LYP 3-21G*, and finally to B3LYP 6-31G*.Molecular dynamics (MD) simulations were performed using AMBER22.[17] The system was prepared in three steps. First, the

antechamber, prepin, and parmchk2 programs in the AmberTools23 package[18] generated the charge and force constants. Minimization was done in five stages, gradually removing restrictions from the protein backbone to the side chain. Each step yields 10,000 steps of steepest descendent and 10,000 steps of conjugate gradient methods. A quick 9-ps *NPT* simulation was conducted to avoid the formation of bubbles during heating. Afterward, a 36-ns *NVT* heating was performed with the temperature increasing gradually from 0 to 300 K. Then another 20-ns simulation was performed to equilibrate the system in the *NPT* ensemble, and the last 2,000 frames were used for distance analysis. The PME method and PBC were used for the simulations, and the Langevin algorithm with a 2.0 ps^{-1} friction frequency coefficient was used for maintaining the temperature.[19] The Berendsen barostat method was used for pressure control with a relaxation time of 1.0 ps.[20] The time step was 1.0 fs, with the SHAKE function constraining the hydrogen atom bonds.[21]

Results and Discussion

Synthesis of (2*R*,3*S*)-3-amino-2-hydroxy-5-methylhex-4-enoyl CoA (4.3)

Characterization of BAPT acyltransferase activity requires acyl CoA substrates such as (2*R*,3*S*)-phenylisoserinyl CoA (**4.2**) and (2*R*,3*S*)-3-amino-2-hydroxy-5-methylhex-4-enoyl CoA (**4.3**) which are not commercially available. The synthesis of isoerninyl CoA thioester substrates by reacting a mixed anhydride and CoA required protecting the reactive amino and hydroxy groups on the propanoid side chain before the CoA coupling with the C13 position of baccatin III.[22] The propanoic side chain substrate is synthesized by hydrolyzing β-lactam analogs to a racemic mixture which then resolute after derivatization with CH_2N_2 and Ac_2O to two enantiomers.[23-26]

Considering the numerous challenges encountered with the organic synthesis of (2*R*,3*S*)-isoserniyl CoA analogs, this approach was abandoned, and a biosynthetic method was considered. Previously substrate specificity studies in the Walker group show that PheAT enzyme is active with (2*R*,3*S*)-isoserine and can convert it to its CoA thioester analog.[27-29] Earlier studies showed

that immobilized CAL-B-catalyzed β-lactam ring cleavage with high enantioselectivities for (2*R*,3*S*)-isoserine analogs.[30] Therefore, we proposed to use phenylisoserine CoA ligase (PheAT) and immobilized CAL-B (lipase B from Candida antarctica) as an alternative method to synthesize isobutenyl isoserine CoA thioester and coupling with taxane analogs by BAPT catalysis to produce the next generation paclitaxel analog precursors (Figure 4.5).

The hydrolysis of β-lactam: 3-acetoxy-4-(2-methyl-1-propen-1-yl) azetidine-2-one (**4.15**) was dissolved diisopropyl ether. Immobilized CAL-B and H_2O were added, and LC/ESI-MS was constructed to assess the production. Selected ion m/z 160.0928 was identified for the $[M + H]^+$ ion for the (2*R*,3*S*)-3-amino-2-hydroxy-5-methylhex-4-enoic acid (**4.16**) (Figure 4.18).

Testing the activity of PheAT: The bio-thioesterification activity of PheAT was tested by incubating purified PheAT with (2*R*,3*S*)-3-amino-2-hydroxy-5-methylhex-4-enoic acid (**4.16**), CoA, ATP, and $MgCl_2.(6H_2O)$. The biosynthetic thioester product was verified by LC/ESI-MS selected-ion monitoring and selected ion m/z 907.09, was identified in the LC/ESI-MS profile and putatively assigned to the $[M-H]^{-1}$ ion for (2*R*,3*S*)-3-amino-2-hydroxy-5-methylhex-4-enoyl CoA (Figure 4.19).

Kinetic Analyses of PheAT with (2*R*,3*S*)-3-amino-2-hydroxy-5-methylhex-4-enoic acid (4.16)

The Michaelis-Menten kinetics parameters of PheAT catalysis were calculated under steady-state conditions by incubating purified PheAT with CoA, ATP, $MgCl_2.(6H_2O)$, and varying concentrations of (2*R*,3*S*)-3-amino-2-hydroxy-5-methylhex-4-enoic acid (**4.16**). These calculated parameters of PheAT for (2*R*,3*S*)-3-amino-2-hydroxy-5-methylhex-4-enoic acid (**4.16**) were used as a guide for the mg-laboratory scale up the biocatalysis production of (2*R*,3*S*)-3-amino-2-hydroxy-5-methylhex-4-enoyl CoA (**4.3**) and confirm its structure by NMR.

Laboratory Scale-Up. The ^1H NMR spectra of purified biocatalysis product (2*R*,3*S*)-3-amino-2-hydroxy-5-methylhex-4-enoyl CoA (**4.3**) show that chemical shifts (δ 4.82) of H2', (δ 4.21) of

(H3'), and (δ 5.12) of (H4') (Figure 4.20) were shifted upfield relative to that for the (2*R*,3*S*)-3-amino-2-hydroxy-5-methylhex-4-enoic acid (**4.16**) (δ 5.18) of (H2'), (δ 4.57) of (H3'), and (δ 5.42) of (H4') (Figure 4.16) suggesting that (2*R*,3*S*)-3-amino-2-hydroxy-5-methylhex-4-enoic acid (**4.16**) biocatalyzed by PheAT. The ^{13}C-NMR chemical shift (δ 198) for the carbonyl carbon (C1') (Figure 4.21) of (2*R*,3*S*)-3-amino-2-hydroxy-5-methylhex-4-enoyl CoA (**4.3**) was shifted downfield compared to that for the (2*R*,3*S*)-3-amino-2-hydroxy-5-methylhex-4-enoic acid (**4.16**) (δ 175) (Figure 4.17) which further confirm the thioesterfication catalysis by PheAT. Moreover, LC/ESI-MS/MS analysis confirms that the biocataylzed product of the correct molecular weight was obtained ($[M - H]^{-1}$ at m/z 907.0951 for (2*R*,3*S*)-3-amino-2-hydroxy-5-methylhex-4-enoyl CoA (**4.3**)) (Figure 4.24).

BAPT Activity Evaluation with Isoserinyl CoA analogs and Baccatin III

First, the activity of BAPT with Mg^{2+} as a cofactor was tested by incubating (2*R*,3*S*)-phenylisoserinyl CoA (**4.17**), purified BAPT, CoA, ATP, and $MgCl_2.(6H_2O)$. The putative product made biocatalytically was screened by LC/ESI-MS selected-ion monitoring. The control assay was done under the same conditions except that $MgCl_2.(6H_2O)$ was omitted. Selected ions m/z 750.31 were identified in the LC/ESI-MS profiles and putatively assigned to the $[M+H]^+$ ion for 3′-*N*-debenzoyl-paclitaxel (**4.4**) (Figure 4.25A).

After confirming that BAPT catalysis coupled phenylisoserinyl CoA with baccatin III, we tested the BAPT catalysis with the isobutenylisosernyl CoA (**4.3**), the next-generation paclitaxel precursors. The coupling of (2*R*,3*S*)-3-amino-2-hydroxy-5-methylhex-4-enoyl CoA (**4.3**) with baccatin III (**4.1**) was done under the same condition as the phenylisosernyl coupling assay. Selected ions m/z 728.33 were identified in the LC/ESI-MS profiles and putatively assigned to the $[M+H]^+$ ion for 3′-*N*-de(*tert*-butoxycarbonyl)-SB-T-1212 (**4.5a**) (Figure 4.26A). In contrast, the BAPT control assay with no Mg ion added to the reaction shows that there are no products detected

for the coupling reaction of baccatin III (**4.1**) with both (**4.2**) and (**4.3**) CoA substrates (Figure xx 4.25B). These findings suggest that Mg^{+2} is required for the BAPT catalysis by interrupting the hydrogen bonding between the C13 hydroxy group and C4 OAc and organizing the amino acid in the active site. Thus Mg^{+2} is needed for the BAPT biocatalysis production.

Molecular Modeling Analysis of the BAPT-Catalyzed (2R,3S)-isoserninyl Transfer Reaction

A homology model of the BAPT was constructed using the SWISS-MODEL[31] based on a native HCT from *Coffea canephora* (PDB ID: 4G0B) within the BAHD family of acyltransferases.[32] The Mg^{2+} ion, the Gaussian-optimized baccatin III and (2*R*,3*S*)-isoserninyl-CoA were docked to the reaction site using AutoDock Vina[33] and UCSF Chimera[33,34] to visualize and analyze all the binding poses. Molecular dynamics simulations in this study conducted a thermodynamics analysis on a series of conformations accessible to flexible baccatin III and (2*R*,3*S*)-isoserninyl-CoA, both docked in BAPT. The intrinsic intramolecular stability of the ion and ligands was calculated within the context of the proximate residues in the enzyme active site. These conformational snapshots aided in finding low-energy, catalytically competent structural conformations.

To understand the role of Mg^{2+} ions in the BAPT catalysis, we constructed two independent simulations. One simulation with BAPT, baccatin III (**4.1**), (2*R*,3*S*)-isobutenylisoserine-CoA (**4.3**), and Mg^{2+} ion as a cofactor, and the other simulation without Mg^{2+} ion (Figure 4.6). The results show that the simulation with Mg^{2+} at the BAPT active site interrupts the hydrogen bonding between the C13-hydroxyl group and the C4-OAc group. Also, the Mg^{2+} ion organizes the acid active site and puts the catalytic β-amino group of the isosernyl CoA (**4.3**) at a close distance (3.861Å) from the acyl acceptor (**4.1**) (C13-hydroxyl group) (Figure 4.6A).

A

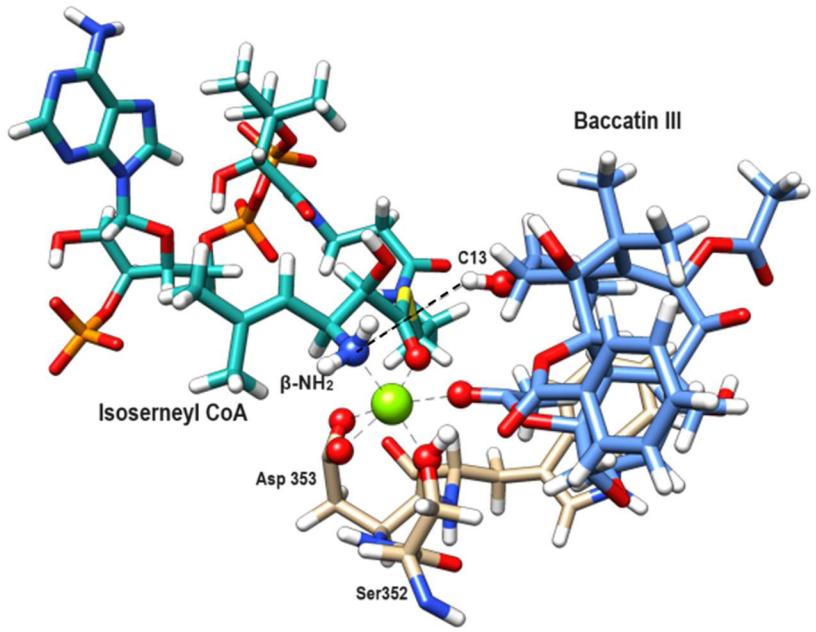

B

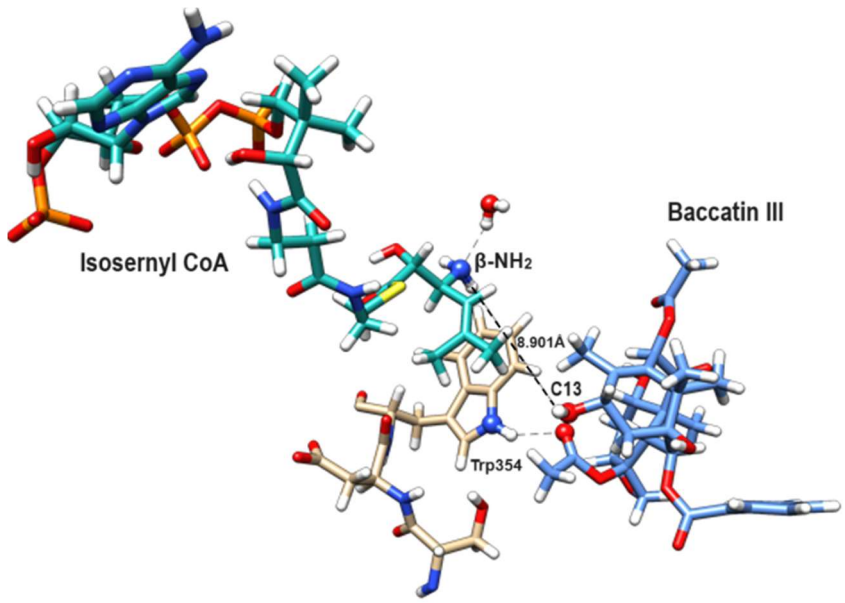

Figure 4.6: MD-simulation comparison of the BAPT enzyme active size (A) with Mg^{2+} ion and (B) and without presence of Mg^{2+} ion.

On the other hand, the simulation with no Mg^{2+} ion at the BAPT active site indicates that other amino acids are either unable to interrupt the hydrogen bond or will like Trp354. Trp354 will slightly disturb the hydrogen bonding between C13 hydroxyl group and the C4-OAc group by forming hydrogen bonding with C4-OAc. However, the Trp354 and C4-OAc interaction will also pull the baccatin III (**4.1**) molecule away from the catalytic center before the intramolecular

hydrogen bond between C4-acetyl and C13-hydroxyl was disassembled. This will put the β-amino group of the isosernyl CoA (**4.3**) at (8.901Å) from the C13-hydroxy group of **4.1** (Figure 4.6B).

This finding supports our hypothesis and experimental results with Mg2+ ions as an important cofactor in the BAPT catalysis not only for interrupting hydrogen bonding but also for increasing the BAPT turnover production by putting the β-amino group of the isosernyl CoA at close range to the C13-hydroxyl group of baccatin III (**4.1**).

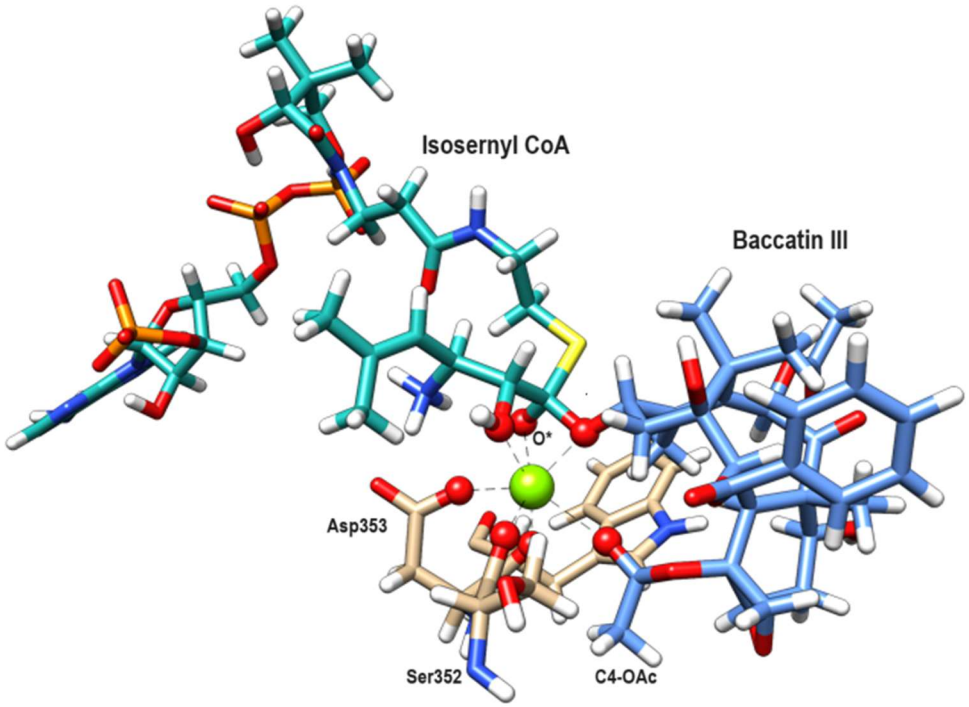

Figure 4.7: MD-simulation of the tetrahedral intermediate form between bacatin III (**4.1**) and (2*R*,3*S*)-isobutenylisoserninyl CoA (**4.3**) in BAPT catalysis with Mg^{2+} ion.

Another simulation was carried out to investigate the geometry and interaction of the tetrahedral intermediate (oxyanion intermediate, see Figure 4.3) during the BAPT catalysis (Figure 4.7). The results show that during the whole 20ns simulation, Mg^{2+} ion act as oxyanion hole by stabilizing the negative charge of the carbonyl oxygen of the isobeutenylisoserine CoA (tetrahedral intermediate) formed after the nucleophilic attack. This strongly proves that other than serving as

an intramolecular hydrogen bond interrupter, Mg^{2+} can also transiently stabilize the tetrahedral intermediate to facilitate the final leaving of the CoA thiol group, which leads to the final product.

Kinetic Evaluation of BAPT with (2*R*,3*S*)-3-amino-2-hydroxy-5-methylhex-4-enoyl CoA (4.3) and taxane analogs ((4.5, 4.6, and 4.7)(a-f))

The K_M and k_{cat} values of the BAPT acylation catalysis reaction were calculated under steady-state conditions by incubating purified BAPT with various concentrations of (2*R*,3*S*)-3-amino-2-hydroxy-5-methylhex-4-enoyl CoA, taxane analogs, and $MgCl_2.(6H_2O)$. The taxane analogs with benzoyl groups at C2 have the high k_{cat} turnover compared to that with 3-F or 3-Cl benzoyl groups (Table 4.1). This is because H has a smaller atomic size than F and Cl which will be less steric hinder in the BAPT active site and therefore increase the production rate. Also, taxane analogs with 3-$OCHF_2$ benzoyl group were faster than that 3-OCF_3 and 3-OCH_3 benzoyl groups. Molecular modeling analysis of the docked taxane analogs with 3-$OCHF_2$, 3-OCF_3, and 3-OCH_3 benzoyl groups show that 3-$OCHF_2$ group has no preferential conformation (in/out) of the plane which make it less steric hinder compared to 3-OCF_3, and 3-OCH_3.[35-37] This unique ability of the 3-$OCHF_2$ group to adopt no preferential conformation might increase the binding affinity to active sites and thus increase the turnover. The docking results indicated that both 3-$OCHF_2$, 3-OCF_3 groups will have VDW interactions with hydrophobic amino acid residues in the binding site compared to 3-OCH_3 group. The ^{1}H NMR spectra of purified biocatalysis products suggests that BAPT selectively acylated C13. The H13 chemical shift (δ 6.19) was shifted downfield for the biocatalized products compared to that for the taxane analogs (δ 4.97) (Figure 4.7).

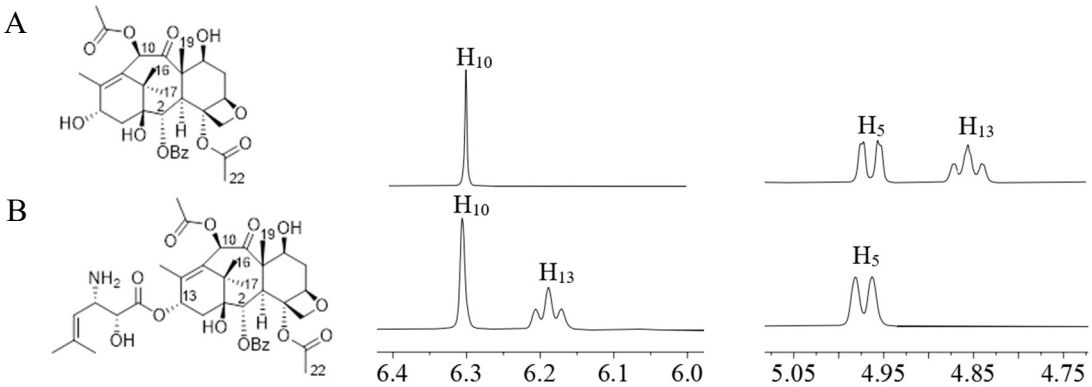

Figure 4.8: Partial ^{1}H NMR of (A) Baccatin III (**4.1**) and (B) 3´-*N*-de(*tert*-butoxycarbonyl)-SB-T-1212 (**4.8a**).

Table 4.1: Relative Kinetics of BAPT with (2*R*,3*S*)-isobutenylisoserinyl CoA and taxane analogs (**4.8**, **4.9**, **4.10**)**a-f**.

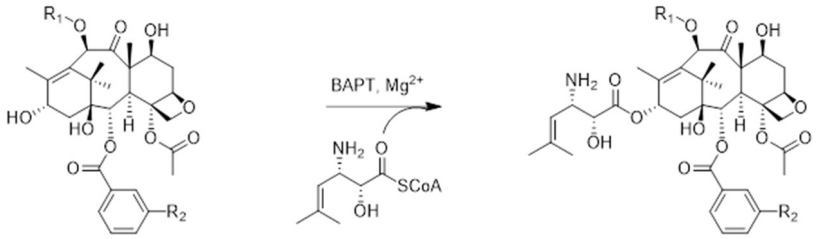

4.5, **4.6**, **4.7** **4.3** **4.8, 4.9, 4.10**

R_1	R_3	Exact mass (Da)	$[M+H]^+$ (*m/z*)	k_{cat} (min^{-1})	K_M (μM)	k_{cat}/K_M (s^{-1} M^{-1})
 **4.5→4.8**	**a**: H	727.32	728.33	1.84 ± 0.12	131 ± 11	234
	b: F	745.31	746.32	1.71 ± 0.34	138 ± 28	206
	c: Cl	761.28	762.29	1.31 ± 0.26	189 ± 15	115
	d: OCH_3	757.33	758.34	0.31 ± 0.05	188 ± 21	27
	e: $OCHF_2$	793.31	794.32	1.02 ± 0.04	159 ± 18	106
	f: OCF_3	811.30	812.31	0.65 ± 0.08	193 ± 23	56
 **4.6→4.9**	**a**: H	741.34	742.35	1.58 ± 0.18	156 ± 35	168
	b: Fl	759.33	760.34	1.36 ± 0.27	147 ± 12	154
	c: Cl	775.30	776.31	1.03 ± 0.05	167 ± 14	102
	d: OCH_3	771.35	772.36	0.25 ± 0.06	242 ± 56	17
	e: $OCHF_2$	807.33	808.34	0.82 ± 0.02	148 ± 22	92
	f: OCF_3	825.32	826.33	0.45 ± 0.03	218 ± 35	34
 **4.7→4.10**	**a**: H	753.34	754.35	1.27 ± 0.12	164 ± 16	129
	b: F	771.33	772.34	1.13 ± 0.06	182 ± 21	103
	c: Cl	787.30	788.31	0.86 ± 0.05	192 ± 17	74
	d: OCH_3	783.35	784.36	0.19 ± 0.01	215 ± 32	14
	e: $OCHF_2$	819.33	820.34	0.61 ± 0.04	144 ± 15	70
	f: OCF_3	837.32	838.33	0.38 ± 0.06	188 ± 42	33

Conclusion

The role of Mg^{2+} ion was investigated to understand the BAPT catalysis mechanisms. It shown that Mg^{2+} ions are effectively disassembling the hydrogen bond between C13-OH and C4-OAc of taxane substrate acyl acceptor. Also, introducing Mg^{2+} ion organized the BAPT active site. Moreover, the BAPT biocatalysis was able to catalytically produce precursors of non-natural next generation pactitaxel with *meta*-substitutions with F, Cl, OCH_3, OCF_3, and $OCHF_2$ groups at the C2-hydroxy benzoate and isobutenylisoserine analog at C13 moiety of the taxane core. The biocatalytic approach described here provides an alternative route to produce the important key intermediates of the next generation taxoids by eliminating the use of highly toxic reagents.

REFERENCES

(1) De Luca, V.; St Pierre, B. The Cell and Developmental Biology of Alkaloid Biosynthesis. *Trends Plant Sci.* **2000**, *5*, 168-173.

(2) D'Auria, J. C. Acyltransferases in plants: a good time to be BAHD. *Curr. Opin. Plant Biol.* **2006**, *9*, 331-340.

(3) Malik, S.; Cusidó, R. M.; Mirjalili, M. H.; Moyano, E.; Palazón, J.; Bonfill, M. Production of the anticancer drug taxol in Taxus baccata suspension cultures: A review. *Process Biochem.* **2011**, *46*, 23-34.

(4) Frense, D. Taxanes: perspectives for biotechnological production. *Appl. Microbiol. Biotechnol.* **2007**, *73*, 1233-1240.

(5) Hampel, D.; Mau, C. J.; Croteau, R. B. Taxol biosynthesis: Identification and characterization of two acetyl CoA:taxoid-O-acetyl transferases that divert pathway flux away from Taxol production. *Arch. Biochem. Biophys.* **2009**, *487*, 91-97.

(6) Jennewein, S.; Wildung, M. R.; Chau, M.; Walker, K.; Croteau, R. Random sequencing of an induced Taxus cell cDNA library for identification of clones involved in Taxol biosynthesis. *Proc. Natl. Acad. Sci.* **2004**, *101*, 9149-9154.

(7) Kaspera, R.; Croteau, R. Cytochrome P450 oxygenases of Taxol biosynthesis. *Phytochem. Rev.* **2006**, *5*, 433-444.

(8) Walker, K.; Schoendorf, A.; Croteau, R. Molecular Cloning of a Taxa-4(20),11(12)-dien-5α-ol-O-Acetyl Transferase cDNA from Taxus and Functional Expression in Escherichia coli. *Arch. Biochem. Biophys.* **2000**, *374*, 371-380.

(9) Walker, K.; Fujisaki, S.; Long, R.; Croteau, R. Molecular cloning and heterologous expression of the C-13 phenylpropanoid side chain-CoA acyltransferase that functions in Taxol biosynthesis. *Proc. Natl. Acad. Sci. U.S.A.* **2002**, *99*, 12715-12720.

(10) Ma, X.; Koepke, J.; Bayer, A.; Linhard, V.; Fritzsch, G.; Zhang, B.; Michel, H.; Stöckigt, J. Vinorine synthase from Rauvolfia: the first example of crystallization and preliminary X-ray diffraction analysis of an enzyme of the BAHD superfamily. *Biochim. Biophys. Acta.* **2004**, *1701*, 129-132.

(11) Ma, X.; Koepke, J.; Panjikar, S.; Fritzsch, G.; Stöckigt, J. Crystal Structure of Vinorine Synthase, the First Representative of the BAHD Superfamily*. *J. Biol. Chem.* **2005**, *280*, 13576-13583.

(12) Nakayama, T.; Suzuki, H.; Nishino, T. Anthocyanin acyltransferases: specificities, mechanism, phylogenetics, and applications. *J. Mol. Catal., B Enzym.* **2003**, *23*, 117-132.

(13) Bayer, A.; Ma, X.; Stöckigt, J. Acetyltransfer in natural product biosynthesis--functional

cloning and molecular analysis of vinorine synthase. *Bioorg. Med. Chem.* **2004**, *12*, 2787-2795.

(14) Chen, J.; Huang, X.; Fang, X.; Yan, C.; Gao, Z.; Shao, H. Disassembly of intermolecular hydrogen bond induced by cations on self-assembled monolayer. *J. Electroanal. Chem.* **2020**, *876*, 114476.

(15) Majerz, I. The influence of potassium cation on a strong OHO hydrogen bond. *Org. Biomol. Chem.* **2011**, *9*, 1466-1473.

(16) Frisch, M. J.; Trucks, G. W.; Schlegel, H. B.; Scuseria, G. E.; Robb, M. A.; Cheeseman, J. R.; Scalmani, G.; Barone, V.; Petersson, G. A.; Nakatsuji, H.; Li, X.; Caricato, M.; Marenich, A. V.; Bloino, J.; Janesko, B. G.; Gomperts, R.; Mennucci, B.; Hratchian, H. P.; Ortiz, J. V.; Izmaylov, A. F.; Sonnenberg, J. L.; Williams; Ding, F.; Lipparini, F.; Egidi, F.; Goings, J.; Peng, B.; Petrone, A.; Henderson, T.; Ranasinghe, D.; Zakrzewski, V. G.; Gao, J.; Rega, N.; Zheng, G.; Liang, W.; Hada, M.; Ehara, M.; Toyota, K.; Fukuda, R.; Hasegawa, J.; Ishida, M.; Nakajima, T.; Honda, Y.; Kitao, O.; Nakai, H.; Vreven, T.; Throssell, K.; Montgomery Jr., J. A.; Peralta, J. E.; Ogliaro, F.; Bearpark, M. J.; Heyd, J. J.; Brothers, E. N.; Kudin, K. N.; Staroverov, V. N.; Keith, T. A.; Kobayashi, R.; Normand, J.; Raghavachari, K.; Rendell, A. P.; Burant, J. C.; Iyengar, S. S.; Tomasi, J.; Cossi, M.; Millam, J. M.; Klene, M.; Adamo, C.; Cammi, R.; Ochterski, J. W.; Martin, R. L.; Morokuma, K.; Farkas, O.; Foresman, J. B.; Fox, D. J.: Gaussian 16 Rev. C.01. Wallingford, CT, **2016**.

(17) D.A. Case, H. M. A. K. B. I. Y. B.-S. S. R. B. D. S. C. T. E. C. I. I. I.; Kollman, P. A.: Amber 2021, University of California, San Francisco. **2021.**

(18) Case, D. A.; Aktulga, H. M.; Belfon, K.; Cerutti, D. S.; Cisneros, G. A.; Cruzeiro, V. W. D.; Forouzesh, N.; Giese, T. J.; Götz, A. W.; Gohlke, H.; Izadi, S.; Kasavajhala, K.; Kaymak, M. C.; King, E.; Kurtzman, T.; Lee, T.-S.; Li, P.; Liu, J.; Luchko, T.; Luo, R.; Manathunga, M.; Machado, M. R.; Nguyen, H. M.; O'Hearn, K. A.; Onufriev, A. V.; Pan, F.; Pantano, S.; Qi, R.; Rahnamoun, A.; Risheh, A.; Schott-Verdugo, S.; Shajan, A.; Swails, J.; Wang, J.; Wei, H.; Wu, X.; Wu, Y.; Zhang, S.; Zhao, S.; Zhu, Q.; Cheatham, T. E., III; Roe, D. R.; Roitberg, A.; Simmerling, C.; York, D. M.; Nagan, M. C.; Merz, K. M., Jr. AmberTools. *J Chem Inf Model* **2023**, *63*, 6183-6191.

(19) Loncharich, R. J.; Brooks, B. R.; Pastor, R. W. Langevin dynamics of peptides: the frictional dependence of isomerization rates of N-acetylalanyl-N'-methylamide. *Biopolymers* **1992**, *32*, 523-535.

(20) Berendsen, H. J. C.; Postma, J. P. M.; Gunsteren, W. F. v.; DiNola, A.; Haak, J. R. Molecular dynamics with coupling to an external bath. *The Journal of Chemical Physics* **1984**, *81*, 3684-3690.

(21) Miyamoto, S.; Kollman, P. A. Settle: An analytical version of the SHAKE and RATTLE algorithm for rigid water models. *J. Comput. Chem.* **1992**, *13*, 952-962.

(22) Loncaric, C.; Merriweather, E.; Walker, K. D. Profiling a Taxol Pathway 10β-

Acetyltransferase: Assessment of the Specificity and the Production of Baccatin III by In Vivo Acetylation in E. coli. *Chem. Biol.* **2006**, *13*, 309-317.

(23) Ojima, I.; Fumero-Oderda, C. L.; Kuduk, S. D.; Ma, Z.; Kirikae, F.; Kirikae, T. Structure–activity relationship study of taxoids for their ability to activate murine macrophages as well as inhibit the growth of macrophage-like cells. *Bioorg. Med. Chem.* **2003**, *11*, 2867-2888.

(24) Ojima, I.; Das, M. Recent Advances in the Chemistry and Biology of New Generation Taxoids. *J. Nat. Prod.* **2009**, *72*, 554-565.

(25) Ojima, I.; Hoon Park, Y.; Ming Sun, C.; Brigaud, T.; Zhao, M. New and efficient routes to norstatine and its analogs with high enantiomeric purity by β-Lactam Synthon Method. *Tetrahedron Lett.* **1992**, *33*, 5737-5740.

(26) Forró, E. New gas chromatographic method for the enantioseparation of β-amino acids by a rapid double derivatization technique. *J Chromatogr A.* **2009**, *1216*, 1025-1029.

(27) Muchiri, R.; Walker, Kevin D. Taxol Biosynthesis: Tyrocidine Synthetase A Catalyzes the Production of Phenylisoserinyl CoA and Other Amino Phenylpropanoyl Thioesters. *Chem. Biol.* **2012**, *19*, 679-685.

(28) Muchiri, R.; Walker, K. D. Paclitaxel Biosynthesis: Adenylation and Thiolation Domains of an NRPS TycA PheAT Module Produce Various Arylisoserine CoA Thioesters. *Biochem.* **2017**, *56*, 1415-1425.

(29) Thornburg, C. K.; Walter, T.; Walker, K. D. Biocatalysis of a Paclitaxel Analogue: Conversion of Baccatin III to N-Debenzoyl-N-(2-furoyl)paclitaxel and Characterization of an Amino Phenylpropanoyl CoA Transferase. *Biochem.* **2017**, *56*, 5920-5930.

(30) Galla, Z.; Beke, F.; Forró, E.; Fülöp, F. Enantioselective hydrolysis of 3,4-disubstituted β-lactams. An efficient enzymatic method for the preparation of a key Taxol side-chain intermediate. *J. Mol. Catal., B Enzym.* **2016**, *123*, 107-112.

(31) Waterhouse, A.; Bertoni, M.; Bienert, S.; Studer, G.; Tauriello, G.; Gumienny, R.; Heer, F. T.; de Beer, T. A P.; Rempfer, C.; Bordoli, L.; Lepore, R.; Schwede, T. SWISS-MODEL: homology modelling of protein structures and complexes. *Nucleic Acids Research* **2018**, *46*, W296-W303.

(32) Levsh, O.; Chiang, Y. C.; Tung, C. F.; Noel, J. P.; Wang, Y.; Weng, J. K. Dynamic Conformational States Dictate Selectivity toward the Native Substrate in a Substrate-Permissive Acyltransferase. *Biochemistry* **2016**, *55*, 6314-6326.

(33) Eberhardt, J.; Santos-Martins, D.; Tillack, A. F.; Forli, S. AutoDock Vina 1.2.0: New Docking Methods, Expanded Force Field, and Python Bindings. *J Chem Inf Model* **2021**, *61*, 3891-3898.

(34) Pettersen, E. F.; Goddard, T. D.; Huang, C. C.; Couch, G. S.; Greenblatt, D. M.; Meng, E. C.; Ferrin, T. E. UCSF Chimera--a visualization system for exploratory research and

analysis. *J. Comput. Chem.* **2004**, *25*, 1605-1612.

(35) Müller, K.; Faeh, C.; Diederich, F. Fluorine in pharmaceuticals: looking beyond intuition. *Science* **2007**, *317*, 1881-1886.

(36) Wang, C.; Wang, X.; Sun, Y.; Taouil, A. K.; Yan, S.; Botchkina, G. I.; Ojima, I. Design, synthesis and SAR study of 3rd-generation taxoids bearing 3-CH3, 3-CF3O and 3-CHF2O groups at the C2-benzoate position. *Bioorg. Chem.* **2020**, *95*, 103523.

(37) Bégué, J.-P.; Bonnet-Delpon, D. Recent advances (1995–2005) in fluorinated pharmaceuticals based on natural products. *J. Fluor. Chem.* **2006**, *127*, 992-1012.

APPENDIX C: CHAPTER 4 SUPPLEMENTARY MATERIALS

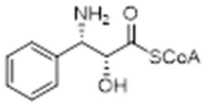

Figure 4.9: Structure of (2*R*,3*S*)-phenylisoserinyl CoA (**4.2**), stander used in the PheAT catalysis. These compounds were synthesized by Dr. Chelsea Thornburg (previous graduate student in Walker group, MSU).

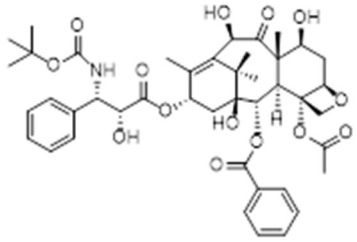

Figure 4.10: Structure of Docetaxel (**4.17**).

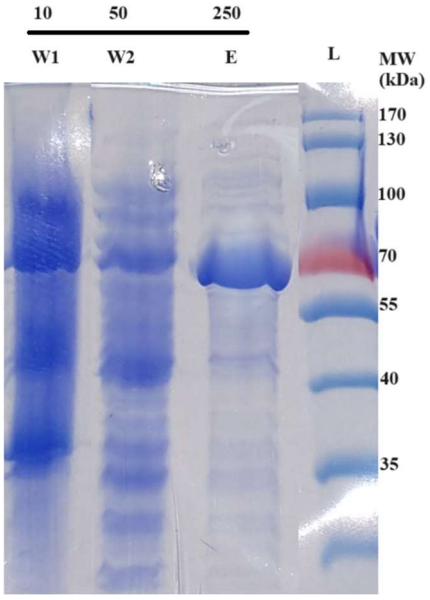

Figure 4.11: Coomassie Blue stained SDS-PAGE gel of aliquots from the fractions collected from Ni-NTA affinity exchange column used to purify the PheAT enzyme. Lanes represent protein contained in the Wash Buffer (W1 and W2); and Elution Buffer (E) fractions. The numbers above the bar are the mM concentrations of imidazole in the respective buffers. Molecular weight references are in the leftmost lane.

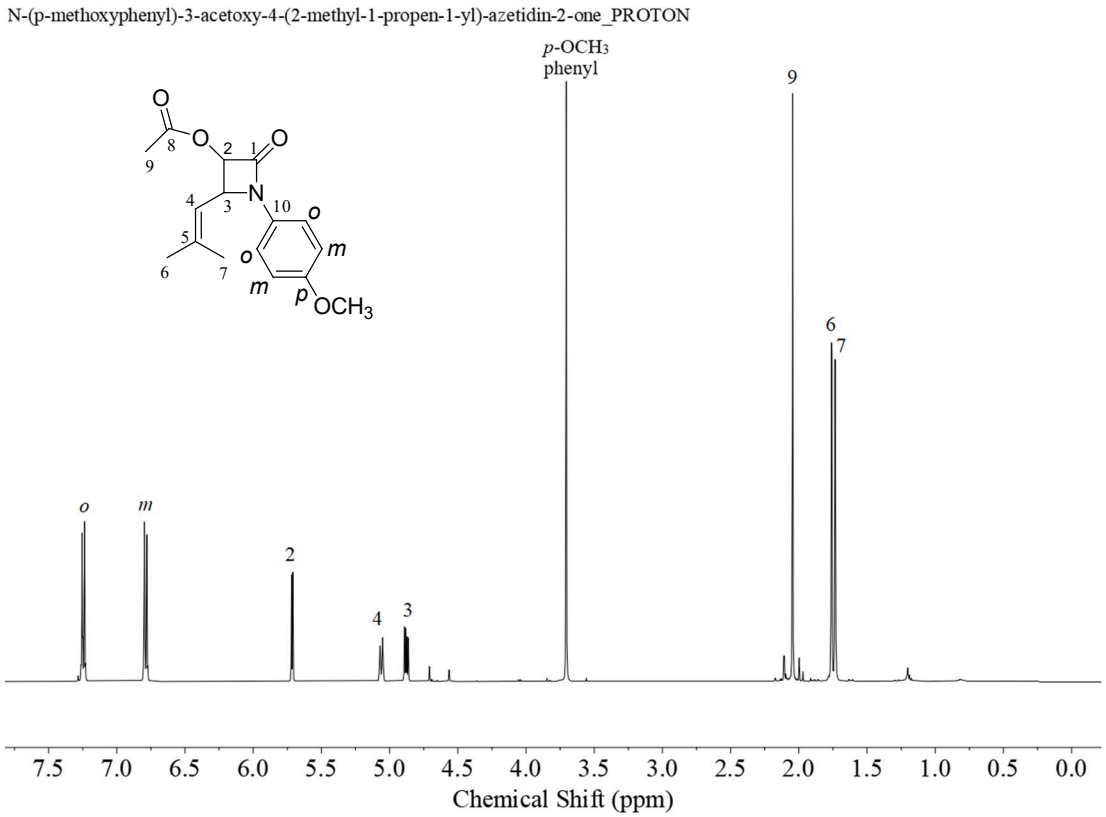

Figure 4.12: 1H NMR of *N*-(PMP)-3-acetoxy-4-(2-methyl-1-propen1-yl)-azetidin-2-one.

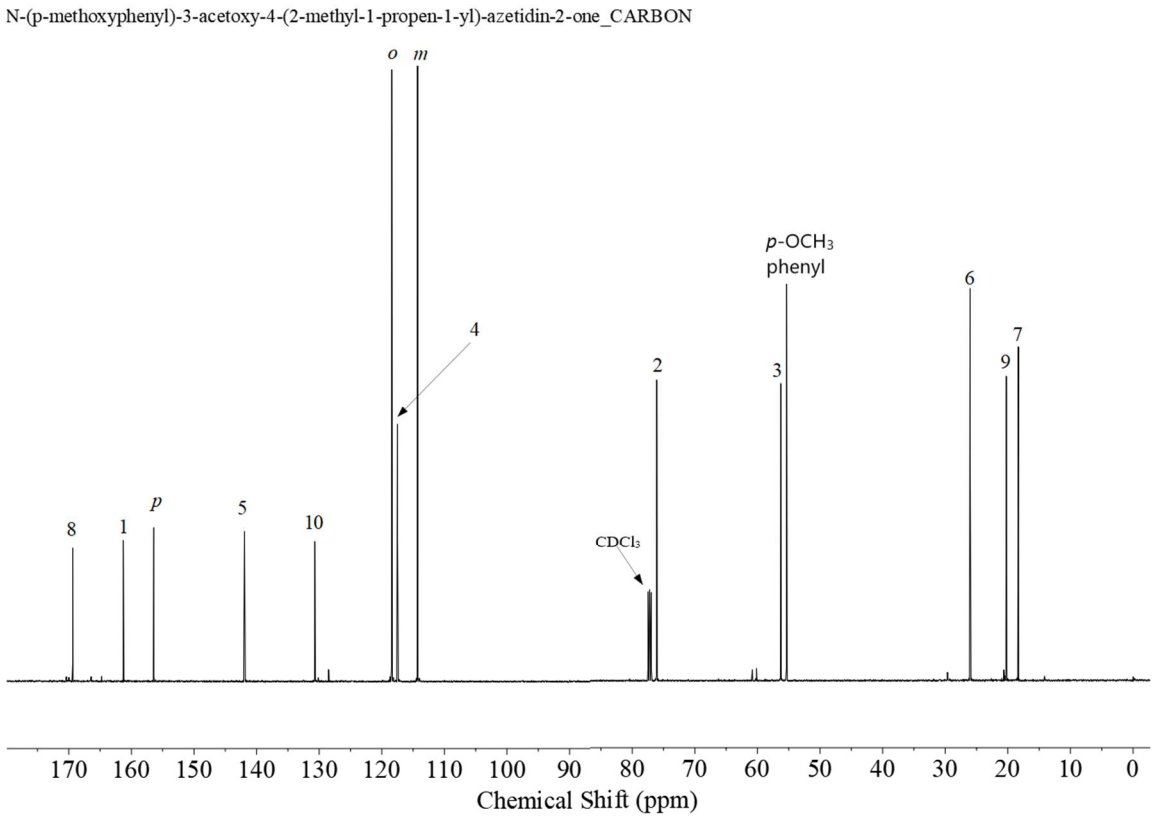

Figure 4.13: ^{13}C NMR of *N*-(PMP)-3-acetoxy-4-(2-methyl-1-propen1-yl)-azetidin-2-one.

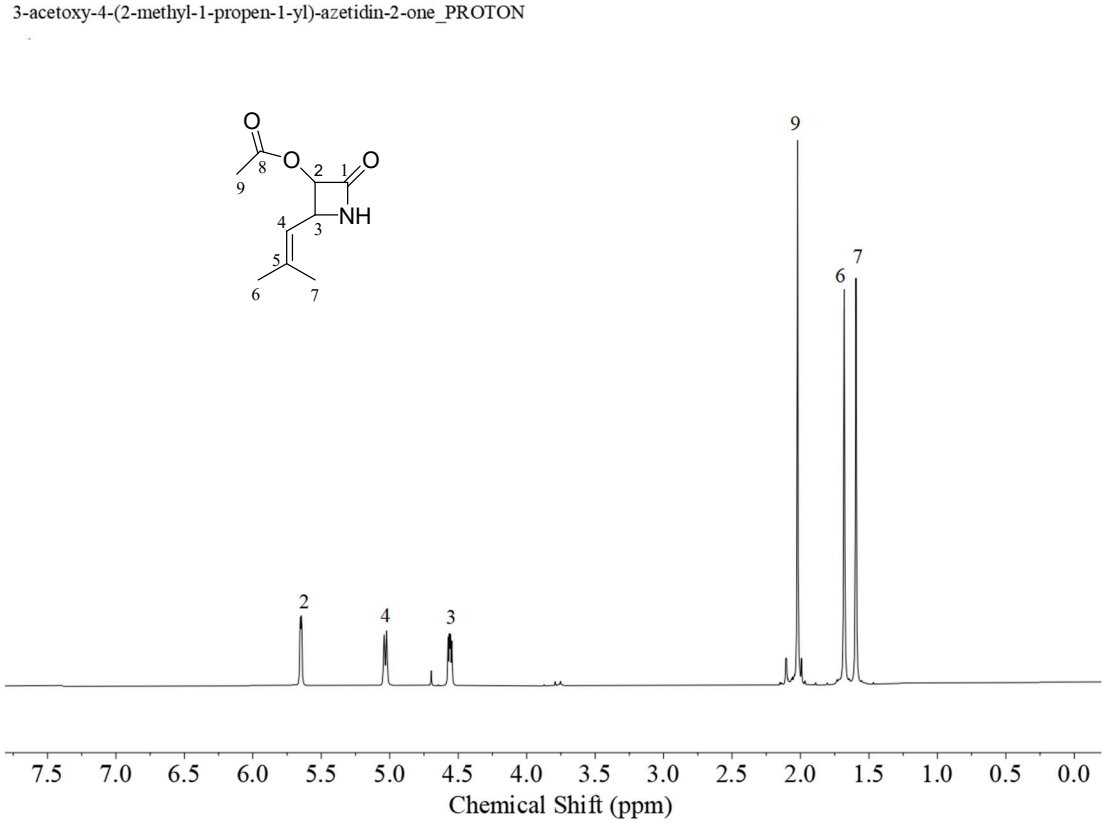

Figure 4.14: ^{1}H NMR of 3-acetoxy-4-(2-methyl-1-propen1-yl)-azetidin-2-one.

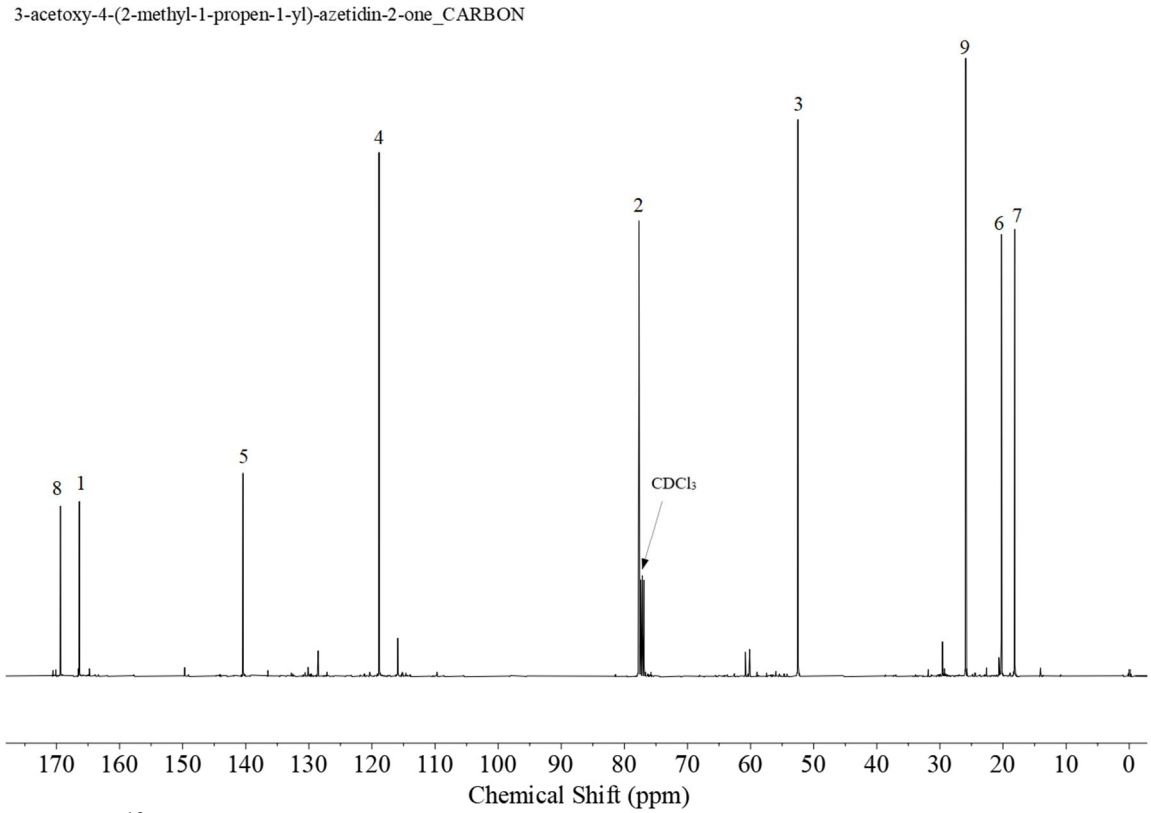

Figure 4.15: ^{13}C NMR of 3-acetoxy-4-(2-methyl-1-propen1-yl)-azetidin-2-one.

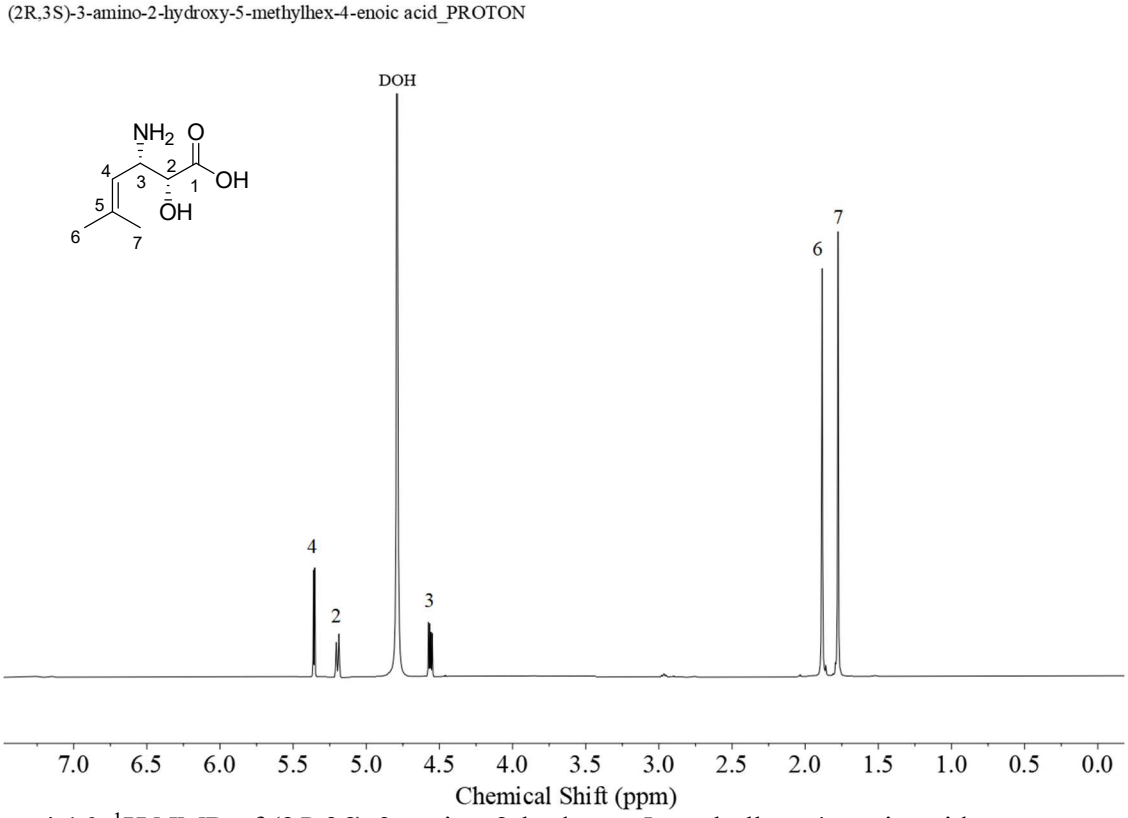

Figure 4.16: ^{1}H NMR of (2*R*,3*S*)-3-amino-2-hydroxy-5-methylhex-4-enoic acid.

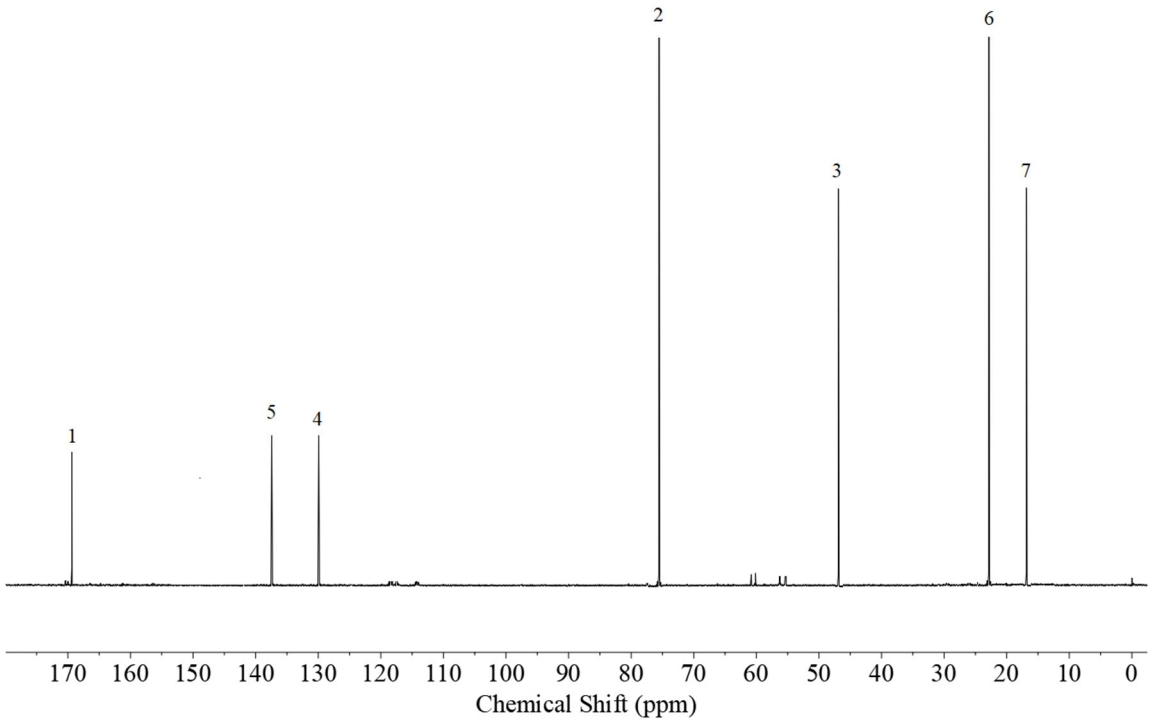

Figure 4.17: ^{13}C NMR of (2*R*,3*S*)-3-amino-2-hydroxy-5-methylhex-4-enoic acid.

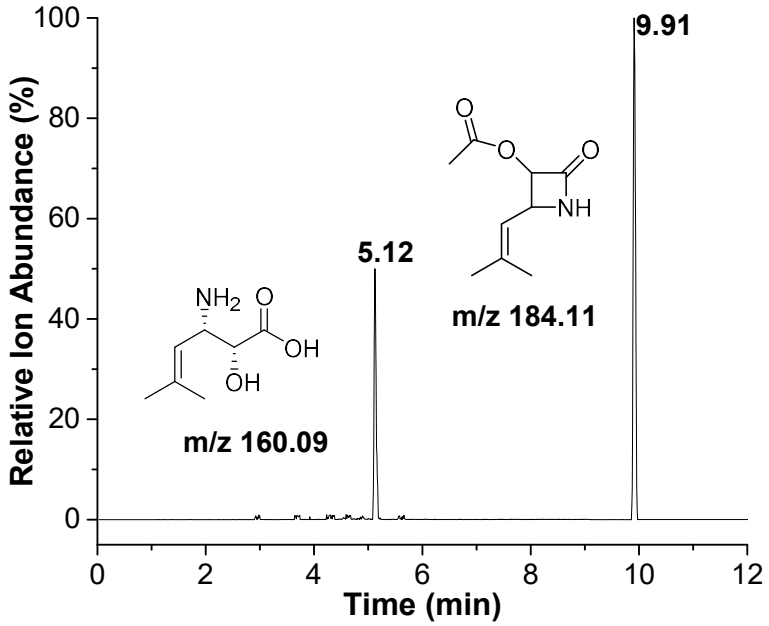

Figure 4.18: LC/ESI-MS (selected ion mode for m/z $[M + H]^+$) of the biocatalytic hydrolysis of 3-acetoxy-4-(2-methyl-1-propen1-yl)-azetidin-2-one to (2*R*,3*S*)-3-amino-2-hydroxy-5-methylhex-4-enoic acid.

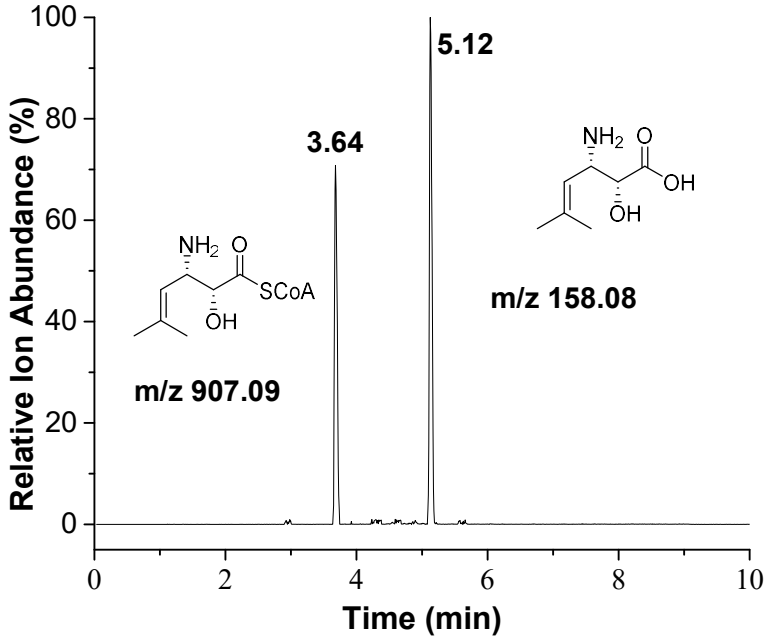

Figure 4.19: LC/ESI-MS (selected ion mode for m/z $[M - H]^-$) of the biocatalytic conversion of (2*R*,3*S*)-3-amino-2-hydroxy-5-methylhex-4-enoic acid to (2*R*,3*S*)-3-amino-2-hydroxy-5-methylhex-4-enoyl CoA.

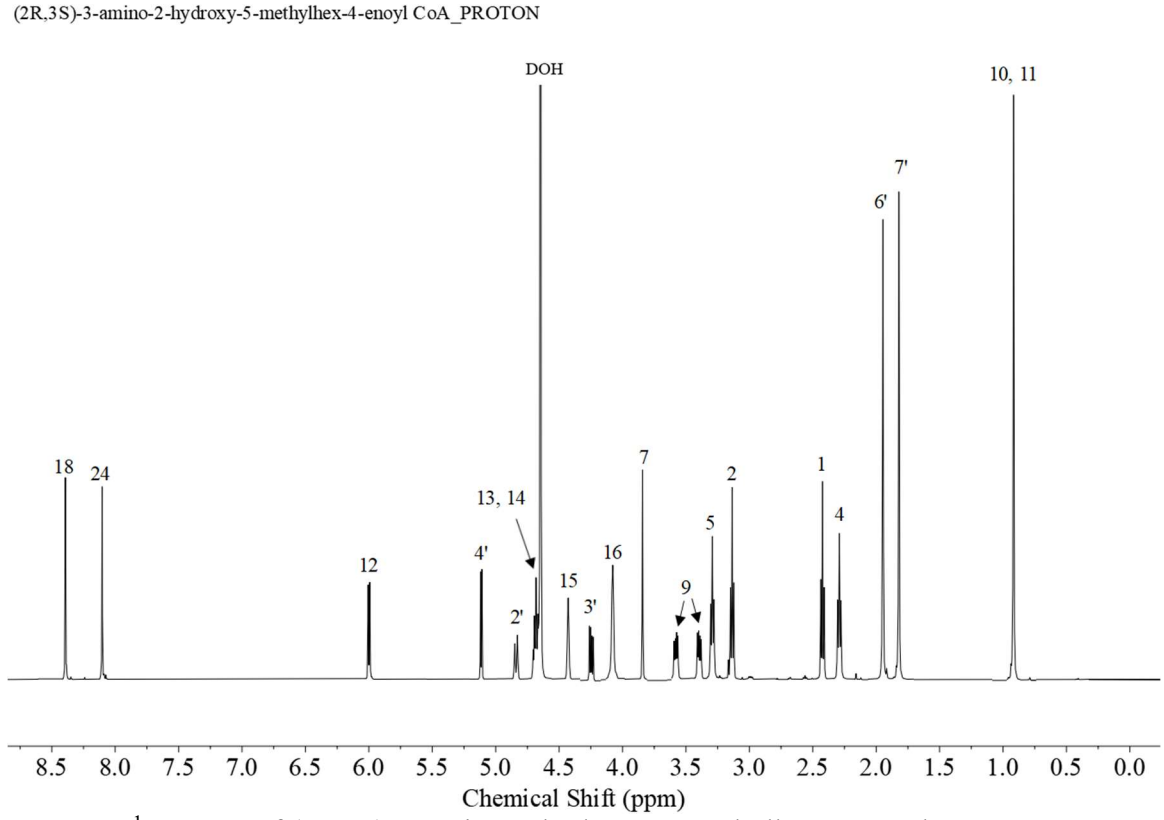

Figure 4.20: ^{1}H NMR of (2*R*,3*S*)-3-amino-2-hydroxy-5-methylhex-4-enoyl CoA.

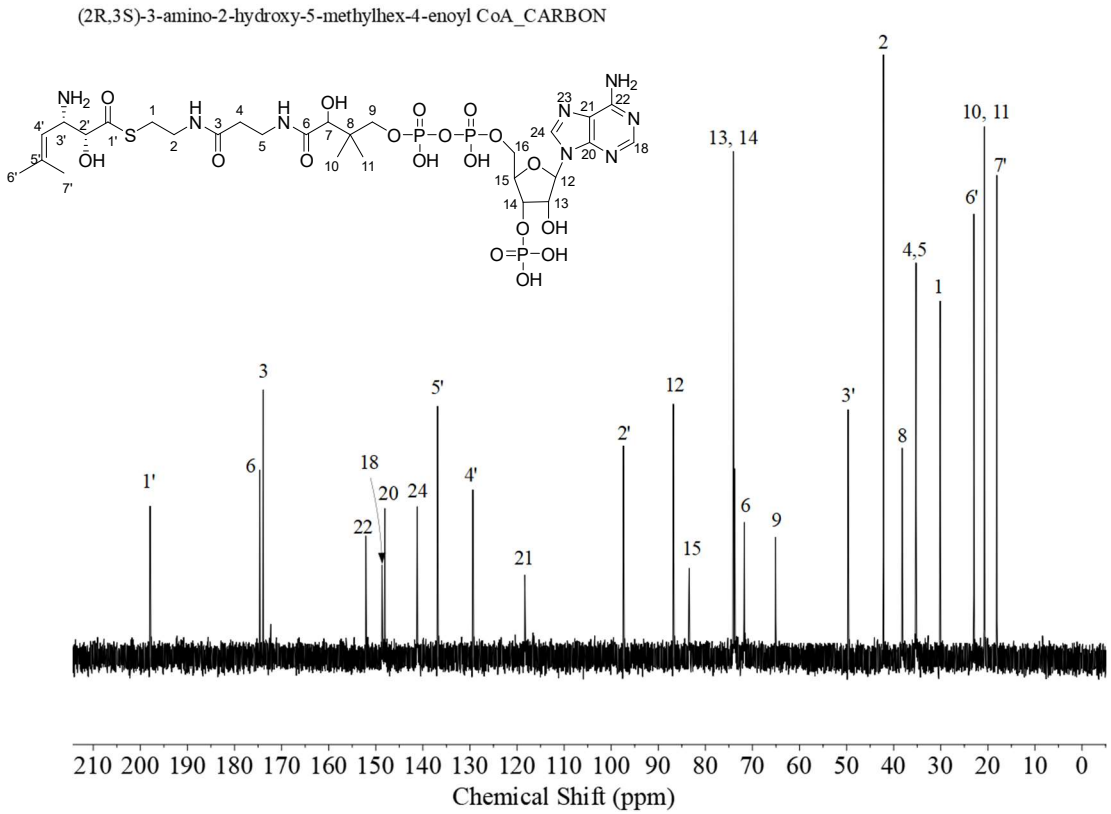

Figure 4.21: ^{13}C NMR of (2*R*,3*S*)-3-amino-2-hydroxy-5-methylhex-4-enoyl CoA.

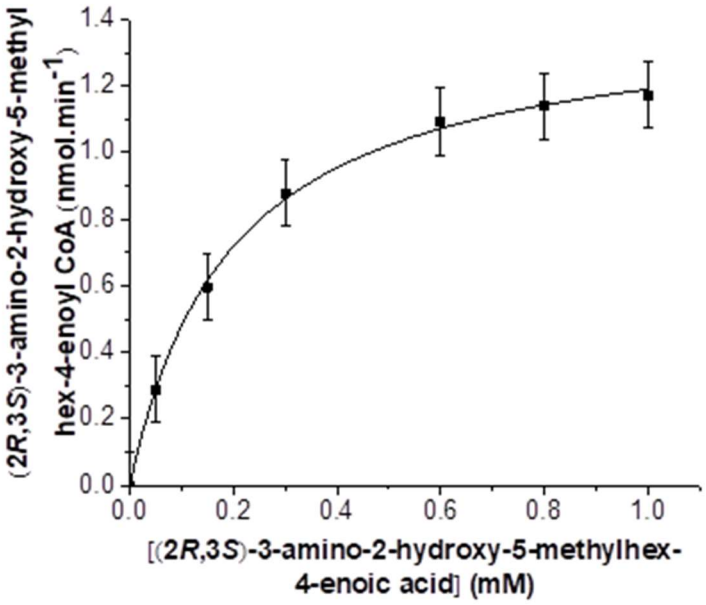

Figure 4.22: Michaelis-Menten kinetics for the turnover of biocatalytic conversion of (2*R*,3*S*)-3-amino-2-hydroxy-5-methylhex-4-enoic acid to (2*R*,3*S*)-3-amino-2-hydroxy-5-methylhex-4-enoyl CoA.

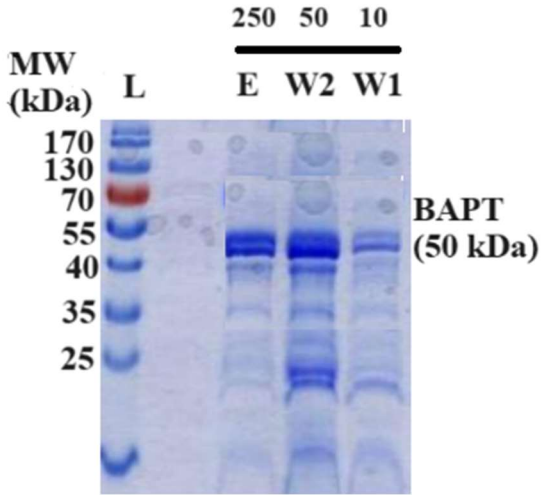

Figure 4.23: Coomassie Blue stained SDS-PAGE gel of aliquots from the fractions collected from Ni-NTA affinity exchange column used to purify the BAPT enzyme. Lanes represent protein contained in the Wash Buffer (**W1** and **W2**); and Elution Buffer (**E**) fractions. The numbers above the bar are the mM concentrations of imidazole in the respective buffers. Molecular weight references are in the leftmost lane.

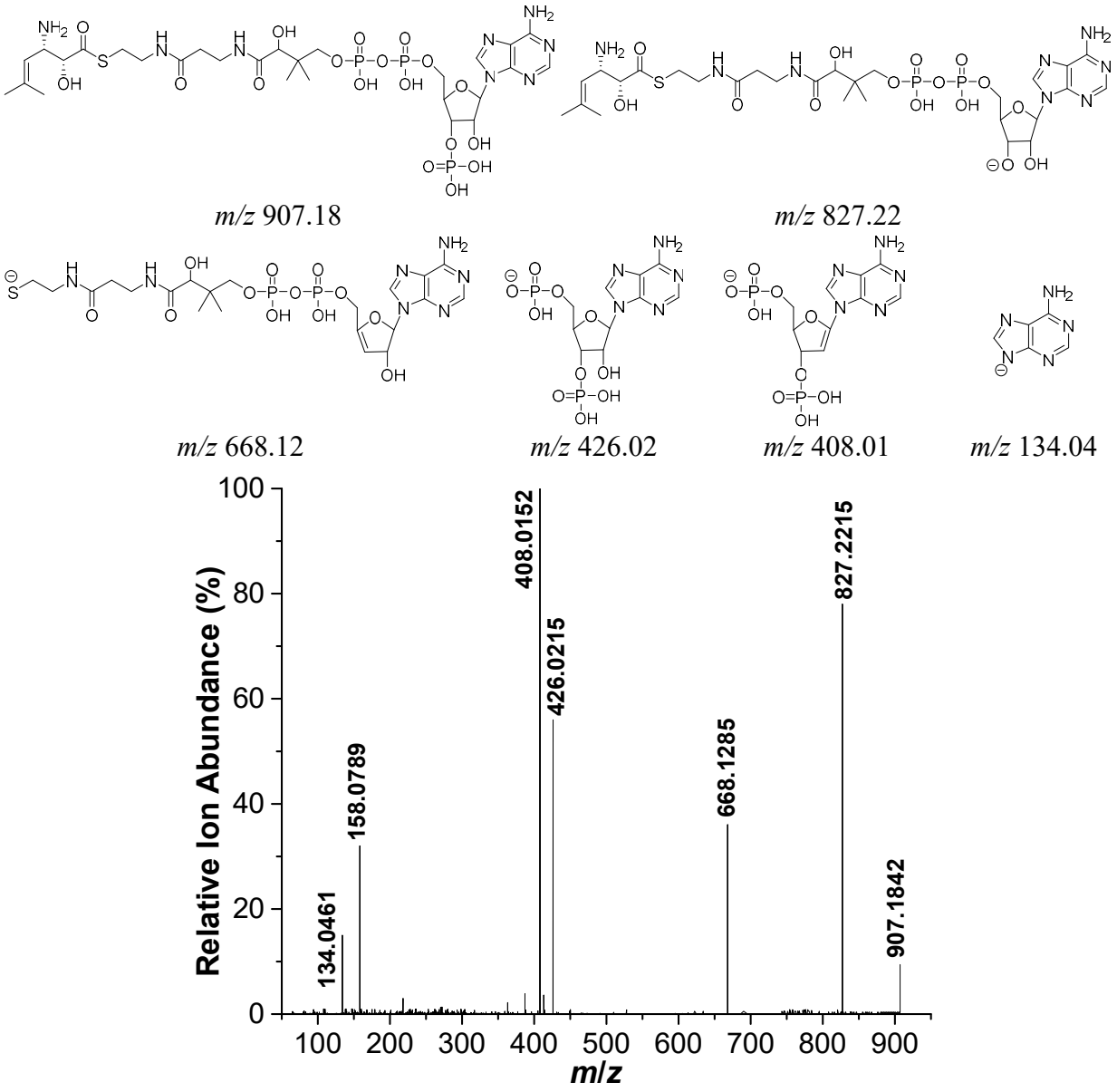

Figure 4.24: LC/ESI-MS/MS (negative-ion mode) of purified (2*R*,3*S*)-3-amino-2-hydroxy-5-methylhex-4-enoyl CoA with peak mass assignments and putative chemical transformations (above spectra).

A

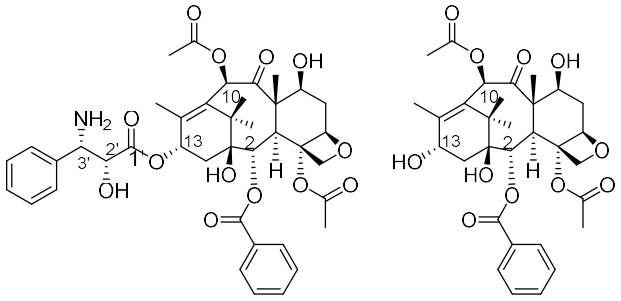

m/z 750.31 *m/z* 587.25

B

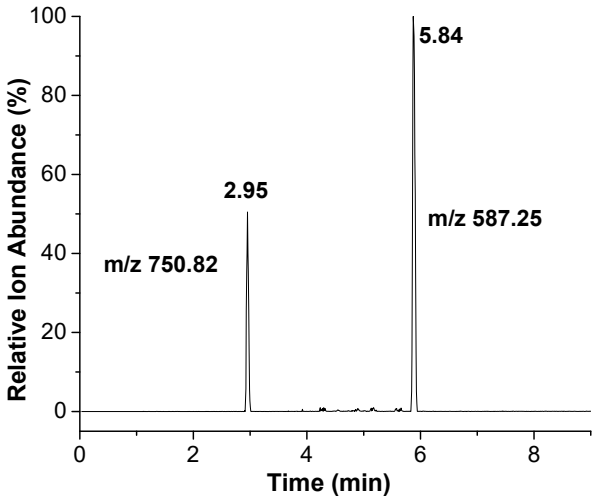

C

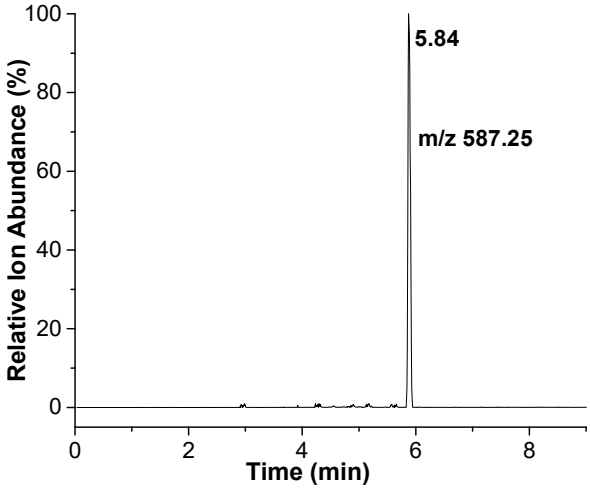

Figure 4.25: (A) Structure of 3′-*N*-debenzoyl-paclitaxel and baccatin III, (B) LC/ESI-MS (selected ion mode for m/z $[M + H]^+$) of the biocatalytic conversion of baccatin III to 3′-*N*-debenzoyl-paclitaxel using Mg^{2+} as cofactor, (c) LC/ESI-MS (selected ion mode for m/z $[M + H]^+$) for control BAPT assay with no Mg^{2+}.

A

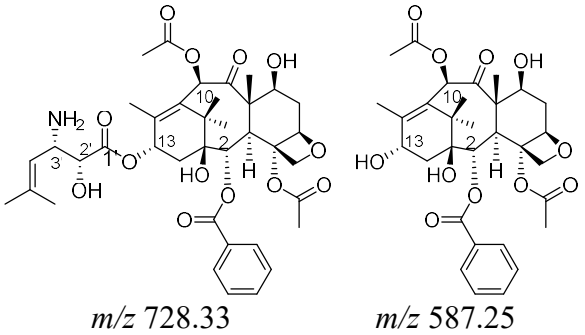

B

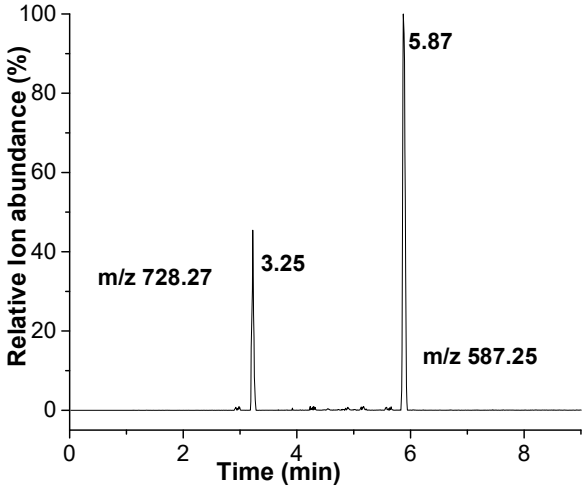

C

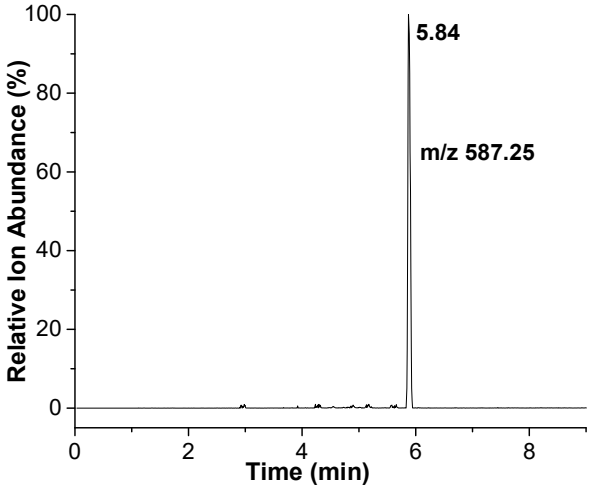

Figure 4.26: (A) Structure of 3′-*N*-de(*tert*-butoxycarbonyl)-SB-T-1212 and baccatin III, (B) LC/ESI-MS (selected ion mode for m/z $[M + H]^+$) of the biocatalytic conversion of baccatin III to 3′-*N*-de(*tert*-butoxycarbonyl)-SB-T-1212 using Mg^{2+} as cofactor, (c) LC/ESI-MS (selected ion mode for m/z $[M + H]^+$) for control BAPT assay with no Mg^{2+}.

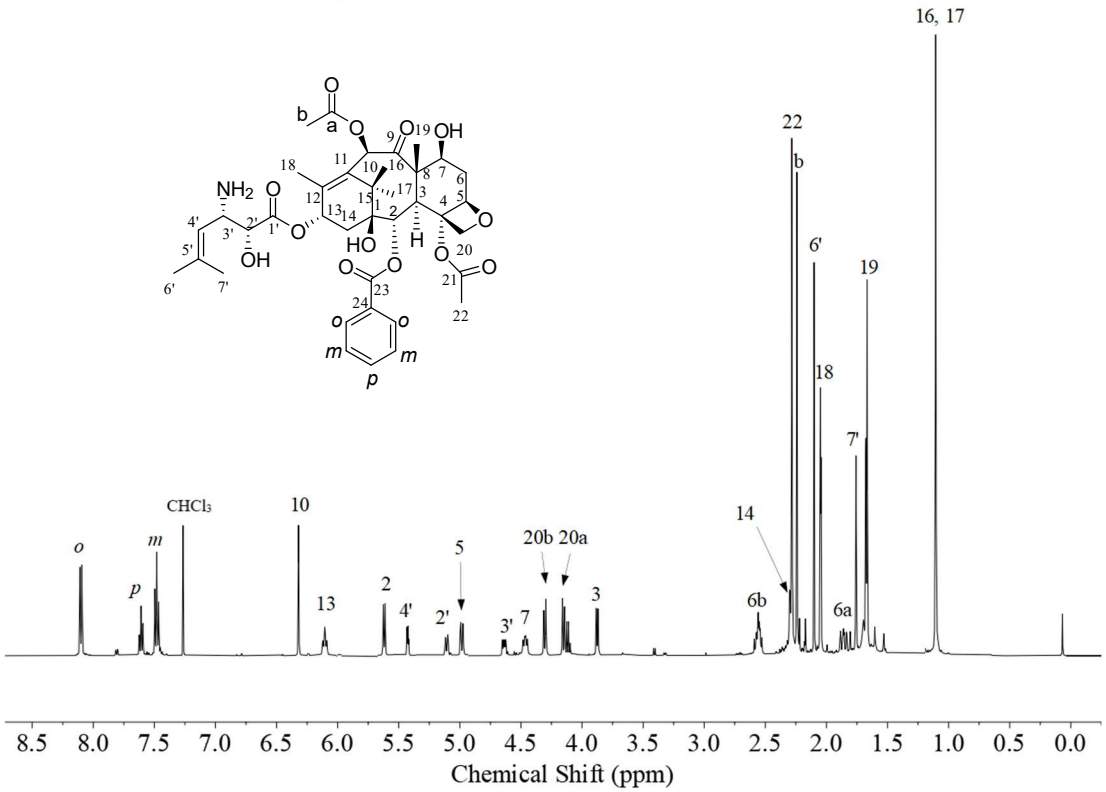

Figure 4.27: ^{1}H NMR of 3'-*N*-de(*tert*-butoxycarbonyl)-SB-T1212.

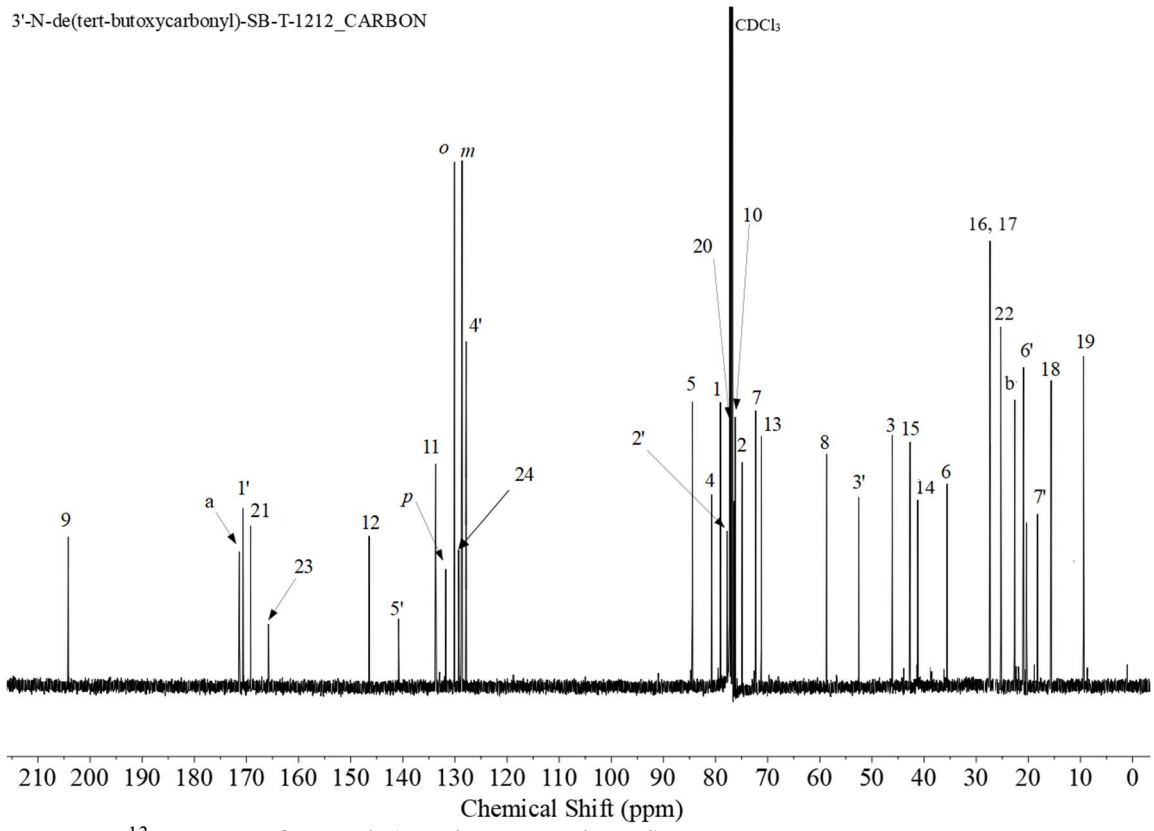

Figure 4.28: ^{13}C NMR of 3'-*N*-de(*tert*-butoxycarbonyl)-SB-T1212.

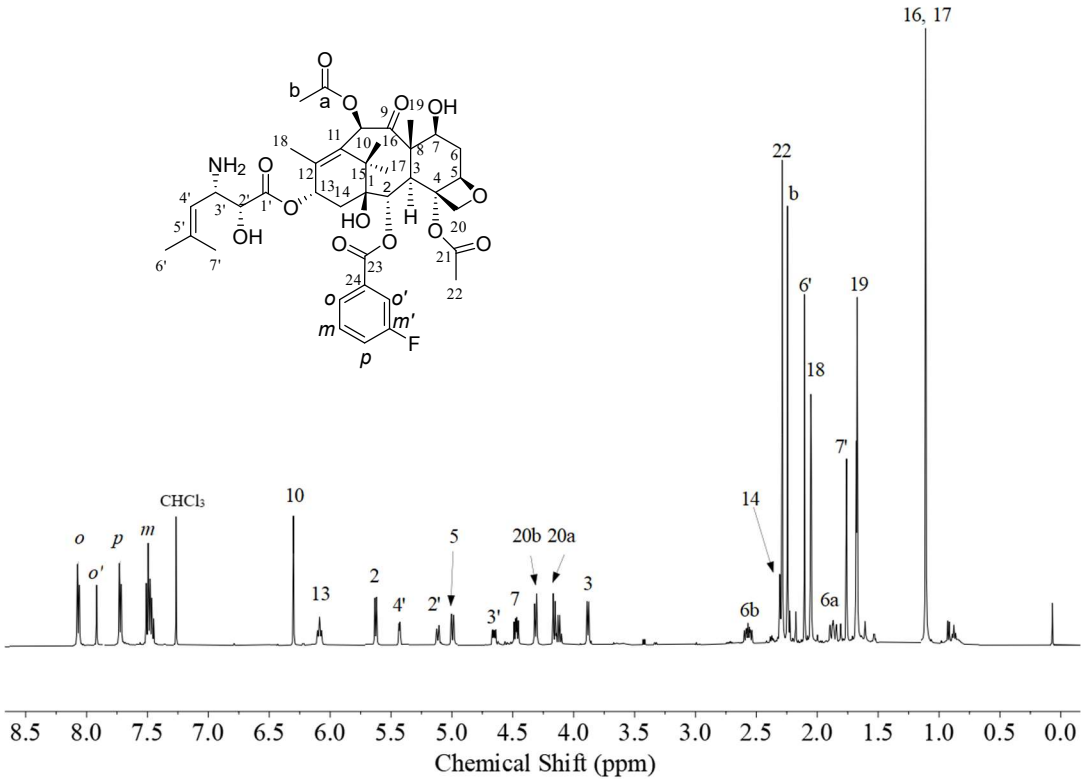

Figure 4.29: ^{1}H NMR of 2-DBz-2-(3-F)Bz-3'-*N*-de(*tert*-butoxycarbonyl)-SB-T1212.

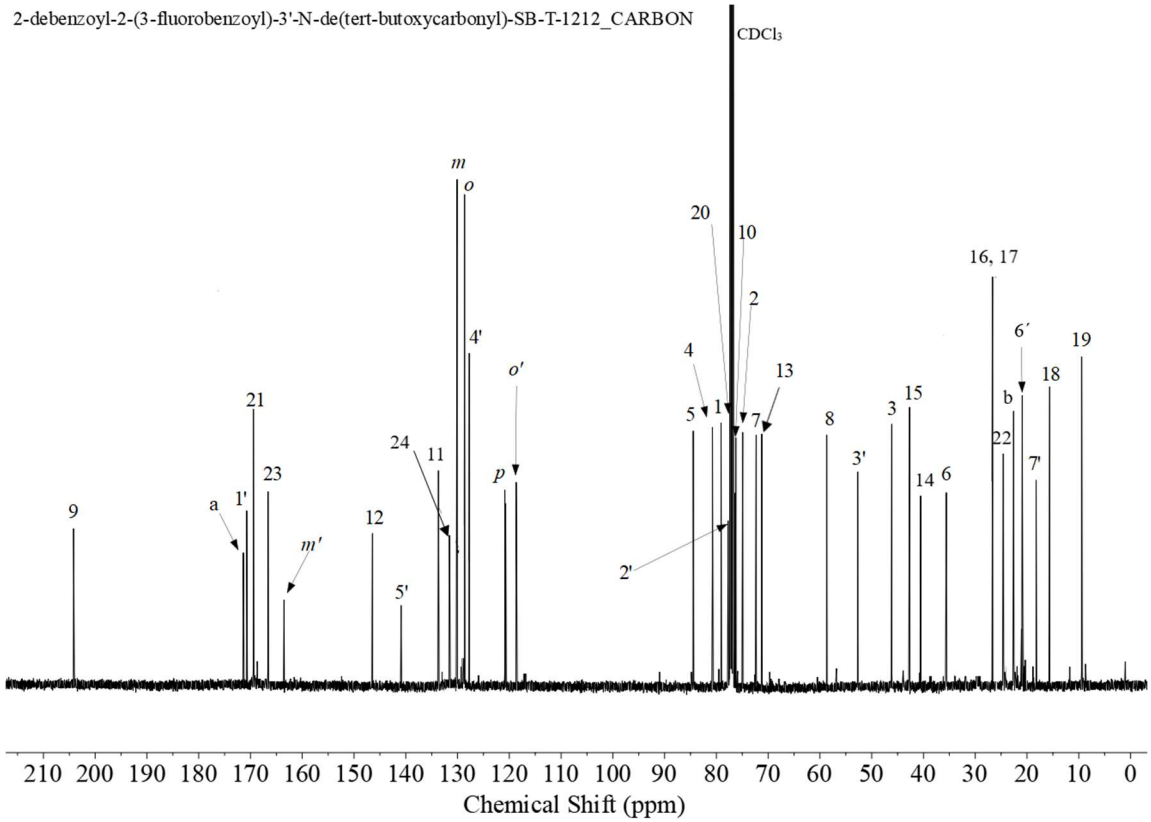

Figure 4.30: ^{13}C NMR of 2-DBz-2-(3-F)Bz-3'-*N*-de(*tert*-butoxycarbonyl)-SB-T1212.

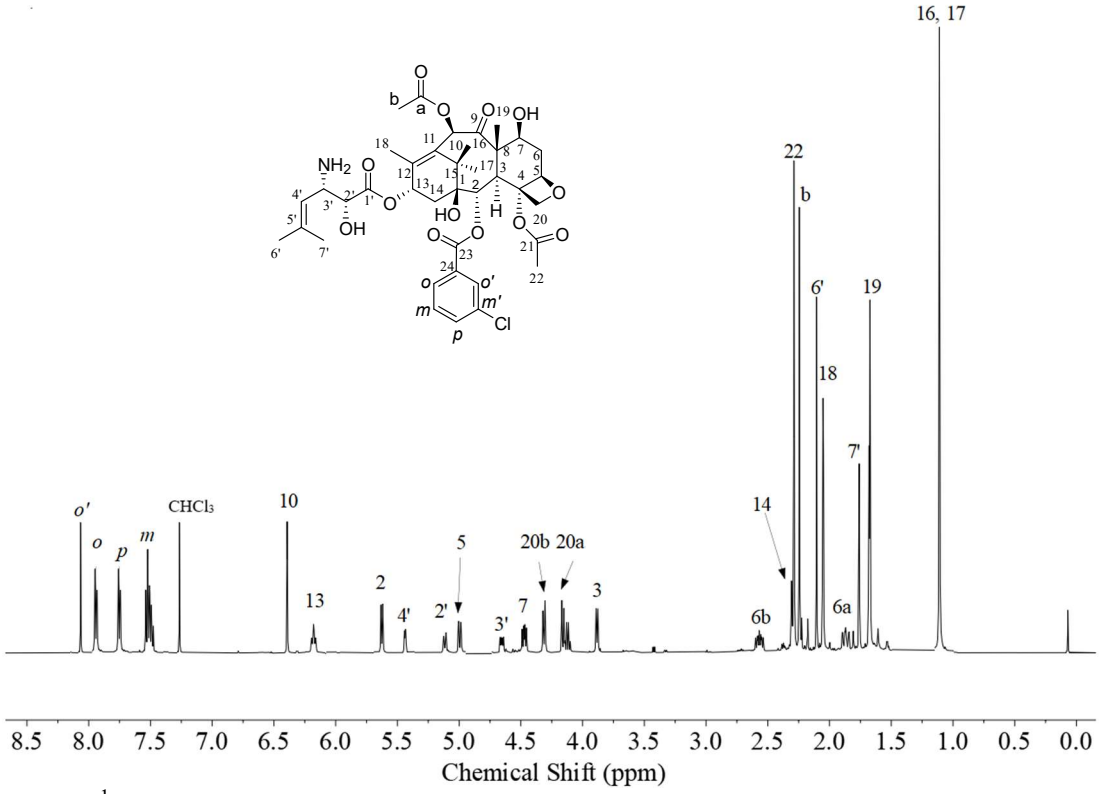

Figure 4.31: ^{1}H NMR of 2-DBz-2-(3-Cl)Bz-3'-*N*-de(*tert*-butoxycarbonyl)-SB-T1212.

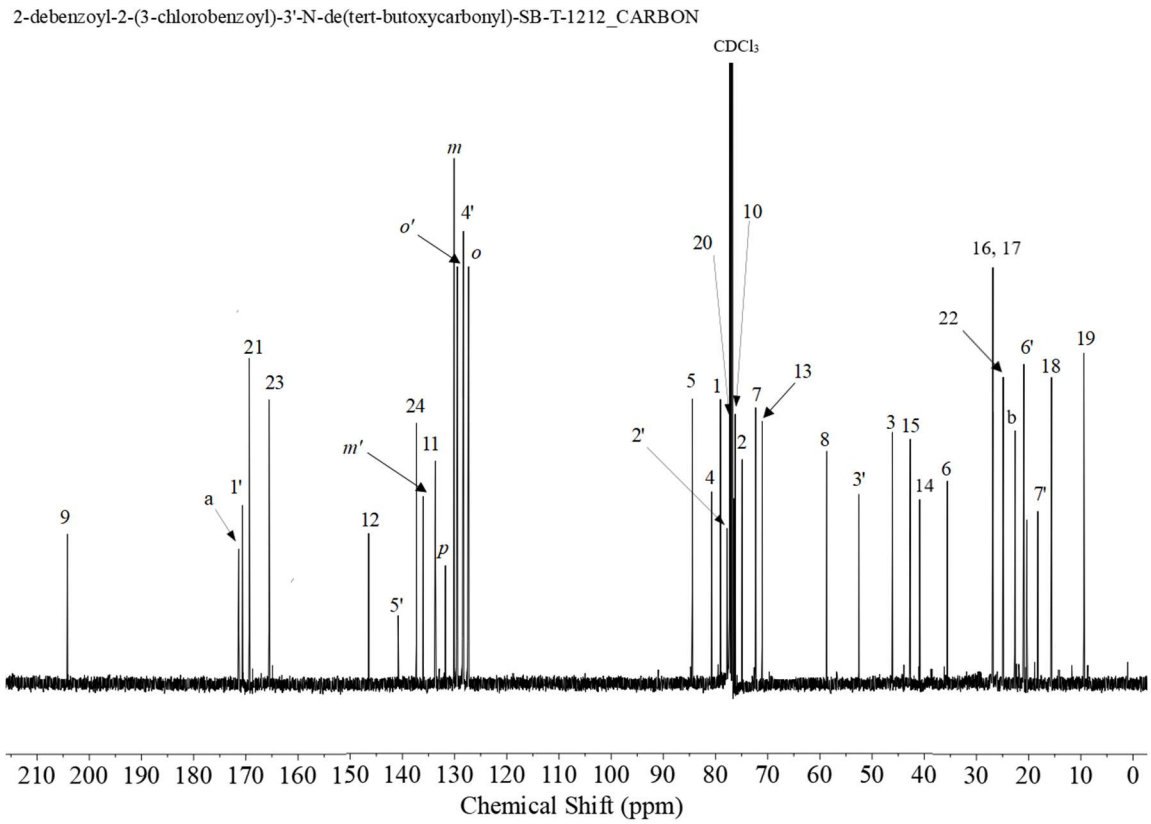

Figure 4.32: ^{13}C NMR of 2-DBz-2-(3-Cl)Bz-3'-*N*-de(*tert*-butoxycarbonyl)-SB-T1212.

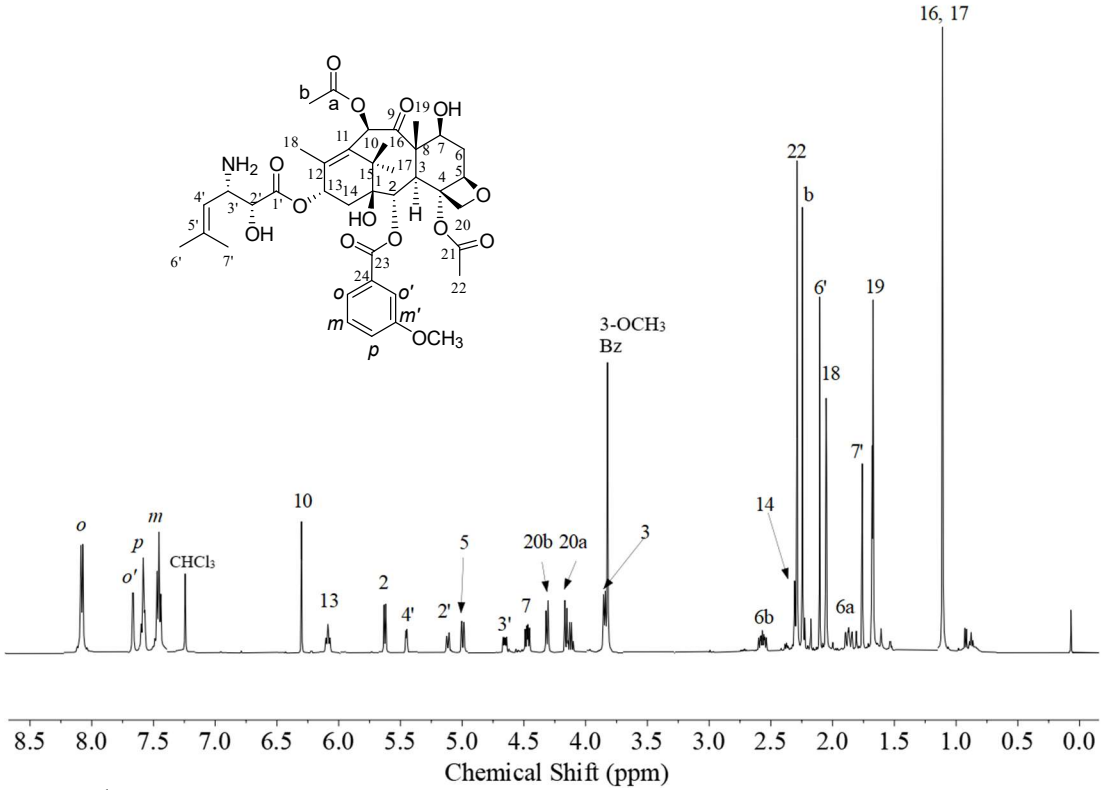

Figure 4.33: ^{1}H NMR of 2-DBz-2-(3-OCH$_3$)Bz-3'-*N*-de(*tert*-butoxycarbonyl)-SB-T1212.

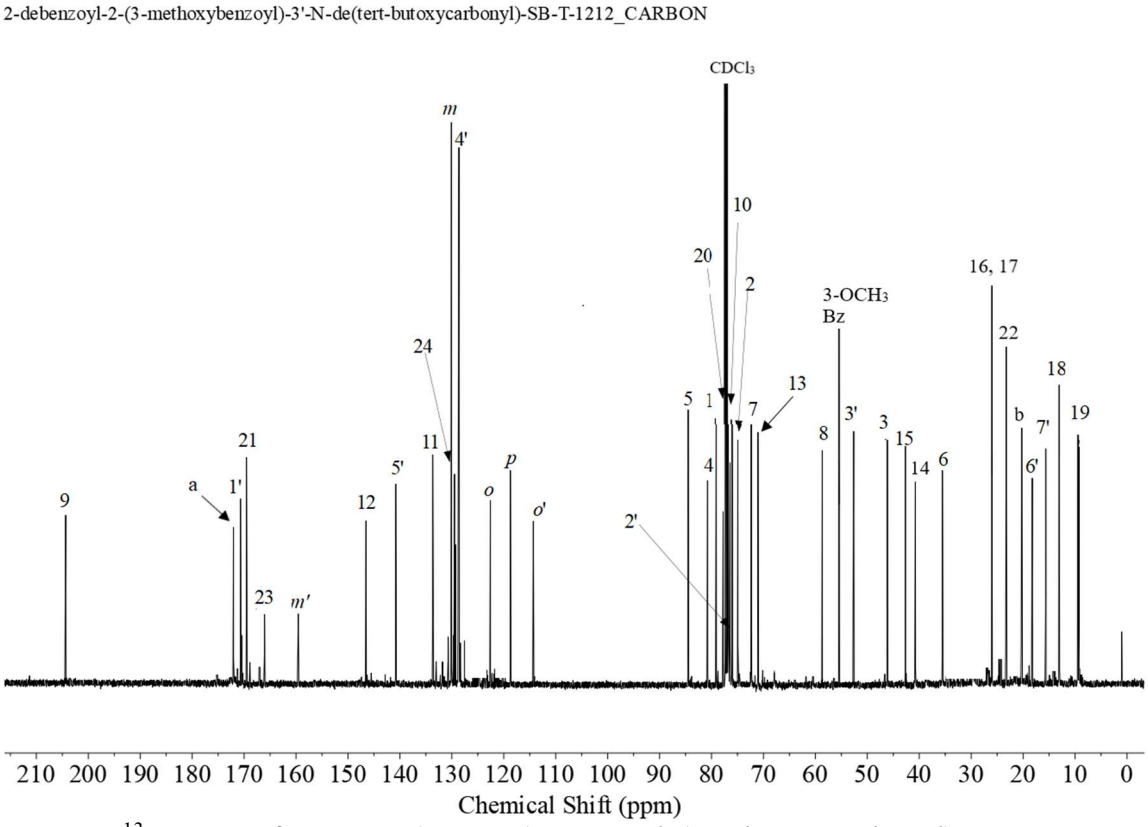

Figure 4.34: ^{13}C NMR of 2-DBz-2-(3-OCH_3)Bz-3'-*N*-de(*tert*-butoxycarbonyl)-SB-T1212.

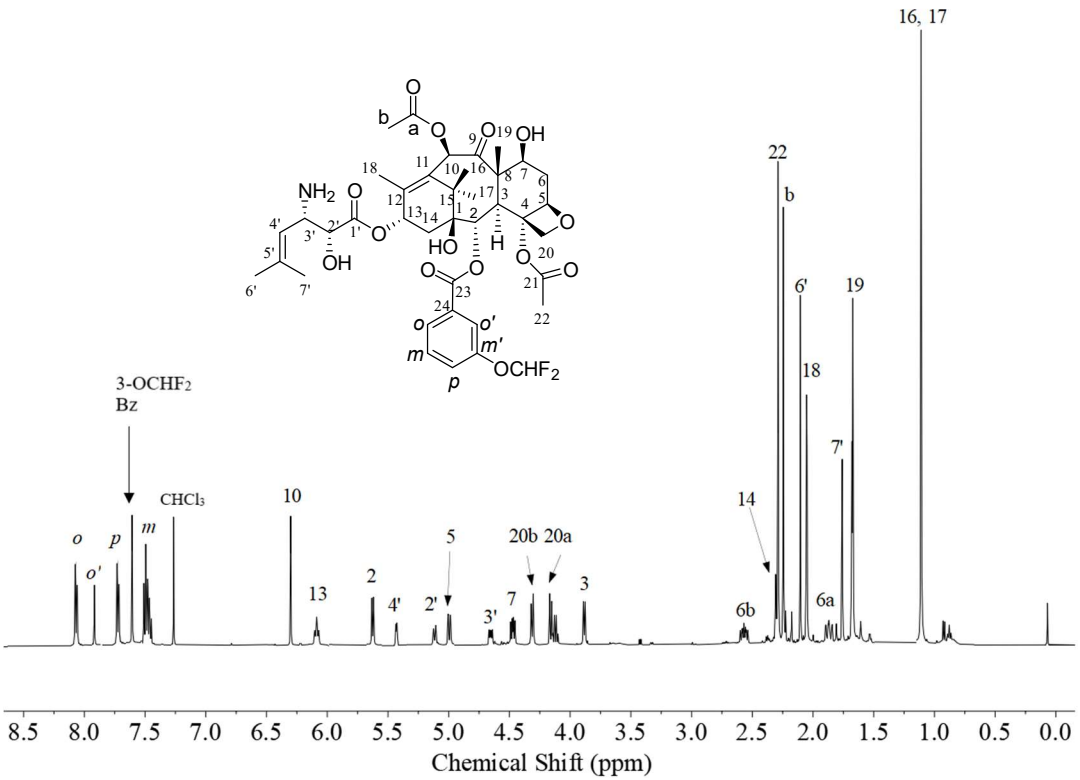

Figure 4.35: ^{1}H NMR of 2-DBz-2-(3-$OCHF_2$)Bz-3'-*N*-de(*tert*-butoxycarbonyl)-SB-T1212.

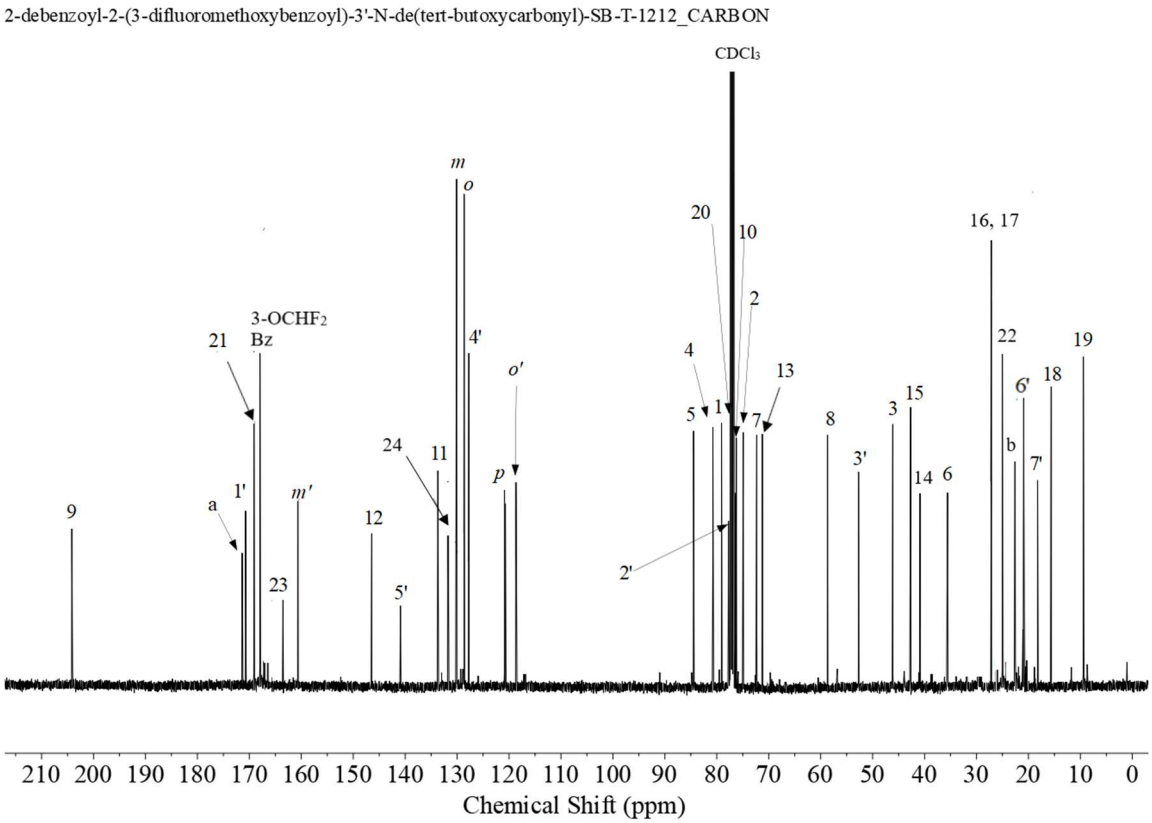

Figure 4.36: ^{13}C NMR of 2-DBz-2-(3-OCHF$_2$)Bz-3'-*N*-de(*tert*-butoxycarbonyl)-SB-T-1212.

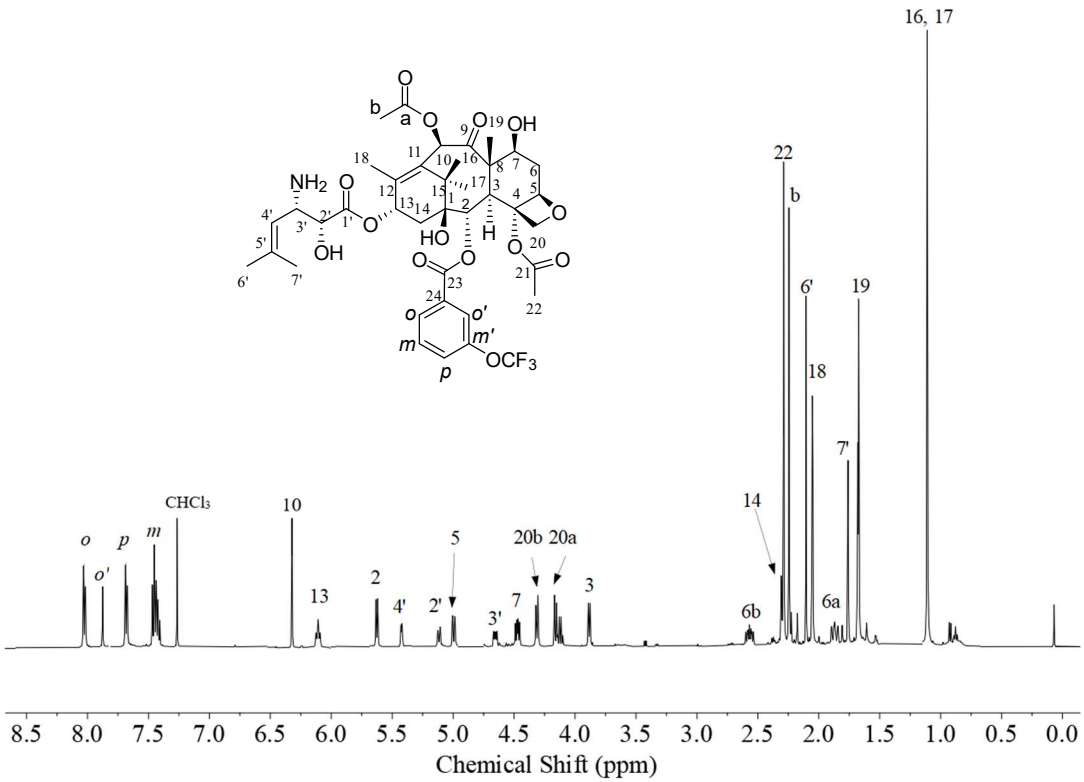

Figure 4.37: ^{1}H NMR of 2-DBz-2-(3-OCF_3)Bz-3'-*N*-de(*tert*-butoxycarbonyl)-SB-T1212.

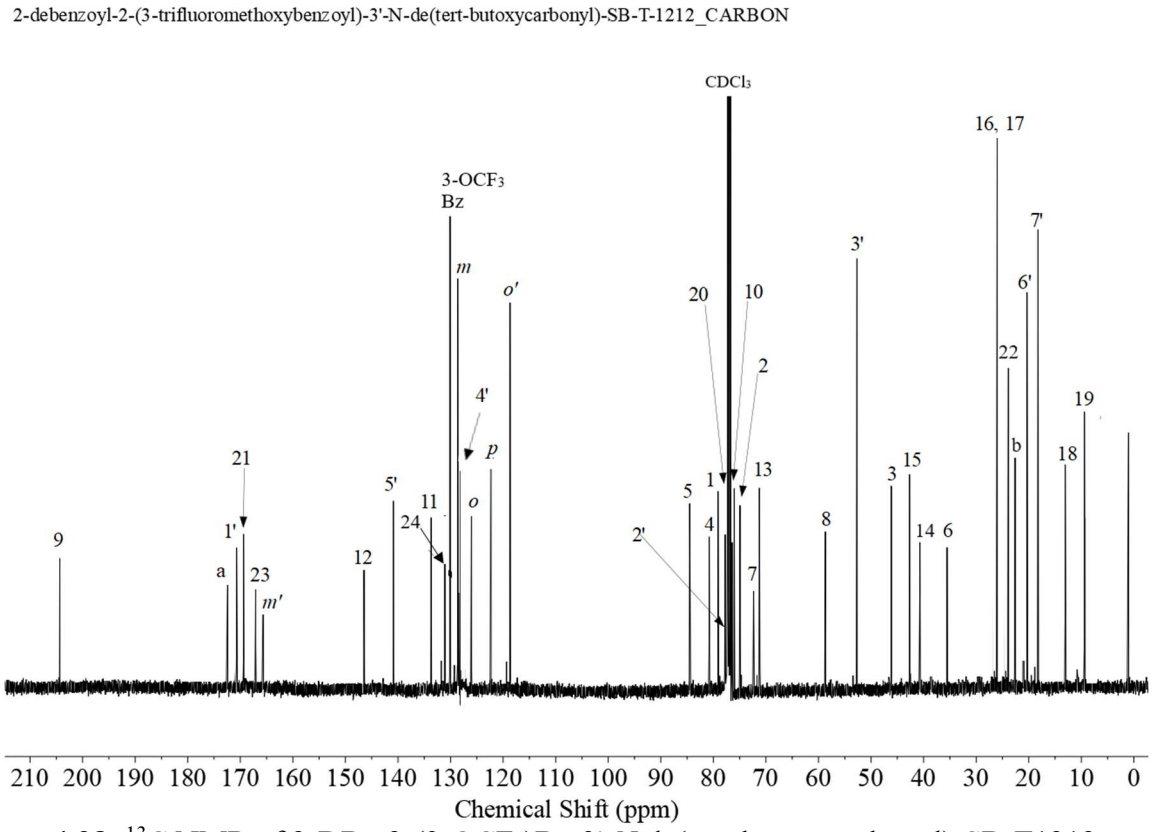

Figure 4.38: ^{13}C NMR of 2-DBz-2-(3-OCF_3)Bz-3'-*N*-de(*tert*-butoxycarbonyl)-SB-T1212.

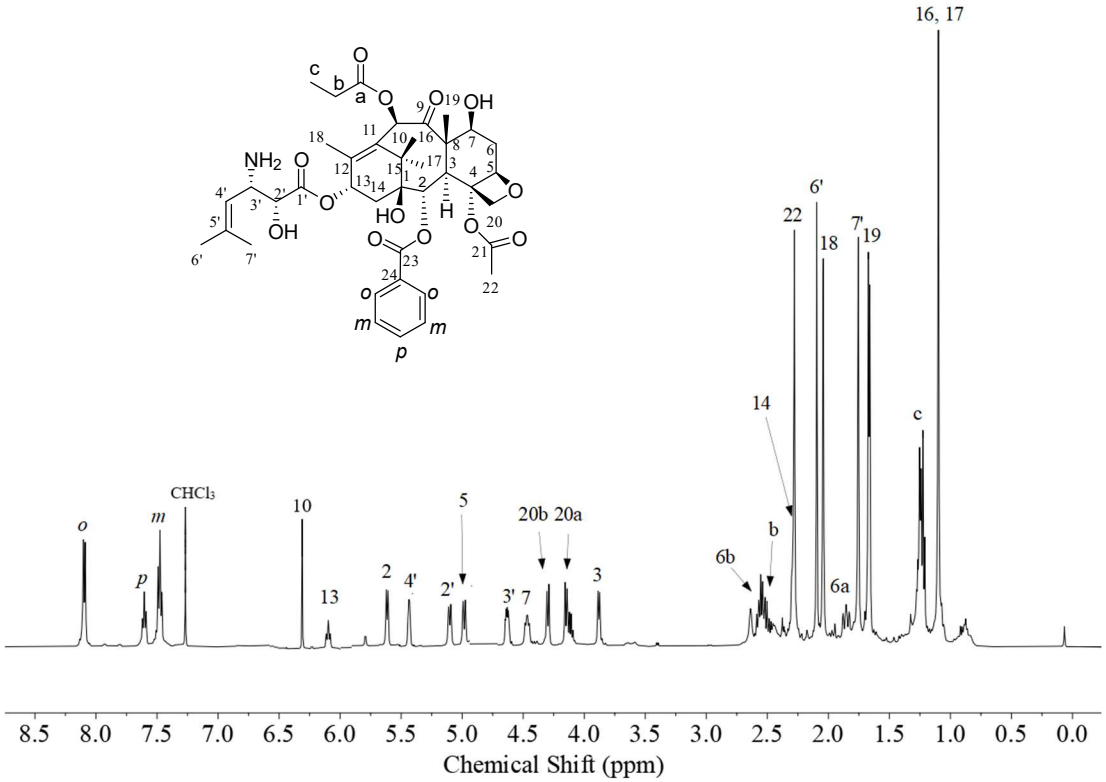

Figure 4.39: ^{1}H NMR of 3'-*N*-de(*tert*-butoxycarbonyl)-SB-T-1213.

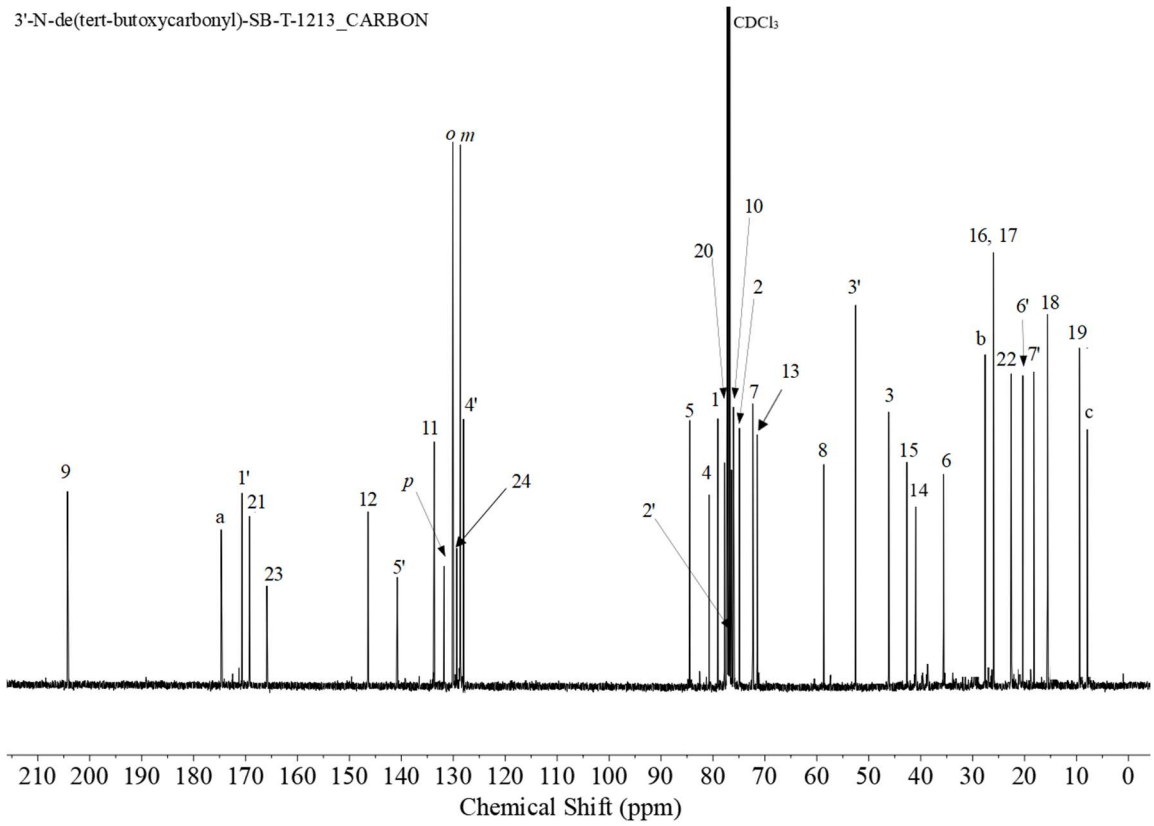

Figure 4.40: ^{13}C NMR of 3'-*N*-de(*tert*-butoxycarbonyl)-SB-T-1213.

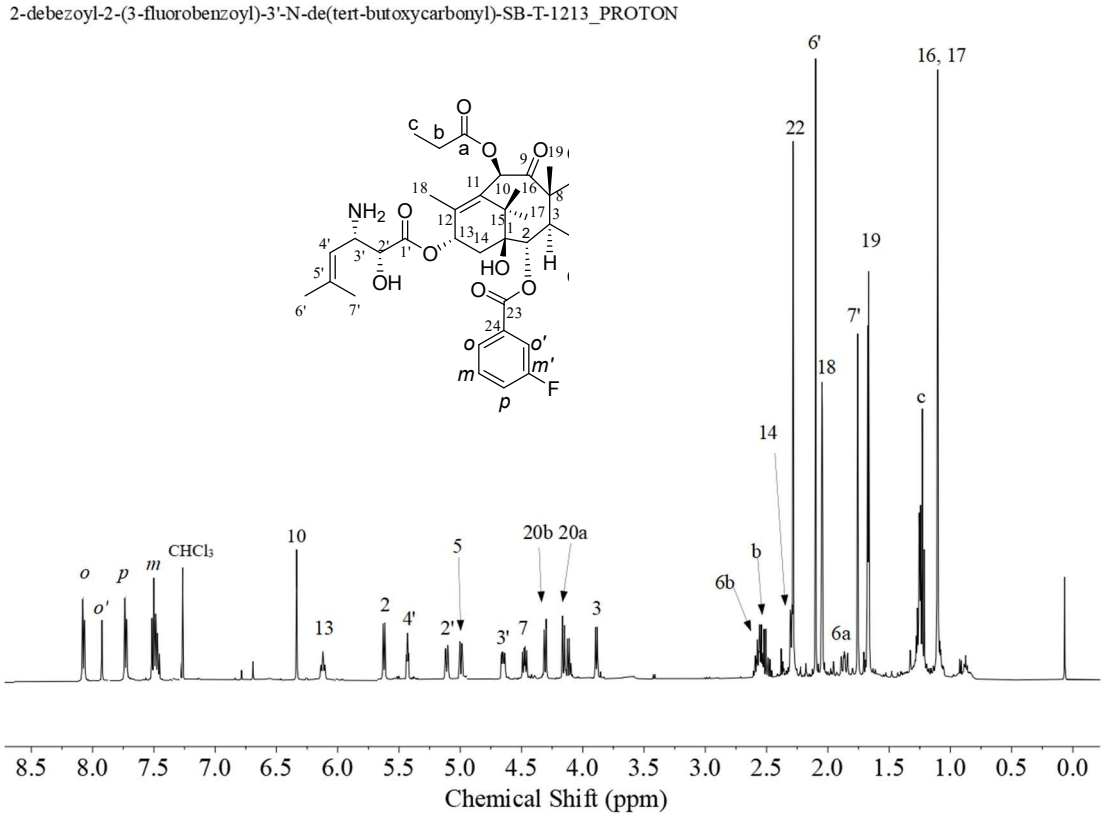

Figure 4.41: ^{1}H NMR of 2-DBz-2-(3-F)Bz-3'-*N*-de(*tert*-butoxycarbonyl)-SB-T1213.

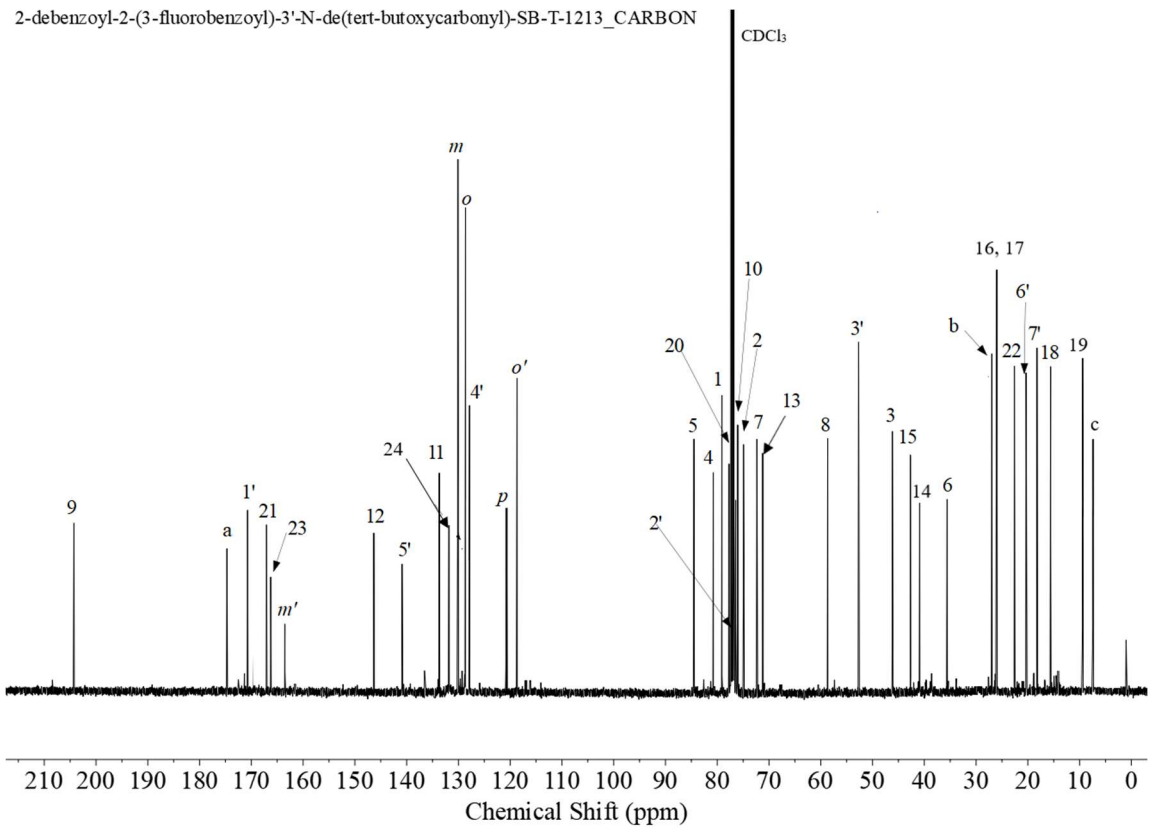

Figure 4.42: ^{13}C NMR of 2-DBz-2-(3-F)Bz-3'-*N*-de(*tert*-butoxycarbonyl)-SB-T1213.

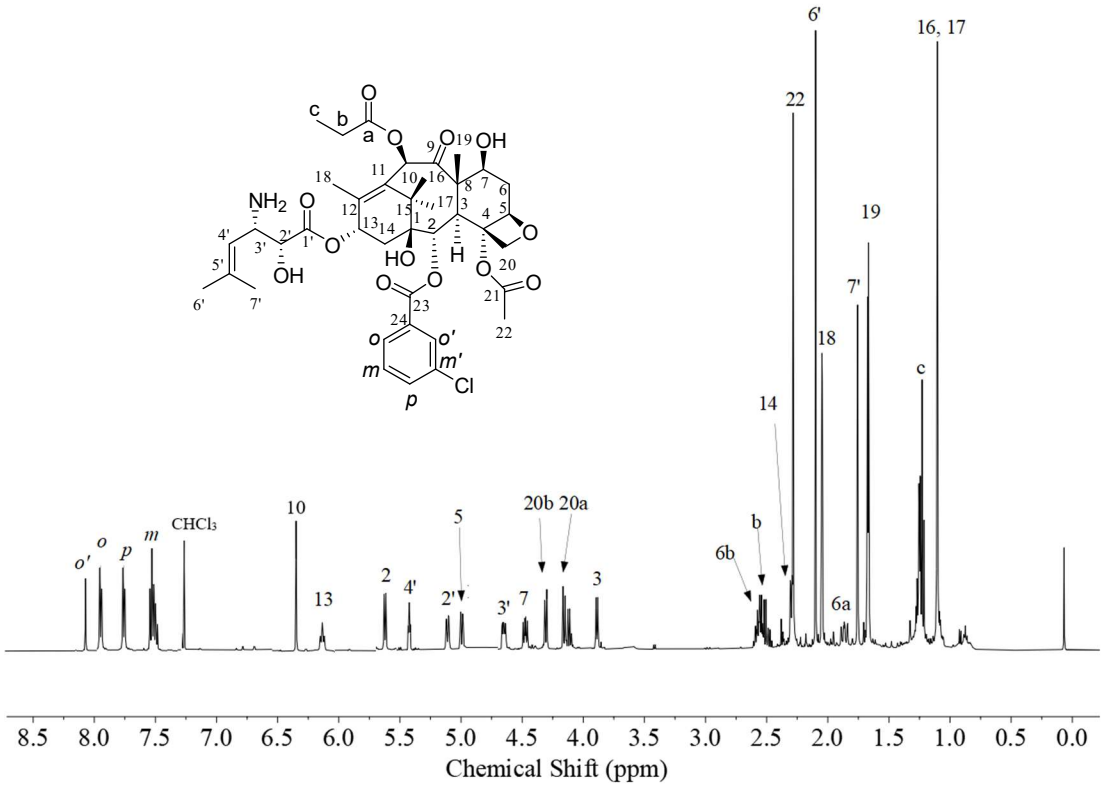

Figure 4.43: ^{1}H NMR of 2-DBz-2-(3-Cl)Bz-3'-*N*-de(*tert*-butoxycarbonyl)-SB-T1213.

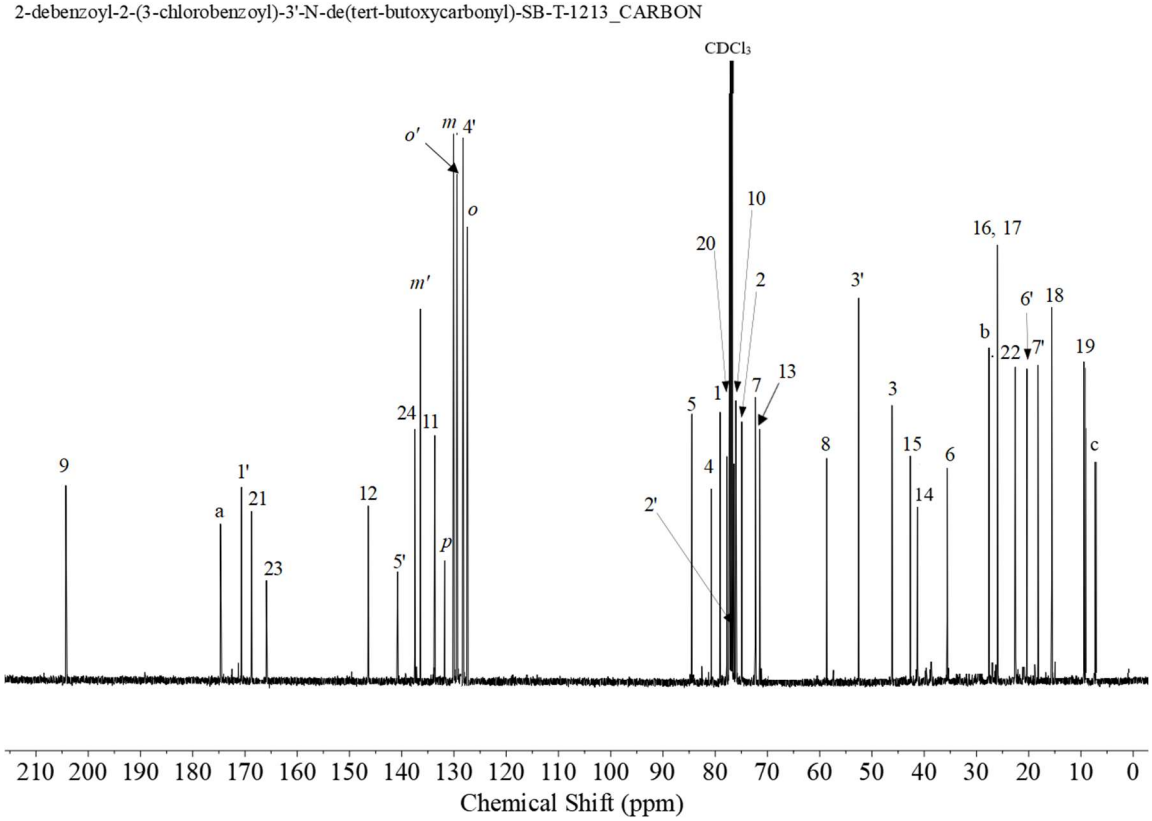

Figure 4.44: ^{13}C NMR of 2-DBz-2-(3-Cl)Bz-3'-*N*-de(*tert*-butoxycarbonyl)-SB-T1213.

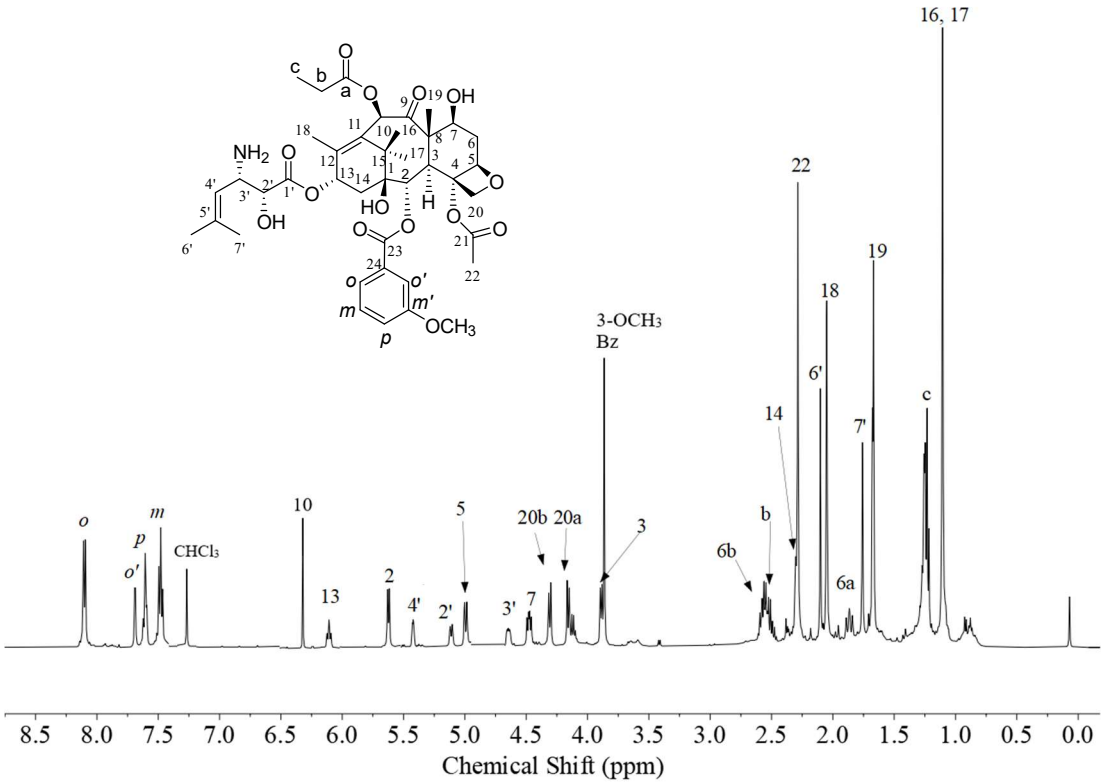

Figure 4.45: ^{1}H NMR of 2-DBz-2-(3-OCH$_3$)Bz-3'-*N*-de(*tert*-butoxycarbonyl)-SB-T1213.

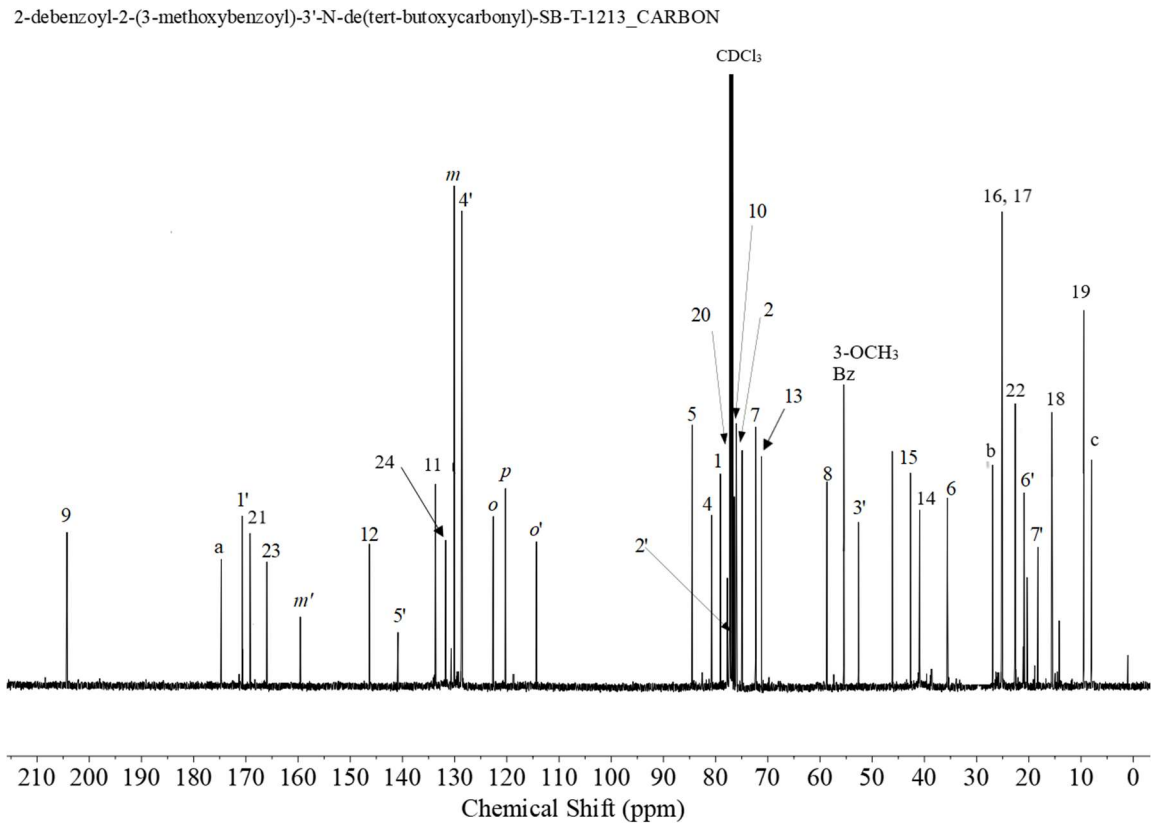

Figure 4.46: ^{13}C NMR of 2-DBz-2-(3-OCH_3)Bz-3'-*N*-de(*tert*-butoxycarbonyl)-SB-T1213.

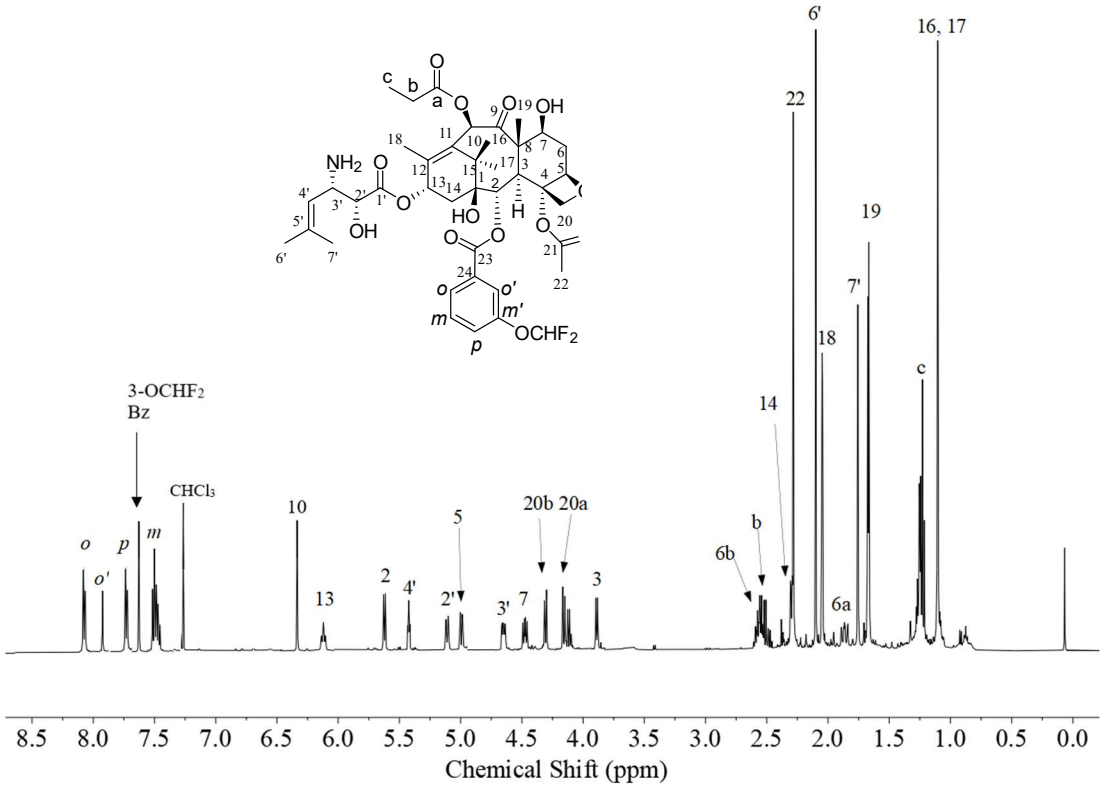

Figure 4.47: ^{1}H NMR of 2-DBz-2-(3-$OCHF_2$)Bz-3'-*N*-de(*tert*-butoxycarbonyl)-SB-T1213.

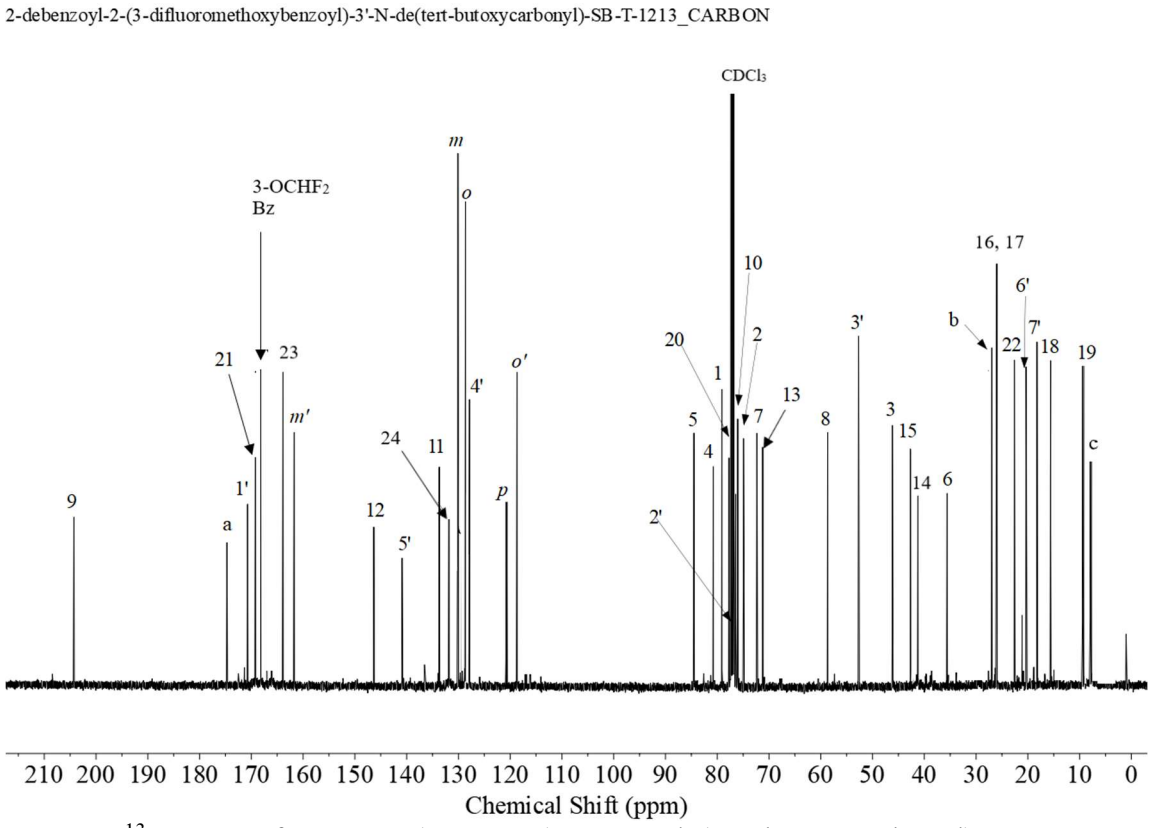

Figure 4.48: ^{13}C NMR of 2-DBz-2-(3-OCHF$_2$)Bz-3'-*N*-de(*tert*-butoxycarbonyl)-SB-T1213.

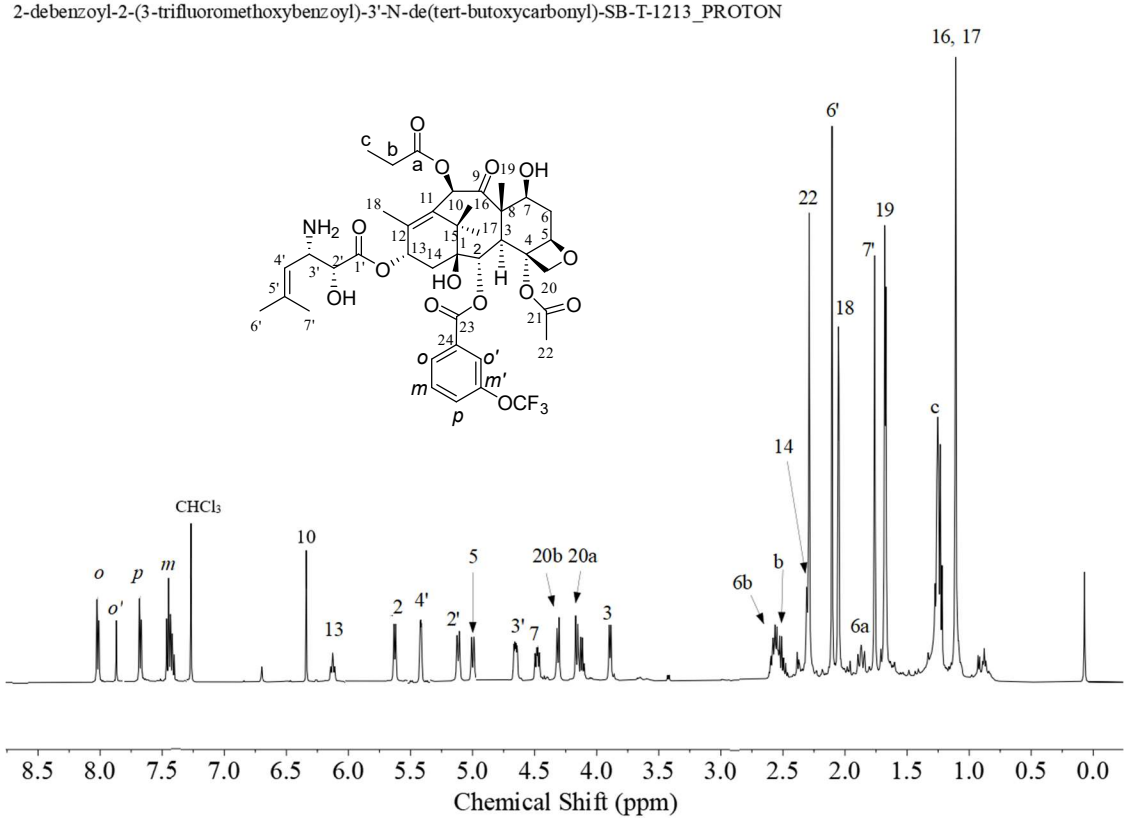

Figure 4.49: ^{1}H NMR of 2-DBz-2-(3-OCF3)Bz-3'-*N*-de(*tert*-butoxycarbonyl)-SB-T1213.

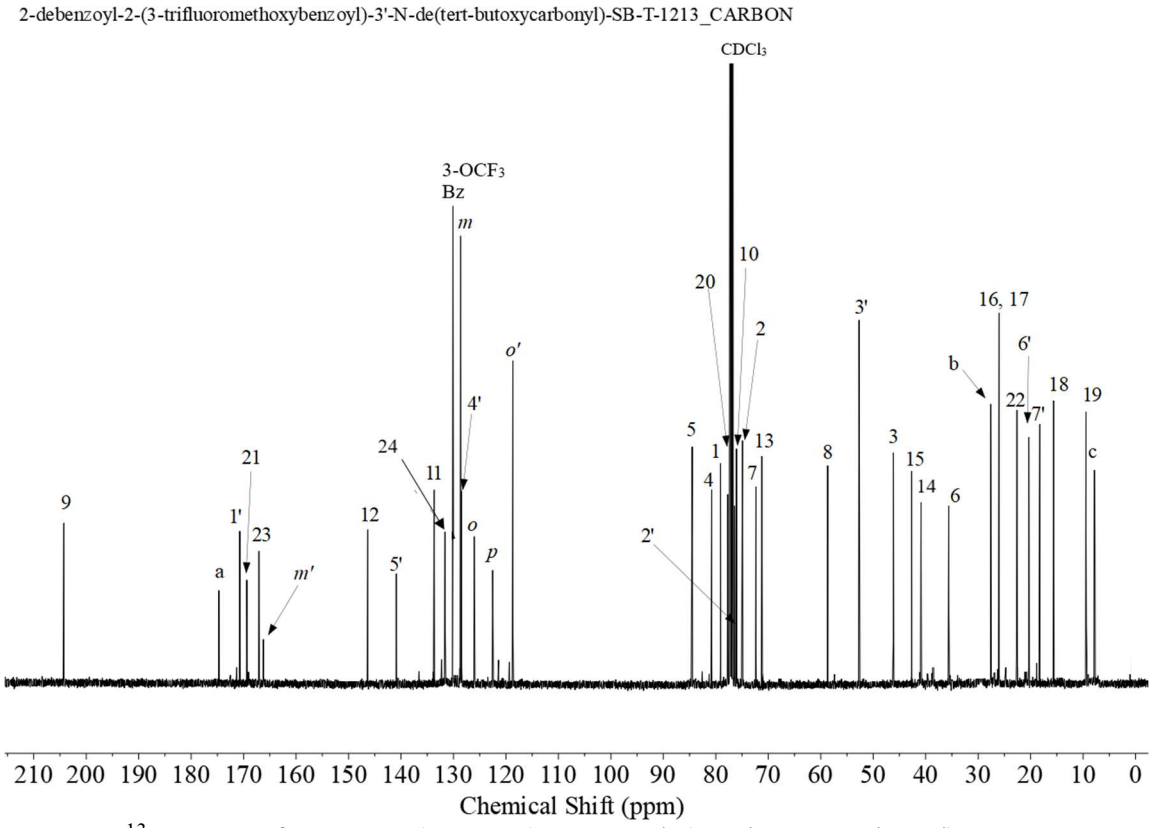

Figure 4.50: ^{13}C NMR of 2-DBz-2-(3-OCF3)Bz-3'-*N*-de(*tert*-butoxycarbonyl)-SB-T1213.

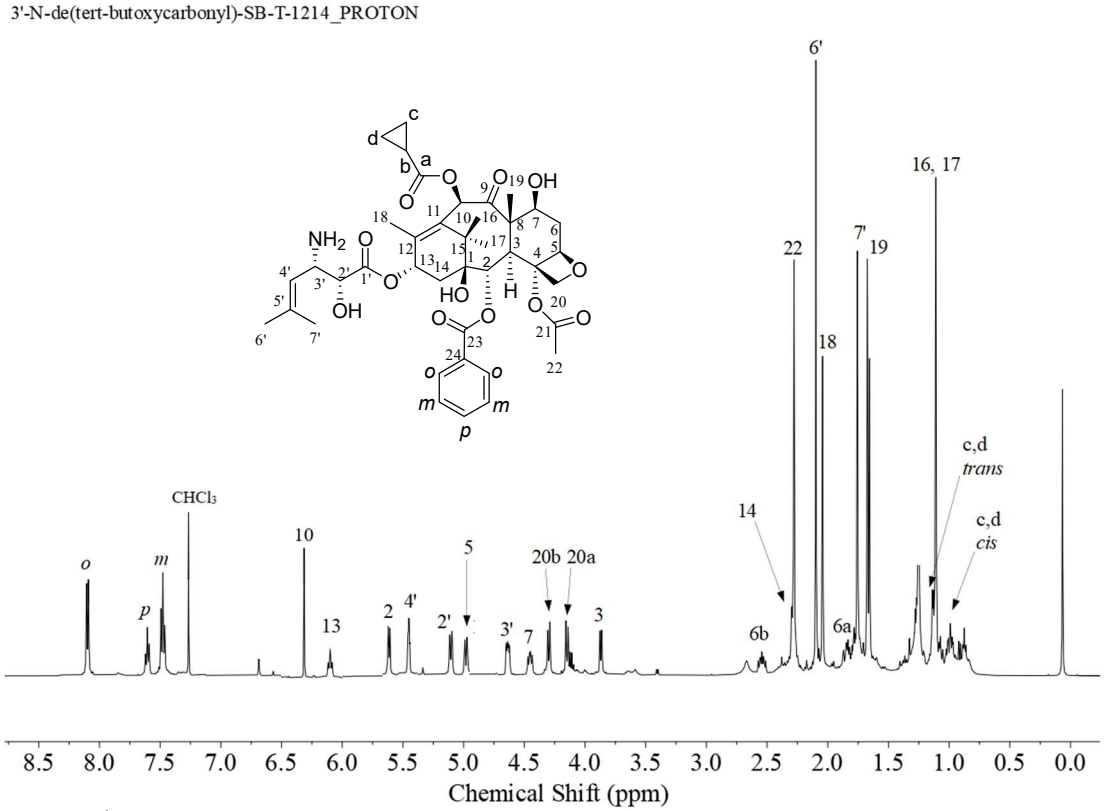

Figure 4.51: ^{1}H NMR of 3'-*N*-de(*tert*-butoxycarbonyl)-SB-T-1214.

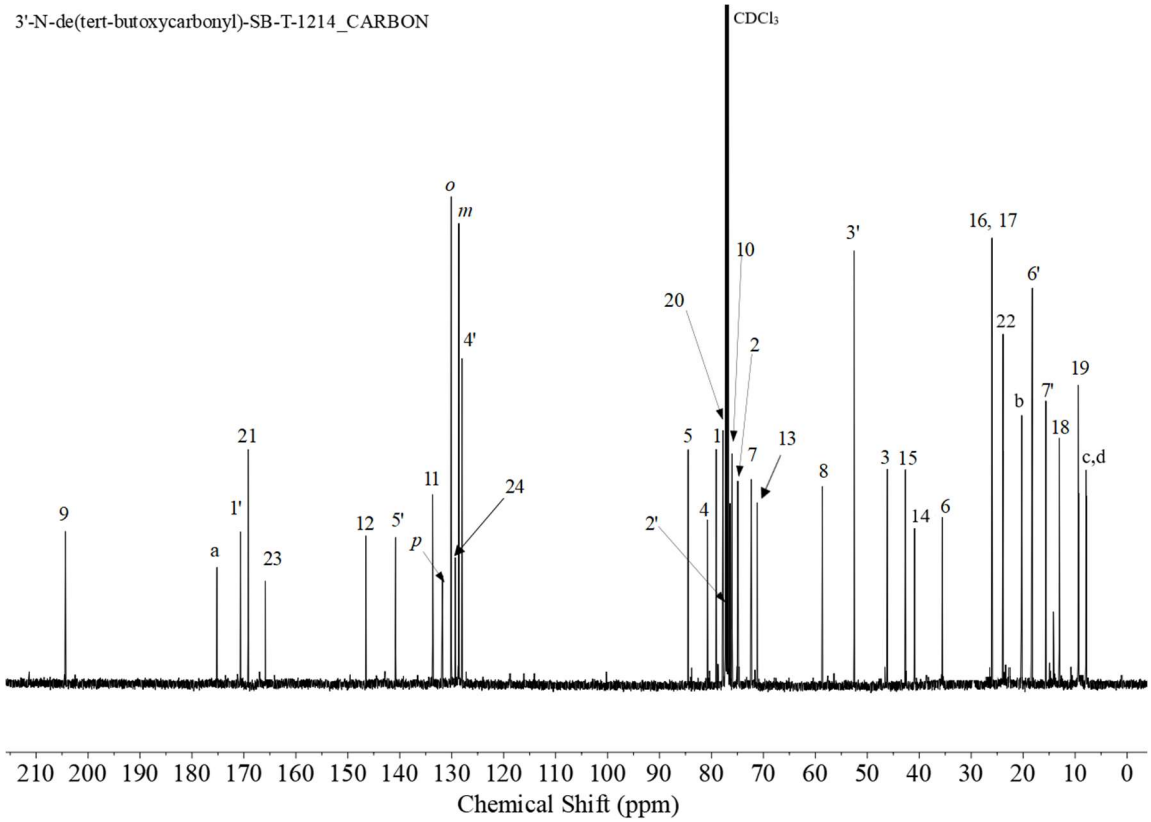

Figure 4.52: ^{13}C NMR of 3'-*N*-de(*tert*-butoxycarbonyl)-SB-T-1214.

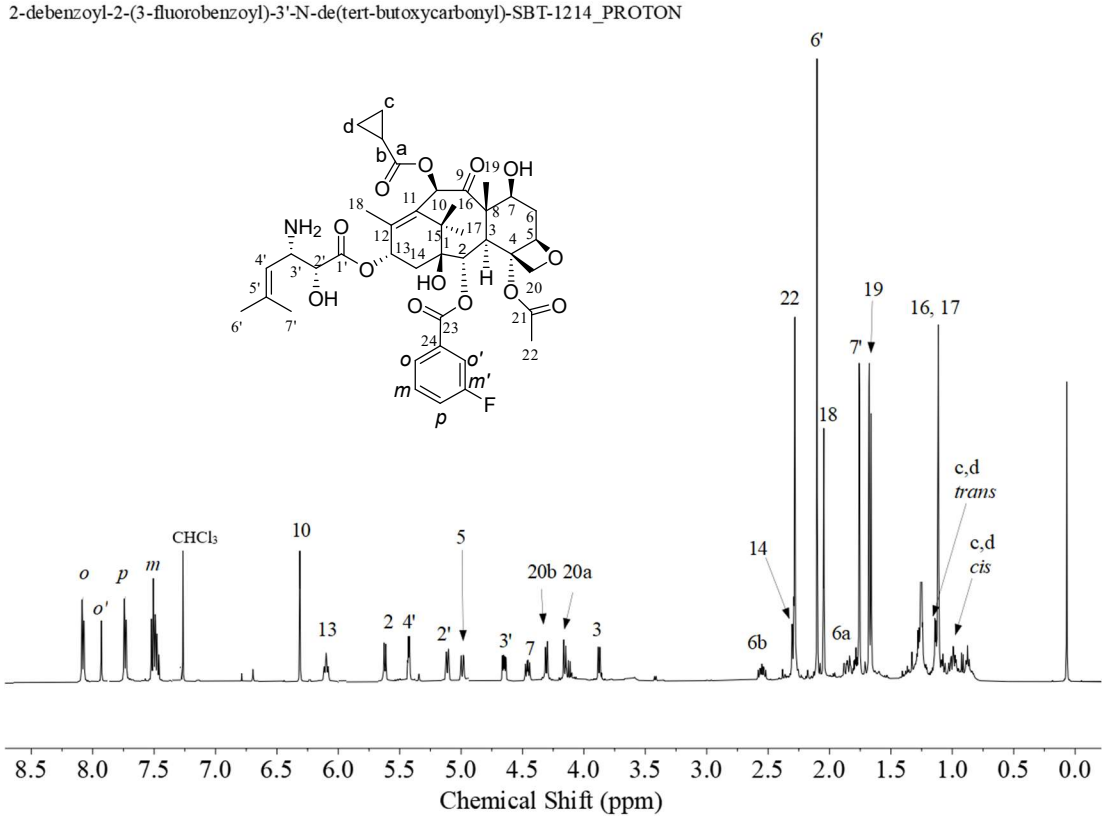

Figure 4.53: ^{1}H NMR of 2-DBz-2-(3-F)Bz-3'-*N*-de(*tert*-butoxycarbonyl)-SB-T-1214.

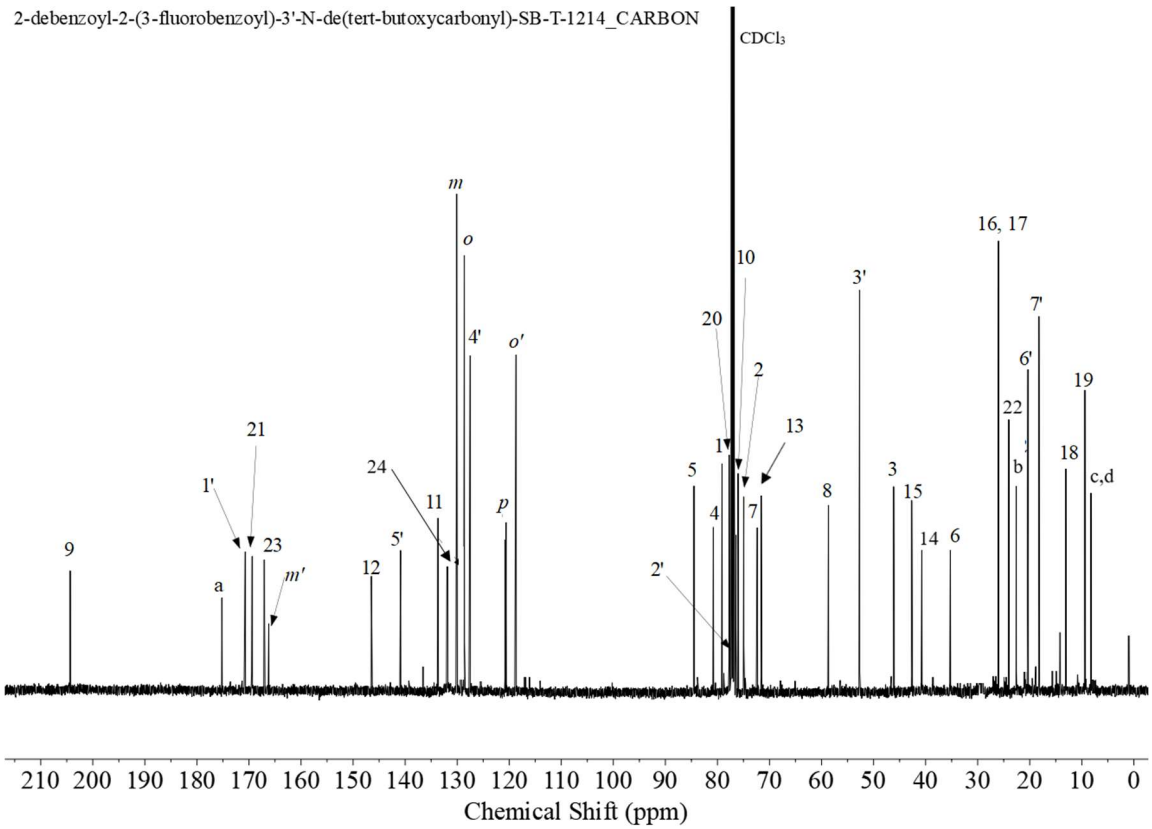

Figure 4.54: ^{13}C NMR of 2-DBz-2-(3-F)Bz-3'-*N*-de(*tert*-butoxycarbonyl)-SB-T-1214.

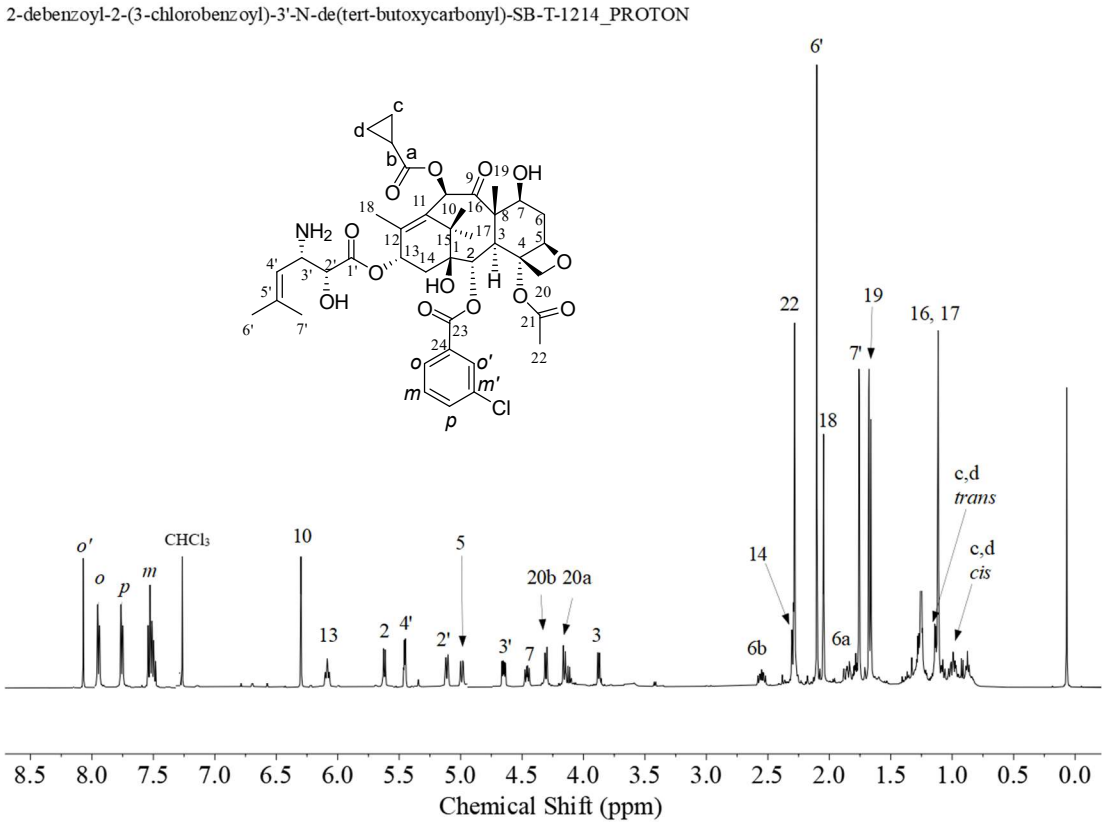

Figure 4.55: ^{1}H NMR of 2-DBz-2-(3-Cl)Bz-3'-*N*-de(*tert*-butoxycarbonyl)-SB-T-1214.

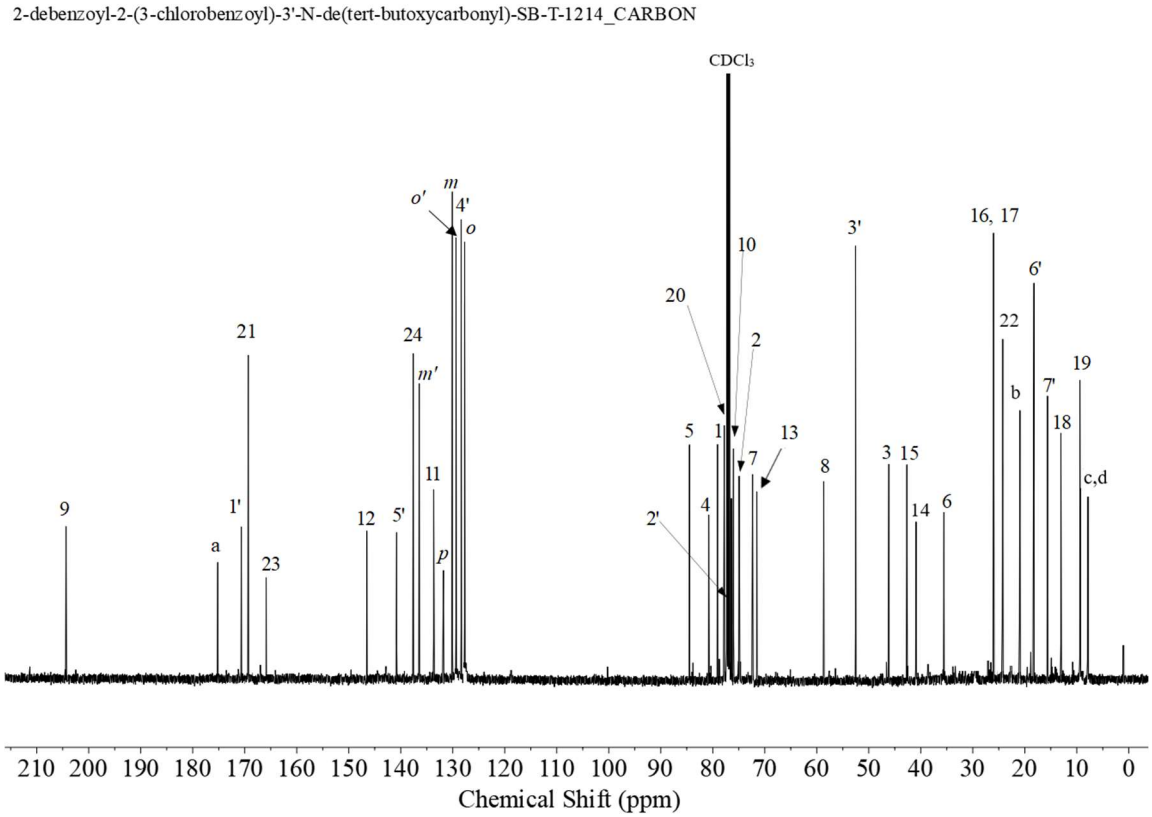

Figure 4.56: ^{13}C NMR of 2-DBz-2-(3-Cl)Bz-3'-*N*-de(*tert*-butoxycarbonyl)-SB-T-1214.

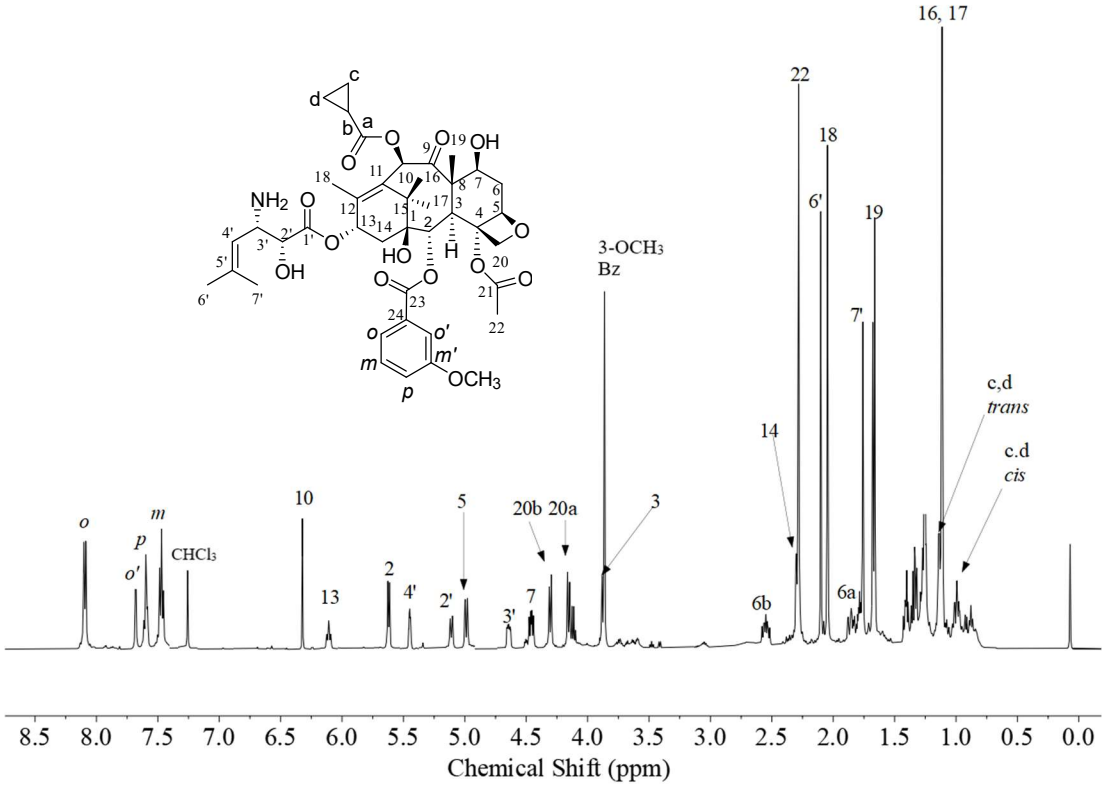

Figure 4.57: ^{1}H NMR of 2-DBz-2-(3-OCH_3)Bz-3'-*N*-de(*tert*-butoxycarbonyl)-SB-T-1214.

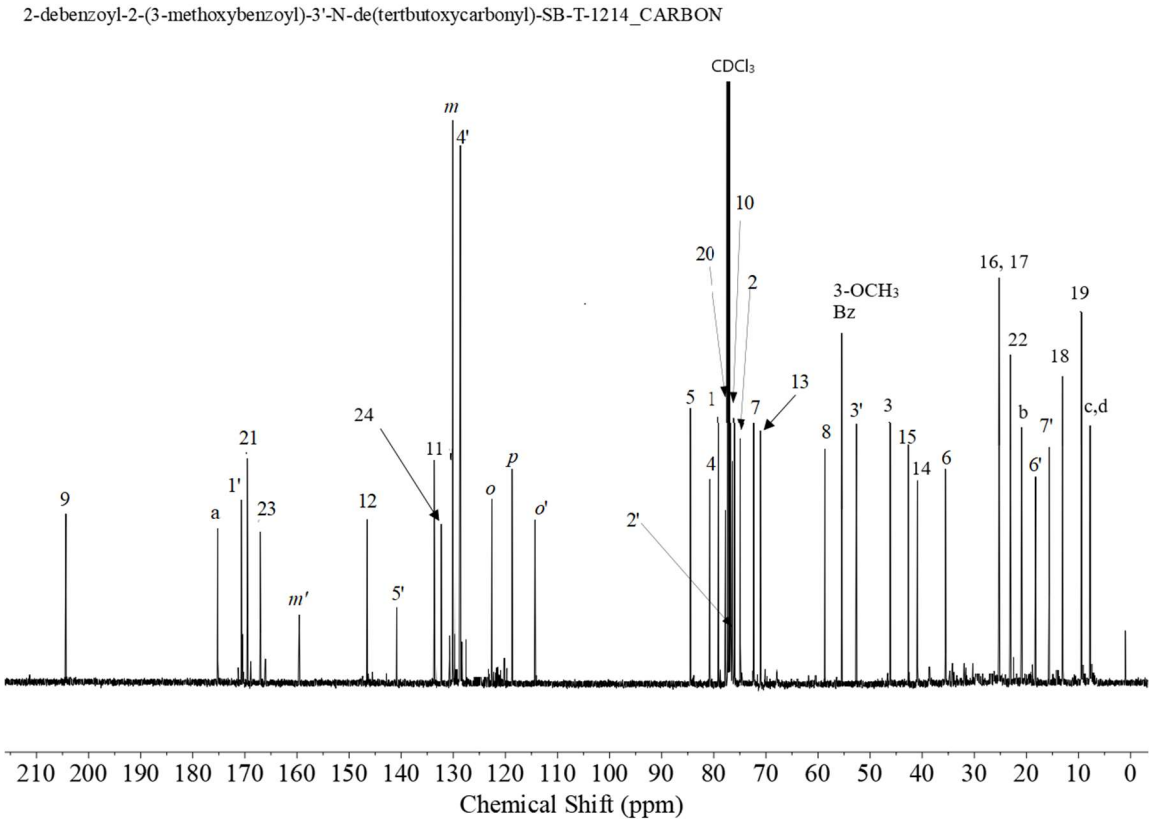

Figure 4.58: ^{13}C NMR of 2-DBz-2-(3-OCH_3)Bz-3'-*N*-de(*tert*-butoxycarbonyl)-SB-T-1214.

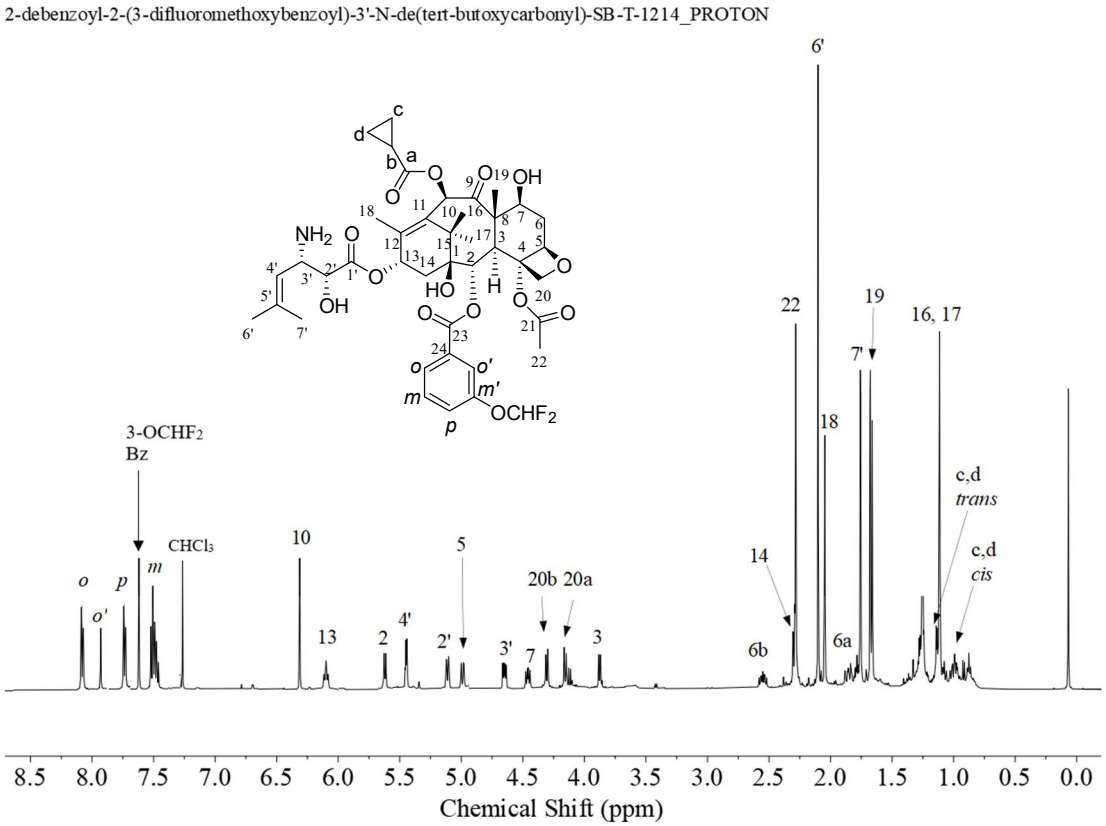

Figure 4.59: ^{1}H NMR of 2-DBz-2-(3-OCHF$_2$)Bz-3'-*N*-de(*tert*-butoxycarbonyl)-SB-T-1214.

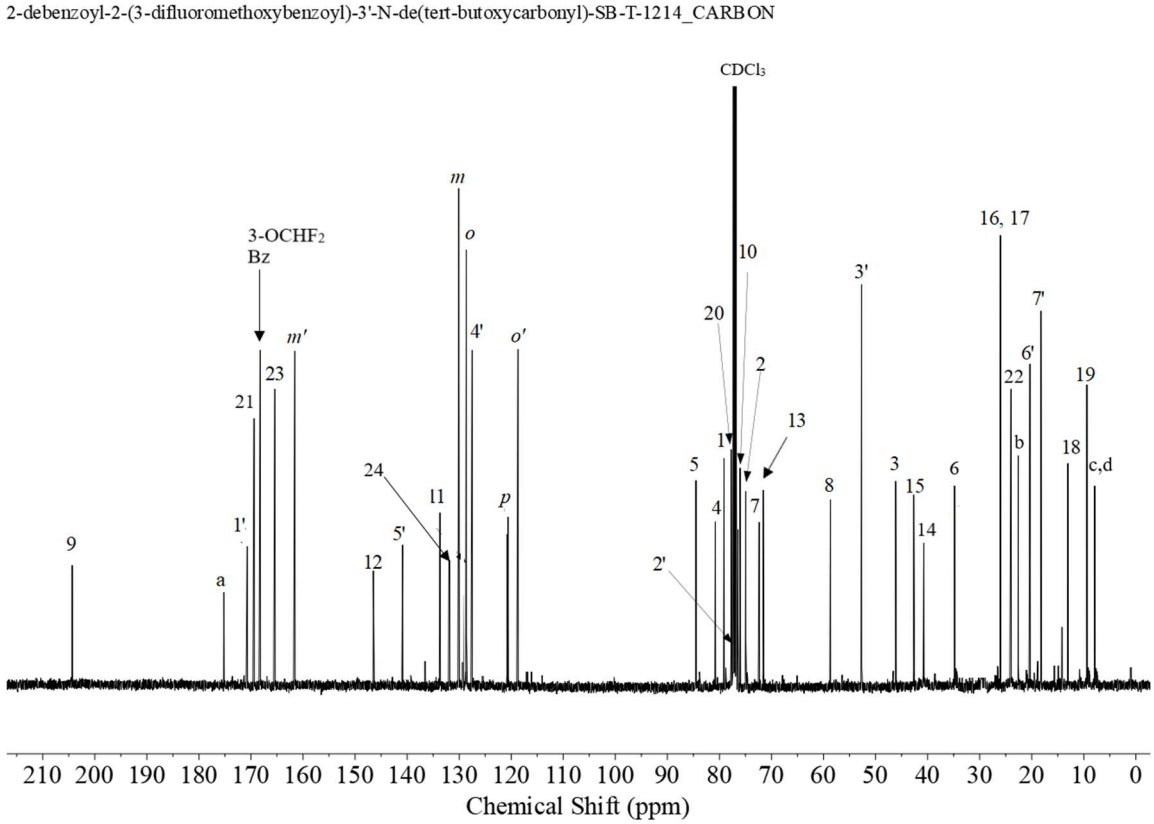

Figure 4.60: ^{13}C NMR of 2-DBz-2-(3-OCHF$_2$)Bz-3'-*N*-de(*tert*-butoxycarbonyl)-SB-T-1214.

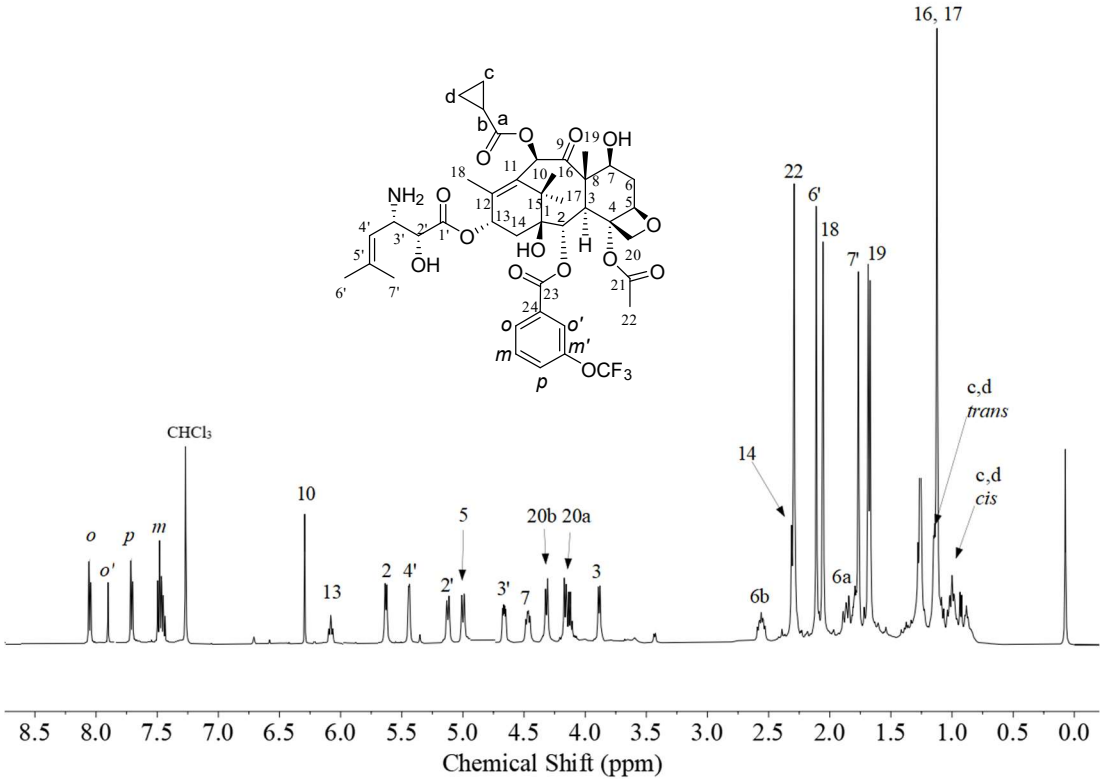

Figure 4.61: ^{1}H NMR of 2-DBz-2-(3-OCF_3)Bz-3'-*N*-de(*tert*-butoxycarbonyl)-SB-T-1214.

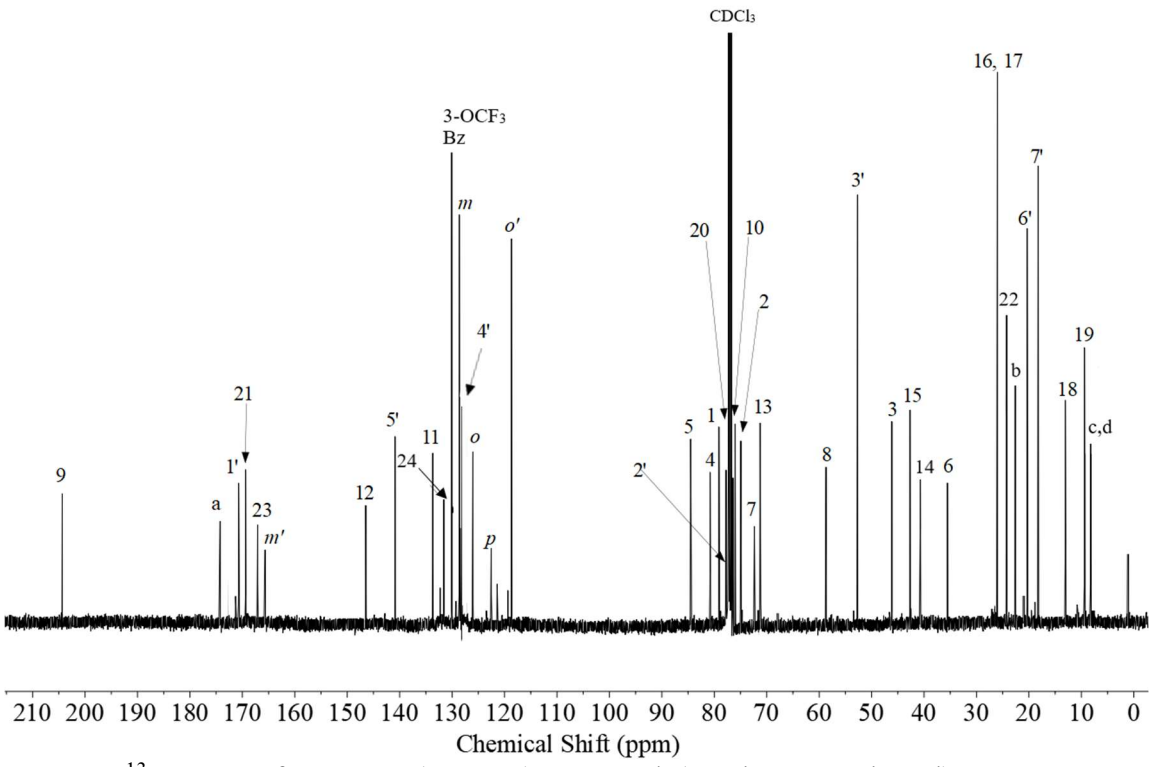

Figure 4.62: ^{13}C NMR of 2-DBz-2-(3-OCF_3)Bz-3'-*N*-de(*tert*-butoxycarbonyl)-SB-T-1214.

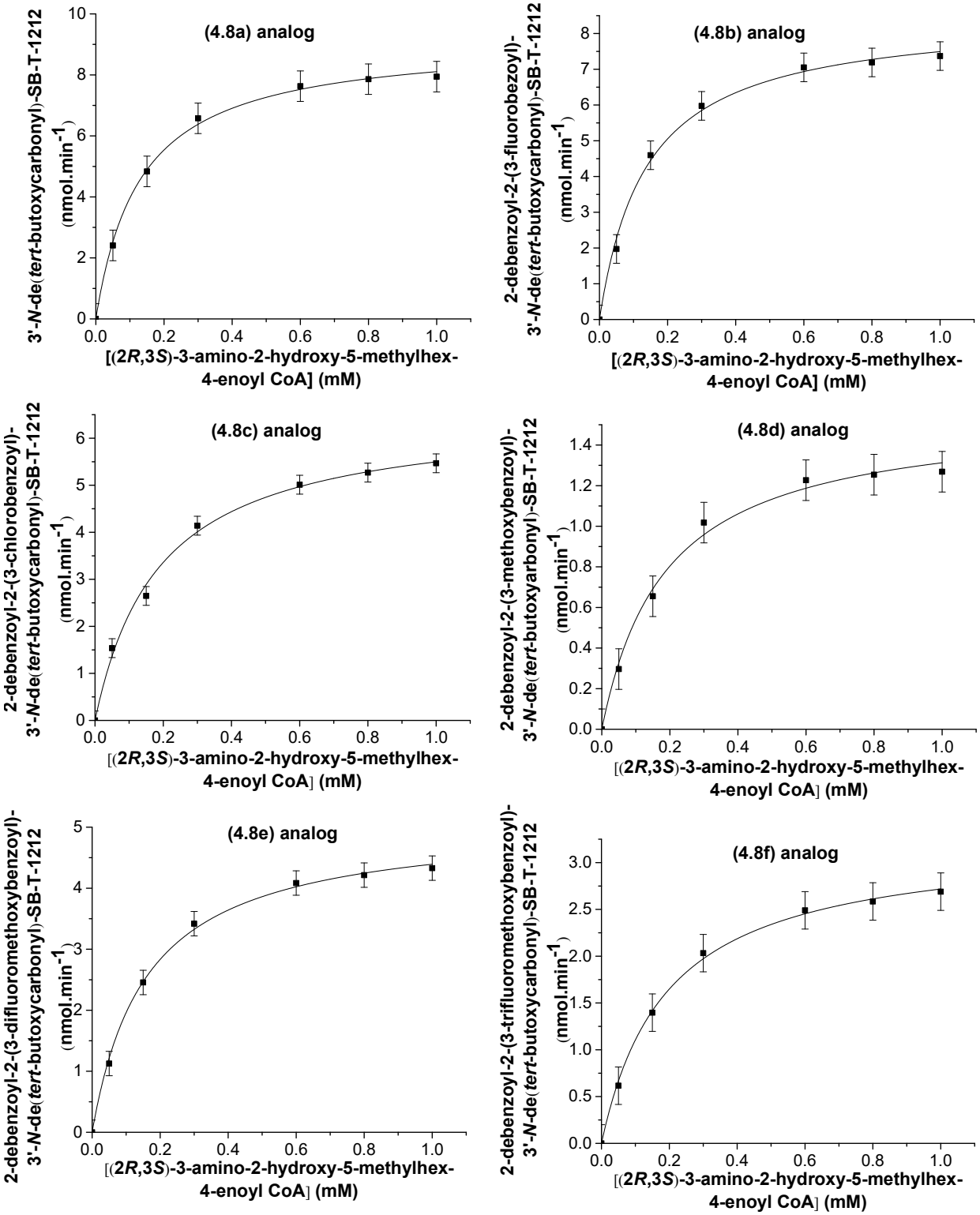

Figure 4.63: Michaelis-Menten kinetics for the turnover of baccatin III to the 3′-*N*-de(tert-butoxycarbonyl)-SB-T-1212 analogues **4.8** (**a**-**f**).

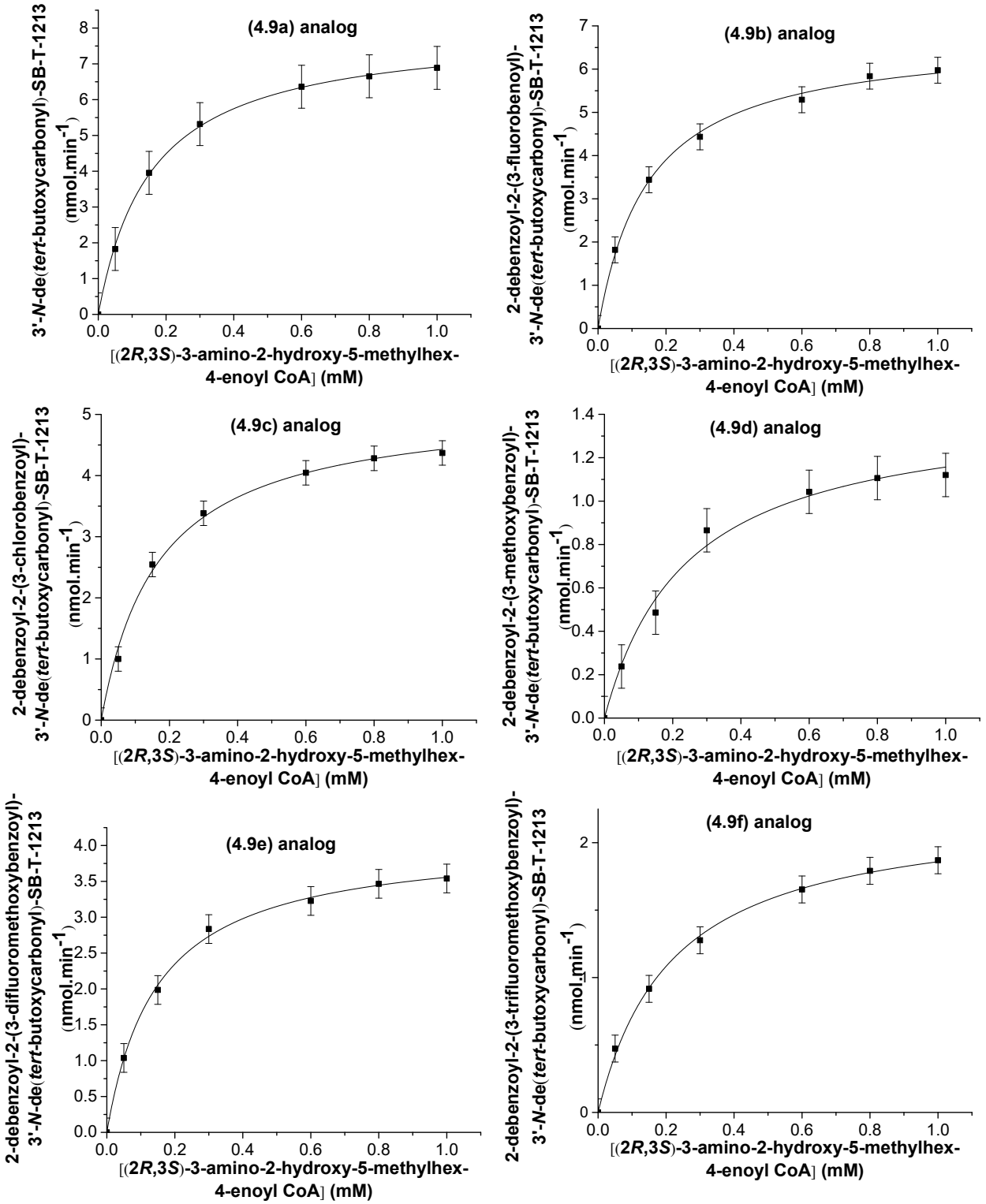

Figure 4.64: Michaelis-Menten kinetics for the turnover of baccatin III to the 3′-*N*-de(tert-butoxycarbonyl)-SB-T-1213 analogues **4.9** (**a**-**f**).

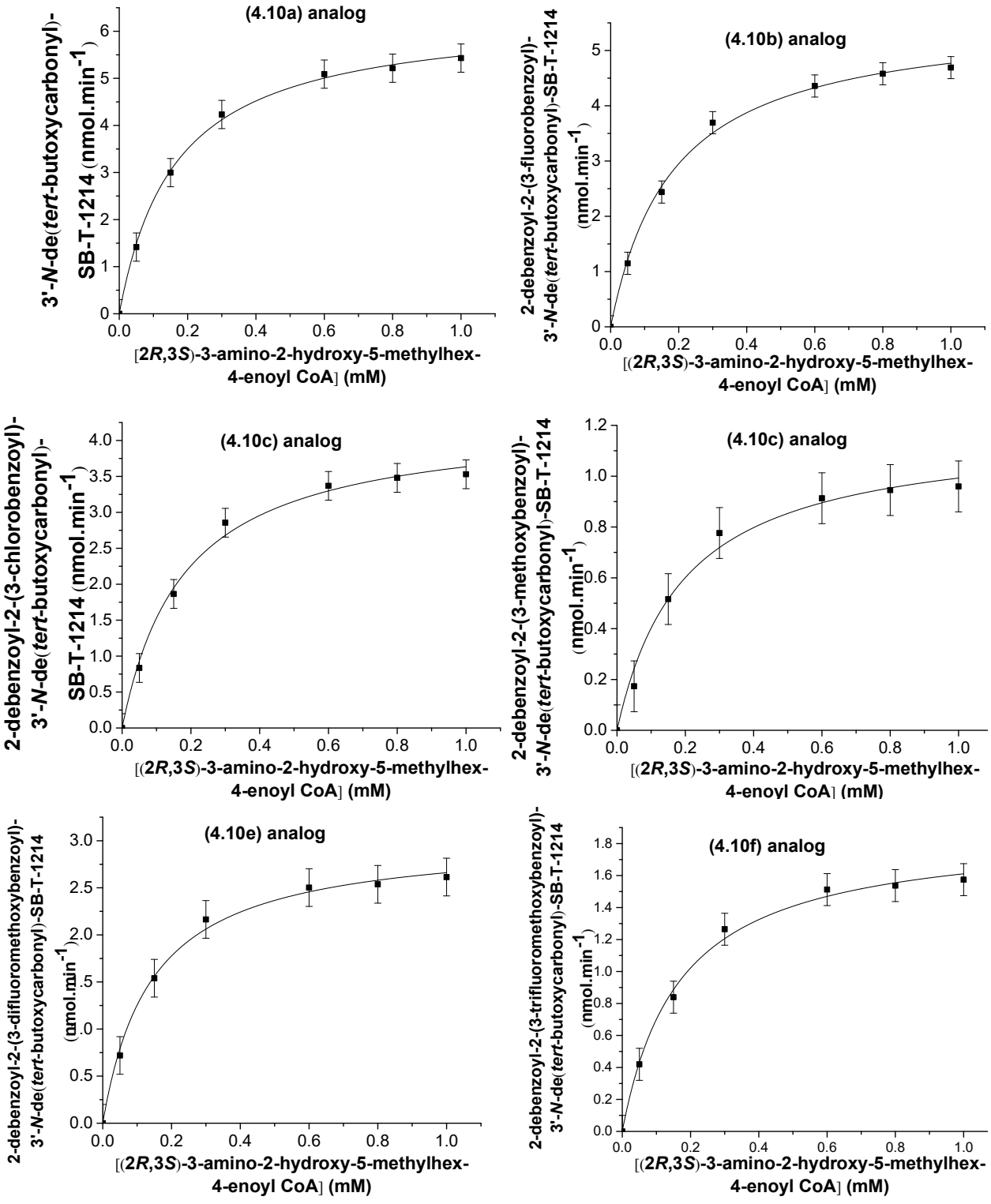

Figure 4.65: Michaelis-Menten kinetics for the turnover of baccatin III to the 3′-*N*-de(tert-butoxycarbonyl)-SB-T-1214 analogues **4.10** (**a**-**f**).

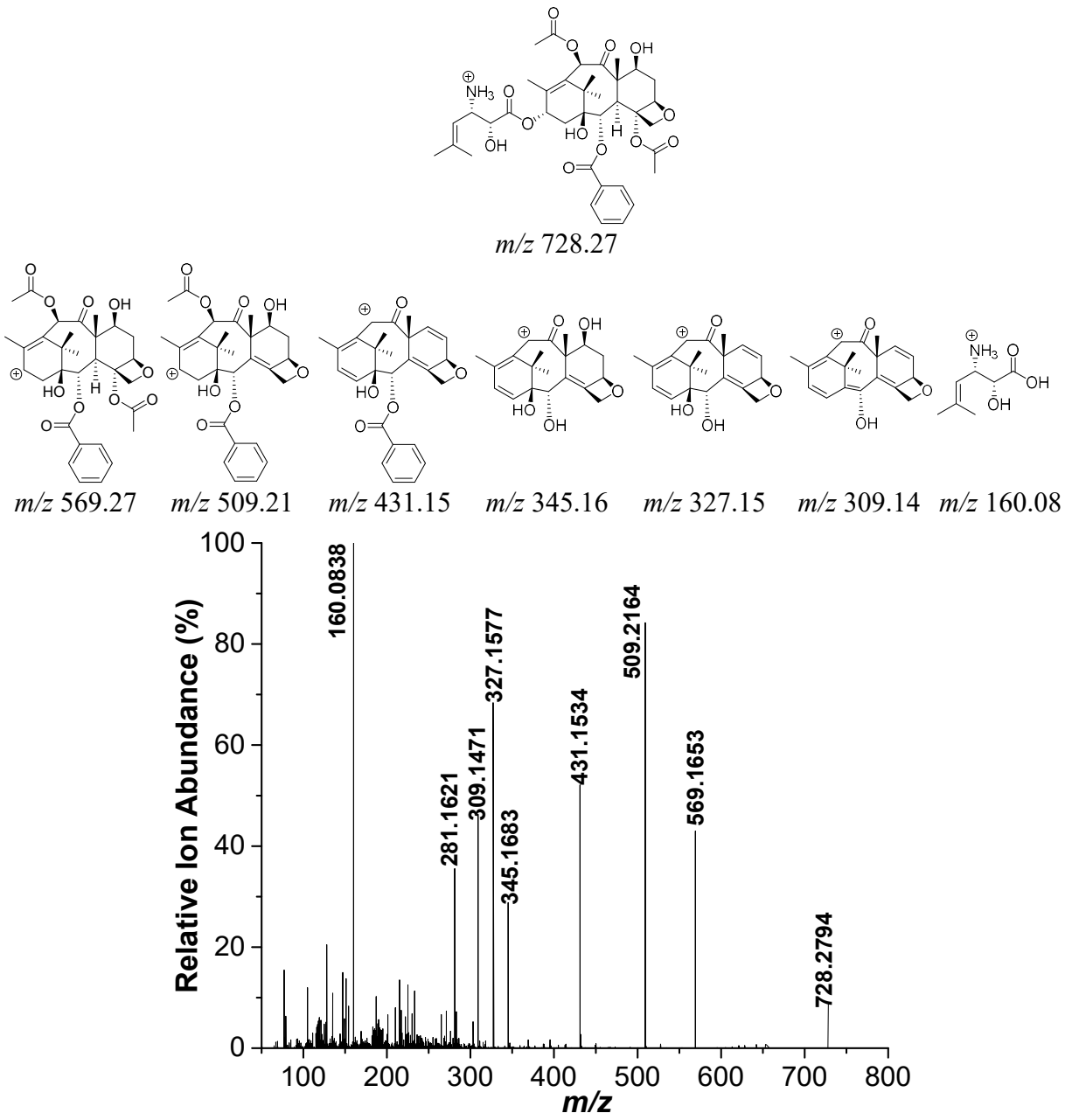

Figure 4.66: LC/ESI-MS/MS (positive-ion mode) of purified 3'-*N*-de(*tert*-butoxycarbonyl)-SB-T-1212 with peak mass assignments and putative chemical transformations (above spectra).

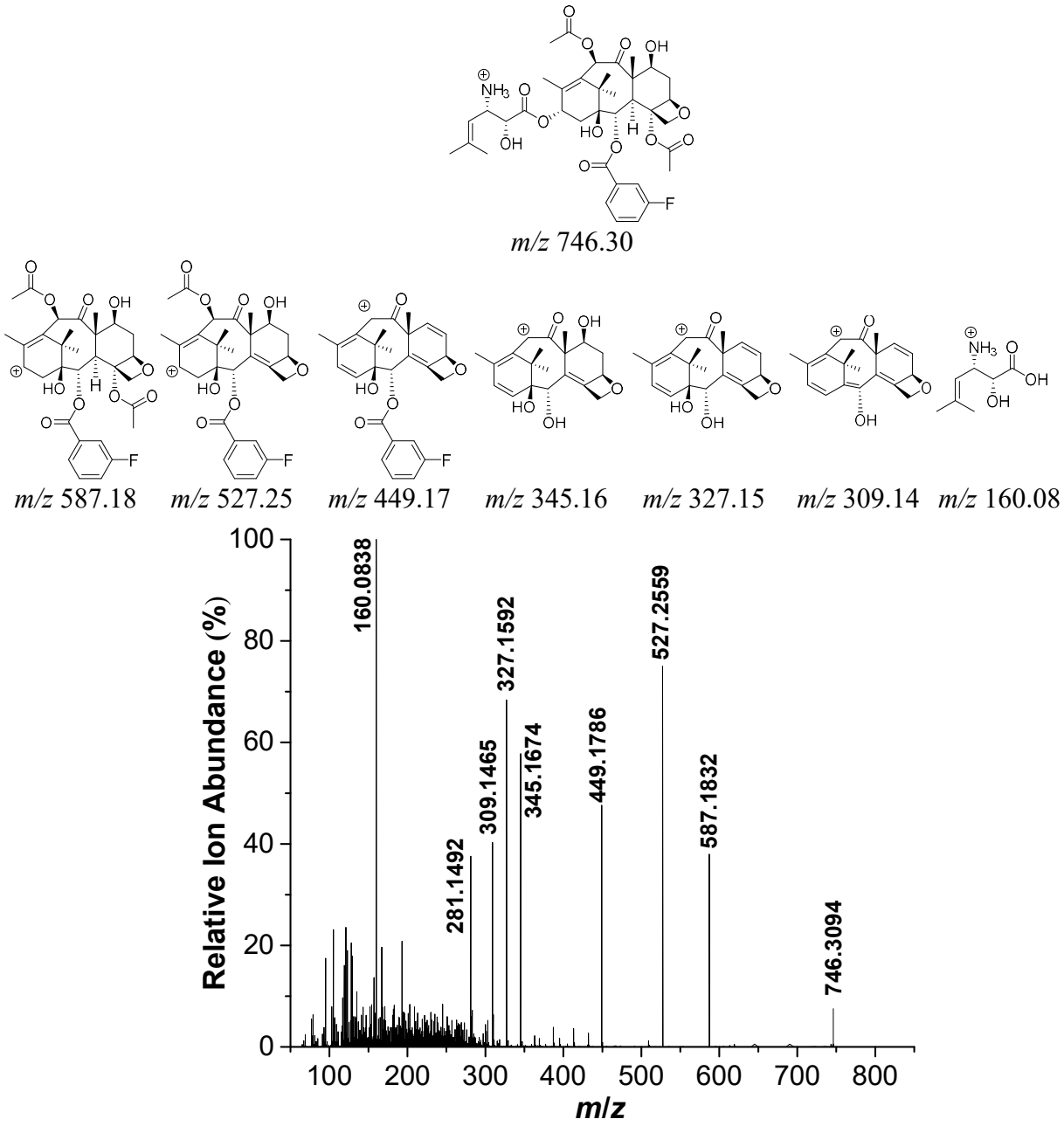

Figure 4.67: LC/ESI-MS/MS (positive-ion mode) of purified 2-DBz-2-(3-F)Bz-3'-*N*-de(*tert*-butoxycarbonyl)-SB-T-1212 with peak mass assignments and putative chemical transformations (above spectra).

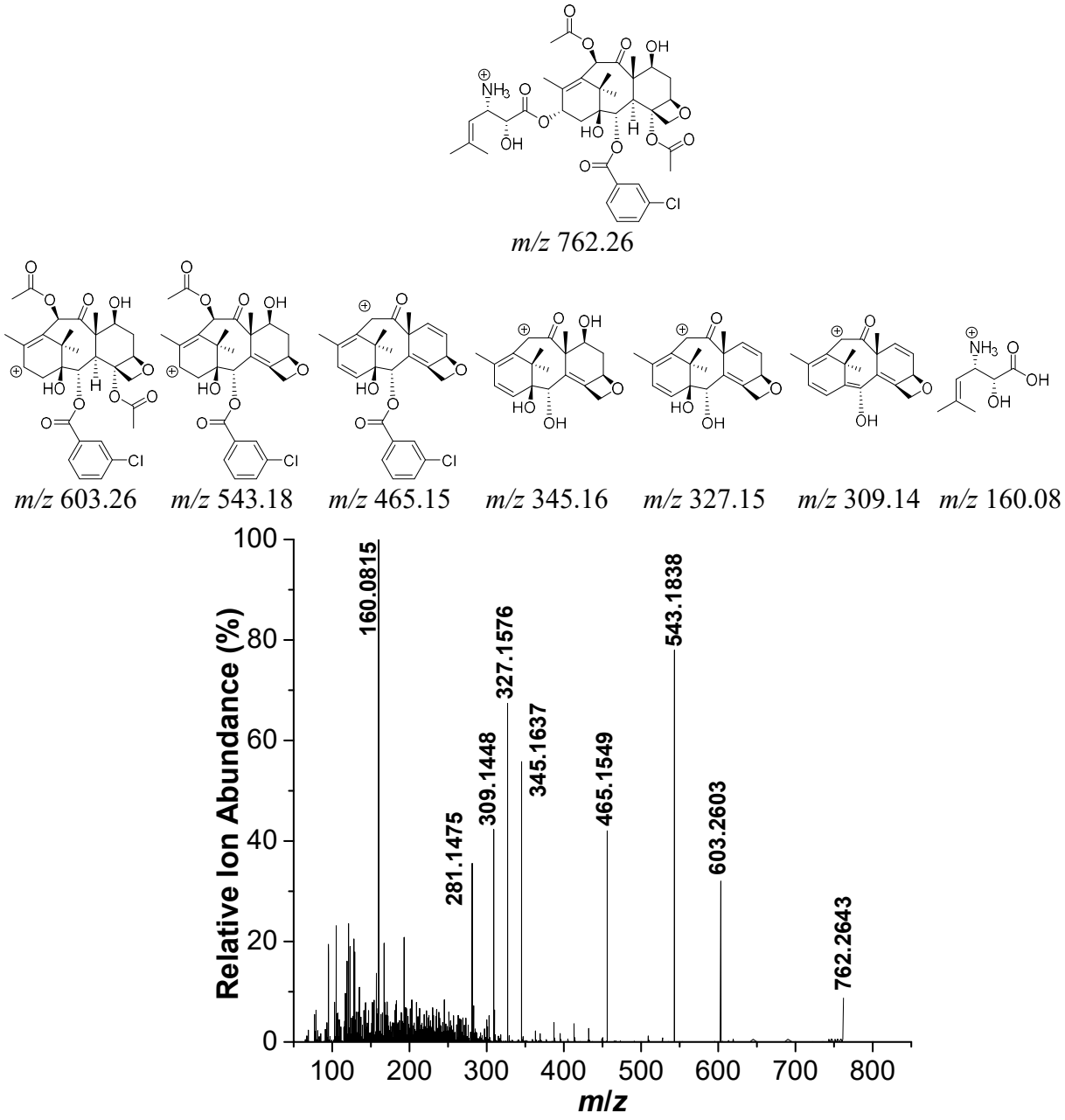

Figure 4.68: LC/ESI-MS/MS (positive-ion mode) of purified 2-DBz-2-(3-Cl)Bz-3'-*N*-de(*tert*-butoxycarbonyl)-SB-T-1212 with peak mass assignments and putative chemical transformations (above spectra).

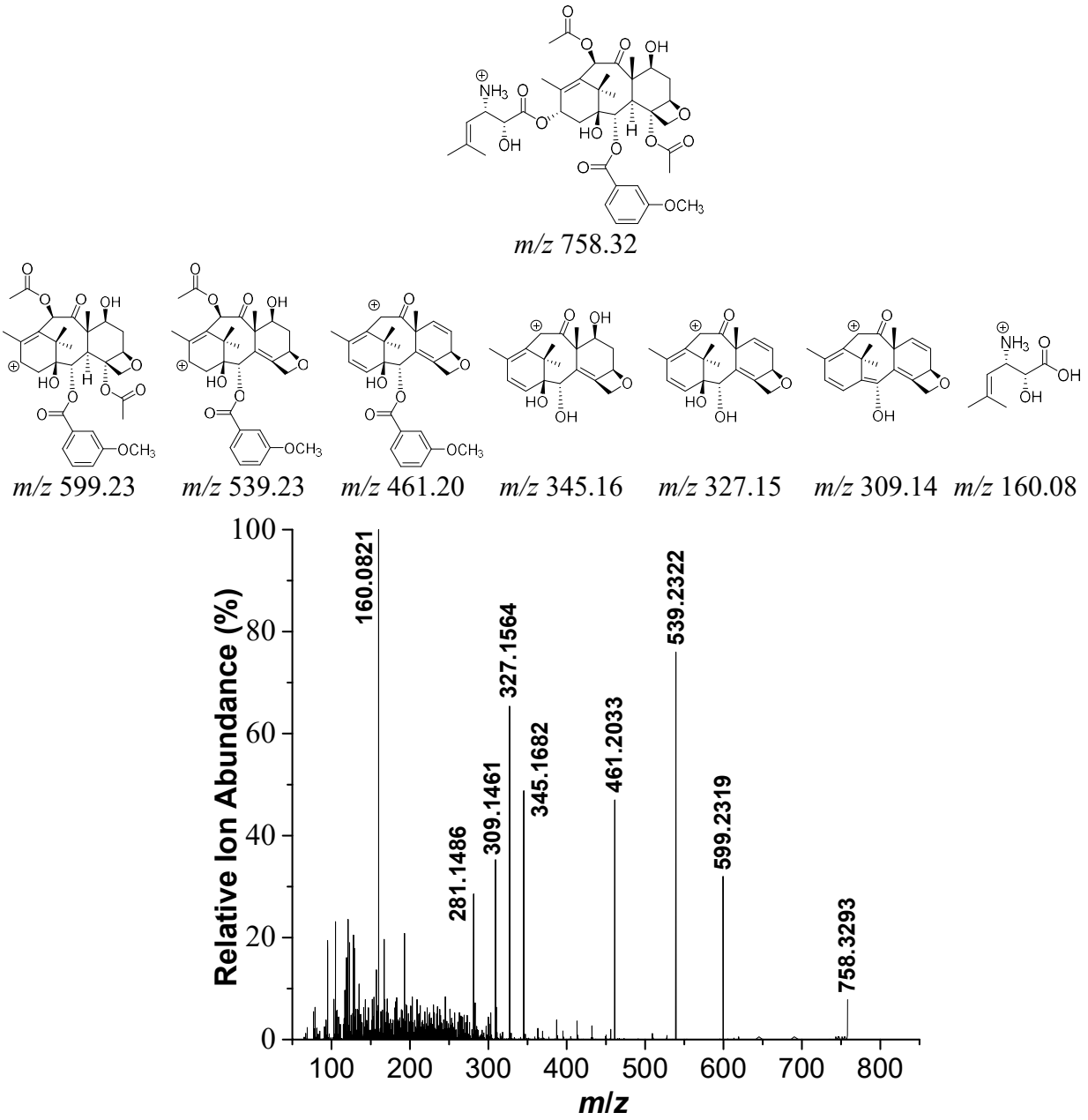

Figure 4.69: LC/ESI-MS/MS (positive-ion mode) of purified 2-DBz-2-(3-OCH_3)Bz-3'-*N*-de(*tert*-butoxycarbonyl)-SB-T-1212 with peak mass assignments and putative chemical transformations (above spectra).

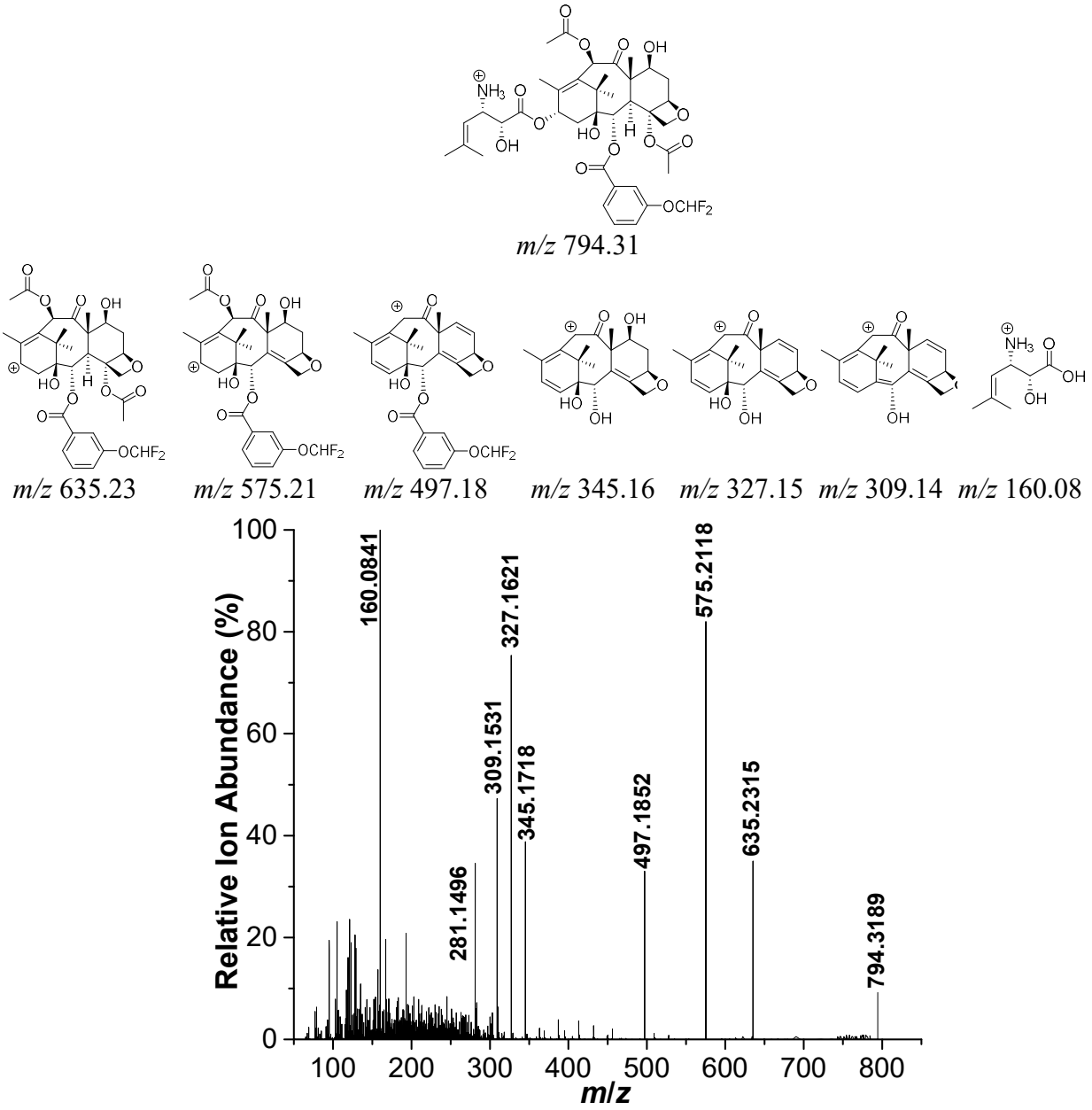

Figure 4.70: LC/ESI-MS/MS (positive-ion mode) of purified 2-Bz-2-(3-$OCHF_2$)Bz-3'-*N*-de(*tert*-butoxycarbonyl)-SB-T-1212 with peak mass assignments and putative chemical transformations (above spectra).

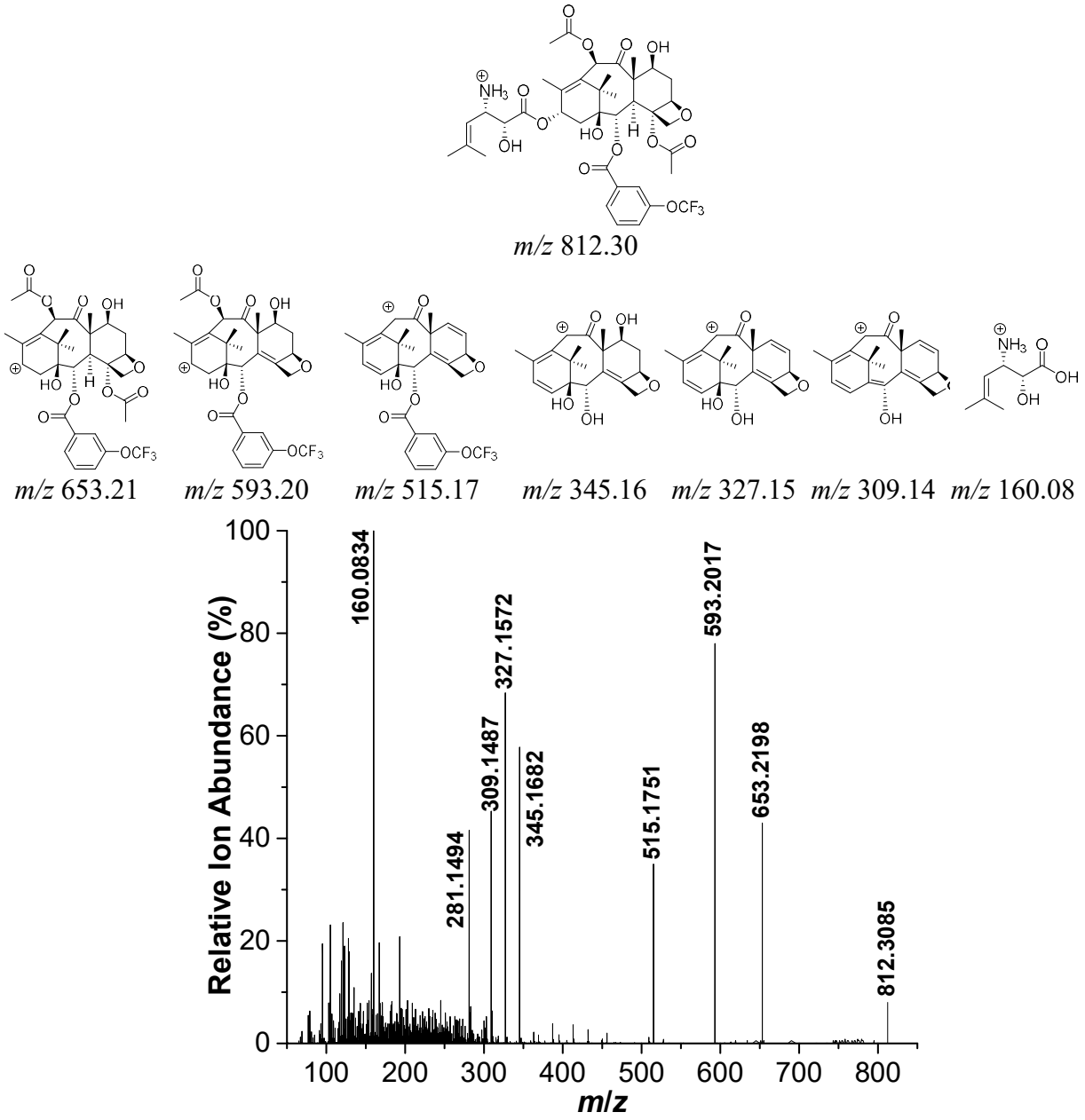

Figure 4.71: LC/ESI-MS/MS (positive-ion mode) of purified 2-DBz-2-(3-OCF_3)Bz-3'-*N*-de(*tert*-butoxycarbonyl)-SB-T-1212 with peak mass assignments and putative chemical transformations (above spectra).

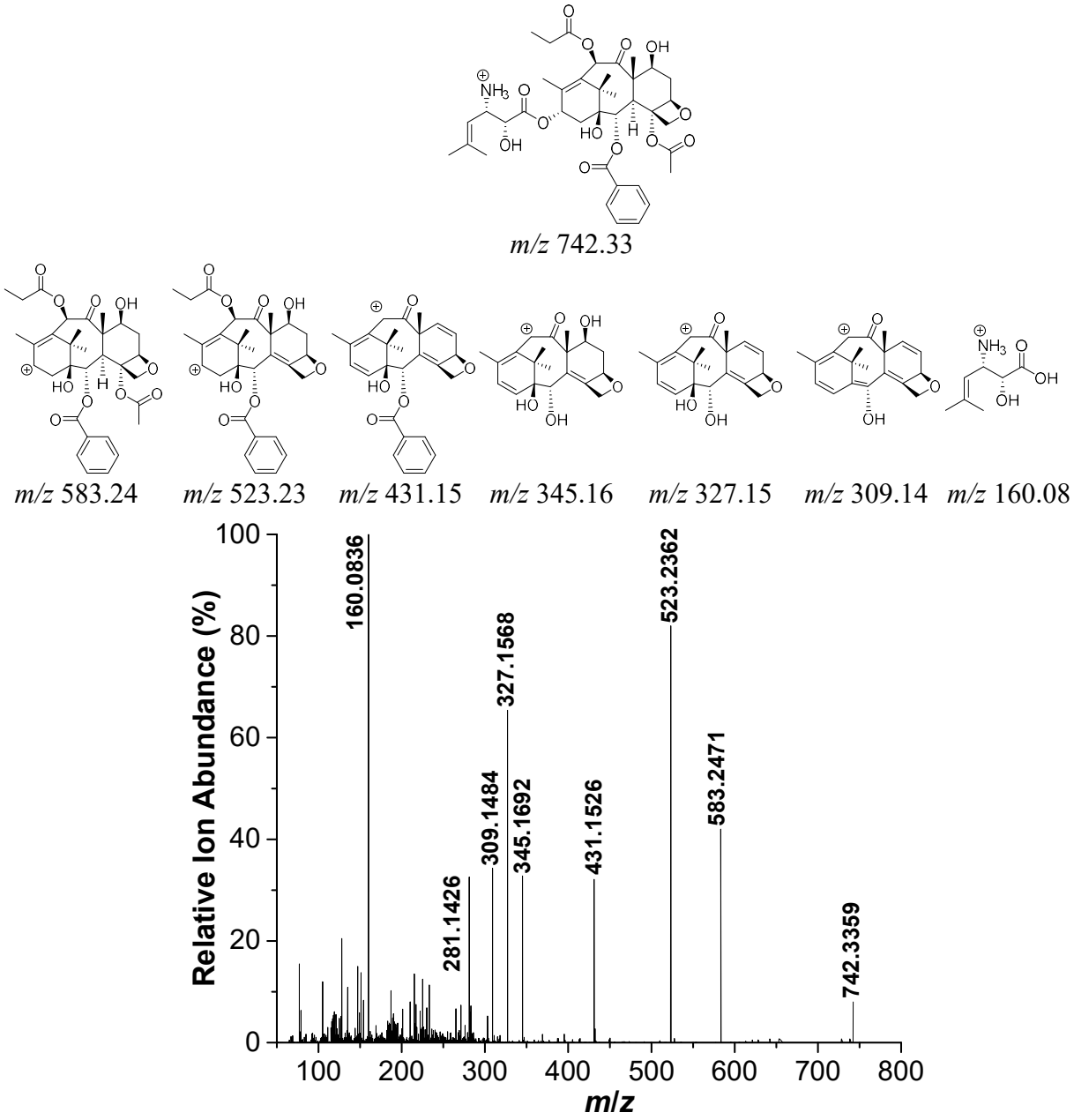

Figure 4.72: LC/ESI-MS/MS (positive-ion mode) of purified 3'-*N*-de(*tert*-butoxycarbonyl)-SB-T-1213 with peak mass assignments and putative chemical transformations (above spectra).

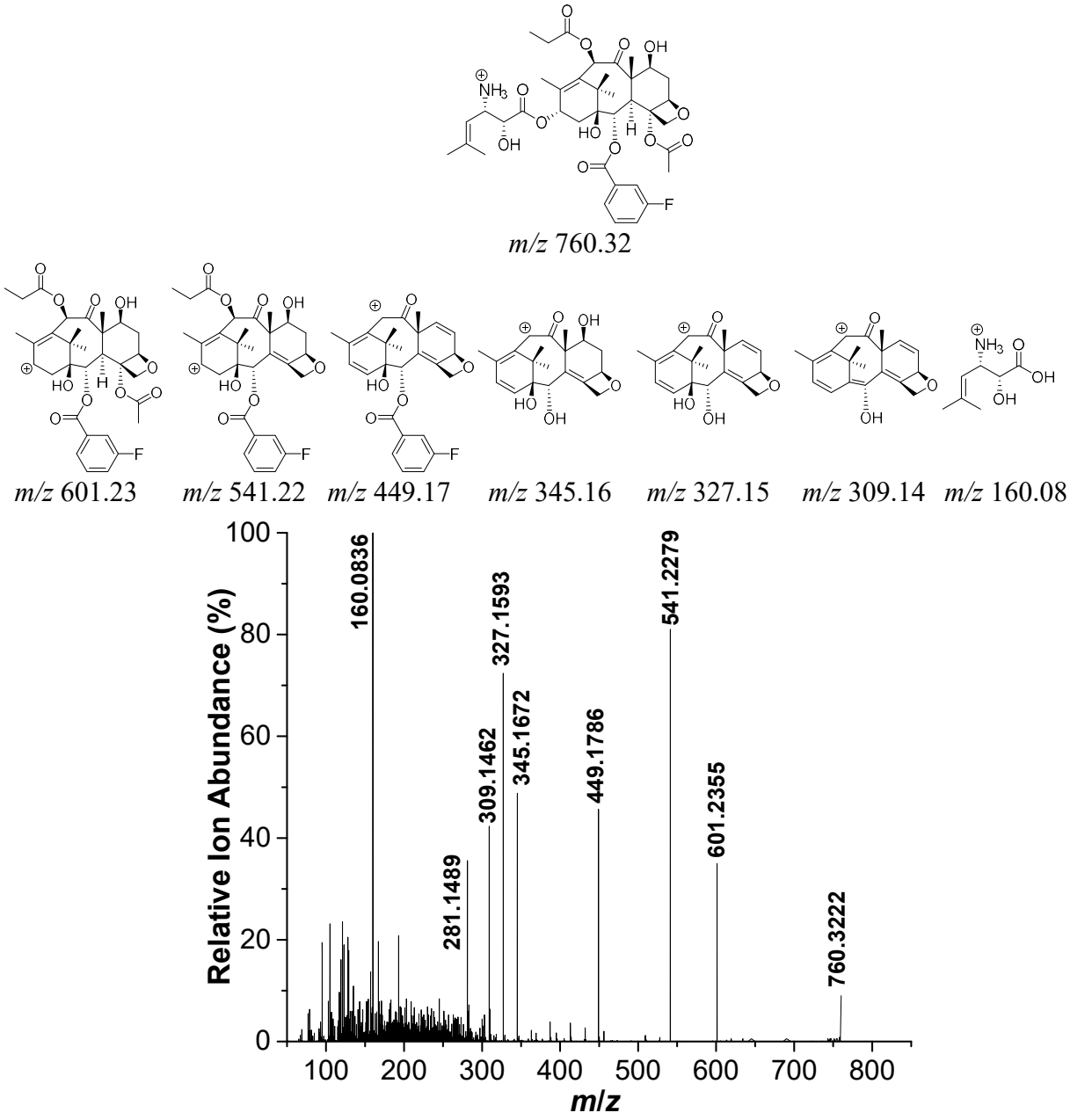

Figure 4.73: LC/ESI-MS/MS (positive-ion mode) of purified 2-DBZ-2-(3-F)Bz-3'-*N*-de(*tert*-butoxycarbonyl)-SB-T-1213 with peak mass assignments and putative chemical transformations (above spectra).

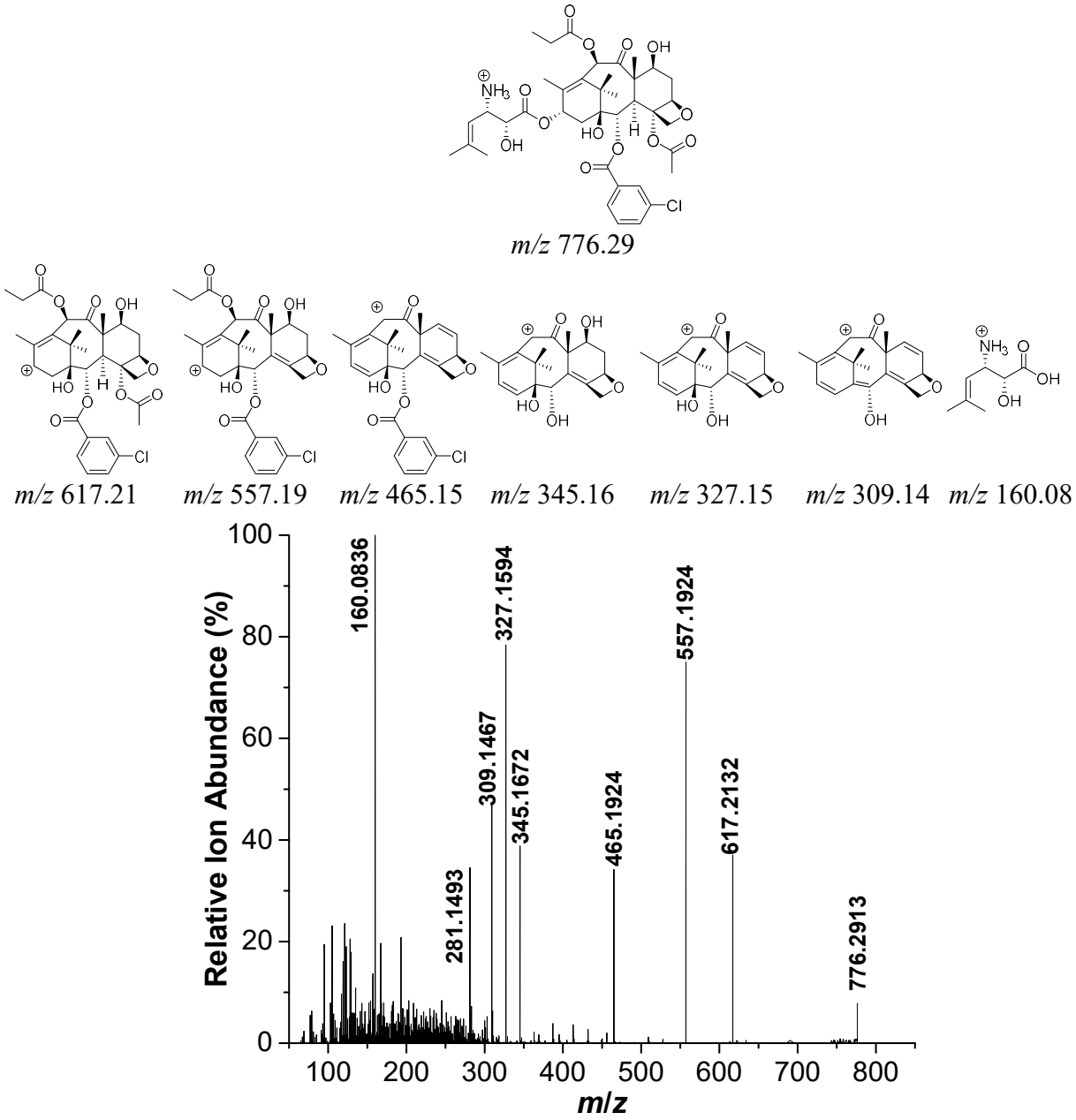

Figure 4.74: LC/ESI-MS/MS (positive-ion mode) of purified 2-DBz-2-(3-Cl)Bz-3'-*N*-de(*tert*-butoxycarbonyl)-SB-T-1213 with peak mass assignments and putative chemical transformations (above spectra).

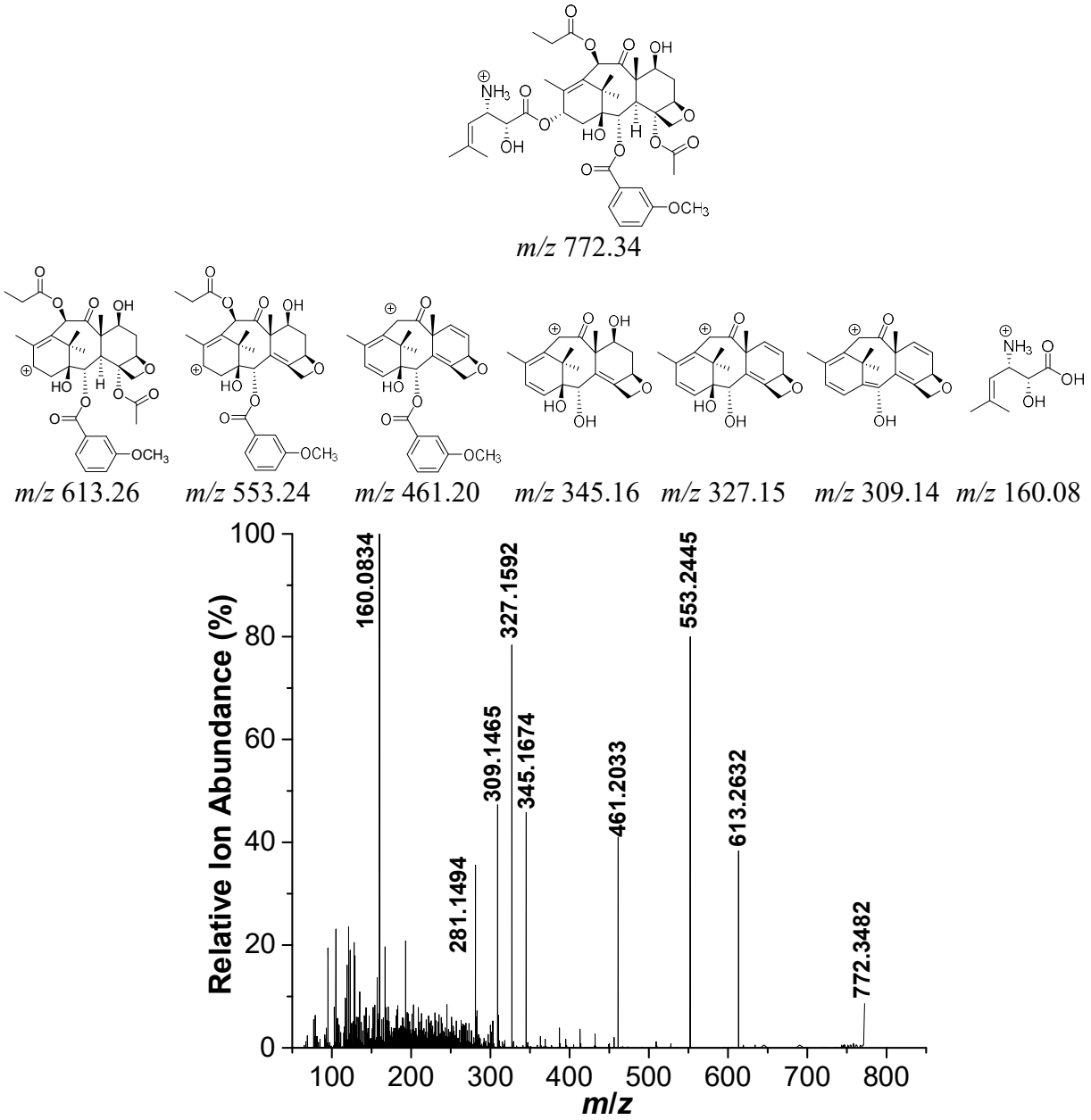

Figure 4.75: LC/ESI-MS/MS (positive-ion mode) of purified 2-DBz-2-(3-OCH_3)Bz-3'-*N*-de(*tert*-butoxycarbonyl)-SB-T-1213 with peak mass assignments and putative chemical transformations (above spectra).

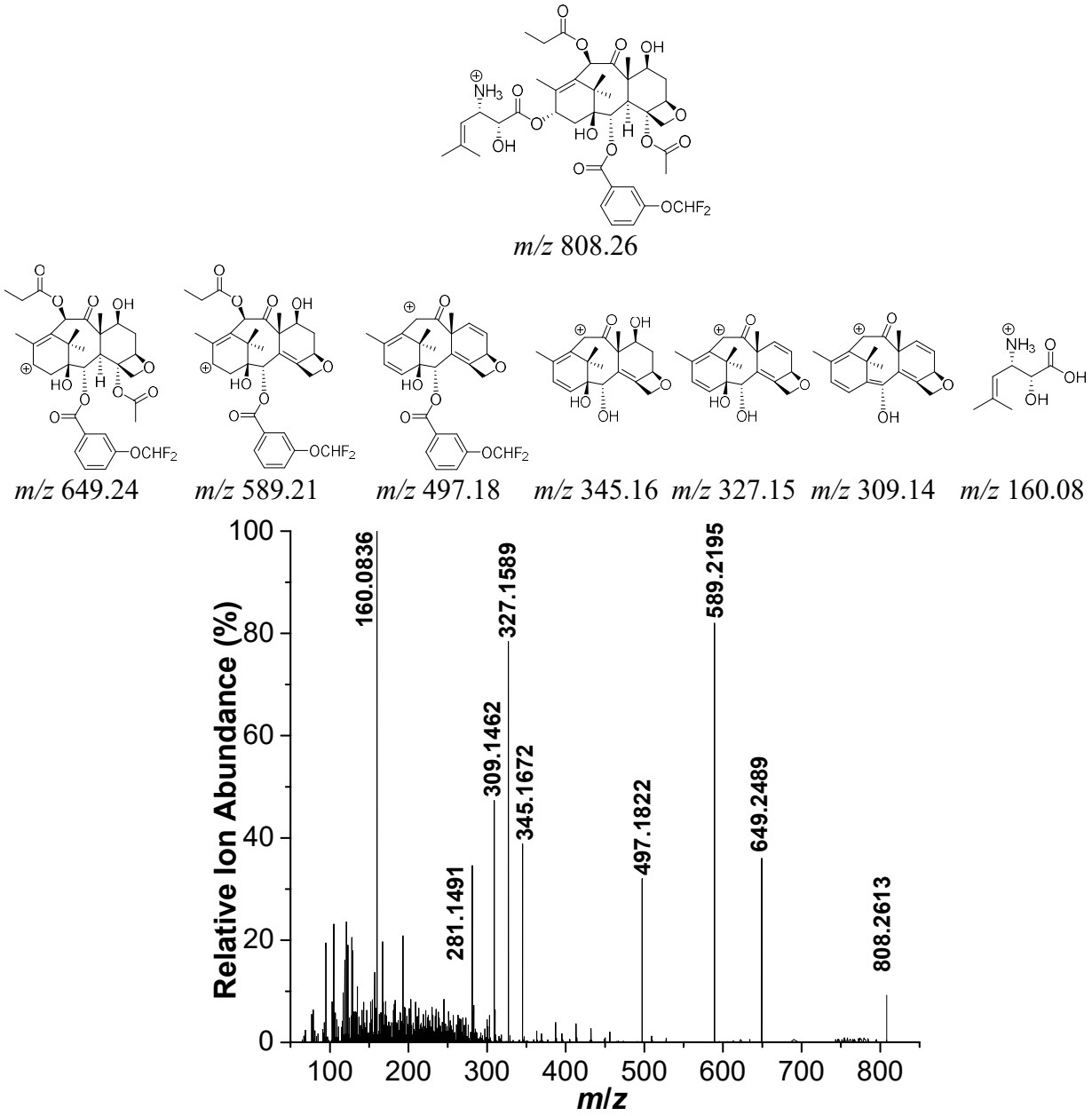

Figure 4.76: LC/ESI-MS/MS (positive-ion mode) of purified 2-DBz-2-(3-$OCHF_2$)Bz-3'-*N*-de(*tert*-butoxycarbonyl)-SB-T-1213 with peak mass assignments and putative chemical transformations (above spectra).

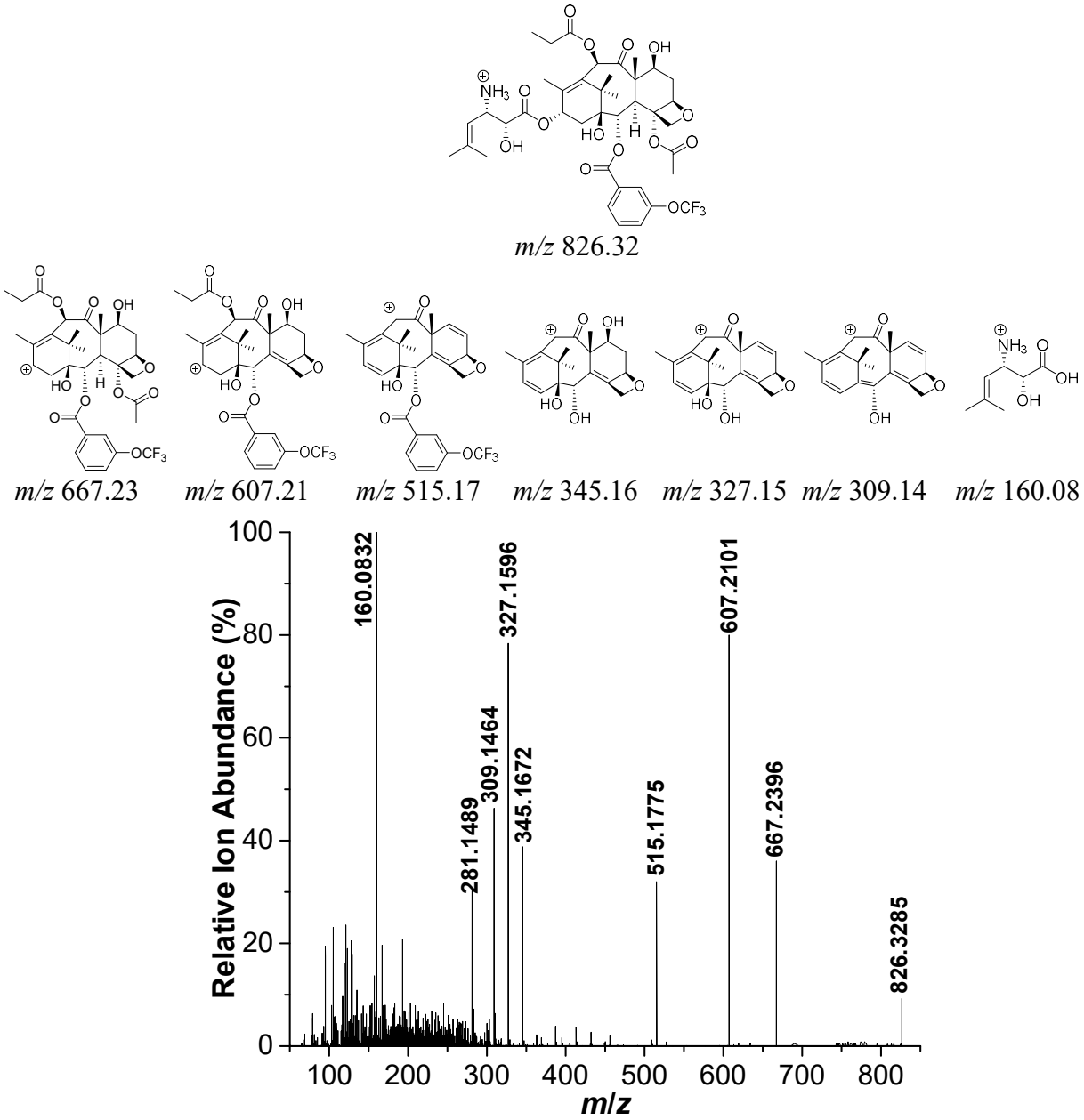

Figure 4.77: LC/ESI-MS/MS (positive-ion mode) of purified 2-DBz-2-(3-OCF_3)Bz-3'-*N*-de(*tert*-butoxycarbonyl)-SB-T-1213 with peak mass assignments and putative chemical transformations (above spectra).

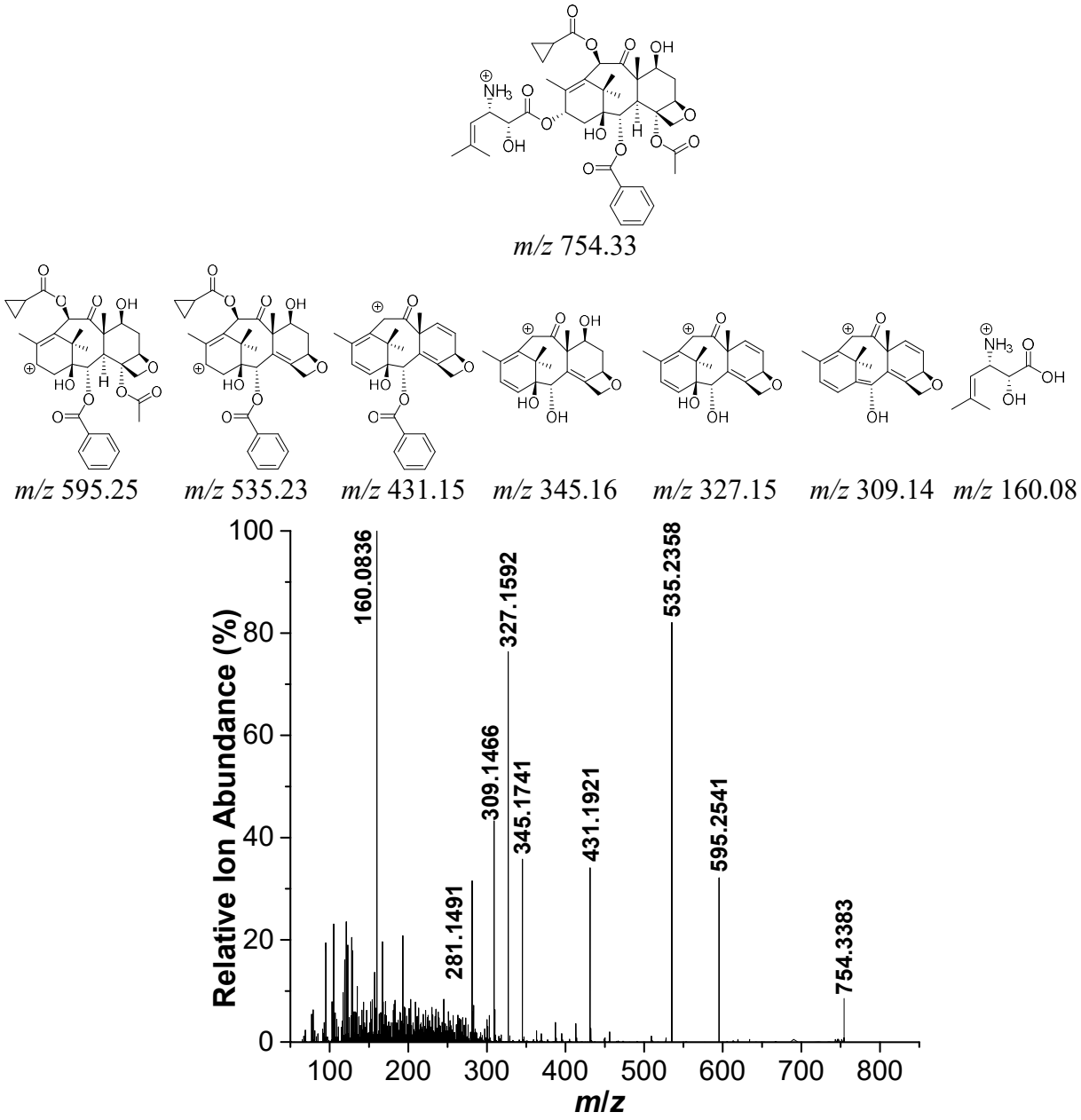

Figure 4.78: LC/ESI-MS/MS (positive-ion mode) of purified 3'-*N*-de(*tert*-butoxycarbonyl)-SB-T-1214 with peak mass assignments and putative chemical transformations (above spectra).

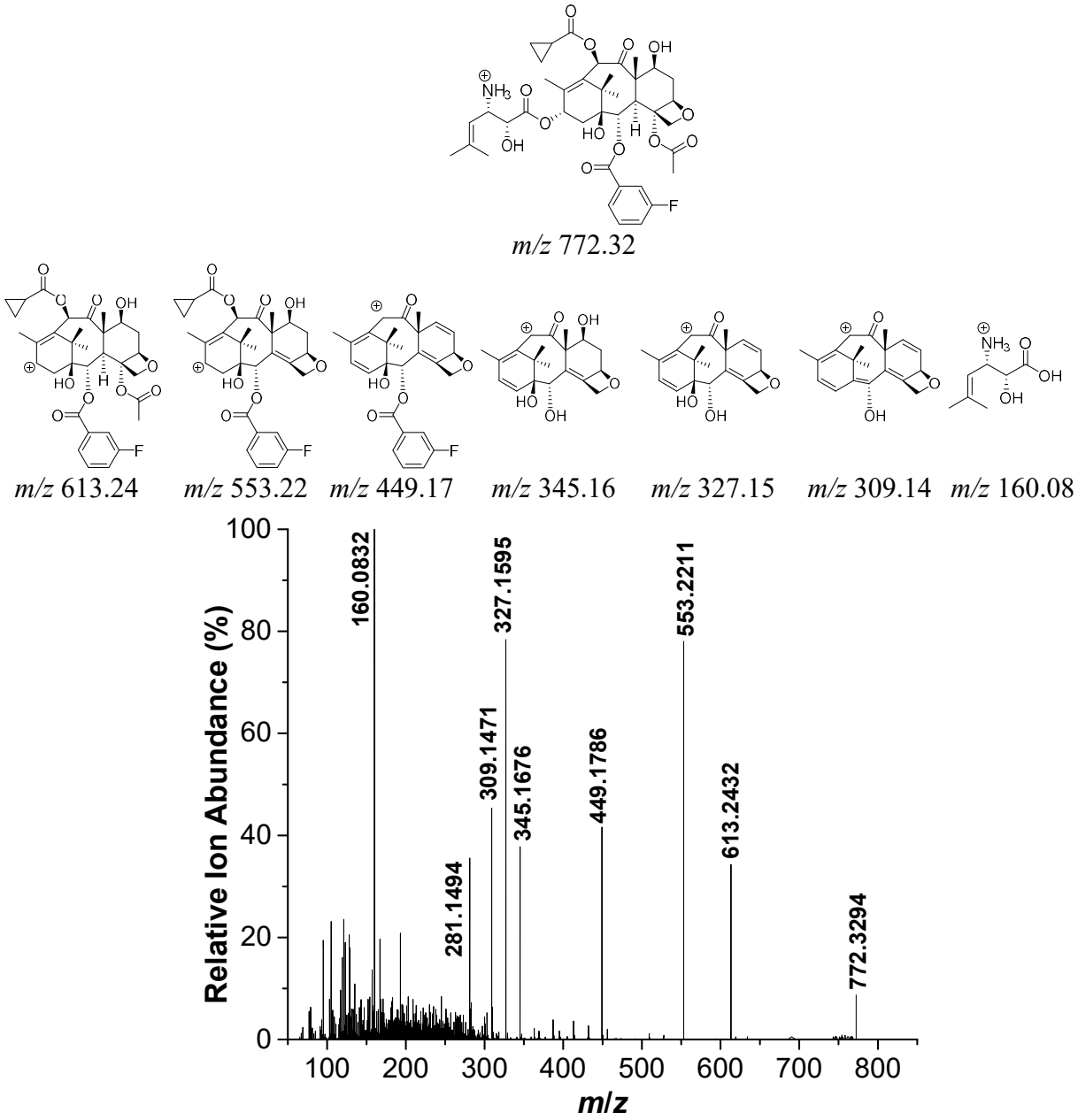

Figure 4.79: LC/ESI-MS/MS (positive-ion mode) of purified 2-DBz-2-(3-F)Bz-3'-*N*-de(*tert*-butoxycarbonyl)-SB-T-1214 with peak mass assignments and putative chemical transformations (above spectra).

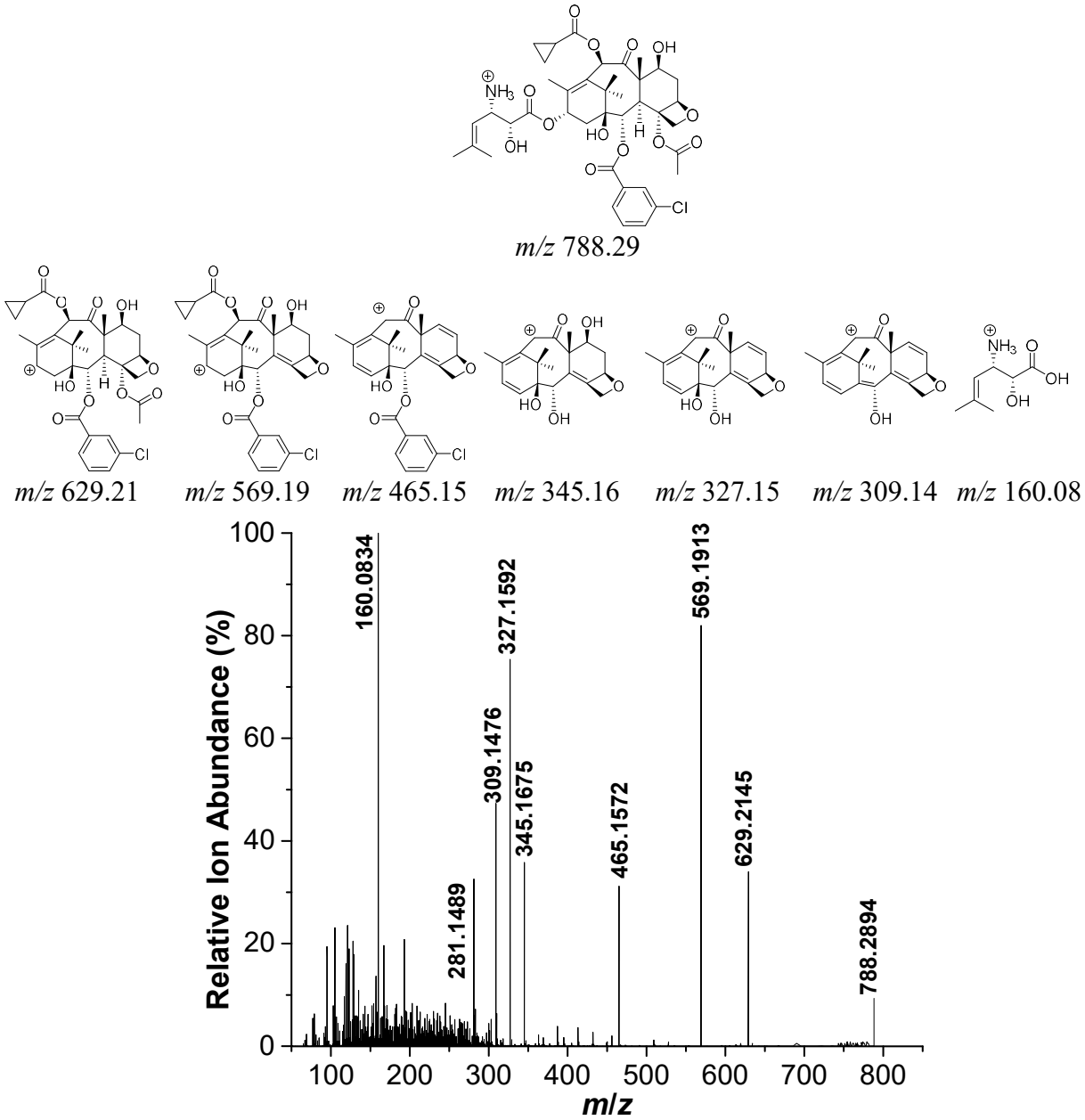

Figure 4.80: LC/ESI-MS/MS (positive-ion mode) of purified 2-DBz-2-(3-Cl)Bz-3'-*N*-de(*tert*-butoxycarbonyl)-SB-T-1214 with peak mass assignments and putative chemical transformations (above spectra).

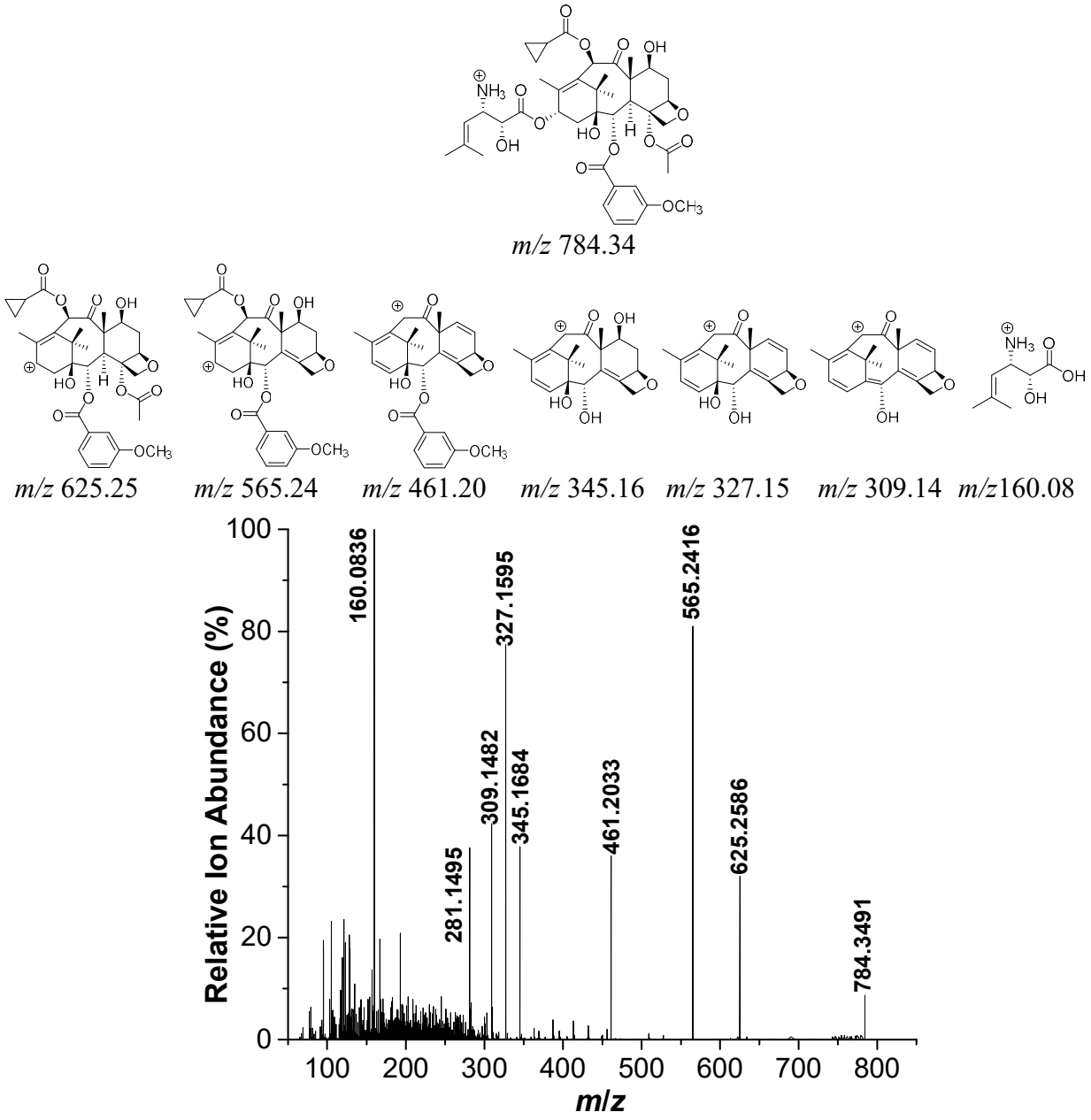

Figure 4.81: LC/ESI-MS/MS (positive-ion mode) of purified 2-DBz-2-(3-OCH_3)Bz-3'-*N*-de(*tert*-butoxycarbonyl)-SB-T-1214 with peak mass assignments and putative chemical transformations (above spectra).

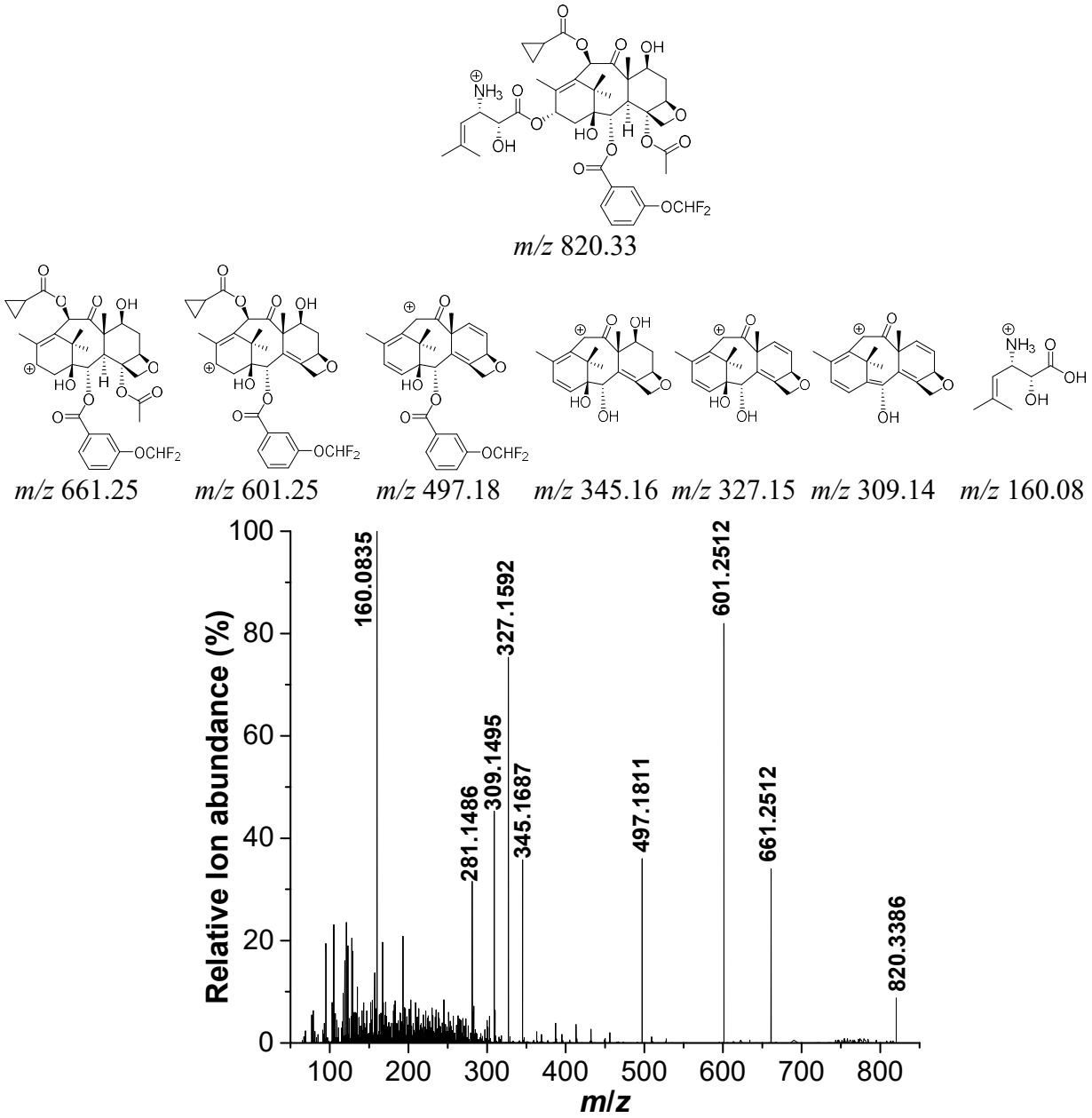

Figure 4.82: LC/ESI-MS/MS (positive-ion mode) of purified 2-DBz-2-(3-$OCHF_2$)Bz-3'-*N*-de(*tert*-butoxycarbonyl)-SB-T-1214 with peak mass assignments and putative chemical transformations (above spectra).

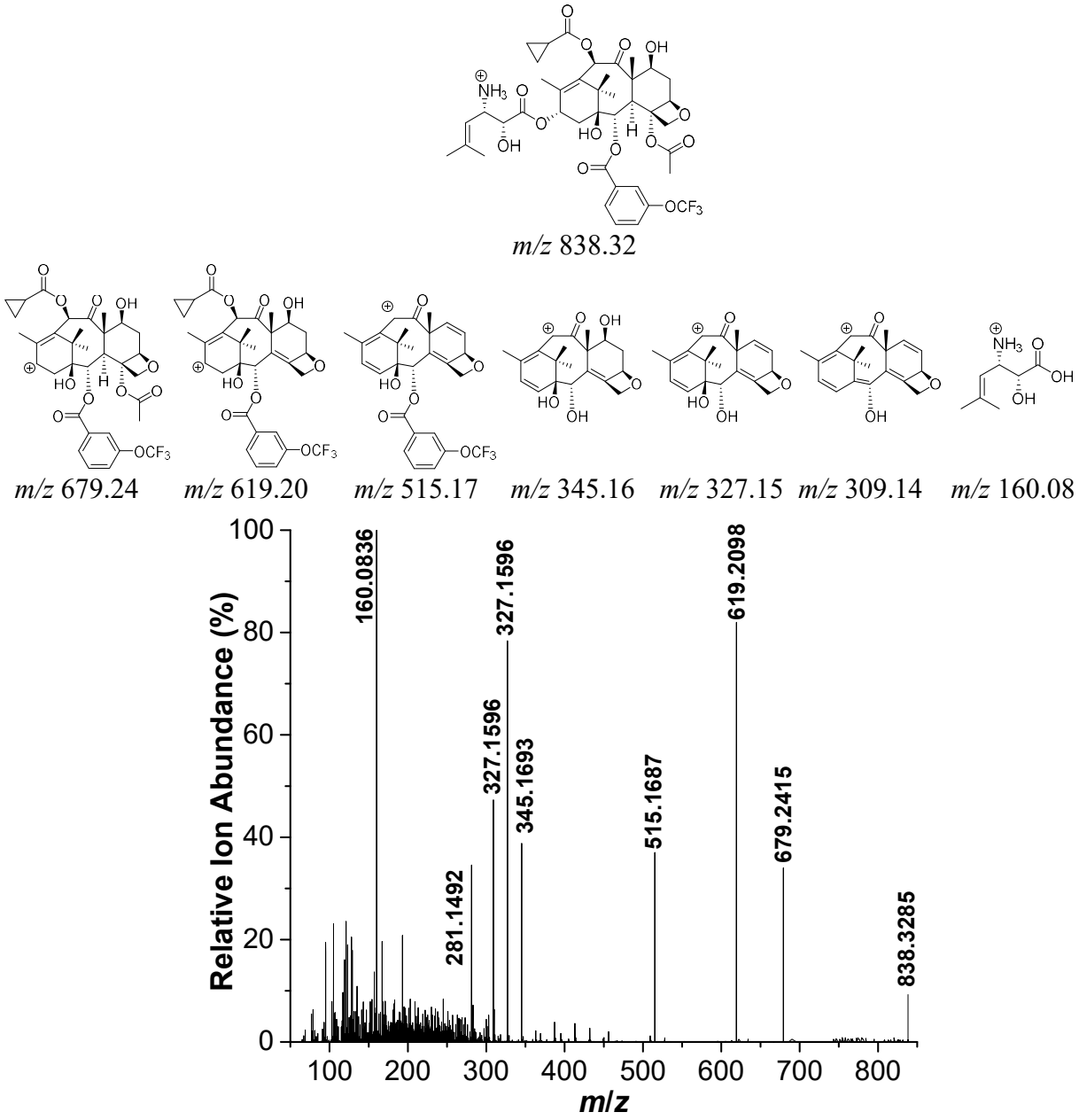

Figure 4.83: LC/ESI-MS/MS (positive-ion mode) of purified 2-DBz-2-(3-OCF_3)Bz-3'-*N*-de(*tert*-butoxycarbonyl)-SB-T-1214 with peak mass assignments and putative chemical transformations (above spectra).

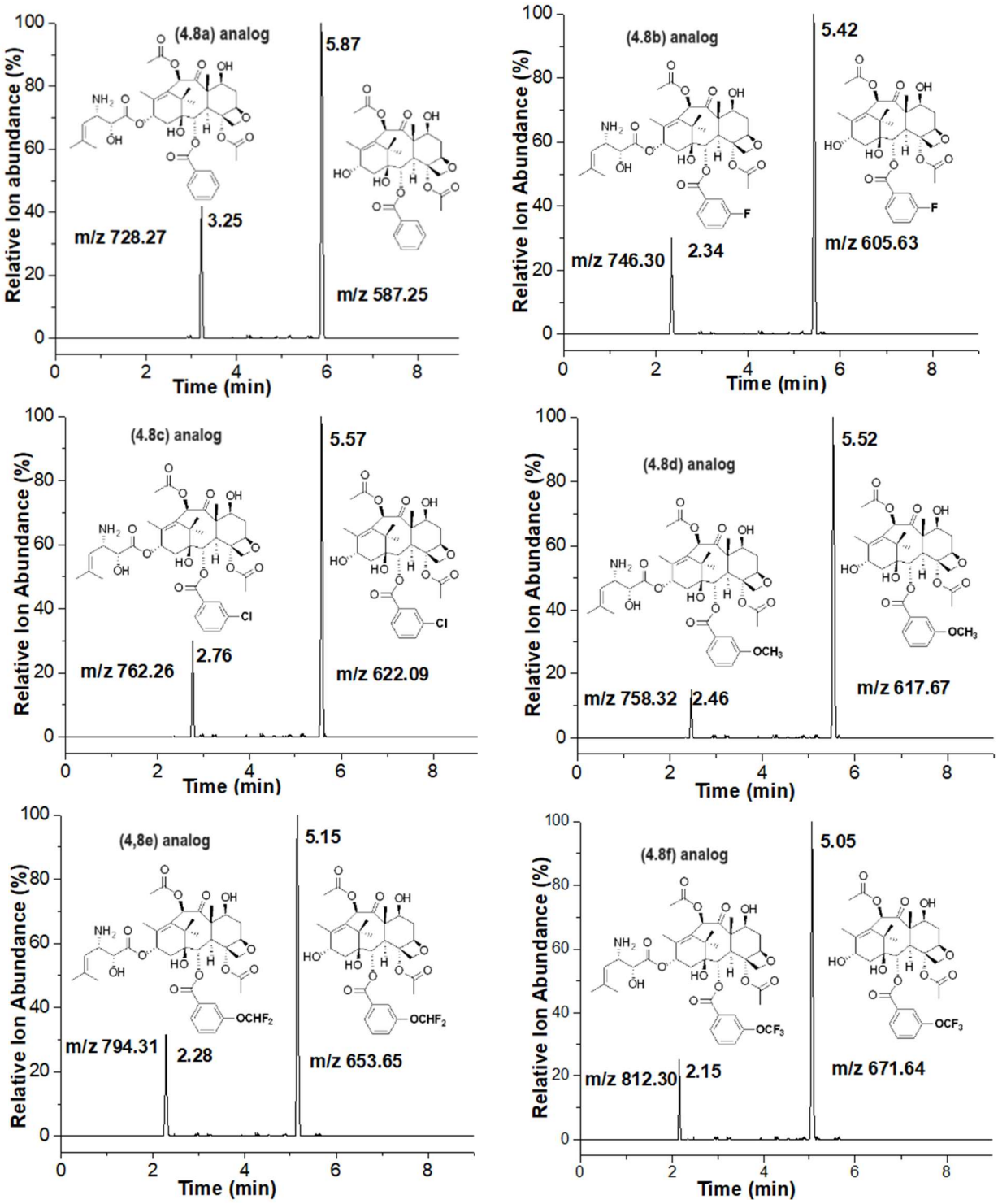

Figure 4.84: LC/ESI-MS (selected ion mode for m/z $[M + H]^+$) of the biocatalytic conversion of baccatin III analogs **4.5(a-f)** to the 3'-*N*-de(*tert*-butoxycarbonyl)-SB-T-1212 analogs **4.8**(**a-f**).

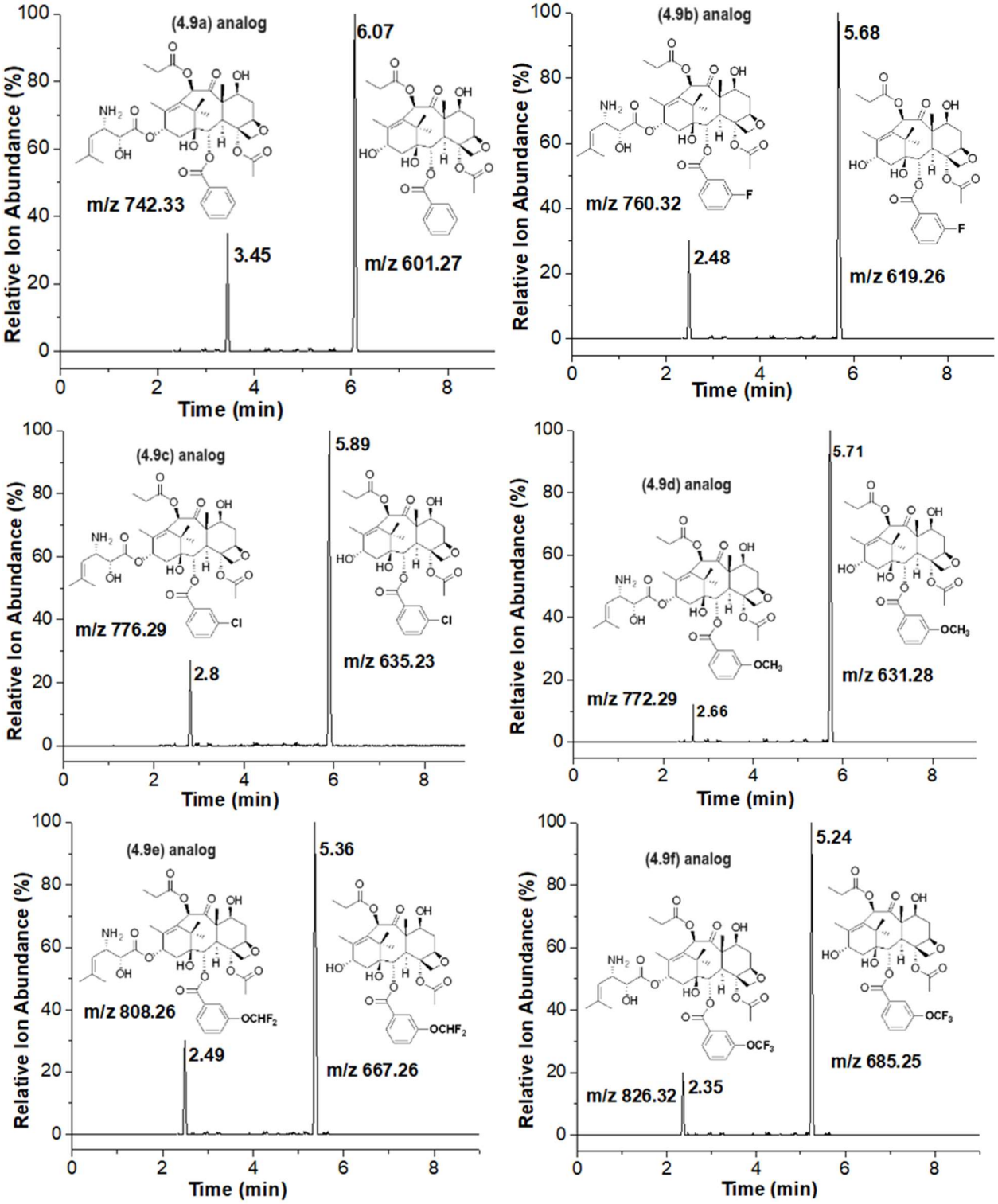

Figure 4.85: LC/ESI-MS (selected ion mode for m/z $[M + H]^+$) of the biocatalytic conversion of 10-PDAB analogs **4.6(a-f)** to the 3'-*N*-de(*tert*-butoxycarbonyl)-SB-T-1213 analogs **4.9**(**a**-**f**).

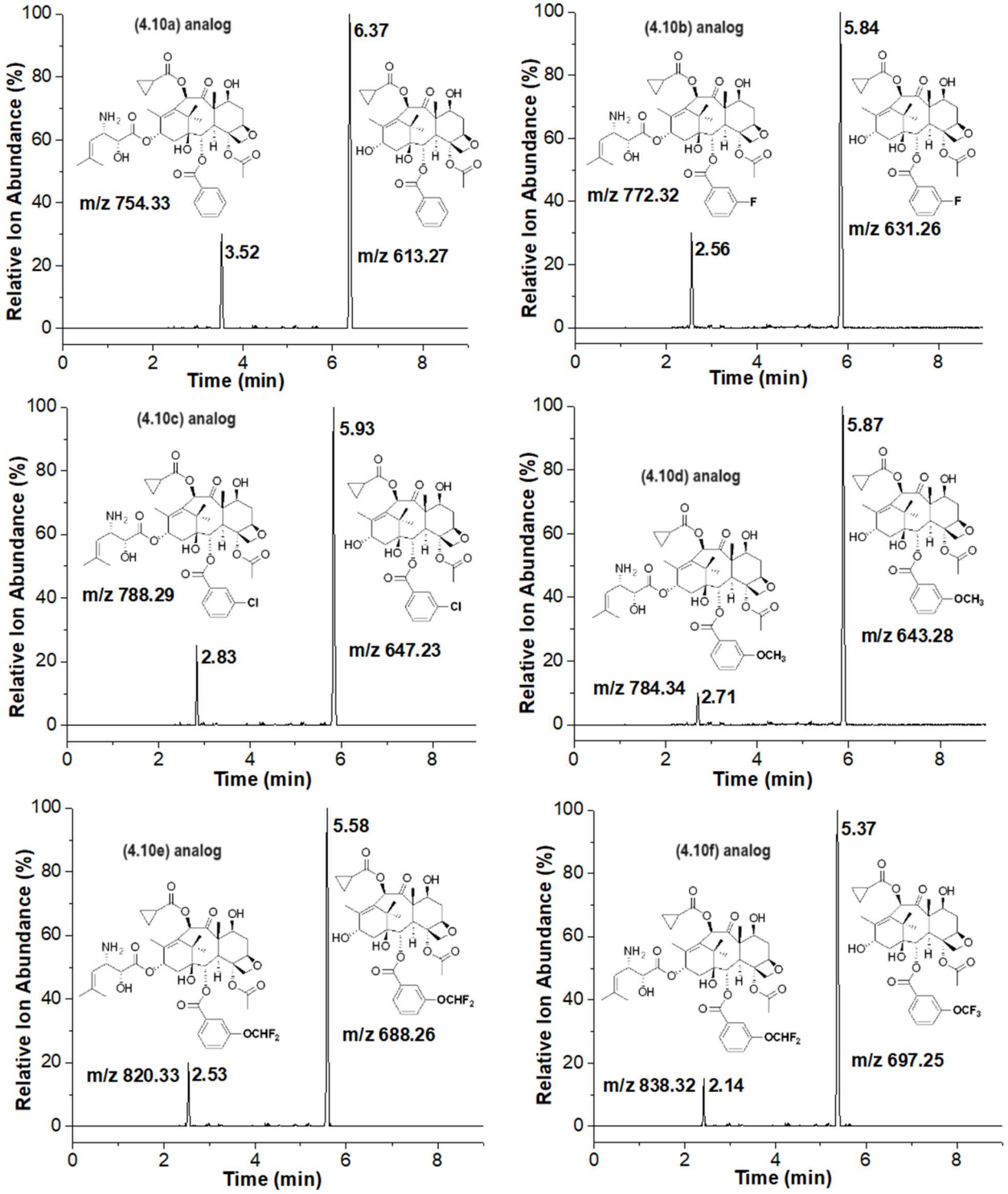

Figure 4.86: LC/ESI-MS (selected ion mode for m/z $[M + H]^+$) of the biocatalytic conversion of 10-CPCDAB analogs **4.7(a-f)** to the 3'-*N*-de(*tert*-butoxycarbonyl)-SB-T-1214 analogs **4.10**(**a-f**).